VOLUME 1 1961

Journal of Quantitative Spectroscopy & Radiative Transfer

OL.
1
961

Editor S. S. PENNER (*Pasadena*)

Associate Editors

W. S. BENEDICT (*Baltimore, Md.*)
LEWIS M. BRANSCOMB (*Washington*)
A. G. GAYDON (*London*)
L. GOLDBERG (*Cambridge, Mass.*)
H. C. HOTTEL (*Cambridge, Mass.*)
J. H. JAFFE (*Rehovoth*)
A. KANTROWITZ (*Everett, Mass.*)
J. LECOMTE (*Paris*)
H. MARGENAU (*New Haven, Conn.*)
R. MECKE (*Freiburg i. Br.*)
R. MEYEROTT (*Palo Alto, Calif.*)
R. W. NICHOLLS (*London, Ontario*)
N. N. SOBOLEV (*Moscow*)
P. SWINGS (*Liège*)
H. TAKEYAMA (*Hiroshima*)
W. M. VAIDYA (*New Delhi*)

PERGAMON PRESS
OXFORD · LONDON · NEW YORK · PARIS

Journal of Quantitative Spectroscopy and Radiative Transfer

Editor

Professor S. S. PENNER, California Institute of Technology, Pasadena, California, U.S.A.

Associate Editors

Dr. W. S. BENEDICT, Johns Hopkins University, Baltimore, Maryland, U.S.A.

Dr. LEWIS M. BRANSCOMB, Chief, Atomic Physics Division, National Bureau of Standards, Washington 25, D.C., U.S.A.

Dr. A. G. GAYDON, Chemical Engineering Department, Imperial College, London, S.W.7., England.

Professor L. GOLDBERG, Harvard University, Cambridge, Massachusetts, U.S.A.

Professor H. C. HOTTEL, Mass. Institute of Technology, Cambridge, Massachusetts, U.S.A.

Professor J. H. JAFFE, The Weizmann Institute of Science, Rehovoth, Israel.

Dr. A. KANTROWITZ, AVCO-Everett Research Lab., Everett, Massachusetts, U.S.A.

Professor J. LECOMTE, Sorbonne, Paris, France.

Professor H. MARGENAU, Yale University, New Haven, Connecticut, U.S.A.

Professor R. MECKE, Universität Freiburg, Freiburg i. Br., Germany.

Dr. R. MEYEROTT, Lockheed Aircraft Corporation, Palo Alto, California, U.S.A.

Professor R. W. NICHOLLS, Department of Physics, The University of Western Ontario, University College, London, Canada.

Professor N. N. SOBOLEV, Lebedev Physical Institute of the U.S.S.R. Academy of Sciences, Moscow, U.S.S.R.

Professor P. SWINGS, Institut d'Astrophysique, Université de Liège, Cointe-Sclessin, Belgium.

Professor H. TAKEYAMA, Department of Physics, Hiroshima University, Hiroshima, Japan.

Dr. W. M. VAIDYA, Assistant Director, Division of Optics, National Physical Laboratory of India, Hillside Road, New Delhi 12, India.

VOL. 1 1961

Publishing Offices:

Pergamon Press Limited, Headington Hill Hall, Oxford, England

Annual Subscription Rates:

(A) For libraries, government establishments, research laboratories, etc.: £7 ($20.00).

(B) For individuals who place their orders directly with the publisher and certify that the journal is for their personal use: £3 10. ($10.00).

Copyright © 1961

Pergamon Press Limited

PERGAMON PRESS LIMITED

HEADINGTON HILL HALL
OXFORD

122 EAST 55TH STREET
NEW YORK 22, N.Y.

Volume 1, Number 1

H. K. WIMMEL: Statistical line broadening in plasmas ... 1
M. LAPP: Shock-tube measurements of the *f*-number of the (O, O)-band of the OH $^2\Sigma$-$^2\Pi$ transitions ... 30
H. SADJIAN, H. K. WIMMEL and H. MARGENAU: Forbidden helium line in a plasma spectrum ... 46
J. C. CAMM, B. KIVEL, R. L. TAYLOR and J. D. TEARE: Absolute intensity of non-equilibrium radiation in air and stagnation heating at high altitudes ... 53
D. ROBINSON and R. W. NICHOLLS: Intensity measurements on overlapped molecular bands ... 76

Volume 1, Number 2

L. D. KAPLAN: The spectroscope as a tool for atmospheric sounding by satellites ... 89
S. S. PENNER, K. G. P. SULZMANN and C. B. LUDWIG: Approximate infrared emissivity calculations for NO at elevated temperatures ... 96
D. B. OLFE: Equilibrium emissivity calculations for a hydrogen plasma at temperatures up to 10,000°K ... 104
J. W. DAIBER and M. J. WILLIAMS: Transition probabilities for nitric oxide in the far ultra violet ... 135
B. H. ARMSTRONG, J. SOKOLOFF, R. W. NICHOLLS, D. H. HOLLAND and R. E. MEYEROTT: Radiative properties of high temperature air ... 143
S. S. PENNER: On iraser detectors for radiation emitted from diatomic gases and coherent infrared sources ... 163

Volume 1, Numbers 3/4

D. B. OLFE: Mean beam length calculations for radiation from non-transparent gases ... 169
H. J. KOSTKOWSKI and A. M. BASS: Direct measurement of line intensities and widths in first overtone band of CO 177
J. POMERANTZ: The influence of the absorption of radiation in shock-tube phenomena ... 185
R. GOULARD: The coupling of radiation and convection in detached shock layers ... 249
R. A. PAPPERT and S. S. PENNER: Approximate continuous opacity calculations for polyelectronic atoms at high temperatures ... 258
R. A. ALLEN, J. C. CAMM and J. C. KECK: Radiation from hot nitrogen ... 269

OL.
1
961

Author Index to Volume I

ALLEN, R. A. 269
ARMSTRONG, B. H. 143
BASS, A. M. 177
CAMM, J. C. 53, 269
DAIBER, J. W. 135
GOULARD, R. 249
HOLLAND, D. H. 143
KAPLAN, L. D. 89
KECK, J. C. 269
KIVEL, B. 53
KOSTKOWSKI, H. J. 177
LAPP, M. 30
LUDWIG, C. B. 96
MARGENAU, H. 46
MYEROTT, R. E. 143
NICHOLLS, R. W. 76, 143
OLFE, D. B. 104, 169
PAPPERT, R. A. 258
PENNER, S. S. 96, 163, 258
POMERANTZ, J. 185
ROBINSON, D. 76
SADJIAN, H. 46
SOKOLOFF, J. 143
SULZMANN, K. G. P. 96
TAYLOR, R. L. 53
TEARE, J. D. 53
WILLIAMS, M. J. 135
WIMMEL, H. K. 1, 46

INFORMATION FOR CONTRIBUTORS

1. Papers dealing with the following subjects will find a preferred publication outlet in JQSRT: theoretical and experimental determinations of *f*-numbers or absolute intensities for atomic and/or molecular systems; theoretical and experimental studies on spectral line shapes and widths; emissivities of heated gases, liquids, and solids; flame temperatures and flame emissivities; emission of radiation from heated gases, liquids and solids and long-range detection of radiating sources; quantitative spectroscopic techniques for environmental studies, particularly those related to rocket flights and satellite exploration; shock-tube studies in which the emphasis is on quantitative spectroscopy; radiant energy emission from plasmas; etc.

2. Manuscripts should be submitted to Professor S. S. Penner, California Institute of Technology, Pasadena, California, U.S.A. Contributors residing outside the U.S.A. should preferably submit their manuscripts through the local member of the Editorial Board. Submission of a manuscript will be taken as a representation that the manuscript has not been copyrighted, published or submitted for publication elsewhere.

3. Manuscripts should preferably be written in English, French or German. Manuscripts should be submitted in duplicate, and should be typewritten (except possibly for mathematical expressions), double spaced with wide margins on substantial white paper. Only one side of each sheet should be used. Contributors are advised to retain an additional copy for themselves as the Editors cannot accept responsibility for damage or loss of papers submitted.

4. The authors are requested to mark those passages which may be printed in small type.

5. Each article should be prefaced by a brief Abstract.

6. Footnotes should be indicated in the text by the following symbols in order, commencing afresh on each page: * † ‡ § || ¶

7. References should be cited in the text with superior numerals in parenthesis: where names are cited these should be in capitals and smali capitals, e.g. HOLTSMARK[1]; CHANDRASEKHAR and VON NEUMANN[2]; CONDON[3].

8. The full references should be listed in the numerical order of citation in the text at the end of the article, and should not be given as footnotes. They should include the names of all the authors and their initials, the order of publication in parenthesis, the full title of the book or standard abbreviated name of the journal (see: *World List of Scientific Periodicals*, 3rd edition (1952), Butterworths, London), the volume number and page: also for books, the publisher and city of publication. Examples:

1. J. HOLTSMARK, *Ann. Physik* **58**, 577 (1919)
2. S. CHANDRASEKHAR and J. VON NEUMANN, *Astrophys. J.* **95**, 489 (1942)
3. E. U. CONDON, *The Theory of Atomic Spectra*, p. 399. The University Press, Cambridge (1957).

9. The illustrations should be sent with the paper, but should not be affixed in place. The proper places for insertion, however, should be indicated in the text. All photographs, graphs and diagrams should be referred to as "Figures" (abbreviated to "Fig.") and should be numbered consecutively. The legends should be typed, correspondingly, on a separate page at the end of the article. The author's name, the figure number, and an indication of its proper orientation should be written lightly on the back of each figure.

10. The photographs should be glossy prints suitable for plates and should be approximately 1·5 times the final size. In general, it is preferable that any lines or letters that are to appear on the photographs be inserted by the publisher. Their position should be drawn on a leaf of drawing paper firmly attached to the photograph, or on an additional print.

Line drawings should be drawn in Indian ink on stiff white paper or on tracing cloth, and should be approximately twice their final size. The letters and symbols should be drawn so as to be clearly legible when reduced. The following standard symbols are readily available to the publisher:

○ ⊙ ● ▲ ▼ △ ▽ ⊡ + ×

11. Particular care should be exercised in identifying mathematical symbols used in equations. Subscripts and superscripts should be set off clearly; Greek symbols should be identified in the margins.

12. Fifty free reprints are available to authors if ordered on the order from accompanying the proofs Additional reprints are available if ordered on this same form.

PRINTED IN GREAT BRITAIN BY THE MENDIP PRESS LIMITED, BATH

VOL
1
196

SUBJECT INDEX

	Page
Absorption coefficient, of Argon continuum	223
— —, of hot air, $T < 12{,}000°K$	146
— —, — — —, $T > 12{,}000°K$	154
— —, — — —, mean	158
— —, of Hydrogen plasma	132
Absorption, continuous in Argon shock	189
—, — — — —, absorption coefficient	223
—, — — — —, density dependence	226
—, — — — —, free-free transitions	203
—, — — — —, frequency dependence	227
—, — — — —, spontaneous emission	193
—, — — — —, temperature effects	236
—, — — — —, transition probability	192
Absorption, influence on shock tube phenomena	185
Air, absorption coefficient $T < 12{,}000°K$	146
—, — —, $T > 12{,}000°K$	154
—, — —, mean	158
—, degree of ionization in shock	237
—, non-equilibrium radiation at high altitude	53
—, radiative properties at high temperature	143
—, effect of O atoms on shock radiation	68
—, radiation from shock wave, 300 A − 1 μ	58
—, — — — —, 1 μ − 9 μ	65
—, radiation transport in hot —	143
—, stagnation heating at high altitude	53
Argon, continuous absorption in shock wave	189
Atmosphere, model	90
—, ozone concentration	93
—, temperature distribution	89
Atmospheric radiation at 15 μ	89
Balmer lines, shape	23
Band intensity, CN violet	86
— —, 0_2^+	83
— —, and rotational line intensity	80
Beam length, mean for non-transparent gases	169
Beryllium atom, Rosseland mean free path	266
Carbon dioxide, atmospheric radiation at 15 μ	89
Carbon monoxide, line intensities	178
— —, line shape	182
— —, line width	179
Coherence loss	7
Coherence time	4
— — and field fluctuation	8
— — reduced	3
Convection, coupling to radiation	249
Cyanogen, (10,10) band intensity	86
Emissivity, of fundamental vibration-rotation band	96
—, of Hydrogen, H_2 vibration-rotation band	108
—, — —, rotational band	111

Emissivity, of Hydrogen, Lyman bands 114
—, — —, Werner bands 114
—, — —, H_2^+ ion 119
—, — —, H^- ion 118
—, — —, H atom 119
—, of NO infra-red 96, 100
—, — —, hemispherical 99
—, of overtone vibration-rotation bands 98

f-value, OH (0,0) band 30
—, N_2^+ first negative bands 269
—, NO γ bands 140
Fluctuation moments 13, 18, 24
Fluorine atom, Rosseland mean free path 266
Fractional band intensity 71
Free-free transitions, In Argon shock 203

Gerdien arc 46

Helium, $4^1D - 2^1P$ line shape 47
—, forbidden line in plasma spectrum 46
—, plasma composition 48
—, Stark effect in plasma 51
Holtzmark integrals 25
Hydrogen, atom, emissivity 119
—, —, Balmer line shape 23
—, negative ion, emissivity 118
—, molecule, emissivity of electronic bands 114
—, —, — of rotational band 111
—, —, — of vibration-rotation band 108
—, molecule ion, emissivity 119
—, plasma, absorption coefficient 132
—, —, emissivity 104
—, —, equilibrium composition 104
—, —, radiancy 129
Hydroxyl radical, *f*-value, for (0,0) band 30
— —, —, errors 44
— —, time constant of formation 35

Intensity, CN(10,10) band 86
—, CO lines 178
—, N_2^+ radiation from shock wave 54
—, NO β system 81
—, O_2^+ bands 83
—, measurement on overlapped bands 71
Ion density in plasma 46
Ionisation, degree of — in argon plasma 237
— potential, reduction in argon shock wave 206, 218
Iraser detectors 163
— —, and vibrational population 165
— —, and vibrational relaxation 164

Line broadening, adiabatic 5
— —, near-statistical 11
— —, Stark 2
— —, statistical 1

Line intensity, and band intensity 80
Line shape 5
— —, in CO 182
— —, contributions to statistical 19, 22
— —, Fourier integral formula 2
— —, Helium 4^1D-2^1P 47
— —, in wings 17
Line width in CO 179
Lyman bands of H_2, emissivity 114

Mean free path, Planck, for Nitrogen 264
— — —, Rosseland, for Beryllium 266
— — —, —, for Fluorine 266
— — —, —, for Nitrogen 264
Model atmosphere 90
Monochromator slit function 40

Nitric oxide, infra-red emissivity 96, 100
—, —, intensities β system 81
— —, f-value, γ system 140
Nitrogen atom, Planck mean free path 264, 265
—, —, Rosseland mean free path 264
Nitrogen molecule-ion, first negative f-value 269
— —, 1st -ve, intensity of radiation from shock 54

OH see under Hydroxyl radical
Opacity, calculations for poly-electronic atoms 258
Oscillator strength, OH (0,0) band 30
—, —, N_2^+ first negative 269
— —, NO bands 140
Overlapped molecular bands, intensities 71
Oxygen, molecule ion, band intensity 83
Ozone, upper atmosphere concentration 93

Planck mean free path 264
Plasma, forbidden lines in spectrum 46
—, ion density 46
Poly-electronic atoms, opacity calculations 258

Radiancy, of hydrogen plasma 129
Radiation, coupling with convection 249
—, from shock wave in air, 300 A to 1 μ 58
—, from shock wave in air, 1 to 9 μ 65
— heating 54
— transport, in hot air 143
Re-entry heating radiation effects 71
Rosseland mean free path, Beryllium 266
— — — —, Fluorine 266
— — — —, Nitrogen 264
Rotational line intensity, and band intensity 80

Satellite radiation heating 54
Shock layer, temperature distribution 252
Shock temperature, effect of radiation absorption 236
Shock tube, for OH f-value 30

VOL.
1
961

Shock waves, in air, non-equilibrium radiation 300 A to 1 μ 58
— —, — —, — — 1 μ to 9 μ 65
— —, — —, effect of O atoms on radiation 68
Slit function, of monochromator 40
Spontaneous emission, from argon shock 193
Stagnation heating, of high altitude air 53
Stark effect in argon shock wave 207
— — in helium plasma 51

Transition probability, of argon continuum 192
— —, for NO in ultra violet 135, 140
— —, for OH (0,0) band 30
Temperature distribution of atmosphere 89
— —, of shock layer 252
Time constant, of OH formation 35

Vibrational distribution, and iraser 165
— relaxation, and iraser 164
Vibration-rotation bands, emissivity 96, 98
—, H_2 108

Werner bands of H_2, emissivity 114

VOL.
1
1961

AUTHOR INDEX

AKRICHE, J. 215
ALEXANDER, E 725
ALPINER, B. P. 305
ATHAY, R. 309 309

BEHRING, W. E. 527
BOLDT, G. 705
BREENE, R. G. 225, 273, 310

CAMBEL, A. B. 249, 297
CARLETON, N. P. 241
CARROLL, P. K. 417
CROSSWHITE, H. M. 97
CURNUTTE, B. 41

DICKERMAN, P. J. 305
DIEKE, G. H. 97
DITCHBURN, R. W. 361
DRESSLER, K. 683
DUNKELMAN, L. 533

FELDMAN, U. 725
FERRELL, R. A. 679
FRAENCKEL, B. S. 725
FRIEDMAN, H. 547
FUJITA, I. 599

GABRIEL, A. H. 491
GARTON, W. R. S. 335
GIVENS, M. P. 629
GOLDEN, S. A. 201
GOLDRING, H. 293
GOTTSCHLICH, C. F. 297
GRENAT, H. 215
GRIEM, H. R. 503
GUTTMAN, A. 1

HARRIS, P. V. 327
HARTMAN, P. L. 579
HASS, G. 637
HEDDLE, D. W. O. 349
HERMAN, L. 215
HERZBERG, G. 319
HINTEREGGER, H. E. 561
HUFFMAN, R. E. 451
HUNTER, R. W. 637

JACOBS, A. 725
JAHODA, F. G. 467

KATO, R. 589
KESSLER, K. G. 713
KIRKPATRICK, H. A. 715
KIVEL, B. 509
KNOPP, C. F. 297
KOLB, A. C. 503

LARRABEE, J. C. 451
LAYZER, D. 309
LILLER, W. 519

MADDEN, R. P. 713
MAKOVSKY, J. 725
MALKMUS, W. 17
MARTON, L. 671
MATSUI, E. 589
MIESCHER, E. 421
MONFILS, A. 321
MOTTL, J. R. 369
MULLIKEN, R. S. 415

NAKAYAMA, T. 369
NAMIOKA, Y. 697
NARDONE, M. L. 273
NEUPERT, W. M. 527
NIBLETT, G. B. F. 491
NICHOLLS, R. W. 433

ONAKA, R. 599
OFFENHEIM, U. P. 293
OSTER, L. 310

PAPALIOLOIS, C. 241
PASSMORE, T. R. 327
PATCH, R. W. 263
PEACOCK, N. J. 491
PENNER, S. S. 263
PRICE, W. 327

RENSE, W. A. 555
RIBE, F. L. 467
ROMAND, J. 691
ROSEN, B. 321

SAWYER, G. A. 467
SHACKLEFORD, W. L. .. 93, 245, 263
STERN, E. A. 679
STRATTON, T. F. 467

TANAKA, Y. 451
TEEGARDEN, K. J. 629
THOMAS, R. N. 309
THOMSON, A. 17
THORNE, ANNE P. 427
THORNTON, J. A. 249
TOMBOULIAN, D. H. 649
TOUSEY, R. 571
TSAO, C. J. 41

UCHIDA, Y. 589

VODAR, B. 393

WALKER, W. C. 613
WATANABE, K. 369
WATSON, R. 301
WEISSLER, G. L. 315, 383, 613
WILKINSON, P. G. 343
WILLIAMS, S. E. 621
WILSON, R. 477

VOL.
1
1961

J. Quant. Spectrosc. Radiat. Transfer. Vol. 1, pp. 1–29. Pergamon Press Ltd. Printed in Great Britain

STATISTICAL LINE BROADENING IN PLASMAS*

H. K. WIMMEL
Laboratory of Marine Physics and Sloane Physics Laboratory
Yale University, New Haven, Connecticut

(*Received* 29 *June* 1960)

Abstract—This paper considers certain fundamental questions encountered in theories of line broadening. It is not so much a contribution to calculational techniques as an attempt at understanding some of the approximations which have been made in more compact and practical approaches to the subject. Its outlook is limited inasmuch as it deals only with the statistical type of line broadening theory.

The conditions under which ion broadening of spectral lines emitted from neutral atoms in plasmas can be described by the statistical theory are investigated by studying the fluctuations of the electric microfield acting on a radiating atom. Classical paths and absence of interaction between perturbers are assumed. The Fourier-integral formula for the line shape reveals three effects that cause deviations from the statistical line shape. Two of them, diabaticity and radiator rotation, are negligible compared to the third, whenever the total deviations are sufficiently small. The third effect, which may be called a phase-shift effect, arises from the frequency modulation in time and the loss of phase coherence occurring in a characteristic time $T_\Phi(F)$, the latter being related to the mean life-time $T_F(F)$ of a given electric microfield F. The correlation function of the spectrum is written as a double ensemble average: first an ensemble average is taken over the frequency shift as a function of time for $t \neq 0$, with the initial frequency shift at $t = 0$ held fixed, and subsequently the expression thus obtained is averaged over all possible initial frequency shifts. On representing the correlation function by a Taylor expansion in time, an expansion for the line shape is obtained that satisfies the wing theorem and likewise reduces to Holtsmark's line shape for high densities and low temperatures. The first-order correction to the statistical line shape is evaulated numerically; it vanishes near the maximum of the Holtsmark line shape (reduced fieldstrength $\beta = 1{\cdot}6$), while the maximal deviations occur in the ranges $\beta \approx 1$ and $\beta \approx 3$, the overall effect being an intensity shift towards larger values of β. The average absolute magnitude of the correction reaches 38 per cent and 16 per cent for the lines H_β and H_γ at $T = 10^4$ °K and $n_{ion} = 10^{17}$ cm^{-3} in the range $0{\cdot}6 < \beta < 10$; however, in these examples diabaticity and radiator rotation are not negligible and may actually alter the magnitude of the correction.

1. INTRODUCTION

STATISTICAL theories of pressure broadening of spectral lines have met with considerable success when applied to gases of high densities or the case of long-range interactions exerted by perturbing particles of low speed. HOLTSMARK[1] developed the first theory of the statistical type for line broadening by electrostatic interactions between radiating and perturbing particles. The concept was extended to more general types of interactions by MARGENAU, KULP, KUHN and LONDON[2–4], who considered perturbations of quantum-mechanical energy levels rather than frequency shifts induced by force-fields; this general theory allowed the application to line broadening by van der Waals interactions. The name *Statistical theory of line broadening* now characterizes those theoretical treatments which follow this general scheme by accounting only for the quasistatic effect of the perturbations and by computing spectral intensities within a line from the probability densities for the occurrence of the appropriate perturber configurations.

Under a wide range of conditions the shape of a spectral line that is emitted from atoms

* Supported by the Air Force Office of Scientific Research and the Office of Naval Research.

or ions in a plasma can be explained by the combined effect of *Stark broadening by ions and electrons*. Ordinarily the ion broadening is treated by a *statistical theory*, while the broadening by electrons is accounted for by an *impact-type theory*. The use of these two theories and the fashion of combining them involve so many simplifications of the physical situation that it becomes very difficult to estimate the magnitude of the error in the theoretical result for the line shape thus obtained.

As a first approach to this problem it appears useful and necessary to investigate the different approximations used and the errors thus produced *separately*. Such preliminary studies will resolve some of the complexities of the general problem of interaction broadening of spectral lines by indicating which of those approximations are especially drastic, and hence facilitate the development of more refined theories of plasma line broadening than are at present available.

The present paper is intended to contribute to this distant goal. It pursues a twofold purpose: to provide a better understanding of the basic assumptions underlying the statistical theory of line broadening, and to give a quantitative estimate of the *range of applicability* of this approach in the case of first-order Stark broadening by ions in a plasma. Both topics deserve closer consideration in view of recent refinements[5] of plasma line broadening theories. The methods employed can easily be adapted to different broadening interactions, but the broadening by first-order Stark effect seems especially suitable as an illustration of the general procedure. In keeping with the above philosophy broadening by electrons is entirely omitted from consideration.

The underlying *assumptions* of the present treatment are: Description of the radiating particles (henceforth called 'radiators') by non-relativistic quantum mechanics; classical treatment of the perturbing particles (henceforth called 'perturbers') and their fields and of the radiation field; infinite mass of the radiators, especially neglect of the Doppler effect. Therefore, the *Fourier-integral line shape formula*[6] in the form presented by BARANGER[7] is the basic intensity formula employed in this paper [equation (2)]. In addition, interactions between the perturbing ions of the plasma are neglected and the electrons are replaced by a homogeneous charge distribution.

The Fourier-integral line shape formula reduces to the statistical or impact-theoretical result under proper conditions[8]. The statistical line shape can be obtained in two ways: (1) At *high densities and low temperatures* the perturbation of the radiators varies 'slowly' in time, hence the variations in time of the perturbation appear to be of minor importance. Complete neglect of the time dependence of the perturbation in the Fourier-integral formula yields then the statistical result; (2) In the *wing* of a single Stark component of a line, i.e., for 'large' values of $|\omega - \omega_0|$ the method of stationary phase seems proper and, asymptotically, yields again the statistical line shape (*wing theorem*)[8].

In both cases it is necessary to assume *adiabaticity* for the radiators, i.e., to omit consideration of transitions between the 'adiabatic states' of the radiators.

A quantitative appraisal of the *validity range* of the statistical approximation has been furnished in the past[9] only with the assumption of either binary collisions or scalarly additive perturbation energies and phase shifts, while the present paper is concerned with *multiple interactions* between a radiating atom that shows linear Stark effect in an electric field, and all the surrounding ions of a plasma. Another advantage of the present treatment lies in the fact that the resulting validity condition for the statistical line shape accounts *simultaneously* for both limiting cases mentioned above.

To illustrate the *crucial point* of our analysis we add a few further remarks, in which we confine ourselves for the sake of simplicity to binary encounters, i.e., we assume for the time being that there exists around each radiator an effective volume in which not more than one perturber is present at the same time. Also we limit our concern for the time being to a single adiabatic Stark state of the upper energy level, neglecting the perturbation of the lower energy level. The quantitative analysis to be given later will of course not be subject to these restrictions.

Of all perturber paths which successively cross the effective volume we now consider only those path elements $(\boldsymbol{r}^*, \boldsymbol{r}^* + \Delta\boldsymbol{r})$ that produce a given electric fieldstrength F^* at the radiator and, according to the statistical approach, thus shift the frequency of the spectral line by the amount $\omega^* - \omega_0 = \mu F^*/h$, ω_0 being the unperturbed frequency, and μ the electric dipole component in field direction of the adiabatic Stark state in question. By proper choice of $|\Delta\boldsymbol{r}|$ the fieldstrength F is then restricted to an interval ΔF about F^*, the frequency ω to an interval $\Delta\omega = (\mu/h) \cdot \Delta F$ about ω^*.

On considering the contribution to line broadening that is caused by a given path element of a *single perturber with specified velocity* $\boldsymbol{v}$, one would expect approximate *validity of the statistical approach* if a $\Delta\omega$ can be chosen such that the following two conditions are fulfilled simultaneously: (a) Fourier analysis of the finite wave train that is emitted while the perturber moves on the path element in question yields a spectral intensity distribution with a half-width small compared to $\Delta\omega$, i.e., $\Delta\omega \times \Delta t > 2\pi$, where Δt is the time interval $|\Delta\boldsymbol{r}|v$ during which ω falls in the interval $\Delta\omega$ period. This condition yields a lower limit for $\Delta\omega$; (b) At the same time $\Delta\omega$ must be small compared to a frequency interval in which the statistical intensity distribution function varies appreciably; this determines an upper limit for $\Delta\omega$.

However, this argument neglects the question of phase coherence and, therefore, does not seem to be complete. For, according to the Fourier-integral formula one should not consider the broadening by a single perturber as an isolated effect, even if the interactions with different perturbers occur separately in time. In order to obtain the *reduced correlation function*, i.e., the correlation function referring to the given frequency ω [equation (20)], one must instead average, for the given path element $(\boldsymbol{r}^*, \boldsymbol{r}^* + \Delta\boldsymbol{r})$, over velocity $\boldsymbol{v}$ and time of passage t_0 of all perturbers.

The reduced correlation function describes, for a given perturbation energy (frequency shift), the *loss of phase coherence with time* of the emitted light wave. This coherence loss is caused by the fact that perturbers which produce exactly the same frequency shift $\omega^* - \omega_0$ at different times t_0 produce different shifts at earlier or later times $t \gtrless t_0$ because of the difference in their velocities $\boldsymbol{v}$. If adiabaticity is guaranteed then the time interval $T_\Phi(F)$ in which the loss of phase coherence occurs will be smaller than the time interval $T_F(F)$ in which the field due to the single effective perturber in question varies appreciably. As will be shown in section (II.5) this holds not only for binary interactions, but for all fields $F > F_0$, where F_0 is the 'normal field' defined in equation (18a). To provide for $T_\Phi < T_F$ for smaller fields ($F < F_0$) the condition of near-statistical broadening must be introduced, as given by equation (1) and (1a) at the end of this section.

It is interesting to compare this situation with the simple *impact assumption* of WEISSKOPF[10]. There one assumes that every adiabatic collision, i.e., every completed passage through a certain effective volume destroys coherence completely. Hence, the characteristic coherence time is identical with the average time interval between two

consecutive collisions. On the other hand the *actual coherence times* for adiabatic interactions, which matter for statistical broadening, are often much shorter, so that they may be associated with given values of interaction energy, fieldstrength, and frequency shift. For this reason and others, mentioned in section (II.5), the concept of *entire adiabatic collisions*, in the sense of completed passages of a perturber, as elementary line-broadening agents does not seem very adequate for charged perturbers even in the frequency regions where the broadening is not statistical. The difficulty does not arise with weak (diabatic) collisions which are essentially responsible for line broadening by electrons at higher temperatures.

The above argument on the validity of the statistical line shape was *incomplete* because the necessary averaging over different perturbers was omitted and arbitrary time intervals Δt were used instead of the physically important coherence times T_Φ. To give a simple *illustration* we may, perhaps, relate the reduced correlation function to the picture of an emitted light wave and say that the coherence time $T_\Phi(F)$ describes the extension in time of a single light wave-train of frequency ω. While using this picture, it must be remembered that neither the reduced correlation function nor the light wave chosen as an illustration can be attributed to the elementary emission act of a single radiator, but describe coherence properties brought about by the stochastic cooperation of all perturbers and radiators. The conclusion suggested by this illustration—and later confirmed by detailed analysis—is that the realization of the following two conditions will guarantee *near-statistical line broadening*, i.e., approximate validity of the statistical theory: (A) The quantity $\Delta\omega(T_\Phi)$, i.e., the possible frequency variation during the coherence time, must be small compared to a frequency interval in which the statistical intensity varies appreciably. This implies

$$T_\Phi \ll T_F, \tag{1}$$

i.e., the coherence time must be small in comparison with the fluctuation time T_F of the electric field, since

$$\Delta\omega(T_\Phi) \approx (\omega - \omega_0)\,(T_\Phi/T_F).$$

(B) Broadening due to the finite extension T_Φ of the wave-trains must not be larger than $\Delta\omega(T_\Phi)$, i.e.,

$$T_\Phi \cdot \Delta\omega(T_\Phi) \gtrsim 2\pi.$$

In view of condition (A) this implies that

$$(2\pi)^{-1}\,(\omega - \omega_0)\,T_\Phi \gg 1. \tag{1a}$$

Hence, the two conditions say that the phase coherence loss must occur in a time that is *short* compared to the field fluctuation time, but *long* compared to the reciprocal Stark shift. It will be shown in section (I.3) that equation (1) and (1a) are practically equivalent in the region of their validity.

In section (II) the general theory for adiabatic and near-statistical line broadening is developed and applied to ion-broadening by linear Stark effect. In section (II.1) the line shape for adiabatic broadening is derived from the Fourier-integral line shape formula. The mechanisms that cause deviations from the statistical line shape are investigated in section (II.2). The relation between coherence times and characteristic field fluctuation times is discussed in section (II.3), while a simple adiabaticity condition is presented in section (II.4). The relations between the conditions of near-statistical broadening and

adiabaticity are discussed in section (II.5). The expansion of the line shape expression in terms of fluctuation moments and derivatives of the statistical line shape function in section (II.6) yields approximate formulas for the line shape that are useful for near-statistical broadening. In section (III) the evaluation of these formulas is carried out for binary interactions [section (III.1)] and in the general case of multiple interactions [section (III.2)]. Finally, in section (IV), numerical results for the deviation of the line shape from the result of the statistical theory are presented and discussed. In three appendices the vanishing of a certain second-order fluctuation moment is demonstrated (App. A), basic relations for an infinite set of Holtsmark integrals are listed (App. B), and the computed functions are tabulated (App. C).

II. THEORY

1. *Adiabatic line broadening*

We use the Fourier-integral line shape formula[6] in the form due to BARANGER[7]. Accordingly the spectral intensity of emission per atom and second is given by

$$I(\omega) = (4\omega^4/3c^3)\, F(\omega),\ \omega > 0 \tag{2}$$

with

$$F(\omega) = \sum_i \sum_f \lim_{T\to\infty} (2\pi T)^{-1} \{ \left| \int_0^T \mathrm{d}t\, e^{i\omega t} < \psi_f(t) | \boldsymbol{\mu} | \psi_i(t) > \right|^2 \}_{Av} \tag{2a}$$

Here ψ_i, ψ_f are initial and final states of a radiator, and $\boldsymbol{\mu}$ is the electric dipole moment operator. The ensemble average indicated by Av refers to all possible motions of the perturbers. For convenience $F(\omega)$ is often referred to as *line shape*, although the actual line shape is given by equation (2).

By introducing the density matrix $\rho(t)$ and the time-development operator $\mathcal{T}(t_1, t_2)$ defined by

$$\mathcal{T}(t_1, t_2)\, \psi(t_2) = \psi(t_1),\ \mathcal{T}^+(t_1, t_2) = \mathcal{T}(t_2, t_1),$$

where the dagger denotes the adjoint operator,
equation (2a) is easily transformed into

$$F(\omega) = \lim_{T\to\infty} (2\pi T)^{-1} \int_0^T \int_0^T \mathrm{d}t_1 \mathrm{d}t_2 e^{i\omega(t_1 - t_2)} \Phi(t_1, t_2), \tag{3}$$

with Φ represented by a trace:

$$\Phi(t_1, t_2) = Tr\{\mathcal{T}(t_1, t_2)\rho(t_2)\boldsymbol{\mu}\mathcal{T}(t_2, t_1)\boldsymbol{\mu}\}_{Av} \tag{4}$$

where the indices i and f now extend over *all* states of the radiator. However, if the summations are restricted to a finite number of states, equation (4) is still useful when understood as a symbolical expression. Clearly

$$\Phi(t_2, t_1) = \Phi^*(t_1, t_2),$$

the star denoting the complex conjugate.

It will be shown in section (II.5) that, for *very small deviations* from the statistical line shape, collision-induced transitions between the adiabatic Stark states play a minor role and need not be taken into account. Although this ideal case is only approximately realized at 'normal' densities and temperatures ($n \approx 10^{17}$ cm^{-3}, $T \approx 10^4$ °K) we shall, for simplicity, make the assumption of adiabaticity henceforth. Therefore we specify our

formulas from the beginning for the case of *adiabatic line broadening*. In evaluating equation (2a) for adiabatic broadening, the system can be considered to be in quasiequilibrium, since the natural lifetime of an excited radiator state is quite large compared to a characteristic coherence time T_Φ. Thus, according to equation (25), we have for $n = 10^{16}$ cm^{-3}, $T = 10^4$ °K, and hydrogen ions as perturbers a fluctuation time T_F smaller than $7{\cdot}8 \times 10^{-13}$ sec, which is to be compared with a typical natural lifetime of 10^{-8} sec ; since we shall consider only the case $T_\Phi < T_F$, we have also $T_\Phi < 7{\cdot}8 \times 10^{-13}$ sec, i.e., a coherence time that is much smaller than the natural lifetime of an excited atomic state.

It follows that $\Phi(t_1, t_2)$, as an ensemble average, depends only on $(t_1 - t_2)$, and, thus, can be replaced by $\Phi(t_1 - t_2) \equiv \Phi(t_1 - t_2, 0)$. On using further the relation

$$\lim_{T\to\infty} (2\pi T)^{-1} \int_0^T \int_0^T dt_1 dt_2 f(t_1, t_2) = (2\pi)^{-1} \int_{-\infty}^{+\infty} f(t)\, dt,$$

which holds for any absolutely integrable function $f(t)$, one may express the line shape by a single rather than a double integral:

$$F(\omega) = (2\pi)^{-1} \int_{-\infty}^{+\infty} e^{i\omega t} \Phi(t) dt, \tag{5}$$

with the *correlation function*

$$\Phi(t) = \Phi^*(-t) = Tr\{\mathcal{T}(t)\rho(0)\boldsymbol{\mu}\mathcal{T}^\dagger(t)\boldsymbol{\mu}\}_{Av} \tag{6}$$

and the time-development operator

$$\mathcal{T}(t) \equiv \mathcal{T}(t, 0)$$

To specify equation (6) for *adiabatic broadening* we use a mixed adiabatic representation of the matrices in the following fashion: The Hamilton operator $H(t)$ of a perturbed radiator defines a complete orthonormal set of adiabatic wave functions

$$U_n(t) = u_n(t) e^{-i\varphi_n(t)} \tag{7}$$

with the phase functions

$$\varphi_n(t) = \int_0^t E_n(t') dt'. \tag{8}$$

Using the *two* sets of functions $U_n(0)$ and $U_n(t)$ we define ordinary and mixed matrix elements, e.g.:

$$\left.\begin{aligned} A^{oo}_{nm} &= \int U_n^*(0) A\, U_m(t) d\tau, \\ A^{it}_{nm} &= \int U_n^*(t) A\, U_m(t) d\tau, \text{ etc.} \end{aligned}\right\} \tag{9}$$

where A is any operator. The matrices that are obtained in this way from the operator A are written as A^{oo}, A^{it}, and so forth. Then equation (6) assumes the following form:

$$\Phi(t) = Tr\{\mathcal{T}^{io}(t)\rho^{oo}(0)\boldsymbol{\mu}^{oo}[\mathcal{T}^{io}(t)]^\dagger \boldsymbol{\mu}^{it}\}_{Av}. \tag{6'}$$

In the *adiabatic approximation*

$$\mathcal{T}^{io}(t) \equiv 1,$$

hence the *adiabatic correlation function* has the form:

$$\Phi_{ad}(t) = Tr\{\rho^{oo}(0)\boldsymbol{\mu}^{oo} \cdot \boldsymbol{\mu}^{it}\}_{Av}. \tag{10}$$

This formula could of course have been derived more directly, i.e., without first introducing the time-development operator, by identifying the $\psi_A(t)$ and $\psi_f(t)$ of equation (2a) with the

$U_n(t)$. However, the presentation given has the advantage of allowing an easier comparison with the treatment by ANDERSON and BARANGER[11].

It is sufficient for our purposes to consider merely the transition between two single Stark levels i and f. The corresponding *adiabatic correlation function* is:

$$\Phi_{if}(t) = \{\boldsymbol{\mu}_{if}(0) \cdot \boldsymbol{\mu}_{fi}(t)\}_{Av}, \tag{11}$$

with the understanding that $\boldsymbol{\mu}_{if}(0)$ and $\boldsymbol{\mu}_{if}(t)$ are given in the $U_n(0)$ and $U_n(t)$ representation, respectively.

2. *Rotation effect and coherence loss*

Further insight in equation (11) is gained by passing over to a u_n-representation in accordance with equation (7) and (8). Then the correlation function becomes

$$\Phi_{if}(t) = \{e^{-i[\varphi_i(t)-\varphi_f(t)]} < u_i(0)|\boldsymbol{\mu}|u_f(0) > \cdot < u_f(t)|\boldsymbol{\mu}|u_i(t) >\}_{Av} \tag{12}$$

According to this formula *two mechanisms* contribute to the decrease of $|\Phi_{if}|$ with time: (a) A loss of phase coherence, which is caused by the random modulation of the radiator frequency by the field. This effect is represented by the exponential in equation (12); (b) Random variation of the direction of the transition moment in time. This effect occurs because the variation of the field orientation induces an equal change of the orientation of the Stark-eigenfunctions; it is represented by the inner product of the transition moments. A possible third mechanism, i.e., collision-induced transitions between the adiabatic states, has already been eliminated by our assumption of adiabaticity.

If we write equation (12) for the case where only the *loss of phase coherence* and the *frequency modulation* contribute, while the rotation is neglected, we obtain:

$$\Phi_{if}(t) = \int_0^\infty d\omega_{if} |\boldsymbol{\mu}_{if}(\omega_{if})|^2 P(\omega_{if}) e^{-i\omega_{if} t} \{e^{-i\Delta\varphi_{if}(t)}\}_{Av(\omega)} \tag{13}$$

with the phase shift

$$\Delta\varphi_{if}(t) = \int_0^t [\omega_{if}(t') - \omega_{if}(0)]\, dt'. \tag{14}$$

Here $\omega_{if} \equiv \omega_{if}(0)$ is the frequency at $t = 0$, and $P(\omega_{if})$ is the statistical frequency distribution function, i.e., the probability density of finding the atom radiating with the frequency ω_{if}, while the statistical *spectral intensity* within a line is generally given by $|\mu_{if}(\omega)|^2 \cdot P(\omega)$ [equation (16)]. In the original formulation of the statistical theory it has always been assumed that the transition moment is independent of the perturbation and, hence, of ω. The average in equation (12) has been written as an average $Av(0)$ for fixed initial frequency $\omega_{if}(0)$, averaged over all the different initial frequencies by the integrating over ω_{if}. In case of *linear Stark effect* the dependence of μ_{if} on ω_{if} may be neglected in first-order approximation.

It will be shown in the following sections that under the conditions considered in this paper, this simplification of equation (12) is permitted. Hence the *line shape* is obtained by substituting equation (13) into (5):

$$F_{if}(\omega) = (2\pi)^{-1} \int_0^\infty d\omega_{if} |\mu_{if}(\omega_{if})|^2 P(\omega_{if}) \times \int_{-\infty}^{+\infty} dt e^{i(\omega_{if} - \omega)t} \{e^{i\Delta\varphi_{if}(t)}\}_{Av(\omega)}, \tag{15}$$

where, for convenience, the sign of the exponents has been changed in accordance with equation (6). For $\Delta\varphi_{if} \equiv 0$ the line shape reduces to *the statistical expression:*

$$F_{if}(\omega) = |\mu_{if}(\omega)|^2 P(\omega); \tag{16}$$

but only *formally*, because $\Delta\varphi_{if} \equiv 0$ contradicts the assumption of the existence of a *time-dependent perturbation*, with which the general theory of line broadening starts. It is, therefore, the purpose of the following considerations to show under what conditions the statistical formula is still a good approximation even though the phase shift $\Delta\varphi_{if}(t)$ cannot be identically zero.

3. *Relation between field fluctuations and coherence times*

If the *correlation time* T_c of the perturbing field is identified with the *fluctuation time*, or *mean life*, T_F of a given fieldstrength, as defined by CHANDRASEKHAR and VON NEUMANN[12] then prevalence of the effect of phase coherence loss over the rotation effect is guaranteed if the fluctuation time is much greater than the *phase coherence time*, i.e., for $T_F \gg T_\Phi$, both of which quantities depend on the instantaneous fieldstrength F. The exact definition of the quantities in question follows.

After CHANDRASEKHAR and VON NEUMANN[12] the *mean life* T_F of a given fieldstrength F is defined as

$$T_F = F\left(\left|\frac{\partial \boldsymbol{F}}{\partial t}\right|^2_{Av(F)}\right)^{-\frac{1}{2}}, \tag{17}$$

with the ensemble average $Av(F)$ taken for fixed F. It is numerically equal to

$$T_F = t_0 \tau(\beta), \tag{18}$$

with $\tau(\beta)$ tabulated[12] as function of $\beta = F/F_0$,

$$F_0 = 2{\cdot}603\, Zen^{\frac{2}{3}}, \tag{18a}$$

and

$$t_0 = 0{\cdot}3201\, n^{-\frac{1}{3}}\left(\frac{m}{3kT}\right)^{\frac{1}{2}} \tag{19}$$

for a Maxwell-Boltzmann velocity distribution (n = number density, Ze = ion charge, m = ion mass, F_0 the *normal field*).

The field correlation time in question, T_c, is defined as the time interval, starting at $t = 0$, in which the ensemble average of the expression

$$|\langle u_i(0)|\boldsymbol{\mu}|u_f(0)\rangle \cdot \langle u_f(t)|\boldsymbol{\mu}|u_i(t)\rangle|$$

decreases by a factor of e, say. Strictly speaking, T_c differs from the ordinary field correlation time since, for linear Stark effect, the expression in equation (12) contains only the *change in direction of the field*, not the change of its magnitude. T_c, by definition, differs also from the fluctuation time T_F; but for the present purpose of comparing the importance of the coherence loss with that of the rotation effect, the identification of both quantities is justified.

Similarly to T_c, the phase coherence time T_Φ is defined as the time interval, starting at $t = 0$, in which the absolute magnitude of the *reduced correlation function*

$$M_{if}(t) \equiv M_{if}^*(-t) = \{e^{i\Delta\varphi_{if}(t)}\}_{Av(\omega)} \tag{20}$$

contained in equation (13) and (15), decreases by a factor of e, say. The calculation of T_Φ under general conditions is complicated. Fortunately, however, it is sufficient for our purpose to calculate T_Φ in an approximate way and only for the case that $T_\Phi \ll T_F$, as will be shown in section (5). The approximation employed consists of two steps. First we assume that for $t = T_\Phi$ the standard deviation of $\Delta\varphi_{if}(t)$ is equal to $\frac{\pi}{2}$, i.e.,

$$\{[\Delta\varphi_{if}(T_\Phi)]^2\}_{Av(i)} \approx \frac{\pi^2}{4} \tag{21}$$

Secondly, because of $T_\Phi \ll T_F$, we assume that the field $F(t)$ can be well described by

$$F(t) = F(0) + t\frac{\partial F}{\partial t}(0). \tag{22}$$

With the aid of equation (17) and

$$\Delta\varphi_{if}(t) = 2\pi h^{-1}(\mu_{ii} - \mu_{ff})\int_0^t [F(t') - F(0)]\,dt', \tag{23}$$

and with the approximation

$$\frac{\partial F}{\partial t} \approx \left|\frac{\partial F}{\partial t}\right|, \tag{24}$$

which leaves the result correct within a factor $\sqrt{3}$ according to CHANDRASEKHAR and VON NEUMANN,[10] T_Φ can be obtained by straightforward calculation as:

$$T_\Phi^2 \approx \frac{hT_F}{2|\mu_{ii} - \mu_{ff}|F}, \text{ if } T_\Phi \ll T_F. \tag{25}$$

Here μ_{ii} and μ_{ff} are the electric dipole components in the field direction for the initial and final state of the radiator. The case $\mu_{ii} = \mu_{ff}$ need not be considered because the corresponding lines show no first-order Stark broadening. The condition $T_\Phi \ll T_F$ for the *prevalence of the effect of coherence loss* over the rotation effect can now be expressed by

$$\frac{T_\Phi}{T_F} \equiv \left(\frac{h}{2|\mu_{ii} - \mu_{ff}|FT_F}\right)^{\frac{1}{2}}$$
$$\equiv \frac{h}{2|\mu_{ii} - \mu_{ff}|FT_\Phi} \ll 1, \tag{26}$$

where T_F is given by equation (18) and (19). Since equation (1a) is identical with equation (26), which itself is approximately equivalent to equation (1), the equivalence of the two conditions given by equation (1) and (1a) has been established for the range of their validity.

4. *Adiabaticity condition*

In considering *small deviations from* the statistical line shape, the effect of *collision-induced transitions* between the adiabatic Stark states may be neglected in comparison with the effect of phase coherence loss if the transition amplitudes remain small compared with 1 for a time interval T_Φ.

To guarantee this for the Stark levels of the upper state one has to require that

$$\left|\int_0^{T_\Phi} \frac{(\partial H/\partial t)_{ij}}{E_i(t) - E_j(t)}\, e^{i[\varphi_i(t) - \varphi_j(t)]}\,dt\right| \ll 1 \tag{27}$$

according to SCHIFF[14]. Here i is the initial Stark level under consideration, and j any other Stark level of the upper state for which $E_i \neq E_j$.

If, in the first-order approximation, $E_i \equiv E_j$ there arises no difficulty because there is always one and only one orthonormal set of functions $u_i(t)$ such that

$$\int u_i^*(t)\dot{u}_j(t)\mathrm{d}\tau \equiv \int u_j^*(t)\dot{u}_i(t)\mathrm{d}\tau \equiv 0 \tag{28}$$

for all pairs (i, j), including $i = j$, for which $E_i(t) \equiv E_j(t)$. This is a generalization for the case of degeneracy of the usual condition[14]

$$\int u_i^*(t)\dot{u}_i(t)\mathrm{d}\tau \equiv 0 \tag{29}$$

which can be fulfilled by merely adjusting the phases of the u_i. Condition (28) says that the u_i can always be chosen in a unique way such that no transitions occur between permanently degenerate states. We shall assume in the following that this has been achieved already for our set of u_i, u_j etc.

It may be worth mentioning that in the case of linear Stark effect (hydrogen-like wavefunctions), which we are considering, the proper set of u_i is constructed in the following manner:

Imagine a coordinate system that rotates with the perturbing field F such that the z-axis points always in the field direction, while the x-axis is identical with the instantaneous rotation axis about which the field vector is rotating, in counter-clockwise fashion. Construct $u_i(t + \mathrm{d}t)$ by rotating $u_i(t)$, without changing its phase, about the x-axis by the same angle $\mathrm{d}\theta = \dot{\theta}\mathrm{d}t$ by which the field vector is rotated. It is easily seen that

$$\dot{u}_i = i^{-1}\dot{\theta}L_x u_i \tag{30}$$

where

$$L_x \equiv \frac{1}{i}\left(y\frac{\partial}{\partial z} - z\frac{\partial}{\partial y}\right) \tag{31}$$

is the angular momentum operator in units of h. A state with the magnetic quantum number m is transformed by L_x into a linear combination of states with $m' = m \pm 1$. On the other hand two Stark-eigenstates u_i, u_j can have the same energy only if the difference of their magnetic quantum numbers is an even number, including zero, as can be seen from the first order Stark correction

$$\Delta E^{(1)} = \frac{3}{2}eFa_0(n - 2k_1 - |m| - 1) \tag{32}$$

in the notation of CONDON and SHORTLEY[15]. From these two facts it follows that in equation (28) $\dot{u}_i$ is always orthogonal to u_j ($j = i$ included), which proves that our construction of the u_i is correct. This consideration shows, by the way, that the splitting between phase coherence loss and rotation effect [section (3)] was done correctly in the case of degenerate states.

If equation (26) is fulfilled for all i, then the adiabaticity condition equation (27) can be *simplified* because the electric field is nearly constant during T_Φ, while the exponential function is rapidly oscillating. Therefore it is sufficient to consider the integral in equation (27) for one period of the exponential, $2\pi/\omega_{ij}$, and the matrix element $(\partial H/\partial t)_{ij}$ can be replaced by its r.m.s. value for a given fieldstrength F, so that we obtain:

$$\frac{2\pi}{|\omega|_{ij}} \cdot \frac{1}{|E_i - E_j|} \cdot \left[\left|\left(\frac{\partial H}{\partial t}\right)_{ij}\right|^2_{Av(F)}\right]^{\frac{1}{2}} \ll 1. \tag{33}$$

On writing equation (33) in terms of the electric field and atomic matrix elements, specifically:

$$\left[\left|\left(\frac{\partial H}{\partial t}\right)_{ij}\right|^2\right]_{Av(F)}^{\frac{1}{2}} = |\mu_{ij}^{\perp}|\left[\left|\frac{\partial F_{\perp}}{\partial t}\right|^2\right]_{Av(F)}^{\frac{1}{2}} \tag{34}$$

$$\approx \frac{1}{\sqrt{3}}|\mu_{ij}^{\perp}|\left[\left|\frac{\partial F}{\partial t}\right|^2\right]_{Av(F)}^{\frac{1}{2}} \tag{35}$$

$$= \frac{1}{\sqrt{3}}|\mu_{ij}^{\perp}|FT_F^{-1}, \tag{36}$$

equation (33) is transformed into the simplified *adiabaticity condition:*

$$\frac{h}{\sqrt{3}\,|\mu_{ii}-\mu_{jj}|FT_F}\cdot\left|\frac{\mu_{ij}^{\perp}}{\mu_{ii}-\mu_{jj}}\right| \ll 1 \tag{37}$$

The index $\perp$ indicates the y-component of $\boldsymbol{\mu}$ and $\boldsymbol{F}$ in the coordinate system introduced above, while the absence of an index indicates the z-component of $\boldsymbol{\mu}$ only, with F retaining its meaning as the absolute magnitude of the electric field. The error introduced by equating the right sides of equation (34) and (35) does not exceed a factor of $\sqrt{2}$. Equation (37) will be further discussed in the next section.

A similar condition may be derived for the Stark levels of the lower state. Since the maximum value of $\mu_{ij}^{\perp}$ increases with the principal quantum number n, adiabaticity for all pairs of levels of the upper state will automatically guarantee the same for the lower state.

5. *Condition of near-statistical broadening*

As has been shown in section (3), the two equations (1) and (1a), originating from the requirement of near-statistical broadening, are practically equivalent to each other and equation (26). Moreover they insure that the effect of phase coherence loss prevails over the rotation effect so that the latter can be neglected. In this section we shall establish, in addition, a close relation between the condition of *adiabaticity*, or rather prevalence of phase coherence loss over the effect of collision-induced transitions, and the condition of *near-statistical broadening* as given by equation (26).

Suppose that equation (26) holds for all i and f, the principal quantum numbers of the upper and lower levels being fixed. This set of conditions is equivalent to the following one, which is obtained by replacing the factor $|\mu_{ii}-\mu_{ff}|$ by $|\mu_{ii}-\mu_{jj}|$, with j denoting a Stark state of the upper level:

$$\frac{h}{2|\mu_{ii}-\mu_{jj}|FT_{\Phi}} \ll 1. \tag{38}$$

Since $T_{\Phi} \ll T_F$, this insures the validity of the adiabaticity condition (37) for small principal quantum numbers n, for which $\mu_{ij}^{\perp}$ and $(\mu_{ii}-\mu_{jj})$ do not differ largely in their orders of magnitude.

Next we ask whether adiabaticity can be expected during one period of the exponential function in equation (27), if the condition of near-statistical broadening [equation (26)] is *not* fulfilled. According to equation (18) and the tabulated values[12] of $\tau(\beta)$, the left side of equation (26) is a monotonically decreasing function of the reduced fieldstrength β,

becoming infinite for $\beta \to 0$, and zero for $\beta \to \infty$. Hence there will always be a range $0 \leq F \leq F_c$ for which equation (26) is violated, while it holds for $F > F_c$. To have the mentioned sort of adiabaticity in the range $0 \leq F \leq F_c$, one must require, in accordance with equation (37), that

$$\frac{h}{\sqrt{3}|\mu_{ii} - \mu_{ff}|} \left\langle \frac{1}{FT_F} \right\rangle_{Av} \ll 1, \tag{39}$$

where the average is restricted to the interval $0 \leq F \leq F_c$, and μ_{ii} has been replaced by μ_{ff}, using the argument above.

In the further discussion *two different cases* have to be distinguished. If F_c is greater than the normal field F_c, then it is appropriate to put

$$\left\langle \frac{1}{FT_F} \right\rangle_{Av} \approx \frac{1}{F_0 T_F(F_0)}.$$

Comparison with equation (26) shows that equation (39) then becomes equivalent to

$$T_{\Phi 0}{}^2 \ll \tfrac{1}{2} T_{F0}{}^2, \tag{40}$$

where the index 0 indicates that the quantities correspond to $F = F_0$. Equation (40), though a somewhat weaker condition than $T_{\Phi 0} \ll T_{F0}$, practically implies validity of equation (26) for $F = F_0$. Hence we have a *contradiction*, from which we infer that for all $F > F_0$ adiabaticity guarantees the validity of equation (26), i.e., near-statistical broadening.

If, on the other hand, $F_c \ll F_0$ we may approximate[16] the probability distribution for β by $H(\beta) \approx \frac{1}{4}\pi^{-1}\beta^2$, put $\tau(\beta) \approx \beta$, and obtain the average involved in equation (39) by a simple integration. The result is

$$7{\cdot}35\, \beta_c\, (T_{\Phi 0}/T_{F0})^2 \ll 1, \tag{41}$$

which even for $\beta_c = 1$ ($F_c = F_0$) requires only the validity of equation (26) for $F \geq F_0$.

The *results* of this section can be summarized as follows: The condition of *near-statistical broadening*, when fulfilled in a certain field range $F > F_c$, *implies adiabaticity* in the same field range at least for small principal quantum numbers. On the other hand adiabaticity for $F > F_0$ always implies the occurrence of near-statistical broadening for this range of fields and hence, in the case of small principal quantum numbers, also adiabaticity for all $F < F_0$, that is for the whole range of fieldstrengths. No inference can be drawn from adiabaticity to near-statistical broadening in the range $F < F_0$.

It seems surprising that under certain conditions adiabaticity is guaranteed even for the very *smallest fieldstrengths*, if this result is compared with the adiabaticity condition obtained from the consideration of binary collisions. The reason seems to be that the latter consideration *overestimates the probability of small fieldstrengths* by referring to a time interval that is either proportional to the perturber distance of nearest approach, or even infinite, while the theories of HOLTSMARK, and CHANDRASEKHAR and VON NEUMANN[17] show that weak fields *occur rarely* and have a very *short lifetime*. Also the time interval for which adiabaticity is required here is defined differently, i.e., either as T_Φ or as $2\pi/(\omega_{ii} - \omega_{jj})$.

It may be worth mentioning that, as a consequence of these results, it follows further that an *impact theory* of line broadening which makes use of *completed adiabatic binary collisions* must be wrong under all circumstances for Stark effect broadening. For, as we saw, adiabaticity means near-statistical line broadening for $F > F_0$, which cannot be

described by an impact theory. On the other hand, fields smaller than F_0 come about by the simultaneous perturbation by many particles; hence an impact theory that makes use of adiabatic collisions cannot be valid in this range either.

6. *Expansion of the line-shape integral in terms of fluctuation moments*

In the next sections we shall study the *deviations from the statistical line shape* under the assumption that the condition of near-statistical broadening be fulfilled, as given by equation (1) and (1a), or (26). This is justified if the deviations from the statistical line shape are very small. Consequently equation (15) represents the simplest line shape formula that is more general than the statistical formula itself. On explicitly introducing the assumption of linear Stark effect we may rewrite the *line-shape formula* (15) as

$$F_{if}(\omega) = (2\pi)^{-1}|\mu_{if}|^2\int_0^\infty d\omega_{if} P(\omega_{if})\int_{-\infty}^{+\infty} dt e^{i(\omega_{if}-\omega)t} M_{if}(t), \tag{42}$$

where $M_{if}(t)$ is the *reduced correlation function* defined by equation (20), and all other quantities are explained in section (1) and (2). To get an approximate expression for the line shape in the case of *near-statistical broadening*, we shall expand the reduced correlation function $M_{if}(t)$ in a Taylor series:

$$M_{if}(t) = \sum_{n=0}^{\infty} \frac{c_{2n} t^{2n}}{(2n)!} + i \sum_{n=0}^{\infty} \frac{c_{2n+1} t^{2n+1}}{(2n+1)!}, \tag{43}$$

where the coefficients are given by

$$c_{2n} = M_{if}^{(2n)}(0); \; c_{2n+1} = -i M_{if}^{(2n+1)}(0). \tag{44}$$

Such an expansion is justified because the perturbing field is nearly constant in the time interval $-T_\Phi \leq t \leq T_\Phi$ from which the main contribution to the time integral in equation (42) arises. Also does it correspond to the way in which one usually derives the *wing theorem*, i.e., to the method of stationary phase.

Denoting the time integral in equation (42) by

$$K(\omega_{if}, \omega) \equiv \int_{-\infty}^{+\infty} e^{i(\omega_{if}-\omega)t} M(t) dt \tag{45}$$

and substituting equation (43), we obtain for $K(\omega_{if}, \omega)$ an expansion in terms of Dirac δ-functions and derivatives:

$$K(\omega_{if}, \omega) = 2\pi \sum_{n=0}^{\infty} \frac{(-1)^n c_{2n}}{(2n)!} \delta^{(2n)}(\omega_{if} - \omega) + 2\pi \sum_{n=0}^{\infty} \frac{(-1)^n c_{2n+1}}{(2n+1)!} \delta^{(2n+1)}(\omega_{if} - \omega). \tag{46}$$

This equation is meaningful as a relation between generalized functions, as defined by LIGHTHILL[18]. Substitution into equation (42) yields:

$$F_{if}(\omega) = |\mu_{if}|^2 \left\{ \sum_{n=0}^{\infty} \frac{(-1)^n c_{2n}}{(2n)!} P^{(2n)}(\omega) + \sum_{n=0}^{\infty} \frac{(-1)^{n+1} c_{2n+1}}{(2n+1)!} P^{(2n+1)}(\omega) \right| \tag{47}$$

i.e., an expansion containing the *statistical frequency distribution function* $P(\omega)$ and its derivatives with respect to ω. It is convenient to introduce a *reduced frequency* β by

$$|\omega - \omega_0| = \beta\omega \tag{48}$$

and to identify β with the synonymous quantity introduced at the beginning of section (III) by putting the 'normal frequency shift'

$$\omega_S = |\mu_{ii} - \mu_{ff}|F_0/\hbar. \tag{49}$$

On denoting the resulting *line shape in the* β*-scale* by $F_{if}(\beta)$ we obtain finally:

$$F_{if}(\beta) = |\mu_{if}|^2\left\{\sum_{n=0}^{\infty}\frac{(-1)^n c_{2n}}{(2n)!}\,\omega_S^{\,2n}H^{(2n)}(\beta) + \sum_{n=0}^{\infty}\frac{(-1)^{n+1}c_{2n+1}}{(2n+1)!}\,\omega_S^{\,-(2n+1)}H^{(2n+1)}(\beta)\right\}. \tag{50}$$

Here $H(\beta)$ is HOLTSMARK's function[19], given by

$$H(\beta) = \frac{2\beta}{\pi}\int_0^{\infty} y e^{-y^3}\sin(\beta y)\mathrm{d}y. \tag{51}$$

The quantity $|\mu_{if}|^2 \cdot H(\beta)$ represents the *statistical line shape* in the β-scale.

To obtain the *coefficients* c_{2n}, c_{2n+1} we substitute equation (20) into equation (44):

$$c_{2n} = \{f^{(2n)}(0)\}_{A\to(0)};\quad c_{2n+1} = -i\{f^{(2n+1)}(0)\}_{A\to(0)} \tag{52}$$

with $f(t)$ defined by

$$f(t) \equiv e^{i\varphi(t)};\quad \varphi(t) = \Delta\varphi_{ii}(t). \tag{53}$$

With the further abbreviation

$$\Delta F(t) \equiv F(t) - F(0) \tag{54}$$

the function $\varphi(t)$ and its first derivative with respect to time are given by

$$\varphi(t) = \frac{\omega_S}{F_0}\int_0^t \Delta F(t')\mathrm{d}t';\quad \varphi^{(1)}(t) = \frac{\omega_S}{F_0}\Delta F(t) \tag{55}$$

according to equation (14) and (49). On observing that

$$f^{(1)} = i\varphi^{(1)}f \equiv \frac{i\omega_S}{F_0}f\cdot\Delta F, \tag{56}$$

we obtain the following *recursion formula* for the time-derivatives of $f(t)$:

$$f^{(n)} = \frac{i\omega_S}{F_0}\sum_{m=0}^{n-1}\binom{n-1}{m}f^{(m)}\Delta F^{(n-m-1)},\ [n \geq 1], \tag{57}$$

where for convenience the common argument t of all functions has been suppressed. For $t = 0$ we have

$$f(0) = 1;\ f^{(1)}(0) = 0; \tag{58}$$

the latter being true because of $\Delta F(0) = 0$. By further observing that the time derivatives of $F(t)$ and $\Delta F(t)$ are identical, we obtain the following recursion formula for the *time derivatives* of $f(t)$ at $t = 0$:

$$f^{(n)}(0) = \frac{i\omega_S}{F_0}\left\{F^{(n-1)}(0) + \sum_{m=2}^{n-2}\binom{n-1}{m} f^{(m)}(0)F^{(n-m-1)}(0)\right\} \tag{59}$$

which is valid for $n \geq 2$, if the summation over m is understood to yield zero for $n - 2 < 2$, i.e., $n \leq 3$. The first eight derivatives have been evaluated according to equation (59) and their ensemble averages taken according to equation (52). By the averaging, all terms that would violate the condition $M_{if}(t) = M_{if}^*(-t)$ drop out because the corresponding probability distributions for these terms are symmetric with respect to time reversal (condition of quasi-equilibrium, mechanical reversibility in time), while the terms themselves are antisymmetrie with respect to time reversal. Hence the following values of the *coefficients* result:

$$\begin{aligned}
&c_0 = 1;\ c_1 = c_2 = 0;\\
&c_3 = \frac{\omega_S}{F_0}\{F^{(2)}\}_{Av(F)};\\
&c_4 = -3\left(\frac{\omega_S}{F_0}\right)^2\{(F^{(1)})^2\}_{Av(F)};\\
&c_5 = \frac{\omega_S}{F_0}\{F^{(4)}\}_{Av(F)};\\
&c_6 = -\left(\frac{\omega_S}{F_0}\right)^2[15\{F^{(1)}F^{(3)}\}_{Av(F)} + 10\{(F^{(2)})^2\}_{Av(F)}];\\
&c_7 = \frac{\omega_S}{F_0}\{F^{(6)}\}_{Av(F)} - 105\left(\frac{\omega_S}{F_0}\right)^3\{(F^{(1)})^2F^{(2)}\}_{Av(F)};\\
&c_8 = -\left(\frac{\omega_S}{F_0}\right)^2[28\{F^{(1)}F^{(5)}\}_{Av(F)} + 56\{F^{(2)}F^{(4)}\}_{Av(F)} + 35\{(F^{(3)})^2\}_{Av(F)}]\\
&\quad + 105\left(\frac{\omega_S}{F_0}\right)^4\{(F^{(1)})^4\}_{Av(F)}.
\end{aligned} \tag{60}$$

Here all averages are taken for fixed fieldstrength F, and the upper bracketed indices indicate derivatives with respect to time. One sees that the c_n describe essentially correlations between the time-derivatives of the field for fixed field F.

If we introduce the reduced fieldstrength β and a *reduced time variable* $s = \omega_F t$, where ω_F is a 'normal' *fluctuation frequency* defined by

$$\begin{aligned}
\omega_F &= \left(\frac{2kt}{m}\cdot\frac{F_0}{Ze}\right)^{\frac{1}{2}}\\
&= 1{\cdot}32\left(\frac{3kT}{m}\right)^{\frac{1}{2}}n^{\frac{1}{6}} \equiv \left(\frac{5}{36}\right)^{\frac{1}{2}}t_0^{-1},
\end{aligned} \tag{61}$$

then the coefficients can be written in the following alternative manner:

$$c_n = \omega_F{}^n\, b_n, \text{ with} \tag{62}$$

$$b_0 = 1;\ b_1 = b_2 = 0;$$

$$b_3 = \left(\frac{\omega_S}{\omega_F}\right)\{\beta^{[2]}\}_{Av(\beta)};$$

$$b_4 = -3\left(\frac{\omega_S}{\omega_F}\right)^2\{(\beta^{[1]})^2\}_{Av(\beta)};$$

$$b_5 = \left(\frac{\omega_S}{\omega_F}\right)\{\beta^{[4]}\}_{Av(\beta)};$$

$$b_6 = -\left(\frac{\omega_S}{\omega_F}\right)^2[15\{\beta^{[1]}\beta^{[3]}\}_{Av(\beta)} + 10\{(\beta^{[2]})^2\}_{Av(\beta)}];$$

$$b_7 = \left(\frac{\omega_S}{\omega_F}\right)\{\beta^{[6]}\}_{Av(\beta)} - 105\left(\frac{\omega_S}{\omega_F}\right)^3\{(\beta^{[1]})^2\beta^{[2]}\}_{Av(\beta)};$$

$$b_8 = -\left(\frac{\omega_S}{\omega_F}\right)^2[28\{\beta^{[1]}\beta^{[5]}\}_{Av(\beta)} + 56\{\beta^{[2]}\beta^{[4]}\}_{Av(\beta)} + 35\{(\beta^{[3]})^2\}_{Av(\beta)}]$$

$$+ 105\left(\frac{\omega_S}{\omega_F}\right)^4\{(\beta^{[1]})^4\}_{Av(\beta)}. \tag{63}$$

where the upper indices in square brackets denote the orders of derivatives with respect to s. Substitution of equation (62) and (63) into equation (50) for the *line shape in the* β*-scale* yields:

$$F_{if}(\beta) = |\mu_{if}|^2\left\{\sum_{n=0}^{\infty}\frac{(-1)^n b_{2n}}{(2n)!}\left(\frac{\omega_F}{\omega_S}\right)^{2n} H^{(2n)}(\beta) + \sum_{n=0}^{\infty}\frac{(-1)^{n+1} b_{2n+1}}{(2n+1)!}\left(\frac{\omega_F}{\omega_S}\right)^{2n+1} H^{2n+1}(\beta)\right\}. \tag{64}$$

Apart from the coefficients b_n this is a *power series* in (ω_F/ω_S). We have to consider, however, that the b_n themselves contain *negative* powers of (ω_F/ω_S). A dimensional study of the recurrence formula (59) shows that the highest negative power of (ω_F/ω_S) contained in a coefficient $b_{4\nu+\alpha}$ ($\alpha = 1, 2, 3, 4$) is of the order $(2 - 2\nu - \alpha)$. Hence we obtain the *zeroth-order approximation* of equation (64) by considering only the term containing $b_0 = 1$ (statistical approximation); we obtain the *first-order approximation* by considering terms containing b_0 to b_4, and the *second-order approximation* from the terms containing b_0 to b_8. A slight dependence on ω_F and ω_S which might be present in the averages for the derivatives of $\beta(s)$ and their products has been neglected as unimportant in these considerations, without proof; yet this assumption appears plausible in dealing with the first few terms of equation (64).

The expansion (64) is the *final form* of our general formula for the *near-statistical line shape*. The *expansion parameter* (ω_F/ω_S) is the ratio of a characteristic fluctuation frequency

VOL. 1 1961

and a characteristic Stark shift and is connected with the quantities describing the state of the plasma by:

$$\left(\frac{\omega_F}{\omega_S}\right)^2 = \frac{2kT}{m} \cdot \frac{\hbar^2}{ZeF_0(\mu_{ii} - \mu_{ff})^2} \tag{65}$$

or

$$\left(\frac{\omega_F}{\omega_S}\right)^2 = 0{\cdot}53 \times 10^8 \frac{T}{(\gamma Z)^2 A n^{\frac{1}{3}}}, \tag{66}$$

where T and n are temperature and number density of the ions, A their atomic weight, Z their charge in units of the proton charge (not the atomic number), and γ expresses the quantity $(\mu_{ii} - \mu_{ff})$ in units of ea_0, with a_0 = Bohr radius. The expansion is therefore good for low temperatures, high densities, large interaction energies (ionic charge, atomic dipole moment), and large ionic mass. If the motion of the radiators had been taken into account, a further requirement would be that the radiator mass is also large.

Of the other quantities contained in equation (64), the function $H(\beta)$ and its derivatives describe the statistics of the reduced frequency β. On the other hand, the ensemble averages over the products of reduced time-derivatives of β, that are contained in the expressions (63) for the b_n, describe the correlations between time-derivatives of the field for given field F, or β, and include the dispersion and other moments of single derivatives. In the following we shall refer to these averages, and to those over the unreduced time-derivatives of the field F, as to the reduced and unreduced *fluctuation moments*. The use of these fluctuation moments is the characteristic feature of the approximation method that led to the near-statistical line shape of equation (64).

III. EVALUATION

1. *Binary interactions, shape of line wings*

It is desirable first to evaluate equation (63) and (64) for *binary interactions*, i.e., far in the wings of a line ($\beta \to \infty$) for the following reasons: While in the general case of multiple interactions (arbitrary β) only the first-order approximation to equation (64) will be considered, it is easy to compute first- and second-order approximations in the binary case. This yields some clue as to how large an error the higher-order terms will introduce, not only in the binary case, but also in the general case [section (III.2)]. We shall also be able to check the general result for multiple interactions by comparing its asymptotic expansion for large β with the binary result.

If we denote the statistical line shape in the β-scale by $S_{if}(\beta)$, the *deviation from the statistical line shape* may be written as

$$F_{if}(\beta) - S_{if}(\beta) = |\mu_{if}|^2 \left(\frac{\omega_F}{\omega_S}\right)^2 \Delta(\beta). \tag{67}$$

Consequently the *relative deviation* from the statistical line shape is given by

$$\frac{F_{if}(\beta) - S_{if}(\beta)}{S_{if}(\beta)} = \left(\frac{\omega_F}{\omega_S}\right)^2 \frac{\Delta(\beta)}{H(\beta)}. \tag{67a}$$

On substituting equation (67) into (64) and remembering that $b_1 = b_2 = 0$, we obtain the second-order approximation for $\Delta(\beta)$

$$\Delta_2(\beta) = \sum_{n=2}^{4} \frac{(-1)^n b_{2n}}{(2n)!} \left(\frac{\omega_F}{\omega_S}\right)^{2n-2} H^{(2n)}(\beta) + \sum_{n=1}^{3} \frac{(-1)^{n+1} b_{2n+1}}{(2n+1)!} \left(\frac{\omega_F}{\omega_S}\right)^{2n-1} H^{2n+1}(\beta) \quad (68)$$

The binary expression for $H(\beta)$ is identical with the first term of its asymptotic expansion[20] for large β, i.e.,

$$H(\beta) \sim 1{\cdot}496\beta^{-\frac{1}{2}}. \quad (69)$$

Accordingly the derivatives are given by

$$H^{(n)}(\beta) \sim 1{\cdot}496\beta^{-\frac{1}{2}} \frac{(-1)^n(2n+3)!}{3 \times 2^{2n+1}(n+1)!} \beta^{-n}. \quad (70)$$

The computation of the *coefficients* b_n is done most easily by first computing the unreduced fluctuation moments contained in the coefficient c_n and then applying equation (62). We derive first the time derivatives of the field $F(t)$ which, according to the binary approximation, is produced by a *single perturber* of velocity v and initial position $r_0 \equiv r(0)$ at $t = 0$. We have

$$F(t) = \frac{F}{1 - 2(v/r_0)|t|\cos\alpha + (v/r_0)^2 t^2}, \quad (71$$

with the abbreviation $F = F(0)$ and $\alpha = \pi - (\sphericalangle r_0, v)$. On using $a = \cos\alpha$, $s = (v/r_0)t$, and restricting ourselves to $t \geq 0$ we obtain

$$F(t) = \frac{F}{1 - 2as + s^2} = AF\left(\frac{1}{s - s_1} - \frac{1}{s - s_2}\right) \quad (72)$$

$$s_1 = e^{i\alpha};\ s_2 = e^{-i\alpha};\ A = (2i\sin\alpha)^{-1}. \quad (73)$$

Consequently the *nth derivative* with respect to t turns out to be:

$$F^{(n)}(t) = (-1)^n n! \left(\frac{v}{r_0}\right)^n \frac{ZeA}{r_0^2} \left[\left(\frac{1}{s - s_1}\right)^{n+1} - \left(\frac{1}{s - s_2}\right)^{n+1}\right] \quad (74)$$

and we obtain for $t = 0$:

$$F^{(n)} \equiv F^{(n)}(0) = n!(Ze)^{-n/2} F^{(n+2)/2} v^n \times \sin[(n+1)\alpha]/\sin\alpha. \quad (75)$$

The *fluctuation moments* contained in equation (60) are then obtained by first forming the products or powers of the derivatives in question and then averaging over all speeds v according to the Maxwell–Boltzmann distribution and over all velocity directions by integrating over $0 \leq \alpha \leq \pi$ with the weight function $\sin\alpha$. The necessary integrations are

somewhat lengthy, but elementary, and are not listed here. The final result for the *coefficients* b_n is in the binary case:

$$b_0 = 1;\ b_1 = b_2 = 0;$$

$$b_3 = \frac{\omega_S}{\omega_F}\beta^2;\ b_4 = -6\left(\frac{\omega_S}{\omega_F}\right)^2\beta^3;$$

$$b_5 = 18\frac{\omega_S}{\omega_F}\beta^3;\ b_6 = -410\left(\frac{\omega_S}{\omega_F}\right)^2\beta^4;$$

$$b_7 = 1350\frac{\omega_S}{\omega_F}\beta^4 - 1470\left(\frac{\omega_S}{\omega_F}\right)^3\beta^5;$$

$$b_8 = -55986\left(\frac{\omega_S}{\omega_F}\right)^2\beta^5 + 1260\left(\frac{\omega_S}{\omega_F}\right)^4\beta^6. \tag{76}$$

Substitution of these coefficients in equation (68) yields the following expression for the *relative deviation from statistical line shape* for the case of binary interactions:

$$\left[\frac{F_{if}(\beta) - S_{if}(\beta)}{S_{if}(\beta)}\right]_{bin} = -\frac{3885}{64}\beta^{-1}\left(\frac{\omega_F}{\omega_S}\right)^2 + \frac{440\ 392\ 953}{8192}\beta^{-2}\left(\frac{\omega_F}{\omega_S}\right)^4 + O\left[\beta^{-3}\left(\frac{\omega_F}{\omega_S}\right)^6\right] \tag{77}$$

The applicability range of this equation will be established from the general result in the next section. If the formula is applicable, the first term is useful for $\beta \geq 10^3\,(\omega_F/\omega_S)^2$, since then the second term is smaller than the first. The first term itself is smaller than 0·06 for this range of β, which means that the formula is good only for deviation smaller than 6 per cent from the statistical line shape. For binary interactions equation (77) also demonstrates, by its dependence on β, the *wing theorem* and the fact that the statistical theory becomes better and better for decreasing temperature and increasing density because of its dependence on (ω_F/ω_S) and equation (66).

2. *General case of multiple interactions*

We shall now evaluate the *deviation from the statistical line shape* for multiple interaction in first-order approximation. According to equation (68) we have

$$\Delta_1(\beta) = \frac{b_3}{3!}\left(\frac{\omega_F}{\omega_S}\right)^3 H^{(3)}(\beta) + \frac{b_4}{4!}\left(\frac{\omega_F}{\omega_S}\right)^4 H^{(4)}(\beta). \tag{78}$$

The coefficients b_3 and b_4 are

$$b_3 = \frac{\omega_S}{\omega_F}\cdot\frac{1}{F_0\omega_F^2}\{F^{(2)}\}_{Av(F)};$$

$$b_4 = -3\left(\frac{\omega_S}{\omega_F}\right)^2\frac{1}{(F_0\omega_F)^2}\{(F^{(1)})^2\}_{Av(F)}. \tag{79}$$

To simplify these expressions further we must introduce a Cartesian coordinate system (ξ, η, ζ) whose ξ-axis is parellel to the direction of $F \equiv F(0)$, while the other axes are not specified. Since this coordinate system does not rotate with the field, in contradistinction

to the coordinate system (x, y, z) introduced in section (II.4), we have to distinguish between F and F_ξ when $t \neq 0$. From the definition of F we obtain the general relations

$$F^{(1)} = \frac{\boldsymbol{F}}{F} \cdot \boldsymbol{F}^{(1)} \tag{80}$$

$$F^{(2)} = \frac{\boldsymbol{F} \cdot \boldsymbol{F}^{(2)}}{F} + \frac{(\boldsymbol{F}^{(1)})^2}{F} - \frac{(\boldsymbol{F} \cdot \boldsymbol{F}^{(1)})^2}{F^3}. \tag{81}$$

On putting $\boldsymbol{F}(0) = (F_\xi, 0, 0)$ this reduces to

$$F^{(1)} = F_\xi^{(1)}, \tag{82}$$

$$F^{(2)} = F_\xi^{(2)} + F^{-1}[(F_\eta^{(1)})^2 + (F_\zeta^{(1)})^2]. \tag{83}$$

On observing that the ensemble average of $F_\xi^{(2)}$ for fixed F is equal to zero (*see Appendix A*) and using the equivalence of the η— and ζ—direction we obtain:

$$\{F^{(2)}\}_{Av(F)} = \frac{2}{F}\{(F_\eta^{(1)})^2\}_{Av(F)}, \tag{84}$$

and in consequence equation (79) transforms into

$$b_3 = \frac{2}{3}\frac{\omega_S}{\omega_F}\frac{1}{(F_0\omega_F)^2}\{(F_\eta^{(1)})^2\}_{Av(F)} \tag{85}$$

and

$$b_4 = -3\left(\frac{\omega_S}{\omega_F}\right)^2\frac{1}{(F_0\omega_F)^2}\{(F_\xi^{(1)})^2\}_{Av(F)}. \tag{85a}$$

The two fluctuation moments have been transformed by CHANDRASEKHAR and VON NEUMANN[21] into expressions containing only one-dimensional integrals:

$$\{(F_\eta^{(1)})^2\}_{Av(F)} = \frac{45}{16}(\omega_F F_0)^2\frac{\beta[Q(\beta) - R(\beta)]}{H(\beta)}, \tag{86}$$

$$\{(F_\xi^{(1)})^2\}_{Av(F)} = \frac{45}{8}(\omega_F F_0)^2\frac{\beta R(\beta)}{H(\beta)}, \tag{87}$$

with

$$Q(\beta) = \frac{2}{\pi}\int_0^\infty y^{-4}e^{-y^2}\sin(\beta y)\mathrm{d}y, \tag{88}$$

$$R(\beta) = \frac{2}{\pi}\beta^{-2}\int_0^\infty y^{-3}e^{-y^2}[\sin(\beta y) - \beta y\cos(\beta y)]\mathrm{d}y. \tag{89}$$

The following relations are useful:

$$Q(\beta) = \frac{3}{2}\beta^{-4}\int_0^\beta x^3 H(x)\mathrm{d}x, \tag{90}$$

$$R(\beta) = \beta^{-2}\int_0^\beta x Q(x)\mathrm{d}x. \tag{91}$$

VOL
1
196

The connection between Chandrasekhar and von Neumann's functions $\tau(\beta)$, $I(\beta)$, $G(\beta)$ and ours is simply

$$Q(\beta) = \beta^{-\frac{1}{2}} G(\beta); \quad R(\beta) = \beta^{-\frac{1}{2}} I(\beta); \tag{92}$$

$$\tau^2(\beta) = \frac{\beta H(\beta)}{Q(\beta)}, \tag{92a}$$

while the constants a and b used by those authors are connected with F_0 and ω_F by

$$a\,b = \frac{45}{32}(\omega_F F_0)^2. \tag{93}$$

Substitution of equation (86) and (87) yields the *coefficients* in the form

$$b_3 = \frac{45}{8}\frac{\omega_S}{\omega_F}\frac{Q(\beta) - R(\beta)}{H(\beta)}, \tag{94}$$

$$b_4 = \frac{135}{8}\left(\frac{\omega_S}{\omega_F}\right)\frac{\beta R(\beta)}{H(\beta)}. \tag{95}$$

By substituting these into equation (78) we obtain finally the *relative deviation from the statistical line shape* in the form:

$$\frac{F_{if}(\beta) - S_{if}(\beta)}{S_{if}(\beta)} = \left(\frac{\omega_F}{\omega_S}\right)^2 \frac{\Delta(\beta)}{H(\beta)} \tag{96}$$

with $\Delta(\beta)$ given in first-order approximation by:

$$\Delta(\beta) = \frac{15}{16}\frac{1}{H(\beta)}\{H^{(3)}(\beta)Q(\beta) - [H^{(3)}(\beta) + \tfrac{3}{4}\beta H^{(4)}(\beta)]R(\beta)\}. \tag{97}$$

To check this formula we may use the following asymptotic expressions (see Appendix B), valid for $\beta \to \infty$:

$$H(\beta) \sim \frac{15}{4}(2\pi)^{-\frac{1}{2}}\beta^{-\frac{7}{2}}, \tag{98}$$

from which we obtain the asymptotic expressions for $H^{(3)}(\beta)$ and $H^{(4)}(\beta)$ by differentiating, and

$$Q(\beta) \sim 2(2\pi\beta)^{-\frac{1}{2}}; \quad R(\beta) \sim \frac{4}{3}(2\pi\beta)^{-\frac{1}{2}}, \tag{99}$$

in accordance with CHANDRASEKHAR and VON NEUMANN[21]. On substituting these expressions into equation (97) we obtain exactly the first-order term of equation (77), i.e., the corresponding expression for the case of binary interactions. The *validity range of the binary formula* (77) is practically determined by the error introduced through the asymptotic expressions for $H^{(3)}(\beta)$ and $H^{(4)}(\beta)$. Comparison of the first and second term in the asymptotic expansion for $H^{(4)}(\beta)$ leads to the conclusion that equation (77) will be applicable for $\beta > 7$.

Formulas that have proved useful in evaluating $\Delta(\beta)$ numerically are listed in *Appendix B*. For $0 \leq \beta \leq 1$ Taylor expansions of the functions $H^{(3)}$, $H^{(4)}$, Q, R were used for numerical computation. In the interval $1 \leq \beta \leq 10$ it was found useful to transform equation (97)

in the following way: By substituting equation (90) into equation (91) and changing the order of integration one obtains

$$R(\beta) = \tfrac{3}{2}Q(\beta) - \frac{H^{(-1)}(\beta)}{\beta^2}\,, \tag{100}$$

with the definition

$$H^{(-1)}(\beta) \equiv \int_0^\beta H(x)\mathrm{d}x. \tag{101}$$

Substitution of equation (92) and (100) into equation (97) yields

$$\Delta(\beta) = \frac{15}{16}\frac{1}{H(\beta)}\left\{\frac{1}{3}\beta^{-\frac{1}{2}}G(\beta)\left[H^{(2)}(\beta) - \frac{3}{2}\beta H^{(4)}(\beta)\right]\right.$$
$$\left. + \beta^{-2}H^{(-1)}(\beta)\left[H^{(2)}(\beta) + \frac{3}{4}\beta H^{(4)}(\beta)\right]\right\}. \tag{102}$$

The functions $H^{(2)}(\beta)$ and $H^{(4)}(\beta)$ were evaluated according to equation (B.14) and (B.15) by *numerical integration* on an I.B.M. 650 electronic computer. The values of $G(\beta)$ were taken from CHANDRASEKHAR and VON NEUMANN[21], the values of $H(\beta)$ from BARANGER and MOZER[5]. From $H(\beta)$ the function $H^{(-1)}(\beta)$ was obtained by numerical integration with a desk computer. The results are listed and discussed in section (IV).

IV. DISCUSSION OF THE RESULTS

The functions $\Delta(\beta)$ and $[\Delta(\beta)/H(\beta)]$ are shown in Fig. 1; one notices that the correction to the statistical line shape vanishes near the maximum of the Holtsmark line shape ($\beta = 1{\cdot}6$), but may contribute appreciably for $\beta \approx 1$ and $\beta \approx 3$, depending on the value of the expansion parameter (ω_F/ω_S). Since the correction is negative for $\beta \approx 1$, but positive for $\beta \approx 3$, the intensity is shifted towards larger values of β as compared to the statistical intensity distribution. For $\beta \to 0$ the correction to the statistical line shape tends to a finite negative value, while the statistical intensity goes to zero. Yet, since the expansion of the line shape and, particularly, the validity of the first-order approximation break down as $\beta \to 0$ in accordance with the β-dependence of (T_Φ/T_F) [see below], the paradox of a negative spectral intensity does not arise for $\beta \to 0$.

Table I shows, as an example, the 'average' value of the absolute magnitude of the relative deviation from the statistical line shape to be expected in the range $0{\cdot}6 \leq \beta \leq 10$ for the hydrogen lines H_β, H_γ, H_δ, and H_ε, at a temperature of 10^4 °K and an ion density of 10^{17} cm^{-3}. The 'average' is obtained somewhat arbitrarily by putting $[\Delta(\beta)/H(\beta)] = 10$ in equation (67a). The associated values of (T_Φ/T_F) at $\beta = 1$ and $(\omega_F/\omega_S)^2$ are shown also. It turns out that (T_Φ/T_F) is only slightly smaller than 1 in these examples, which means that the condition of near-statistical broadening is not very well fulfilled here. Consequently one may expect that the rotation effect and the transitions between adiabatic Stark states will also contribute to the actual deviation from the statistical line shape under these conditions. Also the omission of higher order terms in the expansion for the line shape seems safe only for the H_δ and H_ε lines, if one judges on the basis of the binary expression for the deviation from the statistical line shape [equation (77)]. Nevertheless the average figures obtained can be expected to represent the correct order of magnitude and indicate that for the H_β and H_γ lines the influence of the field fluctuations in time is no longer

VOL 1 196

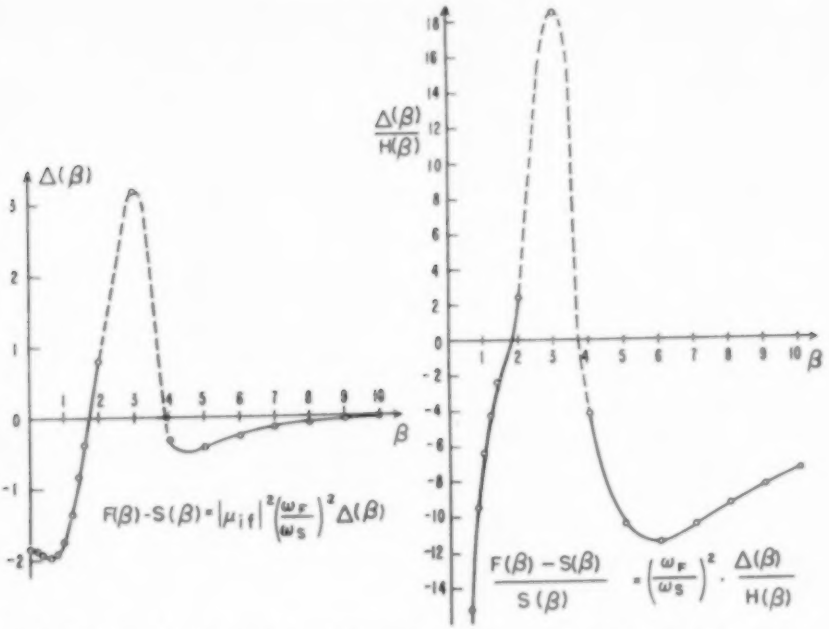

FIG. 1. The functions $\Delta(\beta)$ and $[\Delta(\beta)/H(\beta)]$ for the absolute and relative deviation from the statistical line shape.

negligible under the indicated conditions. By taking into account the thermal motions of the radiators, which we had so far neglected, the average deviation percentages will be increased, while the dependence of the deviation on β may be more or less altered.

TABLE 1. NUMERICAL RESULTS FOR FOUR BALMER LINES OF HYDROGEN AT $T = 10^4$ °K AND $n_{ion} = 10^{17}$ cm^{-3}.

Line	n'_i [a]	$\bar{\gamma}$ [b]	$T_{\Phi 0}/T_{F0}$	$(\omega_F/\omega_S)^2$	$\langle \Delta F/S \rangle$ [c] (%)
H_β	4	8	0·99	$3{\cdot}8 \times 10^{-2}$	38
H_γ	5	12·5	0·79	$1{\cdot}6 \times 10^{-2}$	16
H_δ	6	18	0·66	$0{\cdot}76 \times 10^{-2}$	7·6
H_ε	7	24·5	0·56	$0{\cdot}41 \times 10^{-2}$	4·1

[a] Principal quantum number of the upper Stark state.
[b] $\bar{\gamma} = (n'_i)^2/2$ is the average dipole component in field direction for the upper Stark state, in units of ea_0.
[c] 'Average' absolute magnitude of the first-order correction to the statistical line shape for the range $0{\cdot}6 \leq \beta \leq 10$.

The discrepancy between the statistical and the present approximation may be less important for the result of a line shape calculation that takes into account broadening by both ions and electrons if the different errors introduced by the approximate treatments of both effects happen to cancel one another partially. Since it is not known whether the errors will actually cancel or rather add to one another, further investigations will be required to decide this question.

As mentioned above, our approximation for the deviation from the statistical line shape is valid for $(T_\Phi/T_F) \ll 1$. Since (T_Φ/T_F) varies slowly with β for $\beta \gtrsim 1$, it will often be sufficient to compute this quantity only for $\beta = 1$ through the relation

$$\left(\frac{T_{\Phi 0}}{T_{F0}}\right)^2 = 4{\cdot}98\,\frac{\omega_F}{\omega_S}, \quad [T_{\Phi 0} \ll T_{F0}]. \tag{103}$$

The indices 0 indicate evaluation for $\beta = 1$. For $\beta \to 0$ the approximate expression for (T_Φ/T_F) diverges:

$$\left(\frac{T_\Phi}{T_F}\right)^2 = \frac{\tau(1)}{\beta\tau(\beta)}\left(\frac{T_{\Phi 0}}{T_{F0}}\right)^2 \sim 0{\cdot}877\beta^{-2}\left(\frac{T_{\Phi 0}}{T_{F0}}\right)^2. \tag{104}$$

This relation holds again only for $T_\Phi \ll T_F$. In the range of β where equation (104) yields $(T_\Phi/T_F) \gtrsim 1$, the validity of our approximation for the line shape is no longer guaranteed.

Acknowledgements—The author expresses his sincere thanks to Professor Henry Margenau for his kind interest in this work. Dr. R. E. Gluckstern's advice on some mathematical details, and the numerical computations contributed by Miss S. Cornell and Miss E. Koppelman are gratefully acknowledged. The author is also indebted to the U.S. Government for a *Fulbright Travel Grant*.

APPENDIX A. Vanishing second-order fluctuation moments

We want to prove that

$$\{F_\xi^{(2)}\}_{Av(F)} = 0. \tag{A.1}$$

Proof: The total field component as a function of time is given by the sum of all single ion field components:

$$F_\xi(t) = -Ze\sum_{i=1}^{N}(\xi_i/r_i^3) \tag{A.2}$$

where

$$r_i^2 \equiv r_i^2(t) = \xi_i^2 + \eta_i^2 + \zeta_i^2,$$
$$\xi_i \equiv \xi_i(t) = \xi_i(0) + v_{\xi i}, \text{ etc.} \tag{A.3}$$

If we neglect interactions all $\boldsymbol{v}_i$ are constant in time, and the second time-derivative is given by

$$F_\xi^{(2)} = Ze\sum_i[6v_{\xi i}(\boldsymbol{r}_i\cdot\boldsymbol{v}_i)r_i^{-5} + 3\xi_i v_i^2 r_i^{-5} - 15\xi_i(\boldsymbol{r}_i\cdot\boldsymbol{v}_i)^2 r_i^{-7}] \tag{A.4}$$

The average in (A.1) is to be taken over all $\boldsymbol{r}_i$ compatible with F and over all $\boldsymbol{v}_i$. It suffices to show that averaging over all $\boldsymbol{v}_i$ yields zero. For the Maxwell–Boltzmann velocity distribution

$$\langle v_{\xi i}^2\rangle = \langle v_{\eta i}^2\rangle = \langle v_{\zeta i}^2\rangle = \tfrac{1}{3}\langle v_i^2\rangle; \langle v_{\xi i}v_{\eta i}\rangle = \langle v_{\eta i}v_{\zeta i}\rangle = \langle v_{\xi i}v_{\zeta i}\rangle = 0. \tag{A.5}$$

Hence it follows immediately that

$$\langle F_\xi^{(2)}\rangle = 0 \tag{A.6}$$

where $\langle\ \rangle$ denotes the average over all $\boldsymbol{v}_i$. Since we have made no use of the fact that the ξ-axis is parallel to the field (at $t = 0$), equation (A.6) holds likewise for the η- and ζ-component of $\boldsymbol{F}^{(2)}$, and consequently

$$\{\boldsymbol{F}^{(2)}\}_{Av(F)} = 0. \tag{A.7}$$

APPENDIX B. Holtsmark integrals

The functions $H(\beta)$, $Q(\beta)$, $R(\beta)$ etc. are all related to each other. This is seen in the most convenient way by introducing the following set of *Holtsmark integrals:*

$$S_n(\beta) = \int_0^\infty y^n e^{-y^3} \sin(\beta y) \mathrm{d}y, \; [n > -2], \tag{B.1}$$

$$C_n(\beta) = \int_0^\infty y^n e^{-y^3} \cos(\beta y) \mathrm{d}y, \; [n > -1]. \tag{B.2}$$

The following relations hold: $$\frac{\partial S_n}{\partial \beta} = C_{n+1}; \quad \frac{\partial C_n}{\partial \beta} = -S_{n+1}, \tag{B.3}$$

where for convenience the argument β has been omitted. By partial integration we obtain the recursion formulas:

$$S_n = \tfrac{2}{3}\beta C_{n-\frac{1}{2}} + \frac{2n-1}{3} S_{n-\frac{3}{2}}, \; [n > -\tfrac{1}{2}], \tag{B.4}$$

$$C_n = -\tfrac{2}{3}\beta S_{n-\frac{1}{2}} + \frac{2n-1}{3} C_{n-\frac{3}{2}}, \; [n > +\tfrac{1}{2}]. \tag{B.5}$$

Repeated application of these formulas yields:

$$S_n = -\frac{4}{9}\beta^2 S_{n-1} + \frac{8n-6}{9}\beta C_{n-2} + \frac{(2n-1)(2n-4)}{9} S_{n-3}, \; [n > 1], \tag{B.6}$$

$$C_n = -\frac{4}{9}\beta^2 C_{n-1} - \frac{8n-6}{9}\beta S_{n-2} + \frac{(2n-1)(2n-4)}{9} C_{n-3}, \; [n > 2]. \tag{B.7}$$

For $n = \frac{1}{2}$, two especially interesting formulas arise:

$$S_{\frac{1}{2}} = \tfrac{2}{3}\beta C_0, \tag{B.8}$$

$$C_{\frac{1}{2}} = \tfrac{2}{3} - \tfrac{2}{3}\beta S_0. \tag{B.9}$$

Hence all Holtsmark integrals whose index is an integer or a half-odd-integer greater than $(-\frac{1}{2})$ can be expressed as linear combinations of the four functions, S_0, S_1, C_0, C_1.

The functions used in section (III.2) can be calculated from the Holtsmark integrals by the following relations:

$$H = \frac{2}{\pi}\beta\, S_1, \tag{B.10}$$

$$H^{(-1)} = \frac{2}{\pi}(S_{-1} - \beta C_0), \tag{B.11}$$

$$H^{(2n)} = \frac{2}{\pi}[(-1)^{n+1}(2n)\, C_{2n} + (-1)^n \beta S_{2n+1}], \; [n \geqslant 0], \tag{B.12}$$

$$H^{(2n+1)} = \frac{2}{\pi}(-1)^n [(2n+1)\, S_{2n+1} + \beta\, C_{2n+2}], \; [n \geqslant -1], \tag{B.13}$$

$$Q = \frac{2}{\pi} S_{-\frac{1}{2}} = \frac{2}{\pi}\left(3S_1 + \frac{4}{3}\beta^2 S_0 - \frac{4}{3}\beta\right), \tag{B.14}$$

$$R = \frac{2}{\pi}\left(\frac{2}{3} S_{-\frac{1}{2}} + \beta C_0 - \beta^{-2} S_{-1}\right), \tag{B.15}$$

$$\tau = (\beta H/Q)^{\frac{1}{2}} = (\beta^2 S_1/S_{-\frac{1}{2}})^{\frac{1}{2}}, \tag{B.15a}$$

where again for convenience the common argument β of the functions has been suppressed. These relations are easily obtained from the above equations for the Holtsmark integrals and equation (51), (88) through (91), (100) and (101).

For small and large values of β simple power-series expansions are useful for numerical computation. By expanding the sine and cosine function in equations (B.1) and (B.2) and evaluating the integrals term by term one obtains the following Taylor expansions in β:

$$S_n(\beta) = \frac{2}{3}\sum_{k=0}^{\infty}\frac{(-1)^k}{(2k+1)!}\left(\frac{4k+2n+1}{3}\right)!\beta^{2k+1} \tag{B.16}$$

$$C_n(\beta) = \frac{2}{3}\sum_{k=0}^{\infty}\frac{(-1)^k}{(2k)!}\left(\frac{(4k+2n-1)}{3}\right)!\beta^{2k} \tag{B.17}$$

For large β one uses instead the following asymptotic expansions:

$$S_n(\beta) = \sum_{m=0}^{M}\frac{1}{m!}\left(n+\frac{3}{2}m\right)!\sin\left[\frac{(n+1)\pi}{2}-\frac{m\pi}{4}\right]\times\beta^{-(n+1+\frac{3}{2}m)}+\Delta S_{n,M}, \tag{B.18}$$

$$C_n(\beta) = \sum_{m=0}^{M}\frac{1}{m!}\left(n+\frac{3}{2}m\right)!\cos\left[\frac{(n+1)\pi}{2}-\frac{m\pi}{4}\right]\times\beta^{-(n+1+\frac{3}{2}m)}+\Delta C_{n,M}, \tag{B.19}$$

with $n > -1$ and any integer $M \geqslant 0$. The remainder terms can be estimated by:

$$\left.\begin{matrix}|\Delta S_{n,M}|\\|\Delta C_{n,M}|\end{matrix}\right\} \leq \frac{1}{(M+1)!}\left[n+\frac{3}{2}(M+1)\right]!\left(\frac{\sqrt{3}}{2}\beta\right)^{[n+1+\frac{3}{2}(M+1)]} \tag{B.20}$$

The derivation goes as follows: We define

$$K_n(\beta) \equiv C_n(\beta) + iS_n(\beta). \tag{B.21}$$

Then

$$K_n(\beta) = \int_0^{\infty} y^n e^{-y^3}\, e^{i\beta y}\,\mathrm{d}y. \tag{B.22}$$

In order to be able to expand the first exponential factor we rotate the path of integration in the complex y-plane by an angle of $+60^\circ$, i.e., put

$$y = e^{i\pi/3}t, \text{ with } t \text{ real.}$$

We obtain

$$K_n(\beta) = e^{\frac{1}{2}(n+1)i\pi}\int_0^{\infty} t^n e^{-it^3} e^{\exp(\frac{1}{2}i\pi)\beta t}\mathrm{d}t. \tag{B.23}$$

We then apply, for $x = -it^3$, the Taylor expansion of the exponential function in the following form:

$$e^x = \sum_{m=0}^{M}\frac{x^m}{m!} + R_M(x), \tag{B.24}$$

VOL.
1
1961

where the remainder term is given by the integral representation

$$R_M(x) = \frac{1}{M!}\int_0^x (x-\xi)^M e^{\xi}\,\mathrm{d}\xi. \tag{B.25}$$

Accordingly we write $$K_n(\beta) = K_{n,M} + \Delta K_{n,M}, \tag{B.26}$$

with $$K_{n,M} = e^{\frac{1}{2}(n+1)i\pi}\sum_{m=0}^{M}\frac{(-i)^m}{m!}\int_0^\infty t^{n+\frac{3}{2}m}\times e^{\exp(\frac{2}{3}i\pi)\beta t}\,\mathrm{d}t, \tag{B.27}$$

$$\Delta K_{n,M} = e^{\frac{1}{2}(n+1)i\pi}\int_0^\infty t^n\, R_M(-it^{\frac{3}{2}})\, e^{\exp(\frac{2}{3}i\pi)\beta t}\,\mathrm{d}t. \tag{B.28}$$

By a further rotation of the path of integration through an angle of 30°, i.e., putting

$$t = e^{i\pi/6}s, \text{ with } s \text{ real},$$

the integral in equation (B.27) assumes the form

$$e^{\frac{1}{2}(n+1+\frac{3}{2}m)i\pi}\int_0^\infty s^{n+\frac{3}{2}m}\, e^{-\beta s}\,\mathrm{d}s = (n+\frac{3}{2}m)!\;\beta^{-(n+1+\frac{3}{2}m)}\; e^{\frac{1}{2}(n+1+\frac{3}{2}m)i\pi}$$

whence finally $$K_{n,M} = \sum_{m=0}^{M}\frac{1}{m!}\left(n+\frac{3}{2}m\right)!\; e^{[\frac{1}{2}(n+1)-\frac{1}{4}m]i\pi}\,\beta^{-(n+1+\frac{3}{2}m)}. \tag{B.29}$$

From this, the expansions in equations (B.18) and (B.19) follow at once. The absolute magnitude of the remainder term $\Delta K_{n,M}$ can be estimated by replacing the absolute magnitude of the integral in equation (B.28) by the integral over the absolute value of the integrand. On observing that

$$|R_M(-it^{\frac{3}{2}})| \le \frac{1}{M!}\int_0^{t^{\frac{3}{2}}}(t^{\frac{3}{2}}-\xi)^M\,\mathrm{d}\xi = \frac{1}{(M+1)!}\,t^{\frac{3}{2}(M+1)},$$

we obtain in this way:

$$|\Delta K_{n,M}| \le \frac{1}{(M+1)!}\int_0^\infty t^{n+\frac{3}{2}(M+1)}e^{-\frac{1}{2}\sqrt{3}\beta t}\mathrm{d}t \tag{B.30}$$

or $$|\Delta K_{n,M}| \le \frac{1}{(M+1)!}\left[n+\frac{3}{2}(M+1)\right]!\left(\frac{\sqrt{3}}{2}\beta\right)^{-[n+1+\frac{3}{2}(M+1)]} \tag{B.31}$$

From this the remainder terms $\Delta S_{n,M}$ and $\Delta C_{n,M}$ can be estimated by observing that

$$\left.\begin{matrix}|\Delta S_{n,M}|\\ |\Delta C_{n,M}|\end{matrix}\right\} \le |\Delta K_{n,M}|, \tag{B.32}$$

which yields equation (B.20).

For $n = -1$ we have in place of equation (B.18):

$$S_{-1}(\beta) = \frac{\pi}{2} - \sum_{m=1}^{M}\frac{1}{m!}\left(\frac{3}{2}m-1\right)!\times\sin\left(\frac{m\pi}{4}\right)\beta^{-\frac{3}{2}m} + \Delta S_{-1,M}, \tag{B.33}$$

where $\Delta S_{-1,M}$ can be obtained from equation (B.20).

If only the asymptotic expansions, not the remainder terms, were to be derived, the following method which makes use of generalized functions would be more convenient: According to LIGHTHILL[18]

$$\int_{-\infty}^{+\infty} x^{\alpha}\, He(x)\, e^{j\omega x}\, \mathrm{d}x = \alpha!\, |\omega|^{-(\alpha+1)}\, e^{j\frac{1}{2}\pi(\alpha+1)\operatorname{sgn}\omega}, \tag{B.34}$$

where $\alpha \neq$ integer, while for a non-negative integer n:

$$\int_{-\infty}^{+\infty} x^{n}\, He(x)\, e^{j\omega x}\, \mathrm{d}x = i^{n+1}\, n!\, \omega^{-(n+1)} - \pi\, i^{-n}\, \delta^{(n)}(\omega). \tag{B.35}$$

Here $He(x)$ denotes the Heaviside unit function, which is equal to 1 for $x > 0$ and 0 for $x < 0$, and $\delta(\omega)$ is the Dirac δ-function. If we consider only positive $\omega \geq \omega_0 > 0$ and $\alpha > -1$ the above two relations may be written as one equation:

$$\int_{0}^{\infty} x^{\alpha}\, e^{j\omega x}\, \mathrm{d}x = \alpha!\, \omega^{-(\alpha+1)}\, e^{j\frac{1}{2}\pi j(\alpha+1)}, \quad [\omega > 0;\ \alpha > -1]. \tag{B.36}$$

The use of this relation permits the expansion of the first exponential in equation (B.22) and integration term by term without prior change of the path of integration and yields the expansion of equation (B.29) immediately.

APPENDIX C. Numerical tables

The calculated numerical values of the employed auxiliary functions are given in Tables 2 and 3.

TABLE 2. AUXILIARY FUNCTIONS FOR SMALL VALUES OF β.

β	$H^{(\beta)}$	$H^{(\beta)} + \frac{2}{\pi}\beta H^{(\beta)}$	Q	R
0	0	0	0	0
0·2	−0·89439	−1·4935	0·08421	0·02816
0·4	−1·51991	−2·1568	0·16452	0·05553
0·6	−1·71586	−1·6436	0·23751	0·08139
0·8	−1·48275	−0·2540	0·30067	0·10517
1·0	−0·95920	+1·3009	0·35259	0·12645
1·2	−0·34515	+2·3324	0·39294	0·14500
1·4	+0·182	+2·51	0·42233	0·16077

TABLE 3. AUXILIARY FUNCTIONS FOR $\beta = 0, 1, 2, \ldots 10$.

β	$H^{(-1)}$	S_2	C_4	S_5
0	0	0	+1·852 105 7	0
1	0·10863	+0·736 106 80	−0·701 609 5	+1·927 101 5
2	0·45250	−0·070 188 7	−0·393 154 5	−1·115 230 7
3	0·70837	−0·117 526 1	+0·103 905 7	−0·023 202 0
4	0·83009	−0·036 945 3	+0·047 309 8	+0·059 102 7
5	0·88817	−0·010 564 4	+0·012 584 6	+0·016 681 7
6	0·91959	−0·003 491 9	+0·003 570 9	+0·004 223 9
7	0·93877	−0·001 356 3	+0·001 185 5	+0·001 215 7
8	0·95137	−0·000 601 6	+0·000 455 8	+0·000 406 7
9	0·96017	−0·000 296 0	+0·000 196 9	+0·000 155 0
10	0·96661	−0·000 158 0	+0·000 093 7	+0·000 065 8

REFERENCES

1. J. HOLTSMARK, *Ann. Physik* **58,** 577 (1919); *Physik. Z.* **20,** 162 (1919); **25,** 73 (1924). See also ref. 8.
2. H. MARGENAU, *Phys. Rev.* **40,** 387 (1932); **43,** 129 (1933); **44,** 931 (1933); **48,** 755 (1935); **82,** 156 (1951).
3. M. KULP, *Z. Physik* **79,** 495 (1932); **87,** 245 (1933).
4. H. KUHN, *Phil. Mag.* **18,** 987 (1934). H. KUHN and F. LONDON, *Phil. Mag.* **18,** 983 (1934).
5. M. BARANGER and B. MOZER, *Phys. Rev.* **115,** 521 (1959); **118,** 626 (1960). H. R. GRIEM, A. C. KOLB and K. Y. SHEN, *Phys. Rev.* **116,** 4 (1959). See also ref. 8.
6. P. W. ANDERSON, *Phys. Rev.* **76,** 647 (1949). S. BLOOM and H. MARGENAU, *Phys. Rev.* **90,** 791 (1953).
7. M. BARANGER, *Phys. Rev.* **111,** 494 (1958); *New Developments in the Theory of Pressure Broadening*, the Rand Corporation, Santa Monica, California, ASTIA Document No. AD 150692 (1958). See also A. C. KOLB and H. GRIEM, *Phys. Rev.* **111,** 514 (1958).
8. H. MARGENAU and M. LEWIS, *Revs. Mod. Phys.* **31,** 569 (1959).
9. T. HOLSTEIN, *Phys. Rev.* **79,** 744 (1950). P. W. ANDERSON, *Phys. Rev.* **86,** 809 (1952). Also ref. 8 and G. TRAVING, *Über die Theorie der Druckverbreiterung von Spektrallinien*, Mitteil. Astron. Ges., Sonderheft No. 1 G. Braun, Karlsruhe (1959).
10. V. WEISSKOPF, *Z. Physik* **75,** 287 (1932).
11. See ref. 6 and 7.
12. S. CHANDRASEKHAR and J. VON NEUMANN, *Astrophys. J.* **95,** 489 (1942).
13. Ref. 12, p. 506 and 507.
14. L. I. SCHIFF, *Quantum Mechanics*, p. 213 ff. McGraw-Hill Book Company, New York (1955).
15. E. U. CONDON and G. H. SHORTLEY, *The Theory of Atomic Spectra*, p. 399. The University Press, Cambridge (1957).
16. S. CHANDRASEKHAR, *Revs. Mod. Phys.* **15,** 1 (1943), p. 72 and 73. See also ref. 12 and Appendix B.
17. See ref. 12 and 16.
18. M. J. LIGHTHILL, *Introduction to Fourier Analysis and Generalised Functions*. The University Press, Cambridge (1958).
19. See ref. 12, p. 502 f.; ref. 16, p. 70 ff. Compare Appendix B.
20. See ref. 8 and Appendix B.
21. S. CHANDRASEKHAR and J. VON NEUMANN, *Astrophys. J.* **97,** 1 (1943). Ref. 12, p. 506 ff.
22. See ref. 18, p. 43.

OL.
1
961

J. Quant. Spectrosc. Radiat. Transfer. Vol. 1, pp. 30–45. Pergamon Press Ltd. Printed in Great Britain

SHOCK-TUBE MEASUREMENTS OF THE *f*-NUMBER FOR THE (0, 0)-BAND OF THE OH $^2\Sigma \rightarrow {}^2\Pi$ TRANSITIONS*

M. LAPP†

Daniel and Florence Guggenheim Jet Propulsion Center, California Institute of Technology
Pasadena, California

(*Received* 22 *July* 1960)

Abstract—The *f*-number for the (0, 0)-band of the $^2\Sigma \rightarrow {}^2\Pi$ transitions of OH has been found to be $(0{\cdot}9 \pm 0{\cdot}5) \times 10^{-3}$. A shock tube was used to produce hot gas samples at temperatures from 3300 to 3900°K with equilibrium partial pressures of OH of 0·004 to 0·02 atm. The emission intensities were measured photoelectrically as a function of time behind the reflected shock in a selected spectral interval. These results were then related to the *f*-number by means of an absolute intensity calibration.

1. INTRODUCTION

THE shock tube has been used by a number of investigators in emission and absorption experiments for the determination of *f*-numbers[1]. The purpose of this experiment was the determination of the *f*-number for the (0, 0) vibrational band of the $^2\Sigma \rightarrow {}^2\Pi$ OH electronic transitions. This *f*-number has been measured previously by OLDENBERG and RIEKE[2] and by DYNE[3] for OH produced at equilibrium in furnaces and by CARRINGTON[4] for OH in flames. The use of a shock tube permits the attainment of temperatures in excess of those achieved in furnaces and flames, with correspondingly better known equilibrium OH concentrations.

We have studied the emission from OH (formed behind the reflected shock) in an axial direction within a very small solid angle. All tests were performed with H_2O – Ar mixtures. The gas composition was measured for each test and about 1% H_2O was usually found to be present. The experimental conditions were chosen in such a way that no OH emission could be detected from the gas behind the incident shock wave. The radiation was monitored by a 1P 28 photomultiplier used with a Perkin–Elmer quartz monochromator.

The length of the test gas grows linearly with time for constant reflected shock velocity. This enabled us to determine whether the gas was transparent or self-absorbed. Theoretical estimates of transparency are possible from available information but are often inconclusive because of the absence of accurate data for the line widths. We observed that the emission intensity was essentially a linear function of time after shock reflection, thus indicating that the radiating region was transparent. This emission was related to the *f*-number by an absolute intensity calibration‡ made by imaging a source of known intensity at the shock-tube exit port. In addition, relative intensity calibrations were performed immediately following each run.

* Supported by the Air Force Office of Scientific Research of the Air Research and Development Command, U.S. Air Force, under Contract AF 18(603)–2.

† Present address: General Electric Research Laboratory, Schenectady, New York.

‡ If we had chosen conditions such that the test gas did not radiate in the linear portion of the curves of growth, an absolute intensity calibration would not have been required, since each run would have corresponded to an infinite number of multiple-path experiments. However, the reduction of data would have been more difficult.

II. EXPERIMENTAL APPARATUS

A. The shock tube

The shock tube used for these experiments[5] was constructed of steel tubing of 3 in. inside diam. and $\frac{1}{4}$ in. wall thickness. The low-pressure section was either $78\frac{5}{8}$ or $66\frac{5}{8}$ in. long, depending upon the experimental testing time required. The high-pressure section was 60 in. long. The end plate of the low-pressure section was removable from a threaded mount and contained a $\frac{3}{4}$ in. diameter, $\frac{3}{8}$ in. thick, Linde synthetic sapphire window whose surface was flush with the end wall of the shock tube. Velocity measurements were made by measuring the shock transit time between sputtered platinum thin film heat gages[6]. DuPont mylar diaphragms were used. With mylar, ultraviolet impurity radiation was negligibly small and the experimental scatter of measured incident shock velocities (u_s) was reduced to about $\frac{1}{2}$ per cent. The tube was cleaned between runs by flushing with high-pressure dry nitrogen gas discharged through a hose directed at the tube walls. During preliminary work the tube was cleaned with various solvents.

B. The gas-handling system

The gas-handling system was constructed of copper tubing and solder fittings except that glass systems were used for analysis (cf. section C) and for bubbling Ar through H_2O to produce the test-gas mixtures. The bubblers were connected to a 3 l. storage flask and to a steel mixing bottle containing glass beads. The steel bottle was attached to the system through a flexible metal line that permitted additional mixing of the gases by shaking. The driver gas for these experiments was helium.

The apparatus was evacuated through use of an oil diffusion pump and a mechanical forepump. A Philips gage was used for high vacuum measurements and was calibrated against a McLeod gage. The entire apparatus could be evacuated to approximately 5×10^{-5} mm of Hg with a leak rate of about 0·02 μ of Hg/min. A pressure of less than 10^{-3} mm of Hg with a leak rate of about 1 μ of Hg/min was considered satisfactory.

C. Concentration analysis

Because of strong adsorption of H_2O vapor on the metallic walls, it was found necessary to determine the test-gas composition for each run. This determination was performed by admitting test gas to the shock tube from the manifold while simultaneously withdrawing a sample from another tap in the tube. The initial test-gas pressure (p_1) was recorded on a precision Hg manometer. The analytical method involved freezing of the H_2O vapor from a known volume of test gas. This H_2O was then allowed to evaporate into a small calibrated volume and the concentration determined from the resulting pressure. A check on this procedure was performed by analyzing a 1 % CO_2 – 99 % Ar mixture. The composition was determined with an accuracy of better than one per cent.

D. Electronic equipment

The thin film heat gages mentioned in section A permitted the measurement of u_s by triggering a Berkeley counter with a time resolution of 1 μsec. The step-pulse signal at the heat gages was about 1 mV and was amplified by identical wideband amplifiers. Considering the transit time of an average shock ($u_s \approx 1{\cdot}3$ mm/μsec) past a gage (width $\approx \frac{3}{4}$ mm) to be about 0·6 μsec, the total error in shock velocity measurement was less than $\frac{1}{2}$ %.

The radiant intensity was recorded as a function of time by using either a Tektronix Type 535 or Type 551 oscilloscope with Type D or Type 53/54B plug-in preamplifiers. The oscilloscopes were triggered by a spike pulse from a transistorized 19000-gain trigger amplifier which was fed by the step-pulse output of the second heat gage.

The photomultiplier power supply circuit is shown in Fig. 1. The time constant τ introduced through use of this power supply was measured by the cathode-ray tube method. In this method, an oscilloscope is used as a pulse light source, the cathode-ray tube face being masked off except for a small opening. The sweep traverses this opening rapidly and provides a step pulse of radiation. By placing the photomultiplier close to this light source and by recording its output signal on a second oscilloscope, we obtain the time constant of the electronic circuitry associated with the tube. With a 53/54B preamplifier, τ was found to be about 0·2 μsec. The time constant associated with a 53/54B preamplifier is 0·02 μsec, while that of a Type D preamplifier at 1 mV/cm gain is 0·45 μsec. The latter preamplifier was used for low level photomultiplier output signals and introduced the

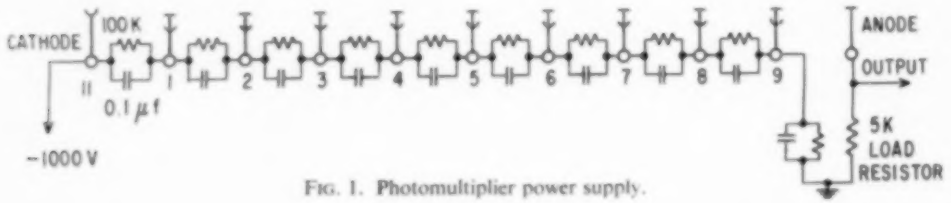

FIG. 1. Photomultiplier power supply.

limiting time response into the system. For the experiments performed, this time response was entirely adequate. Linearity of the photomultiplier output with changes in incident light intensity was checked for the photomultiplier currents used.

E. Exit optics for the shock tube

A schematic diagram of the exit optics is drawn in Fig. 2. All quantitative experiments were performed using a fused quartz prism with the monochromator from a Perkin–Elmer Model 13 spectrophotometer. An RCA 1P 28 photomultiplier was used as detector. Preliminary qualitative data were obtained with a Jarrell–Ash (JACO) Model 8200 $\frac{1}{2}$ meter monochromator and a Hilger small quartz spectrograph. Several front-surface aluminized mirrors, not shown in Fig. 2, were used in the exit optics.

At the wavelengths of interest (≈ 3100Å), the sapphire exit port transmission[7] and the reflectivity of the mirrors[8] were both about 82%. The exact values were not required for reduction of the data since both the calibration radiation and the hot gas radiation share these elements of the optical path. The lenses were made of clear fused quartz; the transmission of 1 cm samples of this material was about 99·8% excluding reflection losses[9].

The exit system solid angle ($\Delta\Omega_E$) used for the quantitative runs was $3{\cdot}40 \times 10^{-5}$sr. This small angle was produced by imaging and recording the hot gas radiation from a volume with cross-sectional area practically equal to the exit port area.

F. Calibration optics

An absolute intensity calibration of the apparatus was performed by imaging a known intensity per unit area at the shock-tube exit plane and comparing the resultant oscilloscope

VOL
1
196

deflection with that from the OH emission during a shock-tube run. The image was produced with the optics shown in the schematic diagram in Fig. 2.

A General Electric 30A/T24/3 tungsten strip filament lamp with a regulated power supply was used as source. The filament had a useful area of 46 × 3 mm. A quartz window was attached to the lamp through a graded tube seal. Each time the lamp was used for a calibration, the filament brightness temperature (T_B) was measured with a Leeds and Northrup optical pyrometer which had been calibrated against a blackbody. A 50 c/s light chopper was placed next to the source aperture in order to permit the use of a.c. amplifiers.

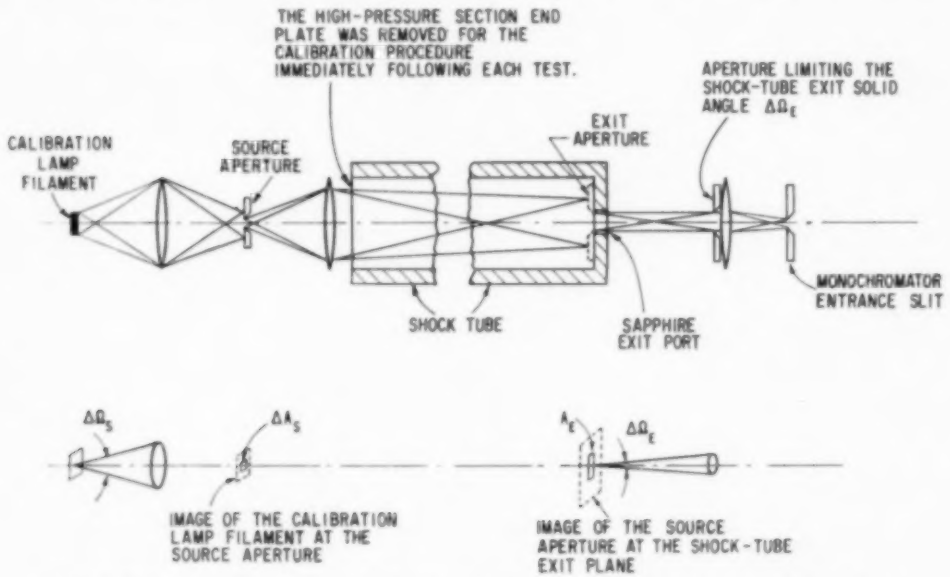
THE HIGH-PRESSURE SECTION END PLATE WAS REMOVED FOR THE CALIBRATION PROCEDURE IMMEDIATELY FOLLOWING EACH TEST.
APERTURE LIMITING THE SHOCK-TUBE EXIT SOLID ANGLE $\Delta\Omega_E$
EXIT APERTURE
CALIBRATION LAMP FILAMENT
SOURCE APERTURE
MONOCHROMATOR ENTRANCE SLIT
SHOCK TUBE
SAPPHIRE EXIT PORT
$\Delta\Omega_S$
ΔA_S
A_E
$\Delta\Omega_E$
IMAGE OF THE CALIBRATION LAMP FILAMENT AT THE SOURCE APERTURE
IMAGE OF THE SOURCE APERTURE AT THE SHOCK-TUBE EXIT PLANE

FIG. 2. Schematic diagram of the shock-tube exit optics and the calibration optics. This optical system was used for relative intensity calibrations and for converting observed intensities to absolute intensities. The source aperture limited the effective source area (ΔA_S). The exit aperture limited the shock-tube exit port area (A_E) and was produced by the image of the monochromator entrance slit at the shock-tube exit plane.

The lamp filament was first imaged (1:1) on an accurately measured source aperture of dimensions 1·519 ± 0·003 × 1·527 ± 0·003 mm. The aperture was then imaged at the shock-tube exit plane by the second lens. The resulting magnification produced an image larger than the exit port. The solid angle of the calibration beam exceeded that subtended by the shock-tube exit optics ($\Delta\Omega_E$). The lenses were carefully positioned according to their focal lengths at 3090Å, thus producing a monochromatically aligned calibration system. The aberrations introduced into the image at the exit port did not affect the accuracy of our experiments significantly since suitable corrections were made (see section III B).

III. EXPERIMENTAL PROGRAM AND DATA ANALYSIS

A. Shock-tube measurements

1. *Experimental gas properties.* Equilibrium computations of the gas properties behind the incident and reflected shocks (state functions) were made through use of relations

expressing the conservation of energy, momentum, and mass and thermochemical data relating to the chemical species present (Ar, H_2O, OH, H_2, O_2, H, O)*. The computations were performed at the Rand Corp. with an IBM 704 program developed for the calculation of shock-wave parameters by Dr. R. E. Duff of Los Alamos†.

The standard notation for state functions is used, as may be seen in Fig. 3. The subscript 1 refers to initial downstream conditions; 2, to conditions behind the incident shock; 3, to conditions behind the contact surface; 4, to the initial upstream conditions; and 5, to conditions behind the reflected shock with speed u_{s_r}. We use p_2 and p_5 for total gas pressures and p_2^* and p_5^* for partial pressures of OH behind the incident and reflected shocks.

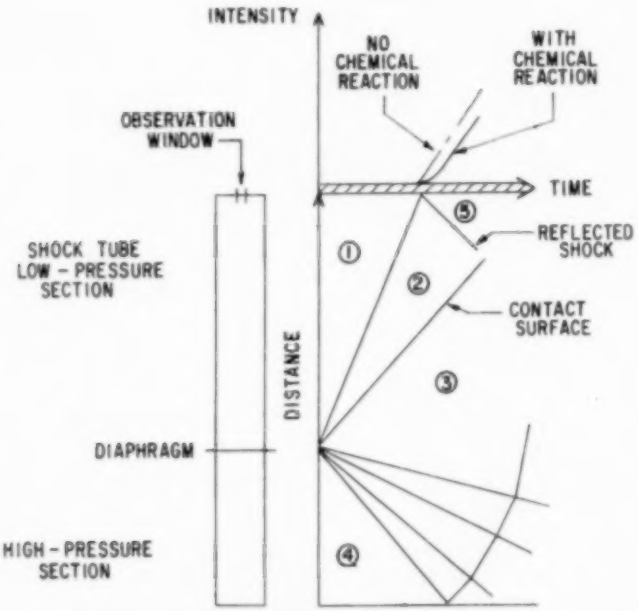

FIG. 3. Representative distance-time plot for the shock-tube experiments.

The initial pressure (p_1) and temperature (T_1), the incident shock speed (u_s), and the initial test-gas composition are all that are needed in order to determine the equilibrium state functions.

All quantitative experiments were made with $p_1 \approx 50$ mm of Hg, and the final data used correspond to 0·67 to 1·40% of H_2O. Computations were made for temperatures behind the reflected shock (T_5) of about 3100 to 4400°K. For these values of T_5, the corresponding lower values of T_2 indicate that the kinetics of the thermal decomposition of H_2O is sufficiently slow[10] to justify the assumption that no significant reaction occurs in the gas behind the incident shock. Estimates made on the basis of data given[10] show

* The heat of formation of OH used was 9·27 kcal/mole.

† Dr. Duff very kindly supplied us with a copy of his IBM deck. The author is grateful to the Rand Corp., and in particular to W. Sibley, for assistance with the machine computations.

VOL. 1 1961

that the time constant for the formation of OH is* about 8000 μsec at 2000°K. Therefore, the state function computations were made by considering no chemical reaction to occur behind the incident shock whereas chemical equilibrium was assumed to exist behind the reflected shock wave.

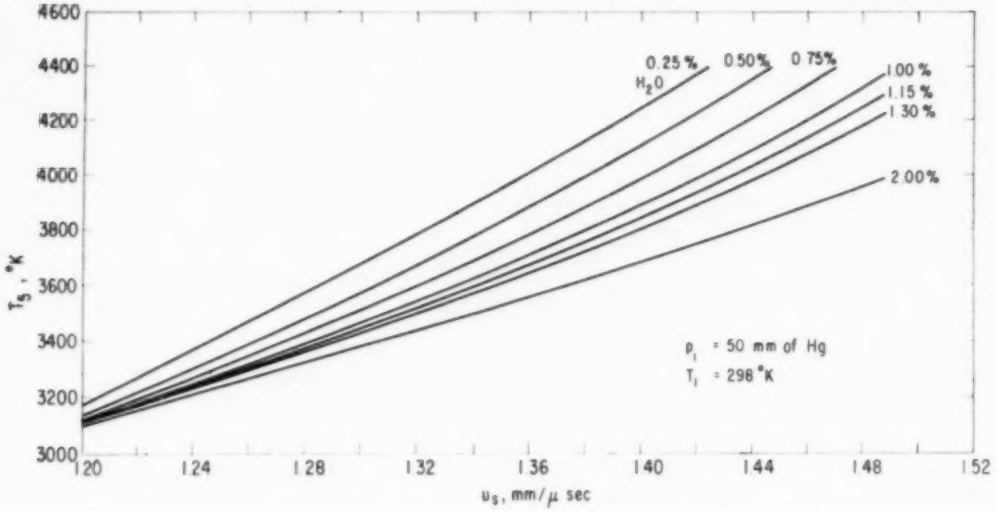

FIG. 4. Temperature T_5 behind the reflected shock as a function of incident shock speed u_s.

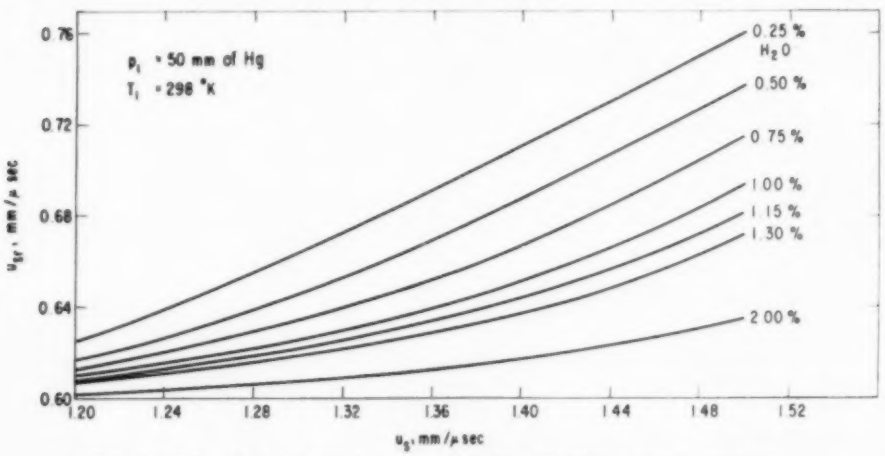

FIG. 5. Reflected shock speed u_{sr} as a function of incident shock speed u_s.

Results of the calculations of T_5, u_{sr} and p_5* as functions of u_s for $p_1 = 50$ mm of Hg† appear in Figs. 4–6.

* Inspection of Fig. 5 of Ref. 10 indicates that the OH concentration profile as a function of distance behind a shock may be represented approximately by an exponential curve.

† The variation of T_5 and u_{sr} with small changes of p_1 is negligible. For example, with $u_s = 1{\cdot}3$ mm/sec and a 1% H_2O test gas, T_5 and u_{sr} decrease about 0·2% for p_1 varying from 50 to 45 mm of Hg. This decrease in p_1 causes a 12% decrease in p_5*.

2. *Qualitative data.* Preliminary experiments were performed to determine (a) the presence of OH radicals in the shocked gas and (b) the presence of any impurities that radiate significantly in the region of the OH emission. Photographic spectra taken with the Hilger spectrograph established the presence of OH in the test gas. Further exploration

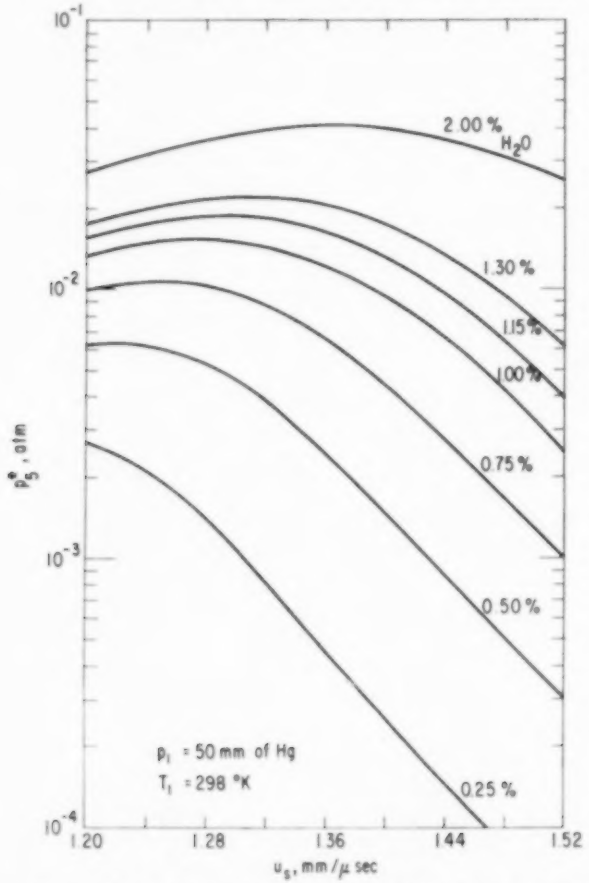

FIG. 6. Partial pressure p_5^* of OH behind the reflected shock as a function of incident shock speed u_s.

of OH and impurity radiation was made through use of the JACO monochromator and a 1P 28 photomultiplier. Runs were made at wavelength settings varying from 3070 to 3093Å with a spectral slit width of 8 Å both with and without H_2O vapor added to the Ar. When the tube was properly cleaned and evacuated, the impurity radiation became negligibly small; on the other hand, H_2O – Ar test gas produced an essentially linear intensity–time profile*. The effects of not cleaning the tube thoroughly after the preceding run (using

* When the reflected shock intersects the contact surface we observe a change in the intensity–time profile and consider the useful experiment to be ended. The testing times of our experiments were limited to about 160 μsec or less in order to ensure the absence of intersection effects.

VOL. 1 1961

mylar diaphragms) and of not pumping the tube for a sufficiently long time were found to be quite similar, both leading to high levels of impurity radiation.

The Perkin–Elmer monochromator was used for quantitative runs since its dispersion exceeded that of the JACO instrument in the spectral region of interest and since the reduction of experimental data was simplified by the observed OH radiation corresponding as nearly as possible to the entire (0, 0)-band $^2\Sigma \rightarrow {}^2\Pi$ transitions of OH. In addition, use of a wide spectral slit width minimizes any errors introduced by slight misalignments. Use of this instrument in Ar and Ar–H_2O runs indicated that, for a 1 mm slit, the impurity level was still negligibly low.

3. *Quantitative data.* A sample oscillogram obtained with the Perkin–Elmer instrument set at 3090Å with a 1 mm slit is shown in Fig. 7. The oscillograms suggested that the OH gas was optically transparent and that the linear intensity rise was produced by the linear

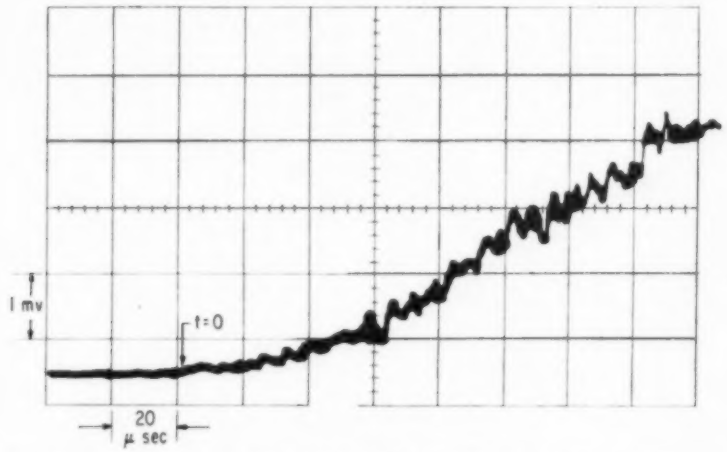

FIG. 7. Oscilloscope trace for run 65 (1·15% H_2O, $p_1 = 50{\cdot}3$ mm of Hg, $u_s = 1{\cdot}27$ mm/μ sec).

growth with time of the optical depth (partial pressure of emitter times geometric path length) $X = p_5^* u_{sr} t$ for u_{sr} = constant. Estimates of the transparency of OH under the conditions of these experiments ($X \approx 0{\cdot}02$ to $0{\cdot}1$ cm-atm, $T_5 \approx 3300$ to 3900°K, $p_5 \approx 7$ to $8\frac{1}{2}$ atm) made by using available estimates of line intensities and half widths[2–4, 11–12] indicate that the gas should be transparent for most of the spectral lines.

The initial non-linear portion of the intensity–time curves arises because a finite time is required to form OH from H_2O behind the reflected shock wave. In Fig. 8, we show the reflected shock at position $x = L$ at time $t = L/u_{sr}$ after reflection. The gas at $x = x'$ has now been in state 5 for a time $t' = (L\text{-}x')/u_{sr}$. The partial pressure of OH at this station is given by $p_5^*(t')$. If we let $B_\lambda^{\bar{}o}$ = the average blackbody steradiancy and α = the integrated intensity of the observed transitions, then we obtain for the (axial) steradiancy (in erg/sec-cm^2-sr) the following explicit relation in the isothermal, transparent-gas approximation:

$$B = B_\lambda^{\bar{}o} \alpha p_5^* \int_0^L h(t')\mathrm{d}x'$$

where $p_5^*(t') = p_5^* h(t')$, p_5^* is the equilibrium value of OH partial pressure, $h(0) = 0$ and $\lim_{t' \to \infty} h(t') = 1$. An appropriate form for $h(t')$ is $1\text{-}\exp(-t'/\tau)$ where τ is defined as the time constant for the reaction (see discussion in section 1). We obtain

$$B = B_\lambda^\circ \alpha p_5^* u_{sr}[t - \tau(1 - e^{-t/\tau})] \; ; \tag{1}$$

thus

$$B \approx B_\lambda^\circ \alpha p_5^* u_{sr}(t - \tau) \quad \text{for } t \gg \tau, \tag{2}$$

$$B = B_\lambda^\circ \alpha p_5^* u_{sr} \tau(1/e) \quad \text{for } t = \tau, \tag{3}$$

$$B \approx B_\lambda^\circ \alpha p_5^* u_{sr}(t^2/2\tau) \quad \text{for } t \ll \tau. \tag{4}$$

Results obtained from equation (1) for $\tau = 30$ μsec are plotted in Fig. 9. The shape of the curve obtained from equation (1) is seen to be similar to that of the oscilloscope trace shown in Fig. 7.

A convenient method for reducing the results of our experiments which does not depend upon detailed knowledge of the chemical kinetics relating to OH formation involves fitting a straight line to the measured intensity–time data. From equation (2) we may then obtain values for $\alpha = B/B_\lambda^\circ p_5^* u_{sr}(t - \tau)$ that are directly proportional to the f-number. We

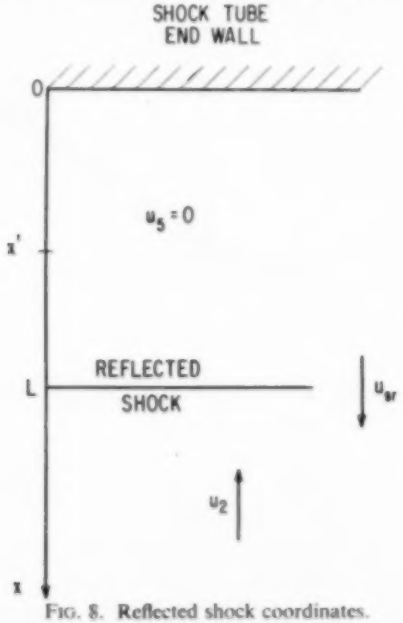

FIG. 8. Reflected shock coordinates.

may, in addition, estimate τ from our data. Our estimates agree within about 20 per cent with values derived from the Los Alamos data[10].

B. Calibration procedures

In order to reduce the experimental data, we performed the following absolute calibrations:

(1) the fraction of the total intensity to which our system responded was estimated, i.e., the instrumental slit function was measured;

(2) an estimate was made of the absolute intensity of the source radiancy that is actually imaged at the shock-tube exit port and recorded by the detector;

(3) the instrumental output was then related to the absolute incident energy flux.

A schematic diagram of the optical system used for intensity calibrations and for converting

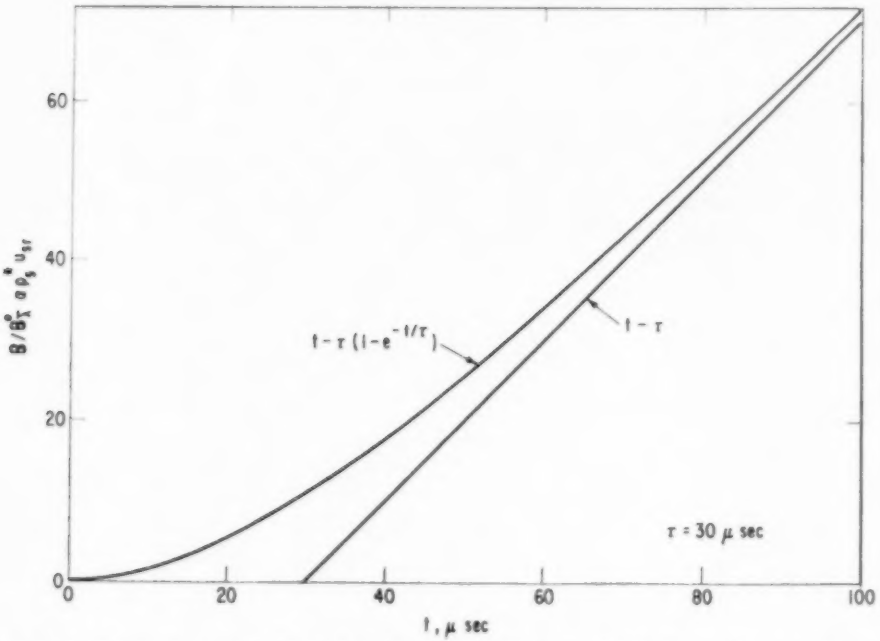

FIG. 9. Schematic diagram of the intensity–time profile for a chemically-reacting gas with characteristic time constant τ.

observed intensities to absolute intensities is shown in Fig. 2. If we let R_T represent the total radiant flux (erg/sec) produced by heated OH, we obtain

$R_T \approx$ [source steradiancy B_S (erg/sec-cm^2-A-sr)]

$\times$ [source solid angle $\Delta\Omega_S$ subtended by the source optics (sr)]

$\times$ [source area ΔA_S (cm^2)] $\times$ [wavelength interval $\Delta\lambda$ (Å)]

$\times$ [intensity loss factor F due to quartz optics, off-axis rays, and the ratio of the shock-tube exit port area to the area of the image made of the source]

$\times$ [ratio Y of the intensity of the shock-tube data in mV per mV of the calibration intensity corresponding to B_S] (5)

The quantity R_T is related to the expression given for B in equations (1) to (4) as follows:

$R_T = B \times$ (solid angle subtended by the receiver optical system)

$\times$ (shock-tube exit area actually viewed).

The effect of the slit function on equation (5) must still be considered.

1. *Monochromator slit function.* A monochromator is characterized by a slit function $g(|\lambda-\lambda_o|, b')$ which indicates the response of the instrument at wavelength λ when it is set at λ_o. Here b' represents all of the instrumental constants. For a prism spectrograph, the entrance slit of which is uniformly filled with radiation, we expect the slit function to be of triangular shape if we neglect small variations of prism dispersion with wavelength. The base of the triangle should be equal to twice the spectral slit width for one-to-one optics of the monochromator entrance and exit slits.

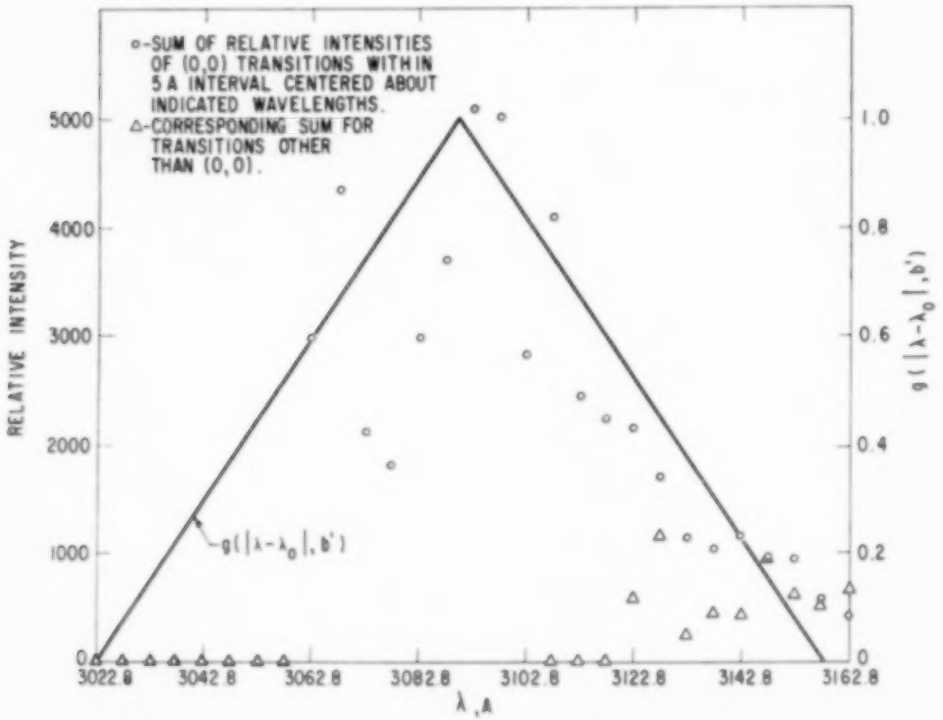

FIG. 10. Relative intensities of OH $^2\Sigma \rightarrow {}^2\Pi$ transitions at 3000°K over a selected portion of the spectrum[11]. Relative intensities lying between 0 and 30 are indicated as 0. The monochromator slit function g is also shown.

An experimental determination of the slit function was performed by imaging a mercury-vapor lamp on the monochromator slits. After selecting a given slit width, several mercury lines were scanned mechanically and the resulting output recorded. Since no strong isolated mercury line exists within the spectral interval used for the shock-tube runs, scans were made of nearby lines. All scans indicated that the slit function base exceeded the ideal value. Repeated scans of the strong line at 4358Å with mechanical slits varying in width from 0·3 to 1·0 mm indicated that the ratio D of the measured slit function base to the calculated value was 1·52 to within 3 per cent. A check on the validity of using this value of D for the spectral region of these experiments was made by scanning the closely

spaced mercury lines at 3131·8, 3131·6 and 3125·7Å with a 1 mm slit width. A value of D almost exactly equal to the value quoted above was obtained.

The prism dispersion at 3090 Å was $2 \times 44{\cdot}7$ Å/mm; thus the base of the triangular slit function for the shock-tube experiments was $1{\cdot}52 \times 2 \times 44{\cdot}7 = 136$ Å. The slit function has been drawn in Fig. 10 together with data from the extensive tabulation of relative intensities of the OH u.v. transitions[11]. These relative intensity data will be discussed in section C. Since the slit function is triangular, its effect upon the calibration procedure is to make the wavelength interval $\Delta\lambda$ in equation (5) equal to $\frac{1}{2}$ of the spectral base of the slit function, i.e., approximately 68 Å.

2. *Determination of the intensity loss factor F.* Since the optics of the calibration bench have been aligned to fit relations derived from paraxial calculations, the computed source intensity per unit area imaged at the shock-tube end plane applies only in the limit as the exit area approaches zero. We correct for the finite area A_E of the shock-tube exit port through use of the factor

$$C = \frac{\text{calibration intensity per unit area at the shock-tube exit plane for exit area } A_E}{\lim_{\left[\begin{smallmatrix}\text{exit}\\ \text{area}\end{smallmatrix}\right] \rightarrow 0} \text{calibration intensity per unit area at the shock-tube exit plane}}$$

In order to determine C, a set of accurately machined apertures of 0·95 to 10·5 mm diam. was placed at the shock-tube end plane. The calibration intensities per unit area were plotted as a function of the exit area and were found to be constant to within a few per cent for diameters less than about 5 mm. The value of C obtained was 0·83.

Another contribution to the loss factor comes from the reflection losses at the quartz surfaces of the calibration bench. The fractional transmissivity Q of these optics is approximately equal to 0·792. Next we consider the fraction U of the source image at the shock-tube exit plane that falls within the exit port area $A_E = 0{\cdot}486$ cm². The magnification of the effective source area $\Delta A_S = 0{\cdot}0232$ cm² was such that $U = 0{\cdot}486/2{\cdot}73 = 0{\cdot}178$. We finally obtain $F = CQU = 0{\cdot}117$.

3. *Relation of shock-tube intensity data to absolute intensity calibration.* We shall now describe how the parameter Y in equation (5) was determined. In order to insure a reasonable lifetime for the calibration lamp, it was operated at its rated current of 30 amp resulting in a filament (source) temperature T_S of about 2090°K as measured by a pyrometer. The source intensity at 2090°K was too low to permit a good absolute calibration at 3090 Å. Therefore relative intensity calibrations were performed at three other wavelengths ($\lambda_o = 3800$, 3920 and 4120 Å) for each run, and these relative intensity calibrations related to an absolute calibration at 3090 Å after all runs had been completed. This absolute calibration was performed by operating the lamp at approximately 40 amp with $T_S = 2440$°K.

We let $R' = FB_S\Delta\Omega_S\Delta A_S\Delta\lambda$ erg/sec and I_c' = the receiver signal in mV for an absolute calibration at 3090 Å and 2440°K. Then R'/I_c' = the absolute energy flux in ergs/sec per mV of receiver output. We also let I = the receiver signal in mV for OH emission as measured from our shock-tube data. Thus, if the photomultiplier sensitivity and the electronic gain did not change with time, $(R'/I_c')I$ = the absolute radiant flux in erg/sec corresponding to the OH emission from a shock-tube run. Since the gain and sensitivity actually change somewhat with time, the relative intensity calibrations were performed immediately

following each run. We let $I_c(\lambda_o)$ = the receiver signal in mV obtained from one of these relative calibrations at λ_o and $T_S = 2090°K$. We also let $I_c^*(\lambda_o)$ = the corresponding signal obtained under the same conditions of photomultiplier sensitivity and electronic gain as existed during the absolute intensity calibration. Therefore, $[I_c^*(\lambda_o)/I_c(\lambda_o)]$ [I] gives the receiver signal for OH emission from the shock tube corrected to the conditions of the absolute calibration. We finally obtain

$$Y = \frac{I_c^*(\lambda_o)}{I_c(\lambda_o)} \frac{I}{I_c'} = \left[\begin{array}{l}\text{the receiver signal } [I_c^*(\lambda_o)/I_c(\lambda_o)][I] \text{ in mV for the flux in erg/sec} \\ \text{emitted from the heated OH in the shock tube divided by the} \\ \text{receiver signal } (I_c') \text{ in mV corresponding to the flux in erg/sec} \\ \text{orginating from the calibration source, for the same amplification} \\ \text{scale and photomultiplier sensitivity.}\end{array}\right]$$

We may now use equation (5) to relate the observed radiant flux in the shock-tube studies to the absolute intensity calibration, viz.,

$$R_T \approx FB_S \Delta\lambda \Delta\Omega_S \Delta A_S [I_c^*(\lambda_o)/I_c(\lambda_o)]\,[I/I_c'] \text{ erg/sec.} \tag{5a}$$

Here B_S = steradiancy of the calibration lamp at 3090 Å and 2440°K = 10·3 erg/sec-cm²-Å-sr,[13] $\Delta\lambda \approx \frac{1}{2}$ the spectral base of the triangular slit function = 68 Å, $\Delta\Omega_S$ = solid angle associated with the calibration source = 0·00400 sr, ΔA_S = source area = 0·0232 cm², and F = intensity loss factor = 0·117. The absolute intensity calibration signals I_c^* were 0·975 mV at 3800 Å, 1·83 mV at 3920 Å, and 3·90 mV at 4120 Å and I_c' was found to be 0·0343 mV. We finally obtain

$$R_T \frac{I_c(\lambda_o)}{I} = \left\{\begin{array}{l}\text{0·216 erg/sec for calibration at 3800 Å} \\ \text{0·406 erg/sec for calibration at 3920 Å} \\ \text{0·865 erg/sec for calibration at 4120 Å}\end{array}\right\}. \tag{5b}$$

C. Calculation of the f-number

The integrated intensity $\alpha_{(0,\,0)} = \int_{(0,\,0)\text{-band}} P_\lambda d\lambda$ is related to the f-number through

$$\alpha_{(0,\,0)} \approx \frac{\pi e^2}{mc^2} \frac{N_1}{p} \lambda_o^2 f \approx 0{\cdot}0227 \frac{273}{T} f \text{ atm}^{-1} \tag{6}$$

where $\lambda_o = 3090$ Å, p = pressure in atm and N_1 = number of molecules per unit volume in the ground state. The induced emission term has been omitted since it is practically unity. Also $N_1 \approx$ total number of molecules per unit volume. The f-number defined by equation (6) is the total f-number for the (0, 0) vibrational band of the $^2\Sigma \rightarrow {}^2\Pi$ transitions of OH.

Since the OH radiators are in the linear part of the curves of growth, we may use equation (2) to relate the partial integrated intensity α' of those OH transitions that make contributions falling within the limits of the slit function to the experimentally measured radiant flux R_T. Thus

$$R_T = B\Delta\Omega_E A_E = B_\lambda^\circ \Delta\Omega_E A_E \alpha' p_{J'}^* u_{v'}(t-\tau). \tag{7}$$

The influence of the slit function upon this result is to replace

$$\alpha' = \sum_{\substack{\text{all OH transitions} \\ \text{for which the slit} \\ \text{function is non-zero}}} S_J$$

by the expression

$$\alpha' = \sum_{\substack{\text{all OH transitions} \\ \text{for which the slit} \\ \text{function is non-zero}}} g(|\lambda - \lambda_0|, b') S_J,$$

where S_J is the integrated intensity of the Jth line at wavelength λ and where λ_0 is the wavelength of the monochromator setting. For the measured triangular slit function and $\lambda_0 = 3090$ Å, we may compute the ratio

$$G = \left[\frac{\displaystyle\sum_{\substack{\text{all OH transitions} \\ \text{for which the slit} \\ \text{function is non-zero}}} g(|\lambda - \lambda_0|, b') S_J}{\displaystyle\sum_{\substack{\text{all (0, 0)-band} \\ \text{transitions}}} S_J} \right] = 0{\cdot}67 \qquad (8)$$

from the tabulated relative intensities[11] (cf. Fig. 10). The variation of G with temperature over our experimental range is negligible. The correct value of the integrated intensity ($\alpha_{(0,\,0)}$) of the (0, 0)-band is then given by

$$\alpha_{(0,\,0)} = \alpha'/G = \alpha'/0{\cdot}67. \qquad (9)$$

Using the values $A_E = 0{\cdot}486$ cm^2 and $\Delta\Omega_E = 3{\cdot}40 \times 10^{-5}$sr, we obtain from equations (6), (7) and (9)

$$f \approx 0{\cdot}0398\ R_T / B_\lambda^{\circ} p_5^{*} u_{s\tau}(t-\tau)\ (273/T_5), \qquad (10)$$

where B_λ° is in erg/sec-cm^2-Å-sr. The f-number may now be computed from our experimental calibration and shock-tube data through use of equation (10) together with the numerical relations given as equation (5b). The result of eight experimental determinations of f with T_5 varying from 3330°K to 3925°K, the composition varying from 0·67% to 1·40% H_2O, and $p_1 \approx 50$ mm of Hg is

$$f = (0{\cdot}90 \pm 0{\cdot}10) \times 10^{-3}$$

for the (0, 0)-band, $^2\Sigma \rightarrow {}^2\Pi$ transitions of OH. The indicated 10% uncertainty represents the r.m.s. scatter of the shock-tube data.

D. Discussion of results and error estimates

Previously published values for the *f*-number are $1{\cdot}2 \times 10^{-3}$ (OLDENBERG and RIEKE[2]), $0{\cdot}6 \times 10^{-3}$ (DYNE[3]) and $1{\cdot}3 \times 10^{-3}$ (CARRINGTON[4]). The computation of these values from the experimental data involved the use of different heats of formation of OH (ΔH_f°) for the determination of OH partial pressures. When converted to our value of ΔH_f°, Oldenberg and Rieke's *f*-number is reduced to about $1{\cdot}0 \times 10^{-3}$ and Dyne's becomes about $0{\cdot}5 \times 10^{-3}$. Carrington's value is only slightly increased, although accurate conversion of his data is complicated by his use of different flames.

Both Oldenberg and Rieke and Dyne produced OH radicals by heating H_2O–O_2 mixtures in a furnace to about 1400 to 1500°K. Densitometer records of photographic absorption spectra were used to provide the absorption coefficient profiles (P_ν) of selected lines. The line integrated intensities (S) were obtained through use of the relation $S_{\text{line}} = \int_{\text{line}} P_\nu d\nu$ and were then corrected by extrapolation to " zero intensity." Carrington's measurements were carried out with various H_2–O_2 and propane–O_2 flames. The *f*-number was measured by the "curve-of-growth" method* in which the total line absorptions are plotted as a function of

$$\log(\text{constant} \times \text{partial pressure of absorbing particles} \times \text{relative line } f\text{-number}).$$

Fitting this experimental curve of growth to an absolute curve of growth[14] then determines the *f*-number by fixing the constant in the expression for the abscissa.

An overall estimate of our experimental accuracy is about $\pm 60\%$ i.e., $f = (0{\cdot}9 \pm 0{\cdot}5) \times 10^{-3}$ although it is difficult to give an exact figure because of uncertainties in the temperature T_5. About half of this error estimate arises from uncertainties in the state functions, intensity calibration procedures, and shock-tube data and half arises from quantities associated with the calibration source and with the definition of the shock-tube exit optics.

Several compensating effects tend to make T_5 somewhat uncertain. (1) Reflected shock velocities u_s, and pressures p_5 in Ar lower than those calculated from the usual gasdynamic relations have been observed experimentally and predicted theoretically[15]. These correspond to lower values of T_5. (2) The OH formed immediately behind the reflected shock is initially at a higher temperature than the calculated equilibrium value of T_5. (3) It is possible that excessive populations of OH in the $^2\Sigma$ state may be produced behind shock fronts as is known to occur in flames. This problem can be settled only by performing a difficult, time-resolved population temperature measurement for the OH radicals formed behind a shock wave. We note that the first effect tends to make our computed *f*-number too small while the second and third effects tend to make it too large.

A rough estimate of the first effect based upon Goldsworthy's theoretical relations and the later experimental references[15] indicates an *f*-number increase of perhaps 20 to 40%. An estimate of the magnitude of the second effect made by calculating the temperature decrease associated with equilibration of the gases after passage of the reflected shock leads to a decrease of the *f*-number of roughly 15%. The errors associated with possible chemiluminescent radiation cannot be estimated theoretically but are presumed to be small[16].

* Dyne also measured the *f*-number by the curve-of-growth method and obtained a value about 10% lower than his best value.

VOL. 1 1961

Acknowledgement—The author is indebted to Dr. S. S. Penner for suggesting this investigation and for helpful discussions and suggestions during the course of the work.

REFERENCES

1. J. Keck, J. Camm and B. Kivel, *J. Chem. Phys.* **28,** 723 (1958); J. Keck, J. Camm and T. W. Wentink, Jr., *Ann. Phys.* **7,** 1 (1959); C. E. Treanor and W. H. Wurster, *J. Chem. Phys.* **32,** 758 (1960).
2. O. Oldenberg and F. F. Rieke, *J. Chem. Phys.* **6,** 439 (1938); also R. J. Dwyer and O. Oldenberg, *J. Chem. Phys.* **12,** 351 (1944).
3. P. J. Dyne, *J. Chem. Phys.* **28,** 999 (1958).
4. T. Carrington, *J. Chem. Phys.* **31,** 1243 (1959).
5. M. Lapp, *Ph. D. Thesis*, California Institute of Technology, Pasadena, California, 1960.
6. J. Rabinowicz, M. E. Jessey and C. A. Bartsch, *J. Appl. Phys.* **27,** 97 (1956).
7. R. W. Kebler, *Optical Properties of Synthetic Sapphire*, Linde Air Products Co., A Division of Union Carbide and Carbon Corp., New York.
8. C. W. Allen, *Astrophysical Quantities*, p. 102, University of London, The Athlone Press, London, 1955.
9. General Electric Co., Willoughby Quartz Plant, Willoughby, Ohio (personal communication).
10. S. H. Bauer, G. L. Schott and R. E. Duff, *J. Chem. Phys.* **28,** 1089 (1958).
11. G. H. Dieke and H. M. Crosswhite, *The Ultraviolet Bands of OH*, Bumblebee Report No. 87, The Johns Hopkins University, 1948.
12. W. E. Kaskan, *J. Chem. Phys.* **28,** 729 (1958); *J. Chem. Phys.* **29,** 1420 (1958).
13. *Tables for the Spectral Radiant Intensity of a Blackbody and of a Tungsten Ribbon*, Rocketdyne Research Report No. 59–32.
14. S. S. Penner, *Quantitative Molecular Spectroscopy and Gas Emissivities*, p. 108, Addison-Wesley Publishing Co., Reading, Mass., 1959.
15. T. A. Brabbs, S. A. Zlatarich and F. E. Belles, *J. Chem. Phys.* **33,** 307 (1960); G. B. Skinner, *J. Chem. Phys.* **31,** 268 (1959); R. A. Strehlow and A. Cohen, *J. Chem. Phys.* **30,** 257 (1959); F. A. Goldsworthy, *J. Fluid Mech.* **5,** 164 (1959); J. P. Toennies and E. F. Greene, *J. Chem. Phys.* **26,** 655 (1957).
16. W. E. Kaskan (personal communication).

J. Quant. Spectrosc. Radiat. Transfer, Vol. 1, pp. 46–52. Pergamon Press Ltd. Printed in Great Britain

FORBIDDEN HELIUM LINE IN A PLASMA SPECTRUM*†

H. SADJIAN
Missile and Space Vehicle Department, General Electric Company, Philadelphia, Pennsylvania
and
H. K. WIMMEL and H. MARGENAU
Sloane Physics Laboratory, Yale University, New Haven, Connecticut

(*Received* 14 *October* 1960)

Abstract—The appearance of forbidden spectral lines in a plasma yields a means of determining the plasma ion density by measuring relative intensities or frequency shifts. A simple static analysis is applied to the He I lines 4^1D–2^1P and yields an ion density of 5×10^{15} cm^{-3} in agreement with other evidence.

1. EXPERIMENTAL PROCEDURE

FORBIDDEN spectral lines are observed in the Stark effect[1]. In a plasma, too, they appear with strengths depending on the ion densities. This paper presents a simple description of a typical instance and the general principles of its analysis.

The line in question is He I $\lambda = 4922$ Å, a 4^1D–2^1P transition, which in the plasma is accompanied by two forbidden lines arising from the transitions 4^1P–2^1P and 4^1F–2^1P, as indicated in Fig. 1. Of the two, the latter is by far the stronger; its normal wave length is 4920·4 Å.

The spectrogram, Fig. 1, was obtained from a high purity Gerdien type[2] arc which consisted of a quartz chamber approximately 3 in. in diam. and 1 in. long. Pure helium gas was introduced tangentially to produce a gas swirl along the chamber axis. The chamber itself had 5/16 in. openings at both ends for introducing the electrodes and to permit venting of the hot gas. Initially, pencil graphite electrodes, attached to $\frac{1}{2}$ in. diam. graphite electrodes outside the chamber, were brought in contact inside the chamber. Thus the arc is struck and the pencil electrodes burn back to the larger electrodes in a few seconds. After electrical equilibrium is attained, the helium arc burns along a column that is $\frac{1}{4}$ in. in diam. and approximately 3 in. long. The unit drew around 300 amp at 200 V.

Spectra obtained from the center of the arc column showed no impurity lines whatsoever; in addition, high speed movies taken with a Fastax camera at 7000 frames per second revealed no perceptible plasma oscillations except in the vicinity of the electrodes outside the chamber. Moreover, spectra obtained over a distance of 1 in. along the column axis displayed a constant steradiancy as determined with a densitometer.

A standard Bausch and Lomb 1·5 meter spectrograph (15 Å/mm) was used to obtain the profiles of the helium lines. The spectrographic slit was oriented parallel to the chamber axis and an achromat served to project an enlarged image on the slit. As the source itself displayed a constant steradiancy over an inch of the column, it was possible to calibrate

* General Electric Company work performed under Air Force Contract AF 04(647)-269.
† Yale University aided by Air Force Office of Scientific Research.

the film by using the helium lines themselves along with a neutral density seven-step filter placed over the slit. The profiles were obtained by densitometering the film and converting the transmission values to their corresponding intensities.

The determination of the temperature posed a problem. The temperature could not be determined from impurity lines as none were present and the introduction of impurities would invariably lower the temperature. Atom–ion ratios could not be used since no helium ion lines appeared in the spectrum.

As it was certain that the helium plasma was at high purity, it was possible to determine the temperature once the ion density was determined. For this purpose a plasma

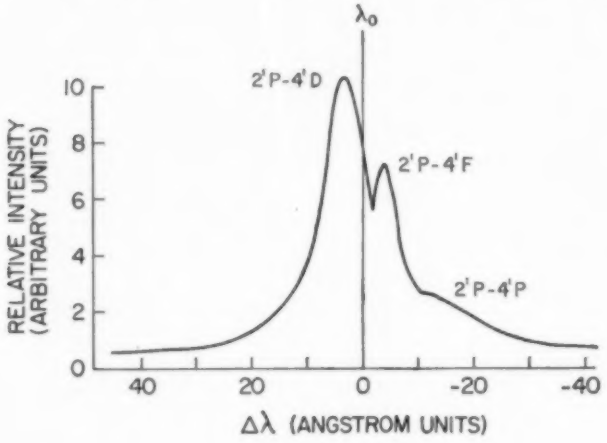

FIG. 1. Experimental line profile of He I, $\lambda_0 = 4921{\cdot}9$ Å, at a temperature of 19,000°K and a He^+ density of 5×10^{16} cm^{-3}.

composition–temperature curve was constructed by use of the Saha equation and the ideal gas law. The method is described elsewhere[3]. The resulting curve is shown in Fig. 2. As can be seen from the curve, once the ion density is known, the temperature is uniquely determined.

In the absence of adequate experimental information relating Stark broadening of the helium lines to the ion density, n_i, the Inglis–Teller relationship was used to determine n_i. As is well known[4, 5],

$$\log_{10} n = 23{\cdot}2 - 7{\cdot}5 \log_{10} g^*$$

where g^* is the highest quantum number observed for a particular spectral series and n is the charge density. Originally, the relationship was derived for hydrogen, but it is equally applicable to the higher terms of helium and many of the alkali and alkali-earth elements.

In the visible-ultraviolet spectrum of helium, six series are observed, 2^1P–n^1S, 2^3P–n^3S, 2^1P–n^1D, 2^3P–n^3D, 2^1S–n^1P and 2^3S–n^3P. In the first two series, the disappearance of lines was masked by other series members; however, in the remaining four series, the highest quantum number observed was $g^* = 7$, yielding an ion density of about 4×10^{16}/cm^3. Perhaps unjustifiably, we have given n here the customary interpretation of $2n_{ion}$ to take into account the electrons. Even though this is an approximate density, it is probably correct to within a factor of 2. Consequently we should expect the true ion density to be

between 3 to 7 $\times$ 10^{16}/cm^3. Referring to Fig. 2, this is seen to correspond to a temperature of 18,000–20,000°K.

II. SIMPLE THEORY

In the following we give a simple theory of shifts and intensities of these components under a static perturbation V. For simplicity we assume that there is only one level (4^1F) from which transitions to 2^1P can be induced by the plasma potential, V. The case of two levels leads to cubic equations but can otherwise be treated by the same method. In a

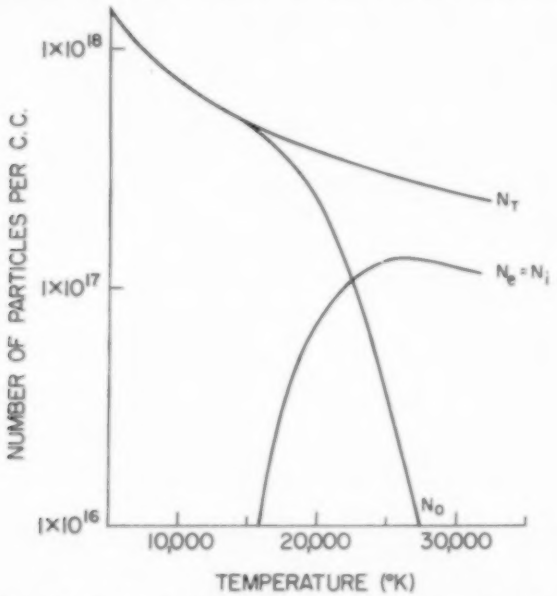

FIG. 2. Composition of the helium plasma versus temperature at a pressure of one atmosphere. *Ne*, *Ni*, *No* are the number densities of electrons, helium ions and neutral helium atoms respectively while N_T is the total particle density.

constant Stark field F, $V = eFr\cdot\cos\theta$; in a nonhomogeneous time-dependent field V is more complicated.

Consider the situation depicted in Fig. 3 where the notation to be used is explained. In the presence of V, Ψ_1^0 and Ψ_2^0 are coupled to form $a_1\Psi_1^0 + a_2\Psi_2^0$, and the levels are pushed apart to become E_1 and E_2. The following results are obtained by simple perturbation theory.

$$\text{Let } \delta \equiv E_2^0 - E_1^0,$$

$$\alpha^2 \equiv 1 + \frac{4|V_{12}|^2}{\delta^2}.$$

$$\text{Then} \quad \left.\begin{aligned} E_1 &= E_1^0 - \frac{\delta}{2}(\alpha - 1);\ \Psi_1 = (2\alpha)^{-\frac{1}{2}}[(\alpha+1)^{\frac{1}{2}}\Psi_1^0 - (\alpha-1)^{\frac{1}{2}}\Psi_2^0] \\ E_2 &= E_2^0 + \frac{\delta}{2}(\alpha - 1);\ \Psi_2 = (2\alpha)^{-\frac{1}{2}}[(\alpha+1)^{\frac{1}{2}}\Psi_2^0 + (\alpha-1)^{\frac{1}{2}}\Psi_1^0] \end{aligned}\right\} \quad (1)$$

Here V_{12} is the matrix element between Ψ_1^0 and Ψ_2^0.

The intensities of the lines in the absence of V are given by

$$I_{10}^{0} = c|\int \Psi_1^{0} \mu \Psi_0 \mathrm{d}t|^2 \equiv I^0$$
$$I_{20}^{0} = c|\int \Psi_2^{0} \mu \Psi_0 \mathrm{d}t|^2 = 0$$

In the presence of V

$$\left.\begin{aligned} I_{10} &= c|\int \Psi_1 \mu \Psi_0 \mathrm{d}t|^2 = \frac{\alpha+1}{2\alpha} I^0 \\ I_{20} &= c|\int \Psi_2 \mu \Psi_0 \mathrm{d}t|^2 = \frac{\alpha-1}{2\alpha} I^0 \end{aligned}\right\} \tag{2}$$

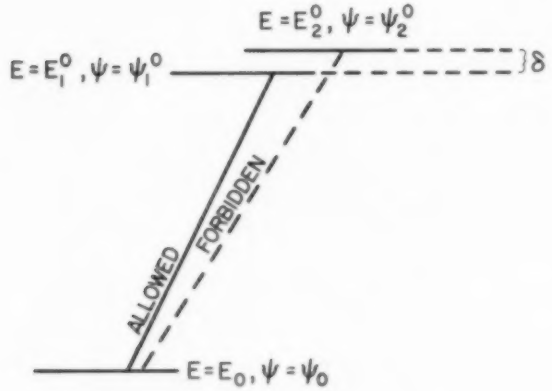

FIG. 3. Levels and state functions for $V = 0$.

Thus the parameter α can be obtained from measurements in two independent ways. For from the intensity ratio (2)

$$\frac{I_{20}}{I_{10}} = \frac{\alpha - 1}{\alpha + 1}\,; \tag{3}$$

$$\frac{E_2 - E_1}{E_2^{0} - E_1^{0}} = \alpha. \tag{4}$$

These results are well substantiated in Fig. 1; viz.

$$\alpha = \frac{\Delta\nu}{\Delta\nu_0} = -\frac{\Delta\lambda}{\Delta\lambda_0} = \frac{7{\cdot}5\ \text{Å}}{1{\cdot}5\ \text{Å}} = 5 \tag{5}$$

$$\frac{I_{20}}{I_{10}} = 0{\cdot}68$$

whereas

$$\frac{\alpha - 1}{\alpha + 1} = \frac{2}{3}$$

Here we have simply taken the intensity peaks to be proportional to the intensities, which is proper because the lines will have approximately equal widths.

VOL.
1
1961

To study the problem in greater detail we must specify the form of V. Let it be EFz, the Stark potential produced by an ion field F. The states are hydrogen-like and can be characterized by quantum numbers n, l, m for the one excited electron. The lower state is a P-state for which m can be 0 and ± 1. Hence the only D and F states which combine with P are those with m-values of 0, 1 and 2. But V couples only states of D and F which have the same m. For each m there will be a different value of $\varkappa$. We define

$$\varkappa_m^2 = 1 + \frac{4}{\delta^2}(V_{DmFm})^2. \tag{6}$$

For hydrogen functions

$$(n, l, m|V|n, l+1, m) = \frac{3}{2} eFa_0 n \left\{\frac{[(l+1)^2 - m^2][n^2 - (l+1)^2]}{4(l+1)^2 - 1}\right\}^{\frac{1}{2}}$$

Hence our

$$(V_{Dm,\,Fm})^2 = |(4, 2, m|V|4, 3, m)|^2 = \frac{9}{4} e^2F^2a_0^2 \cdot 16 \left\{\frac{(9 - m^2) \cdot 7}{35}\right\}$$
$$= \begin{Bmatrix} 324/5 \\ 288/5 \\ 36 \end{Bmatrix} e^2F^2a_0^2 \text{ for } \begin{Bmatrix} m = 0 \\ m = \pm 1 \\ m = \pm 2 \end{Bmatrix} \tag{7}$$

Thus

$$\varkappa_0^2 = 1 + 259{\cdot}2 \left(\frac{eFa_0}{\delta}\right)^2$$
$$\varkappa_1^2 = 1 + 230{\cdot}4 \left(\frac{eFa_0}{\delta}\right)^2$$
$$\varkappa_2^2 = 1 + 144 \left(\frac{eFa_0}{\delta}\right)^2$$

The level shifts are

$$E_m = \frac{\delta}{2}(\varkappa_m - 1),$$

and the intensities

$$I_{Dm} = \frac{\varkappa_m + 1}{2\varkappa_m} I^0, \; I_{Fm} = \frac{\varkappa_m - 1}{2\varkappa_m} I^0.$$

An accurate theory would now require the construction of a diagram showing the level separations for different m, as well as the possible transitions between them ($\Delta m = 0$ for parellel, $|\Delta m| = 1$ for perpendicular polarization). A proper sum over the different intensities must then be taken for all components.

We use here the very crude procedure of averaging the $\varkappa_m^2$:

$$(\varkappa^2_{AV}) = 1 + 211 \left(\frac{eFa_0}{\delta}\right)^2 \tag{8}$$

This, we saw, is 25. Hence one finds

$$eFa_0 = {\cdot}338\delta. \tag{9}$$

We identify F with the "normal" field, $2{\cdot}6\ Zen^{\frac{2}{3}}$, and solve for n, assuming $Z = 1$. Since

$$\delta = h\Delta\nu_0 = -\frac{hc}{\lambda^2}\Delta\lambda = 8{\cdot}3 \times 10^{-8}\Delta\lambda = 12{\cdot}4 \times 10^{-16}\ \text{erg}, \tag{10}$$

we find

$$2{\cdot}6\ e^2a_0n^{\frac{2}{3}} = 4{\cdot}2 \times 10^{-16},$$
$$n = 5{\cdot}2 \times 10^{16}/\text{cm}^3.$$

Thus it seems that even this simplified analysis yields useful results.

III. VALIDITY CONSIDERATIONS

For the following validity investigations we assume an ion density $n = 5{\cdot}2 \times 10^{16}\text{cm}^{-3}$ and a temperature $T = 18000°\text{K}$.

A question arises with respect to our choice of the "normal" field, $F_0 = 2{\cdot}6\ Zen^{\frac{2}{3}}$, instead of the most probable field of the Holtsmark distribution, $F' = 4{\cdot}16\ Zen^{\frac{2}{3}}$. At first glance, the latter seems more appropriate. The picture changes, however, if we take into account the mutual interaction of the perturbing ions and the screening of the ion fields by the electrons. On using BARANGER and MOZER'S[6] high-temperature approximation for the probability distribution of the low-frequency component of the plasma field at a neutral point, one obtains for their parameters the values: $r_0 = 1{\cdot}7 \times 10^{-6}$ cm; Debye length $\lambda = 4{\cdot}1 \times 10^{-6}$ cm; hence $r_0/\lambda \approx 0{\cdot}4$. The most probable field in accord with that value is $F' = 2{\cdot}9\ Zen^{\frac{2}{3}}$, which is very close to the value of the "normal" field used above.

The simple static treatment presented in II is appropriate only if the variations in time of the helium wave function are adiabatic, i.e., if transitions between the adiabatic solutions of the Schrodinger equation are unimportant. We use an approximate condition for adiabaticity given by MARGENAU and LEWIS[15] as a criterion for the validity of the static approach. Accordingly, the quantity $\varphi = 2\pi V\tau/h$ must be larger than 1 to guarantee adiabaticity. Here $V = \mu F$ is a characteristic value of the energy perturbation (μ = atomic dipole moment), while τ is a fluctuation time of the perturbing field defined in a suitable way; under proper conditions, it can be understood as the duration of one collision. The condition $\varphi \gg 1$ holds for degenerate levels, which exhibit linear Stark effect; but it can also be applied to the Helium levels under investigation, since the separation of the unperturbed levels is small in comparison with the matrix elements of the most probable Stark perturbation. We have indeed:

$$|V_{D,F}|_{Av} = 7{\cdot}25eFa_0 = 2{\cdot}45\delta = 2{\cdot}57 \times 10^{-15}\ \text{erg}, \tag{11}$$

according to equations (6) and (8). Hence, equations (1) and (6) show that the corresponding Stark shifts E_i–E_i^0 ($i = 1, 2$) are very close to the ones resulting for degenerate levels. Quantitatively, we have from equations (5) and (10):

$$|E_i - E_i^0| = \frac{\delta}{2}(\alpha - 1) = 2{\cdot}48 \times 10^{-15}\ \text{erg}.$$

this compares well with the energy shift in a linear Stark effect which follows from equations 5 and 11:

$$|E_i - E_i^0| = |V_{D,F}|_{Av} = 2{\cdot}57 \times 10^{-15}\ \text{erg}.$$

In order to evaluate φ, we may use the model of binary collisions between a radiating helium atom and one perturbing (singly-charged) helium ion. On putting (cf. equation 11)

$$V = 7{\cdot}25\, eFa_0, \text{ with } F = \frac{e}{R^2},$$

$$\tau = R \cdot \left(\frac{m}{3kT}\right)^{\frac{1}{2}} = 1{\cdot}7 \times 10^{-12} \text{ sec},$$

we obtain $\varphi = 4{\cdot}2$.

There is of course some doubt about the usefulness of the concept of binary collisions in the case of charged perturbers. Except for the wings of a spectral line, many-particle perturbations are important in a plasma, and the adiabaticity condition should be reformulated accordingly. As will be shown elsewhere[7], an adiabaticity parameter $\varphi(F)$ may be associated with the instantaneous magnitude of the fluctuating plasma field F rather than with a binary "collision", provided the value of F belongs to a well-defined F-interval for which $\varphi \gg 1$. The characteristic time τ is then given by the mean time of occurrence of F, T_F, a quantity that has been introduced by CHANDRASEKHAR and VON NUEMANN[8]. From this viewpoint

$$\varphi = \frac{2\pi V(F) T_F}{h},$$

with

$$T_F = \frac{0{\cdot}32}{n^{\frac{1}{3}}} \left(\frac{m}{3kT}\right)^{\frac{1}{2}} \tau(\beta), \beta = F/F_0$$

The function $\tau(\beta)$ has been tabulated[8]; specifically, $\tau(1) = 0{\cdot}877$, and in consequence $T_F = 0{\cdot}71 \times 10^{-12}$ sec. From this we obtain $\varphi = 1{\cdot}7$.

It is difficult to estimate how the values of φ would be altered by taking into account the mutual interaction of the perturbing ions, and the screening by the electrons. Yet the resulting values of φ seem to indicate that the deviations from adiabaticity are not large, especially not in the wings of the lines; hence the use of a static approach seems justified within the scope of the simple treatment here presented.

Acknowledgement—The authors are indebted to Mr. R. S. HARNER of the General Electric Company for his assistance with the experimental work.

REFERENCES

1. J. S. FOSTER, *Proc. Roy. Soc., Lond.* A.**117**, 137 (1927). J. S. FOSTER and A. DOUGLAS, Monthly Notices **99**, 150 (1939). A. UNSÖLD, *Physik der Sternatosphären*. Springer-Verlag, Berlin (1955).
2. H. GERDIEN and A. LOTZ, *Wiss. Veröff. Siemens*, **2**, 489 (1922).
3. H. C. WOLFE, *Temperature—Its Measurement and Control in Science and Industry*, Vol. II. Reinhold Publishing Corporation, New York (1955), pp. 418–419.
4. D. R. INGLIS and E. TELLER, *Astrophys. J.* **90**, 439 (1939).
5. H. MARGENAU and M. LEWIS, *Revs. Mod. Phys.* **31**, 594 (1959).
6. M. BARANGER and B. MOZER, *Electric Field Distributions in an Ionized Gas*, II. Carnegie Institute of Technology, Dept. of Physics, Pittsburgh 13a, Pennsylvania.
7. H. K. WIMMEL, to be published.
8. S. CHANDRASEKKAR and J. VON NEUMANN, *Astrophys. J.* **95**, 489 (1942).

VOL.
1
1961

J. Quant. Spectrosc. Radiat. Transfer. Vol. 1, pp. 53–75. Pergamon Press Ltd. Printed in Great Britain

ABSOLUTE INTENSITY OF NON-EQUILIBRIUM RADIATION IN AIR AND STAGNATION HEATING AT HIGH ALTITUDES*

J. C. CAMM, B. KIVEL, R. L. TAYLOR and J. D. TEARE
Avco–Everett Research Laboratory, Everett, Massachusetts

(*Received* 4 *November* 1961)

Abstract—The paper presents some attempts to obtain the magnitude of the non-equilibrium radiation behind a normal shock for velocities up to 25,000 ft/sec in air. It is noted that the high non-equilibrium temperatures force one to extend studies further into the u.v. and i.r. than required for equilibrium predictions of significant sources of radiation. For example, to ascertain that the total non-equilibrium radiation is less than 1 W/cm² requires measurements from several hundred angstroms to more than 10 μ. Measurements covering much of this region using (1) monochromator and photocells, (2) bolometers, (3) photoelectric detectors, (4) spectrographs and (5) i.r. photocells are reported. At 23,000 ft/sec the radiation integral normal to the shock is about 0.4 W/cm²-steradian; in air initially at a pressure of 20μ of Hg most of the radiation originates within 5 cm of the shock front. We also report on calculations which show that the effect of ambient atomic oxygen at high altitudes does not introduce any pronounced changes. Application of the results to the problems of satellite heating is made.

OL.
1
961

1. INTRODUCTION

IT is the purpose of this paper to consider the intensity of radiation from the non-equilibrium region at the front of normal shocks in air, and to estimate the importance of this radiation on the calculation of re-entry heating.

A luminous front has been observed at the front of normal shocks in noble gases by KANTROWITZ and co-workers at Cornell University and LAPORTE and co-workers at the University of Michigan.[1] Spectroscopic examination showed that this radiation spike consisted of molecular bands from impurities such as CN and C_2. This radiation disappears as soon as the impurity molecules are dissociated in the high temperature shock. In air, molecules also give rise to the radiation front, but here the non-equilibrium overshoot of temperature plays a major role.

The overshoot of non-equilibrium radiation at the front of strong shock waves in air has been known for some time.[2–7] Our early experiments showed that the intensity overshoot increased rapidly with shock speed; however, because of poor experimental resolution, the magnitude of the radiation was poorly defined. Recently, we have used the 24-inch low density shock tube designed by S. C. Lin, which provides a sufficiently thick shock so that the radiation profile can be resolved. The results reported here, which give a quantitative estimate of the intensity of this radiation at velocities up to 25,000 ft/sec, should be considered preliminary.

One of the important features of the non-equilibrium radiation is that the integrated

* This work was supported jointly by Air Force Ballistic Missile Division, Air Research and Development Command, United States Air Force, Air Force Unit Post Office, Los Angeles 45, California, under Contract No. AF 04(647)-278; Advanced Research Projects Agency, monitored by the Army Rocket and Guided Missile Agency, Army Ordnance Missile Command, United States Army, Huntsville, Alabama, under Contract No. DA-19-020-ORD-4862.

non-equilibrium radiation is independent of density and, consequently, altitude. Since the chemistry and radiation near the shock front are determined by binary collisions (collisions between only two atoms or molecules), the non-equilibrium intensity is proportional to the density while its spatial extent is inversely proportional to density. This leads to a stagnation gas radiation independent of altitude—an effect we will call the "luminous front plateau". The plateau is bounded at low altitudes by the more intense equilibrium radiation and at high altitudes by collision limiting and the truncation of the radiation profile because of the finite shock detachment distance. These altitudes depend on the size of the re-entry body.

Radiation heating of re-entering satellites of low performance may exceed the aerodynamic heating. In a recent report[5] we have discussed the equilibrium radiation heat transfer to the stagnation point and noted the altitudes at which non-equilibrium effects become important. For satellite re-entry there are two reasons for the importance of radiation. First, a large nose radius enhances the radiation while decreasing the aerodynamic heating. Second, at high altitudes, non-equilibrium effects increase the radiation. According to Rose,[8] a radiation heat transfer level as low as 1 W/cm^2 is significant. This is 10% of the aerodynamic heating of a 1 ft radius sphere with 20,000 ft/sec speed at about 60 miles altitude.

In section II we present recent experimental data by Camm which covers the spectral range from the far ultraviolet to the infrared ~ at 8000 Å. Work by Taylor which extends these measurements into the far infrared will be described in section III. Section IV is a discussion of calculations by Teare of the effect of ambient atomic oxygen. Finally, in section V we give a cursory application of the results to the heat transfer problem.

In the remainder of this section, we present some preliminary theoretical considerations which describe the radiation from the non-equilibrium region behind a normal shock and the extent of the wavelength region which must be studied.

We first note that a radiation level of 1 W/cm^2 is possible. Fig. 1 shows results of a typical calculation for properties behind a normal shock having a velocity of 0·716 cm/μsec in air with initial pressure of 0·020 mm Hg. In the figure we plot the concentrations of atomic nitrogen and oxygen. These are seen to start at zero and increase rapidly in a few cm to values approaching their final equilibrium. Also shown is the concentration of nitric oxide which overshoots its final equilibrium value. While the atoms are being dissociated, the temperature drops rapidly from 25,000°K, reaching 15,000°K at ~ 1·5 cm and 10,000°K at ~ 4·5 cm. We also indicate the radiation intensity from the first negative band system of the ionized nitrogen molecule assuming the ions are produced by recombination of ground state atoms and that they radiate in local equilibrium at the translational temperature. This is known from past experience in pure nitrogen to predict too much radiation near the front of the shock but is used as a conservative upper limit in the absence of a reliable theory.[4] The peak intensity is about 2 W/cm^3 and the integrated intensity is about 5 W/cm^2. This result is probably reduced by collision limiting.* To make this correction, we use the experimental[9] de-excitation cross section, $\geqslant 10^{-15}$cm^2, and the radiation lifetime, $\sim 2 \times 10^{-7}$ sec. With these values we estimate that collision limiting reduces the intensity of $N_2^+(1-)$ shown in Fig. 1 by about a factor 6. Consequently, we have a preliminary prediction of ~ 1W/cm^2 from this band system alone. Since there

* Collision limiting[9] occurs when the particle density is so low that there are insufficient collisions to maintain the population of excited states against the drainage by radiation.

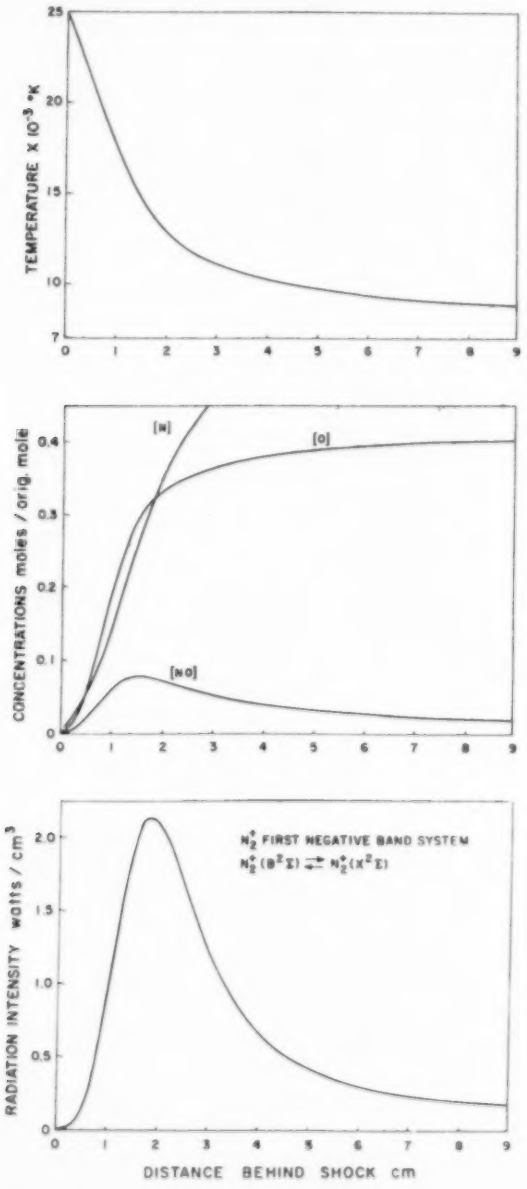

FIG. 1. Properties behind a normal shock in air; (top) translational temperature, (middle) moles per original mole of N, O and NO, (bottom) intensity of N_2^+ first negative assuming equilibrium between radiating and ground state.

are several other possible strong band systems and many lesser ones, we conclude that a radiation level of at least 1 W/cm² is to be expected.

We next consider the wavelength region that must be surveyed. Because of the low power level and high non-equilibrium temperature, we find that the region from several hundred angstroms to $\sim 10\mu$ must be studied.

In Fig. 2 we have drawn the integrated black body radiation for 10,000°K, 15,000°K and 20,000°K. This gives us a conservative but unequivocal limit. On the left we have integrals from the far u.v. as a function of wavelength, and on the right, from the far i.r. It is seen that the integrated radiation from 20,000° black body can exceed 1 W/cm² in the

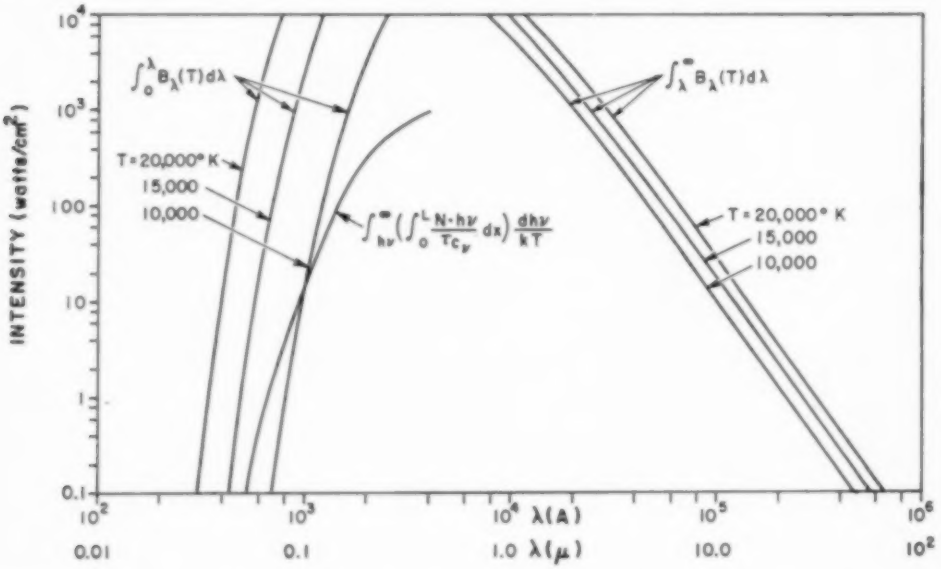

Fig. 2. Integrated Planck intensities from i.r. and u.v. for several temperatures. Also shown is an estimate of the maximum radiation based on an excitation cross-section of 10^{-15} cm² according to equation 1 in text.

region extending from 350 Å in the u.v. to 30μ in the i.r. Other values can be read from the graph but the conclusion is essentially unchanged—one must push his knowledge into both the far u.v. and the far i.r.

We now consider two limitations which somewhat circumscribe the spectral region that must be studied. In the u.v. we consider the finite number of collisions with sufficient energy to produce this radiation. This only increases the cut-off wavelength to about 700 Å. In the i.r. we find an upper limit to the radiation assuming local equilibrium. The many unknowns of the molecular potential wells make our conclusions uncertain, but we conclude that the 9μ limit of our current experiments is reasonable.

At the suggestion of S. C. Lin, we have considered the number of collisions which are sufficiently energetic to produce u.v. radiation. It turns out that we can cover the far u.v. region experimentally (section II) so that this limit is not vital. The main unknown in the estimate is the cross section. We take $Q = 10^{-15}$ cm² which may be considered conservative,

although there is experimental indication that this is not too large.[9] Using the temperature–distance data in Fig. 1, we have evaluated the following integral

$$I \doteq \int_0^L \int_{E_\nu}^{\infty} [N]^2 \bar{v}\, Q\, [e^{-E_\nu/kT}] \frac{E_\nu}{kT}\, dE_\nu\, dx \qquad (1)$$

where $[N] \approx 7 \times 10^{-15}$ cm^{-3} is the particle density behind the shock

$\bar{v} = 3 \times 10^5$ cm/sec is the mean particle speed

$Q = 10^{-15}$ cm^2 is the excitation cross section

kT is the temperature in eV

$E_\nu = h\nu = hc/\lambda$ is the radiation energy

$x =$ is the distance from the shock front in cm

Significant radiation for such high excitation energies can come only from the high temperature region near the shock front. We have chosen the upper limit L to be 2 cm, since the contribution to the integral for $x > 2$ cm can be neglected. Values for I as a function of λ are plotted in Fig. 2. I reaches the value of 1 W/cm^2 at $\lambda \approx 670$ Å, 10 at 860 Å and 100 at 1400 Å. Thus, even the smaller cross sections of 10^{-16} cm^2 and 10^{-17} cm^2 only bring the limit for 1 W/cm^2 to 860 Å and 1400 Å, respectively.

The i.r. limit is more important because our current measurements do not go beyond $\sim 9\mu$ (section III). The upper limit in this case is obtained by assuming local thermodynamic equilibrium. The uncertainty in our calculation is a result of the unknown molecular states which give rise to infrared radiation and the corresponding transition strength. We must estimate the number of infrared molecular bands as well as their emission intensities.

We first determine the emissivity or fraction of black body radiation and then compare this with the black body limits shown in Fig. 2. In order to assure that there is less than 1 W/cm^2 being contributed from the i.r. region beyond 9μ, it is necessary that the emissivity in this region be less than $\sim 0{\cdot}03$.

The emissivity from the front of the shock to thickness x is

$$\varepsilon = 2 \int_0^x \mu\, dx$$

where μ is the gas absorption coefficient composed of contributions from many band systems. Thus

$$\mu = \Sigma_i\, \mu_i = \Sigma_i\, N_i\, Q_i$$

with the density of absorbing molecules given by

$$N_i = \Psi_i\, [N]\, e^{-E_i/kT}$$

where Ψ_i is the fraction of the molecules which can radiate the i^{th} band system and E_i is the energy of the absorbing state. The absorption cross section is given by

$$Q_i = \pi r_0 f_i / \Delta\tilde{\nu} \doteq 10^{-15} f_i\ \text{cm}^2$$

where f_i is the f-number for the i^{th} band system, $r_0 = 2{\cdot}82 \times 10^{-13}$ cm is the classical electron radius, and we have taken $\Delta\tilde{\nu} = 10^3$ cm^{-1} assuming uniform coverage from $\lambda = 10\mu$ to ∞. This value $\Delta\tilde{\nu} = 10^3$ cm^{-1} is not a conservative assumption since the intensity will be slightly higher if the emission strength is concentrated at the shortest wavelength of interest. However, the distribution of molecular rotation will probably

smear a given band preventing such concentration. The amount of this smearing depends on the change of the rotation constant B which is inversely proportional to the moment of inertia. The energy spread

$$\Delta E \approx J^2 hc \Delta B \approx \frac{\Delta B}{B} kT$$

where J is the angular momentum quantum number. For a sharp band system $\Delta B/B$ may be as small as 1/20 (which occurs for the CN violet system) which makes $\Delta E \approx 0{\cdot}1$ eV which corresponds to the width we have taken ($\Delta\tilde{\nu} = 10^3$ cm^{-1}). It is possible that there may be an unusually sharp band near 10μ. In this case the radiation may be increased a factor $\gtrsim 4$.

We have now to enumerate the band systems. Band systems with strong radiation may have f-numbers as high as 0·3 at 1 eV. On the other hand, since $f \propto h\nu$ and we are interested in energies like 0·1 eV and less, we take as a guess $f = 0{\cdot}03$ for strong bands in the far i.r. We postulate that these may occur in N_2 and O_2 at energies $E_i \sim 8$ eV and in NO at $E_i \sim 5$ eV. These will be weak because of the high excitation energy. O_2 may have a weak system at $E_i \sim 1$ eV but this should be strongly forbidden and have an f-value smaller by at least 10^{-2}, because the electronic states are formed from ground state atoms.

Each molecule may have more than one band which radiates in the i.r. We estimate this number to be <10. A canceling effect is that not all of the vibration states of each potential take part. This introduces a factor ($\sim hc\omega_e/kT$) $\sim 1/10$.

In the table we summarize the extreme contributions possible from each molecule.

Table 1

Molecule	Ψ_i	E_i	f_i	ε_i
N_2	·8	8	0·03	0·0024
O_2	·2	8	0·03	0·0006
NO	·1	5	0·03	0·0018
O_2	·2	1	3×10^{-4}	0·0004

$\varepsilon_{total} = \Sigma_i \varepsilon_i = 0{\cdot}005$

The total value of the emissivity indicated above is below the limit 0·03 which will bring the intensity to 1 W/cm^2. The safety factor of 6 is marginal in view of our many assumptions and an exceptionally strong and narrow band system near 10μ might upset the conclusion that radiation beyond 9μ can be neglected.

II. MEASUREMENTS OF NON-EQUILIBRIUM RADIATION FROM 300 to 8000 ANGSTROMS

Spectral intensity measurements were made on air shocks produced in a 24-inch shock tube. Unless stated otherwise, the initial gas pressure was 20μ of Hg and the shock speed 6·8 mm/μsec. Since the maximum gas temperature produced is about 23,000°K, significant amounts of radiant energy might possibly be found at wavelengths as far as 300 Å in the ultraviolet and as far as 25μ in the infrared. This section describes the measurements made in the spectral region of from 300 to 8000 Å. The measurements beyond 8000 Å are described in section III of this report.

The 24-inch shock tube is described by Lin.[10] Untreated room air was used for all tests. The output signals of the radiation detectors were displayed on Tektronix oscilloscopes and the traces photographed using Polaroid cameras. Care was taken that the

electronic rise times were always less than the rise times determined by the system optics.

The detectors used in making these measurements are described below under headings which indicate the wavelength regions in which they produced useful results.

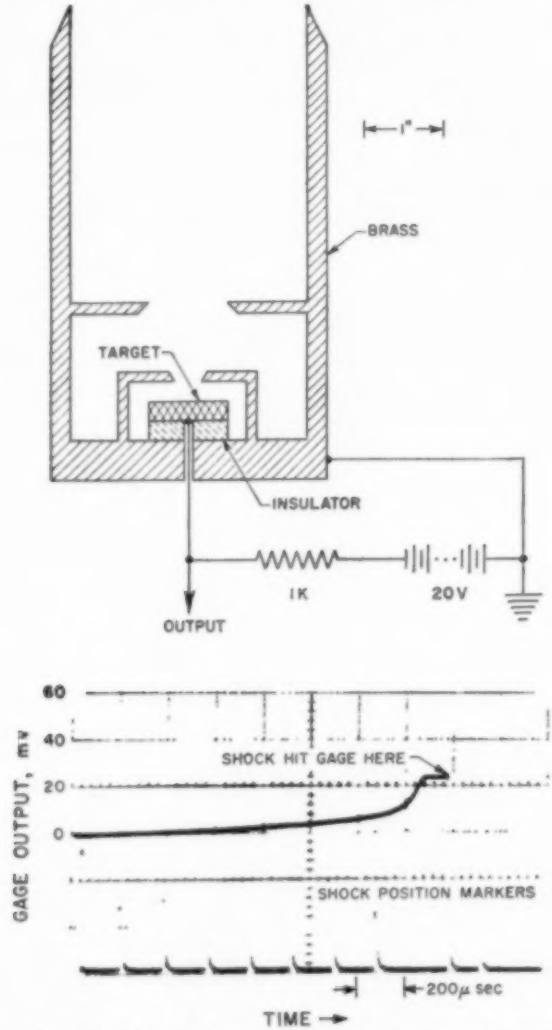

FIG. 3. Upper, schematic diagram of photoelectric gage and associated electrical circuit. Lower, typical oscilloscope trace of the output signal from the photoelectric gage.

300–1500 Å-*Photoelectric gage*

Tungsten and molybdenum were used as the active elements in photoelectric gages to measure the radiation intensity below 1500 Å. A schematic diagram of the gage and the associated electrical circuit is presented in the upper portion of Fig. 3. The tungsten target

was cut from a tungsten electrode. The molybdenum target was cut from a boat used in vacuum evaporation. The gage is supported coaxially inside the shock tube and pointed toward the shock tube diaphragm. When the tube is fired the shock moves toward the gage. The brass case restricts the field of view of the gage so that the radiation input will be constant for a short time. This arrangement also eliminates radiation from the boundary layer at the wall of the tube when the shock nears the gage. When energetic photons from the shock strike the tungsten target, electrons are ejected from the surface and collected by the brass gage body, which has a 20-volt positive potential relative to the target. The

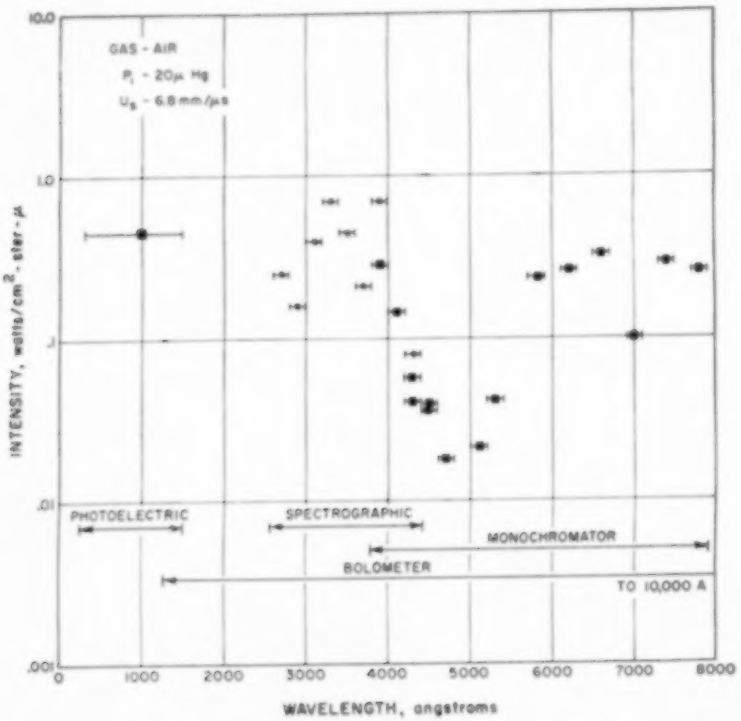

Fig. 4. Measured spectral intensity of a 6.8 mm/μsec shock in air at a pressure of 20 μ of mercury.

resulting current produces a voltage change across the 1000 Ω load resistor. This voltage change is displayed on an oscilloscope and photographed. A typical trace obtained during a run is presented in the lower half of Fig. 3. The plateau is caused when the field of view of the gage is entirely filled by the shock. The maximum photoelectric current is found to be 20 μamp. Using the spectral photoelectric yield curves of tungsten[11] and assuming 1000 Å photons in this region, the measured radiation intensity is 0·45 W/cm²-sr-μ at a shock speed of 6·8 mm/μsec. This result is plotted in Fig. 4. Identical results were obtained using a molybdenum target. If most of the radiation in the 300 to 1500 Å region fell near the 1500 Å limit, the intensity would be many times the given figure.

Since the gage was used in air at a pressure of 20μ of Hg, where the gas mean-free-path

is about 2·5 mm, the electron flow from the target to the brass case was not impeded by the air molecules. Absence of space charge limitation was checked by increasing the bias voltage to 30 V and observing that identical results were obtained.

The observed u.v. radiation is within the upper limit estimates of section I. We have tentatively attributed the radiation to the $b'\,{}^1\Sigma_u^+ \rightarrow X^1\Sigma_g^+$ transition of nitrogen. This will be discussed in greater detail in a future publication by Hammerling.

2300–3500 Å-*Spectrograph*

A Hilger *f*/4 quartz spectrograph was used to measure the radiation from 2300 to 3500 Å. Kodak type 103–0 spectrographic plates were used with an entrance slit of 40 μ. The spectrograph was aligned with its optic axis perpendicular to the axis of the shock tube and the radiation was observed through a fused quartz window which was 0·5 in. thick. The window was mounted flush with the inside wall of the shock tube. The shutter was left open from before the firing of the shock tube until several seconds afterwards. This procedure appears justified due to the fact that monochromator measurements discussed below indicate that all of the detectable radiation is confined to the first few centimeters of the shock in this wavelength region. The resulting spectrum is presented in Fig. 5. A densitometer trace of the spectrogram is also presented in Fig. 5. Using the manufacturer's film specification the densitometer trace was transformed into a relative spectral intensity curve, which is also given in Fig. 5. This curve was normalized to the intensity data at 3500 Å obtained with a monochromator. The resulting spectral intensity curve is plotted in Fig. 4.

Examination of the shock spectrum shown in Fig. 5 shows that much of the observed radiation is due to impurities either in the test gas or at the wall of the shock tube. Previous experience with smaller shock tubes suggests that the wall source is more important, but no definitive tests have been made. In any case, the measurements provide upper bounds of the spectral radiation intensity of air under the test conditions.

3500–8000 Å-*Monochromator*

A Bausch and Lomb monochromator was used to measure the spectral intensity in the spectral region from 3500 to 8000 Å. A schematic diagram of the monochromator and optical system is shown in Fig. 6. The entrance aperture of the monochromator consisted of a hole 1 mm in diameter. This was imaged on the axis of the shock tube with a magnification of 3. The aperture stop of the system was a one-half inch diameter quartz window mounted flush with the inside shock tube wall. The field optic axis was perpendicular to the shock tube axis. The electrical signals from the photomultiplier detectors at the exit slit were displayed on oscilloscopes and the traces photographed. The sweep of the oscilloscope was started just before the arrival of the shock. Typical traces are presented in Fig. 7. The test time was estimated by Lin[12] to be about 40 μsec. It is apparent that most of the radiation comes from the front of the shock. The monochromator was calibrated using a tungsten ribbon filament lamp calibrated at 0·653 μ by the National Bureau of Standards. The spectral intensity of the lamp was determined using the De Vos[13] values for the emissivity of tungsten, the black body radiation intensity equation, and the spectral transmission of the quartz window of the lamp. The measured spectral intensity of the shock from 3500 to 8000 Å is presented in Fig. 4.

We have made some measurements at other pressures and Mach numbers. In Fig. 7,

we compare traces at $p_1 = 20\,\mu$ Hg and $100\,\mu$ Hg in which the sensitivity and sweep speed have been adjusted according to the binary scaling rule. The correctness of the binary scaling is substantiated by the similarity in the two traces. The dependence on shock speed is summarized in section V.

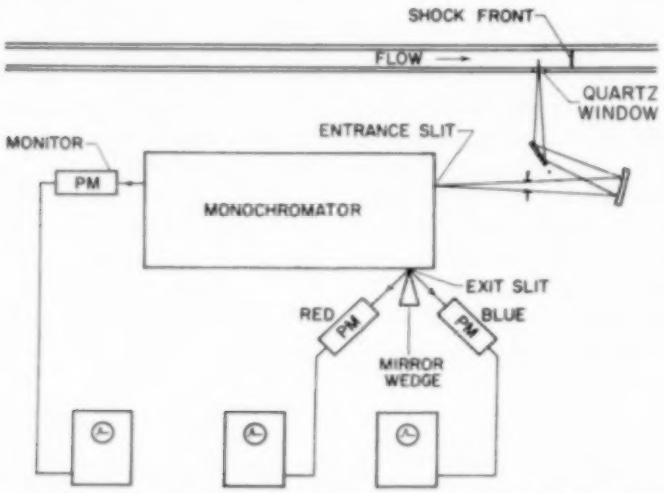

Fig. 6. Schematic diagram of monochromator in position at the shock tube.

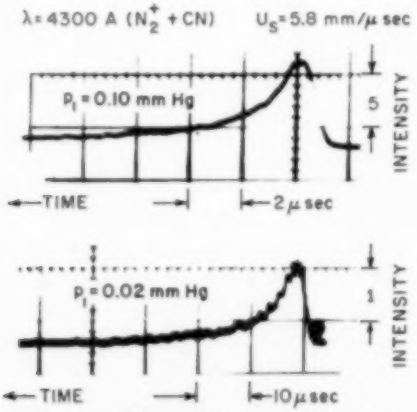

Fig. 7. Typical oscilloscope traces of the output signal from the monochromator, illustrating binary scaling.

1500–10,000 Å-*Bolometer*

A bolometer was used to measure the radiation from 1500 to 10,000 Å. A schematic diagram of the bolometer is presented in Fig. 8. The active element is a vacuum-evaporated aluminum grid about $0{\cdot}2\,\mu$ thick. The resistance of the grid was about 200 Ω. To eliminate photoelectric effects, a $1\,\mu$ dielectric layer of SiO was evaporated over the grid and a $0{\cdot}2\,\mu$ shield layer of aluminum over that. The resistance across the shield

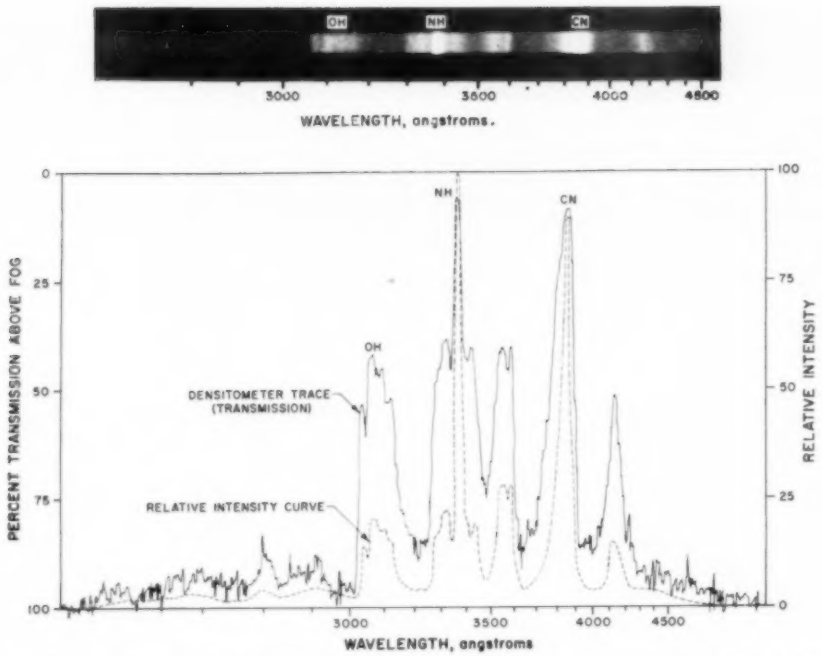

FIG. 5. Spectrum and densitometer trace of spectrogram of a 6·8 mm/μsec shock in air at a pressure of 20μ of mercury. (6 exposures; $f/4$ quartz Hilger spectrograph; 100μ slit; Kodak 103–0 plate; line of sight perpendicular to axis of 24-in diam. shock tube; quartz window).

(facing p. 62)

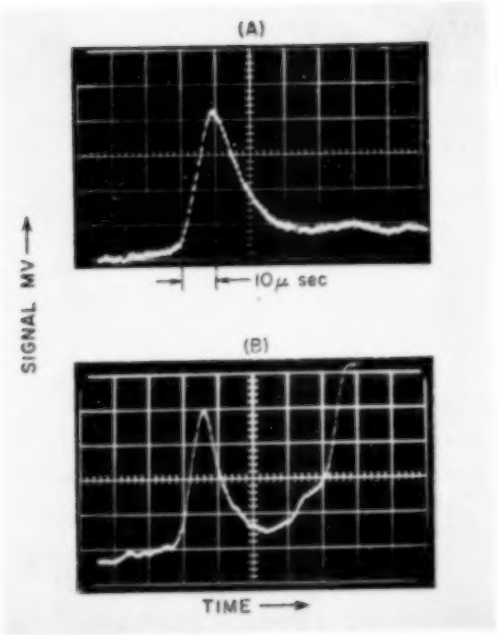

FIG. 11-A. Shock front seen by a PbSe detector (1–2·8 μ). Time increases to the right. Sweep speed — 10 μsec/cm. Shock condition: $P_1 = 20\,\mu$, $M_s = 19{\cdot}9$.

FIG. 11-B. Shock front seen with a Ge detector (2–9 μ). Sweep speed — 10 μsec/cm. $P_1 = 20\,\mu$, $M_s = 20{\cdot}1$.

(facing p. 63)

VOL.
1
1961

was less than an ohm, which was low enough to prevent significant voltage changes on the grid (through capacitance) during the flow of photoelectric current across the shield. Since aluminum is highly reflecting a 0·4 μ layer of carbon was evaporated onto the aluminum shield. The reflectance of the gage was measured to be about 10% at wavelengths below 1 μ and about 60% above. The bolometer was assembled inside a brass case which

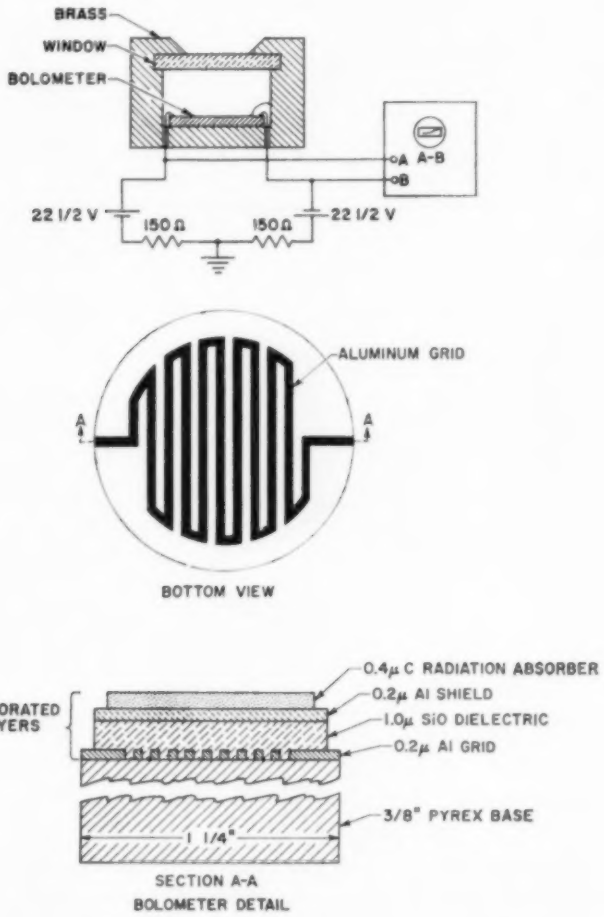

FIG. 8. Schematic diagram of bolometer and associated electrical circuit.

was equipped to take a quartz or calcium fluoride window. The calcium fluoride window was used for these measurements. The thermal delay due to the protective evaporated layers was computed to be less than 15 μ sec.[14] The shield was grounded to the brass case, and the electrical circuit balanced so as to suppress any residual photoelectric effect. The bolometer was mounted coaxially inside the shock tube and facing the diaphragm. The electrical output was displayed on an oscilloscope and photographed. The sweep was triggered prior to the firing of the shock tube. A typical trace is presented in Fig. 9. The

geometry of the gage is such that the shock radiation falling on the gage was constant for about 30 μ sec prior to the time the shock hit the gage. Details of the gage output during this period were obtained by means of an oscilloscope trace with faster sweep than that shown in Fig. 9.

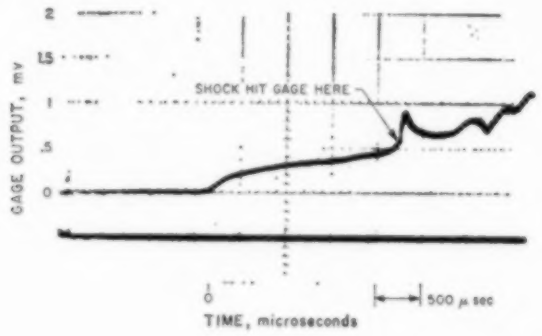

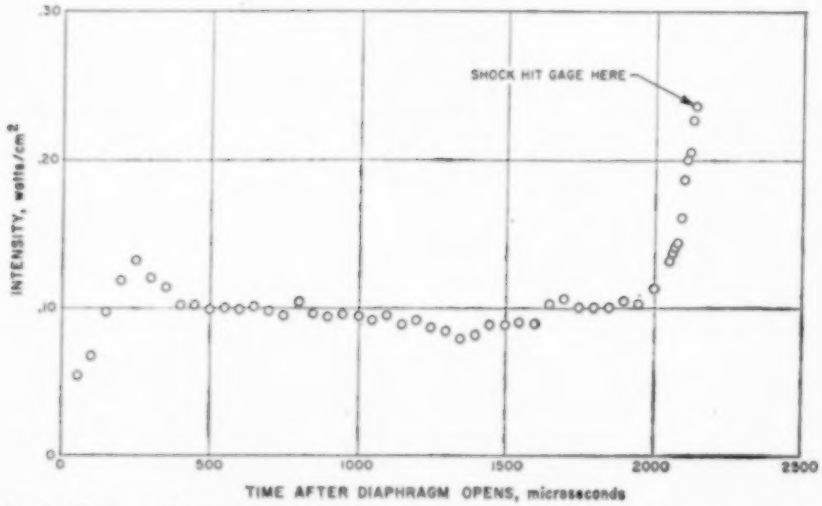

Fig. 9. Upper, typical oscilloscope trace of the output signal from the bolometer. Lower, intensity of the radiation absorbed by the bolometer, computed using the output signal in the upper part of the figure.

The relationship between the heat input q and the electrical output E of the bolometer is given by the equation[15]

$$q(t) = \frac{1}{k''(IR)\pi}\left\{\frac{2E(t)}{\sqrt{t}} + \int_0^t \frac{E(t) - E(\tau)}{(t-\tau)^{3/2}}\,d\tau\right\}$$

where k'' (IR) is a constant depending on the gage and electrical circuit. Inserting the measurement E (t) we obtain the input radiation history, which is presented in Fig. 9. The initial rise in radiation is due to the driver gas. Reflections by the walls of the shock

tube account for some of the observed radiation, and some is due to impurities in the boundary layer of the shock and driver gas. Just before the shock strikes the gage the reflections from the shock are sharply reduced and the shock boundary layer radiation is outside the field of the gage; however, significant amounts of radiation from the driver gas and driver gas boundary layer may still be present. The final value for the heat input just before the shock hits the gage provides an upper bound measurement, which is found to be 0·45 W/cm²-sr. It should be noted that the bolometer has a finite absorptance in the infrared and, consequently, detects some of the radiation outside of the 1300 to 10,000 Å region of highest absorptance. Infrared sources are discussed in section III.

Discussion

We have surveyed the measurements of non-equilibrium radiation between 300 and 8000 Å. Integration of this intensity distribution yields a value of 0·2 W/cm²-sr. This is consistent with the bolometer measurement of 0·45 W/cm²-sr if about one-half of the bolometer measurement is a result of impurity radiation from the boundary layer and the driver gas. Fig. 4 illustrates the spectral distribution at $P_1 = 0{\cdot}020$ mm Hg and shock speed 6·8 mm/μsec.

III. PHOTOMETRIC STUDIES OF INFRARED RADIATION

The availability of sensitive photoconductive detectors with fast response times now makes it possible to measure infrared radiation behind shock waves. Previous measurements in this laboratory have yielded information about the intensity of the continuum infrared radiation from equilibrium shock-heated air under conditions simulating the stagnation point in missile re-entry.[16, 17] The present work describes some preliminary intensity measurements of infrared radiation behind shock fronts in air under non-equilibrium conditions.

Measurements of the radiation history behind the shock front were made over the wavelength range of 1–9 μ. Because of the availability of certain detectors in the laboratory this interval was divided into two regions: (a) 1–2·8 μ and (b) 2–9 μ. Shock waves were generated in the 24-in. diam. low density shock tube. Measurements were made at a nominal Mach number of 20 corresponding to a shock velocity of 6·87 mm/μsec. P_1 was chosen to be 0·020 mm of air. Room air was used without drying or purification.

1–2·8 μ

A schematic of the experimental arrangement is shown in Fig. 10. For this wavelength range an Eastman Kodak PbSe detector was employed. This detector has a useful sensitivity out to 4·5 μ. However, glass filters were used to isolate the 1–2·8 μ region over which the response of the detector is fairly uniform. The shock tube window was made of quartz.

A typical oscilloscope record of a PbSe run is shown in Fig. 11 A. The optical resolution was calculated to be less than 2–3 μsec. However, the PbSe detector has a time constant of about 6–7 μsec and is the limiting factor in resolving the shock front. The rise time of the electronics following the detector (preamplifier and scope) was less than 1 μsec.

In order to calculate the absolute intensity of the radiation the PbSe detector was calibrated against a tungsten strip-filament lamp. An optical pyrometer was used to measure the temperature of the lamp. The emissivity values of DeVos[13] were employed

over the wavelength range of 1–2·8 μ to calculate the intensity of the lamp radiation. An optical system identical to that employed on the shock tube was used for the calibration. Therefore, no corrections for the transmission characteristics of the shock tube window and filters were necessary.

The average of five selected runs over the Mach number range of 19·8–20·2 yields a peak intensity of $1{\cdot}5 \times 10^{-2}$ W/cm³-sr and an integrated intensity through the shock front of 0·15 W/cm²-sr. Because of the preliminary nature of these results no estimate of the uncertainty of this number can be made, but the experimental data have a scatter of ±15%.

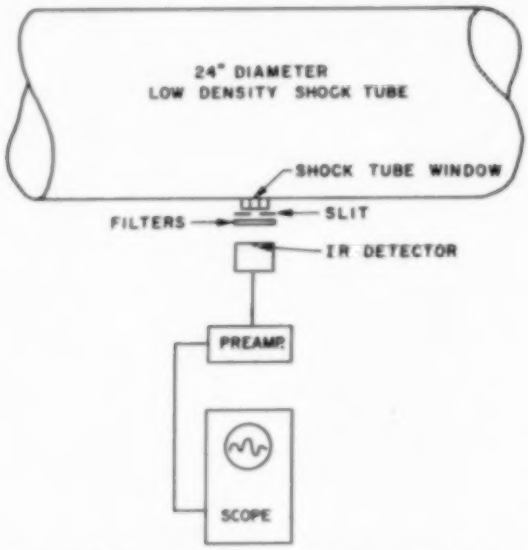

Fig. 10. Diagram of equipment for obtaining i.r. data.

2–9 μ

The experimental arrangement was the same as used in the previous spectral region except that a Westinghouse type 812 gold-doped germanium photoconductive detector was employed. This detector has useful sensitivity out to 9 μ. For this wavelength region a Ge filter blocked radiation at wavelengths shorter than 2 μ. A CaF_2 window was used in the shock tube, and the upper wavelength cut-off was determined by a combination of the transmission of this window and the fall off in sensitivity of the detector.

A sample oscilloscope record of the signal from the detector is shown in Fig. 11 B. In several respects the signal observed in this wavelength region differs from that of the 1–2·8 μ region. First, the rise time of the signal is noticeably shorter which is to be expected in view of the shorter response time of the gold-doped Ge detector.* Secondly, in this wavelength region a spurious signal was observed before the shock arrived at the slit. This signal is believed to be due to radiation scattered off the metal walls of the tube. The effect was reduced by blackening the wall of the shock tube opposite the detector. Finally, a large signal is noticeable about 30 μsec after the shock front passes. 30 μsec

* This detector has a measured response time of less than 0·2 μsec.

is roughly equal to the test time available under these shock conditions, and this signal is believed due to the passage of the contact surface and driver gas by the slit. There is just a hint of this signal in the oscilloscope trace from the PbSe detector (Fig. 11 A) indicating that the driver gas radiates predominantly beyond 3 μ in the infrared.

The absolute intensity of the radiation in the wavelength range of 2–9 μ was calculated by employing the manufacturer's (Westinghouse) calibration of the detector. An average of eight experimental runs over the Mach number range of 19·4–20·4 yields a peak intensity of $1{\cdot}2 \times 10^{-2}$ W/cm³-sr and an intensity integrated through the shock of $8{\cdot}4 \times 10^{-2}$ W/cm²-sr. The experimental data show a scatter of about $\pm 25\%$.

A few runs were made replacing the Ge filter with various narrow band interference filters. These results are shown in Table 2.

TABLE 2. WAVELENGTH DEPENDENCE OF RADIATION

Mach No.	λ (μ)	$\Delta\lambda$ (μ)	Peak Intensity W/cm³-sr $\times 10^3$
19·77	2·53	0·23	0·81
19·40	2·53	0·23	0·68
20·06	3·75	0·14	2·0
20·56	3·75	0·14	2·9
20·17	4·82	0·17	0·64

$\Delta\lambda$ is the band pass of the filter, measured when the transmission has reached 50 per cent of its peak value.

Although these results are sketchy they indicate that at around 3·75 μ there is about three times the radiation intensity per μ as in the other two wavelength regions. It is of interest that 3·75 μ is the same wavelength at which an anomolous band was observed in the study of the radiation intensity from equilibrium air.[17]

Based on the studies of the infrared radiation from equilibrium air, the bulk of the radiation in this wavelength region is expected to be due to free-free scattering of electrons (Bremsstrahlung). Since the Bremsstrahlung is relatively insensitive to temperature and since there is no large overshoot of electron density in the shock front, we can estimate the intensity by comparison with the equilibrium measurements.[16, 17] These experimental observations indicate that the radiation from the i.r. beyond 1 μ is about 3 W/cm³-sr at 8000°K and atmospheric density. The correction for the different particle and electron densities in the present experiment reduces this value by a factor $\sim 3 \times 10^{-7}$, indicating a Bremsstrahlung intensity of $\sim 10^{-6}$ W/cm³-sr. The reason for the difference between this estimate and the present experiment is not understood. Because of the overshoot of NO concentration in the shock front a contribution from the vibration-rotation bands of NO might also be expected, but the estimated intensity indicates a level many orders of magnitude lower than the present measurements.

The intensity observed at 3·75 μ may be attributable to a molecular band. Assuming a radiating temperature of 15,000°K, the observed peak radiation of 3×10^{-3} W/cm³-sr can be explained by 1% of the molecules being capable of a radiative transition to the

ground electronic state with an *f*-number of 0·01. Alternatively, a transition to an excited molecular state would require a higher *f*-number or, because of the Boltzmann factor, a higher percentage of ground state molecules. If a related molecular band occurred beyond 10μ, it is reasonable to expect that its intensity would be appreciably less, corresponding to the lower rate of radiation at lower energies. Thus, the measurements at 3·75μ do not invalidate the arguments made in section I to rule out important radiations beyond 10μ.

It is to be emphasized that further work is necessary to explain the rather large discrepancy between the measurements and current theory. Specific areas that need investigation are the effect of boundary layer radiation, the elimination of spurious scattered radiation, and the magnitude of radiation from impurities and minor constituents of air.

IV. ON THE EFFECT OF ATOMIC OXYGEN AHEAD OF THE BOW SHOCK WAVE

Although the ambient concentration of atomic oxygen is not significant at altitudes below 300,000 ft, it is interesting to determine whether its presence could have any major effect on the non-equilibrium radiation or ionization at higher altitudes. It is clear that the presence of atomic oxygen ahead of the bow shock wave will lead to a higher equilibrium temperature behind the shock, for any given value of shock speed and ambient density. On the other hand, the temperature immediately behind the shock (after translational and rotational equilibrium) will be lower since the partially dissociated gas has a higher specific heat ratio than a diatomic gas.

We have made a numerical investigation of these competing effects, using the various Avco-Everett computational programs which have been devised to aid in the study of relaxation phenomena. The objective has been to determine the physical quantities in the non-equilibrium regions behind strong normal shock waves, by integration of rate equations which describe the various chemical reactions and excitation processes occurring subject to constraints imposed by the conservation relationships. A survey of the work done in this field at Avco-Everett, together with a discussion of the choice of rate constants for the various reactions involved has been published elsewhere.[7] The same choice of rate constants is used in the present comparison.

A phenomenon predicted by our early calculations, and subsequently observed experimentally, was the overshoot of NO concentration above its equilibrium value. This overshoot is produced by the fast atom–molecule interchange reactions which drive the NO population towards a local equilibrium with the oxygen and nitrogen molecules when the molecular concentrations are still in excess of equilibrium. These exchange reactions cannot start producing NO until some oxygen or nitrogen molecules have been dissociated. It is obvious that the presence of ambient atomic oxygen would enhance the initial rate of production of NO behind the shock. This could increase the radiation from the NO β and γ bands. Furthermore, the increased NO production could lead to faster N production, and thus to a higher concentration of N_2^+, and to higher radiation from the first negative band system.

For the present investigation, the conditions chosen are appropriate to an altitude of 100 km, where the density is 10^{-9} g/cm^3, and where approximately one-half of the oxygen is dissociated. However, for convenience in comparison with calculations already made for

VOL.
1
1961

undissociated air, we have specified a density level of $3{\cdot}15 \times 10^{-8}$ g/cm^3, which is appropriate to an initial pressure $P_1 = 0{\cdot}02$ mm Hg in undissociated air. Since all mechanisms are binary within the scale of the figures of this section, and since the concentrations plotted are non-dimensional, it is permissible to scale the results shown in these figures to any

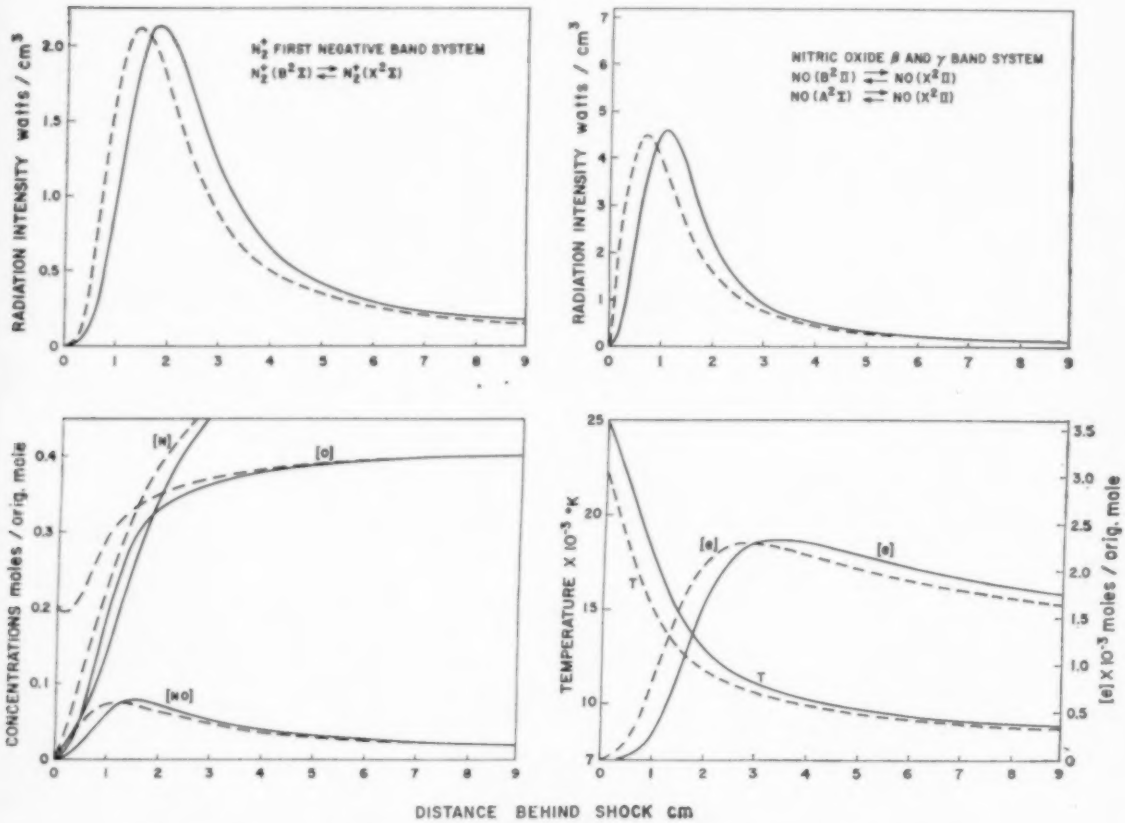

FIG. 12. Relaxation behind shock wave at Mach number $M_s = 20{\cdot}8$ ($U_s = 7{\cdot}16$ mm/μsec). All concentrations are expressed in moles per mole of undissociated gas. Conditions ahead of shock: $\rho_1 = 3{\cdot}15 \times 10^{-8}$ g/c^3, $T_1 = 294$°K, and
——— $P_1 = 0{\cdot}020$ mm Hg, $[O_2] = 0{\cdot}212$, $[N_2] = 0{\cdot}788$.
– – – – – $P_1 = 0{\cdot}022$ mm Hg, $[O_2] = 0{\cdot}112$, $[N_2] = 0{\cdot}788$ and $[O] = 0{\cdot}200$.

desired altitude. To scale from density ρ_1 to ρ'_1 the abscissa of the figure should be multiplied by ρ_1/ρ'_1. The radiation intensity ordinate should be multiplied by ρ'_1/ρ_1.

The comparisons shown in Figs. 12, 13 and 14 illustrate the temperature histories and the concentration histories for NO, O, N and electrons. For each figure we have preserved the values of shock speed and of density ahead of the shock. In calculating the conditions behind the shock, we assume that rotational equilibration is instantaneous for the molecules. In addition, for reasons of computational expediency, we assume that electronic excitation

is instantaneous for any atoms present immediately behind the shock. Also shown are some upper limits to the radiation intensities from NO and N_2^+. For NO, this limit is obtained by assuming the population of the radiating states to be in equilibrium with the ground state population ($B^2\Pi \rightleftarrows X^2\Pi$ and $A^2\Sigma \rightleftarrows X^2\Pi$). Similarly, for the N_2^+ upper limit, we assume that $B^2\Sigma \rightleftarrows X^2\Sigma$, as in the case discussed in section I.

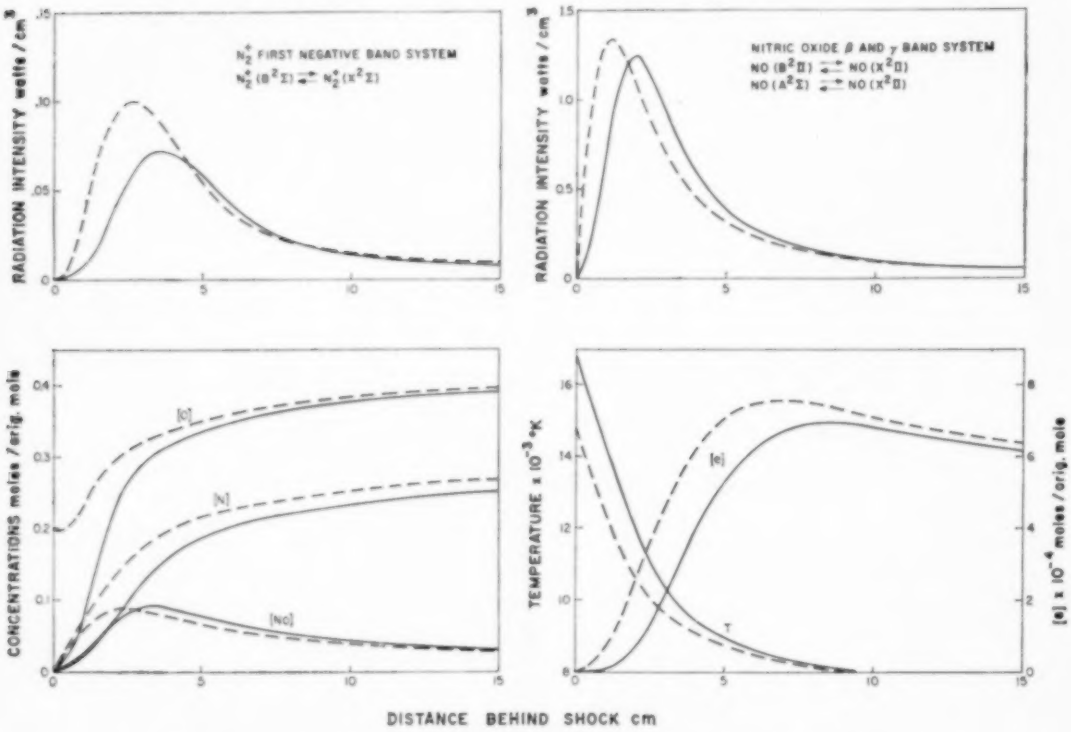

FIG. 13. Relaxation behind shock wave at Mach number $M_s = 17$ ($U_s = 5{\cdot}86$ mm/μsec). All concentrations are expressed in moles per mole of undissociated gas. Conditions ahead of shock: $\rho_1 = 3{\cdot}15 \times 10^{-9}$ g/cm³, $T_1 = 294°$K, and
——— $P_1 = 0{\cdot}020$ mm Hg, $[O_2] = 0{\cdot}212$, $[N_2] = 0{\cdot}788$.
– – – – – $P_1 = 0{\cdot}022$ mm Hg, $[O_2] = 0{\cdot}112$, $[N_2] = 0{\cdot}788$ and $[O] = 0{\cdot}200$.

At the higher Mach numbers (Figs. 12 and 13), the major difference noted in these comparisons is that the presence of atomic oxygen causes the NO concentration to rise linearly with time immediately behind the shock. The peak NO concentration occurs earlier in time, but the magnitude of the overshoot is not greatly affected. At $M_s = 12$ the production of atomic nitrogen is controlled entirely by the atom–molecule interchange reactions rather than by dissociation processes. The ambient atomic oxygen leads to increased activity of the interchange reactions and thus to increased N production. This is reflected in the comparisons of Fig. 14, which show significant changes in the ionization build-up, and in the radiation limit for N_2^+ first negative.

VOL. 1 1961

We conclude that the presence of atomic oxygen in the ambient air should not lead to any dramatic change in either convective or radiative heat transfer, or in the observable radiation intensity, for flight speeds in the range $M_s \approx 15$ to $M_s \approx 21$.

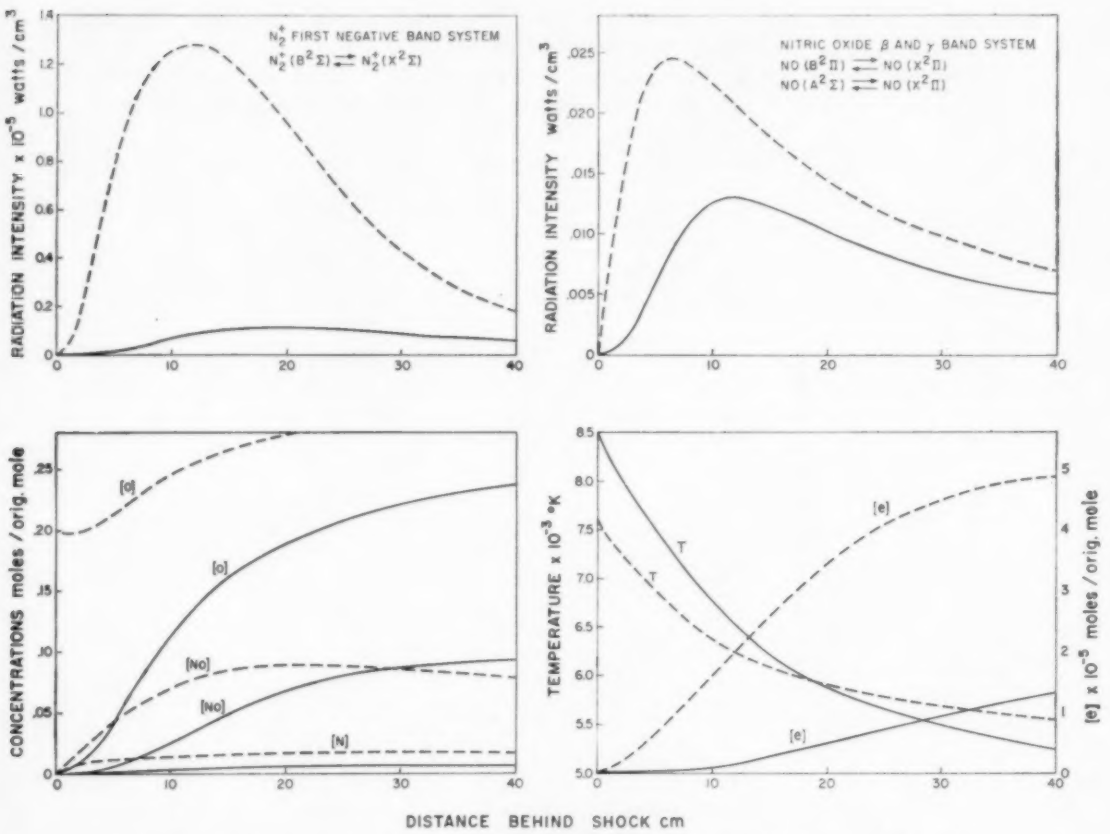

FIG. 14. Relaxation behind shock wave at Mach number $M_s = 12$ ($U_s = 4.13$ mm/μ sec). All concentrations are expressed in moles per mole of undissociated gas. Conditions ahead of shock: $\rho_1 = 3{\cdot}15 \times 10^{-9}$ g/cm^3, $T_1 = 294$°K, and
——— $P_1 = 0{\cdot}020$ mm Hg, $[O_2] = 0{\cdot}212$, $[N_2] = 0{\cdot}788$.
- - - - - $P_1 = 0{\cdot}022$ mm Hg, $[O_2] = 0{\cdot}112$, $[N_2] = 0{\cdot}788$ and $[O] = 0{\cdot}200$.

V. APPLICATION TO RE-ENTRY HEATING

Our understanding of non-equilibrium radiation has been extended with the use of the 24-inch low density shock tube. The new data have not been fully analyzed in terms of our rate constant calculations, and we do not have spectra to determine what fraction of the radiation is an impurity effect. As a result, this work must be considered preliminary. However, in combination with earlier experimental data, we arrive at estimates of the non-equilibrium radiation intensity. With this we make some statements about re-entry radiation heating in the stagnation region.

In Fig. 15 we give the integrated luminous front radiation at $\lambda = 3916$ Å as a function of velocity. The intensity is given in units of W/cm²-sr-μ. We have plotted the log of intensity vs. the reciprocal of the velocity. This is because the radiation, in general, has an exponential dependence on the temperature. There is the question of whether the effective temperature for radiation is proportional to the first or second power of velocity. The data using the first power are slightly more linear.

In preparing Fig. 15, we have resurrected some old data to compare with the new. The points ∇ were from measurements made in 1957 using $P_1 = 1$ mm Hg. These are

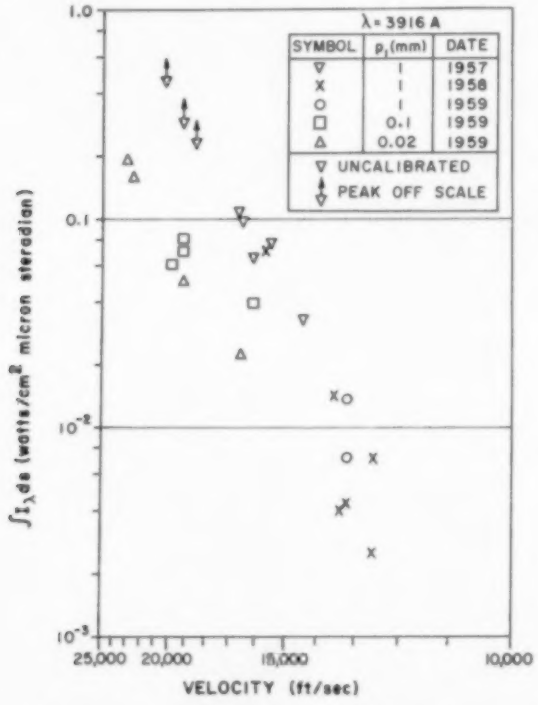

Fig. 15. Integrated luminous front intensity at $\lambda = 3916$ Å as a function of shock speed. The abscissa scale is linear in the reciprocal of the shock speed.

uncalibrated so that they only give velocity dependence information. The points marked with an arrow indicate that the oscillograph signal was off scale at the peak so that the integral is uncertain and may be somewhat larger than indicated (perhaps a factor 1·5). In 1958 we obtained some calibrated measurements at $P_1 = 1$ mm Hg symbolized by X. These are limited to low speeds. The remainder of the points were made recently in connection with this study and are all calibrated. Initial shock tube pressures of $P_1 = 1$, 0·1 and 0·02 mm Hg were used. Some of these were made at 4300 Å and were scaled to 3900 Å by multiplying by a factor 4 (Fig. 4). There is an indication that the $P_1 = 0{\cdot}02$ mm Hg points are slightly lower which may be a collision limiting effect.

To compare with the preliminary discussion of section I of N_2^+ (1–) radiation, we

multiply by 2π for the solid angle (2π is used instead of 4π since we are only interested in that half of the radiation which goes toward the body) and 0·1 micron for the spectral coverage. Then at 0·716 cm/μsec (23,500 ft/sec) we estimate $I = 0{\cdot}4$ W/cm^2 by extrapolating the trend of the data. This is only slightly less than the 1 W/cm^2 upper limit for N_2^+ (1–) indicated in section I. However, this agreement is fortuitous, since our estimate of N_2^+ was too large while NO (β), which is probably important, was not included.

In Figs. 16 and 17 we have applied the results of the luminous front measurements to the problem of re-entry heat transfer. These figures are the same except that Fig. 16 is for

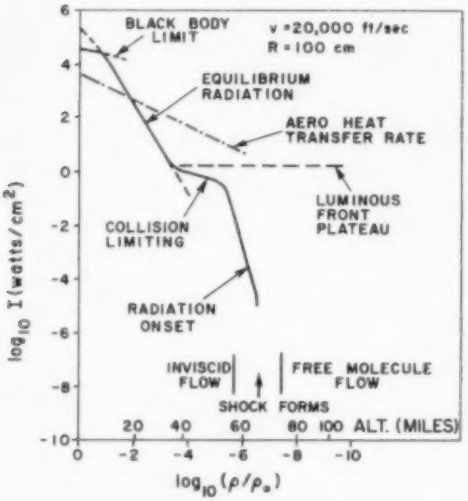

FIG. 16. Comparison of aerodynamic and radiation heat transfer as a function of altitude for flight speed of 20,000 ft/sec and nose radius $R = 100$ cm.

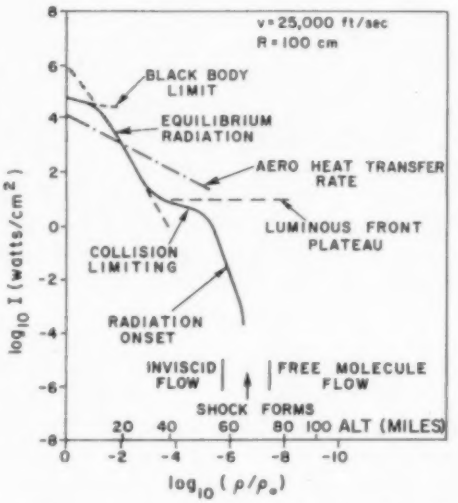

FIG. 17. Comparison of aerodynamic and radiation heat transfer as a function of altitude for flight speed of 25.000 ft/sec and nose radius $R = 100$ cm.

20,000 ft/sec and Fig. 17 for 25,000 ft/sec. The laminar aerodynamic heat transfer rate is estimated according to

$$q_{\text{AERO}} = 10^3 V^3 (\rho_\infty/\rho_0)^{\frac{1}{2}} R^{-\frac{1}{2}}$$

where the velocity (V) is in units of 10^4 ft/sec and the nose radius (R) is in feet. This expression is in agreement with shock tube measurements by ROSE and STARK.[15] The solid line in the figure gives the radiation heat transfer rate to the stagnation point of a spherical body with nose radius 100 cm as a function of altitude. At low altitude the equilibrium radiation reaches the black body maximum. At about 30 miles, the non-equilibrium becomes important and tends to form a plateau, because it is independent of density. Two density dependent corrections become increasingly important as the altitude increases. First, the collision limiting effect decreases the radiation in proportion to the density decrease. Second, the flow goes into the boundary layer and the wake so that the air is cooled and the radiation quenched. This truncates the non-equilibrium region and reduces the radiation. At sufficiently high altitudes, the non-equilibrium radiation does not reach the radiation peak, and the intensity decreases more rapidly with altitude. At still higher

altitudes, a further quenching of the radiation occurs as the boundary layer extends throughout the shock, the shock disappears, and finally the free molecule flow region is reached.

The density dependence of the radiation will now be described. The black body intensity, at low altitudes, decreases as the stagnation temperature decreases corresponding to increased dissociation as density decreases. In the equilibrium region there are three density effects: (1) decreased gas, (2) smaller fraction of molecules, and (3) lower temperature because of increased dissociation. This results in about a density squared dependence.[5] The luminous front plateau as described above is essentially independent of density and will be flat at low altitudes. The radiation onset region depends on the shape of the front of the radiation profile. If the intensity increases linearly with distance behind the start of the shock, then in the collision limited regime the integrated radiation will have approximately a density cubed dependence.

It is seen that the aerodynamic heat transfer above 30 miles is at least a factor 10 greater than the radiation according to our current estimate for $R = 3{\cdot}3$ ft. Hence, radiation heating at $V \leqslant 25$ k ft/sec can be neglected. It should be remembered that the radiation heating on the plateau is independent of R compared to an $R^{-\frac{1}{2}}$ dependence for the aero heat transfer. Thus, radiation becomes relatively more important in comparison with the aerodynamic heating for larger size; however, it is not a rapid effect.

VI. SUMMARY

The program we have described has provided new experimental data which give the order of magnitude of the non-equilibrium radiation. While these data leave much to be desired they will allow preliminary predictions that are suitable for starting engineering programs. Of particular interest is the luminous front plateau which leads to higher radiation intensities at high altitudes. Despite this increase in radiation heat transfer because of the non-equilibrium region, radiation heating remains smaller than aerodynamic heating at high altitudes.

It will be necessary to confirm by further experimentation the magnitude of the non-equilibrium radiation and obtain a more complete understanding of the spectral distribution, collision limiting and the effects of body shape and boundary layer. Analyses of these measurements using the theoretical calculations of relaxation behind shock waves to obtain the basic excitation mechanisms are also required.

Acknowledgement—A. R. Kantrowitz, H. Bethe, M. C. Adams, M. Camac, P. Hammerling, J. C. Keck, S. C. Lin, C. C. Petty and P. Rose have taken an active role in this program. In addition, we thank the staff of AERL for much help.

REFERENCES

1. H. E. Petschek, *Phys. Rev.* **84**, 614A (1951). E. B. Turner, *Phys. Rev.* **99**, 633A (1955). R. J. Rosa, *Ibid.* **99**, 633A (1955).
2. M. Camac, J. C. Camm, S. Feldman, J. C. Keck and C. C. Petty, *Chemical Relaxation in Air, Oxygen and Nitrogen*, Institute of the Aeronautical Sciences, 26th Annual Meeting, New York (1958).
3. J. C. Camm and J. C. Keck, *Bull. Amer. Phys. Soc.*, Series 2, 4, 19 (1959).
4. P. Hammerling, J. D. Teare and B. Kivel, *Non-Equilibrium Electrical and Radiative Properties of High Temperature Air, Nitrogen and Oxygen*, 4th International Conference on Ionization Phenomena in Gases, Uppsala, Sweden (1959). Also Theory of radiation from luminous shock waves in nitrogen, *Phys. Fluids*, **2**, 422 (1959).

5. B. KIVEL, *Radiation from Hot Air and Stagnation Heating*, Avco–Everett Research Laboratory, Research Report 79 (1959), AFBMD–TR–59–20. ASTIA AD 232 836. *J. Aerospace Sci.* **2**, 96 (1961).
6. B. KIVEL, *Radiation from Incident and Reflected Shocks in Air*. Presented at the Symposium Optical Spectrometric Measurements of High Temperatures, Univ. of Chicago (March 1960). Avco–Everett Research Laboratory, AMP 39. *Optical spectrometric measurements of high temperatures*, p. 197 (P. J. Dickerman, Ed.) (Univ. Chicago Press, Chicago) (1961).
7. K. WRAY, J. D. TEARE, B. KIVEL and P. HAMMERLING, *Relaxation Processes and Reaction Rates Behind Shock Fronts in Air and Component Gases*, Avco–Everett Research Laboratory, Research Report 83 (1959), Eighth International Symposium on Combustion, Pasadena, California (1960).
8. P. ROSE, Avco–Everett Research Laboratory, Everett, Mass., Private Communication.
9. J. KECK, J. CAMM, B. KIVEL and T. WENTINK, *Radiation from Hot Air, Part II*, Avco–Everett Research Report 42 (1959). *Ann. Phys.* **7**, 1959.
10. S. C. LIN and W. I. FYFE, *Low Density Shock Tube for Chemical Kinetic Studies*, Avco–Everett Research Report 91 (1960), *Phys. Fluids*, **4**, 238 (1961).
11. G. L. WEISSLER, Photo-ionization in Gases, *Handbuch der Physic*, Vol. XXI, p. 354.
12. S. C. LIN, Avco–Everett Research Laboratory, Everett, Mass. (see Ref. 10).
13. J. C. DE VOS, A New Determination of the Emissivity of Tungsten Ribbon, *Physica* XX, p. 690–714 (1954).
14. H. BROWN, *The Theoretical Response of Heat Transfer Gages Employed in Shock Tubes*, Avco–Everett Research Note 58 (1958).
15. P. H. ROSE and W. I. STARK, Stagnation Point Heat Transfer Measurements in Dissociated Air, *J. Aero. Sci.* **25**, No. 2, 86 (1958).
16. T. WENTINK, W. PLANET, P. HAMMERLING and B. KIVEL, *J. Appl. Phys.* **29**, 742 (1958).
17. R. TAYLOR, *Centinuum Infrared Spectrum of High Temperature Air*, Avco–Everett Research, Report 88 (1960).

OL.
1
961

J. Quant. Spectrosc. Radiat. Transfer. Vol. 1, pp. 76–87. Pergamon Press Ltd. Printed in Great Britain

INTENSITY MEASUREMENTS ON OVERLAPPED MOLECULAR BANDS*

D. ROBINSON† and R. W. NICHOLLS
Department of Physics, University of Western Ontario, London, Canada

(*Received* 27 *July* 1960)

Abstract—The measurement of intensities of molecular band systems is often complicated by the partial overlapping of adjacent bands, making the direct measurement of integrated total band intensities extremely difficult, if not impossible. Several attempts have been made by various authors to overcome the problem, none being universally applicable to any band system.

Two general methods are suggested here. In the first, a known fraction of the band is employed, and in the second, the rotational intensity distribution within a band is interpreted in terms of the total band intensity.

The methods have been tested experimentally and found to be in good agreement for the NO β and 0_2^+ Second Negative Systems where the integrated intensities were independently measured.

1. INTRODUCTION

WHEN measuring the intensities of molecular band systems, one is seldom fortunate enough to have well separated, non-overlapped, bands to analyse; some degree of overlap is often present. It is nevertheless becoming increasingly important to obtain measured intensity distributions of whole band systems. Methods therefore have to be developed which allow for overlap between bands. Two such methods, which have been found to be reliable, are discussed here. They are:

(1) Measurement of a *known* fraction of a band (such as a band head), as indicative of the intensity of the whole band (The Fractional Band Intensity Method). This is particularly applicable to spectra that are not completely resolved.

(2) Measurement of intensity distributions of *individual rotational lines* in bands, from appropriate semilogarithmic plots of which, relative intensities of the bands may be inferred. (The Rotational Line Intensity Method). This is particularly applicable to well resolved spectra, often of complicated rotational structure.

Specific aspects of each of these methods have been used with varying degrees of success by several authors. When a strong band partially overlaps a much weaker one, the error introduced by empirical separation of profiles does not have a very great effect on the measured intensity of the stronger band, but, depending upon the degree of overlap, can make the measured intensity of the weaker band completely unreliable save as a qualitative indication of trends. The most frequently used aspect of the fractional band intensity method has been the assumption that the intensity of the band head is proportional to that of the whole band. JOHNSON and TAWDE[1] have used this assumption on bands of the CN violet system. ORNSTEIN and BRINKMANN[2] on the other hand, in studying the same system, have concluded that because the rotational energy levels are determined by the moment

* Supported in part by the Air Force Cambridge Research Centre and The Defence Research Board of Canada.

† Now at Engineering Centre, University of Southern California, Los Angeles 7, California.

of inertia which itself varies with vibrational quantum number, that the fraction of each band located in the band head is not constant for the whole system but varies for each v'' progression. In the case of the N_2 Second Positive System, TAWDE and PATANKAR[3] claim that the ratio of band head to whole band intensity is not constant while YOUNG [4] has shown that the deviation from constancy for this system is only 6·2 per cent.

In a theoretical treatment of the problem by FLOYD and KING[5], an "effective" and representative quantum number was assigned to the turning point of the P branch which forms the band head of CN Violet Bands. An effective band width $\Delta\lambda$ for the band head was derived, as was an effective fraction of the band formed by the band head. They treated the $^2\Sigma$–$^2\Sigma$ CN Violet System as an effective $^1\Sigma$–$^1\Sigma$ system. It may be noted in passing that when their measured values of relative vibrational transition probabilities for the bands are subjected to the method of FRASER[6] in order to study the variation of electronic transition moment $R_e(r)$ with internuclear separation, most inconsistent results are obtained which do not agree from progression to progression over identical ranges of r. When the data of ORNSTEIN and BRINKMANN[2] for the same system is treated in the same way however, internally very consistent results are obtained from progression to progression. Floyd and King's method may not adequately allow for the correct fraction of the band taken by its head.

PHILLIPS[7] used the intensity distribution of individual rotational lines in a vibrational band to obtain integrated intensities for the C_2 Swan System. He points out that his method may yield uncertain results for intrinsically weak features.

Some of the difficulties of previous work arise from arbitrary choice of effective band head width, overlaps between features in the rotational structure, and complications which arise when extensions are made to systems in which $\Delta\Lambda \neq 0$. Thus the Fractional Band Intensity and Rotational Line Intensity Methods, which are described below, have been developed for more general applicability. The methods have been tested fully using recent measurements[8–10] of total and partial band intensities of the $NO\beta$ and O_2^+ Second Negative Bands.

2. THEORY

2.1. *Fractional band intensities*

The intensity $I_{J'J''}$ of the (J', J'') rotational line of the (v', v'') vibrational band is given by

$$I_{J'J''} = K\frac{N_{v'}}{Q_{v'}} p_{v'v''} \nu^4_{J'J''} S_{J''} \exp(-E_{J'}/kT_{Rot}) \qquad (1)$$

if thermal equilibrium at temperature T_{Rot} obtains in the rotational degrees of freedom.

Here K is a constant depending on units and geometry

$N_{v'}$ is the total population in the level v'

$Q_{v'}$ is the rotational partition function of the level v'

$p_{v'v''}$ is the relative vibrational transition probability whose dependence on rotational angular momentum is often very small (FRASER[11])

$\nu_{J'J''}$ is the frequency of the $(J'J'')$ line, and for a band of small extension may be treated as a constant[11]

$S_{J''}$ is the line strength or Hönl–London factor

$E_{J'}$ is the rotational energy of the upper level J'

k is Boltzmann's constant

The intensity $I_{v'v''}$ of the whole vibrational band is given by

$$I_{v'v''} = KN_{v'} p_{v'v''} \nu^4_{v'v''} \tag{2}$$

where $\nu_{v'v''}$ is an 'average' frequency for the band.

Equations (1) and (2) may be used to compare the sum $I^{AB}_{v'v''}$ of intensities of all the lines in one branch arising from transitions from upper levels which lie between J'_A and J'_B to the total band intensity $I_{v'v''}$.

Thus

$$\frac{I^{AB}_{v'v''}}{I_{v'v''}} = \frac{1}{Q_{v'}} \sum_{J_A}^{J_B} S_{J'} \exp(-E_{J'}/kT_{Rot}) = \frac{1}{Q_{v'}} f_{v'AB} \tag{3}$$

where $f_{v'AB}$ represents the summation and $\nu_{J'J''}$ and $\nu_{v'v''}$ cancel to a good approximation in most cases.

It is often a matter of experimental importance to compare the ratio between two measured fractions $I^{AB}_{v'v''}$, $I^{CD}_{w'w''}$ of two different bands to the ratio between their total intensities $I_{v'v''}$, $I_{w'w''}$. Thus from equation (3)

$$\frac{I^{AB}_{v'v''}}{I^{CD}_{w'w''}} = \frac{I_{v'v''}}{I_{w'w''}} \frac{Q_{w'}}{Q_{v'}} \frac{f_{v'AB}}{f_{w'CD}} \tag{4}$$

When the fraction of the band is made up from parts of each of the P, Q and R branches (viz: $J_1 \rightarrow J_2$ in the P branch, $J_3 \rightarrow J_4$ in the Q branch and $J_5 \rightarrow J_6$ in the R branch), then from equation (4) the ratio of fractional band intensities is related to that for total band intensities by

$$\frac{I^{PQR}_{v'v''}}{I^{PQR}_{w'w''}} = \frac{I_{v'v''}}{I_{w'w''}} \frac{Q_{w'}}{Q_{v'}} \frac{(f^P_{v'\,1,2} + f^Q_{v'\,3,4} + f^R_{v'\,5,6})}{(f^P_{w'\,1,2} + f^Q_{w'\,3,4} + f^R_{w'\,5,6})} = \frac{I_{v'v''}}{I_{w'w''}} \frac{Q_{w'}}{Q_{v'}} \frac{(f^P_{v'} + f^Q_{v'} + f^R_{v'})}{(f^P_{w'} + f^Q_{w'} + f^R_{w'})} \tag{5}$$

In this equation (and in equation (4)), the left hand side is, in principle, measurable, the actual intensity ratio $I_{v'v''}/I_{w'w''}$ is sought and the rest of the right hand side is in principle calculable as follows:

Case (1): *Bands summed over the same range of rotation quantum numbers $J_A \rightarrow J_B$ and not forming a v' progression, ($v' \neq w'$).* In the simple case in which the same range $J_A - J_B$ *in one branch* is measured in each band, the ratio $f_{v'AB}/f_{w'AB}$ is required in equation (3). From equation (3)

$$f_{v'AB} = \sum_{J_A}^{J_B} S_J \exp[-B_{v'} J(J+1)/kT] \tag{6}$$

where $B_{v'} = B_{e'} - \alpha_{e'}(v' + \frac{1}{2})$, is the rotational constant for the level v', and like the other symbols are in standard rotation[12]. In some cases (e.g. O_2 Schumann–Runge System), it is necessary to include the $D_{v'}J^2(J+1)^2$ term in the exponent realistically to represent the rotational energy $E_{J'}$. The ratio of f's for the two bands is then

$$\frac{f_{v'AB}}{f_{w'AB}} = \frac{\sum_{J_A}^{J_B} S_J \exp[-(B_{v'} J(J+1)/kT]}{\sum_{J_A}^{J_B} S_J \exp[-B_{w'} J(J+1)/kT]} \tag{7}$$

VOL. 1 1961

Writing B_1 for $B_{v'}/kT$, B_2 for $B_{w'}/kT$ and δB for $B_1 - B_2$, equation (7) becomes

$$\frac{f_{v'AB}}{f_{w'AB}} = \frac{\sum_{J_A}^{J_B} S_J \exp\left[-(B_2 - \delta B)J(J+1)\right]}{\sum_{J_A}^{J_B} S_J \exp\left[-B_2 J(J+1)\right]} \tag{8}$$

For most band systems, excited say in an electrical discharge, $T \sim 300°\text{K}$ or greater, $\alpha_e = 2 \times 10^{-2}\ \text{cm}^{-1}$, and $J \sim 100$. Thus $\delta B \sim 10^{-4}$ and $\delta BJ(J+1) \ll 1$. A Taylor's series expansion to two terms of the exponential in the numerator is then an adequate approximation.

Thus
$$\frac{f_{v'AB}}{f_{w'AB}} = 1 - \frac{\delta B \dfrac{\partial (f_{w'AB})}{\partial B_2}}{f_{w'AB}} \tag{9}$$

It is shown in an appendix that the summation involved in f may often be replaced as an integral and thereby, in a specific case, how the partial differentiation is accomplished.

In the more complicated case which involves summation over all three branches, equation (5) may be similarly recast as

$$\frac{I^{PQR}_{v'v''}}{I^{PQR}_{w'w''}} = \frac{I_{v'v''}}{I_{w'w''}} \frac{Q_{w'}}{Q_{v'}} \left[1 - \frac{\delta B \dfrac{\partial (f^P_{w'} + f^Q_{w'} + f^R_{w'})}{\partial B_2}}{(f^P_{w'} + f^Q_{w'} + f^R_{w'})} \right] \tag{10}$$

The bracket on the right hand side is less than, but close to, unity and may be evaluated in specific cases using the S_J values given by HÖNL and LONDON[13], HERZBERG[12], HILL and VAN VLECK[14], RUARK and UREY[15] and JOHNSON[16]. The specific evaluation of the coefficient of $I_{v'v''}/I_{w'w''}$ in equation (10) is presented for the $^1\Sigma$–$^1\Sigma$ case in an appendix. The summations have been replaced by integrals with an error of about 0·1%.

It may be noted in passing that in cases where $I_{v'v''}/I_{w'w''}$ and $I^{PQR}_{v'v''}/I^{PQR}_{w'w''}$ can *both* be measured, the coefficient

$$\frac{Q_{w'}}{Q_{v'}} \left[1 - \frac{\delta B \dfrac{\partial f^P_{w'} + f^Q_{w'} + f^R_{w'})}{\partial B_2}}{f^P_{w'} + f^Q_{w'} + f^R_{w'}} \right]$$

can also therefore be measured and used as a proportionality constant for other bands over the same range of J.

Case 2: Bands measured over the same range of rotational quantum numbers $J_A \rightarrow J_B$, and forming a v'' progression ($v' = w'$). In this case, equation (5) reduces to

$$\frac{I^{PQR}_{v'v''}}{I^{PQR}_{v'w''}} = \frac{I_{v'v''}}{I_{v'w''}} \tag{11}$$

because $Q_{v'} = Q_{w'}$ and the quotient of sums of f's reduces to unity. It is an important practical result that the ratio of fractional intensities is identically equal to the ratio of total band intensities when the same fraction of bands is taken in a v'' progression.

Case 3: Bands measured over different ranges of rotational quantum numbers not forming a progression. In this case equation (5) takes the form

$$\frac{I^{PQR}_{v'v''}}{I^{PQR}_{w'w''}} = \frac{I_{v'v''}}{I_{w'w''}} \frac{Q_{w'}}{Q_{v'}} \frac{(f^{P}_{v'\,1,2} + f^{Q}_{v'\,3,4} + f^{R}_{v'\,5,6})}{(f^{P}_{w'\,7,8} + f^{Q}_{w'\,9,10} + f^{R}_{w'\,11,12})}$$

where the numerical subscripts indicate the different ranges of lines measured in each branch (e.g. the P-branch of the $v'v''$ band is measured from J_1 to J_2 etc.). The f-quotient has to be evaluated specifically in each case. The procedure is tedious but direct.

In summary, it is relatively simple to write down the relation between ratios of measured fractional intensities and ratios of the desired total band intensities. In application, the specific form of the coefficients have to be worked out in each case. In principle the method is often applicable to fractions of *unresolved* bands between specific wavelength ranges.

2.2. *Rotational line intensities*

During recent years, photoelectric scanning grating spectrometers have become available which possess sufficient resolution to separate most of the rotational lines of a band except, in some cases, those for low J values close to the band head where the lines are very closely spaced. As is shown below, it therefore becomes possible to make plots derived from measured line intensities ($J > 10$) to measure relative total band intensities. Serious line blends can often be avoided beyond $J = 10$.

From equations (1) and (2) the ratio of the intensities of the J', J'' lines to the v', v'' band is given by

$$\frac{I_{J'J''}}{I_{v'v''}} = \frac{S_{J'}}{Q_{v'}} \exp\left[-B_{v}J'(J'+1)/kT\right] \tag{13}$$

and thus

$$\log \frac{I_{J'J''}}{S_{J'}} = \log \frac{I_{v'v''}}{Q_{v'}} - B_{v}J'(J'+1)/kT \tag{14}$$

In equations (1) and (2) $\nu_{J'J''}$ has been set equal to an "average" $\nu_{v'v''}$ which is an acceptable approximation in most cases. Also, as has been mentioned above, it is sometimes necessary to express the rotational energy term as $B_vJ'(J'+1) - D_vJ'^2(J'+1)^2$ in some cases.

The usual plot of $\log \frac{I_{J'J''}}{S_{J'}}$ vs. $J'(J'+1)$, if it yields a straight line, justifies the assumption of thermal rotational equilibrium. The intercept of the plot on the ordinate axis is $\log \frac{I_{v'v''}}{Q_{v'}}$, and the difference between intercepts of the two plots for the respective (v', v'') and (w', w'') bands is $\log \frac{I_{v'v''}}{I_{w'w''}} + \log \frac{Q_{w'}}{Q_{v'}}$. *Thus relative total band intensities may be derived from relative intercepts, on the ordinate scale, of comparable plots of* $\log \frac{I_{J'J''}}{S_{J'}}$ *vs. Rotational Energy for each band.* (Such plots may be seen in Fig. 2). Measured values of $I_{J'J''}$ for *non-overlapped* lines are of course used in these plots; intensities of blended lines, when plotted, deviate severely from the linear trend of the other points and can thereby be detected and rejected. In principle the rotational line intensity method could also be used in some cases when rotational thermal equilibrium was not achieved in the source. In these cases each of the

VOL. 1 196

plots would be non-linear. If the rotational energy distribution did not accentuate low J values too severely the curves could be extrapolated back to the ordinate axis to obtain the relative ordinates with somewhat of a reduction in accuracy.

3. RESULTS

These methods described above have been applied with success to a number of band systems and examples are presented below for measurements made on the two systems NO β and O_2^+ Second Negative. The band systems were excited in discharge tubes and their intensities measured photoelectrically by a calibrated Leeds and Northrup photoelectric scanning spectrometer. The experimental details have been presented elsewhere [8, 9, 10] Fractional band intensities and also total band intensities have measured and compared with the calculated ratios discussed above, to check the adequacy of the methods quoted above.

3.1. *The fractional band intensity method*

3.1(a). *The NO β system* ($B^2\Pi$–$X^2\Pi$) $v' = 0$ *progression.* The Fractional Band Intensity method (case 2) discussed above, has been used on seven bands ($v' = 0$, $v'' = 5$–11) of this

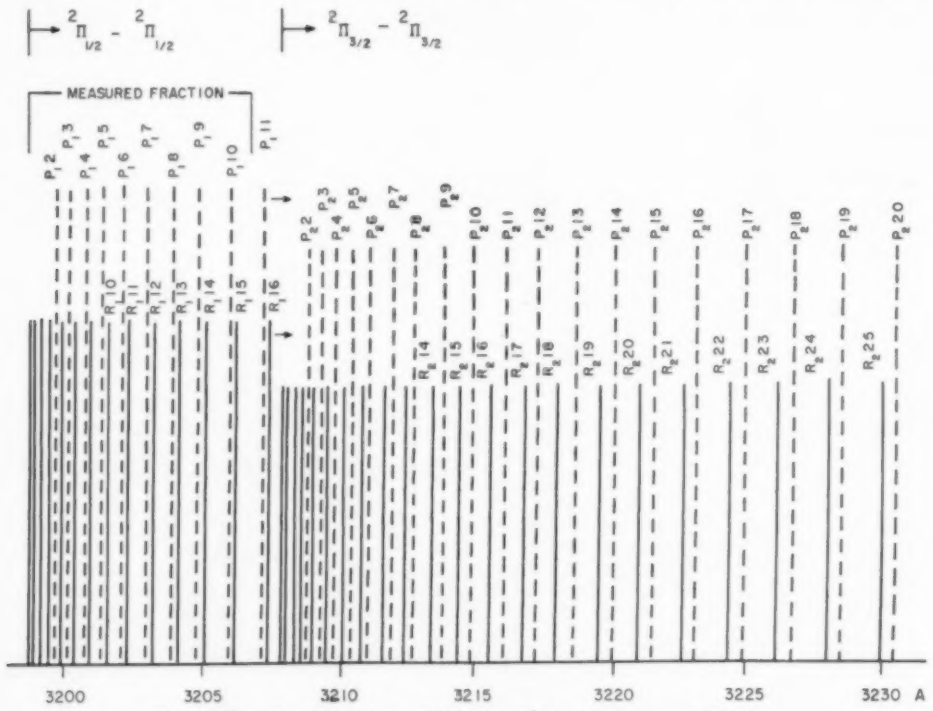

FIG. 1. Rotational structure of NOβ band showing measured fraction.

system over the wavelength region λλ(2748–3801Å). As these bands are relatively isolated it was possible to measure total band intensity[8] in each case in addition to fractional band intensity and to confirm the constancy of the ratios of these for each band. The bands are, as is well known, double headed, and the structure of a typical band is shown in Fig. 1[17]. The fraction chosen was, as indicated in Fig. 1, that which includes the rotational

structure between $J \leqslant 15$ for the R branch and $J \leqslant 10$ for the P_1 branch which is approximately all of the $^2\Pi - {}^2\Pi$ sub band. The total intensities of the bands were also measured. The results of these measurements are shown in Table 1.

TABLE 1. COMPARISON BETWEEN RELATIVE FRACTIONAL BAND INTENSITIES AND RELATIVE TOTAL BAND INTENSITIES FOR NO β SYSTEM.

Band	Relative fractional band intensity*	Relative total band intensity*	Ratio of fractional band intensity to total band intensity†
(0, 5)	0·41	0·55	0·75
(0, 6)	0·90	0·85	1·06
(0, 7)	1·00	1·00	1·00
(0, 8)	0·99	0·97	1·02
(0, 9)	0·83	0·80	1·04
(0, 10)	0·59	0·59	1·00
(0, 11)	0·32	0·35	0·92

* Relative to (0, 7) band

† Ratio of entries of previous two columns

Note: Fractional band intensity $= \sum_{J=1}^{J=15} I_R + \sum_{J=2}^{J=10} I_P$

Good agreement between relative total intensities and relative fractional intensities is seen except in the case of the (0, 5) band, which is weak and which lies in the region of rapid variation of photomultiplier response with wavelength.

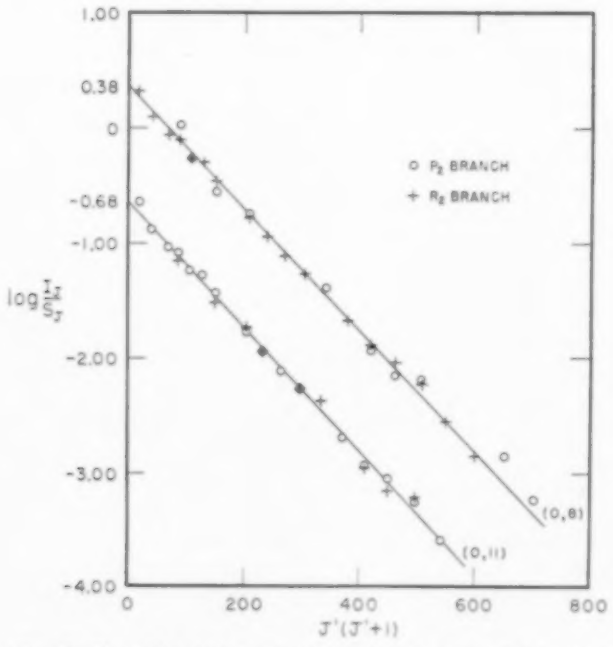

FIG. 2. Plot of $\log I_J/S_J$ vs. $J'(J'+1)$ for the (0, 8) and (0, 11) NOβ bands.

3.1(b). O_2^+ *Second Negative System* ($A^2\Pi - X^2\Pi$) $v' \neq w'$. The Fractional Band Intensity Method (Case 1) was applied here. The bands are double headed, like the NO β bands, and exhibit satellite branches (R_{21}, P_{21}) which are weaker than the main P_1 and R_1 branches because of different coupling cases which operate in each of the electronic states. Contributions from the very weak Q branches are ignored. The detailed rotational structure of these bands has been discussed by STEVENS[18] and BOZÒKY[19]. Steven's vibrational assignments were shown to be in error by two units in v'' which should thus be replaced by $v'' - 2$.

The $^2\Pi_{\frac{1}{2}}$–$^2\Pi_{\frac{1}{2}}$ sub band was the fraction chosen and it included the following lines

R_1 branch $J \leqslant 17$

R_{21} branch $J \leqslant 20$

P_1 branch $J \leqslant 13$

P_{21} branch $J \leqslant 15$

The (0, 6), (0, 7), (1, 5), (1, 6), (1, 7) bands over the wavelength range λλ(3300–3860Å). Fractional band intensities and total band intensities were measured. They are compared in Table 2.

TABLE 2. COMPARISON BETWEEN RELATIVE FRACTIONAL BAND INTENSITIES AND RELATIVE TOTAL BAND INTENSITIES FOR THE O_2^+ SECOND NEGATIVE SYSTEM.

Band	Relative fractional band intensity*	Relative total band intensity*	Ratio of fractional band intensity to total band intensity†
(0, 7)	0·81	0·80	0·99
(0, 6)	0·75	0·76	1·01
(1, 7)	0·73	0·75	1·03
(1, 6)	0·83	0·84	1·01
(1, 5)	1·00	1·00	1·00

* Relative to (1, 5) band

† Ratio of entries of two previous columns

Note: Fractional band intensity $= \sum_{J=0}^{J=15} I_{P_1} + \sum_{J=0}^{J=15} I_{P_{21}} + \sum_{J=0}^{J=17} I_{R_1} + \sum_{J=0}^{J=20} I_{R_{21}}$

Table 2 shows that the Fractional Band Intensities are good measures of Total Band Intensities.

Table 3 presents data on

$$\frac{I^{PQR}_{v'v''}}{I^{PQR}_{w'w''}} \Big/ \frac{I_{v'v''}}{I_{w'w''}} \text{ for the bands.}$$

It will be recalled from equation (12) that the ratio is an experimental measure of $Q_w(f^P_v + f^Q_v + f^R_v)/Q_v(f^P_w + f^Q_w + f^R_w)$. The ratio is in all cases within 4 per cent of unity.

TABLE 3. O_2^+ SECOND NEGATIVE SYSTEM: EXPERIMENTALLY MEASURED VALUES OF

$$\frac{I^{PQR}_{v'v''}}{I^{PQR}_{w'w''}} \Big/ \frac{I_{v'v''}}{I_{w'w''}} = \frac{Q_{w'}(f^P_{v'} + f^Q_{v'} + f^R_{v'})}{Q_{v'}(f^P_{w'} + f^Q_{w'} + f^R_{w'})}$$

Bands	Ratio
$\frac{(0, 7)}{(1, 7)}$	0·96
$\frac{(0, 6)}{(1, 6)}$	1·00
$\frac{(0, 7)}{(1, 6)}$	1·02
$\frac{(0, 6)}{(1, 7)}$	1·02
$\frac{(0, 7)}{(1, 5)}$	1·01
$\frac{(0, 6)}{(1, 5)}$	0·99

3.2. *The rotational line intensity method*[10]

The NO β system was selected to test this method as its rotational structure is well developed, intensities are easily measured line by line and because results on total band intensities are available[8]. JENKINS, BARTON and MULLIKEN[17] give a very complete description of the bands in the $v' = 0$ progression.

Following the discussion of section (2.2.), Fig. 2 shows typical plots of log $I_{J'J''}/S_{J'}$ vs. $J'(J' + 1)$ for the (0, 8) and (0, 11) bands of the system. As is seen they both give rise to lines of equal slope, which confirms the assumption of rotational thermal equilibrium. The differences between intercepts on the ordinate scale are direct measures of relative band intensities. Table 4 presents relative intensity data measured in this way from lines of the P_2 and R_2 branches which fall in the tail of the second sub band. The relative intensities measured in this way are also compared in Table 4 with total band intensities which have been measured previously[8] and very good agreement is noted.

TABLE 4. NO β SYSTEM:
RELATIVE BAND INTENSITIES MEASURED BY THE ROTATIONAL LINE INTENSITY METHOD.

Band	$I^{Rot}_{v'v''}$*	$I_{v'v''}$†	$\frac{I^{Rot}_{v'v''}}{I_{v'v''}}$
(0, 6)	8·9	8·5	1·05
(0, 7)	10·0	10·0	1·00
(0, 8)	9·8	9·7	1·01
(0, 9)	7·6	8·0	·95
(0, 10)	5·7	5·9	·97
(0, 11)	3·4	3·5	·97

* Intensities derived by rotational method arbitrarily scaled to $I_{0,7} = 10$.
† Total integrated intensities arbitrarily scaled to $I_{0,7} = 10$.

4. DISCUSSION

In this paper two methods of measuring the relative total intensity of a band by treatment of intensity measurements of a fraction of it have been discussed and shown to give results which are in excellent agreement with intensities integrated over the whole band profile. These methods are of immediate application to band systems of relatively complicated structure either fully resolved or only partially resolved. The fractional band intensity method is particularly useful when unresolved spectra of only moderate dispersion are available as its application only requires accurate knowledge of the wavelength limits of the band in question. Ideally the applicability of the method should be tested on each band system considered but there seems to be no serious reason to doubt its general applicability.

The rotational line intensity method* is of particular use in the case of bands of interlaced structure of which some of the lines of band tails are resolved sufficiently as to be measureable. It requires the existence of rotational thermal equilibrium which is not a very stringent requirement in many cases. In principle the method is applicable when rotational thermal equilibrium does not exist but in this case the determination of the relative intercepts on the ordinate scale will require extrapolation of a series of curves rather than straight lines and relative accuracy will thereby be reduced somewhat.

Acknowledgements—The authors would like to acknowledge many helpful discussions with Dr. P. A. Fraser. The work was supported in part by contracts with The Air Force Cambridge Research Centre and the Department of Defence Production of Canada and in part by research grants from The National Research Council of Canada, The Ontario Research Foundation and The Defence Research Board of Canada.

REFERENCES

1. R. C. Johnson and N. R. Tawde, *Proc. Roy. Soc.* A **137**, 575 (1932).
2. L. S. Ornstein and H. Brinkmann, *Proc. Acad. Amst.* **34**, 33 (1931).
3. N. R. Tawde and V. S. Patankar, *Proc. Phys. Soc.* **55**, 396 (1943).
4. B. G. Young, *M.Sc. Thesis*, Univ. of Western Ontario (1954).
5. A. L. Floyd and R. B. King, *J. Opt. Soc. Amer.* **45**, 249 (1955).
6. P. A. Fraser, *Can. J. Phys.* **32**, 512 (1954).
7. J. G. Phillips, *Astrophys. J.* **125**, 1953 (1957).
8. D. Robinson and R. W. Nicholls, *Proc. Phys. Soc.* **71**, 957 (1958).
9. D. Robinson and R. W. Nicholls, Scientific Report No. 3 (1958), Contract AF 19 (604)–1718.
10. D. Robinson and R. W. Nicholls, Scientific Report No. 5 (1958), Contract AF 19 (604)–1718.
11. P. A. Fraser, Scientific Report No. 6 (1958), Contract AF 19 (604)–1718.
12. G. Herzberg, *The Spectra of Diatomic Molecules*, Van Nostrand, New York (1950).
13. H. Hönl and F. London, *Z. Phys.* **33**, 803 (1925).
14. E. Hill and J. Van Vleck, *Phys. Rev.* **32**, 250 (1928).
15. A. E. Ruark and H. C. Urey, *Atoms, Molecules and Quanta*, McGraw Hill, New York (1933).
16. R. C. Johnson, *An Introduction to Molecular Spectra*, Methuen, London (1949).
17. F. A. Jenkins, H. A. Barton and R. S. Mulliken, *Phys. Rev.* **30**, 150 (1927).
18. D. S. Stevens, *Phys. Rev.* **38**, 1292 (1931).
19. L. V. Bozòky, *Z. Phys.* **104**, 275 (1937).
20. D. Robinson, *Ph.D. Thesis*, University of Western Ontario (1957).
21. G. R. Hebért, *Ph.D. Thesis*, University of Western Ontario (1960).
22. C. E. Treanor and W. H. Wurster, *J. Chem. Phys.* **32**, 758 (1960).
23. D. Robinson and R. W. Nicholls, *Proc. Phys. Soc.* **75**, 817 (1960).

* The basis and evaluation of the method was first discussed in the 1957 Ph.D. thesis of one of us (D.R.)[20], and was later described in a Scientific Report[10]. The method has recently been employed to measure intensities of O_2 Schumann–Runge bands in emission[21] and in absorption[22]. Intensity measurements have also recently been made upon bands of the CO^+ Comet-Tail and BO α and β systems[23].

APPENDIX

In this appendix we consider the specific application of equation (10) to Σ–Σ transitions in general and the CN Violet ($^2\Sigma$–$^2\Sigma$) system in particular.

For Σ–Σ transitions P and R branches only occur and $S_J^P = J + 1$, $S_J^Q = 0$, $S_J^R = J$. Thus from equation (6)

$$f^P_{vAB} = \sum_{J_A}^{J_B} (J + 1) \exp [- B_v J(J + 1)] \tag{6a}$$

$$f^R_{vAB} = \sum_{J_A}^{J_B} J \exp [- B_v J(J + 1)] \tag{6b}$$

where B_v applies to the vibrational level v.

Negligible error is made by replacing the summations by integrals between the limits $J_A - \frac{1}{2}, J_B + \frac{1}{2}$.

Both integrals then take the form

$$f^{PR}_{vAB} = \frac{1}{2B_v} \{\exp [- B_v(J_A^2 - \tfrac{1}{4})] - \exp [- B_v(\overline{J_B + 1}^2 - \tfrac{1}{4})]\}$$
$$\pm \left(\frac{\Pi}{16B_v}\right)^{\frac{1}{2}} \exp \frac{B_v}{4} \{\operatorname{erf} B_v^{\frac{1}{2}}(J_B + 1) - \operatorname{erf} B_v^{\frac{1}{2}} J_A\} \tag{6c}$$

where $\operatorname{erf} x = (2/\pi)^{\frac{1}{2}} \int_0^x \exp(-S^2) dS$. The positive alternative is taken for f^P_{vAB} and the negative alternative is taken for f^R_{vAB}.

Further

$$\frac{\partial f^{PR}_{vAB}}{\partial B_v} = \frac{1}{2B_v^2} [(1 + L) \exp(-L) - (1 + M) \exp(-M)]$$
$$\pm \frac{1}{4B_v} [(J_B + 1) \exp(-M) - J_A \exp(-L)]$$
$$\pm \left(\frac{\Pi}{16B_v}\right)^{\frac{1}{2}} \exp(B_v/4)\ (\tfrac{1}{4} - \tfrac{1}{2}B_v)\ (\operatorname{erf} B_v^{\frac{1}{2}}(J_B + 1) - \operatorname{erf} B_v^{\frac{1}{2}} J_A) \tag{6d}$$

where $L = B_v(J_A^2 - \frac{1}{4})$; $M = B_v(\overline{J_B + 1}^2 - \frac{1}{4})$

Now in the case of P and R branches only, equation (10) which compares the intensities of the (v', v''), (w', w'') bands takes the form

$$\frac{I^{PR}_{v'v''}}{I^{PR}_{w'w''}} = \frac{I_{v'v''}}{I_{w'w''}} \frac{B_{v'}}{B_{w'}} \left\{1 - \frac{\varkappa(w' - v')}{kT} \frac{\dfrac{\partial}{\partial B_v}(f^P_{w'AB} + f^R_{w'AB})}{f^P_{w'AB} + f^R_{w'AB}}\right\} \tag{10a}$$

As, for large T or small B_v. (See (12) p. 125).

$$\frac{Q_{w'}}{Q_{v'}} = \frac{B_{v'}}{B_{w'}} \text{ and also } \delta B = \frac{\varkappa_e(w' - v')}{kT}$$

An estimate may be made of the fractional band intensity quotient $I^{PR}_{v'v''}/I^{PR}_{w'w''}$ and the total band intensity quotient $I_{v'v''}/I_{w'w''}$ from equation (10a) for the extreme cases of the v', $v'' = (0, 0)$ and w', $w'' = (10, 10)$ bands of the CN Violet system as follows. Here, taking the basic data $B_e = 1{\cdot}9701\ \text{cm}^{-1}$, $\alpha_e = 0{\cdot}02215\ \text{cm}^{-1}$, $k = 0{\cdot}6952\ \text{cm}^{-1}/^\circ\text{K}$; from HERZBERG[12] and assuming $T = 300^\circ\text{K}$ then $B_1 = 0{\cdot}00827$ and $B_2 = 0{\cdot}00933$. Also $B_{v'}/B_{w'} = 0{\cdot}89$. Consequently

$$\frac{\dfrac{\partial}{\partial B_2}(f^P_{v'AB} + f^R_{w'AB})}{(f^P_{v'AB} + f^{w'AB}_R)} = -\frac{(106{\cdot}93\ e^{0{\cdot}00233} + 222{\cdot}93\ e^{-1{\cdot}127})}{e^{0{\cdot}00233} - e^{-1{\cdot}127}} = -49$$

Thus in equation (10a)

$$\frac{B^{v'}}{B_{w'}}\left[1 - \frac{\alpha_e(w^1 - v^1)}{kT}\,\frac{\dfrac{\partial}{\partial B_2}(f^P_{w'AB} + f^R_{w'AB})}{(f^P_{w'AB} + f^R_{w'AB})}\right] = 0{\cdot}89\,(1 + 0{\cdot}005\,w' - v')$$

$$= 0{\cdot}89\,(1 + 0{\cdot}05)$$

$$= 0{\cdot}94$$

as $w' = 10$, $v' = 0$

from which it may be concluded that in this case the ratios of the fractional band intensities are indeed an excellent measure of total band intensity ratio.

VOL.
1
1961

J. Quant. Spectrosc. Radiat. Transfer. Vol. 1, pp. 89–95. Pergamon Press Ltd. Printed in Great Britain

THE SPECTROSCOPE AS A TOOL FOR ATMOSPHERIC SOUNDING BY SATELLITES*

L. D. KAPLAN
Department of Meteorology, Massachusetts Institute of Technology, Cambridge, Massachusetts

(*Received* 2 *December* 1960)

Abstract—A previous suggestion by the author that the atmosphere can be sounded by remote satellite measurements of thermal radiation is discussed in more detail. Preliminary calculations show that the accuracy required to determine the temperature structure to within a degree or two is probably obtainable for fairly large atmospheric layers.

Singer's method of satellite ozone sounding is shown to be an extremely sensitive technique for determining the upper-level ozone distribution in considerable detail.

OL.
1
961

I. INTRODUCTION

IT has been suggested by the author[1] that a detailed analysis of the thermal structure of the atmosphere could be obtained by satellite measurements, at carefully selected frequencies in the 15 μ band of CO_2, of the radiation leaving the top of the atmosphere. Such measurements could provide a continuous global picture of the three-dimensional temperature distribution. This would be of immense value both to the study of the atmospheric circulation and to weather forecasting.

The instrumentation suggested was a grating spectrometer capable of several simultaneous measurements with a spectral resolution of 5 cm^{-1}. For a receiving cone of two degrees, corresponding to a few miles spatial resolution, the energy to be measured is in excess of 10^{-8} W per cm^2, and this can be detected with very high signal–noise ratio. An instrument of this type is now being built for the U.S. Weather Bureau.

Qualitative arguments were given for uniqueness of interpretation and sensitivity of the signals to the detailed thermal structure. These questions have since been investigated more quantitatively, and the results will be presented in this paper. A method for determining the high level ozone distribution from satellite measurements of scattered solar radiation will also be discussed.

It should be noted that the atmospheric models and frequencies chosen for this study will require modification for use in an actual interpretation scheme. The same is perhaps true of the radiation calculations.

II. THE TEMPERATURE SOUNDING

The atmosphere is divided into layers bounded by the isobaric surfaces labelled in Fig. 1, and the outgoing radiation in the vertical direction is calculated for all continuous combinations of temperature distribution shown. The lapse-rates within an individual layer

* Presented at the Helsinki Meeting of the IUGG, 29 July 1960, and at the New York Meeting of the Instrument Society of America, 26 September 1960.

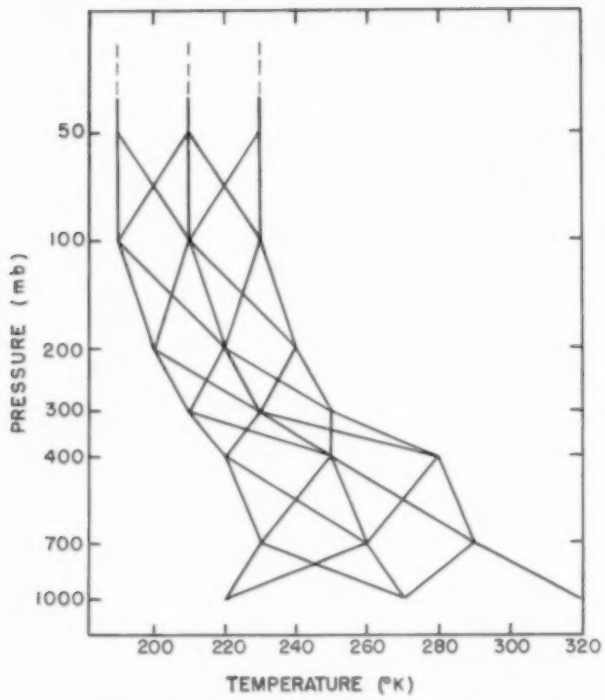

Fig. 1. Temperature variation with pressure for the 'model atmospheres.'

are taken as constant, and the atmosphere is assumed to be isothermal above 50 mb. Each of these model atmospheres emits radiation $\uparrow_{\nu 0}$ whose frequency dependence is a function of the temperature distribution:

$$\uparrow_{\nu 0} = \uparrow_{\nu 0}(T_{50}, T_{100}, \ldots T_{1000}). \tag{1}$$

The ground is assumed to be at 1000 mb, and the CO_2 concentration to be 2·6 mm STP per mb. The calculations were made by the method previously described by the author[2], with minor modifications to reduce computation time.

The problem is to reverse the procedure and determine the temperature structure from the measurement of the outgoing radiation. Since the atmosphere is assumed to be completely specified by the temperature at seven levels, their determination by inversion of the radiative transfer equations requires measurement of outgoing radiation at seven frequencies.

The model which 'best fits' a set of observations of outgoing radiation $\uparrow_\nu$ at the seven frequencies can be chosen by finding the one for which

$$\Sigma(\uparrow_\nu - \uparrow_{\nu 0})^2$$

is a minimum. Intercomparison of the various models by this method shows that any real solution would be unique.

A more detailed solution can then be found by a perturbation technique. At a given

frequency, the observed radiation can be expanded about that of the 'best-fitting' model in terms of temperature departure:

$$\frac{\uparrow_\nu - \uparrow_{\nu o}}{\uparrow_{\nu o}} = \Sigma c_i \Delta T_i + \Sigma c_{ij} \Delta T_i \Delta T_j + \ldots \qquad (2)$$

The coefficients for any one model are obtained by solving (2), using the $\uparrow_\nu$'s from as many other models as there are unknown coefficients.

The $\uparrow$'s and first order coefficients for the middle route are given in Table 1. A comparison of the coefficients shows that regardless of the frequencies chosen, the linear part

TABLE 1. $c_i = d \log_e \uparrow / dT$ (°C)

ν(cm^{-1})	675	685	695	700	705	710	730	745	760
$\uparrow$(c.g.s. units per sr.)	185·0	182·4	199·8	227·8	264·7	301·9	356·8	391·6	444·5
Pressure (mb)									
50	·0145	·0132	·0068	·0038	·0021	·0011	·0005	·0002	0
100	·0057	·0062	·0049	·0030	·0016	·0009	·0004	·0001	0
200	·0018	·0026	·0048	·0037	·0022	·0013	·0006	·0002	0
300	·0001	·0003	·0024	·0029	·0024	·0016	·0009	·0004	0
400	0	0	·0010	·0030	·0042	·0040	·0027	·0017	·0004
700	0	0	·0001	·0009	·0025	·0037	·0040	·0031	·0010
1000	0	0	0	0	·0003	·0015	·0055	·0086	·0135

of (2) forms a set of independent simultaneous equations that can be solved for the ΔT_i's. This solution can then be substituted in the quadratic terms and the process interated until a satisfactory convergence is obtained. Because of the smallness of second-order coefficients (all $c_{ij} < \cdot 0001$) it can be assumed that coefficients of order three or higher can be neglected if there are a sufficient number of models to obtain a reasonable first approximation.

The method was tested by assuming that the other models were observations and solving (2) as described above. The frequencies chosen were the first seven, i.e., 675, 685, 695, 700, 705, 710 and 730 cm^{-1}. Because of the large temperature differences, convergent solutions were not obtained in about one-eighth of the cases, for which neglecting the quadratic terms in the first approximation gave results that departed more from the 'actual' temperature distribution than the middle route did. Actually none of the models are a really close fit, so convergence can be assured with the use of a larger number of model atmospheres.

Typical results for the best cases are given in Table 2. Model No. 1 is one of the models used to determine the coefficients; but models No. 2 and 3 are independent cases. The first row for each model gives the actual temperature distribution. The second row gives the solution of (2), and the third and fourth rows give the solutions after addition of systematic errors of about one-third of one per cent and three per cent, respectively, to the $\uparrow$'s. It is seen that the temperature errors are approximately proportional to the magnitude of the systematic noise, and that even for a signal–noise ratio as low as 30:1 the computed temperatures are accurate to about three or four degrees. The temperature errors are of course also systematic.

Random noise was also added to the $\uparrow$'s, but the resulting errors in computed temperature were much worse. The errors, however, were oscillatory and means over

TABLE 2. COMPARISON OF COMPUTED WITH ACTUAL TEMPERATURES (°K) WITHOUT AND WITH SYSTEMATIC ERRORS. BASIC SIGNAL $\sim 3 \times 10^{-4}$ W/sr.

Pressure (mb)	50	100	200	300	400	700	1000
Middle Route	210·0	210·0	220·0	230·0	250·0	260·0	270·0
zero noise	210·0	210·0	220·0	230·0	250·0	260·0	270·0
$+10^{-7}$ W/sr.	210·2	210·5	220·0	230·5	250·2	260·3	270·1
$+10^{-6}$ W/sr.	211·7	214·8	219·8	235·1	251·5	262·9	270·8
Model No. 1	210·0	230·0	220·0	230·0	220·0	260·0	270·0
zero noise	210·0	229·9	220·2	229·7	220·1	259·9	270·0
$+10^{-7}$ W/sr.	210·2	230·4	220·1	230·2	220·1	260·3	270·1
$+10^{-6}$ W/sr.	211·8	234·3	219·6	234·4	220·8	263·7	271·0
Model No. 2	190·0	190·0	220·0	210·0	250·0	260·0	220·0
zero noise	189·9	190·1	219·9	209·8	250·3	259·8	220·1
$+10^{-7}$ W/sr.	190·2	190·5	220·4	209·8	250·8	259·8	220·3
$+10^{-6}$ W/sr.	192·7	193·9	223·7	210·3	255·4	259·3	222·2
Model No. 3	190·0	190·0	220·0	250·0	250·0	260·0	270·0
zero noise	190·1	189·5	220·4	249·8	250·3	259·8	270·0
$+10^{-7}$ W/sr.	190·3	190·2	220·4	250·4	250·3	260·1	270·1
$+10^{-6}$ W/sr.	192·2	195·8	220·8	255·6	250·5	263·1	270·8

several layers were about the same order as the errors due to the systematic noise. The effect of random errors can undoubtedly be reduced by a more careful choice of the frequencies used, based on an examination of the elements of the inverse matrix. The search for the best frequencies will continue. If it is unsuccessful either the number of atmospheric layers will have to be reduced or the sounding will be smoothed to at least such an extent that superadiabatic lapse-rates are eliminated.

To the extent that cloud and ground reflectivity at 15 μ can be neglected, the outgoing radiation for overcast conditions is the same as with an isothermal layer from the top of the clouds to the ground. Thus the method can be expected to give both the temperature and level of the cloud tops. The outgoing radiation with a non-uniform cloud cover can be obtained by a linear averaging; but the inversion problem would require the use of cloud pictures, taken simultaneously with radiation measurements. An examination of Table 1 will show that FRITZ's suggestions for eliminating the effect of clouds by sounding only the stratosphere[3] will not work, because of the impossibility of finding a sharp enough cut-off for the layered emission. The most accurate results will be obtained for each layer if the entire atmosphere is sounded.

The 15 μ band of CO_2 is overlapped by the rotational water band and the 14 μ ozone band. These effects can be taken into account if the distribution of H_2O and O_3 are known; and the latter can be determined by simultaneous measurements of radiation at frequencies where other bands of these molecules occur.

Once the temperature distribution is known through the CO_2 measurements, the water vapor distribution can be obtained by an analogous inversion of the radiative transfer equation after measurements in the semi-opaque region of the rotational water band or the 6·3 μ band. The transmission in the 15 μ region can then be corrected for the effect of water vapor, and the procedure iterated.

The effect of ozone can be determined similarly by measurements in the 9·6 μ band. Much of the ozone emission, however, will come from the upper stratosphere, and a

detailed knowledge of the ozone distribution at these heights would be desirable. Such knowledge would also be of considerable use in connection with studies of the stratospheric circulation. Even in the strong 9·6 μ band, however, the ozone is too transparent to obtain detailed enough information about the ozone distribution. We must therefore obtain the high level ozone distribution by a more sensitive method. If we at least knew that the high level ozone were in photochemical equilibrium, the temperature distribution in the stratopause region could be estimated by combined measurements in the 9·6 μ ozone band and high-resolution measurements in the strong central Q-branch of the 15 μ CO_2 band.

A method for determining the ozone distribution has been suggested by SINGER and WENTWORTH[4], as a means of studying the circulation of the lower stratosphere. GREENFIELD and KELLOGG have pointed out that large-particle scattering would cause a serious difficulty[5]. Moreover, it is doubtful that any detail in the ozone distribution can be obtained below the ozone maximum. It would be best therefore to choose the CO_2 frequencies where the ozone band does not have strong Q-branch maxima.

As will be seen below, the objections of Greenfield and Kellogg do not apply to a determination of the high-level ozone distribution; and a variant of the Singer–Wentworth procedure will be discussed.

VOL. 1 1961

III. THE OZONE SOUNDING

The ozone distribution in the upper stratosphere can be determined by measurement of scattered solar radiation at several wavelengths between 2600 and 3000 Ångstrom units. The principal is as follows: for a given solar elevation, the radiation scattered in any direction has relative components from each isobaric layer that differ markedly from wavelength to wavelength due to the variation of the ozone absorption coefficient. If measurements of upward radiation are made at carefully selected wavelengths, the radiative transfer equations can again be inverted to give the ozone concentration as a function of pressure.

This method is particularly sensitive for the region above the ozone maximum, where the Umkehr method is least sensitive and balloon measurements most difficult. It is also the region in which the ozone distribution is most likely to be in photochemical equilibrium, and accurate measurements would provide a check on the theory and a determination of the photochemical factors.

We will deliberately restrict ourselves to the upper stratosphere, therefore, so that we can simplify matters by assuming linear, first-order, Rayleigh scattering. The radiative transfer equation then becomes

$$\uparrow_\lambda = \alpha \downarrow_{\lambda 0} \int_0^\infty e^{-(1+\sec\Theta)\int_0^p k_\lambda w \, dx} dp, \tag{3}$$

where $\downarrow_{\lambda 0}$ is the incident solar radiation at wavelength λ, $\uparrow_\lambda$ the corresponding scattered radiation leaving the top of the atmosphere, $\alpha(\Theta)$ the scattering coefficient corresponding to the solar angle and the collection angle of the receiver, k_λ the ozone absorption coefficient, $w = dm/dp$ the ozone concentration, and p the pressure.

To simplify the evaluation of (3), the temperature dependence of k_λ was ignored and the atmospheric layers given in the second column of Table 3 were each assumed to have the constant ozone concentrations given in the first column. DÜTSCH's distribution was followed[6]. For actual use in an ozone distribution determination, a continuous distribution

of ozone should be assumed, and the temperature variation of the absorption coefficient taken into account. For the stratification used in this study, (3) becomes

$$\uparrow_\lambda = \frac{\pi \downarrow_{\nu_0}}{(1 + \sec\Theta)k_\lambda}\left[\frac{1}{w_0} - \sum_{i=0}^{I}\left(\frac{1}{w_i} - \frac{1}{w_{i+1}}\right) e^{-(1+\sec\Theta)k_\lambda \sum_{j=0}^{i} w_j(\Delta p)_j}\right] \tag{4}$$

For the special case of constant composition, it is seen from (4) that the outgoing radiation is inversely proportional to the concentration. This gives an indication of the sensitivity of the method.

The last seven columns of Table 3 give, for the six layers, the calculated value of the relative change in $\uparrow_\lambda$ per relative change in $w = \mathrm{d}m/\mathrm{d}p$, i.e. the quantities c_i in the expansion

$$\frac{\mathrm{d}\uparrow}{\uparrow} = -\sum c_i \frac{\mathrm{d}\, w_i}{w_i} \tag{5}$$

as functions of $(1 + \sec\Theta)k_\lambda$.

The bottom layer was taken to infinity. This is serious only for the $(1 + \sec\Theta)k_\lambda = 16$ column, for which ten per cent of the outgoing radiation is scattered below the 16 mb level. For $(1 + \sec\Theta)k_\lambda = 32$, only one per cent comes from below the 16 mb level. Since the scattering coefficient per atmosphere is of the order of unity, it is obvious from the sharp cut-offs that the assumptions used to derive (3) are reasonable. This is also verified by the results of calculations by J. V. Dave (private communication).

The wave-lengths corresponding to the values of $(1 + \sec\Theta)k_\lambda$ were obtained by interpolation from the VIGROUX tables[7] for an air-mass of one and three, and are given in the second and third rows of Table 3. It is seen that measurements at seven wavelengths

TABLE 3. $c_i = \mathrm{d}\log\uparrow/\mathrm{d}\log w_{o_3}$

$(1 + \sec\Theta)\,k_\lambda$ (cm^{-1} S.T.P.) (base e)		16	32	64	128	256	512	1024
$\lambda(\sec\Theta = 1)$ Å		3010	2960	2910	2860	2780	2630	
$\lambda(\sec\Theta = 3)$ Å			3010	2960	2910	2860	2780	2630
$w = \mathrm{d}m/\mathrm{d}p$	$\uparrow/\downarrow\alpha$(mb)	9·253	5·681	3·560	2·231	1·391	·857	·516
(cm S.T.P./mb)	Δp(mb)							
·0015	0–·5	·01	·02	·04	·09	·16	·29	·47
·0025	·5–1	·02	·04	·06	·11	·17	·23	·21
·0035	1–2	·05	·08	·14	·20	·23	·18	·07
·0050	2–4	·11	·17	·22	·22	·12	·03	·01
·0070	4–8	·21	·23	·17	·06	·01	0	0
·0100	>8	·34	·14	·03	0	0	0	0

are sufficient to give the ozone amounts in the six layers for a wide range of solar angles.

Comparison of Table 3 with Table 1 shows that the ozone determination method can be made to be as sensitive as the temperature sounding method, or even more sensitive.

The inversion will be carried out in a manner analogous to that for the temperature sounding, and the results will be reported in a future paper. It can already be seen from the coefficients in Table 3, however, that the accuracy with which the ozone distribution can be obtained is not an order of magnitude less than the accuracy of the measurements.

VOL
1
196

Acknowledgements—The author is grateful to Mrs. Barbara Grant for programming the calculations, which were done on the digital computer at the MIT Computation Center. The work was supported by the Office of Naval Research.

REFERENCES

1. L. D. KAPLAN, Inference of atmospheric structure from remote radiation measurements, *J. Opt. Soc. Amer.*, **49**, 1004 (1959).
2. L. D. KAPLAN, *A method for calculation of infrared flux for use in numerical models of atmospheric motion*, in B. BOLIN, *The atmosphere and the sea in motion*, p. 170. Rockefeller Institute Press, New York and The University Press, Oxford (1959).
3. S. FRITZ, Satellite meteorology, *Trans. Amer. Geophys. Un.*, **41**, 217 (1960).
4. S. F. SINGER and R. C. WENTWORTH, A method for the determination of the vertical ozone distribution from a satellite, *J. Geophys. Res.*, **62**, 299 (1957).
5. S. M. GREENFIELD and W. W. KELLOGG, Calculations of atmospheric infrared radiation as seen from a meteorological satellite, *J. Met.*, **17**, 283 (1960).
6. H. U. DÜTSCH, *Evaluation of the Umkehr effect by means of a digital electronic computer*, Sci. Report No. 1. Lichtklimatisches Observatorium, Arosa (1957).
7. E. VIGROUX, Absorption de l'ozone à 18° audessous de 3130 Å. *C. R. Acad. Sci.*, **234**, 2529 (1952).

VOL.
1
1961

J. Quant. Spectrosc. Radiat. Transfer. Vol. 1, pp. 96–103. Pergamon Press Ltd. Printed in Great Britain

APPROXIMATE INFRARED EMISSIVITY CALCULATIONS FOR NO AT ELEVATED TEMPERATURES*

S. S. PENNER, † K. G. P. SULZMANN and C. B. LUDWIG
Convair, A Division of General Dynamics Corporation, San Diego 12, California
(*Received* 30 *December* 1960)

Abstract—Analytical expressions are derived for the spectral and total emissivities of diatomic gases at elevated temperatures. Our analytical formulae reproduce the numerical results obtained for NO by Breene with acceptable precision.

I. INTRODUCTION

THE theoretical calculation of gas emissivities has been described in a recent book to which we shall refer henceforth as Q[1]. We shall amplify the published results by deriving analytical expressions for the spectral and (hemispherical) engineering infrared emissivities of diatomic gases at temperatures which are so high that we may assume essentially a continuum distribution of rotational line structure. The results should be applicable in practice whenever the weak line approximation may be used. Our method is similar to a treatment first employed by KIVEL, MAYER and BETHE[2] in emissivity calculations on the ultraviolet bands of NO. This method of treatment for electronic band systems has been refined recently by KECK, CAMM, KIVEL and WENTINK[3] in order to account for the influence of vibrational structure on emissivities.

We shall demonstrate the utility of our formulae for approximate infrared spectral emissivity calculations by showing that the numerical results obtained by Breene for NO in air are reproduced, in good approximation.

II. OUTLINE OF THEORETICAL CONSIDERATIONS

A. Calculation of spectral absorption coefficients and of spectral emissivities for fundamental vibration–rotation bands

Consider transitions between the ground state with vibrational quantum number n'' and rotational quantum number j'' and the upper state n', j'. Since both vibrational levels belong to the same electronic state of a given diatomic molecule, we may write the respective rotational energies (ε_j) in the form

$$\varepsilon_{j''} = j''(j'' + 1)hcBe$$

and

$$\varepsilon_{j'} = j'(j' + 1)hcBe$$

where h is Planck's constant, c is the velocity of light and Be the rotational constant for the given state. The selection rules allow $\Delta j = \pm 1$ except that for asymmetric top

* This work was supported by the Army Rocket and Guided Missile Agency under Contract No. DA-04-495-ORD 3112, ARPA Order No. 39-59, Task 2.
† Consultant; permanent address: Division of Engineering, California Institute of Technology, Pasadena, California.

VOL. 1 1961

molecules the transitions $\Delta j = 0$ are also allowed. We shall assume that the contributions of the Q-branches to the total and spectral emissivities may be neglected at temperatures which are sufficiently high that, for all practical purposes, $j' \simeq j''$. Subject to this last approximation, we note that

$$hc\omega = (\varepsilon_{n'} - \varepsilon_{n''}) \pm 2j'hcBe$$

where ω is the observed wave number for the transition $(n'', j'') \rightarrow (n', j')$ if $\varepsilon_{n''}$ and $\varepsilon_{n'}$ are the corresponding vibrational energies. Hence

$$\varepsilon_{j''} \simeq (j')^2 hcBe = \left(\frac{\omega}{2Be} - \frac{\varepsilon_{n'} - \varepsilon_{n''}}{2hcBe}\right)^2 hcBe$$

and*

$$\frac{df_{n',n''}}{d\omega} = \frac{1}{2} f_{n',n''} \frac{|hc\omega - (\varepsilon_{n'} - \varepsilon_{n''})|}{2BekT} \exp\left\{-\frac{[hc\omega - (\varepsilon_{n'} - \varepsilon_{n''})]^2}{4hcBekT}\right\}. \tag{1}$$

In equation (1), $f_{n',n''}$ is the total f-number for the $n' \rightarrow n''$ transition, k is the Boltzmann constant, and T denotes the temperature. Equation (1) is obtained by assuming that

$$\frac{df_{n',n''}}{d\omega} = \text{constant} \times f_{n',n''} \times \frac{d}{d\omega} \exp(-\varepsilon_{j''}/kT)$$

and determining the constant in such a way that

$$2\left|\int_{\omega-(\varepsilon_{n'}-\varepsilon_{n''})/hc}^{\infty} \frac{df_{n',n''}}{d\omega}\, d\omega\right| = f_{n',n''}.$$

It is now convenient to write

$$f_{n',n''} = f_{n'-n'',0} x^2_{n',n''} \tag{2}$$

where $f_{n'-n'',0}$ is the f-number for the transition from the ground state that falls in the same spectral region as the transition $n' \rightarrow n''$. Using the general relation†

$$P_{\omega_{n',n''}} \simeq \frac{\pi e^2}{mc^2} \frac{N_{n''}}{p} \frac{df_{n',n''}}{d\omega} (1 - e^{-hc\omega/kT})$$

for the spectral absorption coefficient at the wave number ω produced by the vibrational transition $n' \rightarrow n''$ (e and m denote, respectively, the electronic charge and mass; $N_{n''}/p$ represents the total number of molecules in the ground vibrational state per unit volume per unit pressure), we find for the spectral absorption coefficient P_ω the following explicit relation:

$$P_\omega = \sum_{n''} P_{\omega_{n',n''}} \simeq \frac{1}{2} \frac{\pi e^2}{mc^2} f_{n'-n'',0} \frac{N_T}{pQ_v} \frac{hc}{2BekT} [1\text{-}\exp(-hc\omega/kT)]$$
$$\times \sum_{n''} x^2_{n',n''} [\exp(-\varepsilon_{n''}/kT)] |\omega - \omega_{n',n''}| \exp\left[\frac{-hc(\omega - \omega_{n',n''})^2}{4BekT}\right] \tag{3}$$

where N_T/p is the total number of molecules of the emitting species per unit pressure per unit volume.

* Compare Q, p. 398. Equation (1) provides essentially a relation between the local value of the spectral absorption coefficient and the product of (integrated intensity) and (population in the ground state) for a given transition.

† Q, equations (14–7) and (2–19).

Equation (3) takes a particularly simple form to the harmonic oscillator approximation since only the transitions $n' \rightarrow n' - 1$ are allowed in emission and

$$\omega_{n',n''} = \omega_0 = \text{constant},$$

$$\varepsilon_{n''} = (n'' + \tfrac{1}{2})hc\omega_0,\ x^2_{n',n''} = n' = n'' + 1,^{*} \text{ viz.},$$

$$P_{\omega,h.o.} = \frac{1}{2}\frac{\pi e^2}{mc^2} f_{1,0} \frac{N_T}{pQ_v} [1\text{-exp}(-hc\omega/kT)]\,[\exp(-hc\omega_0/2kT)]\,[1\text{-exp}(-hc\omega_0/kT)]^{-2} \times \frac{hc|\omega - \omega_0|}{2BekT}\left[\exp - \frac{hc(\omega-\omega_0)^2}{4BekT}\right] \tag{3a}$$

where the subscript *h.o.* identifies results that are applicable to the harmonic oscillator approximation and $\omega \simeq \omega_0$ for harmonic transitions.†

The spectral emissivities for gases distributed uniformly through the length l at a partial pressure p may be computed readily from equations (3) and (3a). Thus

$$\varepsilon_\omega = 1\text{-exp}(-P_\omega pl) \tag{4}$$

or

$$\varepsilon_{\omega,h.o.} = 1\text{-exp}(-P_{\omega,h.o.}pl). \tag{4a}$$

B. Approximate calculation of spectral absorption coefficients and of spectral emissivities for the first overtone region

We may derive an approximate expression for the spectral absorption coefficient in the first overtone region by noting that equation (3) leads to the relation

$$P_{\omega,overtone} \simeq \frac{1}{2}\frac{\pi e^2}{mc^2} f_{2,0} \frac{N_T}{pQ_v}\frac{hc}{2BekT}[1\text{-exp}(-hc\omega/kT)] \times |\omega - \omega_{2,0}|\left\{\exp\left[\frac{-hc(\omega-\omega_{2,0})^2}{4BekT}\right]\right\}[\exp(-hc\omega_0/2kT)] \times \sum_{n''}[\tfrac{1}{2}(n''+2)(n''+1)]\,[\exp(-n''hc\omega_0/kT)] \tag{5}$$

since‡

$$\chi^2_{n''+2,n''} \simeq \tfrac{1}{2}(n''+2)(n''+1).$$

---

* Q, equation (7–56).

† Equation (3a) is identical with equation (11–141) of Q, viz.,

$$P_{\omega,h.o.} = \bar{P}_{VR} = \frac{\alpha}{4\sqrt{BC}}u' \exp\left(-\frac{u'^2}{4\gamma}\right),$$

which was first obtained by J. A. L. Thomson.

The validity of the preceding identification may be demonstrated as follows. The quantity α in equation (11–141) of Q represents

$$\sum_n \alpha_{n,n+1}$$

where $\alpha_{n,n+1}$ is the integrated absorption for the band corresponding to the transitions $n \rightarrow n+1$. But, according to equation (7–91) of Q,

$$\sum_n \alpha_{n,n+1} \simeq \alpha_{0,1}[1\text{-exp}(-hc\omega_0/kT)]^{-2}.$$

Furthermore [compare equation (2–21) of Q],

$$\alpha_{0,1} = \frac{\pi e^2}{mc^2} f_{1,0}\frac{N_T}{pQ_v}[\exp(-hc\omega_0/2kT)]\,[1\text{-exp}(-hc\omega/kT)];$$

$B = C = Be$, $u' = hc\,|\omega - \omega_0|/kT$, and $\gamma = hcBe/kT$. Thus the identification of equation (3a) with equation (11–141) of Q has been established.

‡ Q, equation (7–95).

Hence

$$P_{\omega,\,overtone} \simeq \frac{1}{2}\frac{\pi e^2}{mc^2}\left(\frac{\alpha_{0,2}}{\alpha_{0,1}}\right)_{rt} f_{1,0}\,\frac{N_T}{pQ_v}\,[\exp(-hc\omega_o/2kT)]$$
$$\times\,[1\text{-}\exp(-hc\omega/kT)]\,\frac{hc|\omega-\omega_{2,0}|}{2BekT}\left[\exp-\frac{hc(\omega-\omega_{2,0})^2}{4BekT}\right] \qquad (6)$$
$$\times\,[1\text{-}\exp(-hc\omega_o/kT)]^{-3}$$

since [see equation (7–91) of Q]

$$\frac{\sum_m \alpha_{m,\,m+2}}{\sum_m \alpha_{m,\,m+1}} \simeq \frac{\alpha_{0,2}}{\alpha_{0,1}}\,[1\text{-}\exp(-hc\omega_o/kT)]^{-1},$$

$$f_{2,0}\,\frac{[1\text{-}\exp(-2hc\omega_o/kT)]}{[1\text{-}\exp(-hc\omega_o/kT)} = \frac{\alpha_{0,2}}{\alpha_{0,1}} f_{1,0}$$

and the constant $f_{2,0}$ is conveniently evaluated from room temperature (rt) data by using the preceding relation, i.e.,

$$f_{2,0} \simeq \left(\frac{\alpha_{0,2}}{\alpha_{0,1}}\right)_{rt} f_{1,0}.$$

The spectral emissivity in the first overtone region is given by the expression

$$\varepsilon_{\omega,\,overtone} = 1\text{-}\exp(-P_{\omega,\,overtone}pl). \qquad (7)$$

C. Approximate calculation of hemispherical engineering emissivities for transparent gases

For transparent gases distributed uniformly throughout the optical depth pl, the emitted spectral radiancy is

$$R_\omega = R_\omega{}^o P_\omega pl$$

where $R_\omega{}^o$ is the spectral blackbody radiancy. Using equation (3a), we obtain the following explicit relation for the fundamental region:

$$R_\omega = \frac{1}{2}\left(\frac{\pi^2e^2}{mc^2}\right)(hc^2\omega^3) f_{n'-n'',0}\,\frac{N_T l}{Q_v Q_r'}\,[\exp(-hc\omega/kT)]\sum_{n''}\chi^2_{n,\,n''}|\omega-\omega_{n',\,n''}|$$
$$\times\,[\exp(-\varepsilon_{n''}/kT)]\left[\exp-\frac{hc(\omega-\omega_{n',\,n''})^2}{4BekT}\right] \qquad (8)$$

where

$$Q_r' = BekT/hc$$

is Be^2 times the rotational partition function. To the harmonic oscillator approximation we find that

$$R_{\omega,\,h.o.} \simeq \frac{1}{2}\left(\frac{\pi^2e^2}{mc^2}\right) hc^2\omega^3 f_{1,0}\,\frac{N_T l}{Q_v Q_r'}\,[\exp(-hc\omega_o/2kT)]\,[\exp(-hc\omega/kT)]$$
$$\times\,[1\text{-}\exp(-hc\omega_o/kT)]^{-2}|\omega-\omega_o|\left[\exp-\frac{hc(\omega-\omega_o)^2}{4BekT}\right]. \qquad (8a)$$

The (hemispherical) engineering emissivity is defined by the expression

$$\varepsilon_{1,0} = \frac{2}{\sigma T^4}\int_0^\infty R_\omega d\omega. \tag{9}$$

Hence, to the harmonic oscillator approximation,

$$\varepsilon_{1,0;\,h.o.} \simeq \frac{15e^2}{\pi^3 mc^2\omega_o}\left(\frac{hc\omega_o}{kT}\right)^4 f_{1,0}\frac{N_T l}{Q_v}[\exp(-3hc\omega_o/2kT)]\,[1-\exp(-hc\omega_o/kT)]^{-2}. \tag{10}$$

Similarly, for the first overtone region,

$$\varepsilon_{2,0} = \frac{2}{\sigma T^4}\int_0^\infty R_{\omega,\,overtone}\,d\omega \tag{11}$$

whence, using equation (6) and the transparent gas approximation,

$$R_{\omega,\,overtone} \simeq \frac{1}{2}\left(\frac{\pi^2 e^2}{mc^2}\right) hc^2\omega^3\left(\frac{\alpha_{0,2}}{\alpha_{0,1}}\right)_{rt} f_{1,0}\frac{N_T l}{Q_v Q_r}[\exp(-hc\omega_o/2kT)]$$
$$\times\,[\exp(-hc\omega/kT)]\,[1\text{-}\exp(-hc\omega_o/kT)]^{-3}|\omega-\omega_{2,0}|\left[\exp\frac{-hc(\omega-\omega_{2,0})^2}{4BekT}\right] \tag{12}$$

and

$$\varepsilon_{2,0} \simeq \frac{15e^2}{\pi^3 mc^2(2\omega_o)}\left(\frac{2hc\omega_o}{kT}\right)^4\left(\frac{\alpha_{0,2}}{\alpha_{0,1}}\right)_{rt} f_{1,0}\frac{N_T l}{Q_v}[\exp\text{-}(5hc\omega_0/2kT)]$$
$$\times\,[1\text{-}\exp(-hc\omega_o/kT)]^{-3}. \tag{13}$$

Comparison of equations (13) and (10) shows that

$$\frac{\varepsilon_{2,0}}{\varepsilon_{1,0;\,h.o.}} \simeq 8\left(\frac{\alpha_{0,2}}{\alpha_{0,1}}\right)_{rt}[\exp(-hc\omega_o/kT)]\,[1\text{-}\exp(-hc\omega_o/kT)]^{-1}. \tag{14}$$

The ratio $\varepsilon_{2,0}/\varepsilon_{1,0;\,h.o.}$ should not be confused with

$$\lim_{pl\to 0}\frac{\int\varepsilon_{\omega,\,overtone}d\omega}{\int\varepsilon_{\omega,\,h.o.}d\omega} = \frac{\int P_{\omega,\,overtone}d\omega}{\int P_{\omega,\,h.o.}d\omega}$$
$$\simeq \left(\frac{\alpha_{0,2}}{\alpha_{0,1}}\right)_{rt}[1-\exp(-hc\omega_o/kT)]^{-2}\,[1-\exp(-2hc\omega_o/kT)] \tag{15}$$

which may be obtained directly by integrating tabulated spectral emissivity data for transparent gases.

III. APPROXIMATE SPECTRAL EMISSIVITY CALCULATIONS FOR NO

Spectral emissivities have been computed for NO in air at various optical depths by using equations (3a) and (4a) for the fundamental region and equations (6) and (7) for the first overtone region. These spectral emissivity data are compared* in Figs. 1–5 with the

* For the purposes of this comparison, we have employed the same integrated intensity estimates as were used by Breene. These numerical results are practically identical with the values reported by PENNER and WEBER[4].

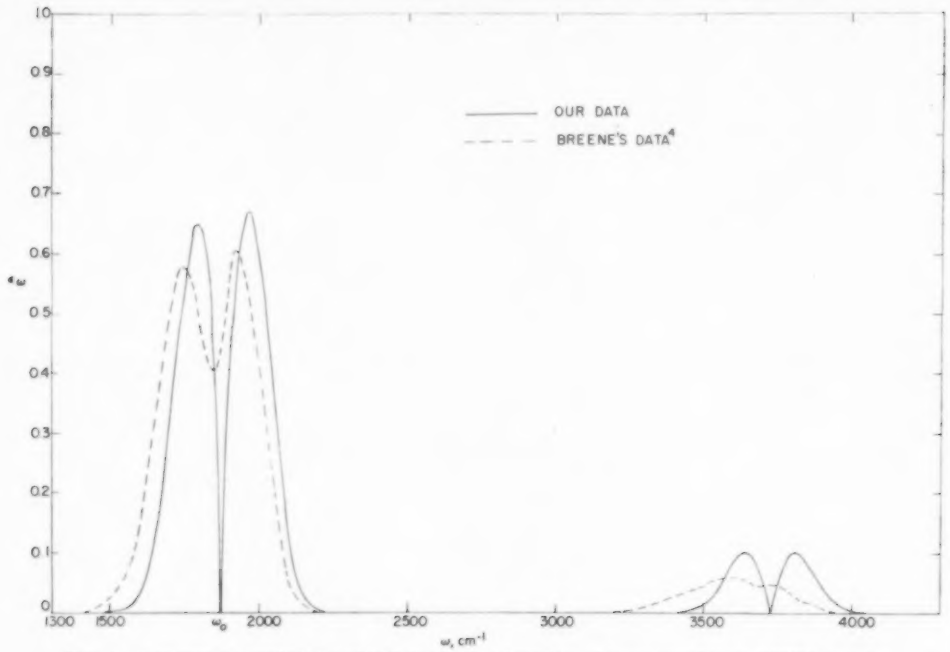

FIG. 1. The spectral emissivity of NO in air as a function of wave number at 3000°K and ten times normal density for an optical depth of 47·1 cm-atmos.

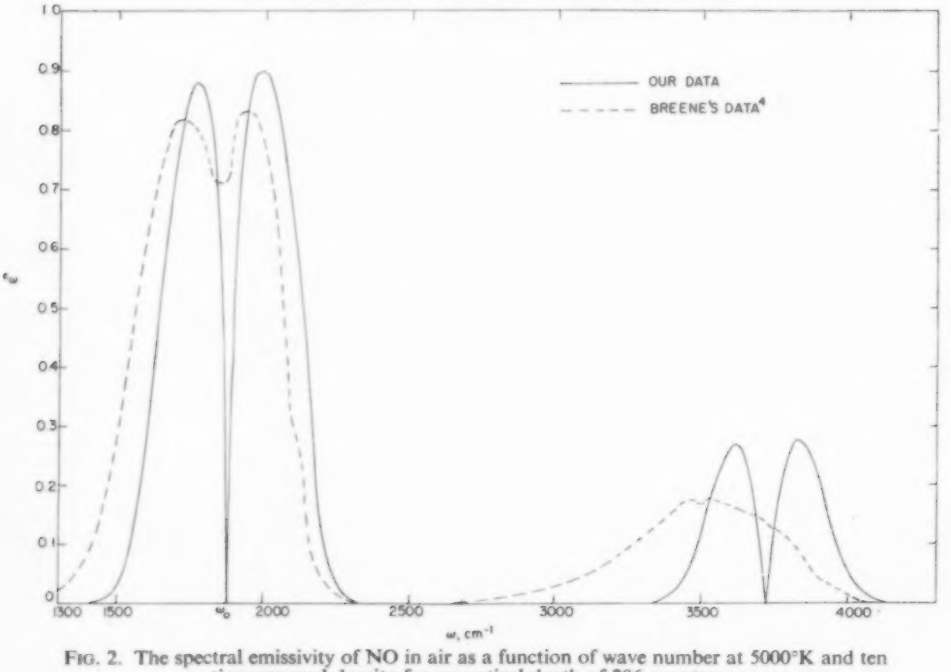

FIG. 2. The spectral emissivity of NO in air as a function of wave number at 5000°K and ten times normal density for an optical depth of 206 cm-atmos.

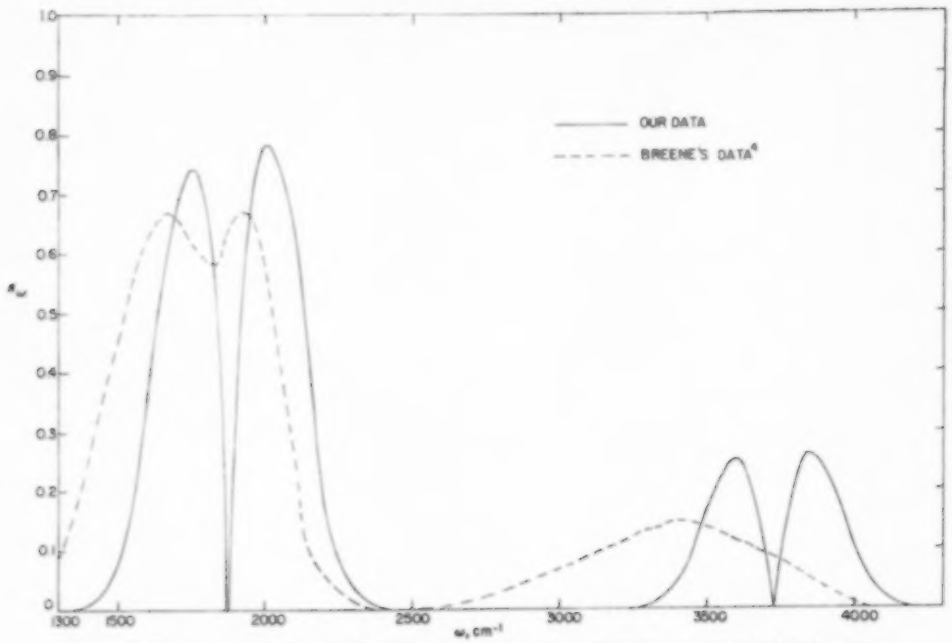

FIG. 3. The spectral emissivity of NO in air as a function of wave number at 7000°K and ten times normal density for an optical depth of 222 cm-atmos.

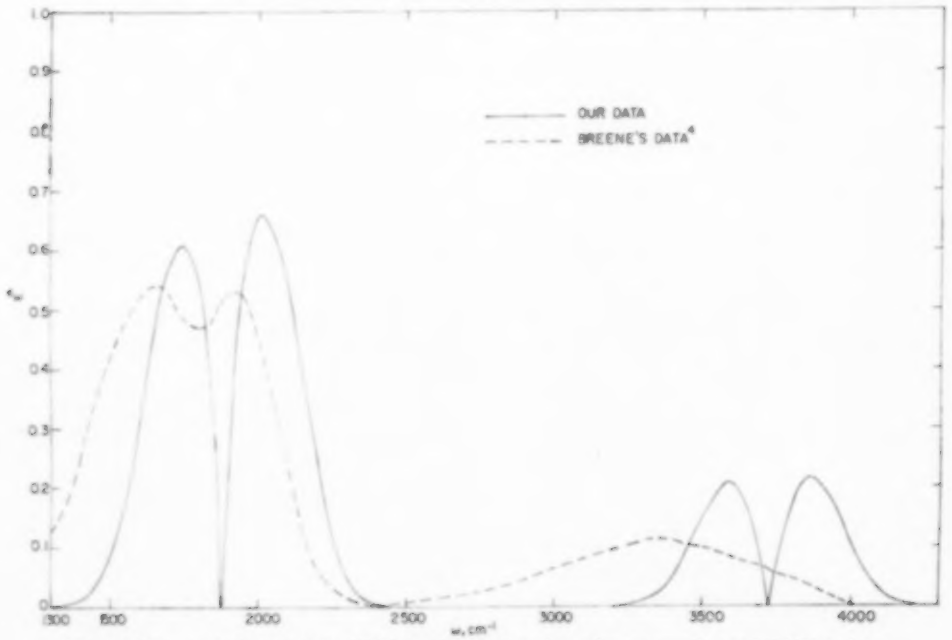

FIG. 4. The spectral emissivity of NO in air as a function of wave number at 8000°K and ten times normal density for an optical depth of 191 cm-atmos.

VOL
1
196

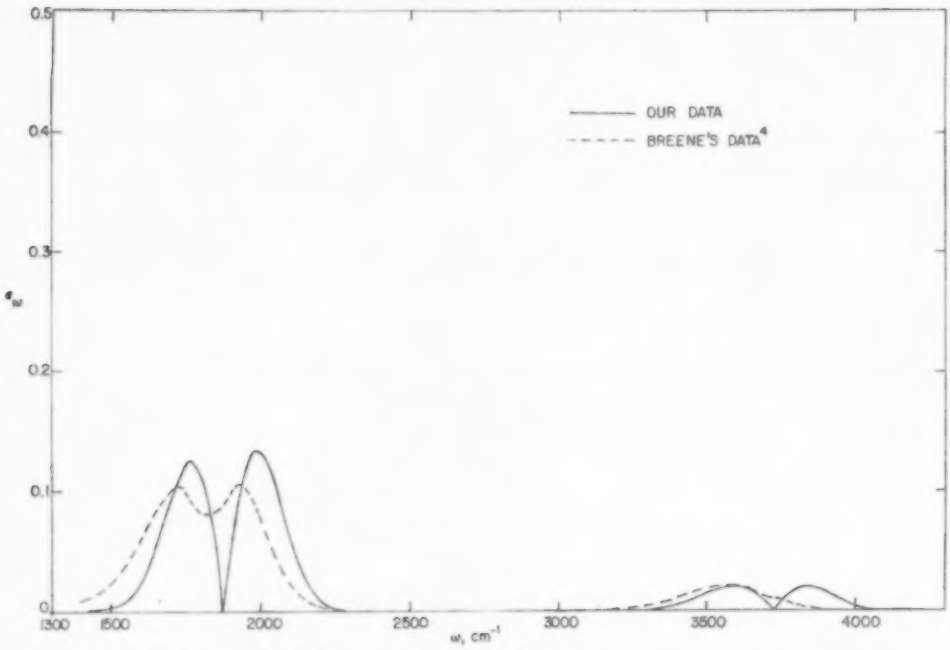

FIG. 5. The spectral emissivity of NO in air as a function of wave number at 5000°K and normal density for an optical depth of 13 cm-atmos.

results of numerical computations performed by BREENE[5]. Reference to Figs. 1–5 shows that our approximate theoretical values for the spectral emissivities agree reasonably well with the results obtained from machine computations. The most notable discrepancy is a small shift toward larger wave numbers for the extrema of the spectral emissivities computed from our formulae. This shift is expected since we have neglected all anharmonicity corrections. Slight errors have also been introduced because we have ignored vibration–rotation interactions. With the suggested modifications, the analysis should yield improved results, albeit at the expense of considerable complication.

The excellent agreement between our calculated estimates and Breene's data for $\int \epsilon_\omega d\omega$ for the fundamental and first overtone bands may be judged by noting, for example, that both of our values at 5000°K for normal density are higher than Breene's by only about 2 per cent.

REFERENCES

1. S. S. PENNER, *Quantitative Molecular Spectroscopy and Gas Emissivities*, Addison–Wesley Publishing Co., Reading, Mass. (1959). A list of errata to this book may be obtained from the author.
2. B. KIVEL, H. MAYER and H. A. BETHE, *Ann. Phys.* **2**, 57 (1957).
3. J. C. KECK, J. C. CAMM, B. KIVEL and T. WENTINK, *Ann. Phys.* **7**, 1 (1959).
4. S. S. PENNER and D. WEBER, *J. Chem. Phys.* **21**, 649 (1953).
5. R. G. BREENE, *J. Chem. Phys.* **29**, 512 (1958).

J. Quant. Spectrosc. Radiat. Transfer, Vol. 1, pp. 104–134. Pergamon Press Ltd. Printed in Great Britain

EQUILIBRIUM EMISSIVITY CALCULATIONS FOR A HYDROGEN PLASMA AT TEMPERATURES UP TO 10,000°K*†

D. B. OLFE‡
Daniel and Florence Guggenheim Jet Propulsion Center, California Institute of Technology
Pasadena, California

(*Received* 4 *December* 1960)

Abstract—The important equilibrium emission processes in a hydrogen plasma have been investigated in the temperature range between 300°K and 10,000°K for pressures up to several hundred atmospheres. Representative emissivity calculations have been carried out for a transparent gas. For a nontransparent gas, the particular case of a total pressure of 100 atmos and a mean beam length of 30 cm has been considered.

Important emissivity contributions are made by the pressure-induced fundamental vibration–rotation band and rotational lines of H_2 at the lower temperatures, i.e., below approximately 4500°K. Above this temperature, the bound-free and free-free transitions of the H^- ion and the continuum and line radiation of the H atom are the most important contributors to the emissivity. The following emission processes also have been investigated: the bound-free transitions of the H_2^+ ion, free-free transitions of colliding H atoms and H^+ ions, electronic transitions of the H_2 molecule, quadrupole vibration–rotation transitions of the H_2 molecule, and vibration–rotation transitions of the HD molecule. In addition, the effects of the lowering of the ionization potentials by the fields of plasma ions and of the very broad wings of the Lyman α-line have been considered.

I. INTRODUCTION

RADIANT-HEAT transfer from a hydrogen plasma is of considerable interest in a number of engineering applications, e.g., power plants utilizing hydrogen as a driving fluid. For these applications it may be necessary to consider pressures up to several hundred atmospheres and temperatures from several hundred °K to many thousands of °K. Accordingly, the emission for temperatures between 300°K and 10,000°K at high as well as low pressures is considered here (see reference 1 for a calculation of the continuous emission above 10,000°K). Above 10,000°K the emissivity will be essentially unity for high pressures and moderate or large mean beam lengths[1] (cf. Fig. 16).

Only equilibrium radiation from a pure hydrogen plasma is considered. However, this work may be adapted easily to the case where other constituents are present.

II. EQUILIBRIUM COMPOSITION

For the calculation of the equilibrium composition it is sufficient to consider the species H_2, H, H^+, e^-, H^- and H_2^+. For low ion densities the equilibrium composition may be calculated using equilibrium constants determined from the dissociation and ionization (Saha) equations. The equilibrium compositions given in Figs. 1–3 were calculated in this manner for total pressures of 1, 10, and 100 atm and temperatures up to 10,000°K.

* This work was supported, in part, by the Office of Naval Research under Contract Nonr–220(03), NR 015 401 and, in part, by the Office of Scientific Research of the Air Research and Development Command under Contracts AF 18(603)–2, and AF 49(638)–984.

† An account of this work was given at the *Symposium on Quantitative Spectroscopy and Selected Military Applications*, March 28–29, 1960, at the California Institute of Technology.

‡ Now Associate Professor of Aeronautics, New York University.

VOL
1
196

In the calculation of the equilibrium composition at low ion densities it is assumed that an electron moves in a potential determined only by the core of a single atom (or ion or molecule), which is true only for an isolated atom. As the ion density is increased, some of the bound electrons become free to pass over to nearby ions because the potential barrier is lowered by the fields of the ions (cf. Fig. 4). Therefore, in addition to the electrons which would be free in a dilute plasma, there exist electrons with a degree of 'freedom' that

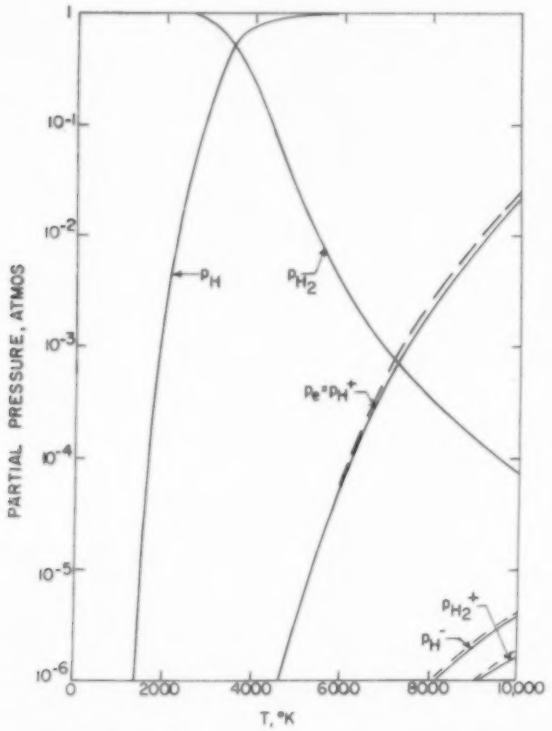

FIG. 1. Equilibrium composition as a function of temperature for total pressure $p_T = 1$ atm. The difference between p_e and p_{H^+} is too small to be shown. The dashed curves include the correction for the lowering of the ionization potential.

depends on their energy and the surrounding ion density. These electrons wander around in the potential troughs between close ions.

In order to retain the concept of regarding any electron as being either bound or free, various simple models have been proposed for the plasma from which a lowering of the ionization potential due to the ion and electron densities may be calculated. UNSÖLD[2] considers the model of an electron passing from an atom to a single perturbing ion, situated at a distance equal to the mean distance between the atom and the perturbing ions. For this model, the lowering of the hydrogen atom ionization potential is

$$\Delta I = 7 \times 10^{-7}(N_i)^{\frac{1}{3}}\text{eV} \qquad (1)$$

where N_i is the number of ions per cm^3. In the treatments by ECKER and WEIZEL[3] and by MARGENAU and LEWIS[4] the electron is considered to be moving in a Debye field with the lowering of the ionization potential obtained by solving the Schrödinger equation.

In addition to the change in equilibrium composition, emissivity calculations will be directly affected by the ion density since the transition probabilities depend on the potential

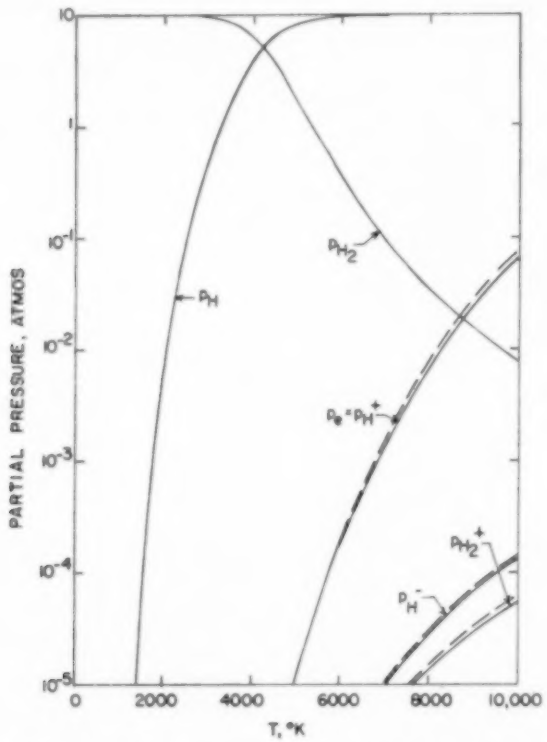

FIG. 2. Equilibrium composition as a function of temperature for $p_T = 10$ atm. The difference between p_e and p_{H^+} is too small to be shown. The dashed curves include the correction for the lowering of the ionization potential.

curves along which the electron moves. This direct effect is proportional to the change in the square of the matrix element, which will not be of a greater order of magnitude than the change in equilibrium composition for the temperatures of interest here. The simple formula of Unsöld may therefore be used to determine under what conditions the effects of ion fields become important.

Since the electron density is determined primarily by the ionization of the hydrogen atom and because the lower effective core charge of the H^- ion produces a smaller change in ionization potential, the change in the ionization potential of H^- is neglected[1]. The change in ionization potential of H_2 is taken to be the same as that of H. In the temperature

VOL. 1 1961

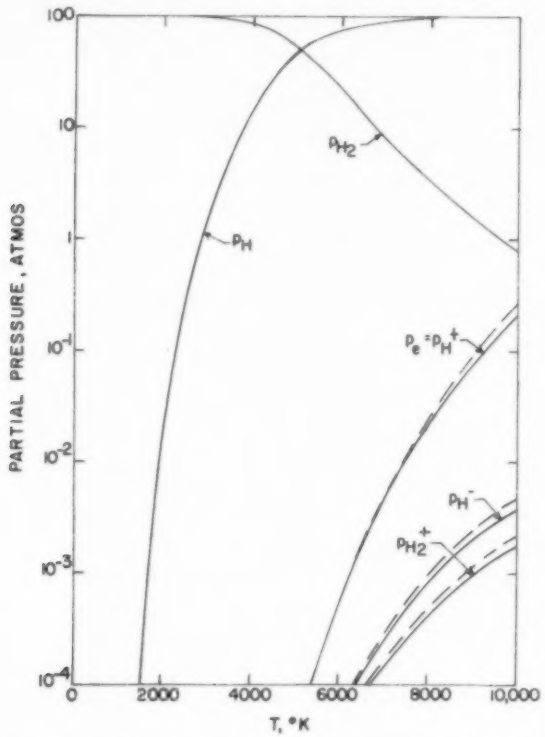

FIG. 3. Equilibrium composition as a function of temperature for $p_T = 100$ atm. The difference between p_e and p_{H^+} is too small to be shown. The dashed curves include the correction for the lowering of the ionization potential.

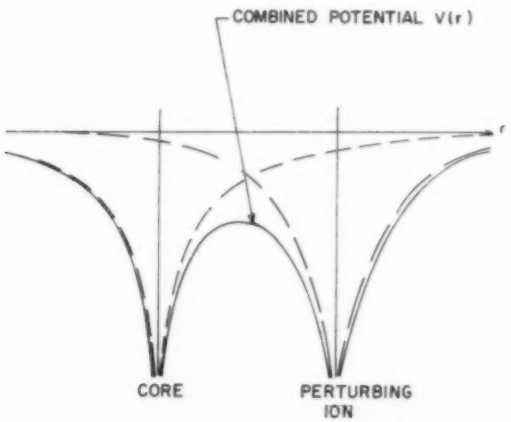

FIG. 4. Potential energy curves for an electron in the field of an atom (or ion or molecule) core and an ion.

range of interest, viz., 5000°K–10,000°K, the partial pressures p_e, p_{H^+}, p_{H^-} and $p_{H_2^+}$ are all much smaller than the total pressure p_T, and $p_e \simeq p_{H^+}$. Therefore,

$$\frac{p_e}{(p_e)_0} \simeq \frac{p_{H^+}}{(p_{H^+})_0} \simeq \frac{p_{H^-}}{(p_{H^-})_0} \simeq \frac{(p_{H_2^+})}{(p_{H_2^+})_0} \simeq \exp\frac{\Delta I}{2kT} \tag{2}$$

where k is the Boltzmann constant, T the temperature, and the subscript zero denotes the partial pressure for no lowering of the ionization potential. Using equation (1) for ΔI, the calculated values of $\exp(\Delta I/2kT)$ are given in Table 1 and the resulting partial pressures

TABLE 1. THE QUANTITY $\exp(\Delta I/2kT)$ FOR VARIOUS TOTAL PRESSURES AND TEMPERATURES

T (°K)	$p_T = 1$ atm	$p_T = 10$ atm	$p_T = 100$ atm
5000	1·01	1·02	1·03
6000	1·03	1·04	1·06
7000	1·05	1·07	1·10
8000	1·07	1·10	1·15
9000	1·09	1·13	1·21
10,000	1·11	1·16	1·27

are given by the dashed curves in Figs. 1–3. Reference to Table 1 shows that the ion densities increase by less than 15 per cent except near the highest temperatures and pressures considered. However, for mean beam lengths of several centimeters or larger, the emissivity is near unity at these high pressures and temperatures (cf. Fig. 16) and, therefore, the emission is not strongly dependent on the partial pressures. Hence serious errors in the emissivity estimates will be introduced only for very small mean beam lengths and at the highest temperatures and pressures considered.

III. EMISSIVITY CONTRIBUTIONS FROM THE HYDROGEN MOLECULE

For a gas at constant temperature and pressure, the total emissivity is given by[5]

$$\varepsilon = \frac{1}{\sigma T^4}\int_0^\infty R_\omega^\circ[1-\exp(-k_\omega l)]\,d\omega \tag{3}$$

where σ is the Stefan–Boltzmann constant, R_ω° is the spectral blackbody radiancy at the wave number ω, l is the mean beam length, and k_ω is the spectral absorption coefficient (in cm^{-1} for l in cm).

For low temperatures, the blackbody radiancy is large only at small wave numbers, where the vibration–rotation bands and rotational lines occur. The H_2 molecule is homonuclear, however, so that ordinary vibrational and rotational transitions are forbidden. Investigation of other emission processes shows that the so-called 'pressure-induced' spectrum will give the dominant contribution to the emissivity at low temperatures and moderate to high pressures.

A. The pressure-induced spectrum

The pressure-induced spectrum consists of vibration–rotation bands and rotational lines resulting from transitions which occur during collisions when dipole moments are induced

VOL.
1
1961

in the colliding molecules. Since the integrated intensities of the overtone bands are much smaller than those of the fundamental[6], and because the blackbody radiancy at the fundamental band is not appreciably less than any of the values at the overtone bands for the temperatures of interest, only the fundamental vibration–rotation band and the pure rotational lines need to be considered for emissivity calculations.

1. *Fundamental vibration–rotation band.* Considerable experimental work has been done on the absorption of the fundamental band at temperatures near 300°K and at lower temperatures[7–9]. The theoretical equations of VAN KRANENDONK[10–12] may be used to extend the experimental results to higher temperatures.

For his theoretical model, Van Kranendonk considers the induced dipole moment to be made up of two parts: a short-range part produced by the overlapping charge clouds of the molecules producing exchange and deformation dipole moments and a long-range part produced by quadrupole induction. The short-range overlap moment is angle-independent, decreasing exponentially with the intermolecular separation R, and may be determined by two parameters which measure the magnitude and the range of the moment. The values of these parameters can be obtained from measurements of the total absorption coefficient and its temperature dependence. The long-range moment is proportional to R^{-4} with an angular dependence characteristic for quadrupolar induction. The magnitude of the long-range induced moment is determined from the known values of the quadrupole moment and average polarizability of the H_2 molecule and their derivatives with respect to internuclear distance in the molecule.

Using the Lennard–Jones 6–12 intermolecular potential, Van Kranendonk obtains

$$\tilde{\alpha}_1 \equiv \frac{c}{\rho_{H_2}^2} \int_{\substack{\text{fundamental} \\ \text{band}}} \frac{k_\omega}{\omega} \, d\omega = \lambda^2 I \tilde{\gamma} + (\mu_1^2 + \mu_2^2) J \tilde{\gamma} \tag{4}$$

where ρ_{H_2} is the density, c the velocity of light and, for the hydrogen molecule, $\lambda = 9{\cdot}04 \times 10^{-3}$, $\mu_1^2 + \mu_2^2 = 7{\cdot}55 \times 10^{-6}$, and $\tilde{\gamma} = 5{\cdot}80 \times 10^{-32}$ sec^{-1} cm^6. The functions I and J are given by the integrals

$$I = 4\pi \int_0^\infty e^{-2(x-1)\sigma/\rho} g_0(x) dx \tag{5}$$

and

$$J = 12\pi \int_0^\infty x^{-8} g_0(x) x^2 dx \tag{6}$$

where $x = R/\sigma$ with σ being the molecular diameter in the Lennard–Jones 6–12 intermolecular potential:

$$V(R) = 4\varepsilon \left[\left(\frac{\sigma}{R} \right)^{12} - \left(\frac{\sigma}{R} \right)^{6} \right] \tag{7}$$

For hydrogen, $\sigma = 2{\cdot}928$Å and $\rho = 0{\cdot}145\sigma$. At high temperatures, the quantum effects in the translational motion of the molecules may be neglected and the distribution function $g_0(x)$ is then given by

$$g_0(x) = \exp \left[- \frac{V(x)}{kT} \right] \tag{8}$$

with $V(x)$ obtained from equation (7). Equation (8) may be used to extend the tabulated[10] classical values of the integrals I and J, denoted by I_{cl} and J_{cl}, to temperatures of several thousand °K (see Fig. 5). At temperatures above 600°K, I_{cl} and J_{cl} are essentially equal to I and J.

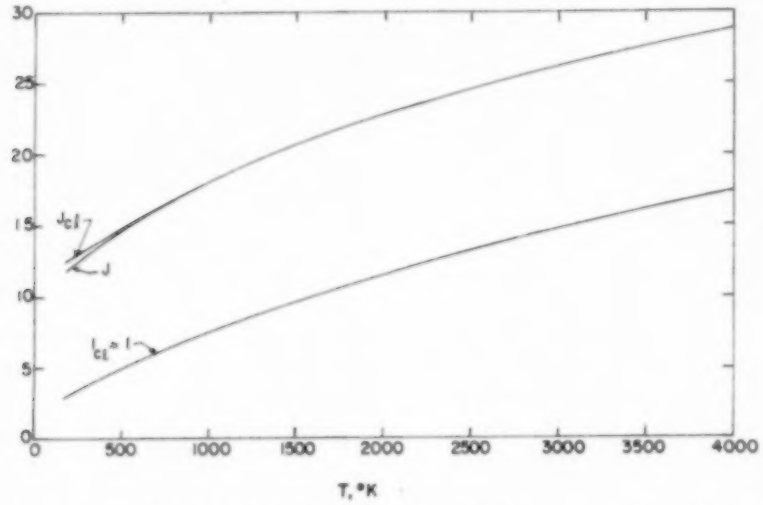

FIG. 5. The integrals I, J, I_{cl}, and J_{cl} for pressure-induced absorption as functions of the temperature.

Since the mean wave number $\bar{\omega}$, defined by

$$\tilde{\alpha}_1 = \frac{c}{\rho_{H_2}^2}\int \frac{k_\omega}{\omega}\,d\omega \equiv \frac{c}{\rho_{H_2}^2}\frac{1}{\bar{\omega}}\int k_\omega d\omega, \tag{9}$$

is nearly constant for the temperatures considered, the following relation is obtained for the integrated intensity of the fundamental band:

$$\alpha \equiv \int k_\omega d\omega = (37{\cdot}2I + 3{\cdot}43J)\left(\frac{p_{H_2}}{T}\right)^2 \text{cm}^{-1} \tag{10}$$

for p_{H_2} in atm and T in °K. In equation (10) the perfect gas relation, which is good to a few per cent for pressures up to 100 atm, has been used[13].

From Fig. 6 it is evident that the fundamental band may be approximated by the box model[5], i.e., by an average absorption coefficient acting over an effective band width $\Delta\omega$ which is proportional to the square root of the temperature. Using this model, the emissivity of the fundamental band may be calculated from the relation

$$\varepsilon = \left(\int_{\Delta\omega} R_\omega^\circ d\omega\right)\left[1\text{-}\exp\left(-\frac{\gamma l}{\Delta\omega}\right)\right]. \tag{11}$$

In the temperature region in which the fundamental band is important, viz., 1000°K $\leq T \leq$ 4500°K, the gas is essentially transparent for values of $p_{H_2}{}^2 l$ less than about 10^5 cm-atm^2.

For the case of a transparent gas, equation (11) constitutes an approximation only in the averaging of the blackbody function over the band.

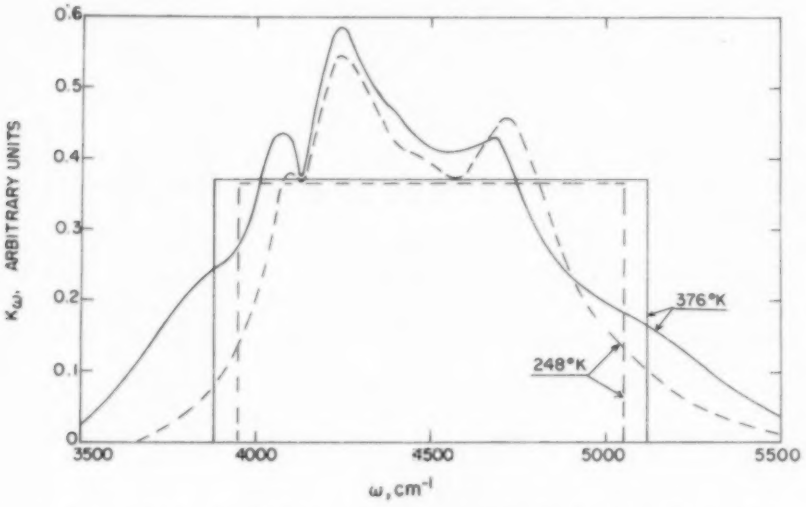

FIG. 6. Box model for the fundamental band compared with the absorption coefficients measured by CHISHOLM and WELSH[9].

2. *Pure rotation spectrum.* Several papers on the pressure-induced rotational spectrum have been published recently[14–17]. In addition to the rotational spectrum, one should also consider the collision-induced translational spectrum corresponding to transitions with no change in the internal quantum numbers. However, the integrated intensity of the translational spectrum amounts to only about 15 per cent of that for the rotational spectrum and occurs primarily at smaller wave numbers[17], corresponding to smaller blackbody radiancies for $T \gtrsim 300°K$; thus the emissivity contribution of the translational spectrum is small. Accordingly, a pure rotational model is used for extrapolation of the experimental integrated intensity to higher temperatures and for determination of the spectral dependence of the absorption coefficient.

In an analysis similar to that used for the fundamental band, VAN KRANENDONK and KISS show that the integrated intensity of the rotational line for the $j \to j+2$ transition may be approximated by[16]

$$\tilde{\alpha}_1(j) \equiv \frac{c}{\rho_{H_2}^2} \int_{j\to j+2 \text{ line}} \frac{k_\omega}{\omega} \, d\omega = L(j)\left[(\lambda_0^2 + 2\lambda_1)I + \overline{\mu}^2 J + \overline{\mu}(\lambda_0 - \frac{2}{\sqrt{3}}\lambda_1)K\right]\tilde{\gamma}' + L(j)L'\mu'^2 J\tilde{\gamma}' \quad (12)$$

where I and J are again defined by equation (5) and (6); now $\rho = 0{\cdot}126\sigma$ and K is defined by the relation

$$K = \frac{2\pi}{\sqrt{5}} \int_0^\infty x^{-4} e^{-(x-1)\sigma/\rho} \, g_0(x) \, x^2 dx; \quad (13)$$

$L(j)$ and L' are given by

$$L(j) = \frac{3(j+1)(j+2)}{2(2j+3)}[P(j) - P(j+2)] \tag{14}$$

and

$$L' = \sum_{j=0}^{\infty} \frac{3(j+1)(j+2)}{2(2j+3)} P(j), \tag{15}$$

respectively, where $P(j)$ is the normalized Boltzmann factor for the rotational state j. The quantities λ and μ are constants describing the overlap and quadrupolar induced moments, respectively, while $\gamma' = (4\pi^2 e^2 \sigma^5/3h)$.

In equation (12) the first term on the right-hand side is the intensity due to the overlap moment alone, the second and fourth terms are produced by the quadrupolar induction effect, while the third term represents the interference effect between quadrupolar and overlap moments. For pure hydrogen the second term contributes about 90 per cent of the total intensity; hence the approximation

$$\tilde{\alpha}_1(j) = \frac{c}{\rho_{H_2}^2} \int_{j \to j+2 \text{ line}} \frac{k_\omega}{\omega} \, d\omega = \overline{\mu}^2 \tilde{\gamma}' L(j) J \tag{16}$$

may be used.

KISS and WELSH have shown[17] that the absorption coefficient $\tilde{k}_\omega \equiv \frac{1}{\omega} k_\omega$ for a rotational line may be represented by a dispersion contour modified on the low-frequency side by a Boltzmann factor and with a half-width proportional to the square root of the temperature. For the temperatures considered here, $T \geqslant 300°K$, the Boltzmann factor in the line contour is nearly unity over most of the line so the absorption coefficient may be represented by

$$k_\omega = \sum_j \frac{\tilde{\alpha}_1(j)}{\pi} \frac{\delta\omega}{(\omega - \omega_j)^2 + \delta^2} \rho_{H_2}{}^2 = \sum_j \frac{\tilde{\alpha}_1(j)}{\pi} \frac{\delta\omega}{(\omega - \omega_j)^2 + \delta^2} \left(\frac{273}{T} p_{H_2}\right)^2 \tag{17}$$

with ω_j denoting the wavenumber at the center of the jth line and δ the line half-width. For $\tilde{\alpha}_1(j)$ in cm^{-1}–amagat^{-2}, p_{H_2} should be expressed in atmos to give k_ω in cm^{-1}. Equation (17) was used to calculate the points shown in Fig. 7 which are compared with the experimental absorption coefficients of KISS *et al*[15]. Figs. 8 and 9 show the computed absorption coefficients using equation (17) at 600°K and 1000°K, respectively. These absorption coefficients are used directly in equation (3) in order to estimate the emissivity contribution of the rotational spectrum.

In the above analysis, the plasma was assumed to be pure H_2. This assumption will not introduce a serious error because emission processes involving only atoms and ions (sections IV–VI) make the dominant contributions to the total emissivity at temperatures high enough for an appreciable fraction of H_2 to be dissociated. It should be noted in this connection that collisions of an H_2 molecule with molecules of other gases, including monatomic gases, produce absorption coefficients that are of the same order of magnitude as the absorption coefficients resulting from collisions with other H_2 molecules[7–9,15]. Therefore H_2–H_2 collisions will contribute most of the pressure-induced emission up to temperatures where atomic and ionic emission processes take over as the dominant contributions to the total emissivity.

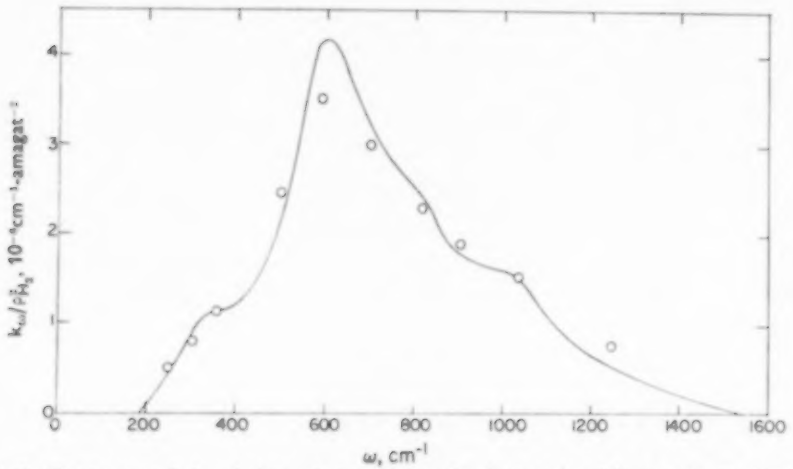

FIG. 7. The pressure-induced absorption coefficient for the rotational lines of H_2 at 300°K as measured by KISS *et al*[151] (curve) and computed from equation (17) (circles).

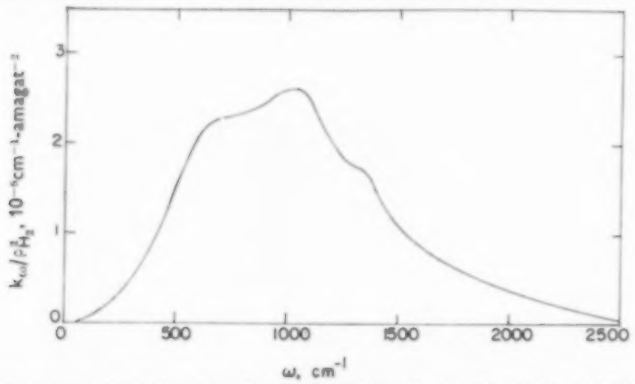

FIG. 8. The pressure-induced absorption coefficient for the rotational lines of H_2 computed from equation (17) for $T = 600$°K.

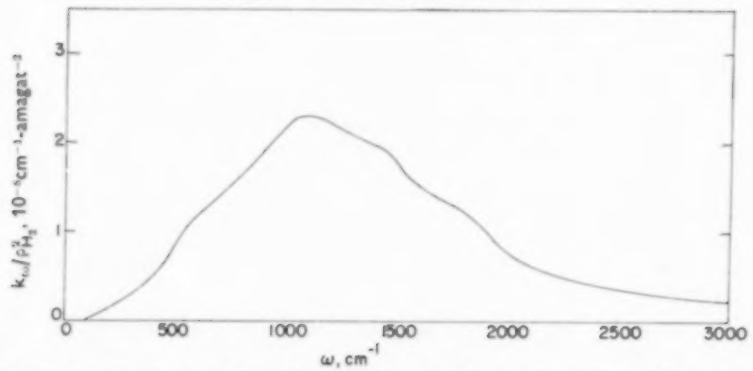

FIG. 9. The pressure-induced absorption coefficient for the rotational lines of H_2 computed from equation (17) for $T = 1000$°K.

B. Electronic transitions

In this section it is shown that the band and continuum spectra resulting from electronic transitions in the hydrogen molecule for moderate and high pressures make a much smaller contribution to the total emissivity than the pressure-induced spectrum in the low-temperature range where the molecular emissivity contributions are important. Reference to the energy level diagram for H_2 in Fig. 10 and consideration of selection rules show that there will be two strong transitions to the ground state, viz., the Lyman and Werner band systems corresponding to the transitions $2p\sigma\,^1\Sigma_u^+ \rightarrow 1s\sigma\,^1\Sigma_g^+$ and $2p\pi\,^1\Pi_u \rightarrow 1s\sigma\,^1\Sigma_g^+$, respectively. Accordingly, these transitions are considered in detail and the emissivity contribution from all other electronic transitions is shown to be less than that from the Lyman bands.

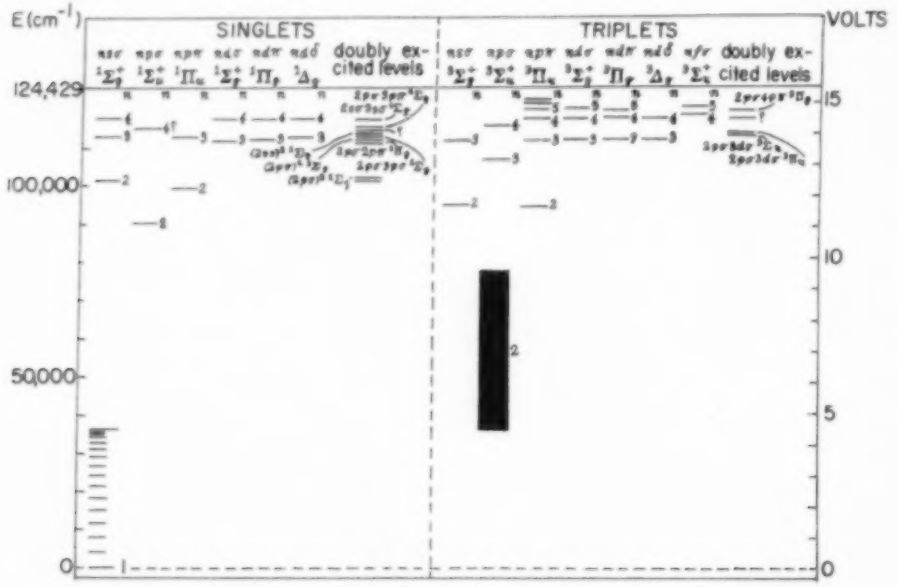

FIG. 10. Energy level diagram of the observed electronic states of the H_2 molecule (after FIG. 160[18]).

1. *The Lyman and Werner bands.* Several calculations of the electronic f-numbers for the Lyman and Werner bands have been made. For the emissivity calculation, the discrepancies between the calculated f-numbers are unimportant. The values[19] $f_{Lyman} \equiv f = 0{\cdot}18$ and $f_{Werner} \equiv f' = 0{\cdot}42$ have been chosen. Since the lower electronic state involved in the Lyman and Werner transitions is the ground state, the sums of the integrated intensities of all the lines belonging to the Lyman and Werner band systems, α and α', respectively, are[5]

$$\alpha \equiv \sum_{\substack{\text{all Lyman} \\ \text{bands}}} (\int k_\omega \mathrm{d}\omega) = \frac{\pi e^2}{m_e c^2} N_{H_2} f = \frac{1{\cdot}17 \times 10^9}{T} p_{H_2}(\mathrm{cm}^{-1}) \qquad (18)$$

VOL. 1 1961

and

$$\alpha' = \frac{\pi e^2}{m_e c^2} N_{H_2} f' = \frac{2{\cdot}73 \times 10^9}{T} p_{H_2}(\mathrm{cm}^{-1}) \tag{19}$$

where e denotes the electronic charge, m_e the mass of the electron, and N_{H_2} the number of molecules per cm³. In equations (18) and (19) the number of molecules in the ground state was set equal to the total number of molecules and the induced emission factor $(1 - e^{-hc\omega/kT})$ was set equal to unity since both of these approximations are valid for the temperature range of interest.

To obtain an upper limit for the emissivity, the form for a transparent gas is used, viz.,

$$\varepsilon \leq \varepsilon_L = \int_0^\infty \frac{R_\omega^\circ}{\sigma T^4} k_\omega \mathrm{d}\omega l. \tag{20}$$

The blackbody function $R_\omega^\circ/\sigma T^4$ is given by

$$\frac{R_\omega^\circ}{\sigma T^4} = \left(\frac{15}{\pi^4}\right) \frac{\left(\frac{hc\omega}{kT}\right)^4 \frac{1}{\omega}}{\exp(hc\omega/kT) - 1}. \tag{21}$$

To obtain an approximate expression for k_ω, a simple treatment is followed[20]. In this treatment, all of the upper vibrational levels are approximated by the lowest vibrational level of the upper electronic state. The absorption coefficient is then roughly proportional to the number of molecules in the lower vibrational state, i.e.,

$$k_\omega \simeq \alpha \left(\frac{hc}{kT}\right) e^{-hc(\omega_1 - \omega)/kT} \tag{22}$$

since $e^{-hc(\omega_1 - \omega_2)/kT} << 1$ for the specified temperature range; ω_1 and ω_2 are the maximum and minimum wave numbers for the band system (cf. Fig. 11). Introduction of equations (21) and (22) into equation (20) yields for the Lyman and Werner bands

$$\varepsilon_L \simeq \frac{1}{4}\left(\frac{15}{\pi^4}\right)\left(\frac{hc}{kT}\right) l \left[\alpha e^{-u_1}(u_1^4 - u_2^4) + \alpha' e^{-u'_1}(u_1'^4 - u_2'^4)\right] \tag{23}$$

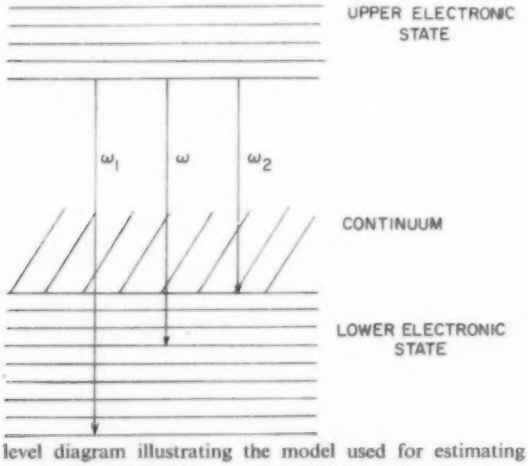

FIG. 11. Energy level diagram illustrating the model used for estimating the emissivity contributions of the Lyman and Werner bands.

since $e^{hc\omega/kT} - 1 \simeq e^{hc\omega/kT}$; $u = hc\omega/kT$; the quantities for the Lyman band system are again unprimed while those for the Werner system are primed.

The preceding analysis tends to give excessively large values for the emissivity contribution of the Lyman and Werner bands because the transparent gas relation was used and because replacing the upper levels by the lowest vibrational level in the upper electronic state means that the actual emission occurs at larger wave numbers than calculated, i.e., the blackbody radiancy at the bands has been overestimated.

The emissivity term $\varepsilon_L/p_{H_2}l$ calculated from equation (23) is given in Table 2. From

TABLE 2. THE EMISSIVITY TERM ε_L/p_{H_2} FOR THE LYMAN AND WERNER BANDS

T (°K)	2000	3000	4000	5000
$\frac{\varepsilon_L}{p_{H_2}}$ (cm^{-1}atm^{-1})	$1{\cdot}6 \times 10^{-20}$	$3{\cdot}6 \times 10^{-12}$	$3{\cdot}5 \times 10^{-8}$	$6{\cdot}9 \times 10^{-6}$

these values it is concluded that the emissivity contribution from the Lyman and Werner bands is generally small compared to the contribution from the pressure-induced spectrum for the temperature and pressure range in which H_2 emission is important. For example, the emissivity contribution of the Lyman and Werner bands is small compared to that of the pressure-induced spectrum for $p_{H_2} \gtrsim \frac{1}{10}$ atm and $T \lesssim 3500$°K; $p_{H_2} \gtrsim 1$ atm, $T \lesssim 3700$°K; $p_{H_2} \gtrsim 10$ atm, $T \lesssim 4000$°K; and $p_{H_2} \gtrsim 100$ atm, $T \lesssim 4300$°K.

2. *The other electronic transitions.* In order to obtain an upper limit for the intensity of all the transitions other than the Lyman and Werner bands, the intensities of various transitions may be compared with that of the Lyman bands. Since the transparent gas approximation was used in the preceding section, the calculated intensity of the Lyman bands may be represented by the simple relation

$$I_{Lyman} = \left(\frac{\pi^2 e^2 h}{m_e}\right) N_u (\bar{\omega}_{Lyman})^3 f_{Lyman} \tag{24}$$

where N_u is the total number of molecules in the upper ($2p\sigma^1\Sigma_u^+$) state and $\bar{\omega}$ is a mean wavenumber for the transition. Considering the intensity $I_{kk'}$ of the electronic transition $k' \rightarrow k$,

$$\frac{I_{kk'}}{I_{Lyman}} = \frac{(N_u)_{k'}}{(N_u)_{Lyman}} \left(\frac{\bar{\omega}_{kk'}}{\bar{\omega}_{Lyman}}\right)^3 \frac{f_{kk'}}{f_{Lyman}} \tag{25}$$

and inserting $f_{Lyman} = 0{\cdot}18$ and $\bar{\omega}_{Lyman} > \omega_{min} \simeq 54{,}000$ cm^{-1}, the following inequality is obtained:

$$\frac{I_{kk'}}{I_{Lyman}} < 10\, e^{-hc\Delta\omega_{k'}/kT} \left(\frac{\omega_{kk'}}{54{,}000}\right)^3 f_{kk'}. \tag{26}$$

Here $hc\Delta\omega_{k'}$ is the energy difference between the $2p\sigma^1\Sigma_u^+$ state and the upper state of the $k' \rightarrow k$ transition.

All transitions to the ground state, other than the Lyman and Werner transitions, will be considered for temperatures less than 5000°K. For these transitions, $\Delta\omega_{k'} \geq 22{,}198$ cm^{-1} and $\omega_{kk'} < 124{,}429$ so that

$$\frac{\sum_{k'} I_{kk'}}{I_{Lyman}} < 0{\cdot}21 \times \sum_{k'} f_{kk'}. \tag{27}$$

VOL. 1 1961

But the sum rule[18] for $f_{kk'}$ requires that $\sum_{k'} f_{kk'} = 1 - f_{Lyman} - f_{Werner} = 0{\cdot}4$. Therefore these transitions contribute less than one tenth of the intensity of the Lyman bands for $T \leq 5000°\text{K}$.

This procedure may be applied to the other transitions since for any electronic state k the sum rule[18]

$$\sum_{\text{all } k'} f_{kk'} = 1 \tag{28}$$

exists for a single emission electron.

In equation (28) the f-numbers for transitions from the state k to lower states k' are included as negative quantities so that the sum of f-numbers from states k' higher than k will be somewhat greater than unity.

The continuum transitions may be included in this analysis if the mean f-number $\bar{f}$, and mean wave number, $\bar{\omega}$, are defined by

$$\int \omega^3 \left(\frac{\mathrm{d}f_{k',\omega}}{\mathrm{d}\omega}\right) \mathrm{d}\omega \equiv \bar{\omega}_{ck'}{}^3 \bar{f}_{ck'} \tag{29}$$

for a transition from the bound upper state k', where $\dfrac{\mathrm{d}f_{k',\omega}}{\mathrm{d}\omega}$ is the f-number per unit wave number. A calculation using equations (26) and (29) yields the result that the intensity of the strong continuum transition $2s\sigma^3\Sigma_g^+ \rightarrow 2p\sigma^3\Sigma_u^+$ is less than or approximately equal to the intensity of the Lyman bands at temperatures below 5000°K. To check this result, the emissivity contribution of the $2s\sigma^3\Sigma_g^+ \rightarrow 2p\sigma^3\Sigma_u^+$ transition was calculated using the mean lifetimes and relative spectral intensities given by JAMES and COOLIDGE[21]. This calculated emissivity contribution is less than a hundredth of the calculated Lyman contribution given in Table 2 for temperatures less than 5000°K.

For all transitions to the $2p\sigma^3\Sigma_u^+$ continuum state, other than the $2s\sigma^3\Sigma_g^+ \rightarrow 2p\sigma^3\Sigma_u^+$ transition, equations (26) and (29) yield

$$\frac{\sum_{k'} I_{ck'}}{I_{Lyman}} < \frac{\sum_{k'} (N_u)_{k'}\, \bar{\omega}_{ck'}{}^3 \bar{f}_{ck'}}{(N_u)_{Lyman} \times (5400)^3 \times 0{\cdot}18} < {\cdot}04. \tag{30}$$

Direct application of equation (26) to the individual transitions for which $n = 2$ in both the upper and lower states shows that these may also be neglected.

Thus all possible transitions between singly excited levels, for which the lower state is below $E = 107{,}770\ \text{cm}^{-1}$, have been considered (cf. Fig. 10). Application of equations (26) and (28) shows that $\sum_{k'} I_{kk'}/I_{Lyman} < 2 \times 10^{-3}$ for any lower state with $E > 107{,}770\ \text{cm}^{-1}$. Since there are fewer than about fifty states with $107{,}770\ \text{cm}^{-1} \leq E \leq 120{,}000\,\text{cm}^{-1}$, it may be concluded that the emission for which these states are the lower states may be neglected. Finally, all lower states with energies between 120,000 cm^{-1} and the ionization energy (124,429 cm^{-1}) will be considered. For any of these states, $\sum_{k'} I_{kk'}/I_{Lyman} < 10^{-6}$. But there will be fewer than 10^5 states in this region whence these transitions may also be neglected.

Transitions involving doubly excited levels may be included in the calculation by using the sum rule of equation (28) with unity replaced by 2. Thus it is concluded that the calculated transparent gas emissivities for the Lyman and Werner bands constitute

approximate upper limits for all electronic transitions at temperatures below 5000°K. In the preceding section it was shown that these upper limits for the emissivity of electronic transitions are below the values for the pressure-induced spectrum at moderate and high pressures and low temperatures, where the molecular spectrum is important.

C. *Quadrupole and* HD *radiation*

In addition to the pressure-induced vibration–rotation spectrum, there will be a quadrupole vibration–rotation spectrum for H_2 and an ordinary dipole vibration–rotation spectrum of the isotopic species HD, where D is the deuterium atom.

1. *Quadrupole spectrum.* Calculations[22, 23] show that the integrated intensity of the fundamental quadrupole vibration–rotation band is about 8×10^{-9} times that of the ordinary fundamental of HCl. The first and second overtone quadrupole bands are about 0·9 and 0·2 times as strong as the fundamental. Accordingly, $\varepsilon_{quadrupole}/p_{H_2}l$ will have a value of about 5×10^{-11} cm^{-1} atm^{-1} at 1000°K. Since the temperature dependence of the emissivity will be roughly the same as that for the pressure-induced spectrum, it may be concluded that the emissivity contribution of the quadrupole spectrum will be small compared to that of the pressure-induced spectrum for pressures greater than about 1/100 atm.

2. *HD Vibration–rotation spectrum.* The calculated ratio of the integrated intensities[22–24] for the fundamental bands of HD and HCl is about $1{:}7 \times 10^5$. Using an abundance ratio of $3{\cdot}1 \times 10^{-4}$:1, the integrated intensity of the HD fundamental in natural hydrogen is about 4×10^{-10} times that of the HCl fundamental. Therefore the HD emissivity contribution may be neglected.

IV. EMISSIVITY CONTRIBUTIONS FROM THE H^- ION

Considerable work has been done on the calculation of the absorption coefficient for the H^- ion for use in astrophysical applications[25–28]. The two processes contributing to the absorption coefficient are the bound-free (photodetachment) transitions represented by the reaction

$$H^- + h\nu \rightarrow H + e^-$$

and the free-free transitions represented by

$$H + e^- + h\nu \rightarrow H + e^-,$$

where e^- represents an electron and $h\nu$ is the absorbed photon.

A. *Bound-free transitions*

CHANDRASEKHAR[25–27] has evaluated the absorption coefficient for bound-free transitions directly by evaluating the matrix element. In the latest calculations[26, 27], the 20-parameter wave function of HART and HERZBERG[29] was used for the bound state. The wave function for the continuous state was first approximated by a plane wave representation of the outgoing electron, then more accurately by the wave function of an electron moving in the static field of a hydrogen atom (Hartree approximation). The accuracy of the calculation was improved by use of the dipole-velocity form of the matrix element[27].

Direct measurements of the bound-free cross section by BRANSCOMB and FITE[30] agree reasonably well with CHANDRASEKHAR's calculations. In a note[25], CHANDRASEKHAR uses

VOL
1
196

the calculations of BRANDSEN *et al*[31] for *p*-waves in the field of a neutral hydrogen atom, which allow for exchange and polarization. This sample calculation indicates that his earlier estimates of the bound-free absorption coefficients should be decreased by about 20 per cent.

B. Free-free transitions

In the earliest evaluations of the free-free absorption coefficient the Born approximation was used to describe the motion of an electron in the field of a hydrogen atom. However, CHANDRASEKHAR[28] showed that the electron velocities in the temperature range considered are too low for a valid application of the Born approximation. For this reason, he calculated the free-free absorption coefficients using the Hartree approximation described above[28].

A calculation of the free-free absorption coefficient using the computations of BRANDSEN *et al.*[31] is being performed by T. and H. OHMURA[32]. Preliminary estimates for the absorption coefficient are 40 to 50 per cent smaller than those of CHANDRASEKHAR and BREEN[28].

The values of the absorption coefficient calculated by Chandrasekhar *et al.* are used in the present emissivity calculation. Since the bound-free contribution to the total emissivity is appreciably greater than that of the free-free transitions, the results should be accurate to better than about 25 per cent.

V. EMISSIVITY CONTRIBUTIONS FROM THE H_2^+ ION

The absorption coefficient of H_2^+ arises from the bound-free transition

$$H_2^+ + h\nu \rightarrow H + H^+$$

and from the free-free transition

$$H + H^+ + h\nu \rightarrow H + H^+.$$

By first evaluating the exact two-center wave functions[33] and the dipole moments[34], BATES calculated the H_2^+ absorption coefficient[35].

Using the absorption coefficients given by Bates, it is found that the H_2^+ contribution to the total emissivity is less than about 5 per cent of the H^- contribution for temperatures less than 10,000°K.

VI. EMISSIVITY CONTRIBUTIONS FROM THE HYDROGEN ATOM

In addition to the line spectrum of the hydrogen atom, there exists a continuum spectrum consisting of the bound-free transitions

$$H + h\nu \rightarrow H^+ + e^-$$

and the free-free transitions (Bremsstrahlung)

$$H^+ + e^- + h\nu \rightarrow H^+ + e^-.$$

A. The continuum spectrum

An expression for the free-free absorption coefficient was first derived by KRAMERS[36] by utilizing the correspondence principle. Subsequent derivations[37–39] have shown that

the quantum-mechanical expression may be written as Kramer's expression times the quantity g_{ff} called the Gaunt factor, which is of the order of unity, viz.,

$$\frac{k_\omega^{ff}}{p_H} = \frac{32}{3\sqrt{3}} \frac{\pi^2 e^6 Ry}{h^3 c^3 kT} \frac{e^{-x_1}}{\omega^3} \left(\frac{1}{2x_1}\right) (1 - e^{-hc\omega/kT}) \cdot g_{ff}(\omega) \tag{31}$$

where Ry is the Rydberg constant for hydrogen and $x_1 = hcRy/kT$. Extrapolation of the results given[40] for $T > 11{,}605°K$ shows that for the temperatures of interest in our calculation $g_{ff}(\omega)$ may be replaced by the mean value $\bar{g}_{ff} \simeq 1{\cdot}24$.

The bound-free absorption coefficient may similarly be written in terms of a simple expression, obtainable from the equation derived from the correspondence principle but multiplied by the Gaunt factor $g_{bf,n}$,[41] viz.,

$$\frac{k_\omega^{bf}}{p_H} = \frac{32}{3\sqrt{3}} \frac{\pi^2 e^6 Ry}{h^3 c^3 kT} \frac{e^{-x_1}}{\omega^3} \left(\sum_{\omega_n > \omega}^{\infty} \frac{e^{x_n}}{n^3} g_{bf,n}(\omega) \right) (1 - e^{-hc\omega/kT}) \tag{32}$$

where $x_n = hcRy/kTn^2$ and $\omega_n = Ry/n^2$. The Gaunt factors $g_{bf,n}(\omega)$ vary from about 0·90 to 1·10[42]; hence the approximation $g_{bf,n}(\omega) \simeq 1{\cdot}00$ may be used.

Using the mean values for the Gaunt factors, the total continuum absorption coefficient for the hydrogen atom becomes

$$\frac{k_{c,\omega}}{p_H} = \frac{32}{3\sqrt{3}} \frac{\pi^2 e^6 Ry}{h^3 c^3 kT} \frac{e^{-x_1}}{\omega^3} \left(\sum_{\omega_n < \omega}^{\infty} \frac{e^{x_n}}{n^3} + \frac{0{\cdot}62}{x_1} \right) (1 - e^{-hc\omega/kT}). \tag{33}$$

Equation (33) was used directly for the calculation of the continuum absorption coefficient, since the temperatures considered here are not high enough to validate the use of UNSÖLD'S[43] approximation, $\sum_{n=5}^{\infty} \frac{1}{n^3} e^{x_n} \simeq e^{x_5} - 1/2x_1$.

B. The line spectrum

The f-number for an atomic line corresponding to a transition between states with principal quantum numbers n and n' is [44]

$$f_{n \to n'} = \frac{64}{3\sqrt{3}} \frac{1}{\pi 2n^2} \frac{1}{\left(\frac{1}{n^2} - \frac{1}{n'^2}\right)} \frac{1}{n^3 (n')^3} g. \tag{34}$$

Except for the Gaunt g-factor, equation (34) may be obtained from the correspondence principle. The f-number values are tabulated[45]. For a transparent gas it is sufficient to know only the f-numbers in order to calculate the emissivity contributions of the atomic lines. On the other hand, if there is appreciable self-absorption, it is necessary to know the line contours in order to calculate the line emissivities. Accordingly, except for the transparent gas case, it is necessary to consider collision-broadened and Stark-broadened line contours. (See PENNER[3] for an account of Doppler broadening, which is important only at low pressures).

1. *Transparent gases.* For a transparent gas, the total emissivity of a single line is

$$\varepsilon_L = \frac{R^\circ_{\omega_0}}{\sigma T^4} S p_H l \tag{35}$$

where $R^\circ_{\omega_0}$ is the blackbody radiancy at the line center and $S = \frac{1}{p_H}\int k_\omega d\omega$ is the line integrated intensity. Here S may be evaluated from the relation[5]

$$S_{nn'} = \frac{\pi e^2}{m_e c^2} f_{n\to n'} n^2 \left(\frac{N_H}{p_H}\right) e^{-(x_1 - x_n)} (1 - e^{-hc\omega_{nn'}/kT}) \tag{36}$$

where the number of atoms per unit volume in the lower state has been approximated by the total number per unit volume N_H.

2. *Collision-broadened lines.* For the temperatures considered here, practically all of the hydrogen atoms are in the ground ($1s$) state. Between these $1s$ atoms and an atom in an np state there will exist a resonance interaction energy which may be approximated by[45]

$$(\Delta E)_{np,\,1s} \simeq \pm \left(\frac{he^2}{8\pi^2 m_e c} \frac{f_{np,\,1s}}{\omega_{1,\,n}}\right) \frac{1}{r^3} \tag{37}$$

where r is the distance between the two atoms, $f_{np,\,1s}$ is the f-number for the transition from lower state $1s$ to upper state np, and $\omega_{1,\,n}$ is the wave number difference between these states. This resonance interaction will account for the collision broadening since the van der Waals interaction energies are much lower, being proportional to r^{-6}. Using the statistical theory of line broadening, MARGENAU and WATSON[45] show that, in the wings of the spectral line for a $1s$–$2p$ transition, equation (37) leads to

$$\frac{k_\omega}{p_H} \simeq \frac{S}{\pi} \frac{b_c}{(\Delta\omega)^2} \tag{38}$$

where the half-width b_c is

$$b_c = \frac{N_H e^2}{12 m_e c^2} \left(\frac{f_{2p,\,1s}}{\omega_{1,\,2}}\right) \tag{39}$$

and $\Delta\omega = (\omega - \omega_0)$ with ω_0 being the wave number at the line center. This result agrees well with

$$b_c = \frac{N_H e^2}{4\pi m_e c^2} \left(\frac{f_{2p,\,1s}}{\omega_{1,\,2}}\right) \tag{40}$$

obtained by WEISSKOPF[46] using a modification of the Lorentz formula.

In the H atom emissivity calculations[47], equation (40) was incorrectly used for the Balmer and Paschen lines. Recalling that the resonance interaction with the perturbing atom in the ground state occurs only when the emitting atom is in an np state, it is possible to add the transitions contributing to a single line and to obtain the appropriate b_c for use in equation (38) for the Balmer line ($n \to 2$):

$$b_c = \left(\frac{N_H e^2}{12 m_e c^2}\right) \frac{1}{4} \left[f_{np,\,2s} \left(\frac{f_{np,\,1s}}{\omega_{1,\,n}}\right) + 3(f_{ns,\,2p} + f_{nd,\,2p}) \left(\frac{f_{2p,\,1s}}{\omega_{1,\,2}}\right)\right] \frac{1}{f_{n,\,2}} \tag{41}$$

where

$$f_{n,\,2} \equiv f_{2\to n} = \tfrac{1}{4} \left[f_{np,\,2s} + 3(f_{ns,\,2p} + f_{nd,\,2p})\right]. \tag{42}$$

In equation (41) the broadening for a given transition is multiplied by the fraction of the total line intensity contributed by the transition. Similarly, for the Paschen line ($n \rightarrow 3$),

$$b_c = \left(\frac{N_H e^2}{12 m_e c^2}\right) \frac{1}{9} \left[(f_{np,\,3s} + 5 f_{np,\,3d}) \left(\frac{f_{np,\,1s}}{\omega_{1,\,n}}\right) + 3(f_{ns,\,3p} + f_{nd,\,3p}) \left(\frac{f_{3p,\,1s}}{\omega_{1,\,3}}\right) \right] \frac{1}{f_{n,\,3}} \tag{43}$$

where

$$f_{n,\,3} \equiv f_{3 \rightarrow n} = \tfrac{1}{9} \left[f_{np,\,3s} + 3(f_{ns,\,3p} + f_{nd,\,3p}) + 5(f_{np,\,3d} + f_{nf,\,3d}) \right]. \tag{44}$$

For the Lyman lines we find

$$b_c = \frac{N_H e^2}{12 m_e c^2} \left(\frac{f_{np,\,1s}}{\omega_{1,\,n}}\right). \tag{45}$$

However, as will be discussed in section VI 4, the very distant parts of the low wave number wings of the Lyman lines are of most interest here and equation (45) is not applicable in this region.

The values of b_c $(12 m_e c^2 / N_H e^2)$ for the Balmer and Paschen lines are given in Table 3.

TABLE 3. THE HALF-WIDTH FACTOR b_c $(12 m_e c^2 / N_H e^2)$ FOR THE BALMER AND PASCHEN LINES COMPUTED FROM EQUATIONS (41) TO (44)

n	Balmer lines	Paschen lines
3	$4{\cdot}36 \times 10^{-6}$	
4	$4{\cdot}05 \times 10^{-6}$	$1{\cdot}74 \times 10^{-6}$
5	$3{\cdot}89 \times 10^{-6}$	$3{\cdot}73 \times 10^{-7}$
6	$4{\cdot}05 \times 10^{-6}$	$1{\cdot}48 \times 10^{-7}$
7	$3{\cdot}85 \times 10^{-6}$	$7{\cdot}45 \times 10^{-8}$
8	$3{\cdot}89 \times 10^{-6}$	$4{\cdot}44 \times 10^{-8}$

Insertion of the absorption coefficient given by equation (38) into the general expression for the total emissivity, equation (3), yields

$$\varepsilon = \frac{R^{\circ}_{\omega_0}}{\sigma T^4} 2 \sqrt{S b_c p_H l}. \tag{46}$$

Since equation (38) describes only the wings of the spectral line, equation (46) applies only when l is large enough to lead to blackened line centers. Specifically[5], equation (35) applies for $S p_H l / 2\pi b_c \leq 2/\pi$ and equation (46) for $S p_H l / 2\pi b_c \gtrsim 2/\pi$, with the actual emissivity never exceeding either expression.

3. *Stark-broadened lines.* The absorption coefficient in the wings of a line broadened by the Stark effect is[5]

$$\frac{k_\omega}{p_H p_e} = \frac{321 c_l \omega_0^{\,5}}{kT^2} n^2 \left(\exp\left[-\frac{Ryhc}{kT} \left(1 - \frac{1}{n^2}\right) \right] \right) \frac{1}{(\omega - \omega_0)^{5/2}} \tag{47}$$

where ω_0 is the wave number at the line center, n is the principal quantum number of the lower state, and c_l is a constant. Values of c_l for the first four Balmer lines are given (in references 5 and 44, while more complete data are given in reference 48).

Using equation (47) to evaluate the total emissivity for the line, one obtains

$$\varepsilon = \frac{R^{\circ}_{\omega_0}}{\sigma T^4} 2\Gamma(3/5) \left[\frac{321 c_l \omega_0^{\,5}}{kT^2} n^2 \left(\exp\left[-\frac{Ryhc}{kT} \left(1 - \frac{1}{n^2}\right) \right] \right) p_H p_e l \right]^{2/5}$$

$$= \frac{R^{\circ}_{\omega_0}}{\sigma T^4} A (p_H p_e l)^{2/5} \tag{48}$$

where Γ denotes the Gamma function. For pure Stark broadening, equation (48) is applicable for $p_H l/(p_e)^{2/3} \geq (A/S)^{5/3}$ while the transparent gas relation, equation (35), is applicable for $p_H l/(p_e)^{2/3} \leq (A/S)^{5/3}$, with the actual emissivity never exceeding either expression.

If desired, the more elaborate Stark broadening theories may be used[49], rather than the simple Holtsmark formula given in equation (47).

4. *The Lyman α-line.* If the simple collision and Stark broadening theories discussed above are used to compute the profile of the Lyman α-line, the absorption coefficient far out in the wings will be appreciable because of the large intensity of the Lyman α-line. Even though the center of the Lyman α-line is at 82,258 cm^{-1}, the absorption coefficient of the low wave number wing computed from the simple broadening theories is large enough at low wave numbers, where the blackbody radiancy is large, to account for the major portion of the total emitted intensity of the hydrogen plasma from approximately 4000°K to 8000°K. However, this conclusion is erroneous because these simple relations for collision and Stark broadening are not applicable at very large wave number distances from the line center.

Broadening in the far wings will result from either close encounters between an H atom and an H^+ ion (Stark broadening) or between two H atoms (collision broadening). The absorption coefficient for the H atom and H^+ ion encounters may be approximated by

$$k_\omega = g' \left(\frac{4\pi^2 e^2}{m_e c^3}\right) r^2 \left(\frac{dr}{d\omega}\right) e^{-\frac{hc\omega_l}{kT}} \left(1 - e^{-\frac{hc\omega}{kT}}\right) N_H N_{H^+} f_{lu} \qquad (49)$$

which is given by the semi-classical treatment of BATES[35] and, equivalently, by the statistical theory. Quantal calculations by BUCKINGHAM *et al*[50] show that the semi-classical treatment gives reliable results at the temperatures and wave numbers of interest. Equation (49) gives the absorption coefficient for transitions between two potential curves, with $hc\omega_l$ denoting the energy of the lower potential curve and $hc\omega$ the energy difference between the two potential curves at the atom–ion separation r. The factor g' represents the ratio of the statistical weight of the lower curve to the sum of the weights of all possible curves. To obtain the total absorption coefficient, the transitions between all potential curves which contribute intensity at ω must be included. For broadening of the Lyman α-line we must consider upper curves which merge into the $n = 2$ state of the H atom and lower curves which merge into the $n = 1$ state when $r \to \infty$. To avoid the laborious f-number calculations from the H_2^+ wave functions, we obtain an upper limit for k_ω by setting f_{lu} and g' equal to unity and consider the two permissible curves which give the maximum value of $r^2 \left(\frac{dr}{d\omega}\right) e^{-hc\omega_l/kT}$ at wave number ω. Use of the data[33] on potential curves shows that the repulsive curves $2p\sigma_u$ and $2p\pi_u$ should be used for the lower and upper curves, respectively, for $\omega < 71{,}000$ cm^{-1}. Computation shows that this upper limit for the absorption coefficient is much less than the absorption coefficient of the H^- ion for $\omega < 71{,}000$ cm^{-1} and may therefore be neglected. The term $e^{-hc\omega_l/kT}$, which accounts for the repulsion between the H atom and H^+ ion, is the important factor in reducing the absorption coefficient in the outer part of the low wave number wing to such an extent that it becomes unimportant.

Equation (49) may be used to compute the wing absorption coefficient for encounters between two H atoms (collision broadening) if N_{H^+} is replaced by N_H. Setting f_{lu} and g'

equal to unity and using the $2s\sigma^3\Sigma_g^+$ and $2p\sigma^3\Sigma_u^+$ potential curves of the H_2 molecule given by COLLIDGE and JAMES[51] in the calculation of an upper limit, one finds that the repulsion term $e^{-hc\omega_i/kT}$ again reduces the absorption coefficient sufficiently to make it become unimportant in the outer part of the low wave number wing.

It may therefore be concluded that the contribution of the Lyman lines to the total emissivity may be neglected, except at very low pressures when the lines start to become transparent.

A. Summation of the emissivity contributions

To sum emissivity contributions one must add the absorption coefficients for the various processes and use this sum as the total absorption coefficient k_ω in equation (3). For a transparent gas this will be equivalent to adding directly the emissivities of the various emission processes.

At high temperatures, when both continuum and line radiation may be important, it is convenient to utilize the total line emissivities directly since these can be easily calculated from equations (35), (46), and (48). For this purpose, equation (3) may be written in the form

$$\varepsilon = \int \frac{R^\circ_\omega}{\sigma T^4}\left(1\text{-}\exp\left[-\left(k^c{}_\omega + \sum_i k_\omega{}^{line\ i}\right)l\right]\right)d\omega \tag{50}$$

$$= \int \frac{R^\circ_\omega}{\sigma T^4}(1\text{-}\exp\left[-k^c{}_\omega l\right])d\omega + \int \frac{R^0{}_\omega}{\sigma T^4}\exp\left[-k^c{}_\omega l\right]\left(1\text{-}\exp\left[-\sum_i k_\omega{}^{line\ i} l\right]\right)d\omega$$

where $k^c{}_\omega$ is the spectral absorption coefficient for the continuum spectrum while $k_\omega{}^{line\ i}$ is that for the ith line. Since the continuum absorption coefficient is essentially constant over a line width, and since the important lines do not overlap, equation (50) may be written as

$$\varepsilon = \varepsilon_c + \sum_i (\exp\left[-k^c{}_{\omega_i} l\right])\varepsilon^{line\ i} \tag{51}$$

where ω_i is the wave number at the center of the ith line. Thus the total emissivity is equal to the continuum emissivity ε_c plus the line emissivities $\varepsilon^{line\ i}$ decreased by the transmissivity for continuum absorption at the line centers.

B. Representative calculations

First the component emissivities for a transparent gas, applicable over large ranges of T, p_T, and l, will be considered. The emissivity for $p_T = 100$ atm and $l = 30$ cm has also been calculated. An addition, component absorption coefficients are presented for use in radiative transfer problems.

1. *Transparent gases.* For a transparent gas, the emissivity of a component is given simply by a temperature dependent function times the mean beam length and the particular partial pressure(s) representative of the transitions involved.

The transparent gas emissivity term $(\varepsilon_{H_2})_L/p^2{}_{H_2}l$ for the H_2 molecule is given in Fig. 12. This figure supplies the actual H_2 emissivity for values of $p^2{}_{H_2}l$ for which there is little self-absorption. Since the absorption coefficient for H_2 varies rather gradually and covers a

VOL. 1 1961

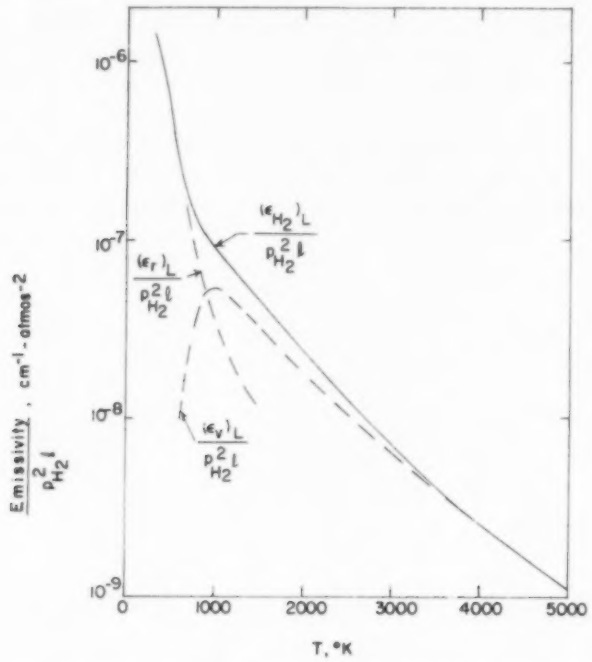

FIG. 12. The transparent gas emissivity term $(\varepsilon_{H_2})_L/p^2_{H_2}l$ as a function of the temperature. This term is the sum of the contributions from the pressure-induced rotational spectrum, $(\varepsilon_r)_L/p^2_{H_2}l$, and from the pressure-induced fundamental vibration–rotation band, $(\varepsilon_v)_L/p^2_{H_2}l$.

large portion of the blackbody curve, there will be little self-absorption for $(\varepsilon_{H_2})_L \lesssim 10^{-2}$. Thus Fig. 12 gives the actual H_2 emissivity down to 300°K for $p^2_{H_2}l \lesssim 10^4$ cm-atm², down to 1000°K for $p^2_{H_2}l \lesssim 10^5$ cm-atm², etc.

Similarly, for the H^- and H_2^+ ions, Fig. 13 presents the emissivity term $(\varepsilon_{H^-} + \varepsilon_{H_2^+})_L/p_e p_H l$ in the temperature range 3000°K to 10,000°K. In this temperature range, $(\varepsilon_{H^-})_L$ is more than ten times greater than $(\varepsilon_{H_2^+})_L$. Since the sum of the absorption coefficients for H^- and H_2^+ varies gradually over a large wave number range, the criterion for the gas to be transparent to a mixture of H^- and H_2^+ is $(\varepsilon_{H^-} + \varepsilon_{H_2^+})_L \lesssim 10^{-2}$. For example, it may be observed from Fig. 13 that the sum of the H^- and H_2^+ contributions to the emissivity at 5000°K is $0{\cdot}144 p_e p_H l$ if $p_e p_H l \lesssim 0{\cdot}1$.

Using equation (33) for the continuum absorption coefficient of the H atom, the expression for the emissivity of a transparent gas, equation (20), may be integrated directly to yield

$$\frac{(\varepsilon_{H,c})_L}{p_H l} = \left(\frac{160}{\pi^4\sqrt{3}}\right)\frac{\pi^2 e^6 Ry}{(kT)^4}\, e^{-x_1}\left[\sum_{n=1}^{\infty}\frac{1}{n^3} + \frac{0{\cdot}62}{x_1}\right] \tag{52}$$

and

$$\frac{(\varepsilon_{H,c})'_L}{p_H l} = \left(\frac{160}{\pi^4\sqrt{3}}\right)\frac{\pi^2 e^6 Ry}{(kT)^4}\, e^{-x_1}\left[\sum_{n=2}^{\infty}\frac{1}{n^3} + \frac{0{\cdot}62}{x_1}\right] \tag{53}$$

where the prime denotes the emissivity exclusive of the Lyman continuum. The value of the sum $\sum_{n=1}^{\infty} \frac{1}{n^3}$ is 1·20206. These emissivity terms are given in Fig. 14 along with the maximum absorption coefficient $k_{B,\omega}/p_H$ in the Balmer continuum. When $p_H l \lesssim 10^{-2}/(k_{B,\omega}/p_H)$, equation (53) may be used to give the actual emissivity of the H atom continuum, exclusive of the Lyman continuum. For the conditions of interest, the Lyman continuum

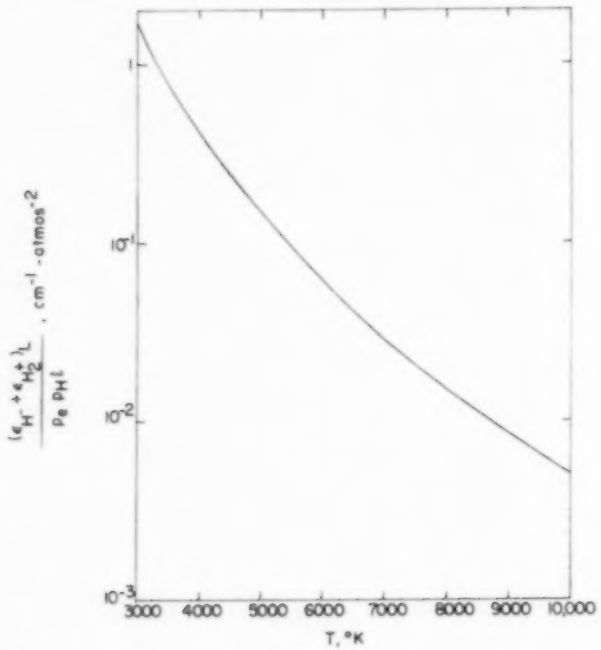

FIG. 13. The transparent gas emissivity term $(\epsilon_{H^-} + \epsilon_{H_2^+})_L/p_e p_H l$ as a function of temperature.

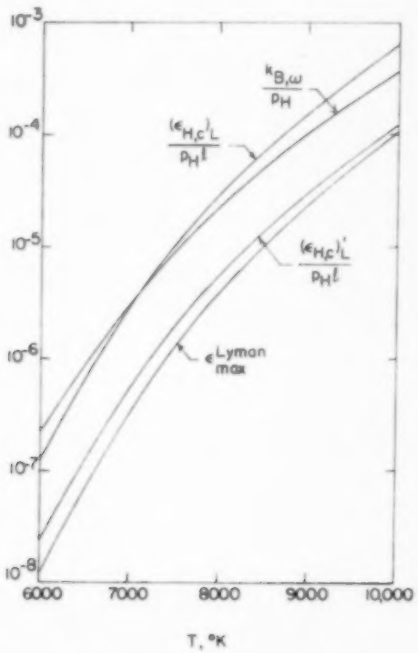

FIG. 14. The transparent gas emissivity terms $(\epsilon_{H,c})_L/p_H l$ and $(\epsilon_{H,c})'_L/p_H l$ in cm^{-1} atm^{-1}, the maximum value of the Balmer continuum absorption coefficient $k_{B,\omega}/p_H$ in cm^{-1} atm^{-1}, and $\epsilon^{Lyman}_{max} = \int_{Ry}^{\infty} R^{\circ}_{\omega}\, d\omega$ as functions of the temperature.

region is generally far from transparent. The maximum emissivity contribution possible from the Lyman continuum, viz.,

$$\epsilon^{Lyman}_{max} = \frac{1}{\sigma T^4} \int_{Ry=109{,}678\ cm^{-1}}^{\infty} R^0_{\omega}\, d\omega, \tag{54}$$

is also given in Fig. 14. Considering $T = 6000°K$, for example, it is evident from Fig. 14 that equation (53) will give the actual emissivity of the H atom continuum for $10 \lesssim p_H l \lesssim 10^6$ cm-atm.

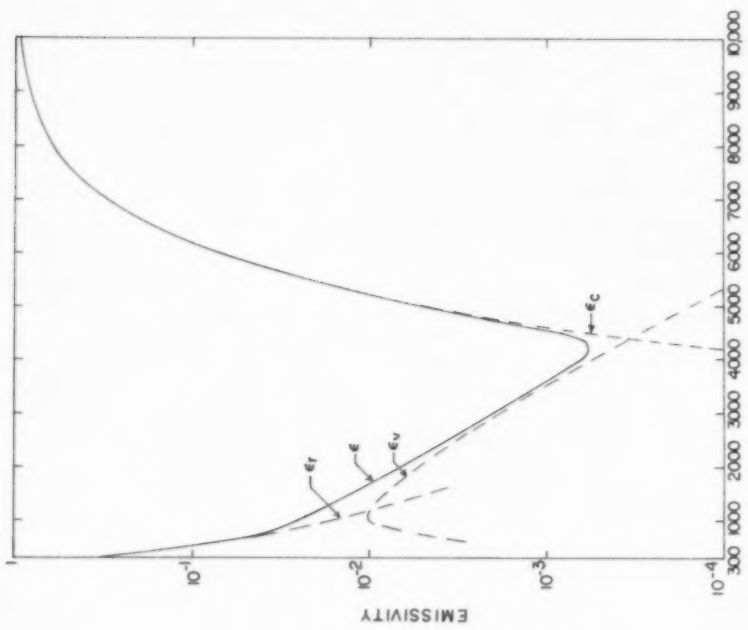

FIG. 16. The total emissivity ε of a hydrogen plasma for $p_T = 100$ atm and $l = 30$ cm. The dashed lines indicate emissivity contributions from the pressure-induced rotational lines ε_r and fundamental band ε_v and from the continuum spectrum ε_c.

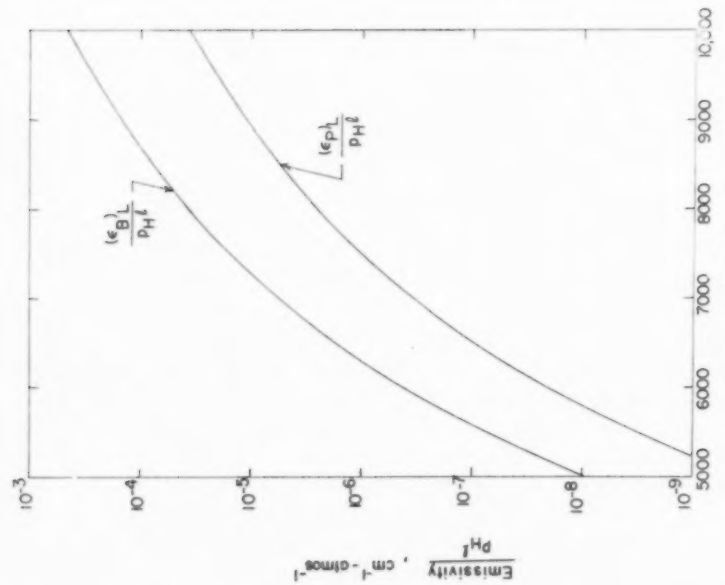

FIG. 15. The transparent gas emissivity terms $(\varepsilon_B)_L/p_H l$ and $(\varepsilon_P)_L/p_H l$ for the Balmer and Paschen lines, respectively.

The transparent gas emissivity terms for the Balmer and Paschen lines computed from equations (35) and (36) are presented in Fig. 15. A given line will be approximately transparent if the emissivity computed from equation (35) is less than one or both of the values computed from equations (46) and (48), i.e., when one or both of the inequalities $Sp_H l/2\pi b_c \lesssim 2/\pi$ and $p_H l/(p_e)^{2/3} \lesssim (A/S)^{5/3}$ hold. The Lyman α-line will be far from transparent at most optical depths of interest. The emissivity contribution of the Lyman α-line can be estimated from the analysis of section VI B 4, and proves to be negligibly small except for very small optical depths. The emissivity contributions of the Brackett series, Pfund series, etc., are negligibly small.

2. *Calculation for a total pressure of* 100 *atm and a mean beam length of* 30 *cm.* In Fig. 16 results are shown of an emissivity calculation for $p_T = 100$ atm and $l = 30$ cm for

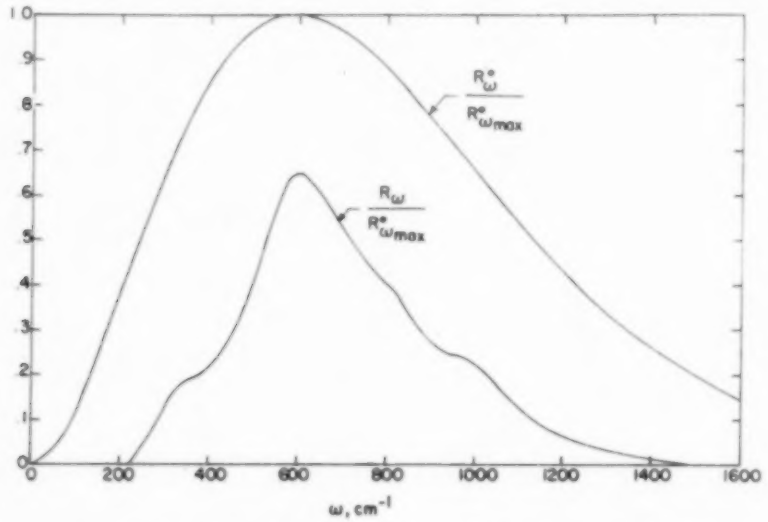

FIG. 17. The relative radiancy $R_\omega/R^\circ_{\omega_{max}}$ at 300°K for the pressure-induced rotational spectrum with $p_T = 100$ atm and $l = 30$ cm. The relative blackbody radiancy $R^\circ_\omega/R^\circ_{\omega_{max}}$ is shown for comparison.

$T = 300$°K to 10,000°K. At temperatures below about 1200°K, the pressure-induced rotational spectrum of H_2 provides the dominent emissivity contribution. The spectral radiancies at 300°K and 600°K are compared with the blackbody radiancies in Figs. 17 and 18. The dominant emissivity contribution is provided by the pressure-induced fundamental vibration–rotation band between 1200°K and 4400°K, and by the continuum radiation from 4400°K up to 10,000°K. The continuum radiation is primarily from the H^- bound-free and free-free transitions with the bound-free transitions of the H atom starting to become important at the higher temperatures. In Figs. 19–23 we show the spectral radiancy of the continuum spectrum. In Figs. 19–21 the division of the H^- continuum radiation into the sum of a contribution from free-free transitions and from bound-free transitions is evident. In Figs. 21–23 the Balmer bound-free continuum is observable. The emissivities of the atomic lines, decreased by the transmissivity of the

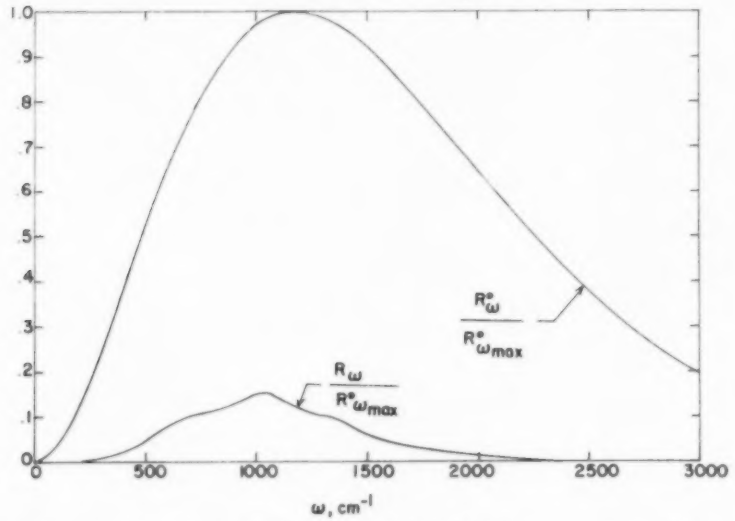

FIG. 18. The relative radiancy $R_\omega/R^\circ_{\omega_{max}}$ at 600°K for the pressure-induced rotational spectrum with $p_T = 100$ atm and $l = 30$ cm. The relative blackbody radiancy $R^\circ_\omega/R^\circ_{\omega_{max}}$ is shown for comparison.

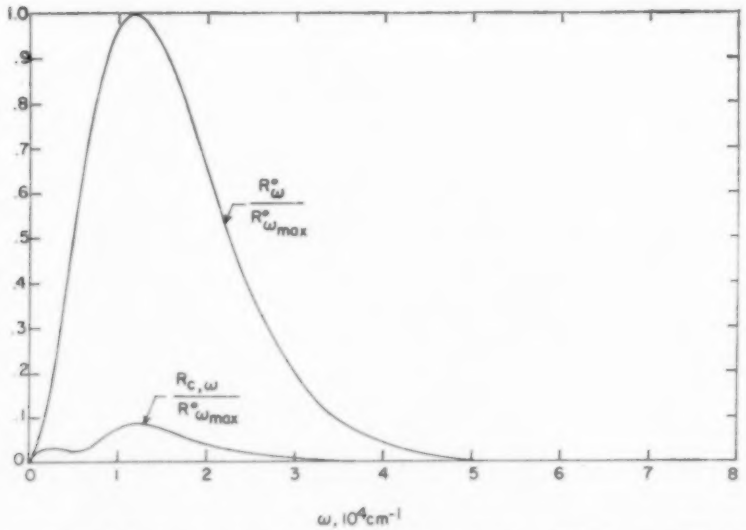

FIG. 19. The relative continuum radiancy $R_{c,\omega}/R^\circ_{\omega_{max}}$ for $T = 6000$°K, $p_T = 100$ atm and $l = 30$ cm compared with the relative blackbody radiancy $R^\circ_\omega/R^\circ_{\omega_{max}}$.

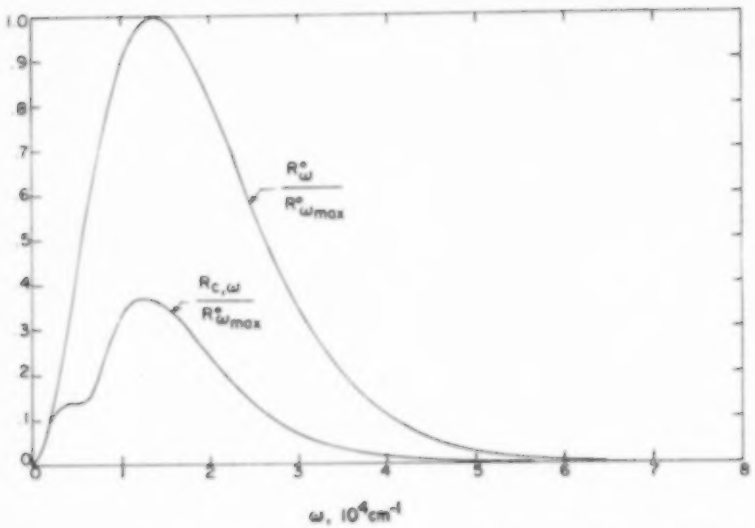

FIG. 20. The relative continuum radiancy $R_{c,\omega}/R^\circ_{\omega_{max}}$ for $T = 7000°K$, $p_T = 100$ atm and $l = 30$ cm compared with the relative blackbody radiancy $R^\circ_\omega/R^\circ_{\omega_{max}}$.

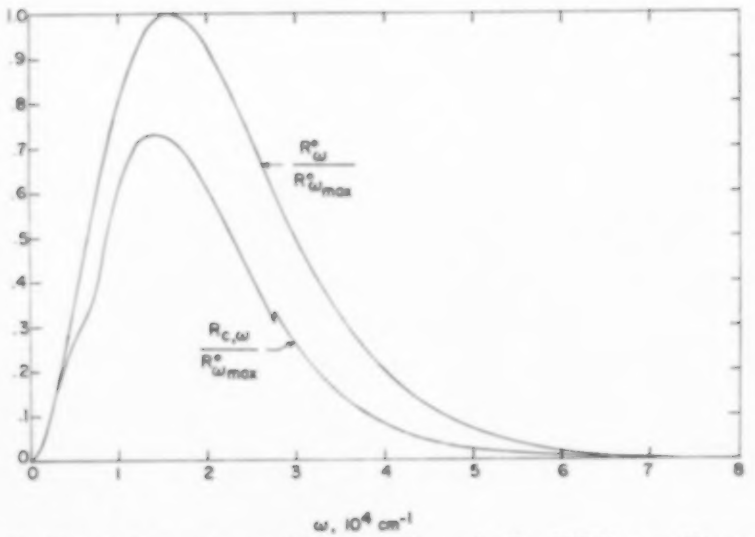

FIG. 21. The relative continuum radiancy $R_{c,\omega}/R^\circ_{\omega_{max}}$ for $T = 8000°K$, $p_T = 100$ atm and $l = 30$ cm compared with the relative blackbody radiancy $R^\circ_\omega/R^\circ_{\omega_{max}}$.

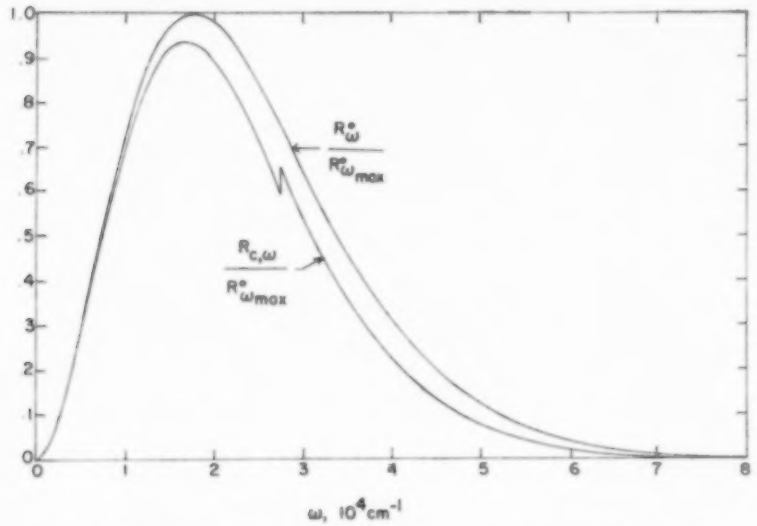

FIG. 22. The relative continuum radiancy $R_{c,\omega}/R^{\circ}_{\omega_{max}}$ for $T = 9000$°K, $p_T = 100$ atm and $l = 30$ cm compared with the relative blackbody radiancy $R^{\circ}_{\omega}/R^{\circ}_{\omega_{max}}$.

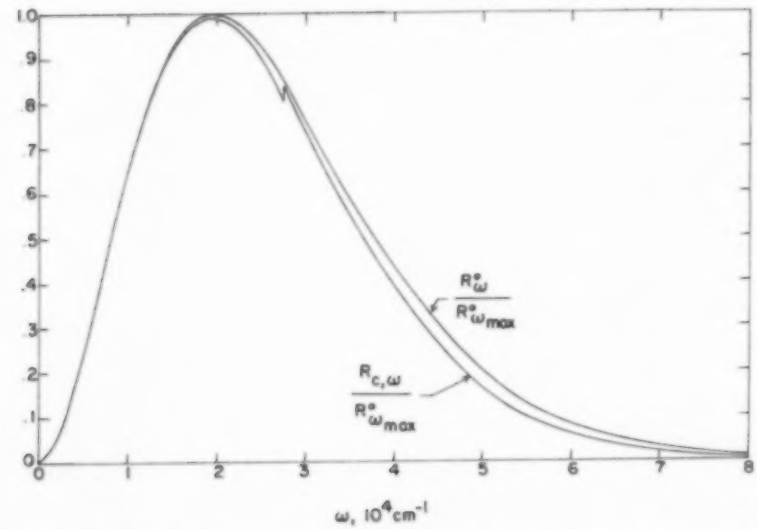

FIG. 23. The relative continuum radiancy $R_{c,\omega}/R^{\circ}_{\omega_{max}}$ for $T = 10{,}000$°K, $p_T = 100$ atm and $l = 30$ cm compared with the relative blackbody radiancy $R^{\circ}_{\omega}/R^{\circ}_{\omega_{max}}$.

continuum [cf. equation (51)], amount to less than a few per cent of the continuum emissivity.

Since the absorption coefficient for the H^- ion is proportional to $p_e p_H$ and that for the H atom is proportional to p_H, the H atom spectrum will become more important at lower total pressures.

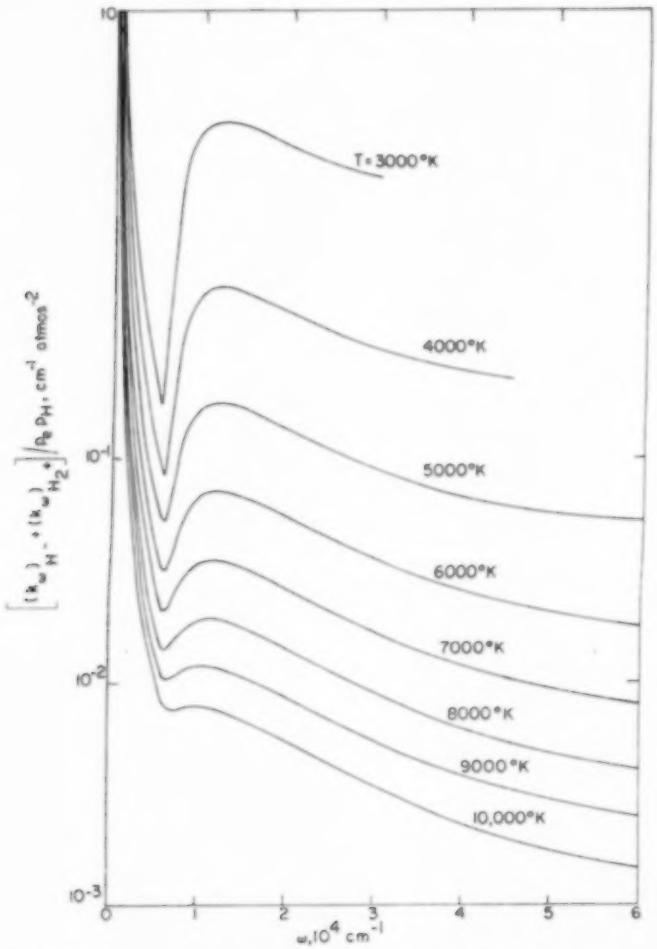

FIG. 24. The absorption coefficient term $[(k_\omega)_{H^-} + (k_\omega)_{H_2^+}]/p_e p_H$ at various temperatures.

3. *The absorption coefficient.* For the solution of many problems in radiative transfer it is necessary to know the spectral absorption coefficients directly, i.e., it may not be sufficient to know just the total isothermal emissivities. The spectral absorption coefficients for the various emission processes may be obtained by the procedures described in this paper.

The absorption coefficient for the pressure-induced rotation spectrum is given by equation (17) and is plotted in Figs. 7–9 for three different temperatures. At temperatures

VOL. 1 1961

near room temperature, the absorption coefficient for the pressure-induced vibration–rotation spectrum is given in Fig. 6, while approximate values at higher temperatures may be obtained by use of the box model, as discussed in section III A 1. The absorption coefficient term $[(k_\omega)_{H^-} + (k_\omega)_{H_2^+}]/p_e p_H$ is given in Fig. 24 for temperatures from 3000°K to 10,000°K. In Fig. 25, the absorption coefficient term $(k_{c,\omega})_H/p_H$, calculated from

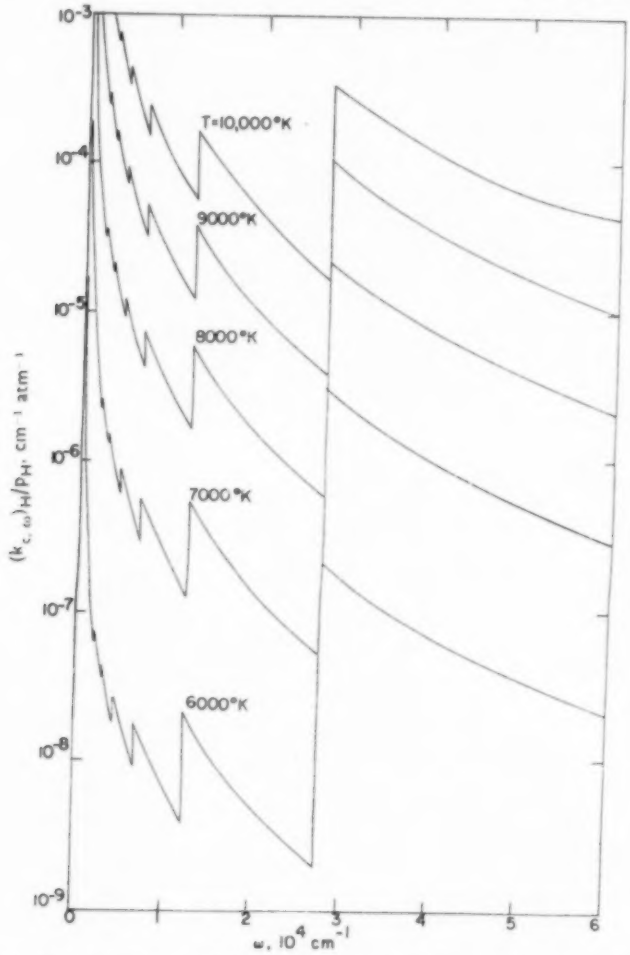

FIG. 25. The absorption coefficient term $(k_{c,\omega})_H/p_H$ at various temperatures.

equation (33), is presented for temperatures from 6000°K to 10,000°K. The absorption coefficient in the wings of the atomic spectral lines may be calculated from equations (38) and (47) for collision-broadening and Stark-broadening, respectively (see Ref. 5 for a discussion of Doppler-broadening).

Acknowledgement—The author is indebted to Dr. S. S. PENNER for suggesting this investigation and for helpful discussions and suggestions during the course of the work.

REFERENCES

1. F. MASTRUP, *J. Opt. Soc. Amer.* **50**, 32–35 (1960).
2. A. UNSÖLD, *Z. Astrophys.* **24**, 355–362 (1948).
3. G. ECKER and W. WEIZEL, *Ann. Phys., Lpz.* **17**, 126–140 (1956).
4. H. MARGENAU and M. LEWIS, *Rev. Mod. Phys.* **31**, 569–615 (1959).
5. S. S. PENNER, *Quantitative Molecular Spectroscopy and Gas Emissivities*, Addison-Wesley Publishing Co., Reading, Mass. (1959).
6. M. MIZUSHIMA, *Phys. Rev.* **77**, 150–151 (1950).
7. W. F. J. HARE and H. L. WELSH, *Canad. J. Phys.* **36**, 88–103 (1958).
8. H. P. GUSH, A. NANASSY and H. L. WELSH, *Canad. J. Phys.* **35**, 712–719 (1957).
9. D. A. CHISHOLM and H. L. WELSH, *Canad. J. Phys.* **32**, 291–312 (1954).
10. J. VAN KRANENDONK, *Physica* **24**, 347–362 (1958).
11. J. VAN KRANENDONK, *Physica* **23**, 825–837 (1957).
12. J. VAN KRANENDONK and R. B. BIRD, *Physica* **17**, 953–967, 968–975 (1951).
13. NBS Circular 564, *Tables of Thermal Properties of Gases*, 1 November (1955).
14. J. P. COLPA and J. A. A. KETELAAR, *Molec. Phys.* **1**, 14–22, 343–357 (1958).
15. Z. J. KISS, H. P. GUSH and H. L. WELSH, *Canad. J. Phys.* **37**, 362–376 (1959).
16. J. VAN KRANENDONK and Z. J. KISS, *Canad. J. Phys.* **37**, 1187–1198 (1959).
17. Z. J. KISS and H. L. WELSH, *Canad. J. Phys.* **37**, 1249–1259 (1959).
18. G. HERZBERG, *Molecular Spectra and Molecular Structure I. Spectra of Diatomic Molecules*. Van. Nostrand, New York (1953).
19. H. SHULL, *J. Chem. Phys.* **20**, 18–21 (1952).
20. B. KIVEL, H. MAYER and H. BETHE, *Ann. of Phys.* **2**, 57–80 (1957).
21. H. M. JAMES and A. S. COOLIDGE, *Phys. Rev.* **55**, 184–190 (1939).
22. H. M. JAMES and A. S. COOLIDGE, *Astrophys. J.* **87**, 438–459 (1938).
23. G. HERZBERG, *Astrophys. J.* **87**, 428–437 (1938).
24. G. C. WICK, *R. C. Accad. Lincei.* **21**, 708–714 (1935).
25. S. CHANDRASEKHAR and D. D. ELBERT, *Astrophys. J.* **125**, 633–635 (1958).
26. S. CHANDRASEKHAR, *Astrophys. J.* **128**, 114–123 (1958).
27. S. CHANDRASEKHAR, *Astrophys. J.* **102**, 395–401 (1945).
28. S. CHANDRASEKHAR and F. H. BREEN, *Astrophys. J.* **104**, 430–445 (1946).
29. J. F. HART and G. HERZBERG, *Phys. Rev.* **106**, 79–82 (1957).
30. L. M. BRANSCOMB and W. L. FITE, *Phys. Rev.* **93**, 651 (1954).
31. B. H. BRANDSEN, A. DALGARNO, T. L. JOHN and M. L. SEATON, *Proc. Phys. Soc. Lond.* **71**, 877–892 (1958).
32. T. OHMURA and H. OHMURA, *Astrophys. J.* **131**, 8–11 (1960).
33. D. R. BATES, K. LEDSHAM and A. L. STEWART, *Phil. Trans.* **A246**, 215–240 (1953).
34. D. R. BATES, *J. Chem. Phys.* **19**, 1122–1124 (1951).
35. D. R. BATES, *Mon. Not. R. Astr. Soc.* **112**, 40–44 (1952); **111**, 303–314 (1951).
36. H. A. KRAMERS, *Phil. Mag.* **46**, 836–871 (1923).
37. J. A. GAUNT, *Proc. Roy. Soc. Lond.* **A126**, 654–660 (1930).
38. A. W. MAUE, *Ann. Phys., Lpz.* **13**, 161–190 (1932).
39. A. SOMMERFELD, *Atombau und Spektrallinien*, Vieweg, Braunschweig (1939).
40. J. GREENE, *Astrophys. J.* **130**, 693–701 (1959).
41. D. H. MENZEL and C. L. PEKERIS, *Mon. Not. R. Astr. Soc.* **96**, 77–111 (1935).
42. H. MAYER, Los Alamos Scientific Laboratory Report LA-647 (1947).
43. A. UNSÖLD, *Physik der Sternatmosphären*, Springer, Berlin (1938).
44. L. H. ALLER, *Astrophysics*, p. 133, The Ronald Press, New York (1953).
45. H. MARGENAU and W. W. WATSON, *Rev. Mod. Phys.* **8**, 22–53 (1936).
46. V. WEISSKOPF, *Z. Phys.* **75**, 287–301 (1932).
47. H. AROESTE and W. C. BENTON, *J. Appl. Phys.* **27**, 117–121 (1956).
48. A. B. UNDERHILL and J. H. WADDELL, NBS Circular 603 (1959).
49. H. MARGENAU and M. LEWIS, *Rev. Mod. Phys.* **31**, 569–615 (1959).
50. R. A. BUCKINGHAM, S. REID and R. SPENCE, *Mon. Not. R. Astr. Soc.* **112**, 382–386 (1952).
51. A. S. COOLIDGE and H. M. JAMES, *J. Chem. Phys.* **6**, 730–734 (1938).

VOL.
1
1961

J. Quant. Spectrosc. Radiat. Transfer. Vol. 1, pp. 135–142. Pergamon Press Ltd. Printed in Great Britain

TRANSITION PROBABILITIES FOR NITRIC OXIDE IN THE FAR ULTRAVIOLET*

J. W. DAIBER and M. J. WILLIAMS†
Cornell Aeronautical Laboratory, Inc., P.O. Box 235, Buffalo 21, New York

(*Received* 7 *December* 1960)

Abstract—Nitric oxide was heated in a shock tube up to 2200°K behind the reflected shock wave. Absorption spectra of the (0, 1), (0, 2), (0, 3) and (1, 4) bands of the gamma system were photographed, using a continuum light source and a medium quartz spectrograph. The NO was diluted in an argon bath in volume ratios from 0·08 to 10 per cent. This was necessary for two reasons. First, it was essential to photograph the spectra before the NO decomposed detectably. An earlier study by Freedman and Daiber verified that argon dilution slows the NO decomposition rate because of reduction in NO partial pressure. The effectiveness of this dilution was confirmed by the absence of O_2 absorption on the resulting spectrograms. Secondly, high pressures were used to obliterate the rotational structure, and at the required pressures pure NO is totally absorbing. The wavelength-integrated absorption coefficients for each band were determined. From these data, the electronic oscillator strength was calculated to be 0·0034 ± 25 per cent. This value is greater than the 0·0024 derived by Weber and Penner and the 0·0022 derived by Bethke from gas cell measurements at room temperature of the γ (v', 0) sequence in the vacuum ultraviolet, and the value of 0·001 ± 50 per cent based on the emissivities of 4000°K air by Keck *et al.* For the NO beta system, which was not observed on any spectrogram, the electronic oscillator strength was inferred to be less than 0·006. This value does not discriminate between Keck's 0·006 and Bethke's 0·0015.

I. INTRODUCTION

THE emissivity of air depends on the energy-level populations, spectral line shape and oscillator strengths for each of its chemical constituents. For gases in equilibrium the population distribution is given by statistical mechanics but it is necessary to resort to experiment for the oscillator strengths and the dependence of line width on temperature and density.

For air between 2000 and 5000°K, the optically-important radiators in the ultraviolet are the Schumann–Runge system of oxygen and the nitric oxide β and γ systems. A detailed study of line widths and transition probabilities for the Schumann–Runge system of oxygen has been reported[1]. MARMO[2], MAYENCE[3] and LAMBREY[4] measured nitric oxide absorption coefficients in the region from 1600 to 2300 Å. However, because the pressure-broadening of the rotational lines was insufficient to remove the effect of finite slit width, the oscillator strengths could not be determined[5–8]. Sufficient pressure-broadening was attained by WEBER and PENNER[9] and BETHKE[10]. Using gas cells filled with NO in an inert diluent and photometric technique, they measured the absorption of the first few bands of the γ system $v'' = 0$ sequence in the vacuum ultraviolet and determined an electronic absorption oscillator strength. In addition, Bethke reported an electronic oscillator strength based on measurements of the absorption of the $v'' = 0$ sequence of the NO β system.

* Supported by the Combustion Dynamics Division of the AFOSR.
† The authors wish to express their thanks to Dr. Walter H. Wurster for his help and advice.

The gas cell technique is limited to measurements at or very near room temperature. Consequently the higher vibrational states in the lower electronic level are not populated and the oscillator strengths for the v' progressions can not be determined directly at these temperatures. It is these bands which are important in high temperature air emissivity calculations and consequently it is desirable to measure directly the transition probabilities for these bands.

In the present study, nitric oxide, carefully purified and premixed with argon, was heated by shock-tube techniques to temperatures from 1500°K to 2200°K at total densities from 16 to 33 atm. The absorption spectrum behind the reflected shock was then photographed using a short-duration, high-intensity light source. The β bands were not observed because the transitions for which the initial vibrational levels were appreciably populated had very small Franck–Condon factors[11]. The oscillator strengths of the γ (0, 1), γ (0, 2), γ (0, 3), γ (1, 3) and γ (1, 4) bands were obtained from the calibrated absorption spectrograms.

II. THEORY

When the absorbing gas is of uniform temperature and density along the optical path, and when its radiation is negligible compared with the radiation from the flash lamp, as in the present experiments, the spectral transmission may be written

$$I_{\tilde{\nu}}/I_{0_{\tilde{\nu}}} = \exp\{-\tau_{\tilde{\nu}}\}$$

where $I_{0_{\tilde{\nu}}}$ is the initial intensity of radiation of wave number $\tilde{\nu}$, $I_{\tilde{\nu}}$ is the transmitted intensity and $\tau_{\tilde{\nu}}$ is the spectral absorption coefficient. The integral of the absorption coefficient over a single vibrational band,

$$\int_{v',v''} \tau_{\tilde{\nu}} d\tilde{\nu} = \int_{v',v''} \ln(I_{0_{\tilde{\nu}}}/I_{\tilde{\nu}}) d\tilde{\nu},$$

is related to the vibrational oscillator strength $f_{v',v''}$, by the expression [12]

$$\int \tau_{\tilde{\nu}} d\tilde{\nu} = (\pi e^2/mc^2)\, N_{v''} f_{v',v''} X$$

where

$$\pi e^2/mc^2 = 8{\cdot}85 \times 10^{-13}\ \text{cm}$$

X is the pathlength, and $N_{v''}$ is the number density of absorbing molecules in the lower level for the transition.

Assuming that the total wave function is separable into the product of vibrational and electronic wave functions and that the electronic transition integral is constant for the band system, the electronic oscillator strength is [10]

$$f_{v',v'')_{\text{el}} = f_{v',v''} \frac{\sum_{v'} \tilde{\nu}_{v',v''}\, q_{v',v''}}{\tilde{\nu}_{v',v''}\, q_{v',v''}}$$

where $\tilde{\nu}_{v',v''}$ is an average wave number for the band and $q_{v',v''}$ is the overlap integral squared. Since the set of overlap integrals for $v'' > 0$ is not sufficiently complete to permit an accurate evaluation of the summation

$$\sum_{v'} \tilde{\nu}_{v',v''}\, q_{v',v''} \tag{1}$$

the wave number of the (0, 0) band head[9], $\tilde{\nu}_{0,0} = 4{\cdot}43 \times 10^4\ \text{cm}^{-1}$, is substituted. Once the electronic oscillator strength is known, vibrational oscillator strengths for other bands of the system can be determined from this equation.

VOL
1
196

The ultraviolet γ bands of nitric oxide correspond to $A^2\Sigma^+ \leftrightarrow X^2\Pi$ transitions. Because the lower state has two levels, $^2\Pi_{\frac{3}{2}}$ and $^2\Pi_{\frac{1}{2}}$, separated by 121·1 cm^{-1}, each γ band consists of two sub-bands. Each sub-band has six branches, two of which form heads. Wavelengths of rotational lines for eight of the twelve branches of the (0, 2), (0, 3) and (0, 4) bands have been listed by GUILLERY[13]. The mean line spacing for these listed lines in the region about 250 cm^{-1} behind the long-wavelength sub-band heads is 2 cm^{-1}.

In order to obtain accurate measurements of the contour of absorption spectra, it is necessary to avoid distortion due to the slit function. This could be accomplished by using a very narrow spectrograph slit, were it not for the lower limit on the slit function width. In addition, analysis of each individual line of such a complex spectrum would be impractical. An alternative is to pressure-broaden the lines so that they are broad when compared with the slit function and/or they overlap sufficiently to obliterate the rotational structure.

The half-width of γ-band lines collision-broadened in pure NO is approximated by the expression[14]

$$b_c)_{\text{NO-NO}} \approx (0{\cdot}10\ \text{P})/(\text{T}/300)^{\frac{1}{2}}$$

where the pressure is in atmospheres. Assuming an NO–A collision diameter approximately half that of the NO–NO collision diameter, the half-width of γ-band lines collision-broadened by argon is

$$b_c)_{\text{NO-A}} \approx \tfrac{1}{4} b_c)_{\text{NO-NO}}$$

For a mean line spacing of 2 cm^{-1}, the rotational structure should be blended if $b_c)_{\text{NO-A}}$ is $\sim$ 1 cm^{-1}. At 2000°K, this would require pressures of the order of 100 atm, which are easily obtainable using conventional shock-tube techniques.

III. EXPERIMENTAL CONSIDERATIONS

The shock tube was used to heat mixtures of nitric oxide and argon to high temperatures at known thermodynamic conditions. A beam from a high-intensity light source was passed through this gas into a spectrograph. The resulting spectrogram was analyzed with a densitometer and the absorption of the NO γ bands determined.

The shock tube used in this study was used in previous studies of radiative properties of hot gases[1]. The driver gas was helium and the test gas in the driven section was nitric oxide diluted in argon. The vacuum pump to each section of the tube had a liquid-nitrogen cold trap at its intake to prevent oil vapors from reaching the tube; in addition, the impurity level of the tube was kept to an absolute minimum by thoroughly swabbing the tube with alcohol after each run.

The nitric oxide was purified by passing it through a soda-lime trap to remove any nitrogen dioxide it contained. Then the NO was mixed with argon in separate tanks to form mixtures containing from 0·08% to 10% (by volume) of nitric oxide. These gases were allowed to stand at least 24 hr to insure a homogeneous mixture.

With the optical pathlength of the present shock tube, 6·35 cm, increasing the density of NO to produce the necessary pressure broadening would result in absorption too great to permit measurements. Hence, an inert argon bath was used to pressure-broaden the individual lines in the NO spectrum. The decomposition kinetics of nitric oxide were studied separately[15]. The results indicated that at 2000°K the reaction rate for NO–NO collisions was 200 times that for NO–A collisions. Thus the use of the argon diluent had

the further advantage of slowing the decomposition reaction. None of the spectrograms from which data were taken showed any oxygen absorption indicating that the species concentrations and thermodynamic variables were maintained at the chemically-frozen shock values for the duration of the testing time.

The measured wave speed exhibited a slight attenuation and was consequently extrapolated linearly to the end wall. The conditions of the gas behind the reflected shock wave were calculated by using an IBM program[16] which included vibrational, but not chemical, equilibrium. Because of the attenuation in the wave speed, the error in the time between stations resulted in an uncertainty of $\pm 50^{\circ}$K in the gas temperature behind the reflected shock wave.

The output of the end wall pressure transducer was displayed on a dual-beam oscilloscope. This record was only used to determine the length of the testing time. The other beam of this oscilloscope displayed the output of a current probe in the lamp housing. This record then served as an independent verification of the time of the lamp flash, and consequently insured that the absorption measurements were made in a gas of known thermodynamic state.

The light source used for the absorption measurements was a short-duration high-intensity argon flash lamp[1]. The light output lasted for less than 20 μsec and gave continuum radiation from 2200 Å through the visible region of the spectrum. Spectrograms of the lamp flash showed slight variations in the time-integrated intensity. For this reason background flashes were taken before and after the run. Agreement in the measured output of these flashes were accepted as an indication of an equal intensity of incident radiation on the gas sample during the experiment.

Parallel rays from the flash lamp were passed through the shock tube and focused on a 6-mm-by-approximately-25-μ slit of an f/10 Bausch and Lomb medium-quartz spectrograph. This slit width was chosen on the basis of spectrograms of a low-pressure mercury lamp because it is the maximum slit setting consistent with minimum spectral line width (approximately 3 cm^{-1}).

The photographic plates used for the spectrograms were Kodak-Type 103–0. These plates were developed for 9 min in D–19 at 68° F. In spite of this forced development, the gradient was only $\sim 0{\cdot}4$ in the wavelength region of interest. The forced development did have the beneficial effect of extending the linear region to emulsion densities as low as 0·1. The plates were calibrated by inserting known filters in the flash-lamp beam. Thus a calibration was possible without assuming a reciprocity relation for the plate.

The photographic plates were analyzed with the aid of a Jarrell–Ash recording microphotometer. The scanning-beam width was set at 3 μ, which is sufficiently narrow to record the spectrogram without loss in resolution.

The conditions of the experiments were adjusted so as to keep the spectrogram density at values corresponding to the linear part of the characteristic curve. Hence, the integrated absorption coefficient could be determined directly from the relation

$$\int \tau_{\tilde{\nu}} d\tilde{\nu} = \int (\Delta D_{\tilde{\nu}}/S) d\tilde{\nu}$$

where $\Delta D_{\tilde{\nu}}$ is the difference in emulsion density between the absorption spectrum and the background and S is the slope of the characteristic curve at the weighted center of the band.

Assuming the dispersion curve linear over the extent of the band, a plot of $\Delta D_{\tilde{\nu}}$ vs. $\tilde{\nu}$ was drawn on linear paper (Fig. 1) and the area beneath the curve measured to obtain $\int \Delta D_{\tilde{\nu}} d\tilde{\nu}$.

IV. RESULTS: GAMMA BAND SYSTEM

From a single plate, measurable data could be obtained for only one band because of the relatively wide spacing of vibrational energy levels. The absorption of adjacent bands was either undetectable or extended into the region of nonlinear plate response. This is illustrated in Fig. 2, which is a spectrogram with data for the γ (0, 4) band.

A densitometer record of a spectrogram is shown in Fig. 1. The total line width ($2\,b_c$) due to pressure broadening by the argon is approximately 3·2 cm^{-1} for the conditions of this run. The conditions of the other runs give similar results. This indicates that the

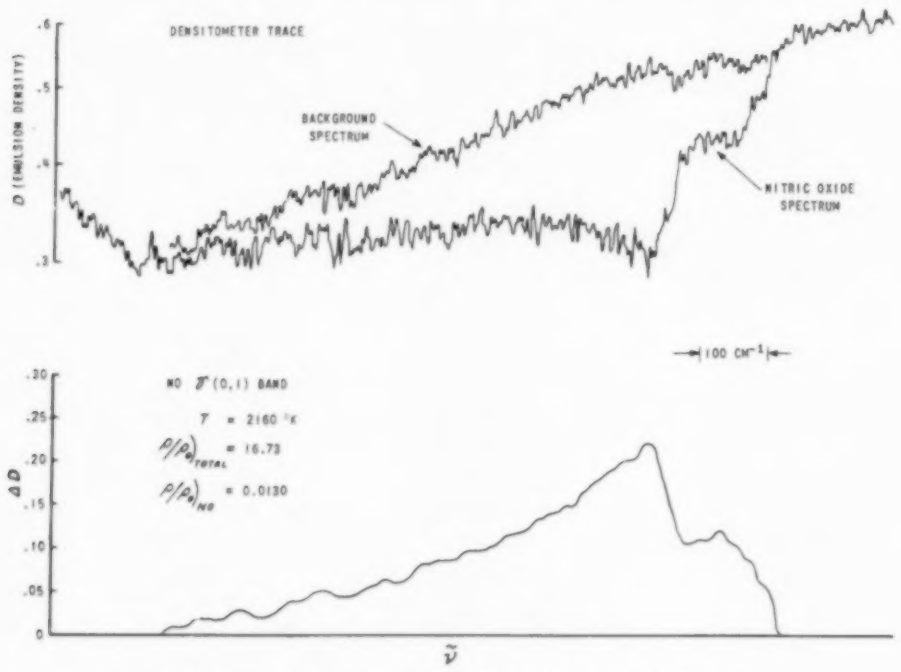

FIG. 1. Absorption spectrum of the nitric oxide gamma (0, 1) band.

overlapping due to collision broadening is such that the slit function is no longer of critical importance.

The bands for which measurable absorption was achieved are the γ (0, 1), γ (0, 2), γ (0, 3) and the overlapping γ (1, 3) and γ (1, 4). Because of the large pathlength used (6·35 cm), the absorption of the γ (0, 0) band for all attainable conditions was too great. At the highest temperatures and concentrations permissible (to forestall decomposition reactions), the γ (0, 4) band was weakly absorbing. In addition, it was strongly overlapped by the γ (1, 5) and γ (2, 6) bands and hence no quantitative analysis was attempted for these transitions.

In all cases the γ (0, 1) and γ (0, 2) bands appeared to be free of overlapping from other bands. However, the γ (1, 3) band does overlap the γ (0, 2) band. The calculated overlap integral[11] of the γ (1, 3) band is $\sim$ 0·3 of the γ (0, 2) overlap integral. However, at 2000°K

the ratio of populations of the third to the second vibrational level is ~ 0·28. Thus the relative intensities of the two bands should be ~ 0·08. The contribution of the γ (1, 3) band, therefore, should not be expected to be separable from that of the γ (0, 2). The total absorption in the region of the γ (0, 2) band was attributed to the γ (0, 2) and γ (1, 3) bands and the electronic oscillator strength, $f_{v',v'})_{el}$, was computed assuming its variation for these overlapping bands to be negligible. The γ (0, 3) and γ (1, 4) absorption was treated similarly, although in this case the overlap was easily discernible. The results are given in Table 1. The conditions given in the table are those behind the reflected shock, where ρ_0 is density at standard temperature and pressure.

Table 1. Oscillator-strength determinations for NO gamma system

Bands	T (°K)	$\frac{\rho}{\rho_0})_{Total}$	$\frac{\rho}{\rho_0})_{NO}$	$\int \tau_\nu d\bar{\nu}$ (cm^{-1})	f_{el}
γ (0, 1)	2160	16·73	0·0130	$3{\cdot}13 \times 10^2$	$3{\cdot}4 \times 10^{-3}$
	1970	20·81	0·0107	$2{\cdot}64 \times 10^2$	$3{\cdot}7 \times 10^{-3}$
	1970	18·52	0·0143	$3{\cdot}16 \times 10^2$	$3{\cdot}3 \times 10^{-3}$
γ (0, 2), γ (1, 3)	1960	18·57	0·0619	$3{\cdot}51 \times 10^2$	$3{\cdot}6 \times 10^{-3}$
	2070	20·00	0·0666	$3{\cdot}67 \times 10^2$	$3{\cdot}1 \times 10^{-3}$
γ (0, 3), γ (1, 4)	1620	32·60	3·26	$1{\cdot}54 \times 10^3$	$3{\cdot}8 \times 10^{-3}$
	1715	29·58	2·96	$1{\cdot}54 \times 10^3$	$3{\cdot}1 \times 10^{-3}$
	1520	18·29	0·914	$2{\cdot}78 \times 10^2$	$3{\cdot}2 \times 10^{-3}$

For the higher vibrational states, the major source of inaccuracy is associated with the uncertainty in estimating the shock wave velocity and hence the temperature at which the experiments were performed. In the third vibrational level of the ground state, an error of 50° at 2000°K causes $\Delta N_{v'}/N_{v'}$ to be 10 per cent, whereas in the second vibrational level the error is only 5 per cent which is comparable to the uncertainty in the total density. The plate calibration is reliable to within approximately 10 per cent. There are additional small errors in the percentage of NO mixed with the argon, the initial pressure level in the shock tube, and the values of the overlap integrals. Consequently, we estimate that the uncertainty in the electronic oscillator strength is $\pm$25 per cent.

V. RESULTS: BETA BAND SYSTEM

In most cases the bands of the NO beta system are superimposed near the heads of NO gamma bands. However, a few occur far in the tails and thus should be more easily detectable. Of these, the strongest are those which have relatively-large overlap integrals and originate from relatively more populous vibrational levels of the $X^2\Pi$ state. Only the β (0, 4) band at 2625 Å has the optimum conditions for detection at temperatures less than 2000°K. Since the gamma and beta systems share the same lower electronic level, the γ (0, 4) band originates from the same level as this beta band. Therefore, a spectrogram taken at conditions designed to enhance the γ (0, 4) band should be most likely to emphasize the β (0, 4) band. At temperatures required to sufficiently populate the fourth vibrational level of the lower state, decomposition reactions may have altered somewhat the density of NO molecules by the time the spectrogram is taken. Although this precludes the use of these spectrograms for determining absolute oscillator strengths, a comparison of bands originating from the same lower level is still valid. Nevertheless, a close inspection of these

OL.
1
961

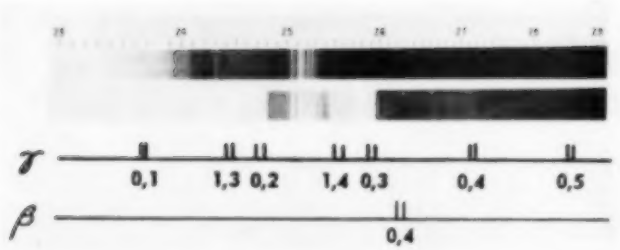

FIG. 2. Spectrogram showing the absorption of nitric oxide. The upper trace is that of the lamp and shows the quartz lines. T = 1620°K, $(\rho/\rho_0)_{total} = 32{\cdot}6$, $(\rho/\rho_0)_{NO} = 3{\cdot}26$. The wavelength scale is in 100's of Angstroms.

(*facing p.* 140)

VOL.
1
1961

spectrograms, which clearly showed γ (0, 4) absorption, failed to reveal the beta system band (see Fig. 2).

The beta band heads tend to be obscured because they are less sharp than the gamma band heads. It can be shown that the ratio of the intensity in the first 100 cm^{-1} (approximately $\frac{1}{2}$ mm on the spectrogram) of the three branches of one sub-head to the total branch intensities at 2000°K is 1·8 times greater for the gamma bands than for the beta bands.

The ratio of the electronic oscillator strengths for the beta and gamma bands is given by

$$f_{el})_\beta / f_{el})_\gamma = (\int \tau d\tilde{\nu}/q_{0,4})_\beta / (\int \tau d\tilde{\nu}/q_{0,4})_\gamma$$

Since both transitions start from the same lower level, the population ratio is unity. Using $\tilde{\nu}_{0,0})_\beta$ (determined by extrapolation from tabulated wavelengths to be $4{\cdot}55 \times 10^4$ cm^{-1}) and $\tilde{\nu}_{0,0})_\gamma$ in place of the summations (1), the factor

$$(\tilde{\nu}_{0,0}/\tilde{\nu}_{0,4})_\beta / (\tilde{\nu}_{0,0}/\tilde{\nu}_{0,4})_\gamma$$

is also unity. Taking the ratio of the maximum absorption as an indication of the relative total absorption of the β (0, 4) and γ (0, 4) bands, then

$$\int_\beta \tau d\tilde{\nu} / \int_\gamma \tau d\tilde{\nu} \approx 1{\cdot}8[(\Delta D/S)^\beta_{max.}/(\Delta D/S)^\gamma_{max.}]$$

One of the spectrograms showed the γ (0, 4) band to have a maximum absorption of $\Delta D = 0{\cdot}15$ with an average emulsion density, D, of 0·4. At 2625 Å this same spectrogram had a noise level with an approximate amplitude of $\Delta D = 0{\cdot}01$. It was then estimated that the β (0, 4) band could have been discriminated from the noise if the maximum absorption corresponded to a ΔD of 0·03. Therefore, taking into account the ratio of calibration slopes,

$$\int_\beta \tau d\tilde{\nu} / \int_\gamma \tau d\tilde{\nu} < 0{\cdot}49$$

The overlap integral ratio[11, 17] is

$$q_{0,4})_\gamma / q_{0,4})_\beta = 3{\cdot}6$$

Hence, the relative electronic oscillator strength is

$$f_{el})_\beta < 1{\cdot}8\, f_{el})_\gamma$$

or

$$f_{el})_\beta < 0{\cdot}006$$

VI. COMPARISON WITH PRIOR RESULTS

Electronic oscillator strengths have been measured for NO band systems at wavelengths in the interval between 1700 Å and 5000 Å. The results are summarized in Table 2.

TABLE 2. COMPARISON WITH PRIOR RESULTS

	$f_{el})_\gamma \times 10^3$	Experimental range (Å)	$f_{el})_\beta \times 10^3$	Experimental range (Å)
WEBER and PENNER[9]	2·4 ± 0·4	2000–2280	—	—
BETHKE[10]	2·2 ± 0·1	1700–2280	1·5 ± 0·1	1700–2280
KECK *et al.*[18]	1 ± 0·5	2500–2700	6 ± 2	3500–5000
Present results	3·4 ± 0·8	2300–2730	$\lesssim 6$	2630

The measurements of KECK *et al.* were obtained from emission spectra of heated air. This procedure involves the removal of the contributions of other radiating species and attributes the remainder to NO. It is thus subject to errors in the knowledge of transition probabilities for the other components. Since Bethke measured absorption of bands originating from $v'' = 0$ only, he was able to use the summation (1) in the reduction of his data. Therefore his reported value of 0·0024 has been adjusted for comparison with the other results.

There is reasonable agreement among the values of $f_{el})_{\gamma}$ given by references 9 and 10 for the bands in the vacuum ultraviolet and those of the present report for bands in the far ultraviolet. The upper limit for $f_{el})_{\beta}$ established by the discussion of the preceding section is in accord with both of the previously measured values and therefore gives no basis for preferring either.

REFERENCES

1. C. E. TREANOR and W. H. WURSTER, *J. Chem. Phys.* **32,** 758 (1960).
2. F. F. MARMO, *J. Opt. Soc. Amer.* **43,** 1186 (1953).
3. J. MAYENCE, *Ann. Phys., Paris* (Ser. 12) **7,** 453 (1952).
4. M. LAMBREY, *Ann. Phys., Paris* (Ser. 10), **14,** 95 (1930).
5. S. P. ERKOVICH, *Optika i Spektroskopiia,* **6,** 193 (1959).
6. S. S. PENNER, *J. Opt. Soc. Amer.* **50,** 627 (1960).
7. R. F. HUGHES, *J. Opt. Soc. Amer.* **50,** 740 (1960).
8. S. P. ERKOVICH and YU. V. PISAREVSKY, *Optika i Spektroskopiia* **8,** 160 (1960).
9. D. WEBER and S. S. PENNER, *J. Chem. Phys.* **26,** 860 (1957).
10. G. W. BETHKE, *J. Chem. Phys.* **31,** 662 (1959).
11. W. R. JARMAIN, P. A. FRASER and R. W. NICHOLLS, *Astrophys. J.* **118,** 228 (1953).
12. G. HERZBERG, *Spectra of Diatomic Molecules.* (2nd Ed.), van Nostrand, New York (1950).
13. M. GUILLERY, *Z. Phys.* **42,** 121 (1927).
14. S. S. PENNER, *Quantitative Molecular Spectroscopy and Gas Emissivities,* p. 403. Addison–Wesley Publishing Co., Reading, Mass. (1959).
15. E. FREEDMAN and J. W. DAIBER, *J. Chem. Phys.* **34,** 1271 (1961).
16. Program supplied by R. E. Duff, Los Alamos Scientific Laboratory, Los Alamos, New Mexico.
17. R. W. NICHOLLS, P. A. FRASER and W. R. JARMAIN, *Combustion and Flame* **3,** 13 (1959).
18. J. KECK, J. CAMM, B. KIVEL and T. WENTINK, *Ann. Phys.* **7,** (1959).

VOL.
1
196

J. Quant. Spectrosc. Radiat. Transfer. Vol. 1, pp. 143–162. Pergamon Press Ltd. Printed in Great Britain

RADIATIVE PROPERTIES OF HIGH TEMPERATURE AIR

B. H. ARMSTRONG, J. SOKOLOFF, R. W. NICHOLLS*, D. H. HOLLAND and R. E. MEYEROTT
Lockheed Aircraft Corporation, Missiles and Space Division, Palo Alto, California

(*Received* 27 *January* 1961)

1. INTRODUCTION

INTEREST in the radiative properties of high temperature air has been greatly stimulated in recent years by several practical problems, such as the state of the air surrounding a re-entry body, radiation from nuclear detonations etc. As a result, a considerable amount of effort has been expended in calculations of opacities, equations of state, and other quantities related to the general problem. Reports of this work are generally quite detailed and contain extensive tables. Consequently, the work appears to be too bulky to publish *in toto*. In this paper we therefore present a summary of the theoretical work in this field performed during the last five years. Primary emphasis is given to the work performed at this laboratory[1–3], with occasional comparisons of results and methods with those of other workers.†

In section II the equation of radiation transport is discussed, and it is shown that the quantity of primary interest is the absorption coefficient μ_ν. Expressions for the Planck and Rosseland mean absorption coefficients are given, and their use in limiting cases discussed. In section III the calculation is separated into two parts, the calculation of occupation numbers and the calculation of cross-sections. Qualitative variations with temperature and density are discussed, and it is shown that the problem is essentially different at low temperatures, where molecular absorption dominates, and high temperatures, where atomic and electronic effects are most important. The methods and results of the low temperature calculation are presented in section IV, and those for the high temperature calculation in section V. These results are used in calculations of mean absorption coefficients, which are presented in section VI.

II. RADIATION TRANSPORT

Each volume element in a mass of high temperature gas is simultaneously emitting and absorbing radiation of all frequencies. It is the balance between these processes which determines the local radiation flux within the gas, as well as the flux which escapes. Let the flux of radiation per unit frequency interval about ν, per unit solid angle in the direction $\vec{\Omega}$, and per unit area normal to the direction $\vec{\Omega}$, be denoted by $I_\nu(\vec{\Omega})$. Similarly, denote the energy radiated by a unit mass of gas per unit frequency per unit solid angle by $j_\nu(\vec{\Omega})$.

---

* On leave of absence from University of Western Ontario.

† References 1, 2 and 3 are reports of work sponsored by the Air Research and Development Command under Contracts AF 29(601)–524, AF 29(601)–2774, and AF 19(604)–3893.

If the absorption coefficient of the gas for radiation of frequency ν is $\varkappa_\nu$ cm^2 g^{-1}, the flow of radiation through the gas is governed by the equation of radiation transfer

$$\frac{1}{\rho}\frac{dI_\nu(\vec{\Omega})}{ds} = j_\nu(\vec{\Omega}) - \chi_\nu I_\nu(\vec{\Omega}) \tag{1}$$

where s denotes length measured in the direction $\vec{\Omega}$.

If the gas is in local thermodynamic equilibrium, i.e., if at each point in the gas a temperature T can be defined such that the characteristics of the gas in the neighbourhood of the point are those of a gas in equilibrium at that temperature, j_ν is given by

$$j_\nu = \varkappa_\nu' B_\nu(T) + e^{-\frac{h\nu}{kT}} \varkappa_\nu I_\nu \tag{2}$$

where

$$\varkappa_\nu' = \varkappa_\nu\left(1 - e^{-\frac{h\nu}{kT}}\right) \tag{3}$$

and B_ν is the Planck distribution function, which is the value I_ν would have within an enclosure in thermodynamic equilibrium at temperature T. The following discussion is limited to gases in local thermodynamic equilibrium.

Substitution of (2) into (1) yields

$$\frac{1}{\rho}\frac{dI_\nu}{ds} = \chi_\nu'(B_\nu - I_\nu) \tag{4}$$

From this equation it is clear that one parameter characteristic of the gas suffices to specify completely its radiative properties, namely

$$\mu_\nu' = \rho\varkappa_\nu' \tag{5}$$

the absorption coefficient of the gas.

In many problems the spectral distribution of the radiation is not of primary concern. For these cases an appropriately defined mean value of the absorption coefficient is useful. The manner in which the mean value is calculated depends on the characteristics of the problem under consideration. A limiting case of interest is that of an optically thin sample of gas, i.e., a sample whose dimensions are small compared with the mean free path of radiation in the gas. Consideration of this case leads to the definition of the Planck mean absorption coefficient. At the opposite extreme is the case of an optically thick gas sample, which is conveniently analyzed in terms of the Rosseland mean. These two limiting cases are discussed below and the respective mean absorption coefficients are derived.

Consider the radiation from an isolated thin slab of gas. We assume that everywhere within the gas $I_\nu << B_\nu$. Neglect of I_ν relative to B_ν in (4) yields an equation which can immediately be integrated to yield

$$\delta I_\nu = \frac{\mu_\nu' B_\nu \delta x}{\cos\theta} \tag{6}$$

where δI_ν is the intensity at the surface of the slab in the direction at angle θ to the normal of the slab and δx is the slab thickness. The approximation made in deriving the solution is justified provided $\mu_\nu'\delta x << 1$ for all ν, which is just the condition that the slab be optically thin. The total radiation flux F per unit area leaving one face of the slab, regardless of its direction and frequency, is found by integrating $I_\nu \cos\theta$ over frequency and over solid

angle. The cos θ factor must be inserted because I_ν is the flux per unit area normal to the direction of propagation. The result of the integration is

$$F = \int\int I_\nu \cos\theta \mathrm{d}\Omega \mathrm{d}\nu = 2\pi\delta x \int \mu_\nu' B_\nu \mathrm{d}\nu \tag{7}$$

since I_ν is zero for directions with a component directed inward along the normal. The corresponding radiation emitted by a perfect radiator in equilibrium at temperature T is σT^4. The emissivity ε of the gas is the ratio of its total radiation to that emitted by a black body at the same temperature, hence

$$\varepsilon = \frac{2\pi\delta x \int \mu_\nu' B_\nu \mathrm{d}\nu}{\sigma T^4} \tag{8}$$

The quantity $\varepsilon/\delta x$, the emissivity per unit length, is usually quoted. It can be written as

$$\frac{\varepsilon}{\delta x} = \frac{2\pi}{\sigma T^4} \int \mu_\nu' B_\nu(T) \mathrm{d}\nu = 2\overline{\mu}_e(T) \tag{9}$$

where

$$\overline{\mu}_e(T) = \frac{\int \mu_\nu' B_\nu(T) \mathrm{d}\nu}{\int B_\nu(T) \mathrm{d}\nu} = \frac{\pi \int \mu_\nu' B_\nu(T) \mathrm{d}\nu}{\sigma T^4} \tag{10}$$

is the Planck mean absorption coefficient, sometimes referred to as the emission mean absorption coefficient.

If the dimensions of the gas sample are large compared with the mean free path, radiation cannot move freely from one part of the gas to another. Under these conditions the transfer of radiation is most conveniently treated in the diffusion approximation. We define the radiation flex vector $\vec{F}$

$$\vec{F} = \int\int I_\nu(\vec{\Omega}) \vec{e}_\Omega \mathrm{d}\Omega \mathrm{d}\nu \tag{11}$$

where $\vec{e}_\Omega$ is a unit vector in the $\vec{\Omega}$ direction. The total net radiant energy, regardless of frequency, crossing an element of area $\vec{dA}$ is then $\vec{F} \cdot \vec{dA}$. It can be shown that in the diffusion approximation

$$\vec{F} = -\frac{4\pi}{3} \frac{1}{\overline{\mu}_R} \int_0^\infty \vec{\nabla} B_\nu \mathrm{d}\nu \tag{12}$$

where $\overline{\mu}_R$, the Rosseland mean absorption coefficient, is defined by

$$\frac{1}{\overline{\mu}_R} = \frac{\int_0^\infty \frac{1}{\mu_\nu'} \frac{\mathrm{d}B_\nu}{\mathrm{d}T} \mathrm{d}\nu}{\int_0^\infty \frac{\mathrm{d}B_\nu}{\mathrm{d}T} \mathrm{d}\nu} \tag{13}$$

The Rosseland mean opacity, frequently referred to simply as the opacity, is defined by $\overline{\kappa}_R = \frac{\overline{\mu}_R}{\rho}$. The condition for validity of (12) is that the fractional variation in temperature be small in a distance of one mean free path for all frequencies of interest, hence

$$\frac{1}{\mu_\nu'} \frac{|\nabla T|}{T} << 1. \tag{14}$$

In the following sections the current status of our knowledge of the absorption coefficient of high temperature air is discussed, and recently computed values of the above-mentioned mean absorption coefficients are presented.

III. THE ABSORPTION COEFFICIENT OF AIR

The absorption of radiation in a gas occurs by virtue of elementary interactions between the radiation and the individual particles of which the gas is composed. This is true unless the gas is relatively dense and highly ionized, in which case absorption may occur by excitation of collective modes involving many particles simultaneously. In the following discussion it is assumed that the conditions are such that collective effects play no significant role, so that only the elementary interactions involving a single gas particle need be considered.

Let the number density of particles of type s in the state J be denoted by N_{sJ}, and let the cross-section for absorption of a photon of frequency ν by a particle of type s in a transition which carries the particle from the state J to the state J' be denoted by $\sigma_{sJJ'}(\nu)$. Then the absorption coefficient μ_ν is given by

$$\mu_\nu = \sum_{sJJ'} N_{sJ}\,\sigma_{sJJ'}(\nu) \tag{15}$$

where the sum is extended over all particle species s and their initial and final states J and J'. It should be noted that μ_ν as given by (15) is related to μ_ν' as given by (4) through

$$\mu_\nu' = \left(1 - e^{-\frac{h\nu}{kT}}\right)\mu_\nu \tag{16}$$

The density of particles of type s in state J may be written

$$N_{sJ} = N_s P_{sJ} = N P_s P_{sJ} \tag{17}$$

where N_s is the density of particles of type s, N is the density of particles of all types, P_{sJ} is the probability that a particle of type s is in the state J, and P_s is the probability that a particle chosen at random is of type s.

From the above discussion it is clear that calculation of the absorption coefficient naturally falls into two distinct parts. One is the calculation of the probabilities P, a problem in statistical mechanics which has nothing to do with the radiation field; the second is calculation of the cross-sections σ, a problem in the quantum theory of radiation which can be undertaken without reference to the various particle densities. The problems encountered in performing these calculations vary markedly with variations in temperature and density. For this reason it is convenient to discuss the problem with respect to several distinct temperature-density regions characterized by qualitative differences in the effects which are dominant in determining μ.

Cold air consists almost exclusively of N_2 and O_2, hence at sufficiently low temperatures only the cross-sections of these two molecules need be considered. As the temperature is raised, N_2 and O_2 interact to form the various oxides of nitrogen. For example, at normal density and temperature in the range 0·4 to 1 eV, NO is formed and plays a significant role in determining the absorption coefficient. In addition to the formation of new molecular species, ionization and dissociation of the molecules also occur. Thus, at around 0·6 eV, important contributions are made by N_2^+ and O^-. At temperatures of about 1 eV, dissociation is practically complete, and as the temperature is further increased the main contribution

comes from atoms, ions, and free electrons. The problem of obtaining cross-sections for molecular species is much more difficult than the corresponding atomic problem, hence the point at which the molecular density becomes so low that molecules may be neglected in the absorption coefficient calculation constitutes a natural division of the problem into two parts.

A similar division occurs in the statistical mechanical calculations. In some temperature–density regions the interactions among particles may be neglected without introducing serious errors into the calculation of occupation numbers for the various species. At sufficiently high densities, however, the effects of interparticle interactions must be included, with a consequent increase in the difficulty of performing the calculations.

As a rather arbitrary demarcation between the regions where molecular effects may be neglected and where they make a significant contribution, we choose a concentration of 10^{-6} molecules per initial air atom. This molecular density gives rise to a contribution to the absorption coefficient at 12,000°K which is generally less than 2 per cent of the atomic contribution over the optical frequencies. From GILMORE's tables[5] and from other results[2], the temperature–density points corresponding to this demarcation may be found. The

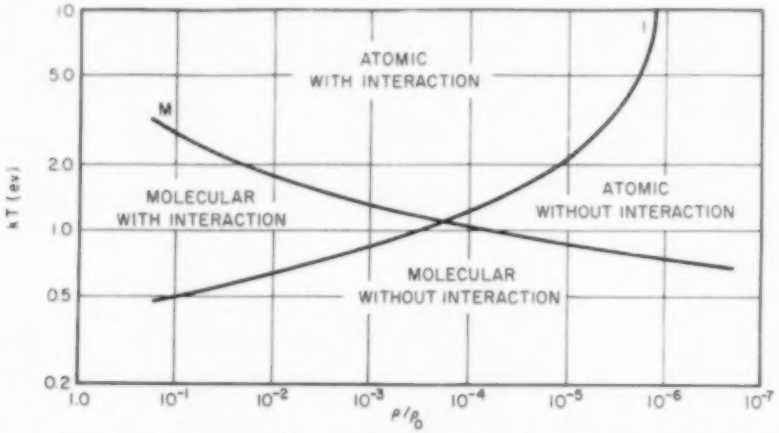

FIG. 1. Subdivion of temperature–density plane into molecular and atomic regions and into regions where interaction can and cannot be neglected.

curve labeled *M* in Fig. 1 is the locus of these points, and divides the temperature–density plane into two regions labeled atomic and molecular.

The curve labeled *I* in Fig. 1 divides the plane into two regions according to whether the interactions among particles may or may not be neglected. Again an arbitrary criterion has been selected for determining the curve, namely, that the Coulomb interaction energy between ions be 1/50 of their thermal kinetic energy, i.e.,

$$\frac{\bar{z}^2 e^2}{r} = \frac{1}{50}\left(\frac{3}{2}kT\right) \tag{18}$$

where r, the average distance between ions, is obtained from

$$\frac{4}{3}\pi r^3 = \frac{1}{N_i} \tag{19}$$

with N_i the number density of ions. The curve shown is obtained from (18) after some smoothing.

Further subdivisions over the parameter ranges may also be made. In Fig. 2 the temperature ranges over which the various processes make significant contributions are

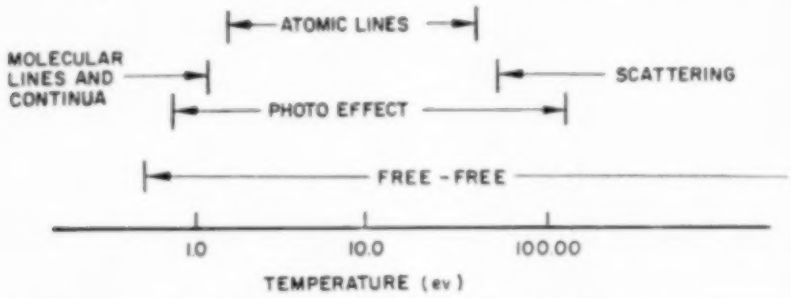

Fig. 2. Effects which contribute to the absorption coefficient of air as a function of temperature.

indicated, without reference to the density dependence of the effects. From this figure a graph of "knowledge" versus temperature may be constructed, and is shown in Fig. 3. At low temperatures, good experimental information is available, while at high temperatures, the theory is in relatively good shape. The lack of knowledge indicated in the middle range

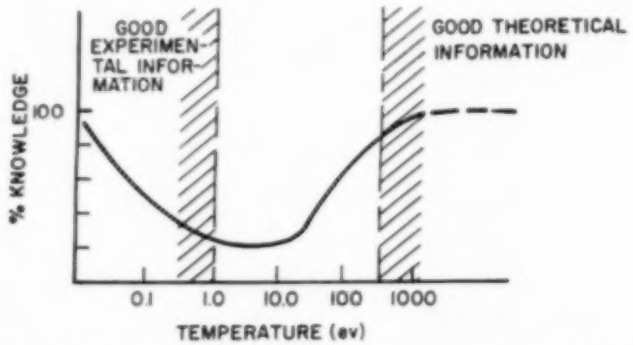

Fig. 3. Graph of "knowledge" versus temperature of the absorption coefficient of air.

results primarily from a lack of knowledge of atomic line absorption. This and other deficiencies are discussed in more detail below.

IV. CALCULATION OF THE ABSORPTION COEFFICIENT AT LOW TEMPERATURES

Two separate calculations of the absorption coefficient of hot air have been performed at Lockheed. The first deals with air at temperatures in the range 1000°K to 12,000°K and densities of ten normal to 10^{-6} normal. The wavelength range covered in this calculation is 1167 Å to 19837 Å, corresponding to a photon energy range of about 0·6 to 10 eV.

At the lowest temperatures considered, very little dissociation has occurred, hence the main contribution to the absorption coefficient arises from molecular transitions. For the

wavelength range under consideration, absorption occurs by excitation of the molecular bands associated with electronic transitions. As the temperature is increased, some of the molecules become ionized, thus giving rise to new band systems to contribute to the absorption. The electrons produced by the ionization of molecules can also contribute to the absorption by the process of inverse bremsstrahlung (free-free transitions). Some of the electrons react with oxygen to form O^-, which makes a further contribution, since radiation may now be absorbed in the photodetachment of electrons from O^-. Finally, at the highest temperatures considered in the low temperature calculation, sufficient dissociation of the molecules has occurred to permit a significant contribution from the photoelectric effect in atomic oxygen and nitrogen. In Table 1 the transitions included in the calculations at

TABLE 1. TRANSITIONS CONSIDERED IN LOW TEMPERATURE ABSORPTION COEFFICIENT CALCULATIONS. (CHECK MARK DENOTES INCLUSION).

	Temperature (° K)						
Transition	12,000	8,000	6,000	4,000	3,000	2,000	1,000
NO(β) $X\,^2\Pi \rightarrow B^2\Pi$	√	√	√	√	√	√	√
NO(γ) $X\,^2\Pi \rightarrow A^2\Sigma$	√	√	√	√	√	√	√
O_2(S–R) $X\,^3\Sigma_g^- \rightarrow B^3\Sigma_u^-$	√	√	√	√	√	√	√
$N_2(1^+)$ $A^3\Sigma_u^+ \rightarrow B^3\Pi_g$	√	√	√	√	√		
$N_2(2^+)$ $B^3\Pi_g \rightarrow C^3\Pi_u$	√	√	√	√	√		
$N_2^+(1^-)$ $X\,^2\Sigma_g^+ \rightarrow B^2\Sigma_u^+$	√	√	√	√	√		
O^- photodetachment	√	√	√				
e free-free	√	√	√				
N, O photoelectric	√						

various temperatures are shown. Only discrete molecular transitions were included in the calculations, whereas continuous transitions only were included in the case of the photoelectric effect, photodetachment, and of course, free-free transitions.

The contribution of the molecular bands was found by calculating an average absorption coefficient over a set of frequency intervals corresponding to photon energy increments of 0·25 eV. The mean value in such an interval is

$$\bar{\mu}_{\Delta\nu} = \frac{\pi e^2}{mc\Delta\nu} \sum_{\Delta\nu} N_{Lv'} f_{Lu} g_{v'v''} \tag{20}$$

where the sum is extended over all bands in $\Delta\nu$. The population of a lower state is denoted by $N_{Lv'}$, and the Franck–Condon factor for the v'–v'' band by $g_{v'v''}$. The effective oscillator strength for the transition is denoted by f_{Lu}, where

$$f_{Lu} = \frac{8\pi^2 m}{3he^2}\,\nu_{Lu}\,R_e^2(r) \tag{21}$$

and $R_e(r)$ is the electronic transition moment, which in general depends on the internuclear separation r.

The equilibrium composition of dry air, as given by GILMORE[5], was used in the calculation of the population factors $N_{Lv'}$. From Gilmore's tables the density of the various molecular and ionic species are first obtained and the numbers $N_{Lv'}$ next calculated on the

assumption that the various species are distributed over their vibrational levels according to the Maxwell–Boltzmann distribution. In the case of N_2 it was necessary to extend Gilmore's tables to lower temperatures.

The Franck–Condon factors $g_{v'v''}$ were taken from the calculated values given in various publications[6–14]. Since the sum of the q values over one of the indices holding the other fixed is generally close to unity, the neglect of molecular transitions to the continuum is a good approximation. The sum rule is not satisfied for the O_2 Schumann–Runge transitions, however, hence a considerable error may have been introduced by neglect of the Schumann–Runge continuum.

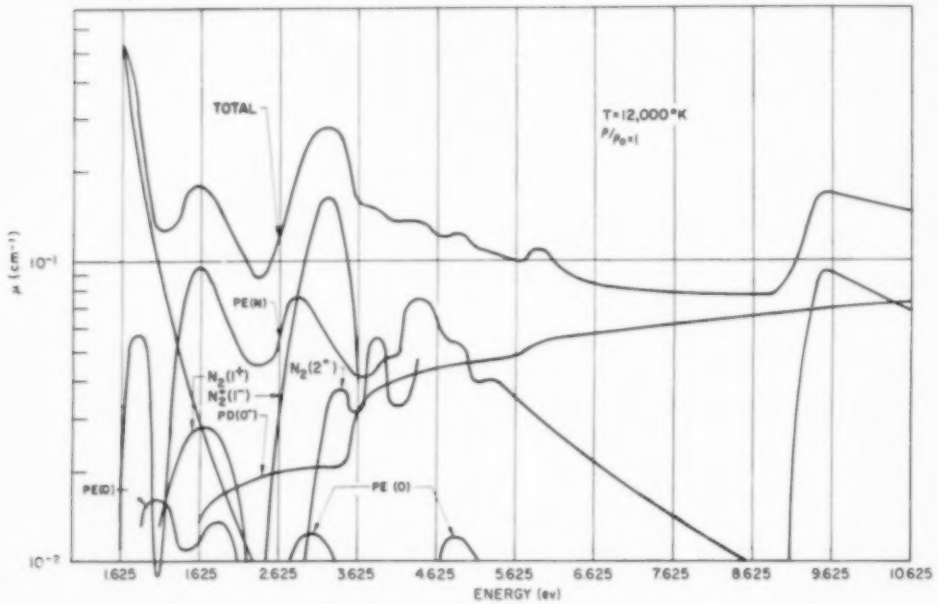

FIG. 4. Absorption coefficient versus photon energy: $T = 12{,}000°K$, $\rho/\rho_0 = 1$.

From (21) it is clear that f_{Lu} is not in general a well defined quantity for a given electronic transition. Its treatment, as such, for a particular initial state is a good approximation only if the dominant transitions are to final states such that:

(1) Only a narrow range of frequencies is involved, so that ν_{Lu} is well defined.

(2) The r dependence of R_e does not give rise to a significant variation of R_e^2 among the dominant vibrational transitions. This may result either from a weak dependence of R_e on r, or because the overlap integrals in $g_{v'v''}$ project out a narrow range of r.

A narrow range of frequencies favors the validity of both conditions (1) and (2). Unfortunately, final states in the continuum play an important role in the Schumann–Runge transition, thus leading to ambiguity in the definition of f and violation of the q sum rule, if only discrete states are considered. These uncertainties no doubt have a great deal to do with the wide range of f values quoted in the literature for the O_2 Schumann–Runge transition[15–20]. The values quoted for the other transitions appear to be more reliable, although still open to some question. The f values used in the calculations were taken from

VOL. 1 1961

various published experimental results[15–24]. In particular, the measurement of Ditchburn and Heddle, which includes the continuum transitions, was assumed for O_2 (S–R), and those of KECK *et al.*[17] for the others.

In spite of the above-mentioned uncertainties, the calculated contributions to the absorption coefficients are believed to be accurate to within an order of magnitude.

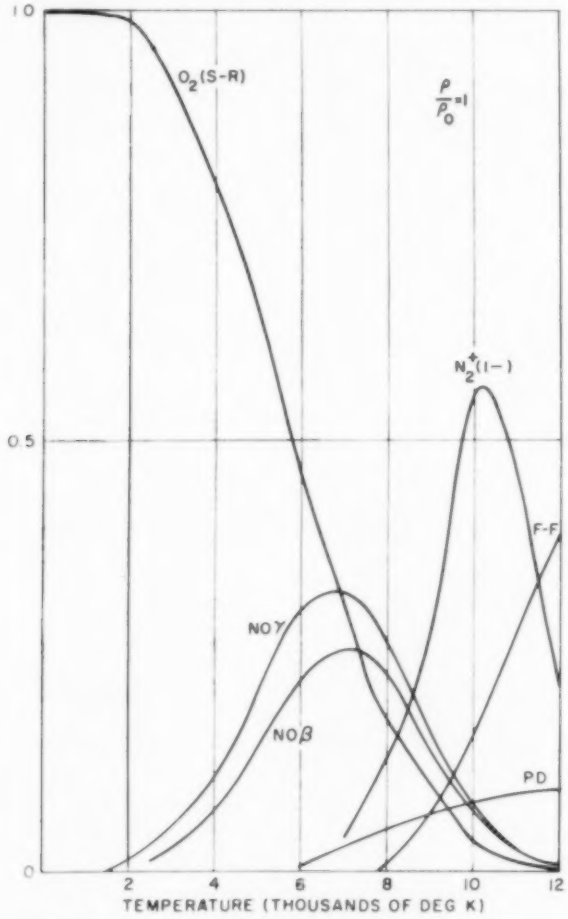

FIG. 5. Relative contribution of transitions: $\rho/\rho_0 = 1$.

Furthermore, the calculated values can easily be scaled to include new and more accurate measurements of the *f*-numbers.

The contribution of O^- was obtained from the measured photodetachment cross-section of BRANSCOMB *et al.*[25, 26] at low energies and the calculated cross-sections of BATES and MASSEY[27, 29] at higher energies. The free-free contribution was calculated under the assumption that only positive ions were effective as the third body in the absorption of a photon by a free electron. The absorption coefficient was then obtained from the Kramers formula, corrected by the gaunt factor as tabulated by BERGER[30].

The most important photoelectric transitions in this work take place from initial states with principal quantum number $n \geq 3$. These excited states are assumed to be nearly hydrogenic, hence the cross-section for absorption of a photon of frequency ν in a transition from a particular initial state varies as ν^{-3}. The cross-section can be written

$$\sigma_{PE} = \frac{\pi e^2}{mc} \frac{df}{d\nu} \tag{22}$$

where f is the f-number. Therefore $\frac{df}{d\nu}$ varies as ν^{-3} for hydrogenic transitions. The total oscillator strength for hydrogenic continuum transitions is approximately 0·2[31]. It follows that

$$\frac{df_i}{d\nu} \simeq \frac{0{\cdot}4\ \nu_i^2}{\nu^3} \tag{23}$$

where ν_i is the absorption edge of the i^{th} transition. The contribution of this transition to the absorption coefficient is

$$\mu \simeq 0{\cdot}4 \frac{\pi e^2}{mc} N_i \frac{\nu_i^2}{\nu^3} \tag{24}$$

where N_i is the density of particles in the i^{th} state. Since the requirement $n \geq 3$ implies excitation energies of 10 eV or higher, the occupation numbers will be negligible at all but the highest temperatures, hence the photoelectric contribution was ignored for all but 12,000°K in the low temperature range calculation. At this temperature dissociation is virtually complete over most of the density range considered, hence only N and O were included in the calculations.

Representative results of the calculations are presented in Figs. 4, 5, 6 and 7. The ordinate in Fig. 5 is the ratio of the maximum value, regardless of wavelength, of the contribution from a given process at a particular temperature and density to the sum of such maxima for all processes at that temperature and density. From the figures it is seen that at the lowest temperatures O_2 Schumann–Runge dominates with the two NO band systems just beginning to appear. In the intermediate range, the NO overtakes the O_2, while the first negative band system of N_2^+ dominates in the visible region. At the high end of the temperature range the continuous absorption takes over, with the free-free transitions dominating in the infrared and the photoelectric effect on N and O dominating the visible and ultraviolet, respectively.

The calculations described above are believed to give a reasonably good picture of the absorption coefficient over the range of parameters included. Nevertheless, considerable room for improvement remains. A major source of uncertainty in the calculations is lack of precise knowledge of the electronic f-numbers in molecular transitions. This question is discussed in some detail in the report of MEYEROTT *et al.*[1]. Improvements in this area must await better experimental data, or possibly the results of reliable machine calculations. The agreement between theory and experiment in the case of O^- photodetachment has recently been improved by the work of KLEIN and BRUECKNER[32]. These results should be included in future calculations. The role of neutral particles in free-free transitions should be investigated. An electron undergoing such a transition must interact with another particle to conserve momentum. The interaction with neutral particles is less

VOL.
1
1961

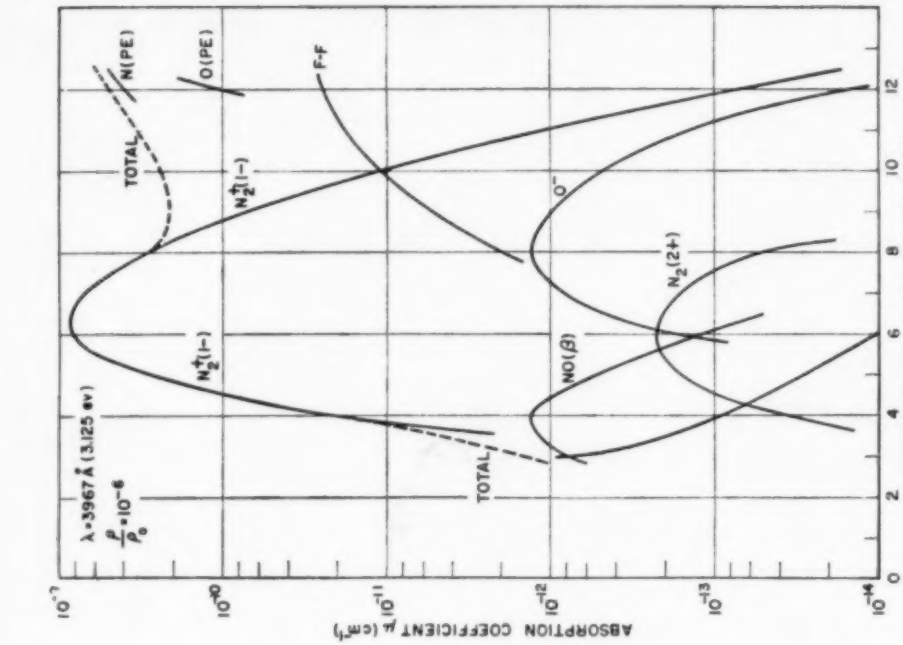

FIG. 7. Absorption coefficient for $\lambda = 3967$Å, $\rho/\rho_0 = 10^{-6}$.

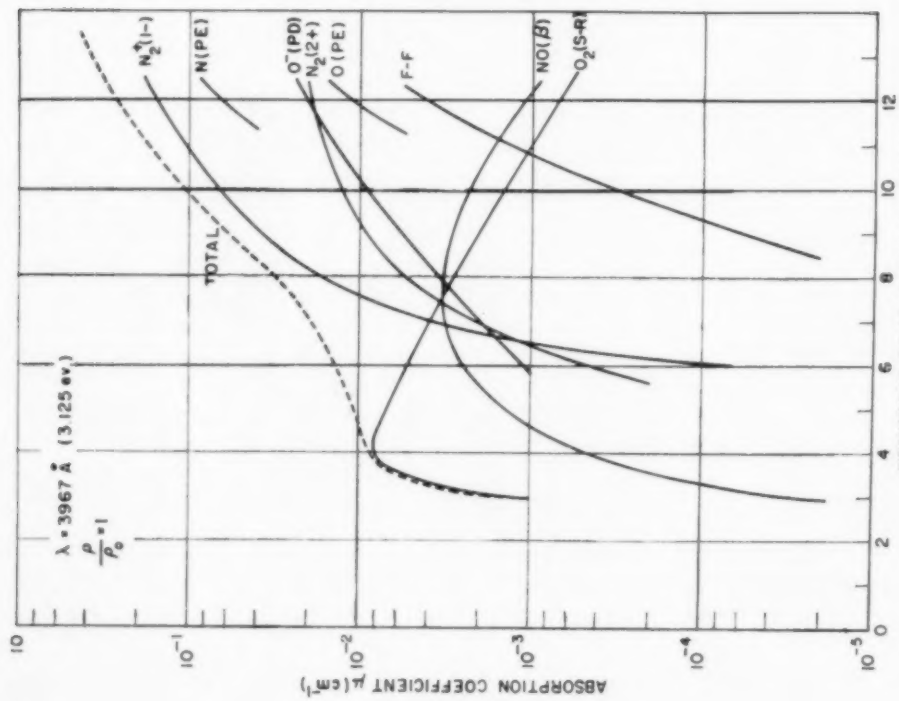

FIG. 6. Absorption coefficient for $\lambda = 3967$Å, $\rho/\rho_0 = 1$.

effective, because of its short range, than the interaction with ions. Because of the large density of neutral particles, however, they may still play an important role in the free-free transitions. In recent calculations, KIVEL AND BAILEY[33] attempt to take the neutral particles into account, and find their contribution dominates that of the ions. This calculation is open to some question, however, and further work in this area should be performed. The calculation of the photoelectric contribution is based on the assumption that the positive ion is created in a definite state. This is in general incorrect, so that while the calculation is adequate for the total contribution, it predicts the wrong wavelength dependence.

In addition to the approximations and uncertainties mentioned above, several omissions should be pointed out. Absorption by NO_2 was not included in the calculations. Comparison of the calculated results with measurements in NO_2 by DIEKE *et al.*[34] indicate that the overall contribution of NO_2 is small. However, in many practical applications, all wavelengths below 3000 Å are absorbed in cold air. The transmitted radiation thus lies in the near ultraviolet and visible region of the spectrum, in which the NO_2 contribution is important, and should be carefully investigated in future studies. There is also a possibility that N_2O_3 contributes at low temperatures, and this also should be investigated. Another omission is the N_2^+ Meinel band system, which overlaps the N_2 first positive system, and probably makes some contribution in the photographic infrared.

V. CALCULATION OF THE ABSORPTION COEFFICIENT AT HIGH TEMPERATURES

As previously pointed out, the calculation of absorption coefficients falls into two parts, the calculation of occupation numbers and the calculation of cross-sections. In the low temperature calculation discussed in the preceding section, the occupation numbers were taken from Gilmore's tables. For the high temperatures presently under consideration, the occupation numbers must be calculated, however, since Gilmore's results extend only to 24,000°K. Over much of the region of interest, the interaction of bound and free electrons are important in determining the occupation numbers, hence these interactions must be included in the calculation.

A statistical mechanical calculation of occupation numbers, which includes the interaction of bound and free electrons, has been performed at Lockheed[2]. In this calculation the volume containing the gas is divided into sub-volumes, called ion spheres. Each ion sphere contains one ion and, on the average, sufficient free electrons to render it neutral. A state J of the ion sphere is characterized by the number N_J of bound electrons in the ion sphere.

The probability that an ion sphere chosen at random is in the state J is given by the grand canonical ensemble expression

$$P_J = \frac{e^{-\alpha n_J - \beta E_J}}{\mathcal{Z}(\alpha, \beta)} \tag{25}$$

where $\mathcal{Z}(\alpha, \beta)$ is the partition function. The energy E_J is the sum of the bound-free interaction energy and the energy of the bound electrons moving in the field of the nucleus. Thus E_J may be written

$$E_J = E_J^0 + \lambda n_J \tag{26}$$

where λ is the bound-free interaction energy per bound electron. The remainder of the

energy, E_J^0, is assumed to be the same as that of an isolated ion in the same state, and hence is obtainable from spectroscopic data. The values used were those contained in Moore's tables, supplemented by estimates of the missing values.

The value taken for λ is

$$\lambda = \frac{3}{2}\frac{\bar{n}_f + e^2}{a} \tag{27}$$

where $\bar{n}_f$ is the average number of free electrons per ion sphere and a is the radius of the ion sphere. This value of λ is a rough intuitive estimate; we are now engaged in an attempt to determine the validity of this estimate.

In terms of

$$\alpha_B = \alpha + \lambda\beta \tag{28}$$

(25) becomes

$$P_J = \frac{e^{-\alpha_B n_J - \beta E_J^0}}{Z(\alpha_B, \beta)} \tag{29}$$

For a given temperature, the density can be calculated from α_B.

In calculating cross-sections, we again make the assumption of hydrogenic wave functions, as in the derivation of (24) for the low-temperature case. In that derivation, however, the assumption was tacitly made that the ejection of an electron from a definite initial state resulted in an ion in a definite state, i.e., that a single absorption edge is related to a given initial state. This is clearly not in general the case, since the electrons remaining bound in the ion may be in any of several states.

Consider, for example, the ejection of a $2p$ electron from the state $1s^2 2s 2p^3 (^3P)$ of NII. The final state is not unique, but consists of a linear combination of ^4P, ^2P, ^2D, and ^2S terms of the $1s^2 2s 2p^2$ configuration of NIII. These terms have quite different energies as shown in Fig. 8. Thus it is clear that the ejection of the $2p$ electron leads to four distinct photoelectric edges rather than just one, as assumed in the low-temperature calculation.

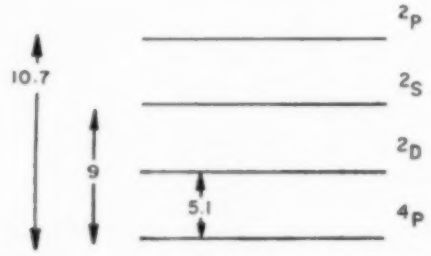

FIG. 8. Terms of the configuration : $1s^2\ 2s\ 2p^3$ of NIII.

In the high-temperature calculation, this multiplicity of edges is taken into account, with a resulting increase in the accuracy of the spectral dependence of the absorption coefficient. In the transition considered above, the transition probabilities (not amplitudes) can be represented symbolically by

$$1s^2 2s 2p^3\,(^3P) \rightarrow 1s^2 2s 2p^2 \left[\frac{4}{9}\,^4P + \frac{1}{18}\,^2P + \frac{5}{18}\,^2D + \frac{2}{9}\,^2S\right] \tag{30}$$

The coefficients of the various terms in the transition amplitudes are called fractional parentage coefficients, and the total photoelectric cross-section for a specific LS term can be written in terms of them. The formal result is

$$\sigma(LS \rightarrow L'S') = \frac{32\pi^4 e^2 m^2 v\nu}{3h^3 c} [C_{l+1}(R_{nl}^{v,\,l+1})^2 + C_{l-1}(R_{nl}^{v,\,l-1})^2] \tag{31}$$

where

$$C_{l\pm1} = \frac{[(l + \tfrac{1}{2}) \pm \tfrac{1}{2}]\,[F(LS \rightarrow L'S']^2}{2l + 1} \tag{32}$$

and ν is the light frequency, v the electron velocity. The fractional parentage coefficients $F(LS \rightarrow L'S')$ have been extensively tabulated in the literature and general formulas exist for their calculation.

The formula actually used in the computation of the contribution to the absorption coefficient of a transition from a state J to a state J' in which a photon of frequency ν is absorbed is

$$\mu_{JJ'} = \left(\frac{P_J\, \rho\, A_0}{M}\right)\left(\frac{24\, he^2}{3\sqrt{3}\, mc}\right)\left(\frac{I_n^2}{nh^3\nu^3}\right)[F(J \rightarrow J')^2\,(g_{nl}^{m,\,l+1} + g_{nl}^{m,\,l-1})^2 \tag{33}$$

The first term in this expression is the density of particles in state J, written in terms of the density ρ, molecular weight M, and Avogadro's number A_0. I_n denotes the ionization potential for an electron in a state with principal quantum number n. The g are gaunt factors, tabulated values of which are given by BETHE and SALPETER[31] and by ARMSTRONG and KELLY[40].

The values of I_n were taken to be the difference in energies of the initial and final states of the bound structure, without including any interaction with free electrons or neighboring ions. The position of the edge, however, was taken to be the difference including interactions. From (26), we have for the initial and final states

$$E_i = E_i^\circ + \lambda n_i$$
$$E_f = E_f^\circ + \lambda(n_i - 1)$$

Hence the energy ΔE corresponding to the edge is

$$\Delta E = E_f - E_i = E_f^\circ - E_i^\circ - \lambda \tag{34}$$

As an illustration of our results, the absorption coefficient of air for several temperatures in the range 2 to 20 eV and 1 atm pressure are shown in Fig. 9.

The use of coulomb wave functions in calculating the radial dipole integrals is a poor approximation in many cases. The energy level diagram of OV shown in Fig. 10 illustrates the problem. The exchange splitting of the ^1P and ^3P terms is of the same order of magnitude as the electrostatic interaction which lifts them above the ground state ^1S term. Under such conditions, a hydrogenic approximation to the radial integral does not even make sense. The approximation improves as one considers levels of higher excitation. Since the highly excited levels contribute to absorption toward the low frequency end of the spectrum the accuracy is best there and decreases with increasing frequency. The error is probably a maximum in the frequency region between the K-edge and the last L-edge. A few spot checks indicate an error in this region of a factor of two or three.

In the preceding discussion, and in the results presented in Fig. 9, the contribution of

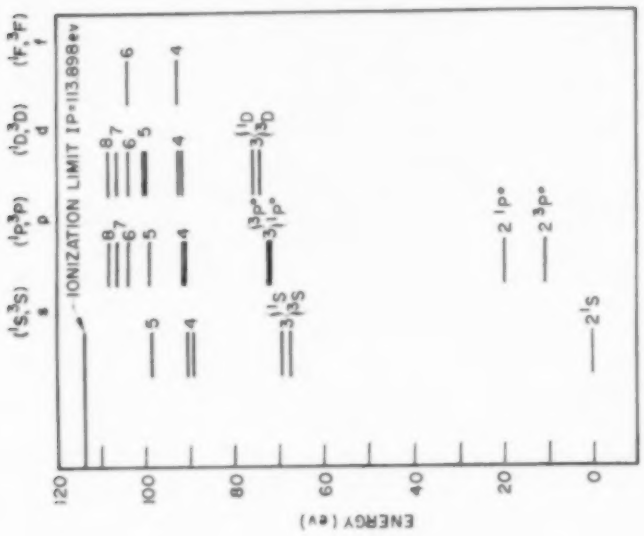

FIG. 10. Energy level diagram of OV $1s^22snl$.

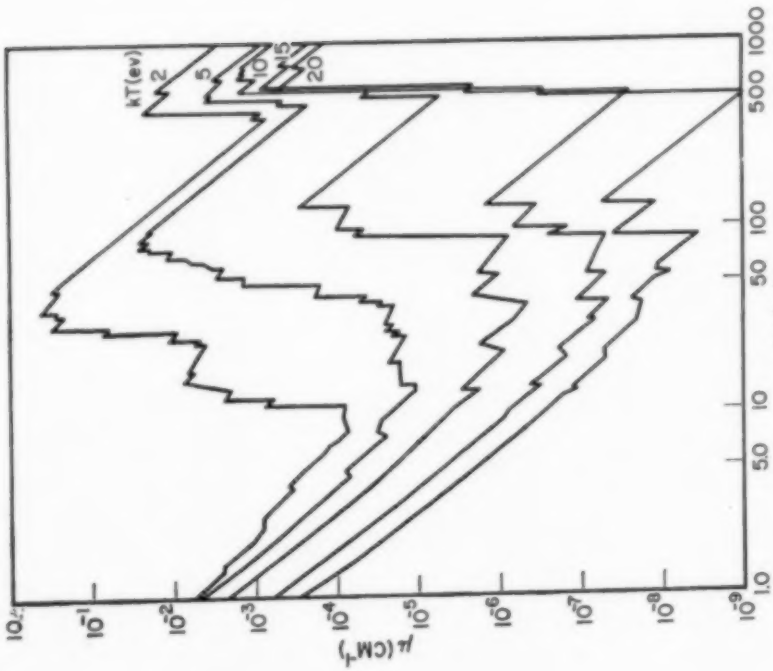

FIG. 9. Absorption coefficients (cm^{-1}) of air as a function of photon energy: pressure 10^5 dynes/cm^2 (1 atm).

discrete transitions has been omitted. Inclusion of line effects is a very difficult problem; no adequate theory presently exists for the calculation under the conditions considered here. Some indication of the importance of discrete transitions is obtained from the calculation of their contribution to the Planck mean absorption coefficient discussed in the next section. The results of that calculation indicate a large contribution from discrete transitions, and for temperatures of 5–10 eV and $\rho/\rho_0 < 10^{-1}$, the mean absorption coefficient is determined almost completely by the line contribution.

These results clearly imply that line effects must be included in future calculations of mean absorption coefficients. To do so is not extremely difficult, since the mean can be calculated with sufficient accuracy without detailed knowledge of line widths and positions. For many problems, however, the knowledge of only the mean is not sufficient, and detailed knowledge of the spectral dependence of μ_ν is required. In such cases, the line widths and positions must be known in greater detail than for the calculation of the means.

The possibility exists that even with accurate detailed knowledge of μ_ν, our position from a practical point of view would not be improved. Complete knowledge of μ_ν would be useful for calculations of radiation transport, for instance, only if the large number of discrete transitions can be grouped together in some way which renders them tractable for practical calculations, without destroying the accuracy of the calculations. The situation here is to be contrasted with that in the low temperature region, where discrete molecular transitions dominate. The situation there is generally much less complicated, since accurate experimental determinations of line widths and positions have been or can be made. The systematics of the lines are relatively well known, and can be described analytically with considerable accuracy.

VOL.
1
1961

VI. MEAN ABSORPTION COEFFICIENTS

From the absorption coefficients obtained by the methods outlined in the preceding sections, it is a straightforward matter to obtain the Planck and Rosseland mean absorption coefficients. The result for the Planck mean in the low temperature case is shown in Table 2.

TABLE 2. PLANCK MEAN ABSORPTION COEFFICIENT (CM^{-1}) AT LOW TEMPERATURES. (SUPERSCRIPTS DENOTE MULTIPLICATION BY CORRESPONDING POWER OF TEN.)

$\bar{\mu}_e$

T	Density							
	10^{1}	10^{0}	10^{-1}	10^{-2}	10^{-3}	10^{-4}	10^{-5}	10^{-6}
1000° K	$1{\cdot}077^{-10}$	$3{\cdot}401^{-12}$	$1{\cdot}077^{-13}$	$3{\cdot}401^{-15}$	$1{\cdot}077^{-16}$	$3{\cdot}401^{-18}$	$4{\cdot}682^{-20}$	$1{\cdot}479^{-21}$
2000° K	$7{\cdot}366^{-9}$	$7{\cdot}371^{-10}$	$7{\cdot}366^{-11}$	$7{\cdot}366^{-12}$	$7{\cdot}311^{-13}$	$7{\cdot}189^{-14}$	$6{\cdot}802^{-15}$	$5{\cdot}697^{-16}$
3000° K	$1{\cdot}8227^{-4}$	$1{\cdot}780^{-5}$	$1{\cdot}651^{-6}$	$1{\cdot}306^{-7}$	$6{\cdot}636^{-9}$	$1{\cdot}616^{-10}$	$3{\cdot}001^{-12}$	$6{\cdot}915^{-14}$
4000° K	$1{\cdot}463^{-2}$	$1{\cdot}137^{-3}$	$5{\cdot}651^{-5}$	$1{\cdot}477^{-6}$	$3{\cdot}302^{-8}$	$9{\cdot}372^{-10}$	$3{\cdot}680^{-11}$	$2{\cdot}164^{-12}$
6000° K	$2{\cdot}906^{-1}$	$9{\cdot}443^{-3}$	$2{\cdot}761^{-4}$	$1{\cdot}144^{-5}$	$9{\cdot}069^{-7}$	$6{\cdot}699^{-8}$	$2{\cdot}532^{-9}$	$8{\cdot}027^{-11}$
8000° K	$5{\cdot}900^{-1}$	$2{\cdot}149^{-2}$	$1{\cdot}122^{-3}$	$6{\cdot}037^{-5}$	$2{\cdot}062^{-6}$	$6{\cdot}347^{-8}$	$1{\cdot}915^{-9}$	$2{\cdot}6^{-10}$
12,000° K	$2{\cdot}606^{0}$	$1{\cdot}315^{-1}$	$8{\cdot}283^{-3}$	$6{\cdot}267^{-4}$	$4{\cdot}584^{-5}$	$2{\cdot}051^{-6}$	$3{\cdot}799^{-8}$	$4{\cdot}230^{-10}$
18,000° K	$6{\cdot}51^{1}$	$5{\cdot}77$			$2{\cdot}11^{-4}$			

These values were obtained from the results of MEYEROTT *et al.*[1], with the exception of those for 18,000°, which are an extension of these calculations. The value for $T = 8000°$, $\rho/\rho_0 = 10^{-6}$ includes the photoelectric contribution, which was not included in reference 1.

The approximation to the true absorption coefficients is very poor below about 6000°, since in this temperature range the main contribution to the Planck mean comes from very long wavelengths, which were not included in the calculation. A calculation of the Planck mean by KIVEL and BAILEY[33] leads to results greater than those shown in Table 2 by factors as large as 10^9 at 1000° K. The reason for this is their inclusion of the NO vibrational–rotational bands, which dominate at low temperatures. By 3000°, the two

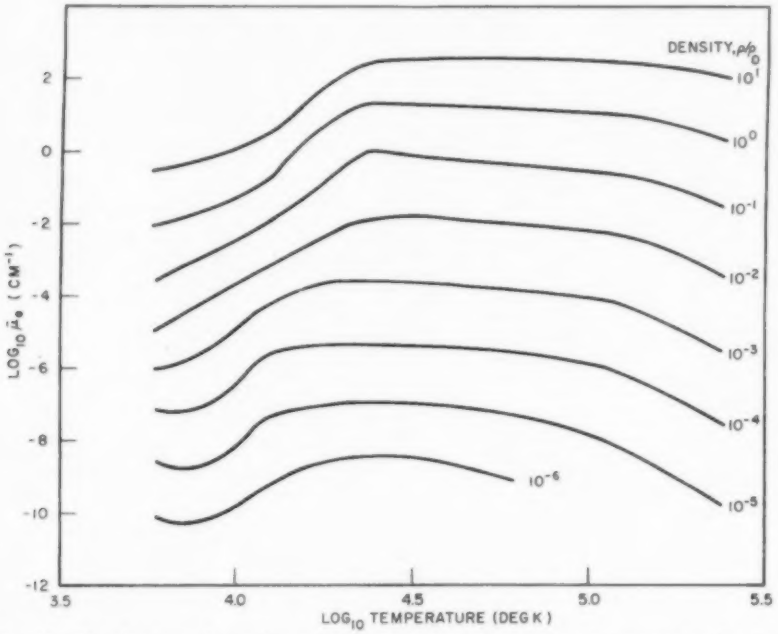

FIG. 11. Planck mean absorption coefficient of air as a function of temperature for various densities ($\rho_0 = 1{\cdot}293 \times 10^{-3}$g/cm^3).

calculations differ by only a factor of ten or a hundred, and above 6000° are in substantial agreement.

The contribution to the Planck mean of the continuous absorption coefficient at high temperatures has been calculated according to the methods discussed in the preceding section. The results of this calculation together with the low temperature results are shown in Fig. 11. To get some idea of the relative importance of discrete transitions, the line contribution has been separately calculated for nitrogen.* In Tables 3 and 4 the line contribution and the total of line plus continuous are presented for various values of temperature and the density parameter α. The relationship between α and density is given in Table 5. The discrete contribution was computed with the help of various sum rules and the radial integrals tabulated by BATES and DAMGAARD[41], supplemented by the formulas of BURGESS and SEATON[42]. An attempt was made to include all transitions which

* The work on the line contribution was sponsored by the Air Research and Development Command under Contract AF 29(601)-2774 and has not been reported elsewhere.

contribute as much as 1 per cent to the mean absorption coefficient. This necessitated inclusion of about 700 multiplets, supermultiplets, and transition arrays of the ions of nitrogen.

The results of the calculation of the Rosseland mean are presented in Fig. 12. The mean free path rather than the absorption coefficient is plotted. Only the continuous contribution

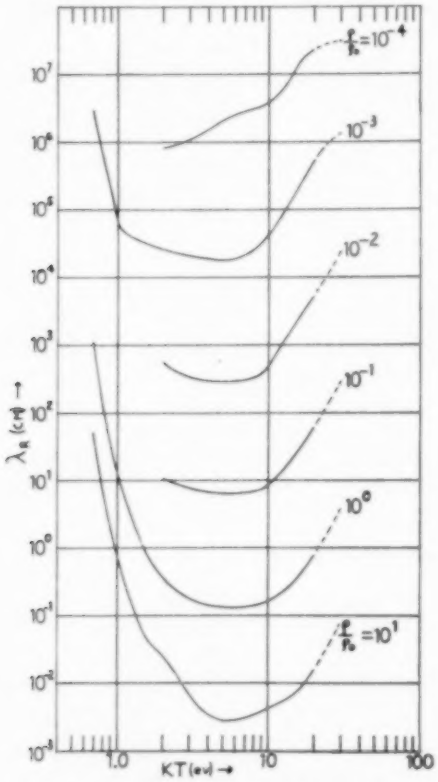

FIG. 12. Rosseland M.F.P. $\bar{\lambda}_R$, Air.

TABLE 3. THE DISCRETE CONTRIBUTION TO THE PLANCK MEAN ABSORPTION COEFFICIENT (CM^{-1}) FOR NITROGEN.

$\bar{\mu}_c$

kT (eV)	α					
	6	9	11	13	15	17
2	$5{\cdot}80^{2}$	$4{\cdot}95^{0}$	$4{\cdot}72^{-1}$	$5{\cdot}38^{-2}$	$5{\cdot}51^{-3}$	$5{\cdot}68^{-4}$
5	$8{\cdot}24^{2}$	$1{\cdot}55^{1}$	$1{\cdot}29^{0}$	$1{\cdot}19^{-1}$	$1{\cdot}05^{-2}$	$6{\cdot}87^{-4}$
10	$8{\cdot}40^{2}$	$8{\cdot}94^{0}$	$3{\cdot}84^{-1}$	$1{\cdot}03^{-2}$	$1{\cdot}96^{-4}$	$3{\cdot}54^{-6}$
15	$5{\cdot}56^{2}$	$3{\cdot}23^{0}$	$6{\cdot}35^{-2}$	$1{\cdot}15^{-3}$	$2{\cdot}03^{-5}$	$3{\cdot}64^{-7}$
20	$2{\cdot}68^{2}$	$1{\cdot}22^{0}$	$2{\cdot}17^{-2}$	$3{\cdot}82^{-4}$	$6{\cdot}81^{-6}$	$1{\cdot}24^{-7}$

TABLE 4. THE TOTAL PLANCK MEAN ABSORPTION COEFFICIENT (CM^{-1}), INCLUDING LINES, FOR NITROGEN.

$\bar{\mu}_e$

kT (eV)	α					
	6	9	11	13	15	17
2	$7{\cdot}08^{2}$	$5{\cdot}25^{0}$	$4{\cdot}77^{-1}$	$5{\cdot}39^{-2}$	$5{\cdot}51^{-3}$	$5{\cdot}68^{-4}$
5	$9{\cdot}94^{2}$	$1{\cdot}59^{1}$	$1{\cdot}30^{0}$	$1{\cdot}19^{-1}$	$1{\cdot}05^{-2}$	$6{\cdot}87^{-4}$
10	$1{\cdot}05^{3}$	$9{\cdot}40^{0}$	$3{\cdot}93^{-1}$	$1{\cdot}05^{-2}$	$1{\cdot}99^{-4}$	$3{\cdot}60^{-6}$
15	$7{\cdot}67^{2}$	$3{\cdot}61^{0}$	$7{\cdot}00^{-2}$	$1{\cdot}25^{-3}$	$2{\cdot}22^{-5}$	$4{\cdot}05^{-7}$
20	$4{\cdot}29^{2}$	$1{\cdot}45^{0}$	$2{\cdot}52^{-2}$	$4{\cdot}39^{-4}$	$7{\cdot}91^{-6}$	$1{\cdot}55^{-7}$

TABLE 5. DENSITY OF NITROGEN AS A FUNCTION OF α AND kT.

ρ (g/cm^3)

kT (eV)	α					
	6	9	11	13	15	17
2	$5{\cdot}44^{-3}$	$7{\cdot}34^{-5}$	$7{\cdot}71^{-6}$	$8{\cdot}96^{-7}$	$9{\cdot}07^{-8}$	$9{\cdot}22^{-9}$
5	$5{\cdot}94^{-3}$	$1{\cdot}28^{-4}$	$1{\cdot}22^{-5}$	$1{\cdot}31^{-6}$	$1{\cdot}51^{-7}$	$1{\cdot}74^{-8}$
10	$9{\cdot}55^{-3}$	$2{\cdot}05^{-4}$	$2{\cdot}03^{-5}$	$2{\cdot}28^{-6}$	$2{\cdot}86^{-7}$	$3{\cdot}77^{-8}$
15	$1{\cdot}29^{-2}$	$2{\cdot}96^{-4}$	$3{\cdot}23^{-5}$	$4{\cdot}00^{-6}$	$5{\cdot}19^{-7}$	$6{\cdot}89^{-8}$
20	$1{\cdot}64^{-2}$	$4{\cdot}17^{-4}$	$4{\cdot}82^{-5}$	$6{\cdot}08^{-6}$	$7{\cdot}95^{-7}$	$1{\cdot}06^{-7}$

is included. The results include calculations by GILMORE[43] in the temperature range 0·7 to 1·5 eV. Calculations by KARZAS and LATTER[44] at temperatures greater than 20 eV yield results which fit into these curves very smoothly, hence the smooth extrapolation, indicated by a dotted line, is included.

REFERENCES

1. R. E. MEYEROTT, J. SOKOLOFF and R. W. NICHOLLS, *Absorption Coefficients of Air*, Geophysics Research Paper No. 68, Air Force Cambridge Research Center, Bedford, Mass. (1960).
2. B. H. ARMSTRONG, D. H. HOLLAND and R. E. MEYEROTT, *Absorption Coefficients of Air from* 22,000° *to* 220,000°, Air Force Special Weapons Center Report TR 58–36, Kirtland Air Force Base, Albuquerque, N.M. (1958).
3. B. H. ARMSTRONG, *Mean Absorption Coefficients of Air, Nitrogen, and Oxygen from* 22,000° *to* 220,000°, Lockheed Missiles and Space Division. Report LMSD 49759, Palo Alto, California (1959).
4. S. CHANDRASEKHAR, *Introduction to the Study of Stellar Structure*. University of Chicago Press (1939).
5. F. R. GILMORE, *Equilibrium Composition and Thermodynamic Properties of Air to* 24,000°K, Rand Corp Research Memorandum RM–1543. Santa Monica, California (1955).
6. W. R. JARMAIN and R. W. NICHOLLS, *Canad. J. Phys.* **32**, 201 (1954).
7. R. W. NICHOLLS, *Ann. Geophys.* **14**, 208 (1958).
8. R. W. NICHOLLS, *J. Atmos. Terr. Phys.* **12**, 211 (1958).
9. W. R. JARMAIN, P. A. FRASER and R. W. NICHOLLS, *Astrophys. J.* **118**, 22 (1953).
10. R. W. NICHOLLS, *The Airglow and the Aurorae* (E. B. ARMSTRONG and A. DALGARNO) (Editors), Pergamon Press, New York (1956).
11. B. KIVEL, H. MAYER and H. BETHE, *Ann. Phys.* **2**, 57 (1957).
12. P. A. FRASER, W. R. JARMAIN and R. W. NICHOLLS, *Astrophys. J.* **119**, 286 (1954).
13. W. R. JARMAIN, P. A. FRASER and R. W. NICHOLLS, *Astrophys. J.* **122**, 55 (1955).

14. R. W. NICHOLLS, P. A. FRASER and W. R. JARMAIN, *Combustion and Flame*, **3**, 13 (1959).
15. R. W. DITCHBURN and D. W. O. HEDDLE, *Proc. Roy. Soc.* A, **220**, 61 (1953).
16. R. W. DITCHBURN and D. W. O. HEDDLE, *Proc. Roy. Soc.* A, **226**, 509 (1954).
17. J. C. KECK, J. C. CAMM, B. KIVEL and T. WENTINK, *Ann. Phys.* **7**, 1 (1959).
18. K. WATANABE, E. C. Y. INN and M. ZELIKOFF, *J. Chem. Phys.* **21**, 1026 (1953).
19. C. F. TREANOR and N. H. WURSTER, *Measured Transition Probabilities for the Schumann–Runge System of Oxygen.* Cornell Aeronautical Laboratories Report AF OSR TN 59–964 (1959).
20. G. W. BETHKE, *J. Chem. Phys.* **31**, 669 (1959).
21. J. C. KECK, B. KIVEL and T. WENTINK, *Emissivity of High Temperature Air.* AVCO Research Report No. 8 (1959).
22. D. WEBER, *Absolute Intensities and Line Width Measurements*, California Institute of Technology, Report No. 23 (1957).
23. D. WEBER and S. S. PENNER, *J. Chem. Phys.* **26**, 860 (1957).
24. R. G. BENNETT and F. N. DALBY, *J. Chem. Phys.* **31**, 434 (1959).
25. L. M. BRANSCOMB and S. J. SMITH, *Phys. Rev.* **98**, 1127 (1955).
26. L. M. BRANSCOMB, D. S. BURCH, S. J. SMITH and S. GELTMAN, *Phys. Rev.* **111**, 504 (1958).
27. D. R. BATES and H. S. W. MASSEY, *Proc. Roy. Soc.* A, **239**, 269 (1943).
28. D. R. BATES, *Mon. Not. R. Astr. Soc.*, **106**, 128 (1946).
29. D. R. BATES and H. S. W. MASSEY, *Phil. Trans.* **192**, 1 (1947).
30. J. M. BERGER, *Astrophys. J.* **124**, 550 (1956).
31. H. BETHE and E. E. SALPETER, *Quantum Mechanics of One and Two Electron Systems*, Academic Press, New York (1957).
32. M. M. KLEIN and K. A. BRUECKNER, *Phys. Rev.* **111**, 1115 (1958).
33. B. KIVEL and K. BAILEY, *Tables of Radiation from High Temperature Air*, AVCO Research Report No. 21 (1957).
34. G. H. DIEKE, D. R. HEATH and W. PETTY (private communication).
35. C. MOORE, *Atomic Energy Levels*, NBS Circular 467 (1949).
36. D. R. BATES, *Mon. Not. R. Astr. Soc.* **106**, 432 (1946).
37. B. H. ARMSTRONG, *Proc. Phys. Lond.* **74**, 136 (1959).
38. D. H. MENZEL and L. GOLDBERG, *Astrophys. J.* **84**, 1 (1936).
39. H. P. KELLY and B. H. ARMSTRONG, *Astrophys. J.* **129**, 786 (1959).
40. B. H. ARMSTRONG and H. P. KELLY, *J. Opt. Soc. Amer.* **49**, 949 (1959).
41. D. R. BATES and A. DAMGAARD, *Phil. Trans.* **242**, 101 (1949).
42. A. BURGESS and M. J. SEATON, *Mon. Not. R. Astr. Soc.* **120**, 121 (1960).
43. F. GILMORE, Rand Corp. (private communication).
44. W. KARZAS and R. LATTER, Rand Corp. (private communication).

VOL
1
196

NOTES AND DISCUSSION

The Editors of the Journal of Quantitative Spectroscopy and Radiative Transfer welcome the submittal of brief, original contributions on timely topics. These manuscripts will generally be published promptly and without editorial review if they are submitted through one of the Associate Editors of JQSRT.

J. Quant. Spectrosc. Radiat. Transfer. Vol. 1, pp. 163–168. Pergamon Press Ltd. Printed in Great Britain

ON IRASER DETECTORS FOR RADIATION EMITTED FROM DIATOMIC GASES AND COHERENT INFRARED SOURCES

S. S. PENNER*

Physics Section, Convair
A Division of General Dynamics Corporation, San Diego, California

(*Received* 2 *January* 1961)

Abstract—The principles involved in the construction of a detector based on the use of an infrared maser (i.e., an iraser) are described for diatomic molecules. The use of iraser detectors holds promise for increasing detector sensitivity over more conventional detector devices for a selected number of diatomic emitters, namely, for molecules with relatively distant rotational line spacing such as HCl or HF. The iraser device may also be used as a multi-wavelength, coherent infrared source.

I. INTRODUCTION

MASERS have found interesting recent applications in a large number of different fields[1]. In an important paper, SCHAWLOW and TOWNES[2] have examined theoretically the problems involved in extending the use of maser techniques to the optical and infrared regions of the spectrum. Following conventional usage, we shall refer to these devices as lasers (for visible or light masers) and irasers (for infrared masers), respectively. The extension of maser techniques to other regions of the spectrum than the microwave region has been discussed independently by PROKHOROV[3] and DICKE[4]. More recent contributions are described also in a symposium publication[5]. All of the published new developments of maser techniques contain theoretical studies on atomic systems. The present analysis appears to be novel in two respects, namely, (a) it is confined to a molecular system and (b) it does not involve the use of selective filters.

The proposed iraser detector or coherent infrared light source is shown schematically in Fig. 1. The device consists essentially of a highly reflecting cylinder with elliptical cross-

---

* Consultant; permanent address: Daniel and Florence Guggenheim Jet Propulsion Center, California Institute of Technology, Pasadena, Calif. The author is indebted to Mr. K. G. Sulzmann for checking the numerical work.

section at the foci of which are centered two long cylindrical tubes containing the same gas. In our example, one of the tubes contains the diatomic gas at low temperature (T_0) and low pressure whereas the other tube contains the gas at an elevated temperature (T_g). Tube materials and pressures for the cold gas are to be chosen in such a way that, at the steady state, (a) the rotational population distribution is equilibrated at the translational temperature of the tube, (b) surface deactivation of vibrationally excited species is unimportant, and (c) the radiative lifetimes of the vibrationally excited emitters are short compared with the time required for vibrational deactivation by gas-phase collisions. Under the specified conditions, the excessively large population of vibrationally excited emitters that is present in the cold-gas tube will hopefully produce measurable stimulated emission on irradiation with infrared radiation of appropriate frequencies and will therefore function either as a highly sensitive detector of radiant energy emitted from heated gases or as a source of coherent infrared radiation, i.e., it will operate as an iraser.

II. VIBRATIONAL RELAXATION IN CYLINDRICAL CHAMBERS CONTAINING ISOTHERMAL, DILUTE GASES

The problem of vibrational relaxation in cylindrical chambers containing isothermal, dilute gas mixtures has been studied for CO in a previous note[6]. The following remarks will be restricted to CO but are easily extended to other molecular emitters.

Wall de-excitation becomes unimportant when the following approximate relation is satisfied:

$$\tau\gamma >> 5.$$

Here

$$\tau = L^2/D$$

and

$$\gamma = A_{1\to 0} + k_{1\to 0}$$

where τ is a characteristic diffusion time if L denotes the chamber diameter in a cylindrical tube and D stands for the diffusion coefficient of vibrationally excited molecules through the gas mixture; $A_{1\to 0}$ is the Einstein coefficient for spontaneous emission from the first excited vibrational levels to the ground state of CO; $k_{1\to 0}$ is the frequency of collisional deactivation in the gas mixture. However, since we require rotational equilibration at the wall temperature, we cannot satisfy the inequality $\tau\gamma >> 5$ and must instead rely on the utilization of a surface material that is highly ineffective in promoting vibrational deactivation.

We shall choose the gas pressure in such a way that

$$k_{1\to 0} << A_{1\to 0}.$$

Since

$$k_{1\to 0} \simeq 5 \times 10^5\, p \text{ sec}^{-1}$$

at room temperature if the probability of de-excitation on collision[7] is 10^{-4}, it follows that

$$k_{1\to 0} << A_{1\to 0}$$

if

$$p << 6{\cdot}6 \times 10^{-5} \text{ atm}.$$

The preceding considerations suggest that, for $p \simeq 10^{-5}$ atm, $k_{1\to 0}$ is small compared with $A_{1\to 0}$: the diffusion time to the wall may then be approximated by the relation

$$\frac{L^2}{D} \simeq \frac{L^2}{5 \times 10^{-2} p^{-1}} = \frac{L^2}{5 \times 10^3}$$

if p is in atm and L in cm. Thus the diffusion time will be smaller than the radiative life $1/A_{1\to 0} \simeq 3 \times 10^{-2}$ sec if

$$L \lesssim 12 \text{ cm}.$$

Hence rotational equilibrium should obtain in cylinders with diameters of the order of a few cm.

For HCl, the pressure required to make $k_{1\to 0} << A_{1\to 0}$ may well be smaller than for CO and, in this case, the desired value of L might be as large as 10 cm for the rotationally equilibrated system.

III. THE STEADY-STATE DISTRIBUTION OF VIBRATIONALLY EXCITED MOLECULES IN THE IRASER TUBE

The hot-gas tube in the iraser assembly may be a low-pressure discharge tube. For the sake of the following illustrative discussion, we shall assume that the hot-gas tube acts like an equilibrium source at 3000°K.

In order to determine the steady-state concentration of the excited molecular species in the iraser tube, it is necessary to solve the complete set of coupled differential equations allowing for all possible radiative transitions that are consistent with the selection rules. Following conventional approximation procedures in preliminary maser studies[8], we shall content ourselves here with a zeroth-order approximation which is motivated by the fact that the assumed hot-gas source will emit strong radiant intensities only for resonance frequencies corresponding to transitions between the ground and first excited vibrational levels and is much weaker for more highly excited levels. We shall focus our attention on the 7, 1 level, i.e., on the seventh rotational level of the first vibrationally excited state.

Allowing for the selection rule $\Delta j = \pm 1$ and considering only the $n = 0$ and $n = 1$ levels, we obtain the following steady-state condition:

$$N_{7,1}\left[A_{7,1\to 6,0} + A_{7,1\to 8,0} + B_{7,1\to 6,0}\rho(\nu_{7,1;6,0}) + B_{7,1\to 8,0}\rho(\nu_{7,1;8,0})\right] = N_{8,0}B_{8,0\to 7,1}\rho(\nu_{8,0;7,1}) + N_{6,0}B_{6,0\to 7,1}\rho(\nu_{6,0;7,1}). \quad (1)$$

Here $N_{j,n}$ denotes the number of molecules per unit volume in the jth rotational and nth vibrational state, the Einstein coefficients A and B are appropriately identified by subscripts, and $\rho(\nu_{j,n;j',n'})$ denotes the incident volume density of radiant energy at the frequency $\nu_{j,n;j',n'} = \nu_{j',n';j,n}$ corresponding to the transition $j, n \rightleftharpoons j', n'$. But*

$$\frac{B_{8,0\to 7,1}}{B_{7,1\to 8,0}} = \frac{15}{17}, \frac{B_{6,0\to 7,1}}{B_{7,1\to 6,0}} = \frac{15}{13}, \frac{A_{7,1\to 6,0}}{B_{7,1\to 6,0}} = \frac{8\pi h}{c^3}(\nu_{7,1\to 6,0})^3,$$

$$\frac{A_{7,1\to 8,0}}{B_{7,1\to 8,0}} = \frac{8\pi h}{c^3}(\nu_{7,1\to 8,0})^3, \frac{N_{6,0}}{N_{8,0}} = \frac{13}{17}\exp(30hcB_e/kT_o)$$

* For justification of all the relations involving Einstein coefficients and matrix elements see, for example, PENNER[9].

if T_0 denotes the temperature of the iraser tube. Use of the preceding relations in equation (1) leads to the expression

$$\frac{N_{7,1}}{N_{8,0}} = \frac{\frac{13}{17}\frac{15}{13}[\exp(30hcB_e/kT_0)] + \frac{B_{8,0\to7,1}}{B_{7,1\to6,0}}\frac{\rho(\nu_{8,0;7,1})}{\rho(\nu_{7,1;6,0})}}{\left[1+\frac{8\pi h}{c^3}\frac{(\nu_{7,1;6,0})^3}{\rho(\nu_{7,1;6,0})}\right] + \left[1+\frac{8\pi h}{c^3}\frac{(\nu_{7,1;8,0})^3}{\rho(\nu_{7,1;8,0})}\right]\frac{B_{7,1\to8,0}}{B_{7,1\to6,0}}\frac{\rho(\nu_{7,1;8,0})}{\rho(\nu_{7,1;6,0})}}.$$

If we now assume that the pressure and pathlength of the gas in the hot-gas source at the temperature T_g are sufficiently high, then we may approximate the volume density of radiation produced by the hot-gas source by the spectral blackbody value at the spectral line centers. In this case,

$$1+\frac{8\pi h}{c^3}\frac{(\nu_{j,n;j',n'})^3}{\rho(\nu_{j,n;j',n'})} = \exp(h\nu_{j,n;j',n'}/kT_g) \simeq \exp(hc\omega_e/kT_g)$$

and

$$\frac{\rho(\nu_{7,1;8,0})}{\rho(\nu_{7,1;6,0})} = \left(\frac{\nu_{7,1;8,0}}{\nu_{7,1;6,0}}\right)^3 \frac{(\exp h\nu_{7,1;6,0}/kT_g)-1}{(\exp h\nu_{7,1;8,0}/kT_g)-1} \simeq 1.$$

Finally, $B_{j,1\to j+1,0} = \text{constant} \times (j+1)$ and $B_{j,1\to j+1,0} = \text{constant} \times j$.

Hence

$$\frac{N_{7,1}}{N_{8,0}} \simeq \frac{(15/17)\exp(30hcB_e/kT_0) + (15/17)(8/7)}{[\exp(hc\omega_e/kT_g)][1+(8/7)]}. \tag{2}$$

A necessary condition for operation of an iraser is the requirement that the effective steady-state concentration in the excited state exceeds that in the ground state. Thus, for example, we must satisfy the condition $N_{7,1}/N_{8,0} > (15/17)$. Since it is impractical to raise T_g significantly above 3000°K and to lower T_0 significantly below the boiling point of the substance, it is apparent from equation (2) that it will generally not be possible to operate the specified type of iraser unless B_e is relatively large.

The proposed scheme will not lead to a useful iraser system for CO. Thus, for $T_0 = 300$°K, $T_g = 3000$°K, we find that

$$\left(\frac{N_{7,1}}{N_{8,0}}\right)_{CO} \simeq 0{\cdot}36$$

since $B_e = 1{\cdot}9313\ \text{cm}^{-1}$ and $\omega_e = 2170\ \text{cm}^{-1}$. Even if T_0 is decreased to a value just above the boiling point of CO, i.e., we set $T_0 = 100$°K, we still find that $(N_{7,1}/N_{8,0})_{CO} < 1$.

For HCl, $B_e = 10{\cdot}59\ \text{cm}^{-1}$, $\omega_e = 2990\ \text{cm}^{-1}$, and we can reduce T_0 to 200°K. In this case we find that

$$\frac{N_{7,1}}{N_{8,0}} \simeq 1{\cdot}08,$$

and

$$N_{7,1} \simeq 1{\cdot}6 \times 10^{12}\ \text{cm}^{-3} \text{ at } 200\text{°K and } 10^{-5}\ \text{atm}$$

where we have assumed that roughly 50 per cent of the HCl molecules remain in the ground vibrational state. If T_0 is set equal to 150°K, we find that

$$\left(\frac{N_{7,1}}{N_{8,0}}\right)_{HCl} \simeq 2{\cdot}19.$$

Results similar to those derived for HCl are obtained for HF.

IV. MINIMUM NUMBER OF EXCITED MOLECULES REQUIRED FOR MASER-TYPE OSCILLATION

The number of vibrationally excited molecules in the upper state in excess of the number in the ground state present at the steady-state is almost equal to $N_{7,1}$ only for very large values of $N_{7,1}/N_{8,0}$. SCHAWLOW and TOWNES[2] have derived an expression for the critical condition at oscillation. For the present application, their result may be written in the form

$$\left(\frac{\pi L^2}{4} l\right)\left(N_{7,1} - \frac{15}{17} N_{8,0}\right) \geq \frac{h(1-\alpha)\mathcal{A}}{16\pi^2 \mu^2}\left(\frac{2kT_0}{\pi m}\right)^{\frac{1}{2}} \tag{3}$$

where l is the length of the iraser tube, h is Planck's constant, α is the wall reflectivity at the frequency under study, $\mathcal{A}$ is the surface area of the walls, μ^2 represents the square of the matrix element for the transition giving rise to a given spectral line, m is the mass of the emitting molecule, and k stands for Boltzmann's constant. Equation (3) holds under conditions where Doppler broadening makes the dominant contribution to the spectral line width. We find that

$$(\mu^2)_{HCl} = |R_{7,1;\,8,0}|^2_{HCl} = 2{\cdot}8 \times 10^{-38} \text{ erg-cm}^3.$$

Hence, for $\alpha = 0{\cdot}99$ and $T_0 = 200°K$,

$$\frac{h(1-\alpha)\mathcal{A}}{16\pi^2 \mu^2}\left(\frac{2kT_0}{\pi m}\right)^{\frac{1}{2}} \simeq 3 \times 10^{11}\mathcal{A} = 3 \times 10^{11}\,\pi L l.$$

Thus, oscillation will result if

$$1{\cdot}2 \times 10^{11}\frac{\pi L^2 l}{4} \geq 3 \times 10^{11}\,\pi L l$$

or

$$L \geq 10 \text{ cm}$$

and it appears that the critical condition for oscillation leads to requirements for the chamber diameter that may be difficult to reconcile, for the particular level examined by us, with the condition that a rotationally equilibrated population distribution is to be maintained (compare section II).

V. METHODS FOR UTILIZATION OF THE IRASER DEVICE

As a detector, the iraser device sketched in Fig. 1 can presumably be used in one of two ways. Thus we imagine steady-state operation in which we look for amplification of photons arriving in the direction of the iraser tube axis. Since induced emission occurs in the direction of the incident photons, the detector should show a significant response to the external light source under the specified steady-state conditions.

The iraser detector may also be operated as a pulsed system. In a sense, an upper state with a radiative life of the order of 10^{-3} sec may be considered to be metastable in view of the fact that detector response times of the order of 10^{-6} sec are easily achieved in the infrared regions of the spectrum. After a steady-state distribution has been obtained in the iraser, the rate of decay of the excited states may be studied; the decay rates should be very different with and without a sufficiently intense external radiation source. For a sufficiently small cross-sectional area of the observed iraser volume and a sufficiently small solid angle, the characteristic decay time without external source should be of the order of the radiative life time. On the other hand, with a sufficiently intense external source

emitting photons of the desired frequency in the preferred direction, the de-excitation time should be greatly shortened.

The iraser device should operate as a multi-wavelength, coherent, infrared light source under the influence of an external source emitting suitable frequencies.

In conclusion, it appears appropriate to stress the necessity for experimental studies of the proposed iraser device. An intelligent program will, no doubt, lead to extensive modifications of the scheme sketched in Fig. 1 although it appears likely that the essential

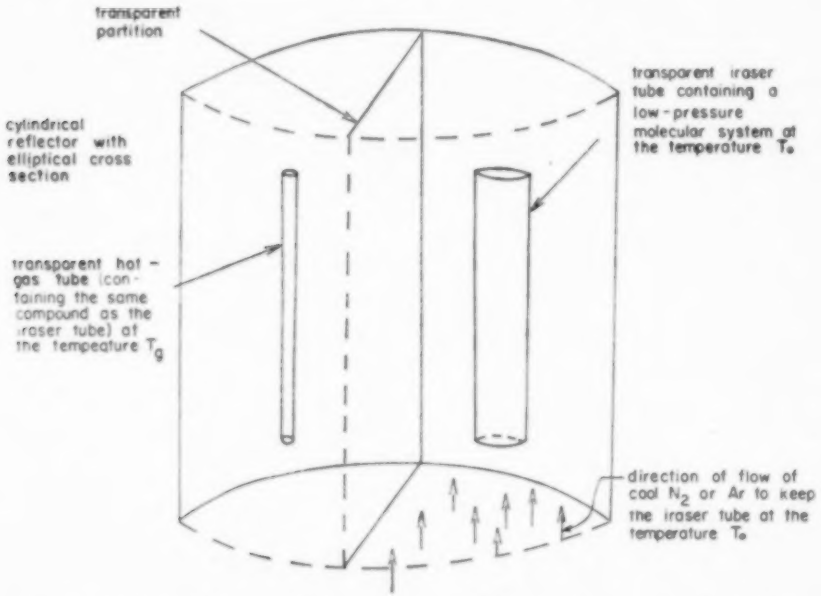
transparent partition
transparent iraser tube containing a low-pressure molecular system at the temperature T_o
cylindrical reflector with elliptical cross section
transparent hot-gas tube (containing the same compound as the iraser tube) at the tempeature T_g
direction of flow of cool N_2 or Ar to keep the iraser tube at the temperature T_o

FIG. 1. Schematic diagram of an iraser detector or coherent infrared light source.

features, namely, rotational equilibration at low temperature and a vibrational population distribution determined by steady-state conditions on exposure to a hot-gas source, will remain unaltered.

REFERENCES

1. J. R. SINGER, *Masers*, John Wiley, New York (1959).
2. A. L. SCHAWLOW and C. H. TOWNES, *Phys. Rev.* **112**, 1940 (1958).
3. A. M. PROKHOROV, *J. Exp. Theor. Phys.* **34**, 1658 (1958).
4. R. H. DICKE, U.S. Patent 2,851,652, 9 September (1958).
5. *Quantum Electronics—A Symposium*, C. H. TOWNES (Editor), Columbia University Press, New York (1960).
6. S. S. PENNER, D. B. OLFE and M. LAPP, *ASME Heat Transfer Symposium*, New York City, November (1960); see also S. S. PENNER, D. B. OLFE and T. A. JACOBS, *Technical Note No.* 13, Contract AF 18(603)–2, California Institute of Technology, Pasadena, May (1960).
7. G. SHERRAT and E. GRIFFITHS, *Proc. Roy. Soc.* **147** A, 292 (1934); D. BENDER, *Ann. Physik* **38**, 199 (1940).
8. N. BLOEMBERGEN, *Phys. Rev.* **104**, 324 (1956).
9. S. S. PENNER, *Quantitative Molecular Spectroscopy and Gas Emissivities*, Addison–Wesley Publishing Co., Reading, Mass. (1959).

VOL. 1 1961

J. Quant. Spectrosc. Radiat. Transfer. Vol. 1, pp. 169–176, Pergamon Press Ltd. Printed in Great Britain

MEAN BEAM LENGTH CALCULATIONS FOR RADIATION FROM NON-TRANSPARENT GASES*

D. B. OLFE†
Daniel and Florence Guggenheim Jet Propulsion Center
California Institute of Technology, Pasadena, California

(*Received* 1 *December* 1960)

Abstract—The mean beam length for radiation from a non-transparent gas may depend on the temperature, pressure and absorbing properties of the gas, as well as on the geometry of the enclosure. Mean beam lengths are studied for the following types of band structure: (1) bands composed of non-overlapping, collision-broadened lines; (2) bands which may be approximated by constant average absorption coefficients acting over effective band widths; and (3) bands composed of randomly distributed, collision-broadened lines. The temperature and pressure dependence of the mean beam length is studied for these types of band structure and expressions for the mean beam length are obtained for some simple enclosure geometries.

I. INTRODUCTION

FOR THE calculation of the radiant-energy flux from a gas volume, it is convenient to use the concept of the mean beam length.[1]

The radiant-energy flux from an isothermal gas volume to a portion of its confining surface is given by[1]

$$H = \frac{\sigma T^4}{\pi} \int_A \int_\rho \int_\Omega \cos\varphi \frac{d\varepsilon(\rho)}{d\rho} d\Omega d\rho dA \equiv \sigma T^4 A \varepsilon(L) \tag{1}$$

which defines the mean beam length L. In equation (1), σ is the Stefan-Boltzmann constant, T the temperature, $d\Omega$ the solid angle subtended by a differential gas volume, ρ the distance between the differential area dA on the enclosure surface and the differential gas volume, φ the angle between ρ and the normal to dA, and $\varepsilon(\rho)$ the total hemispherical emissivity for a gas of beam length ρ.

In equation (1), the integral over ρ may be carried out directly to yield

$$\varepsilon(L) = \frac{1}{A\pi} \int_A \int_\Omega \cos\varphi \, \varepsilon(r) d\Omega dA \tag{2}$$

where r is the total length of gas across the enclosure in the direction of the differential gas volume.

For some simple geometries, the radiation will be uniform over the entire surface of the enclosure and equation (2) will reduce to

$$\varepsilon(L) = \frac{1}{\pi} \int_\Omega \cos\varphi \, \varepsilon(r) d\Omega. \tag{3}$$

* This work was supported by the Office of Naval Research under Contract No. NR-220(03), NR015401.
† Now Associate Professor of Aeronautics, New York University, New York City, N.Y.

In the special case of a transparent gas, the emissivity will be directly proportional to the beam length, and equation (2) becomes

$$L^\circ = \frac{1}{A\pi} \int_A \int_\Omega \cos\varphi \, r \, d\Omega dA. \tag{4}$$

For radiation to the entire surface area A of the enclosure, equation (4) reduces to[1] $L^\circ = 4\,V/A$ where V is the total gas volume. Equation (4) shows that the mean beam length L° for a transparent gas is simply a function of the geometry of the enclosure and does not depend on the conditions or properties of the emitting gas. For a non-transparent gas, it is of interest to relate the mean beam length L, which generally does depend on the gas conditions and properties, to the mean beam length L° for a transparent gas.

II. GENERAL REMARKS ON THE TEMPERATURE AND PRESSURE DEPENDENCE OF THE RATIO L/L° FOR ARBITRARY ENCLOSURE SHAPES

In order to determine the ratio L/L°, the form of the emissivity $\varepsilon(r)$ must be known for the particular gas considered. The form of the emissivity depends on the band and line structure of the emitting gas. For most cases of interest, the band structure may be described by one of the following three models.[2] (1) Bands composed of non-overlapping collision-broadened lines, (2) bands which may be approximated by constant average absorption coefficients acting over effective band widths and (3) bands composed of randomly distributed, collision-broadened lines.

A. Bands composed of non-overlapping, collision-broadened lines

For bands composed of non-overlapping, collision-broadened lines the emissivity $\varepsilon(r)$ will be approximately proportional to r for small r (transparent gas) and approximately proportional to $\sqrt{r}$ for large r. In the first case, $L = L^\circ$ by definition for the transparent gas. When most of the beam lengths across the enclosure are large enough for the square root dependence to be valid, equations (2) and (4) yield

$$L/L^\circ = \frac{\left(\frac{1}{A\pi} \int_A \int_\Omega \cos\varphi \sqrt{r} \, d\Omega dA\right)^2}{\frac{1}{A\pi} \int_A \int_\Omega \cos\varphi \, r d\Omega dA} \tag{5}$$

which depends only on the geometry of the enclosure. Therefore, for bands composed of non-overlapping, collision-broadened lines the ratio L/L° is unity for small enclosures and a constant, independent of temperature and pressure, for large enclosures. Of course the gas properties and temperature determine the size of the enclosure at which the transition occurs from L/L° of unity to the value given by equation (5). This occurs when $\varepsilon(r)$ changes from the linear relation in r to the square root relation, i.e., when[2] $\bar{S}pr/4b_c$ is approximately unity, where $\bar{S}$ is the average line integrated intensity (cm^{-2}–$atm.^{-1}$), given by $\frac{1}{p}\int k_\omega \, d\omega$, p is the partial pressure (atm.) of the emitting gas, and b_c is the collision half-width (cm^{-1}). Since b_c is proportional to the total pressure, the transition is independent of pressure for a pure gas.

B. Bands approximated by average absorption coefficients

For the case of constant average absorption coefficients $\bar{k}$ acting over the band widths $\Delta\omega$, the emissivity of the ith band is given by[2]

$$\varepsilon_i(r) = \frac{R^\circ_{\omega_i}}{\sigma T^4}\,\Delta\omega_i[1\text{-}\exp(-\bar{k}_i r)] \tag{6}$$

where $R^\circ_{\omega_i}$ is the blackbody radiancy evaluated at the wave number ω_i of the band center. In order to investigate the temperature and pressure dependence of L/L°, it is convenient to consider first the value L_i obtained by using only the emissivity $\varepsilon_i(r)$ of the ith band in equation (2). Use of equation (6) in equation (2) yields

$$[1\text{-}\exp(-\bar{k}_i L_i)] = \frac{1}{A\pi}\int_A\int_\Omega \cos\varphi\,[1\text{-}\exp(-\bar{k}_i r)]\,\mathrm{d}\Omega\mathrm{d}A \tag{7}$$

or

$$\frac{L_i}{L^\circ} = -\frac{1}{\bar{k}_i L^\circ}\ln\left[1 - \frac{1}{A\pi}\int_A\int_\Omega \cos\varphi\left(1\text{-}\exp\left[-\bar{k}_i L^\circ\left(\frac{r}{L^\circ}\right)\right]\right)\mathrm{d}\Omega\mathrm{d}A\right]. \tag{8}$$

Now for temperatures low enough for the Boltzmann population factor to be neglected, $\bar{k}_i$ has the temperature and pressure dependence[2]

$$\bar{k}_i \propto p(T)^{-\frac{1}{2}}. \tag{9}$$

Reference to equation (4) shows that, for a given enclosure geometry, the value of r/L° in a given direction is independent of enclosure size. Thus L_i/L° is a unique function of $p(T)^{-\frac{1}{2}}L^\circ$. Using brackets to denote functional dependence, this result may be expressed by

$$\frac{L_i}{L^\circ}\left\{T_2, p_2, L^\circ\right\} = \frac{L_i}{L^\circ}\left\{T_1, p_1, \left(\frac{p_2}{p_1}\right)\left(\frac{T_1}{T_2}\right)^{\frac{1}{2}} L^\circ\right\}. \tag{10}$$

The ratio L_i/L° will increase with increasing temperature for a given value pL° since L_i/L° is a decreasing function of $p(T)^{-\frac{1}{2}}\,L^\circ$.

Since the total emissivity of non-overlapping* bands is simply the sum of the band emissivities, the ratio L/L° may be determined from

$$\sum_i \varepsilon_i(L) = \sum_i \varepsilon_i(L_i) \tag{11}$$

where $\varepsilon_i(L)$ and $\varepsilon_i(L_i)$ are computed from equation (6).

Since the relative importance of the various blackbody functions $R^\circ_{\omega_i}$ changes with temperature, in the general case of two or more bands of unequal intensity the temperature dependence of L/L° will not be the same as that given by equation (10) for L_i/L° (however the pressure dependence will be the same). For bands of equal intensity, L will of course be equal to L_i.

---

* Overlapped bands may be broken up into smaller non-overlapped (just touching) "bands" with constant average absorption coefficients.

C. Bands composed of randomly distributed collision-broadened lines

The Mayer-Goody statistical model* may be used to calculate the emissivity of a gas with a complex spectrum that may be approximated by bands composed of randomly distributed lines. Using this model, the emissivity of the ith band is

$$\varepsilon_i(r) = \frac{R^\circ_{\omega_i}}{\sigma T^4}\,\Delta\omega_i\left[1\text{-}\exp\left(-\frac{\bar{A}_i(r)}{d_i}\right]\right) \tag{12}$$

where

$$\bar{A}_i(r) = \int_0^\infty\int_0^\infty P(\bar{S}_i, S)\,[1\text{-}\exp(-k_\omega r)]\,\mathrm{d}\omega\mathrm{d}S \tag{13}$$

is the mean value of the total absorption of an isolated line averaged over all possible integrated intensities with $P(\bar{S}, S)\mathrm{d}S$ denoting the probability that the integrated intensity lies between S and $S + \mathrm{d}S$ and d being the mean line spacing. For collision-broadened lines, $\bar{A}_i(r) \simeq \bar{S}pr$† or $\bar{A}_i(r)/d_i = \bar{S}pr/d_i = \bar{k}_i r$ for $r \lesssim 4b_c/\bar{S}p$ and $\bar{A}_i(r) \simeq$ constant $\times\, 2\sqrt{\bar{S}b_c pr}$ for $r \gtrsim 4b_c/\bar{S}p$ (the constant is equal to unity for equally intense lines, i.e., for $P(\bar{S}, S) = \delta(S - \bar{S})$).

Using

$$d \propto T^{-\tau_i} \tag{14}$$

for the temperature dependence of d (τ_i is a constant for a given gas) and the usual temperature and pressure dependences of the other quantities,‡ the following results are obtained:

$$\frac{L_i}{L^\circ}\left\{T_2, p_2, L^\circ\right\} = \frac{L_i}{L^\circ}\left\{T_1, p_1, \left(\frac{p_2}{p_1}\right)\left(\frac{T_1}{T_2}\right)^{\frac{1}{2}} L^\circ\right\} \tag{15}$$

for $L^\circ \lesssim 4b_c/\bar{S}p$, and

$$\frac{L_i}{L^\circ}\left\{T_2, p_2, L^\circ\right\} = \frac{L_i}{L^\circ}\left\{T_1, p_1, \left(\frac{p_2}{p_1}\right)^2\left(\frac{T_1}{T_2}\right)^{2-\tau_i} L^\circ\right\} \tag{16}$$

for $L^\circ \gtrsim 4b_c/\bar{S}p$. The mean beam length may be obtained from the L_i values by use of equation (11). The pressure dependence of L will be the same as that of L_i, whereas the temperature dependence will be the same only in the case of equal band intensities. A calculation (see section III–A and Fig. 1) shows that the value of L/L° for H_2O in a spherical enclosure increases more rapidly with temperature (fixed L°) than L_i/L° does. This result is produced by the increased importance of the weak bands at high temperatures, especially for the large values of L°.

III. CALCULATION OF L/L° FOR SOME SIMPLE ENCLOSURE GEOMETRIES

In order to investigate mean beam lengths further, specific enclosure geometries must be considered. In this section some simple geometries will be considered for which analytical expressions may be obtained for the mean beam length.

---

* See, for example, reference 2.

† This relation states that an isolated line of mean intensity is transparent. Thus the L_i/L° expression [equation (15)] derived from this relation will be very near unity in its region of validity.

‡ See reference 2.

A. Spherical enclosure

Since the radiation will be uniform over the entire surface of the sphere, equation (3) may be used. If D is the diameter of the sphere, equation (3) becomes

$$\varepsilon(L) = 2\int_0^{\pi/2} \cos\varphi \sin\varphi \;\; \varepsilon(D\cos\varphi) \;\; \mathrm{d}\varphi. \tag{17}$$

Changing the variable to $r = D\cos\varphi$, equation (17) may be written as

$$\varepsilon(L) = \frac{2}{D^2}\int_0^D r\varepsilon(r)\mathrm{d}r. \tag{18}$$

Equation (18) is in a convenient form for use with tabulated hemispherical emissivities $\varepsilon(r)$.

For a transparent gas, $\varepsilon(r)$ is proportional to r, and equation (18) yields $L^\circ = \frac{2}{3}D$.

The emissivity $\varepsilon(r)$ of non-overlapping collision-broadened lines is proportional to $\sqrt{r}$ for large r. Use of equation (18) yields $L = \frac{16}{25}D$ or $L/L^\circ = \frac{24}{25}$ for large r. Thus L/L° is very nearly unity for all values of r provided the lines are non-overlapped.

The band emissivity $\varepsilon_i(r)$ given by equation (6) may be used in equation (18) to determine L_i and L for bands approximated by average absorption coefficients. The following results are obtained:

$$\frac{L_i}{L^\circ} = -\frac{3}{2x_i}\ln\left[1 - g(x_i)\right]$$

and

$$\sum_i \frac{R^\circ_{\omega_i}}{\sigma T^4}\Delta\omega_i(1 - e^{-\bar{k}_i L}) = \sum_i \frac{R^\circ_{\omega_i}}{\sigma T^4}\Delta\omega_i\, g(x_i) \tag{19}$$

where

$$g(x_i) = \left[1 + 2e^{-x_i}\left(\frac{1}{x_i} + \frac{1}{x_i^2}\right) - \frac{2}{x_i^2}\right]$$

and

$$x_i = \bar{k}_i D.$$

The above results are also valid at small values of r for bands composed of randomly distributed collision-broadened lines (cf. section II–C). At large values of r, the following results are obtained for randomly distributed lines [using $P(\bar{S}, S) = \delta(\bar{S} - S)$*]:

$$\frac{L_i}{L^\circ} = \frac{3}{2y_i^2}\left(\ln\left[1 - h(y_i)\right]\right)^2$$

and

$$\sum_i \frac{R^\circ_{\omega_i}}{\sigma T^4}\Delta\omega_i(1 - e^{-c_i\sqrt{L}}) = \sum_i \frac{R^\circ_{\omega_i}}{\sigma T^4}\Delta\omega_i h(y_i) \tag{20}$$

where

$$h(y_i) = \left[1 + 4e^{-y_i}\left(\frac{1}{y_i} + \frac{3}{y_i^2} + \frac{6}{y_i^3} + \frac{6}{y_i^4}\right) - \frac{24}{y_i^4}\right],$$

$$c_i = \frac{\sqrt{\bar{S}_i b_c p}}{d_i}, \text{ and } y_i = c_i\sqrt{D}.$$

* It is well known that the emissivity is practically independent of the precise form of $P(\bar{S}, S)$.

The spectrum of H_2O may be approximated by bands composed of randomly distributed lines. Using values given in reference 2 for the necessary parameters ($\gamma_i = 1$), equation (20) was used to calculate L/L° for H_2O at large values of L°. The results (discussed in section II–C) are given in Fig. 1.

B. Enclosure consisting of two infinite parallel planes

Use of equation (3) yields

$$\varepsilon(L) = 2\int_0^{\pi/2} \cos\varphi \sin\varphi \; \varepsilon(h/\cos\varphi)\, d\varphi \tag{21}$$

or

$$\varepsilon(L) = 2h^2 \int_h^\infty \varepsilon(r)\frac{dr}{r^3} \tag{22}$$

where h is the distance between the infinite parallel planes.

For a transparent gas, equation (22) reduces to $L^\circ = 2h$. At large values of r when

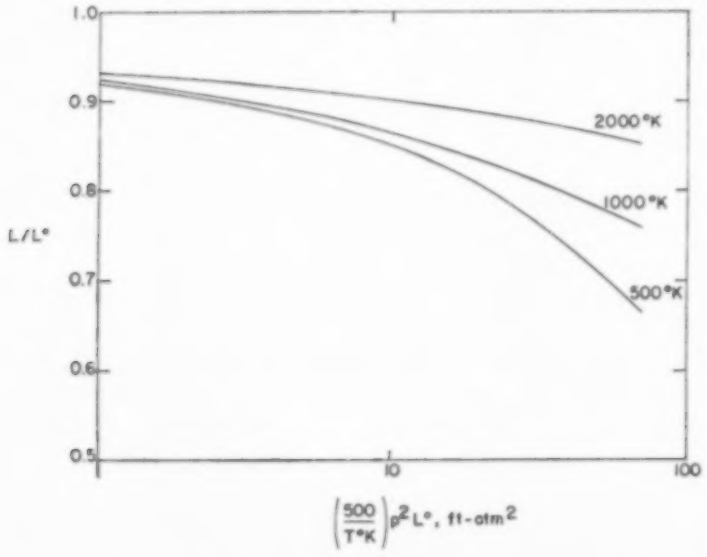

FIG. 1. The mean beam length ratio L/L° for H_2O in a spherical enclosure as a function of $(500/T°K)\,p^2L^\circ$.

$\varepsilon(r)$ for non-overlapping collision-broadened lines is proportional to $\sqrt{r}$, equation (22) reduces to $L = \frac{1}{2}^\circ h$ or $L/L^\circ = 8/9$.

The following result holds for bands approximated by average absorption coefficients:

$$\sum_i \frac{R^\circ_{\omega_i}}{\sigma T^4}\Delta\omega_i\,(1 - e^{-\bar{k}_i L}) = \sum_i \frac{R^\circ_{\omega}}{\sigma T^4}\Delta\omega_i\,[1 - 2E_3(x_i)] \tag{23}$$

where $x_i = \bar{k}_i h$ and $E_3(x_i)$ represents the case $n = 3$ for the tabulated[3] integral

$$E_n(x_i) = \int_0^1 \mu^{n-2} e^{-x_i/\mu} \, d\mu. \tag{24}$$

For randomly distributed collision-broadened lines at large r, the following result is obtained:

$$\sum_i \frac{R^\circ_{\omega_i}}{\sigma T^4} \Delta\omega_i (1 - e^{-c_i\sqrt{L}}) = \sum_i \frac{R^\circ_{\omega_i}}{\sigma T^4} \Delta\omega_i [1 - 4E_5(y_i)] \tag{25}$$

where $E_5(y_i)$ is given by equation (24) with x_i replaced by y_i and $n = 5$. The terms c_i and y_i are defined by

$$c_i = \frac{\sqrt{5} b_c p}{d_i} \quad \text{and} \quad y_i = c_i \sqrt{h}.$$

C. Enclosure consisting of an infinite circular cylinder

For bands composed of non-overlapping collision-broadened lines at large values of L°.

$$L/L^\circ = \left[\frac{\Gamma(5/4)}{\Gamma(7/4)}\right]^4 = 0{\cdot}9460 \tag{26}$$

where Γ denotes the Gamma function and $L^\circ = d$ with d being the diameter of the circular cylinder.

The following result holds for bands approximated by average absorption coefficients:

$$\sum_i \frac{R^\circ_{\omega_i}}{\sigma T^4} \Delta\omega_i (1 - e^{-\bar{k}_i L}) = \sum_i \frac{R^\circ_{\omega_i} \Delta\omega_i}{\sigma T^4} f(x_i) \tag{27}$$

where $x_i = \bar{k}_i d$ and $f(x_i)$ represents the tabulated[4] double integral

$$f(x_i) = \frac{4}{\pi} \int_0^{\pi/2} \int_0^{\pi/2} \left[1\text{-}\exp\left(-x_i \frac{\cos\psi}{\cos\chi}\right)\right] \cos^2\chi \cos\psi \, d\chi \, d\psi. \tag{28}$$

D. Radiation to the center of the base of a finite circular cylinder

The transparent gas mean beam length is given by

$$L^\circ = 2\,[h(1\text{-}\cos\varphi_\circ) + R(1\text{-}\sin\varphi_\circ)] \tag{29}$$

where $\varphi_\circ = \tan^{-1}(R/h)$ with R and h denoting the cylinder radius and height, respectively.

For bands composed of non-overlapping collision-broadened lines at large values of L°,

$$L/L^\circ = \left(\frac{8}{9}\right) \frac{(\sqrt{H}\,[1 - (\cos\varphi_\circ)^{\frac{3}{2}}] + \sqrt{R}\,[1\text{-}(\sin\varphi_\circ)^{\frac{3}{2}}])^2}{H(1\text{-}\cos\varphi_\circ) + R(1\text{-}\sin\varphi_\circ)}. \tag{30}$$

The mean beam length for bands approximated by average absorption coefficients may be computed from the following expression:

$$\sum_i \frac{R^\circ_{\omega_i}}{\sigma T^4} \Delta\omega_i (1 - e^{-\bar{k}_i L}) = \sum_i \frac{R^\circ_{\omega_i}}{\sigma T^4} \Delta\omega_i \left[\Phi(\bar{k}_i H) - \Phi(\bar{k}_i R) + \Phi(\bar{k}_i \sqrt{H^2 + R^2})\right] \quad (31)$$

where

$$\Phi(z) = e^{-z} - ze^{-z} - z^2 \int_{-\infty}^{z} \frac{e^{-z'}}{z'} \, dz' \quad (32)$$

is tabulated on p. 109 of reference 4.

Acknowledgement—Acknowledgement is gratefully extended to Dr. S. S. PENNER for suggesting this investigation.

REFERENCES

1. W. H. MACADAMS, (Editor), *Heat Transmission*, Chapter 4, Radiant-Heat Transmission, by H. C. HOTTEL, McGraw-Hill, New York, 1954.
2. S. S. PENNER, *Quantitative Molecular Spectroscopy and Gas Emissivities*, Addison-Wesley Publishing Co., Reading, Mass., 1959.
3. V. KOURGANOFF, *Basic Methods in Transfer Problems*, pp. 264–266, Clarendon Press, Oxford, 1952.
4. M. JAKOB, *Heat Transfer*, Vol. 2, pp. 103–105, John Wiley, New York, 1957.

VOL.
1
1961

J. Quant. Spectrosc. Radiat. Transfer. Vol. 1, pp. 177–184. Pergamon Press Ltd. Printed in Great Britain

DIRECT MEASUREMENT OF LINE INTENSITIES AND WIDTHS IN THE FIRST OVERTONE BAND OF CO

H. J. KOSTKOWSKI and A. M. BASS
National Bureau of Standards, Washington 25, D.C.

(*Received* 30 *January* 1961)

Abstract—The absolute intensities and widths of self-broadened lines in the first overtone band of carbon monoxide were measured directly with a small grating monochromator to an estimated accuracy of 5 per cent. The intensities were obtained at CO pressures below one atmosphere and the widths at pressures from 2½ to 20 atm. Slit function corrections were made using the results of a paper[1] previously published by the authors. The intensities were found to fit the results of the rotation-vibration interaction calculation of HERMAN and WALLIS.[2] Spectral transmission calculations assuming a Lorentz shape for all the lines fit the observed data up to 20 atm. pressure.

SPECTRAL line intensities and widths are of basic importance for the solution of many technical problems. For example, they are useful for determining temperatures of hot gases or flames and necessary for the calculation of radiative transfer in a gas. Moreover, these parameters, when correlated with theory, furnish information on the structure of the radiating species and their interaction through collisions with their neighbors.

This paper reports on the direct measurement of absolute line intensities and widths in the $0 \rightarrow 2$ rotation-vibration band of carbon monoxide. CO is of particular interest because of its frequent occurence in practical hot gas systems and the availability of a quantum mechanical calculation[2] of the rotation-vibration interaction and its effect on the intensities.

Previous work on the intensities and widths of individual vibration-rotation lines is rather meager. In the case of the 0–2 band of CO, relative line intensities in emission have been reported by EATON[3] and line widths, using equivalent width measurements, have been reported by EATON and THOMPSON[4]. No measurements on the absolute intensities of these lines have been reported though PENNER and WEBER[5,6] calculated absolute line intensities from their measurement of the 0–2 band intensity.

INSTRUMENTATION

The experimental set-up utilized a modified Perkin Elmer doublepass spectrometer with 13 cycle modulation. The prism and Littrow mirror were replaced by a 2½ in. × 3 in., 7500 lines per inch plane grating blazed at 3 μ. The grating drive was modified to permit the grating to be rotated at speeds 1/4 that originally available. A cooled PbS detector was used. The cooled detector consisted of a 2 mm × 0·2 mm cell mounted in a specially designed Dewar having a capacity of about 300 cm³, sufficient for 10 hr. operation on a single filling of dry ice and acetone. A pair of ellipsoidal mirrors formed a three times reduced image of the exit slit on the cooled detector. The optics of the spectrometer were adjusted until the observed profile of the 2·05 μ helium line obtained from a 5 mm Hg

pressure electrodeless discharge was symmetrical and of minimum width. Using a 500 W projection lamp as a source it was possible to obtain a spectral slit width of 0·25 cm^{-1} at 4200 cm^{-1} with a signal to noise ratio of about 500.

Gas absorption cells of lengths from 1 cm to 100 cm and known to $\frac{1}{2}$ per cent or better were used. Cells of conventional design, (glass or quartz tubes with glass or quartz windows either cemented or fused to the ends) were used for measurements at pressures less than 2 atm. For measurements at higher pressures, transmission cells were constructed of stainless steel, based on the design of WELSH, *et al*[7]. With these cells windows of synthetic sapphire ($\frac{7}{8}$ in. diam., $\frac{1}{2}$ in. thick) were used. The pressure-tight seal was made by squeezing a gold 0-ring gasket between the polished optically flat surface of the window and the polished optically flat surface of the hardened steel "lens ring".

Line intensity data were taken at pressures from 1/4 to 1 atm. and line width data from $2\frac{1}{2}$ to 20 atm. Pressure measurements were made with Wallace and Tiernan pressure gauges calibrated at the National Bureau of Standards to an accuracy of 1 per cent or better. Measurements were made at a gas temperature of 27°C (Int. 1948). The temperature was determined with a calibrated copper–constantan thermocouple placed in the absorption cells prior to the actual spectral measurements. The temperature is considered reliable to 1 or 2°C. The CO used was analyzed mass spectrometrically. It consisted of 98·8 $\pm$ 0·3 mol per cent CO, 0·9 mol per cent hydrogen and the remainder nitrogen, oxygen, carbon dioxide and iron pentacarbonyl.

LINE INTENSITIES

The procedure for determining the absolute intensity of an absorption spectral line was to scan over the line with the absorption cell first containing CO and then evacuated; compute the spectral absorption coefficient from the measured spectral transmission; numerically integrate the observed absorption coefficient over the line and apply the appropriate slit function correction to the resulting integral or intensity. The following equations define the observed absorption coefficient and intensity.

$$T_{obs}(\nu) = \frac{I^{obs}(\nu)}{I_o^{obs}(\nu)} = e^{-k_{obs}(\nu)pl} \tag{1}$$

$$S_{obs} = \int_{line} k_{obs}(\nu)d\nu \tag{2}$$

$I^{obs}(\nu)$ and $I_o^{obs}(\nu)$ are the signal outputs or recorder deflections at a spectrometer frequency setting ν with CO in the absorption cell and the cell evacuated respectively. $k_{obs}(\nu)$ is the observed absorption coefficient, p the CO pressure in atmospheres, l the geometrical path length of the cell in centimeters and S_{obs} the observed line intensity. Integrations were performed using Simpson's rule. Accurate values of $I_o^{obs}(\nu)$ were obtained by setting the spectrometer for the wavelength of the trough between the line of interest and an adjacent line and successively letting CO into the evacuated cell and pumping it out. Under the conditions of pressure and path length for which the intensity data were taken, the trough absorption was always less than the noise which was about 0·2 per cent of the signal. Therefore, it was assumed that the transmission in the troughs was unity and the observed $I_o^{obs}(\nu)$ was fitted to the $I^{obs}(\nu)$ runs to make this identically true.

The observed line intensities were corrected for the effect of the instrumental slit

function, the contribution from the wings and the presence of isotopic CO lines. The cell path length was chosen so that the peak absorption of the line under observation was calculated (using best estimate of widths and intensities obtained in preliminary investigations and other studies and assuming a Lorentz line shape) to be about 30 per cent. This corresponded to an observed peak absorption of 15 per cent or less and often about 5 per cent. The slit function corrections were made using previously published graphs[1] and a spectral slit width to line half-width ratio obtained experimentally in a manner to be described later. The slit width correction to the intensity ranged from 1 to 7 per cent, and wing corrections, assuming a Lorentz line shape, ranged from 2 to 5 per cent. The total correction, which resulted in an intensity greater than that observed, ranged from 4 to 9 per cent and was usually about 6 or 7 per cent. Four to six intensity determinations were made for each line reported and the precision was such that the standard deviation of a single determination about the mean was about $2\frac{1}{2}$ per cent. Experimentally determined intensities were obtained for 20 lines and are listed in Table 1.

In order to obtain the intensities of CO lines in the 0–2 band which were not measured and in order to check the validity of existing calculations on relative line intensities, attempts were made to fit the simple rotor[8], OPPENHEIMER[9] and HERMAN–WALLIS[2] calculations to the experimentally determined intensities Only the Herman–Wallis results fit the observed intensities within the experimental error.

The intensity of a line resulting from a transition $J'' \rightarrow J'$ in the first overtone band of CO may be expressed as,[2]

$$S^{J'}_{J''}(m) = |m| \nu^{J'}_{J''} F(m) e^{-\frac{E_{J''}}{kT}} K \tag{3}$$

where the double prime refers to the lower energy level. K is a constant for all the lines in the band, $E_{J''}$ is the energy of the J'' rotational level, T is the Kelvin temperature, $F(m)$ is a correction factor for rotation-vibration interaction where m equals $-J''$ for the P lines and $J''+1$ for the R lines, and $\nu^{J'}_{J''}$ is the frequency in wave numbers of the transition $J'' \rightarrow J'$. Using the physical constants of the CO molecule obtained by PLYLER, BENEDICT and SILVERMAN,[10] Herman–Wallis give for $0 \rightarrow 2$ band of CO

$$F(m) = 1 + 0{\cdot}00528m + \varepsilon(m, m^2) \tag{4}$$

where $\varepsilon(m, m^2)$ represents small correction terms. For lines $m = 21$ and 35 the small correction terms effect $F(m)$ by less than 1·0 and 2·0 per cent respectively and were therefore neglected. Using this expression for $F(m)$, K in equation (3) was calculated for each of the twenty observed lines and found to be constant within the experimental error. The value found was $3{\cdot}80 \times 10^{-6}$ atm^{-1} cm^{-1} with a standard deviation of a single value about the mean of 2·6 per cent. Using this value of K, line intensities up to $J'' = 35$ were calculated and are reported in Table 1. The line intensities in Table 1 differ from those obtained by PENNER and WEBER,[5,6] from the total band intensity, by 7 per cent to 70 per cent depending on the line.

We estimate the line intensities reported here to be accurate to 5 per cent.

LINE WIDTHS

Most of the measurements of CO line widths were made at pressures of 5 and 10 atmospheres of CO. The procedure for obtaining data for line widths was similar to that

for obtaining intensities. However, the method of analysis was different. In the case of line intensities, the pressure was sufficiently low so that each line was well isolated from its neighbors. That is, the overlap was very small. At the pressures used for line width measurements the overlap was not small and had to be subtracted before the width of a line could be determined. The manner in which this was performed was first to assume a Lorentz line shape and to calculate the ratio of the total overlap at the peak of a line to the total absorption coefficient in an adjacent trough.

$$\frac{\text{Total overlap of absorption coefficient at peak of line } i}{\text{Total absorption coefficient at trough between lines } i \text{ and } i\text{–}1} = \frac{\sum_{j=1,\neq i}^{\infty} k_j(\nu_i)}{\sum_{j=1}^{\infty} k_j(\nu_{i,i-1})}$$

$$= \frac{\sum_{j=1,\neq i}^{\infty} \frac{S_j \alpha_j/\pi}{(\nu_i - \nu_j)^2 + \alpha_j^2}}{\sum_{j=1}^{\infty} \frac{S_j \alpha_j/\pi}{(\nu_{i,i-1} - \nu_j)^2 + \alpha_j^2}} \tag{5}$$

where $k_j(\nu_i)$ and $k_j(\nu_{i,i-1})$ are the absorption coefficients of line j evaluated at the peak of line i and the trough between lines i and i–1 respectively. To perform this calculation, the previously determined intensities and the widths obtained from preliminary data and subsequent successive approximations were used. Though the overlap does depend strongly on the assumption of a Lorentz line shape or on the particular widths used, the ratio in equation (5) does not. Therefore the ratio can be calculated with considerably greater accuracy than the overlap. The second step in obtaining the overlap at the peak of a line is to determine experimentally the total absorption coefficient in the trough adjacent to the line in question, i.e. the denominator of equation (5). Since the absorption coefficient in the troughs of the CO lines varies only slightly over the extent of the spectral slit width ($\sim$0·25 cm^{-1}), the denominator of equation (5) can be measured directly and without a correction. Finally, utilizing the calculated ratios and the experimentally determined denominators, the numerator or overlap can be computed. Since the width of a line is defined as that width at which the peak absorption coefficient of the line has decreased to half its maximum value, the overlap ratio in the vicinity of the half-width must also be calculated. In this manner, the observed absorption coefficient at the peak and in the vicinity of the half-width of a line due to that line alone were obtained, and the observed width of the line measured. The pooled standard deviation of each of the determinations of α_j^{obs} about their respective means was 1·3 per cent.

The actual half-widths α_j were obtained from the observed half-widths α_j^{obs} through the equation

$$\frac{\alpha_j^{obs} - \alpha_j}{\alpha_j} = \text{Correction factor} \tag{6}$$

in which the correction factor was obtained from Figs. 2 and 3 of reference (1). In order to utilize Fig. 2, the ratio of spectral slit width to line half-width is required. This was

TABLE 1. EXPERIMENTAL AND CALCULATED ABSOLUTE INTENSITIES FOR THE FIRST OVERTONE BAND OF CO AT A TEMPERATURE OF 300°K. CALCULATED VALUES WERE OBTAINED USING THE HERMAN–WALLIS FORMULAE AND THE EXPERIMENTALLY DETERMINED K.

J''	$S_{J''}$ (atm^{-1} cm^{-2})			
	P Branch		R Branch	
	Experimental	Calculated	Experimental	Calculated
0			160×10^{-4}	163×10^{-4}
1		158×10^{-4}	317	321
2	313×10^{-4}	303		467
3		428		592
4	532	527	658	691
5		598		760
6		638		797
7		651	810	805
8	633	638		785
9		604		742
10		555	695	682
11	516	495		610
12		430		532
13		365	465	453
14	306	301		376
15		243	301	306
16		192		243
17	141	148		189
18		112	143	144
19		82·8		107
20		59·7		77·9
21	40·0	42·3	56·5	55·7
22		29·4		39·0
23		20·0	26·9	26·8
24	13·3	13·3		18·0
25		8·72	12·3	11·9
26		5·56		7·65
27		3·50	4·88	4·86
28		2·15		3·02
29		1·30		1·84
30		0·770		1·10
31		0·446		0·642
32		0·254		0·371
33		0·142		0·209
34		0·0778		0·116
35		0·0418		0·0629

obtained, as described in reference (1), by measuring the observed width of a line at two pressures differing by a factor of 2 and using Fig. 9 of reference (1). The slit width to line half-width ratio was also determined by measuring the observed width of a line with two spectral slit widths differing by a factor of two and using Fig. 10 of the same reference. The ratio of two for the spectral slit widths was obtained by alternately adjusting the slits and scanning over the 2·05μ helium line obtained from a low pressure microwave discharge. This line is considered to have a width at least ten times less than the instrumental spectral slit width, and therefore its scan should be very close to the slit function. Table 2 gives some typical data for the P4 and R3 lines using both the pressure and slit width variation methods. This procedure was carried out for a number of lines, and Table 3 gives experimental α_j's as a function of m together with interpolated α_j's obtained from a smooth curve fitted to the experimental values.

Although the observed line widths depend on the assumed line shape because the

TABLE 2. TYPICAL DATA FOR OBTAINING $\Delta\nu/\alpha$ BY THE PRESSURE OR SLIT WIDTH VARIATION METHOD.

Line	Pressure variation						Spectral slit width variation					
	α^{obs} (cm^{-1})		$\frac{\Delta\nu}{\alpha^{5\cdot07}}$	Correct. factor	$\alpha^{5\cdot07}$ (cm^{-1})	$\Delta\nu$ (cm^{-1})	$\alpha^{5\cdot07}_{obs}$		$\frac{2\Delta\nu}{\alpha^{5\cdot07}}$	Correct. factor	$\alpha^{5\cdot07}$ (cm^{-1})	$\Delta\nu$ (cm^{-1})
	Pressure (atm.)						Spect. slit wid. (cm^{-1})					
	5·07	10·14					$2\Delta\nu$	$\Delta\nu$				
P4	0·442	0·817	0·831	0·128	0·392	0·33	0·499	0·442	1·118	0·201	0·415	0·23
R3	0·438	0·830	0·661	0·088	0·403	0·27	0·501	0·438	1·205	0·225	0·408	0·25

TABLE 3. EXPERIMENTAL LINE HALF-WIDTHS FOR THE FIRST OVERTONE BAND OF CO AT 5·07 ATM OF CO PRESSURE AND A TEMPERATURE OF 300°K.

$\lvert m\rvert$	Experimental	Smoothed and interpolated
1	0·452 cm^{-1}	0·452 cm^{-1}
2		0·428
3		0·409
4	0·395	0·395
5		0·382
6		0·371
7		0·361
8	0·350	0·352
9		0·344
10		0·336
11		0·330
12		0·324
13		0·318
14	0·315	0·312
15		0·308
16		0·302
17		0·297
18		0·292
19	0·285	0·288
20		0·284
21	0·278	0·279
22	0·275	0·275

overlap ratios do, the dependence as mentioned before is not great. Under the present experimental conditions, if the CO line shapes had an inverse 3/2 power rather than the assumed inverse squared frequency dependence, the observed line widths would be in error by about 10 per cent. Furthermore Fig. 1 of reference (1) shows that the correction factor does not depend greatly on line shape. So even if the line shape were not known, the present technique would be useful. Moreover, in the case of CO, measurements to be discussed in the next section confirm at least an approximate Lorentz line shape. Taking these factors into account together with the precision available, the uncertainty of the CO line half-widths reported in column 3 of Table 3 is considered to be about 5 per cent.

LINE SHAPES

To obtain an idea of the shape of the spectral lines as reflected at the troughs of the lines, the absorption coefficients determined from the observed transmissions were compared to those calculated using the values of intensity and width reported in this paper and

TABLE 4. COMPARISON OF EXPERIMENTAL AND CALCULATED TROUGH ABSORPTION COEFFICIENTS AS A FUNCTION OF PRESSURE.

Spectral position	Pressure (atm)	kpl*		
		Experimental	Calculated	Difference (%)
RO–P1 (Midpoint)	5·07	0·0180	0·0185	−2·8
	10·24	0·0712	0·0741	−4·1
	20·48	0·269	0·272	−1·1
	40·72	0·832	0·906	−8·9
R18–R19 (Midpoint)	5·07	0·0498	0·0464	+6·8
	10·24	0·172	0·169	+1·7
	20·99	0·488	0·507	−3·9
	40·72	1·00	1·13	−13·0
P21–P20 ($2{\cdot}25\,cm^{-1}$ from P21)	5·07	0·00450	0·00454	−0·9
	10·24	0·0181	0·0181	0·0
	20·95	0·0683	0·0669	+2·1
	40·72	0·195	0·199	−2·1

assuming a Lorentz line shape. Table 4 gives the results of this comparison. Except for the case of 40 atm. pressure, the agreement is within the experimental error and supports the assumption of a Lorentz shape. The disagreement at 40 atm has not been explained.

Line half-widths were also obtained from the measured value of the absorption coefficients at the peak of a few lines. Taking account of overlap as previously described and correcting $k_j^{obs}(\nu_j)$ from graphs in reference (1), the half-width was calculated from

$$\alpha_j = S_j/\pi k_j(\nu_j) \tag{7}$$

which assumes a Lorentz line shape. The widths obtained in this manner for R3 at 5 and 10 atm pressure were 6 and 11 per cent lower than the values obtained directly. For P4, these widths were 1 and 5 per cent less than those obtained directly. These results further confirm a Lorentz line shape for the CO lines and, in general, confirm the overall consistency of the methods of this paper.

SUMMARY

The absolute intensities and half-widths of lines in the first overtone band of CO have been determined to an estimated accuracy of 5 per cent by direct measurements of these parameters and corrections for overlap and slit function. Agreement between the observed and calculated transmissions at the troughs and peaks of the CO lines has confirmed a Lorentz line shape and linear pressure dependence for the width of the lines for pressures from $2\frac{1}{2}$ per cent to 20 atm. Because the spectral slit width of the spectrometer used was about $0{\cdot}25\ cm^{-1}$ the data on line widths had to be obtained at pressures of 2 to 20 atm. However, with spectral slit widths as small as $0{\cdot}025\ cm^{-1}$ now available and $0{\cdot}1\ cm^{-1}$ common-place, this method should be applicable for a large number of molecules and at pressures below one atmosphere. Moreover, the lower pressures should make possible a greater accuracy because of the reduced overlap which is approximately proportional to the square of the pressure.

* Cell length, l, equals 4·77 cm.

Acknowledgements—The authors wish to thank Mrs. JACQUELINE KIMREY and Mr. RAYMOND BAYER for their help in the computations and some of the data taking and Mr. GEORGE E. BEALE, JR., for his help in maintaining and modifying much of the apparatus used.

REFERENCES

1. H. J. KOSTKOWSKI and A. M. BASS, *J. Opt. Soc. Amer.* **46**, 1060 (1956).
2. R. HERMAN and R. WALLIS, *J. Chem. Phys.* **23**, 637 (1955).
3. D. R. EATON, *Can. J. Phys.* **38**, 390 (1960).
4. D. R. EATON and H. W. THOMPSON, *Proc. Roy. Soc. A*, **251**, 475 (1959).
5. S. S. PENNER and D. WEBER, *J. Chem. Phys.* **19**, 807, 817 (1951).
6. S. S. PENNER and D. WEBER, *Infrared Intensity and Line-Width Measurements on Carbon Monoxide*, Report No. 9-2, Jet Propulsion Lab., Calif. Inst. of Tech., Pasadena, Calif. (1950).
7. H. L. WELSH, P. E. PASHLER and A. F. DUNN, *J. Chem. Phys.* **19**, 340 (1951).
8. G. HERZBERG, *Spectra of Diatomic Molecules*, D. Van Nostrand Co., New York (1950).
9. J. R. OPPENHEIMER, *Proc. Camb. Phil. Soc.* **23**, 327 (1926).
10. E. K. PLYLER, W. S. BENEDICT and S. SILVERMAN, *J. Chem. Phys.* **20**, 175 (1952).

VOL.
1
196

J. Quant. Spectrosc. Radiat. Transfer. Vol. 1, pp. 185–248. Pergamon Press Ltd. Printed in Great Britain

THE INFLUENCE OF THE ABSORPTION OF RADIATION IN SHOCK TUBE PHENOMENA*

J. POMERANTZ†
U.S. Naval Ordnance Laboratory, White Oak, Silver Spring, Maryland

(*Received* 9 *February* 1961)

Abstract—A theoretical investigation is made of the influence of the absorption of continuum radiation on the gas flow variables behind a strong shock wave advancing into argon at room temperature. A derivation of the emission formula for the total continuum radiation from an ionized gas brings out the need for knowing the amount that the ionization potential is lowered in a plasma. A review of the literature led to the choice of Ecker and Weizel's expression for the ionization potential lowering. Numerical results obtained by combining this expression with the usual shock equations are presented for the equilibrium conditions that are assumed to exist at the plane of maximum luminosity.

The absorption at a point behind the plane of maximum luminosity depends on the energy emitted from every element of the luminous region, modified by the absorption along the paths from the emitting elements to this point. The energy emitted from an element depends on the as yet unknown conditions at the element. Thus, the absorption at a point depends on the knowledge of the complete structure of the luminous region that we are seeking to determine. A "relaxation" method for finding the rate of absorption per unit mass is presented. In principle, the method is quite general. Here it is used to find the energy absorped at points in a "shock tube" of finite length and infinite optical cross section, i.e., there is essentially no contribution of radiative energy to a point from points in the same cross section sufficiently far removed. Moreover, the luminous region in this "tube" is assumed to be stratified into plane parallel layers in each of which uniform conditions exist. The absorption term found by this method is introduced into the energy equation. The ionization potential that is present in the energy equation is regarded, of course, as a variable. To obtain an expression for the variation of the degree of ionization with distance, it is necessary to combine the energy equation with the differential forms of the following equations: the equation of state, the Saha equation, the equation for the lowering of the ionization potential, and the conservation equations of mass-flow and momentum. The resulting expression together with similar expressions for the other variables constitute a system of differential equations which were solved (on an IBM computer) both with and without the inclusion in the energy equation of the term for the absorbed energy. Numerical calculations accurate as far as third-order terms showed that the assumptions underlying the "relaxation" method were valid.

Results are presented for shock waves of about Mach number 17 advancing into argon at densities of both 1/76 and 1/10 atm, and for a shock wave of Mach number 16 advancing into 1/2 atm of argon. It is found that for a given Mach number the effect of the absorption of energy is to bring the variables to an essentially constant value in a distance which depends on the density ahead of the shock. The greater the density, the shorter is this distance, and the closer is the magnitude of this constant value to the initial value at the plane of maximum luminosity.

A method is also presented for finding the absorption energy near the center line of a shock tube of finite optical depth. Thus, the influence of the absorption of energy on the flow variables behind the plane of maximum luminosity may be determined for this case, too.

---

* This work was supported in part by the Army Ballistic Missile Agency and in part by the Bureau of Naval Weapons.

† This report is based on a thesis submitted in 1958 by the author to the University of Maryland in partial fulfillment of the requirements for the degree of Doctor of Philosophy in physics.

I. INTRODUCTION

DURING the past decade the shock tube has become a widely used and important tool in the physics of gases at high temperatures. The shock tube is being used to study the kinetics of the approach to thermal equilibrium[1–5], the equation of state of gases[6], the determination of dissociation potentials[6], the electrical conductivity of ionized gases[7], magneto-hydrodynamic phenomena[7–9], atomic and molecular spectra and various radiation phenomena[4, 5, 10–15]. The flow behind the shock front is essentially one dimensional, i.e., except for a thin boundary layer along the tube wall, the pressure, temperature, density, and degree of ionization are constant over any cross section. This makes the shock tube of particular value as a source of spectroscopic light from a gas whose temperature and electron density behind a primary or reflected shock may be calculated from the initial conditions ahead of the shock and the easily determined speed of the primary shock. Shock tube measurements of the broadening of spectral lines at temperatures comparable to that of stellar atmospheres may be used by the astrophysicist to help determine the structure of stellar atmospheres[14]. Experimental and theoretical studies in connection with the shock tube might also help the astrophysicist in the understanding of novae.

Some studies of the shock tube have concerned themselves primarily with the non-equilibrium region directly behind the shock wave, that is, with the processes that occur in the approach to equilibrium. The complexity of the non-equilibrium phenomena involved depends on the strength of the shock wave and on the type of gas. In a diatomic gas, the very high translational energy at the shock front gradually goes into rotational and vibrational energy, and into dissociating the molecules. At still stronger shocks the atoms of the dissociated gas become ionized. In monatomic gases, there is no loss of energy to vibration and dissociation, and the phenomena of ionization may be studied without the complications of vibrational and dissociational relaxation. However, although substantial progress has been made, the kinetics of the approach to equilibrium is not fully understood even for a simple, monatomic gas such as argon[5].

A typical measurement of the intensity of the continuum radiation for a relatively weak shock wave of Mach number 11·4 advancing into argon at a pressure of 1 cm Hg shows that there is essentially no rise in radiation during the first 8 μsec of flow, and the intensity then rises rapidly during the next 11 μsec to a maximum (see Figs. 10(a) and (b) of reference 5) This maximum "equilibrium luminosity" is considered to correspond to the conditions calculated for the thermal equilibrium of an ionized monatomic shock behind the shock. The time required to reach this equilibrium decreases markedly with increasing Mach number, and it decreases with increasing density of the gas ahead of the shock. An increase of the impurity content of the gas will also cause a decrease in the time required to reach equilibrium.[5, 15] This theoretical investigation will not concern itself with this narrow non-equilibrium region, but rather with the broad region behind the plane of equilibrium luminosity.

PETSCHEK *et al.*[13] and TURNER[15] find that the luminosity decreases with distance behind the point of equilibrium luminosity until the cooling of the gas by radiation losses has decreased the electron density and temperature to the point where the luminosity cannot be detected by the particular measuring equipment, or until the luminosity is quenched at the colder interface of the driver gas. The rate of cooling of hot argon has been determined from experiments concerning the time variation of (1) the continuum radiation[13], (2) the

VOL.
1
1961

line shift[13], and (3) the electrical conductivity of the gas[7]. They concluded that the dominant heat loss under their experimental conditions was the continuum radiation. Their data and the data of ELENBAAS[16] and RYABININ *et al.*[17], just to mention a few, show that the intensity of continuum radiation becomes dominant at increasing temperatures.

Calculations by the writer showed that for shocks of strengths less than about Mach 17 advancing into argon at the density corresponding to the pressure of 1/76 atm, the absorption of continuum radiation is small. PETSCHEK *et al.*[13] thus appeared justified in neglecting self-absorption in calculating the effect of cooling on the gas dynamic variables behind the maximum luminosity front. Conditions, however, change rapidly with increasing density. For example, at a wavelength of 5000Å the intensity of the radiation is diminished about 100 times more in passing through 7 cm of the gas at thermal equilibrium behind a Mach 17 shock wave advancing into 1/10 atm of argon, than it is diminished for 7 cm of gas behind a Mach 17 shock wave advancing into 1/76 atmosphere of argon. Furthermore, the absorption of the continuum radiation in denser media will be shown to result in a marked decrease in the cooling rate.

Interest in such higher densities has been increasing because high densities are necessary to achieve Reynolds number simulation. The Reynolds number $R\,(=\rho Ud/\mu)$ is the appropriate parameter involving viscosity which leads to dynamic similarity of geometrically similar flows. The symbol ρ denotes the density, U the velocity past a fixed obstacle having a representative dimension d, and μ is the coefficient of viscosity. Thus, it is desirable that the density in an experiment involving a model should be increased in exactly the same proportion that exists between the full size of the body and that of the model. The need to simulate another flow parameter, the Mach number (U/a) where a is the velocity of sound, more specifically, the need for high *flow* Mach numbers behind the shock front has led to the addition to the conventional shock tube of a diverging nozzle and an enlarged, constant area test section[18, 19]. The nozzle converts the low Mach number (no higher than Mach 3), very high temperature flow behind a shock wave in the shock tube into a high Mach number, low free-stream temperature flow in the larger diameter tube. However, this is accompanied by a very large drop in the initial density, which from the standpoint of Reynolds number simulation is undesirable. Furthermore, the task of measuring pressures and observing optical effects becomes more difficult at the resulting lower densities in the test section. This can be remedied by having as large an initial density as the means of driving the shock will permit. It is thus evident that absorption of radiation will play an important role as stronger drivers for the higher densities are constructed.

A method for calculating the variation in the gas dynamical variables when only the emission of radiation is taken into account has been given by PETSCHEK *et al.*[13]. Thus, if absorption is neglected, the rate of energy loss per unit volume due to emission that enters into the equation of energy is a function of the temperature and electron density of only that element of volume for which the change in variables is being computed. However, if both emission and absorption are considered, then the expression for the absorption of energy that enters into the equation of energy depends on the radiation emitted from every element of the luminous region, modified by the absorption along the paths from each emitting element to the point in question. In other words, the absorption at a point depends on the complete structure of the luminous region which one is seeking to determine.

The principal problem of this theoretical investigation was to find a way of taking this

absorption into account and to show how this will modify the variation of the flow variables behind the maximum luminosity front. This is done in Part V for a "shock tube" of infinite radius, or what is equivalent, for one whose radius is of essentially infinite optical depth. Such a tube would be one in which there is essentially no contribution of radiative energy to a volume element from points in the same cross section that are sufficiently far removed. Furthermore, in Part VI is presented a method for finding the effect of the absorption of continuum radiation at points near the center line of a shock tube of finite optical depth. Numerical calculations were not performed, however, for this case.

A secondary, but nevertheless very important, problem was (1) the choice of a formula which expressed the lowering of the ionization potential in a plasma (hot ionized gas) as a function of the conditions in the plasma, and (2) the determination of the effects that this variable ionization potential has on the conditions at the plane of maximum luminosity and at points behind this plane.

The conditions in the hot ionized monatomic gas at the point of maximum luminosity are generally assumed to correspond to the equilibrium conditions behind the shock as determined from the Rankine–Hugoniot conservation equations for mass-flow, momentum, and energy, together with the equation of state and the Saha equation.[15] Also, it has been recognized by some workers in the field of plasmas[46, 47, 52] that the ionization potential χ appearing in the Saha equation and in the formula for the emission of continuum radiation will be lowered by the presence of ions and electrons from the value which strictly speaking is applicable to an isolated atom. However, the literature discloses that use of the lowered ionization potential has not been made by shock tube researchers when they calculate the equilibrium conditions behind a shock wave. There is, moreover, as already has been implied, some question as to what the ionization potential should be. Part III contains a discussion of the work done by various authors in finding the lowered ionization potential. The formula given by ECKER and WEIZEL[52] is chosen as the most promising. However, further experimental investigations are needed to verify this formula.

The effect of the variable ionization potential on the equilibrium conditions behind shock waves in argon have been determined in Part IV by an iterative process. The results obtained are compared with those for a fixed ionization potential. Also given are results which show the manner in which the ionization potential varies with the Mach number of the shock and the initial density ahead of the shock.

The steady-state, one dimensional equation of energy for a very hot gas contains a term for the ionization energy which involves the ionization potential. To find the manner in which the temperature, degree of ionization, pressure, density, flow velocity, and the ionization potential vary with distance behind the shock front, it is necessary to combine the differential forms of the equations of the ionization potential, state, and ionization equilibrium (Saha), and the conservation equations of mass and momentum with the equation of energy. The resulting system of equations are presented in Part V.

These equations are solved both with and without the inclusion in the energy equation of the term for the absorbed energy. Results are presented for shock waves of about Mach number 17 advancing into argon at densities of both 1/76 and 1/10 atm, and for a shock of Mach number 16 advancing into 1/2 atm of argon.

A derivation will be given in Part II of the formula for the emission of continuum radiation from a partially ionized gas. A clear derivation of this formula from the emission point of view could not be found in the literature, and it was considered desirable to present

VOL.
1
196

such a derivation starting with the time-dependent perturbation theory such as is given in Chapters VIII and X of Schiff's "Quantum Mechanics."

II. TRANSITION THEORY AND THE EMISSION OF CONTINUUM RADIATION

1. *Introduction*

In a semiclassical treatment of radiation a plausible and correct account of the effect of an external radiation field on a system of particles can be given for absorption and induced emission.[20] The electromagnetic field is treated classically and the particles by quantum mechanics. But the theory does not give the influence of the particles on the field, and thus does not predict the spontaneous emission. However, it follows from the theory of quantum electrodynamics (p. 400, reference 20) that the spontaneous emission may be regarded as an emission induced by the "zero-point" oscillations of the electromagnetic field. If the proper intensity of the zero-point field is found, then the semiclassical formula for induced emission may be used to obtain the correct expression for the spontaneous emission.

Many authors have contributed to the development of expressions for the emission and absorption of discrete and continuum radiation.[22–27] It is not always easy to find the exact connections between their methods of treatment. In the following pages we attempt to give a straightforward deduction of the equations we shall need, starting from the treatment presented in Schiff's book.

OL.
1
961

2. *Perturbation theory*

The effect of electromagnetic radiation on an atom can be found by the use of time-dependent perturbation theory. The transition probabilities between one quantum state and another for bound electrons or free electrons (in the vicinity of an atom) are obtained by the use of the Schrödinger wave equation

$$\frac{ih}{2\pi}\frac{\partial\psi}{\partial t} = (H_0 + H')\psi. \tag{1}$$

Here H_o represents the unperturbed Hamiltonian

$$H_0 = \frac{-h^2}{8\pi^2\mu}\Delta + V(\mathbf{r}), \tag{2}$$

while H' represents the first order perturbation due to the radiation field:

$$H' = \frac{ieh}{2\pi\mu c}\mathbf{A}\cdot\text{grad}. \tag{3}$$

A is the vector potential of this field. For the case of a polarized plane wave with propagation vector **k** and angular frequency ω we write the components of **A** in the form

$$A_j[\exp\{i(\mathbf{k}\cdot\mathbf{r} - \omega t + \alpha)\} + \exp\{-i(\mathbf{k}\cdot\mathbf{r} - \omega t + \alpha)\}],$$

where the A_j are the amplitude factors. Since the vector potential **A** is perpendicular to **k**, we have

$$A_1 k_1 + A_2 k_2 + A_3 k_3 = 0.$$

Moreover,

$$\omega = 2\pi\nu = c\sqrt{(k_1^2 + k_2^2 + k_3^2)} = 2\pi c/\lambda,$$

where ν is the frequency of the radiation in $\sec^{-1}$ and λ is the wavelength.

By calculating the electric field strength vector **E**, the magnetic field strength vector **H** and the Poynting vector, it is found that the average over a period of oscillation of the energy transmitted by the wave through a surface perpendicular to **k** of unit area in unit time, is given by

$$\frac{\omega^2}{2\pi c}(A_1^2 + A_2^2 + A_3^2).$$

This quantity is the radiation intensity associated with the plane wave.

In a radiation field we never deal with absolutely plane waves having a single frequency, but with radiation within a solid angle $d\tilde{\omega}$ and having a range of angular frequencies $d\omega$. The intensity of polarized radiation within $d\tilde{\omega}$ and $d\omega$ is represented by

$$I(\omega)\, d\omega\, d\tilde{\omega}.$$

We therefore take

$$A_1^2 + A_2^2 + A_3^2 = \frac{2\pi c}{\omega^2} I(\omega)\, d\omega\, d\tilde{\omega}. \tag{4}$$

In order to solve equation (1), we introduce the normalized eigenfunctions $U_n \exp(-2\pi i E_n t/h)$ of H_o with the corresponding (discrete or continuous) eigenvalues E_n and put:

$$\psi = Sa_n(t)U_n(x_1, x_2, x_3) \exp(-2\pi i E_n t/h). \tag{5}$$

The symbol S denotes both a summation over the discrete set of eigenfunctions and an integration over the continuous set. Any complete orthonormal set of functions such as U_n possesses the orthonormality property:

$$\int U_n^* U_m\, d\tau = \delta_{nm} \text{ or } \delta(n - m), \tag{6}$$

where the integration is over the entire space. The symbol δ_{nm} is the Kronecker delta that equals unity if $n = m$ and is zero otherwise, and applies if either n or m, is one of a discrete set, or when both belong to the discrete set. The function $\delta(n - m)$ is the Dirac delta function $\delta(x)$ (Schiff p. 50) with the properties: $\delta(n - m) = 0$ if $n \neq m$, and

$$\int \delta(n - m)\, dx = 1,$$

where the region of integration includes the point $x = 0$, and it applies if both n and m belong to a continuous set. In either case, for an arbitrary function f there holds the relation:

$$Sf_m \int U_n^* U_m\, d\tau = f_n.$$

The connection between the above notation and the notation which employs eigendifferentials will be considered later.

Upon substitution of equation (5) into (1) and use of the relation $H_o U_n = E_n U_n$, we obtain

$$S \frac{ih}{2\pi} \frac{da_n}{dt} U_n \exp\left(\frac{-2\pi i E_n t}{h}\right) = Sa_n H' U_n \exp\left(\frac{-2\pi i E_n t}{h}\right).$$

VOL
1
196

We multiply from the left with U_m^*, integrate over all space, and making use of the orthonormality properties of the U's, obtain

$$\frac{da_m}{dt} = \frac{2\pi}{ih} Sa_n \exp(i\omega_{mn}t) \int U_m^* H' U_n d\tau, \tag{7}$$

where ω_{mn} is defined as $$\omega_{mn} = \frac{2\pi(E_m - E_n)}{h}.$$

Now, in nearly all cases of interest, the wavelength of the radiation is very much greater than the linear dimensions of the region where the functions U_m and U_n make a substantial contribution to the integral. We can therefore, as a good approximation, set $\exp i\,\mathbf{k}\cdot\mathbf{r}$ equal to unity, since $\mathbf{k}\cdot\mathbf{r}$ will be quite small. The integral in equation (7) is then given by

$$\int U_m^* H' U_n d\tau = \frac{ieh}{2\pi\mu c}\int U_m^*\left(A_1\frac{\partial}{\partial x_1} + A_2\frac{\partial}{\partial x_2} + A_3\frac{\partial}{\partial x_3}\right) U_n d\tau \cdot$$
$$\cdot [\exp(-i\omega t + i\alpha) + \exp(i\omega t - i\alpha)]. \tag{8}$$

In order to transform this expression we first consider the integral

$$\mathscr{I} = \iiint dx_1\, dx_2\, dx_3\, x_1(U_n \Delta U_m^* - U_m^* \Delta U_n).$$

We observe that $$\int dx_2\, x_1 \left(U_n \frac{\partial^2 U_m^*}{\partial x_2^2} - U_m^* \frac{\partial^2 U_n}{\partial x_2^2}\right) = 0$$

and $$\int dx_3\, x_1 \left(U_n \frac{\partial^2 U_m^*}{\partial x_3^2} - U_m^* \frac{\partial^2 U_n}{\partial x_3^2}\right) = 0,$$

as is easily verified by integration by parts.
Hence $\mathscr{I}$ simplifies to

$$\mathscr{I} = \iiint dx_1\, dx_2\, dx_3\, x_1 \left(U_n \frac{\partial^2 U_m^*}{\partial x_1^2} - U_m^* \frac{\partial^2 U_n}{\partial x_1^2}\right).$$

Integration by parts gives

$$\mathscr{I} = \iiint dx_1\, dx_2\, dx_3 \left\{-U_n \frac{\partial U_m^*}{\partial x_1} - x_1 \frac{\partial U_n}{\partial x_1}\frac{\partial U_m^*}{\partial x_1} + U_m^* \frac{\partial U_n}{\partial x_1} + x_1 \frac{\partial U_n}{\partial x_1}\frac{\partial U_m^*}{\partial x_1}\right\} =$$
$$= 2\iiint dx_1\, dx_2\, dx_3\, U_m^* \frac{\partial U_n}{\partial x_1}. \tag{I}$$

On the other hand $$\Delta U_n = \frac{8\pi^2\mu}{h^2}\{VU_n - E_n U_n\},$$

and $$\Delta U_m^* = \frac{8\pi^2\mu}{h^2}\{VU_m^* - E_m U_m^*\}.$$

Multiplying the first equation above by U_m^*, and the second by U_n and subtracting, we can write

$$\mathscr{I} = -\iiint dx_1\, dx_2\, dx_3\, x_1 \frac{8\pi^2\mu}{h^2}(E_m - E_n) U_n U_m^* =$$
$$= -\frac{4\pi\mu\omega_{mn}}{h}\int U_m^* x_1 U_n\, d\tau. \tag{II}$$

Hence, from (I) and (II)

$$\int U_m^* \frac{\partial U_n}{\partial x_1} \mathrm{d}\tau = -\frac{2\pi\mu\omega_{mn}}{h} \int U_m^* x_1 U_n \mathrm{d}\tau, \tag{III}$$

and therefore

$$\int U_m^* \left(A_1 \frac{\partial}{\partial x_1} + A_2 \frac{\partial}{\partial x_2} + A_3 \frac{\partial}{\partial x_3} \right) U_n \mathrm{d}\tau = -\frac{2\pi\mu\omega_{mn}}{h} \int U_m^* (A_1 x_1 + A_2 x_2 + A_3 x_3) U_n \mathrm{d}\tau. \tag{9}$$

With regard to equation (4) we write

$$\int U_m^* (A_1 x_1 + A_2 x_2 + A_3 x_3) U_n \mathrm{d}\tau = W \sqrt{I(\omega)}\, \mathrm{d}\omega\, \mathrm{d}\tilde{\omega}, \tag{10}$$

so that

$$\int U_m^* \left(A_1 \frac{\partial}{\partial x_1} + A_2 \frac{\partial}{\partial x_2} + A_3 \frac{\partial}{\partial x_3} \right) U_n \mathrm{d}\tau = -\frac{2\pi\mu\omega_{mn}}{h} W \sqrt{I(\omega)}\, \mathrm{d}\omega\, \mathrm{d}\tilde{\omega}.$$

We assume that at time $t = 0$ the system is in the single state n, i.e., $a_n = 1$, all other a being zero at that time, and that the perturbation starts at $t = 0$. *The state* n *may be either discrete or continuous*[21] (see p. 197, reference 20).

Then equation (7) becomes

$$\frac{\mathrm{d}a_m}{\mathrm{d}t} = -\frac{2\pi e\omega_{mn}}{hc} W [\exp i(\omega_{mn} t - \omega t + \alpha) + \exp i(\omega_{mn} t + \omega t - \alpha)] \cdot \sqrt{I(\omega)\, \mathrm{d}\omega\, \mathrm{d}\tilde{\omega}}.$$

Integration from 0 to t gives

$$a_m = \frac{2\pi i e\omega_{mn}}{hc} W \left[\frac{\exp [i(\omega_{mn} - \omega)t + i\alpha] - \exp (i\alpha)}{\omega_{mn} - \omega} + \right.$$
$$\left. + \frac{\exp [i(\omega_{mn} + \omega)t - i\alpha] - \exp (-i\alpha)}{\omega_{mn} + \omega} \right] \cdot \sqrt{I(\omega)\, \mathrm{d}\omega\, \mathrm{d}\tilde{\omega}}. \tag{11}$$

3. *Transition probability in general*

The probability of finding the system in the state m is negligible unless either $(\omega_{mn} - \omega)$ or $(\omega_{mn} + \omega)$ is nearly zero; i.e., unless $\omega \cong \omega_{mn}$ or $\omega \cong -\omega_{mn}$. These two cases correspond to the absorption of radiative energy and to induced emission of radiative energy, respectively. Thus, the probability of a transition to a higher state ($E_m = E_n + h\nu$) or to a lower state ($E_m = E_n - h\nu$) is given by

$$|a_m|^2 = \frac{4\pi^2 e^2 \omega_{mn}^2}{h^2 c^2} |W|^2 I(\omega)\, \mathrm{d}\omega\, \mathrm{d}\tilde{\omega} \left[\frac{(e^{i(\omega_{mn} \mp \omega)t} - 1)(e^{-i(\omega_{mn} \mp \omega)t} - 1)}{(\omega_{mn} \mp \omega)^2} \right] =$$
$$= \frac{4\pi^2 e^2 \omega_{mn}^2}{h^2 c^2} |W|^2 I(\omega)\, \mathrm{d}\omega\, \mathrm{d}\tilde{\omega} \left[\frac{4 \sin^2 1/2(\omega_{mn} \mp \omega)t}{(\omega_{mn} \mp \omega)^2} \right].$$

For t different from zero this is a highly fluctuating function of ω when ω is close to either ω_{mn} or $-\omega_{mn}$, while on the other hand it decreases rapidly to zero when ω goes away from either one of these values. Following the treatment presented by Schiff, to whom we refer for its motivation, we shall integrate the right hand side of the equation with respect to ω over a narrow region around either ω_{mn} or $-\omega_{mn}$. In this integration $I(\omega)$ and W can be treated as constant, and in view of the rapid convergence of the integral it is

VOL
1
196

permissible to take the limits as $\omega = -\infty$ and $\omega = +\infty$. The right hand side then acquires the factor t. Dividing by t, we obtain

$$\frac{|a_m|^2}{t} = \frac{8\pi^3 e^2 \omega^2}{h^2 c^2} |W|^2 I(\omega)\, d\tilde{\omega}. \tag{12}$$

The quantity on the left hand side is interpreted as the mean increase of the probability that the system arrives in the state m during the interval of time t, or, in other words, as the transition probability from the state n to the state m in unit time. Equation (12) is valid for both absorption and induced emission.

We must now consider radiation coming from all directions and with all directions of polarization. This means that the vector **A** can have all directions in space with equal probability. Returning to equation (10), we introduce

$$y_j = \int U_m^* x_j U_n \, d\tau, \ (j = 1, 2, 3), \tag{13}$$

and

$$|r_n^m|^2 = y_1^2 + y_2^2 + y_3^2. \tag{13a}$$

Equation (10) then gives

$$A_1 y_1 + A_2 y_2 + A_3 y_3 = W \sqrt{I(\omega)\, d\omega\, d\tilde{\omega}},$$

from which

$$W^2 = \frac{(A_1 y_1 + A_2 y_2 + A_3 y_3)^2}{I(\omega)\, d\omega\, d\tilde{\omega}}.$$

The mean value of W over all directions of $\vec{\mathbf{A}}$ is given by

$$|W^2|_{\text{mean}} = \frac{A^2}{3} \frac{y_1^2 + y_2^2 + y_3^2}{I(\omega)\, d\omega\, d\tilde{\omega}} = \frac{2\pi c}{3\omega^2} |r_n^m|^2, \tag{14}$$

where use is made of equation (4). If we now integrate equation (12) with respect to $d\tilde{\omega}$ over the sphere, we have for radiation coming from all directions

$$\frac{|a_m|^2}{t} = \frac{64\pi^5 e^2}{3h^2 c} I(\omega) |r_n^m|^2. \tag{15}$$

4. *Spontaneous emission*

As mentioned previously, it follows from the theory of quantum electrodynamics that we may regard the spontaneous emission as the emission induced by the zero-point oscillations of the electromagnetic field. The proper expression for the intensity of the zero-point field is found as follows: Consider radiation of angular frequency $\omega = 2\pi\nu$ within an interval $d\omega = 2\pi d\nu$. Each quantum of radiation has the energy $h\nu$ and momentum $h\nu/c$. The number of single quanta contained within the frequency interval $d\nu$, within a volume V, having all possible directions of propagation, and two directions of polarization for each direction of propagation, is given by

$$2 \frac{4\pi (h\nu/c)^2 \, d(h\nu/c) V}{h^3} = \frac{8\pi \nu^2 d\nu V}{c^3}.$$

The energy per unit volume, obtained by multiplying by $h\nu$, is

$$\varepsilon_\nu d\nu = \frac{8\pi h \nu^3}{c^3} d\nu.$$

The radiation intensity corresponding to this energy is

$$I(\nu)d\nu = \frac{2h\nu^3}{c^2}\,d\nu,$$

or in terms of $\omega = 2\pi\nu$:

$$I(\omega)\,d\omega = \frac{h\omega^3}{8\pi^4c^2}\,d\omega.$$

Hence

$$I(\omega) = \frac{h\omega^3}{8\pi^4c^2} = \frac{h\nu^3}{\pi c^2}.$$

The transition probability per unit time, for a spontaneous transition from a state n to a lower state m is, therefore, found by inserting this $I(\omega)$ into equation (15). We obtain

$$A_n^m \equiv \frac{|a_m|^2}{t} = \frac{64\pi^4e^2\nu^3}{3hc^3}\,|r_n^m|^2 \tag{16}$$

(cf. Schiff, equation (36–22). A_n^m is Einstein's coefficient of spontaneous emission.

5. *Normalized eigenfunctions for the discrete case*

To evaluate $|r_n^m|^2 = (y_1^2 + y_2^2 + y_3^2)$ for a hydrogen-like atom with nuclear charge Ze for transitions between two discrete states, between a discrete and a continuous state, or between two continuous states, we must have the normalized energy eigenfunctions for the discrete and for the continuous spectrum.

The normalized eigenfunction corresponding to the principal quantum number n, azimuthal quantum l, and magnetic quantum m for the *discrete case* ($E_n < 0$) is[20, 22, 23]

$$U_{nlm} = R_{nl}(r)\;Y_{lm}(\theta, \varphi), \tag{17}$$

where the normalized spherical harmonic Y_{lm}, expressed in terms of the associated Legendre function $P_l^m(\cos\theta)$, has the form

$$Y_{lm} = \frac{1}{\sqrt{2\pi}}\sqrt{\frac{2l+1\,(l-|m|)!}{2\quad(l+|m|)!}}\,P_l^m(\cos\theta)\,e^{im\varphi}, \tag{18}$$

and the radial function is the real function:

$$R_{nl} = N_r \exp(-rk_n)r^l\,F(-n_r, 2l+2, 2rk_n). \tag{19}$$

Here

$$k_n = \frac{1}{an} \text{ and } n_r = n - l - 1 = \frac{1}{k_n a} - l - 1,$$

where

$$a = \frac{a_0}{Z} = \frac{h^2}{4\pi^2\mu Ze^2}.$$

The symbol a_0 is interpreted in the old Bohr quantum theory as the radius of the smallest electronic orbit of the hydrogen atom. The function F is defined by

$$F(\alpha, \beta, z) = \frac{\Gamma(\beta)}{\Gamma(\alpha)}\sum_{s=0}^{\infty}\frac{\Gamma(\alpha+s)\,z^s}{\Gamma(\beta+s)\,s!}.$$

where Γ is the well-known gamma function. The relation between this function and the

perhaps more familiar associated Laguerre polynomial $L_{n+l}^{2l+1}(2rk_n)$ is (compare the R_{nl} of Schiff's equation (16.24) with that of Stobbe's equation (3)):

$$F[-(n-l-1), 2l+2, 2rk_n] = (-1)\frac{(2l+1)!\,(n-l-1)!}{[(n+l)!]^2} L_{n+l}^{2l+1}(2rk_n).$$

The value of the normalization factor, N_r, is found from the normalizing condition given by equation (6), taking into account that the functions Y_{lm} are already normalized. The condition thus becomes

$$\int (R_{nl})^2 r^2 \, dr = 1,$$

and one obtains

$$N_r = \frac{2^{l+1} k_n^l}{(2l+1)!\, n^2 a^{3/2}} \sqrt{\frac{(n+l)!}{(n-l-1)!}}. \tag{20}$$

The energy eigenvalues E_n are given by

$$E_n = \frac{-h^2}{8\pi^2 \mu a^2 n^2} = -\frac{2\pi^2 \mu Z^2 e^4}{h^2 n^2}, \tag{21}$$

so that

$$k_n = \frac{2\pi}{h}\sqrt{-2\mu E_n}.$$

6. *Normalized eigenfunctions for the continuous case*

The normalized eigenfunction for the continuous set ($E > 0$) may be written

$$U_{clm} = R_{cl}(r)\; Y_{lm}(\theta, \varphi), \tag{22}$$

where Y_{lm} is given, as before, by equation (18), and R_{cl} now is the complex function,

$$R_{cl} = N_r\, e^{i\varkappa r} r^l \quad F(-n_r, 2l+2, -2i\varkappa r),$$

with the radial quantum number

$$n_r = \frac{i}{\varkappa a} - l - 1.$$

The function F, the energy E, and the now complex radial quantum number are found from the expressions of these quantities for the discrete case by replacing n by $(i/a\varkappa)$ and and k_n by $-i\varkappa$. Thus, from equation (21), we find that

$$E = \frac{h^2}{8\pi^2 \mu} \varkappa^2. \tag{23}$$

For future use it is convenient to introduce $k = 1/a\varkappa$ (which thus stands for n/i). We then have

$$E = \frac{h^2}{8\pi^2 \mu a^2 k^2} = \frac{2\pi^2 \mu Z^2 e^4}{h^2 k^2}. \tag{23a}$$

It may be observed that this is the energy of the free electron when it has escaped from the field of the atom. Writing v for the speed of the free electron, we obtain

$$E = 1/2 \mu v^2.$$

Hence from equation (23)

$$\varkappa = \frac{2\pi\mu v}{h},$$

which can be regarded as the propagation number of the free electron.

The symbol c was provisionally chosen above to emphasize that c is a continuously variable parameter, as opposed to the discrete nature of l and m. The parameter c is taken as E, n_r, $\varkappa$, and k by different authors ; it must be a function of E.

The normalization of the coefficient $N_r(c)$ occurring in the function U_c must again be based upon equation (6), which for the present case has the form:

$$\int U_{c'}^* U_c \mathrm{d}\tau = \delta(c' - c).$$

Since in this form the condition is not easily handled, we multiply it by $\mathrm{d}c'\,\mathrm{d}c$ and integrate over two small intervals Δc, $\Delta c'$, chosen out of a complete set of non-overlapping intervals into which the domain for c can be divided. (For simplicity we use a notation as if the domain for c would be a line, but the result holds when this domain is a multidimensional space, provided integration with respect to $\mathrm{d}c'$ or $\mathrm{d}c$ is understood to be a multiple integration of an order corresponding to the number of dimensions of the c-space). Carrying out the integration in two steps, we have first:

$$\int \left\{ U_{c'}^* \left(\int_{\Delta c} U_c \,\mathrm{d}c \right) \right\} \mathrm{d}\tau = \begin{cases} 1, \text{ when } c' \text{ is within } \Delta c. \\ 0, \text{ when } c' \text{ is outside } \Delta c. \end{cases}$$

Hence performing the second integration, we find:

$$\int \left\{ \left(\int_{\Delta c'} U_{c'}^* \,\mathrm{d}c' \right) \left(\int_{\Delta c} U_c \,\mathrm{d}c \right) \right\} \mathrm{d}\tau = \begin{cases} \Delta c, \text{ when } \Delta c' \text{ and } \Delta c \text{ coincide.} \\ 0, \text{ when } \Delta c' \text{ and } \Delta c \text{ do not coincide.} \end{cases} \tag{24}$$

This is the form of the normalization condition given by FUES.[24] It is understood that the Δc must approach the limit zero.

It may be observed that certain authors (e.g., pp. 75–84 of reference 21) introduce auxiliary functions $\bar{U}_c$ defined by

$$\bar{U}_c = \lim_{\Delta c \to 0} \frac{1}{\sqrt{\Delta c}} \int_{\Delta c} U_c \,\mathrm{d}c,$$

which are called "eigendifferentials". It is then possible to write equation (24) as follows:

$$\int \bar{U}_{c'}^* \, \bar{U}_c \,\mathrm{d}\tau = \delta_{c'c},$$

which has the same form as the normalization condition for the discrete eigenfunctions.

In view of the arbitrariness in the choice of the parameter c, to which reference has been made before, the normalization obtained by the application of equation (24) it not unique, but depends on the choice of the parameter. Between eigenfunctions normalized with respect to two different parameters α and β there exists the general relation (p. 667 of reference 22)

$$|U_\alpha|^2 \Delta\alpha = |U_\beta|^2 \Delta\beta. \tag{25}$$

In the following we use $\varkappa$ as the continuous parameter. Since the functions Y_{lm} are

already normalized, it follows from equation (24) that the equation for the determination of $N_r(\varkappa)$ can be written:

$$\int_0^\infty r^2\,\mathrm{d}r\left\{N_r^2(\varkappa)\left|\int_{\Delta\varkappa} R_{\varkappa,l}\,\mathrm{d}\varkappa\right|^2\right\} = \Delta\varkappa. \tag{26}$$

The following result is obtained (p. 666, reference 22):

$$N_r(\varkappa) = \frac{2^l\varkappa^{l+1}}{(2l+1)!}\exp\left(\frac{\pi}{2a\varkappa}\right)\sqrt{\frac{2}{\pi}}\,\Gamma\left(l+1+\frac{i}{a\varkappa}\right) =$$

$$= \frac{2^l\varkappa^{k+1}}{(2l+1)!}\exp\left(\frac{\pi}{2a\varkappa}\right)\sqrt{\frac{2a\varkappa\prod_{s=0}^{l}\left(S^2+\dfrac{1}{a^2\varkappa^2}\right)}{\sinh\pi/a\varkappa}}. \tag{27}$$

7. *Transition probabilities for hydrogen-like atoms*

We return to equation (16) for the transition probability. When the transition takes place between a discrete state nlm and another discrete state $n'l'm'$, we shall write:

$$A_{nlm}^{n'l'm'} = \frac{64\pi^4e^2\nu^3}{3hc^3}\,|r_{nlm}^{n'l'm'}|^2, \tag{28}$$

where r is the resultant of the matrix elements:

$$y_j = \int \mathrm{d}r\, r^3\, R_{n'l'}(r)R_{nl}(r)\iint \sin\theta\mathrm{d}\theta\mathrm{d}\varphi\cos(r, x_j)\,Y_{l'm'}(\theta,\varphi)\,Y_{lm}(\theta,\varphi). \tag{29}$$

Similar expressions can be written for the transition from a continuous state to a discrete state, or from one continuous state to another. The transition probability per unit time per atom from a continuous state $\varkappa lm$ to a discrete state is

$$A_{\varkappa lm}^{n'l'm'} = \frac{64\pi^4e^2\nu^3}{3hc^3}\,|r_{\varkappa lm}^{n'l'm'}|^2\Delta\varkappa, \tag{30}$$

where the interval $\Delta\varkappa$ is introduced since the transition occurs from a range $\Delta\varkappa$. Similarly

$$A_{\varkappa lm}^{\varkappa'l'm'} = \frac{64\pi^4e^2\nu^3}{3hc^3}\,|r_{\varkappa lm}^{\varkappa'l'm'}|^2\Delta\varkappa\Delta\varkappa' \tag{31}$$

gives the transition probability per unit time for a transition from the range $\Delta\varkappa$ to the range $\Delta\varkappa'$.

The z-component of r (with $\cos(r, z) = \cos\theta$) can be written as

$$z_{nlm}^{n'l'm'} = R_{nl}^{n'l'}\int_0^\pi P_{l'm'}(\theta)\,P_{lm}(\theta)\cos\theta\sin\theta\,\mathrm{d}\theta\int_0^{2\pi}\frac{1}{2\pi}\,\mathrm{e}^{i(m-m')\varphi}\mathrm{d}\psi,$$

and is equal to zero unless $m = m'$ and $l' = l \pm 1$. Here

$$R_{nl}^{n'l'} = \int R_{n'l'}(r)\,R_{nl}(r)\,r^3\,\mathrm{d}r.$$

The matrix elements of the other components of r, combined as $(x \pm iy)$, is

$$(x \pm iy)_{nlm}^{n'l'm'} = R_{nl}^{n'l'}\int_0^\pi P_{l'm'}P_{lm}\sin\theta\sin\theta\,\mathrm{d}\theta\int_0^{2\pi}\frac{1}{2\pi}\,\mathrm{e}^{i(m\pm1-m')\varphi}\,\mathrm{d}\psi.$$

The matrix element of $(x + iy)$ vanishes unless $m' = m + 1$ and $l' = l \pm 1$, and the matrix element of $(x - iy)$ vanishes unless $m' = m - 1$ and $l' = l \pm 1$.

The integrals with respect to the spherical harmonics, etc., in these formulas are given by various authors.[22, 25]

The integral $R_{nl}^{n'l-1}$ has been evaluated for the different types of transitions.[22, 23] For the discrete-discrete transitions:

$$R_{nl}^{n'l-1} = \frac{(-)\,1^{n'-l}a}{4(2l+1)!}\sqrt{\frac{(n+l)!(n'+l-1)!}{(n-l-1)!(n'-l)!}}\left(\frac{4nn'}{(n-n')^2}\right)^{l+1}\left(\frac{n-n'}{n+n'}\right)^{n+n'}\cdot$$
$$\cdot\left\{F\left(-n_r, -n'_r, 2l, -\frac{4nn'}{(n-n')^2}\right) - \left(\frac{n-n'}{n+n'}\right)^2 F\left(-n_r-2, -n'_r, 2l, -\frac{4nn'}{(n-n')^2}\right)\right\} \quad (32)$$

Since $R_{nl}^{n'l}$ is symmetrical with respect to the upper and lower indices, the formula for $R_{nl}^{n'l+1}$ can easily be obtained from the one given above. For the free-bound transitions (from a continuum state to a discrete state):

$$R_{\varkappa l}^{nl-1} = \frac{(-1)^{(n'-l)i}}{8\varkappa^{3/2}(2l-1)!}\sqrt{\frac{(n'+l-1)!\,2\prod_{s=1}^{l}\left(S^2+\frac{1}{(a\varkappa)^2}\right)}{(n'-l)!\qquad \sinh \pi/a\varkappa}}\cdot\left\{\exp\left[\frac{1}{a\varkappa}\left(\frac{\pi}{2}-2\tan^{-1}\frac{\varkappa}{k_n}\right)\right]\right\}\cdot$$
$$\cdot\left(\frac{4\varkappa k_n}{k_n^2+\varkappa^2}\right)^{l+1} G^{n'_r-1}\left\{F\left(-n_r, -n'_r, 2l, 1-\frac{1}{G^2}\right) - G^2 F\left(-n_r-2, -n'_r, 2l, 1-\frac{1}{G^2}\right)\right\}, \quad (33a)$$

with $$G = \frac{k_n + i\varkappa}{k_n - i\varkappa} = e^{-2i\tan^{-1}(\varkappa/k_n)};$$

and
$$R_{\varkappa l}^{n'l+1} = \frac{(-1)^{(n'-l+1)}\,a}{8\varkappa^{1/2}(2l+1)!}\sqrt{\frac{(n'+l+1)!\,2\prod_{s=1}^{l}\left(S^2+\frac{1}{(a\varkappa)^2}\right)}{(n'-l-2)!\qquad \sinh \pi/a\varkappa}}\cdot$$
$$\cdot\left\{\exp\left[\frac{1}{a\varkappa}\left(\frac{\pi}{2}-2\tan^{-1}\frac{\varkappa}{k_n}\right)\right]\right\}\cdot$$
$$\cdot\left(\frac{4\varkappa k_n}{k_n^2+\varkappa^2}\right)^{l+2} G^{n'_r}\left\{I\left(-n_r, -n'_r, 2l+2, 1-\frac{1}{G^2}\right) - G^2 F\left(-n_r, -n'_r-2, 2l+2, 1-\frac{1}{G^2}\right)\right\}. \quad (33b)$$

For free-free transitions:

$$R_{\varkappa l}^{\varkappa' l-1} = \frac{i}{8\varkappa\varkappa'(2l-1)!}\sqrt{\frac{\prod_{s=1}^{l}\left(S^2+\frac{1}{(\varkappa a)^2}\right)}{\varkappa a\sinh \pi/\varkappa a}}\sqrt{\frac{\prod_{s'=1}^{l-1}\left(S'^2+\frac{1}{(\varkappa a)^2}\right)}{\varkappa' a\sinh \pi/\varkappa' a}}\cdot$$
$$\cdot\, e^{\pi/2a\left|\frac{1}{\varkappa'}-\frac{1}{\varkappa}\right|}\left(\frac{4\varkappa\varkappa'}{(\varkappa+\varkappa')^2}\right)^{l+1}\left|\frac{\varkappa-\varkappa'}{\varkappa+\varkappa'}\right|^{\frac{i}{\varkappa a}-\frac{i}{\varkappa' a}}\cdot$$
$$\cdot\left\{F\left(l+1+\frac{i}{\varkappa a}, l-\frac{i}{\varkappa' a}, 2l, \frac{4\varkappa\varkappa'}{(\varkappa+\varkappa')^2}\right) -\right.$$
$$\left. - \left(\frac{\varkappa+\varkappa'}{\varkappa-\varkappa'}\right)^2 F\left(l-1+\frac{i}{\varkappa a}, l-\frac{i}{\varkappa' a}, 2l, \frac{4\varkappa\varkappa'}{(\varkappa+\varkappa')^2}\right)\right\}. \quad (34)$$

Since $R_{\varkappa l}^{\varkappa' l'}$ again is symmetrical with respect to the upper and lower indices it is sufficient to have an expression for the case that $l - 1$ is in the upper index. In equations (32)–(34) the function F is the ordinary hypergeometric function:

$$F(\alpha, \beta, \gamma, Z) = 1 + \frac{\alpha\beta}{1!\gamma} Z + \frac{\alpha(\alpha+1)\beta(\beta+1)}{2!\gamma(\gamma+1)} Z^2 + \ldots$$

8. *Mean transition probability*

The total transition probability from a given state nlm to all possible states with different quantum number m', having a given n' and $l' = l + 1$, without regard to the direction of the emitted radiation, is found to be (see p. 433, reference 25):

$$\frac{l+1}{2l+1} (R_{nl}^{n'l+1})^2,$$

and similarly the probability for transitions to the states specified by n' and $l' = l - 1$, is

$$\frac{l}{2l+1} (R_{nl}^{n'l-1})^2.$$

The summation over the admissible values of m' having already been carried out in deducing these results, we arrive at the following result for the transition from a given state nlm to all possible states having a given n':

$$\sum_{l', m'} |r_{nlm}^{n'l'm'}|^2 = \frac{l+1}{2l+1} (R_{nl}^{n'l+1})^2 + \frac{l}{2l+1} (R_{nl}^{n'l-1})^2. \tag{35}$$

If we are interested in the mean value for the transition from discrete states with a given principal quantum number n and arbitrary l to other states with principal quantum number n', we first multiply the above equation by $2l + 1$ for each given l (the number of m states), then sum with respect to l from 0 to $n - 1$, and finally divide by n^2 (the total number of states). If we also consider the spin, we have to multiply equation (35) by two and divide by the weight for a discrete state $\tilde{\omega}_n = 2n^2$.

We then obtain for discrete-discrete transitions

$$A_n^{n'} = \frac{64\pi^4 e^2 \nu_{nn'}^3}{3hc^3} \frac{a^2}{\tilde{\omega}_n} S_n^{n'} = \frac{4h^3 \nu_{nn'}^3}{3\mu^2 Z^2 e^2 c^3} \frac{1}{\tilde{\omega}_n} S_n^{n'}. \tag{36}$$

In anticipation of a later generalization of the above equation, we note that for free-discrete and free-free transitions there must be introduced the factors $\Delta\varkappa$, and $\Delta\varkappa\Delta\varkappa'$ respectively, in the same way as was done in equations (30) and (31). Here $S_n^{n'}$ is a dimensionless quantity defined by

$$S_n^{n'} = \frac{1}{a^2} \sum_{l=0}^{n-1} \left\{ (2(l+1)(R_{nl}^{n'l+1})^2 + 2l(R_{nl}^{n'l-1})^2 \right\}. \tag{37}$$

The frequency $\nu_{nn'}$, in terms of the Rydberg number R, is

$$\nu_{nn'} = RZ^2 \left(\frac{1}{n'^2} - \frac{1}{n^2} \right) \tag{38}$$

where $R = 2\pi^2 \mu e^4 / h^3$.

The value of $S_n^{n'}$ for discrete-discrete transitions is evaluated by McLEAN[26] in terms of the quantities

$$J(l, l-1) = \frac{l}{2a^2}\left(\frac{1}{n'^2} - \frac{1}{n^2}\right)^4 (R_{nl}^{n'l-1})^2,$$

and

$$J(l, l+1) = \frac{l+1}{2a^2}\left(\frac{1}{n'^2} - \frac{1}{n^2}\right)^4 (R_{nl}^{n'l+1})^2.$$

We then have

$$\left(\frac{1}{n'^2} - \frac{1}{n^2}\right)^4 S_n^{n'} = 4\sum_{l=0}^{n-1}\{J(l, l-1) + J(l, l+1)\} \equiv 4J. \tag{39}$$

McLean finds (p. 867) that J defined by equation (39) is an odd function of n and n', and that it is symmetrical with respect to n and n'. Thus

$$J = J_n^{n'} = J_{n'}^{n}.$$

McLean also shows that

$$J = \frac{2^4(n-n')^{2n+2n'-1}}{n^2n'^2(n+n')^{2n+2n'}}\,\Delta(n, n'), \tag{40}$$

where

$$\Delta(n, n') = \left\{\left[F\left(-n+1, -n', 1, -\frac{4nn'}{(n-n')^2}\right)\right]^2 - \left[F\left(-n'+1, -n, 1, -\frac{4nn'}{(n-n')^2}\right)\right]^2\right\}.$$

From equations (39) and (40) we thus obtain

$$S_n^{n'} = 2^6 D\left|\frac{(n-n')^{2n+2n'-1}}{n^2n'^2(n+n')^{2n+2n'}\left(\frac{1}{n'^2} - \frac{1}{n^2}\right)^4}\right|\Delta(n, n'). \tag{41}$$

In this expression a "normalization" factor D has been inserted, which is equal to unity for the discrete-discrete transition treated by McLean.

In order to obtain convenient expressions for free-bound and free-free transitions, MENZEL and PEKERIS[27] generalized McLean's results. They find that equations similar to (36) and (38) to (41)* hold also for free-bound and free-free transitions provided: (1) n and n' are replaced by ik and ik', respectively, as needed, where k and k' are real positive numbers lying in the range 0 to ∞; (2) the weight $\tilde{\omega}_k$ in equation (36) is properly defined for continuous states; and (3) the "normalization" factors for free-bound and free-free transitions are taken respectively equal to

$$D_2 = 1/[1 - \exp(-2\pi k)] \tag{42}$$

---

* Menzel and Pekeris actually express their results in terms of an oscillator strength $f_n^{n'}$ which is related to $S_n^{n'}$ by

$$f_n^{n'} = \frac{1}{3\tilde{\omega}_{nn'}}\left(\frac{1}{n'^2} - \frac{1}{n^2}\right) S_n^{n'}.$$

VOL
1
196

and

$$D_3 = \frac{\exp(2\pi k')}{[1 - \exp(-2\pi k)]\,[1 - \exp(-2\pi k')]} \tag{43}$$

The weight $\tilde{\omega}_k$ for the continuous states depends on the definition of the number of atoms in a continuous state.[27] If this number is defined as the number of atoms per cm^3 whose electrons in hyperbolic orbits have velocities at infinity ranging from v to $v + \mathrm{d}v$ divided by the total number of atoms having electrons in hyperbolic orbits, that is, by the number of positive ions N_i in unit volume, then

$$\tilde{\omega}_k = \tilde{\omega}_e \frac{4\pi\mu^3 v^2 \mathrm{d}v}{N_i h^3} = \frac{\tilde{\omega}_e}{N_e} \frac{\varkappa^2}{2\pi^2}\,\mathrm{d}\varkappa = -\frac{\tilde{\omega}_e}{N_e} \frac{2^5\pi^4\mu^3 Z^3 e^6}{h^6 k^4}\,\mathrm{d}k. \tag{44}$$

Here $\tilde{\omega}_e$ has been written for the electron weight, although it is equal to just 2.

It is useful to write

$$S_n^{n'} = g\, S_n^{n'*}. \tag{45}$$

where

$$S_n^{n*} = \frac{2^6}{\sqrt{3}\pi} \frac{1}{\left(\frac{1}{n'^2} - \frac{1}{n^2}\right)^4} \left|\frac{1}{n^3 n'^3}\right| \tag{46}$$

expresses the chief content of $S_n^{n'}$ and

$$g = \pi\sqrt{3}\, D \left|\left(\frac{n - n'}{n + n'}\right)^{2n + 2n'} \frac{nn'}{(n - n')}\, \Delta(n, n')\right| \tag{47}$$

is a quantity usually close to unity. The values of g_{I}, g_{II}, and g_{III} corresponding to discrete-discrete, free-bound, and free-free transitions, respectively, have been computed by Menzel and Pekeris.

9. *Energy emitted in the discrete spectrum*

If we combine equations (36), (38), (45), (46), and (47), we obtain the discrete-discrete transition probability

$$A_n^{n'} = \frac{2^{11}\pi^5 \mu e^{10} Z^4}{3\sqrt{3} h^6 c^3} \frac{1}{\tilde{\omega}_n} \frac{1}{n^3 n'^3 \left(\frac{1}{n'^2} - \frac{1}{n^2}\right)} g_{\mathrm{I}}. \tag{48}$$

The total energy emitted per second by N_n atoms/cm^3 in state n by spontaneous transitions to state n', is

$$N_n A_n^{n'} h\nu_{nn'}, \tag{49}$$

and the total energy emitted in the discrete spectrum is

$$\sum_n \sum_{n'} N_n A_n^{n'} h\nu_{nn'}. \tag{50}$$

10. *Emission by free-bound transition*

The mean transition probability from a continuum state k within a range $\mathrm{d}k$ to a discrete state n' is

$$A_k^{n'} = \frac{4h^3\nu_{kn}^3}{3\mu^2 Z^2 e^2 c^3} \frac{1}{\tilde{\omega}_k} S_k^{n'}\,\mathrm{d}k, \tag{51}$$

with $\tilde{\omega}_k$ given by equation (44) and $S_k^{n'}$ by equation (41). It is noted that $A_k^{n'}$ is a finite rather than a differential quantity, since $\tilde{\omega}_k$ contains the differential dk. We now substitute equations (38) and (45) into equation (51) and obtain

$$A_k^{n'} = \frac{2^{11}\pi^5\mu e^{10}Z^4}{3\sqrt{3}h^6c^3}\,\frac{1}{\tilde{\omega}_k}\,\frac{1}{k^3n'^3\left(\frac{1}{n'^2}+\frac{1}{k^2}\right)}g_{II}\,dk. \tag{52}$$

The energy emitted per unit time by N_k atoms per cm_3 whose electrons in hyperbolic orbits possess velocities at infinity ranging from v to $v + dv$ is

$$N_k\,dk\,A_k^{n'}\,h\nu_{kn'}. \tag{53}$$

According to the generalized Boltzmann's law, N_k is related to N_o, the total number of neutral atoms irrespective of state, by

$$N_k dk = \frac{N_0}{N_i}\,\frac{b_1\tilde{\omega}_e}{b_0}\,\frac{4\pi\mu^3v^2dv}{h^3}\exp\left(-\frac{\chi_0}{k_BT}-\frac{m_ev^2}{2k_BT}\right) = N_o\,\frac{b_1}{b_0}\tilde{\omega}_k\exp\left(-\frac{\chi_0}{k_BT}-\frac{m_ev^2}{2k_BT}\right), \tag{54}$$

where k_B is Boltzmann's constant; b_0 is the partition function for the neutral atoms (i.e., atoms having electrons in discrete states):

$$b_0 = \sum\tilde{\omega}_{n'}\exp\left(-E_{n'}/k_BT\right) = \sum\tilde{\omega}_{n'}\exp\left(-\frac{\chi_0}{k_BT}+\frac{hRZ^2}{n_1^2k_BT}\right), \tag{55}$$

while b_1 is the partition function for the ionized atoms. If the ionized atoms have no excited states, b_1 reduces to $\tilde{\omega}'$, the weight of the ground level of the ion. (See p. 74–79 of reference 28). (The subscript B used here to avoid confusion with other k's will be omitted in subsequent sections.)

We then obtain from the preceding equations:

$$N_k dk A_k^{n'} h\nu_{kn'} = \frac{N_0b_1}{b_0}\,\frac{2^{10}\pi^5\mu e^{10}Z^4}{3\sqrt{3}h^6c^3}\,\frac{1}{n'^3}\exp\left(-\frac{\chi_0}{k_BT}-\frac{hRZ^2}{k^2k_BT}\right)\cdot\frac{2hRZ^2}{k^3}\,g_{II}\,dk, \tag{56}$$

since

$$\nu_{kn'} = RZ^2\left(\frac{1}{n'^2}+\frac{1}{k^2}\right). \tag{57}$$

We also have

$$-\frac{hRZ^2}{k^2} = -h\nu_{kn'}+\frac{hRZ^2}{n'^2}, \tag{58}$$

and if we define ν by

$$h\nu = 1/2mv^2 = hRZ^2/k^2,$$

then

$$d\nu_{kn'} = d\nu = -\frac{2RZ^2}{k^3}\,dk. \tag{59}$$

If we are interested in a given emission frequency, of magnitude ν_{kn}, we can by the use of equations (58) and (59) transform equation (56) into an equation involving the variables n' and ν. We have then for the radiation in the interval $d\nu$

$$N_k dk A_k^{n'} h\nu_{kn'} = \frac{N_0b_1}{b_0}\,\frac{2^{10}\pi^5\mu e^{10}Z^4}{3\sqrt{3}h^5c^3}\,\frac{1}{n'^3}\exp\left(\frac{-\chi_0}{k_BT}+\frac{hRZ^2}{n'^2k_BT}-\frac{h\nu_{kn'}}{k_BT}\right)g_{II}d\nu. \tag{60}$$

The total emission in the interval $d\nu$ is found by summing equation (60) over n' for the free-bound emission under consideration, $\nu_{kn'}$, being kept constant. The summation

should extend from some limiting value n'_0 to $n' = \infty$. The lower limiting value n'_0 may be obtained from equation (57) by setting $k = \infty$, i.e.,

$$\nu = \nu_{kn'} = RZ^2 \frac{1}{n'^2_0}. \tag{61}$$

If no level exists which satisfies equation (61), then the next higher level may be used. If, as in the case of complex spectra (see p. 90, reference 27 and p. 608–609, reference 46), we may replace the summation by an integration, then

$$\sum_{n'_0}^{\infty} \frac{1}{n'^3} \exp\left(\frac{hRZ^2}{n'^2 k_B T}\right) g_{II} \simeq \int_{n'_0}^{\infty} \frac{dn'}{n'^3} \exp\left(\frac{hRZ^2}{n'^2 k_B T}\right) g_{II} = \frac{k_B T}{2hRZ^2}\left[\exp\left(\frac{hRZ^2}{n'^2_0 k_B T}\right) - 1\right] \bar{g}_{II},$$

with $\bar{g}_{II}$ (see reference (27) given by:

$$\bar{g}_{II} \simeq 1 - 0{\cdot}1728\left(\frac{\nu}{RZ^2}\right)^{1/3}\left(1 - \frac{2kT}{h\nu}\right) - e^{-h\nu/kT}\left[1 + 0{\cdot}1728\left(\frac{\nu}{RZ^2}\right)^{1/3}\left(1 + \frac{2kT}{h\nu}\right)\right].$$

The total free-bound emission per cm³ in the interval dν is thus

$$\sum_{n'_0}^{\infty} N_k A_k^{n'} dk\, h\nu_{kn'} = \frac{N_0 b_1}{b_0} \frac{2^{10}}{3\sqrt{3}} \frac{\pi^5 \mu e^{10} Z^4}{h^5 c^3} \frac{k_B T}{2hRZ^2} \cdot$$

$$\cdot \exp\left(\frac{-\chi_0}{k_B T}\right)\left[\exp\left(\frac{hRZ^2}{n'^2_0 k_B T}\right) - 1\right] \exp\left(\frac{-h\nu}{k_B T}\right) \bar{g}_{II}\, d\nu. \tag{62}$$

If the lower states above n'_0 are not close together, it is not permissible to replace the whole summation by an integration. In this case, the terms are first summed until a value n^* is reached which can be used as the lower limit of the integration. The integrated equation is similar in form to equation (62) with n'_0 replaced by n^* and $\bar{g}_{II} = \bar{g}_{II}(n'_0, \nu)$ replaced by $\bar{g}^*_{II} = \bar{g}^*_{II}(n^*, \nu)$. Thus, in general, we obtain for the total free-bound emission per cm³ in the interval dν

$$\sum_{n'_0}^{\infty} N_k A_k^{n'} dk\, h\nu_{kn'} = \frac{N_0 b_1}{b_0} \frac{2^{10}\pi^5 \mu e^{10} Z^4}{3\sqrt{3}h^5 c^3} \exp\left(\frac{-\chi_e^0 - h\nu}{k_B T}\right)\left\{\sum_{n'_0}^{n^*-1} \frac{1}{n'^3} \exp\left(\frac{hRZ^2}{n'^2 k_B T}\right) g_{II} + \right.$$

$$\left. + \frac{k_B T}{2hRZ^2}\left[\exp\left(\frac{hRZ^2}{n^{*2} k_B T}\right) - 1\right]\bar{g}^*_{II}\right\} d\nu. \tag{62'}$$

11. *Emission by free-free transition*

The mean free-free transition probability from state k within a range dk to a state k' within a range dk' is (see equations 36, 41, 45, 46, and 47):

$$A_k^{k'} = \frac{4h^3 \nu_{kk'}^3}{3\mu^2 Z^2 e^2 c^3} \frac{1}{\bar{\omega}_k} S_k^{k'} dk dk' = \frac{2^{11}\pi^5 \mu e^{10} Z^4}{3\sqrt{3}h^6 c^3} \frac{1}{\bar{\omega}_k} \frac{1}{k^3 k'^3} \frac{1}{\left(\frac{1}{k^2} - \frac{1}{k'^2}\right)} g_{III} dk dk'. \tag{63}$$

The free-free emission per unit time by N_k atoms/cm³ whose electrons in hyperbolic orbits have velocities at infinity ranging from v to $v + dv$ is

$$N_k dk A_k^{k'} h\nu_{kk'}, \tag{64}$$

where

$$\nu_{kk'} = RZ^2\left(\frac{1}{k^2} - \frac{1}{k'^2}\right). \tag{65}$$

If we use equation (54) for $N_k \mathrm{d}k$, we obtain

$$N_k \mathrm{d}k A_k^{k'} h\nu_{kk'} = \frac{N_0 b_1 2^{10}\pi^5 \mu e^{10} Z^4}{b_0 \quad 3\sqrt{3}h^5 c^3} \exp\left(\frac{-\chi_0}{k_B T} - \frac{hRZ^2}{k^2 k_B T}\right) \frac{2RZ^2}{k^3 k'^3} g_{\mathrm{III}} \,\mathrm{d}k \,\mathrm{d}k'.$$

The above equation is transformed in a manner similar to that employed for free-bound transition to

$$\frac{N_0 b_1}{b_0} \frac{2^{10}\pi^5 \mu e^{10} Z^4}{3\sqrt{3}h^5 c^3} \exp\left[\frac{-\chi_0}{k_B T} - \frac{h\nu}{k_B T} - \frac{hRZ^2}{k'^2 k_B T}\right] \frac{1}{k'^3} g_{\mathrm{III}} \,\mathrm{d}\nu \mathrm{d}k'. \tag{66}$$

The total free-free emission per cm^3 in the interval $\mathrm{d}\nu$ is obtained by integrating the above expression with respect to k' from 0 to ∞, again keeping $\nu_{kk'}$ constant. We obtain

$$\int_{k'=0}^{k'=\infty} N_k \mathrm{d}k A_k^{k'} h\nu_{kk'} \mathrm{d}k' = \frac{N_0 b_1}{b_0} \frac{2^{10}\pi^5}{3\sqrt{3}} \frac{\mu e^{10} Z^4}{h^5 c^3} \frac{k_B T}{2hRZ^2} \exp\left(-\frac{\chi_0}{k_B T} - \frac{h\nu}{k_B T}\right) \bar{g}_{\mathrm{III}} \,\mathrm{d}\nu, \tag{67}$$

where $\bar{g}_{\mathrm{III}}$ (see reference 27) is given by:

$$\bar{g}_{\mathrm{III}} = 1 + 0{\cdot}1728\left(\frac{\nu}{RZ^2}\right)^{1/3}\left[1 + \frac{2kT}{h\nu}\right].$$

If we sum equations (62) and (67), which together give the total free-bound and free-free emission for the case of complex spectra, and use the definition of R, we obtain

$$\frac{2b_1}{b_0} \frac{2^7\pi^3 e^6 Z^2}{3\sqrt{3}h^3 c^3} N_0 kT \exp\left(-\frac{\chi_0}{k_B T} - \frac{h\nu}{k_B T}\right)\left\{\bar{g}_{\mathrm{II}}\left[\exp\left(\frac{hRZ^2}{n_0^2 k_B T}\right) - 1\right] + \bar{g}_{\mathrm{III}}\right\} \mathrm{d}\nu. \tag{68}$$

If we let

$$\gamma = \frac{\tilde{\omega}_e b_1}{b_0} = \frac{2b_1}{b_0},$$

and note that by equation (61)

$$h\nu = \frac{hRZ^2}{n_0^2},$$

then we may write for the total continuum radiation per cm^3 per unit frequency

$$\varepsilon_\nu = \gamma \frac{128\pi^3}{3\sqrt{3}} \left(\frac{e^2}{hc}\right)^3 Z^2 N_0 kT \, e^{-\chi_0/kT} \bar{g}, \tag{69}$$

where

$$\bar{g} = \bar{g}_{\mathrm{II}}(1 - e^{-h\nu/kT}) + \bar{g}_{\mathrm{III}} e^{-h\nu/kT}.$$

The behaviour of $\bar{g}$ will be discussed in section V.

However, in the general case, equations (62′) and (67) are summed, and a much stronger

VOL.
1
1961

frequency dependent expression for the total continuum radiation per cm³ per unit frequency is obtained:

$$\varepsilon_\nu = \frac{\gamma 2^9\pi^5\mu e^{10}Z^4}{3\sqrt{3}\ h^5c^3} N_o \exp\left(\frac{-\chi_0 - h\nu}{k_BT}\right) \sum_{n_0'}^{n^*-1} \frac{1}{n'^3} \exp\left(\frac{hRZ^2}{n'^2k_BT}\right) g_{II} +$$

$$+ \gamma \frac{128\pi^3}{3\sqrt{3}} \left(\frac{e^2}{hc}\right)^3 Z^2 N_o kT \exp\left(\frac{-\chi_0 - h\nu}{k_BT}\right) \left\{\bar{g}_{II}^* \left[\exp\left(\frac{hRZ^2}{n^{*2}kT}\right) - 1\right] + \bar{g}_{III}\right\}. \quad (69')$$

12. *Discussion of the continuum radiation equation*

In order that equation (69) be applicable to an atom which has more than one electron it is necessary to introduce an effective nuclear change Z_{eff}. We know that an electron moving in the field of an atom other than hydrogen is not influenced by the total charge Ze on the nucleus since the electron is screened from the nucleus by the other electrons. The effective charge Z_{eff} e which the electron experiences may be written formally as $(Z-S)$e, where S is called the screening constant. An empirical set of rules for finding S, devised by Slater, and theoretically justified by Gambás and Gáspár, is set forth in reference 29. By the use of these rules, $Z_{\text{eff}} = 1$ for an argon electron with principal quantum number $n \geq 5$, $Z_{\text{eff}} = 1$ also for a $4d$ or $4f$ electron, $Z_{\text{eff}} \simeq 2$ for a $4s$ or $4p$ electron, and $Z_{\text{eff}} = 6{\cdot}75$ for a $3p$ electron. PETSCHEK *et al.*[13] used $Z_{\text{eff}} = 1$ for argon when they worked with equation (69). Here, too, $Z_{\text{eff}} = 1$ will be used.

The symbol γ was introduced for $2b_1/b_0$, where b_1 and b_0 were the internal partition functions for the ion and atom respectively. However, the partition functions for an isolated atom or ion diverge[30] if the infinite number of possible discrete energy states are included. As is seen from equation (55), the exponential factor for the higher states approaches a finite limit but the statistical weight increases indefinitely. The higher terms become arbitrarily large and the series diverges. One has to consider the presence of other neutral and charged particles in the gas to obtain convergence. ALPHER[31], who recently investigated methods of computing partition functions found "no unique and universally accepted procedure" for finding b_1 and b_0. A very simple computing approach which is considered to yield as satisfactory results for shock wave calculations as any more elaborate method, is to suppress all electron orbits whose classical major axis

$$a_n = a_o n^2/Z \quad (70)$$

exceeds half the average separation of particles in the gas. Only terms with $n_i \leq n$ contribute to the bound state partition sums. An adjustment in the statistical weight of the outermost bound orbit is made to allow for the fact that generally a_n will not equal the average separation of the particles.[32]

Actually, one need not be concerned with the partition function *directly* as far as equation (69) is concerned, since equation (69) can be combined with the Saha equation in a form often given, namely,

$$\frac{N_I N_e}{N_o} = \frac{N_e^2}{N_o} = \gamma \frac{(2\pi\mu kT)^{3/2}}{h^3} e^{-\chi_0/kT} \quad (71)$$

to yield

$$\varepsilon = \frac{64\pi^{3/2}}{3\sqrt{6}} \frac{e^6}{\mu^{3/2}c^3} Z_{\text{eff}}^2 \frac{N_e^2}{(kT)^{1/2}} \bar{g} \quad (72)$$

where N_I and N_e are the ion and electron densities respectively, and $N_I = \int N_k \, dk$. Indirectly, however, knowledge of the partition function does enter in the use of the above radiation formula in shock wave calculations, since the Saha equation has to be used in finding the equilibrium density N_e behind a shock wave. Similarly, an equation (72′) is obtained by combining equations (69′) and (71).

Equation (70) indicates that the radius corresponding to $n = \infty$ is infinite. Thus by the definition of χ_0 an electron from an isolated atom is removed to infinity upon ionization. It appears natural to suppose that a restriction upon the principal quantum number n that arises in connection with the partition function, should be reflected in some manner in a lowering of the ionization potential from this cause alone. Many references, however, which discuss the computation of the partition functions which occur in the Saha equation (71), have no comment about χ_0, perhaps because at low temperatures and low pressures the resulting change in χ_0 is insignificant. Conversely, any considerations which result in a lowering of χ_0 should provide a direct restriction on the partition function. Furthermore, any lowering in the ionization potential χ_0 must also be inserted in the radiation equation (69).

The complex question of what the amount of the lowering of the ionization potential should be and its consequences will be considered in the next chapter. There is also the question whether an "effective lowering of χ_0" as introduced in equation (69) is greater than the lowering which should be introduced in the Saha equation.

III. THE LOWERING OF THE IONIZATION POTENTIAL

Part II dealt with the emission and absorption of continuum radiation from a partially ionized gas consisting of N_o neutral atoms per cm^3 and $N_I(=N_e)$ ions and electrons per cm^3. A formula for the total continuum radiation was developed which contained the ionization potential χ_0. This part will consider the lowering of the ionization potential that occurs in a thermally ionized gas and its consequences. Such a gas can be called a neutral plasma.

1. *Line broadening*

The Stark effect due to the microfield of the ions and the collision broadening due to electrons cause a shift and broadening of spectral levels. This broadening is evident at temperatures and degrees of ionization characteristic of the heated, compressed gas behind even such weak shocks as a Mach 8 shock advancing into argon at several cm Hg pressure. With increasing Mach number and thus increasing ionization, the lines broaden more and shift further to the red.[13, 15]

The separations ΔE between the higher energy levels are small, and

$$\Delta E = E_{n+1} - E_n = \frac{e^2}{2a_0}\left[\frac{1}{n^2} - \frac{1}{(n+1)^2}\right] \cong \frac{e^2}{a_0 n^3} \tag{1}$$

where n is the principal quantum number, e is the electric charge, and a_0 is the first Bohr radius. When the spread due to the microfield of the broadened lines become equal to ΔE, the lines will have merged into one another and can be considered as having merged into the continuum. The above is the explanation advanced by INGLIS and TELLER[33] for the observation that both in stellar atmospheres and in the laboratory[34] under conditions involving high density of ions (in electric discharges) the lines of hydrogen-like spectra remain normal up to a certain quantum number, after which the lines abruptly merge into the continuum.

2. *The Stark effect*

Before going further it is advantageous to review the Stark effect. In 1913, Stark showed that the Balmer lines of hydrogen are split into many components when excited by a strong electric field F. When viewed at right angles to the field, some components are observed to be polarized perpendicular to the field (σ-components), and others plane polarized parallel to the electric field (π-components). The electric field removes the degeneracy characteristic of the Coulomb field possessed by the hydrogen atom by causing each level to change its energy by an amount that depends on l. (The ground state ($n = 1$, $l = 0$, $m = 0$) is not degenerate).

For atoms other than hydrogen in an external electric field, the first-order correction to the energy vanishes for any eigenstate of the unperturbed energy, and the second-order contribution yields an energy shift proportional to F^2, for permissible Stark effect transitions: $\Delta l = \pm 1$, $m' = m$.[35] For hydrogen, however, let us consider, for example, the case where $n = 2$. Here transitions occur between $l = 0$ and $l = 1$ for the case $m = 0$. For $m = \pm 1$ no such transitions can occur, and these levels may be treated by non-degenerate perturbation theory to give a very small quadratic effect. For $l = 0$ and $l = 1$, $m = 0$, the energy level is split into two levels, and the shift is *linear* in F. The net effect is that the original line is split into three parts. Now $\Delta m = 0$ leads to polarization along the axis of the field, and $\Delta m = \pm 1$ leads to polarization normal to the field axis. Therefore, when we view light at right angles to the field, we see the unshifted $\Delta m = \pm 1$ component, and the two shifted components polarized parallel to the field. The higher levels will show more involved patterns for the Stark shift, since more degenerate levels will be involved.

In the neutral plasma composed of (positive) ions and electrons which we are considering, the electric field at any point changes rapidly in direction and intensity. We must, therefore, consider the probability distribution of the field rather than a given external electric field strength. This distribution will smear out each of the Stark components. Holtsmark tackles the problem of finding this field probability distribution.

HOLTSMARK[36, 37] considers an emitting or absorbing atom, designated as the 0 atom, surrounded by a large number $1 \ldots N$ of disturbing atoms, molecules, or ions. If the disturbing atoms were at rest, there would result a constant electric field at 0, and thus a Stark splitting of the emitted lines. Since the atoms are constantly in motion, the field keeps changing in direction and magnitude, and we obtain a broadening of the lines, rather than some particular splitting. A probability will correspond to each of the various configurations of the system. The Stark splittings also occur with these varying probabilities.

Holtsmark assumes that the broadening molecules are all of the same kind, i.e., the perturbers are all electrons, or all ions of the same type, or all polar molecules of the same type, etc. Holtsmark considers these molecules in general as being made up of a number of charges e_s. A reference frame is established at the center of each molecule, and we wish to determine the potential at a point x, y, z (r) due to *these* charges located at positions r_s. We denote the separation distance between the point r and the sth charge by R_s. The potential φ at r due to the charges e_s is

$$\varphi = \Sigma \frac{e_s}{R_s} = \frac{\Sigma e}{r} + \frac{\boldsymbol{r} \cdot \Sigma e_s \boldsymbol{r}_s}{r^3} - \frac{1}{2r^3}\left\{\Sigma\, e_s r_s^2 - 3\Sigma \left(e_s \frac{(\boldsymbol{r} \cdot \boldsymbol{r}_s)^2}{r^2}\right)\right\} + \ldots \qquad (2)$$

Holtsmark considers three cases: (1) none of the terms disappear, (2) the first term is zero, (3) the first and second terms disappear. In the first case, because of the rapid convergence of the series for $r \gg r_s$, the condition Holtsmark is interested in, the first term predominates, and we have an ion field producer with

$$\varphi = \frac{\Sigma e_s}{r} = \frac{e}{r}. \tag{3}$$

In the second case, the second term predominates and we have

$$\varphi = \frac{\boldsymbol{r} \cdot \Sigma e_s \boldsymbol{r}_s}{r^3} = \frac{\boldsymbol{r} \cdot \boldsymbol{m}}{r^3}, \tag{4}$$

where $\boldsymbol{m}$ denotes a dipole moment. Similarly, for the third case only a quadrupole potential results.

For each of the three cases Holtsmark then obtains the probability $W(X_0, Y_0, Z_0)\,dX_0\,dY_0\,dZ_0$, that a particular electric field strength F_0 with components lying between X_0 and $X_0 + dX_0$, Y_0 and $Y_0 + dY_0$, Z_0 and $Z_0 + dZ_0$, results from a situation where there are present N perturbers per cm³.

For ions, Holtsmark gives $W(F_0)\,dF_0$ in terms of

$$\beta = F_0/F_{n(\text{ion})} \tag{5a}$$

where

$$F_n = 2{\cdot}61\, N^{2/3} e\,. \tag{5b}$$

For the *dipole perturbers*, he finds that

$$W(F_0)dF_0 = \frac{4}{\pi} \frac{\beta^2 d\beta}{(1+\beta^2)^2} \tag{6}$$

where

$$\beta = F_0/F_{n(\text{dipole})} \tag{7}$$

with $F_{n(\text{dipole})} \equiv$ " normal field strength" $\equiv 4{\cdot}54|\boldsymbol{m}|N$.

In our case e is the charge on the ions which is equal to the charge of the electron, and N is the number of ions per cm³. Holtsmark develops two expressions for $W(F_0)dF_0$: one

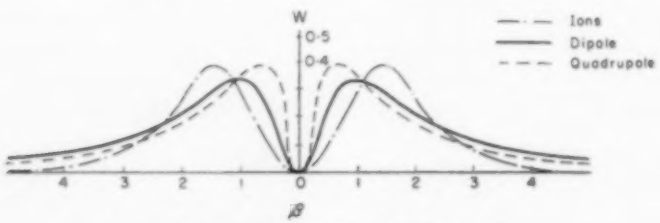

FIG. 1. Rough sketch of $W(F_0)$ vs. β.

valid for small values of β and another for large β. A rough plot of $W_0(F_0)$ vs. β based on a little later work of HOLTSMARK[38] is given in Fig. 1. The positions of the maxima indicate that the ion yields the greatest relative broadening, and the dipole the next. It is to be emphasized that Holtsmark's formulas consider electrostatic actions only, and the effect of the motion of the ions or electrons is neglected.

3. *Nearest neighbor distribution*

CHANDRASEKHAR[39] considers the Holtsmark distribution in connection with the gravitational field arising from an ideal random distribution of stars. The gravitational field is, of course, mathematically similar to that just discussed for the electric field due to ions. Chandrasekhar first derives the Holtsmark distribution in an exact manner, but then derives a distribution based on the assumption that the force acting is entirely due to its nearest neighbor. He shows that the nearest neighbor distribution agrees with the exact solution over most of the range of F, and that the highest fields are produced only by the nearest neighbor. The nearest neighbor approximation leads to serious errors only for weak fields which arise from a more or less symmetrical, average configuration of the ions about the one under consideration. The average nearest-neighbor distance r_0 between ions for a random distribution is shown to be

$$r_0 = 0{\cdot}554\, N^{-1/3}$$

where N is the average number of the particles per unit volume (p. 87, reference 39). For comparison we mention the approximate average distance that Unsöld uses in a nearest neighbor calculation, which we will consider later:

$$r_0 = \left(\frac{4\pi}{3} N\right)^{-1/3} = 0{\cdot}620\, N^{-1/3}.$$

Chandrasekhar also draws attention to the fact that the Holtsmark distribution predicts relatively too high probabilities for F as $F \to \infty$. This results as a consequence of the assumption of complete randomness in the ion distribution for *all* elements of volume, which cannot be true for the regions in the very neighborhoods of the individual ions.

4. *The results of Inglis and Teller*

We now return to the considerations of Inglis and Teller who are concerned with a first-order Stark effect. For hydrogen and for high-series terms of the alkali spectra, the perturbation energy is $3/2\ a\ \mathrm{e}\ F$, where $a = n^2 a_0/Z_{\mathrm{eff}}$ is the semi-major axis of the nth orbit and $Z_{\mathrm{eff}} = 1$. Two levels will merge (see equation 1) if

$$3ae F/2 = \Delta E/2 = \mathrm{e}^2/2a_0 n^3.$$

Thus
$$F = \mathrm{e}/3a_0^2 n^5. \tag{8}$$

From Holtsmark's results Inglis and Teller deduced (see Fig. 1) that the most probable value F_0 of F for ions occurs at

$$\beta \cong 1{\cdot}4 = F_0/F_n = F_0/2{\cdot}61 N^{2/3}\,\mathrm{e}.$$

Consequently,
$$F_0 \cong 3{\cdot}7 N \mathrm{e}^{2/3}. \tag{9}$$

Substituting this value of F_0 in equation (8) gives the approximate relation

$$N_n^{7.5} = 0{\cdot}027 a_0^{-3} = 1{\cdot}824 \times 10^{23} \tag{10}$$

which may also be written (with $a_0 = 0{\cdot}529 \times 10^{-8}$cm) as

$$\log_{10} n = \frac{23{\cdot}26 - \log N}{7{\cdot}5}. \tag{11}$$

Equation (10) or (11) gives the last principal quantum number n observed in a series as a function of the particle density N of the perturbers.

Inglis and Teller also consider the influence of electrons on line broadening. They conclude that for temperatures lower than $T = (10^5/n)^\circ K$ the electrons contribute to the broadening through the same static Stark effect. In this case, the sum of the electrons and ions, i.e., $2N$, appears in equations (10) and (11) since $N_e = N_I =$ the number of electrons per cm^3.

The experimental work of Mohler on the caesium discharge was performed under conditions where $nT \leq 10^5$. As we have just seen, under these conditions both the electrons and ions contribute to Stark broadening. Mohler, indeed, found that his experimental results fitted the curve

$$\log_{10} n = \frac{23{\cdot}06 - \log 2N_e}{7{\cdot}5} \tag{12}$$

which contains $2N_e$ for the number of broadeners.

At somewhat higher temperatures, the positive ions alone cause static Stark broadening, and the electrons contribute by means of collisions only. However, the collision broadening due to electrons decreases inversely with their velocity (or as $T^{-1/2}$) and thus at very high temperatures only the ions alone enter equations (10) and (11).

Transitions from the merged levels to lower ones give rise to continuum rather than line radiation. PETSCHEK *et al.*[13] consider the continuum to have been lowered by an amount $\Delta\chi_m$ due to the merging, as far as the radiation equation (69) is concerned. (However, they did not consider the Inglis and Teller result directly applicable to argon.) Thus, a $\Delta\chi_m$ can be found from the relation

$$\Delta\chi_m = \frac{e^2Z^2}{2a_0n^2} = 13{\cdot}595\frac{Z^2}{n^2}\,(\text{eV}) \tag{13}$$

with n given in equation (11). With $Z = 1$,

$$\log_{10} \Delta\chi_m(\text{eV}) = -\,5{\cdot}069 + 4/15 \log_{10} N. \tag{14}$$

This $\Delta\chi_m$ is not a lowering of the ionization potential in the sense of ionization and as such would not appear in the Saha equation. The other $\Delta\chi$ given in this part can be considered as expressions for the lowering of the ionization potential which may appear in the Saha equation.

It is noted that Holtsmark's theory was developed for a single type of particle acting as broadener. Inglis and Teller simply add the effect of slow moving electrons to the field of the ions, without considering any possible interaction between the ions and electrons.

5. *Corrections to Holtsmark's theory*

ECKER[40] points out that in a system made up of ions and electrons, the interference between the electrons and ions must be considered, and he refers to the DEBYE and HÜCKEL[41] theory according to which each charge is surrounded by a cloud of predominantly opposite charge. Instead of the Coulomb field

$$F = e\frac{r}{r^3}, \tag{15}$$

VOL. 1 196

use should be made of

$$F = \frac{er}{r^2}\left(\frac{1}{r} + \frac{1}{D}\right) e^{-r/D}, \tag{16}$$

where the shielding distance D is given by

$$\frac{1}{D^2} = \frac{4\pi e^2}{k} \sum_s \frac{N_s Z_s^2}{T_s} \tag{17}$$

and Z_s are the charge numbers, N_s the charge densities, and T_s the temperatures.

It is noted that Debye's work is limited in its applicability by the assumption of undisturbed superposition of the changes caused by the individual ions. This assumption is tied up with the necessary requirement in the derivation of equation (16):

$$\frac{Z_i Z_s e^2}{DkT} \ll 1. \tag{18}$$

Rather than use formula (16), Ecker employs the often-used approximation

$$\left.\begin{aligned} F &= \frac{er}{r^3} \qquad r < D \\ F &= 0 \qquad r > D \end{aligned}\right\} \tag{19}$$

(for $T = 14{,}100°\text{K}$ and $N_e = N_i = N = 2{\cdot}2 \times 10^{18}/\text{cm}^3$, we have $D \cong 8 \times 10^{-8}$ cm). Charges beyond the distance D contribute only a negligible amount to the microfield at a point. Ecker now develops a new calculation of the probability distribution for the field strength giving attention to the number δ of charges contained in the Debye zone at equilibrium. The probability density can be expressed in terms of

$$\beta = F/F_n \tag{20}$$

where F_n practically has the same value as given by equation (7), Ecker's coefficient being $(4\pi/3)^{2/3} = 2{\cdot}59$.

The expression for the probability density is of a complex nature and required machine calculation. Satisfactory curves of $\omega(\beta)$ vs. β were obtained for $\delta \geq 5$. But because of the approximation (19), Ecker had to make certain adjustments in the curves for $\delta \leq 5$ so that no quantitative significance can be attributed to them. A rough sketch of Ecker's result is reproduced in Fig. 2. Fig. 2 shows that δ strongly influences the probability

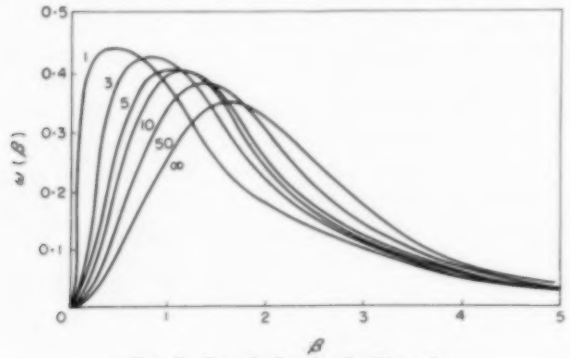

FIG. 2. Rough sketch of $\omega(\beta)$ vs. β.

density $\omega(\beta)$, and that the deviations from Holtsmark's theory ($\delta = \infty$) are greatest for small δ.

Since

$$\delta = (4\pi/3)D^3N \tag{21}$$

for a system with $N_e = N_I = N$, and $Z_e = Z_I = 1$, and $T_e = T_I$, we have from equation (17)

$$\delta = \frac{1}{6\sqrt{\pi}}\left(\frac{kT}{2e^2}\right)^{3/2}\frac{1}{N^{1/2}} = 490\,\frac{T^{3/2}}{N^{1/2}}. \tag{22}$$

The writer finds that for $T = 14{,}100°\text{K}$ and $N = 2{\cdot}2 \times 10^{18}/\text{cm}^3$ which are the approximate conditions behind a Mach 16 shock wave advancing into 1/10 atm argon, that $\delta = 0{\cdot}55$ This value is lower than the lowest value, $\delta = 1$ that Ecker considered. Even though there may be some doubt about the exact value of the most probable field, if Ecker's calculations are broadly correct, a large deviation from the Holtsmark probability is to be expected.

In a recent note to the Astrophysical Journal, HOFFMAN and THEIMER[42] have independently examined the question of a shielding correction to Holtsmark's theory of line broadening. They state that it is well known that Holtsmark's theory of Stark broadening is not fully confirmed by experiments and that recent attempts to improve the theory have centered about the time dependence of the electronic microfield (velocity broadening).[43–45] As none of the recent theories of line broadening are found to be decisive, they investigate in an approximate manner the effect of the Debye shielding. The results they present are similar to Ecker's, that is, the peak of the curves shift to lower values of β for decreasing δ.

VOL.
1
1961

6. *Unsöld's result*

In 1938, UNSÖLD[46] was aware that at high pressures in gas discharges the levels near the ionization limit were so broadened and overlapped that they formed a continuum. He, therefore, formally introduced the lowering of the ionization potential $\Delta\chi$ into the radiation equation (69) of section II but gave no method for finding it until the year 1948.[47] His approach is perhaps the simplest and most straightforward. He first finds for a partially ionized gas the last level n that may be regarded as discrete. He states that FERMI[48], AMALDI and SEGRÉ[49] and FÜCHTBAUER *et al.*[50] have shown experimentally and theoretically that highly excited states are not perturbed much by the presence of a high density of neutral atoms. The effect of neutral atoms are therefore neglected. Also for large enough values of the principal quantum number, the levels may be regarded as hydrogen-like.

Unsöld considers the perturbation of an atom (or ion) of effective charge Z by an ion of effective charge Z_1. He assumes that at any given time only one ion comes close enough to an atom to make a major contribution. Let the nuclei be r cm apart (see Fig. 3), and let the maximum potential be located r_1 cm from Z and ρ cm from Z_1, so that $r_1 + \rho = r$. The maximum potential energy of an electron V_m is given by

$$V_m = -\left(\frac{Ze^2}{r_1} + \frac{Z_1e^2}{\rho}\right). \tag{23}$$

Classically an electron can be considered free when it gets over this potential hill with zero

kinetic energy. If the potential energy at Z due to Z_1 is also taken into consideration (see Fig. 3), the lowering of the ionization, $-\Delta\chi$, becomes

$$-\Delta\chi = -\left(\frac{Ze^2}{r_1} + \frac{Z_1e^2}{\rho} - \frac{Z_1e^2}{r}\right). \tag{24}$$

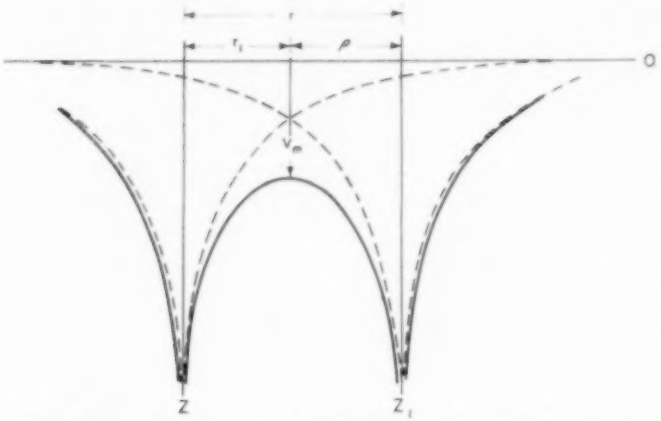

FIG. 3. Potential energy curves of electron in fields of atom and ion.

With the use of the relation

$$\frac{Ze^2}{r_1^2} = \frac{Z_1e^2}{\rho^2}, \tag{25}$$

we have

$$\Delta\chi = \frac{e^2}{r}(Z + 2\sqrt{ZZ_1}). \tag{26}$$

An electron in a highly excited state of an unionized atom moves in a Coulomb field of a charge equal to $Z = 1$. Still retaining an effective charge Z, we may set

$$\Delta\chi = \frac{e^2Z^2}{2a_0n^2}. \tag{27}$$

From equations (26) and (27), we obtain

$$n^2 = \frac{r}{2a_o}\,\frac{Z}{(1 + 2\sqrt{Z_1/Z})}. \tag{28}$$

Expressing the mean distance r between ions by

$$r = (4\pi N_e/3)^{-1/3} \tag{29}$$

where $N_1 = N_e$ is the ion density, and now taking $Z = Z_1 = 1$, we obtain

$$n^2 = 1/6a_0(4\pi N_e/3)^{-1/3}. \tag{30}$$

This can also be written as

$$\log_{10} n = 3{\cdot}645 - 1/6 \log_{10} N_e, \tag{31}$$

which substituted in equation (27) gives

$$\log(\Delta\chi) = -6{\cdot}158 + 1/3 \log_{10} N_e, \tag{32}$$

where $\Delta\chi$ is expressed in electron volts.

Instead of relying upon this simple deduction, which essentially restricts itself to the consideration of the effect of a single nearest neighbor, other authors MARGENAU and KELLY[51], and ECKER and WEIZEL[52, 53] have returned to the consideration of the Debye screening effect. The work of these authors will be discussed in the next two sections.

7. *The results of Margenau and Kelly*

Margenau and Kelly presented a paper entitled "Disappearance of Spectral Lines with High Quantum Numbers in a Plasma" on 2 February 1957 at the New York City meeting of the American Physical Society[51]. They kindly made available a copy of the material presented. Proceeding in the manner of DEBYE and HÜCKEL[41], they find that the potential V_0 of an electron in a plasma at a distance r from an ion of charge $+Ze$ is

$$V_0 = \frac{A \exp(-r/D)}{r}, \tag{33}$$

where D is given by

$$D^2 = \frac{kT}{4\pi Ne^2(1+Z)}. \tag{34}$$

The potential V_0 is valid only where $ZeV/kT \ll 1$. If the ion is regarded as a sphere with point charge $+Ze$ at the center and zero density elsewhere inside, the resulting inner potential V_i is given by

$$V_i = -\frac{Ze^2}{r} + B. \tag{35}$$

The inner potential is valid for a region which is taken to extend from $r = 0$ to D. The outer potential V_0 is valid for $r > D$. The constants A and B are determined from the continuity of the potential and electric intensity at $r = D$, and we obtain

$$V_i = -\frac{Ze^2}{r} + \frac{Ze^2}{2D} \tag{36}$$

and

$$V_0 = -\frac{Ze^2}{2}(2{\cdot}718\ldots)\frac{\exp(-r/D)}{r}. \tag{37}$$

With V_i as the potential, approximate energies are calculated from the wave equation

$$\nabla^2\psi_n + \frac{8\pi^2\mu}{h^2}\left[\left(E_n - \frac{Ze^2}{2D}\right) + \frac{Ze^2}{r}\right]\psi_n = 0, \tag{38}$$

where the ψ_n are the hydrogenic wave functions. The approximate energies are thus given by

$$E_n = -\frac{e^2}{2a_0}\frac{Z^2}{n^2} + \frac{Ze^2}{2D}. \tag{39}$$

VOL. 1 1961

These energies are now corrected by adding a perturbation energy E_n' which Margenau and Kelly find to have a very small effect on the levels. They therefore find the last discrete level by setting E_n of equation (39) equal to zero. Thus

$$n^2 = \frac{ZD}{a_0}. \tag{40}$$

This is the equivalent of setting the Bohr radius $n^2 a_0/Z$ equal to the Debye shielding length D. Setting $Z = 1$ and using equation (34), one finds that the last discrete level n is given by

$$\log_{10} n = \frac{17{\cdot}93 + \log_{10} T - \log_{10} N}{4}, \tag{41}$$

which corresponds to

$$\Delta\chi = \frac{e^2}{2a_0}\frac{1}{n^2} = 13{\cdot}595\,\frac{a_0}{D}\,(\text{eV}). \tag{42}$$

The n given by equation (40) was previously found by a different method by ECKER and WEIZEL[52], who gave the inequality

$$n^2 \leq \frac{ZD}{a_0}. \tag{43}$$

8. *The results of Ecker and Weizel*

ECKER and WEIZEL[52, 53] approached the determination of the lowering of the ionization potential $\Delta\chi$ by deriving a "Saha equation" for a plasma in which the power in the exponential term consists of the sum of two parts, i.e., $\exp -(\chi - \Delta\chi)$ (compare equation (71) part II). As is well known, the Saha equation may be derived from the equilibrium condition:

$$\left(\frac{\partial G}{\partial \alpha}\right)_{T,p} = 0, \tag{44}$$

where G is the Gibbs thermodynamic function

$$G = U - TS + pV. \tag{45}$$

If the usual expressions for the internal energy U and entropy S for a partially ionized monatomic gas given by Ecker and Weizel alone are used in equation (44), only χ_0 would appear in the exponent. However, with the inclusion in U of the total mean electrostatic interaction energy of the ensemble on ions and electrons, U_w, a decrease of the ionization potential is obtained.

The exact interaction energy U_w for $\alpha\bar{N}$ electrons and $\alpha\bar{N}$ ions is formally given by the expression

$$U_w = 1/2 \int_1 \cdots \int_{2n} \sum_{ij} \pm \frac{e^2}{|r_i - r_j|}\, W(r_1 \ldots r_{2n})\, dr_1 \ldots dr_{2n}, \tag{46}$$

where the sum is taken over the electrons and ions, and the integration is taken over the totality of configurations of these particles. The symbol $W(r_1 \ldots r_{2n})$ gives the probability density of these particles in configuration space. The symbol $\bar{N}$ denotes the original number of unionized atoms and α, the degree of ionization. The sign $+$ or $-$ is used according

to whether like or unlike charges are under consideration. In general, it follows from equation (44) that the ionization energy for a plasma is

$$\chi_0 + \frac{1}{\bar{N}} \frac{\partial U_w}{\partial \alpha}. \tag{47}$$

Since an exact evaluation of U_w seemed extremely difficult, Ecker and Weizel proposed the following approximation:

$$U_w = U_a + U_p = -\left\{\frac{2e^2\bar{A}}{r_o} + \frac{e^2(1+\sqrt{2})}{D\sqrt{8}}\right\} \bar{N}\alpha. \tag{48}$$

with

$$r_0 = \left(\frac{V}{\bar{N}\alpha}\right)^{1/3} = N_e^{-1/3}, \tag{49}$$

the mean distance between ions, V the volume of the plasma, and

$$D = \sqrt{\frac{kT}{4\pi(1+Z)e^2} \frac{V}{\bar{N}\alpha}}, \tag{50}$$

the familiar Debye-shielding length.

The first term, U_a corresponds to the energy of a cubic crystal with a mean Madelung coefficient $\bar{A}$[54]. It represents the interaction between charges when the Debye polarization is neglected. In the course of time the ions and electrons take on various configurations of different probability of occurrences, to each of which there corresponds some Madelung coefficient, A. The weighted mean of these A, is $\bar{A}$. The number 2 occurs in this term because A is defined in terms of the nearest neighbor separation between negative and positive charges.

The second term U_p is the result of the polarization of the plasma so that the mean distance between unlike charges is decreased and that of like charges increased. For a neutral plasma with ions of approximately the same mass, U_p would be e^2/D. The factor $(1+\sqrt{2})/\sqrt{8}$ comes about because electrons contribute to the polarization of the neighborhood of an electron only, whereas both ions and electrons contribute to the polarization of the neighborhood of an ion.

We obtain for $\frac{1}{\bar{N}} \frac{\partial U_w}{\partial \alpha}$,

$$-\Delta\chi = -\left(\frac{8}{3}\frac{e^2\bar{A}}{r_0} + \frac{3}{4}\frac{(1+\sqrt{2})}{\sqrt{2}}\frac{e^2}{D}\right) \tag{51}$$

which in terms of electron-volts can be written with the help of equations (48) and (49) as

$$\Delta\chi\,(\text{eV}) = 0{\cdot}67\sqrt[3]{\frac{Ne}{10^{18}}} + 0{\cdot}38\sqrt{\frac{Ne}{T10^{14}}} \tag{52}$$

provided we adopt the value 1·76 for $\bar{A}$.

The particular choice of 1·76 for $\bar{A}$ which corresponds to a body centered ionic crystal, introduces some uncertainty with it. O. Theimer went so far as to suggest that $\bar{A}$ should be approximately zero.[55] However, as Ecker and Weizel pointed out in their reply to

VOL.
1
196

Theimer, Theimer had assumed the stochastic independence of the particles. With this assumption

$$W(r_1 \ldots r_{2n}) = \overset{1 \ldots 2n}{\Pi} W_0(r_i) = \left(\frac{1}{V_i}\right)^{2n}, \tag{53}$$

and if one further assumes a spherical volume, $V = 4\pi R^3/3$, then it follows from equation (46) that

$$U_w = -\frac{18}{15} \bar{N} \alpha \frac{e^2}{R}. \tag{54}$$

Theimer proceeding a little differently, obtained

$$U_w = -\frac{3}{2} \bar{N} \alpha \frac{e^2}{R}.$$

Since $R \gg r_0$, Theimer deduced that $\bar{A} \sim 0$.

However, the probability densities of the single charges are not stochastically independent. States with positive energy hardly occur in contrast with negative energy states. The energy obtained therefore under the assumption of stochastic independence is too large. With increasing density, the ensemble of particles approaches a state of uniform distribution which resembles that of a crystal.

The above discussion explains why Ecker and Weizel choose the value of U_w given by equation (50). However, as Ecker and Weizel acknowledge, the uncertainty in $\bar{A}$ remains.

9. *Justification for choice of Ecker and Weizel's formula*

We now note the remarkable similarity between Ecker and Weizel's first term in equation (51), which with $\bar{A} = 1{\cdot}76$ can be written with the help of equation (49) as

$$\Delta\chi = 4{\cdot}69\, e^2 N_e^{1/3} + \ldots \tag{55}$$

and Unsöld's equation (26), which combined with equation (29), (with $Z = Z_1 = 1$) can be written as

$$\Delta\chi = 4{\cdot}83\, e^2 N_e^{1/3}. \tag{56}$$

There is only a 3 per cent difference between these formulas. Thus as far as any practical computations are concerned it does not matter whether equation (55) or (56) is chosen for the first term in equation (51). For those who may regard the use of an $\bar{A}$ as somewhat arbitrary, the development of Unsöld furnishes essentially the same result. Furthermore, the effect of the ions in a plasma on a given atom in an excited state may logically be divided into *a nearest neighbor interaction*, such as that treated by Unsöld, and *the interaction with the rest of the medium*. The latter is the Debye polarization effect which is expressed by the second term in equation (51). There is precedent for such a viewpoint in the work of GASIOROWICZ, NEWMAN, and RIDDEL.[56] Thus, equation (52) in its entirety, follows from a development which does not invoke a mean Madelung coefficient.

There is no question that a lowering of the ionization potential $\Delta\chi_s$ which appears in the Saha equation would also appear in the continuum radiation equation, since the Saha equation determines the number of free electrons. There remains the possibility that beneath the level corresponding to $\Delta\chi_s$, there might exist a region of broadened lines which

would contribute to the continuum emission but not contribute to the degree of ionization of the plasma. However, it will be assumed here that such contribution is small, more precisely, that $\Delta\chi$ determined by equation (52) gives the approximately correct lowering of the ionization potential for both the Saha and the continuum radiation equation. Consequently, we may now write the continuum radiation equation (69) as

$$\varepsilon = \gamma \frac{128\pi^3}{3\sqrt{3}} \left(\frac{e^2}{hc}\right)^3 Z^2 N_0 kT e^{-(\chi_0 - \Delta\chi)/kT} \bar{g} \tag{57}$$

and also introduce the $\Delta\chi$ in equation (69′). Since the same lowering is introduced in the Saha equation (71) of part II there is no change in equation (72) of part II.

IV. THE EFFECT OF A VARIABLE IONIZATION POTENTIAL ON EQUILIBRIUM CONDITIONS BEHIND THE SHOCK FRONT

1. *Calculation of equilibrium conditions*

One of the places where use of the lower ionization potential must be made is in the calculation of the equilibrium conditions behind a normal shock wave. For a monatomic gas these equilibrium conditions are determined by the equations for the conservation of mass flow, momentum, and total energy across the shock, together with the equation of state, the Saha equation and the equation for the ionization potential. Assuming no ionization in front of the shockwave the conservation equations take the form:

$$\rho_1 u_1 = \rho_0 u_0 \tag{1}$$

$$p_1 + \rho_1 u_1^2 = p_0 + \rho_0 u_0^2 \tag{2}$$

$$5/2(1 + \alpha_1)RT_1 + \alpha_1 \frac{\chi}{m_A} + \frac{u_1^2}{2} = 5/2RT_0 + \frac{u_0^2}{2}, \tag{3}$$

where the subscript zero refers to the conditions ahead of the shock and the subscript one refers to the equilibrium condition behind the shock. The flow velocity u is taken with respect to the shock wave. The pressure p_1 is

$$p_1 = (1 + \alpha_1)\, \rho_1 RT, \tag{4}$$

where ρ is the density and R is the gas constant per unit mass. The symbol m_A refers to the mass of the atom. The degree of ionization is denoted by α and χ is the ionization potential expressed in ergs.

The Saha equation which is needed to relate α to p and T can be written as

$$\frac{\alpha^2}{1 - \alpha^2} p = \frac{(2\pi m_e)^{3/2} k^{5/2}}{h^3} \frac{2b_1}{b_0} T^{5/2} e^{-\chi/kT}. \tag{5}$$

It is assumed that the number of doubly ionized atoms is negligible. Also, at the temperatures involved here, the radiation pressure and radiation energy density are negligible in comparison with the pressure and energy density of the gas and need not be included in equations (2) and (3).

The ionization potential χ is equal to the ionization potential χ_0 for an isolated atom diminished by $\Delta\chi$ due to the surrounding plasma, i.e.,

$$\chi = \chi_0 - \Delta\chi.$$

Making use of equation (52) of section III, we have for argon (expressed in eV),

$$\chi(\text{eV}) = 15{\cdot}76 - 0{\cdot}67\sqrt[3]{N_e/10^{18}} - 0{\cdot}38\sqrt{N_e/(T10^{14})}. \tag{6}$$

The conditions ρ_0, p_0, T_0, and $\alpha_0 = 0$ in the undisturbed gas ahead of the shock are known, and the specification of either u_0 or the Mach number of the shock, or of one of the variables (e.g., T_1) behind the shock, permits one to solve equations (1) to (6). These equations may be solved in many ways. The one used for calculation with a desk calculator was the following. A given Mach number is specified and equations (1) and (5) are solved with $\chi = \chi_0$. From the approximate values of α, p, and T thus found, an N_e given by

$$N_e = \frac{\alpha}{1+\alpha}\frac{p}{kT} \tag{7}$$

is determined. By the use of equation (6) this approximate value of N_e yields the first approximation of χ. Equations (1) to (5) are then solved with this approximate value of χ and a new N_e determined which is used to find the second approximation of χ. This process is repeated till χ and the other variables are obtained to any desired accuracy. In a typical case three iterations furnished a value of α_1 which differed less than one-half per cent from the value determined with much greater accuracy by a high speed computer.

The solutions of equations (1) to (6) with the high speed computer were obtained by two methods. One of these was the iteration method described above carried out to greater accuracy. The other method involved specifying T_1 (not the Mach number) and solving simultaneously two equations in α and χ obtained by combining equations (1) to (6). Both methods yielded the same results.

In these calculations for argon, b_0 of equation (5) was taken equal to 1. For the densities here considered the more exact values of b_0 are less than 1·011 for temperatures from 7,000°K to 16,000°K.[1] For b_1 the often-used approximation $b_1 = 6$ was employed. A comparison with Bond's more exact calculations shows that b_1 varies from 5·63 — 5·76 in the range 10,000°K — 16,000°K and that

$$b_1 \cong 4 + 2e^{-E_1/kT} \tag{8}$$

is a good approximation to b_1. However, for the range of values here given, solutions of equations (1) to (5) obtained with $b_1 = 6$ yield values for α_1 which are only 1 per cent higher than those obtained with b_1 given by equation (8).

Apart from their role in the Saha equation, b_0 and b_1 appear also in the following expression for the energy per unit mass of the excited states of the atom and ion, respectively:

$$(1-\alpha)RT^2\frac{\mathrm{d}(\ln b_0)}{\mathrm{d}T} + \alpha RT^2\frac{\mathrm{d}(\ln b_1)}{\mathrm{d}T}. \tag{9}$$

This energy in the excited states has been neglected in equation (3). Lin[57] estimated that the specific enthalpy contributed by both the above terms at a temperature of 16,000°K amounts to 1·7 per cent of the specific enthalpy given by

$$5/2RT(1+\alpha) + \alpha\frac{\chi}{m_A}$$

in equation (3) and decreases with decreasing temperature.

2. *The variation of $\Delta\chi$ with Mach number*

Before seeing the effect of $\Delta\chi$ on the equilibrium conditions behind the shock front, it is interesting to see how much $\Delta\chi$ varies with the Mach number of a shock. This is shown in Table 1 for argon at three different initial densities. As expected from the dependence

TABLE 1. IONIZATION LOWERING $\chi_0 - \chi = \Delta\chi$ (eV), FOR ARGON AS A FUNCTION OF SHOCK MACH NUMBER AND INITIAL PRESSURE. $T_0 = 294°K$

M_s	Initial pressure (atm)		
	1/76	1/10	1/2
11	0·265	0·469	0·734
12	0·353	0·660	1·093
13	0·437	0·842	1·447
14	0·516	1·017	1·792
15	0·592	1·186	2·129
16	0·667	1·351	2·459
17	0·740	1·511	2·752
18	0·810	1·667	3·068
19	0·879	1·818	3·372
20	0·946	1·966	

of $\Delta\chi$ on electron density, we observe that $\Delta\chi$ increases (χ decreases) with increasing Mach number and with the increasing initial gas density.

3. *Comparison of results for fixed and variable χ*

The manner in which the degree of ionization α_1 varies with Mach number when $p_0 = 1/2$ atm is shown in Fig. 4 for two cases: (1) χ is a constant (15·76 eV) and (2) χ is given by equation (6). We note that because the ionization potential decreases with increasing Mach number, the degree of ionization under these circumstances increases with increasing Mach number more than for the case of a fixed χ. Furthermore, as more energy ($\alpha\chi/m_A$) is taken from the gas with an increase of ionization, we would expect the gas temperature to be lower for the case of the varying ionization potential. This is what we find in Fig. 5, where the temperature is shown as a function of Mach number for χ fixed, and for χ varying. The effect of $\Delta\chi$ on pressure is small. For example, at Mach number 17·06 the pressure for the case of the varying ionization potential is less than one per cent greater than the pressure obtained for χ constant.

The equilibrium values of α, T, and p for χ fixed and χ varying are presented in Tables 2–5 for Mach numbers from about 11 to 20, for initial pressure of 1/10 and 1/76 atm. The same variation observed in Figs. 4 and 5 may be seen to occur for the cases given in these tables.

V. ABSORPTION AND EMISSION OF CONTINUUM RADIATION IN A SHOCK TUBE. A CROSS SECTION OF INFINITE OPTICAL DEPTH

1. *Introduction*

Time resolved measurements on an oscillogram of the intensity of the continuum radiation behind a shock wave in argon show in a typical case (see Fig. 10(a) and (b) of reference 5) that for a shock wave of Mach number 11·4 advancing into argon at a pressure of 1 cm Hg, there is essentially no rise in radiation during the first 8 μsec of flow (laboratory

VOL
1
196

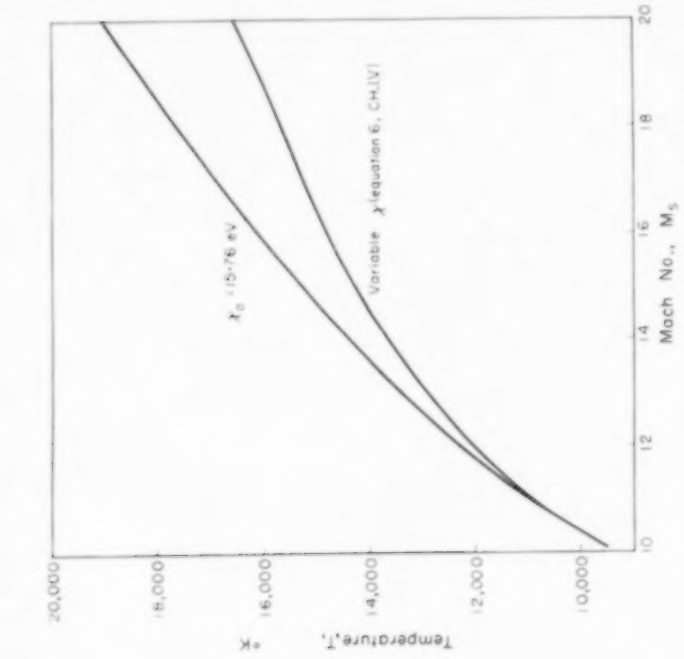

FIG. 5. The effect of the varying ionization potential on temperature for shocks of different strengths advancing into 1/2 atm of argon.

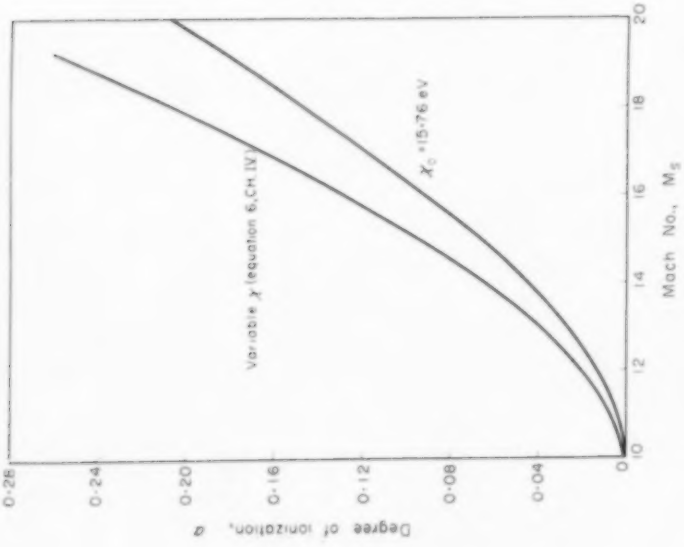

FIG. 4. The effect of the varying ionization potential on α for shocks of different strengths advancing into 1/2 atm of argon.

TABLE 2. EQUILIBRIUM VALUES OF α, T, AND p FOR ARGON AS A FUNCTION OF MACH NUMBER; THE IONIZATION POTENTIAL IS A *variable*, $p_0 = 1/10$TH ATM AND $T_0 = 294°K$

M_s	α	$T(°K)$	p (10^6 dyne/cm^2)
20·00	0·2879	15900	59·65
19·07	0·2476	15500	53·90
18·15	0·2105	15100	48·53
17·06	0·1690	14600	42·42
16·02	0·1331	14100	37·00
15·06	0·1028	13600	32·29
14·02	0·0733	13000	27·51
12·97	0·0472	12300	23·02
11·96	0·0266	11500	19·12
11·15	0·0137	10700	16·26

TABLE 3. EQUILIBRIUM VALUES OF α, T, AND p FOR ARGON AS A FUNCTION OF MACH NUMBER; THE IONIZATION POTENTIAL (15·76 eV) IS *fixed*, $p_0 = 1/10$TH ATM AND $T_0 = 294°K$

M_s	α	$T(°K)$	p (10^6 dyne/cm^2)
20·06	0·2426	17200	59·65
19·16	0·2110	16700	54·09
18·10	0·1759	16100	47·89
17·08	0·1441	15500	42·23
16·10	0·1158	14900	37·13
15·03	0·0872	14200	31·91
14·05	0·0633	13500	27·41
13·03	0·0417	12700	23·13
12·05	0·0241	11800	19·32
11·05	0·0106	10700	15·87
10·73	0·00749	10300	14·88
10·30	0·00420	9700	13·59
10·03	0·00273	9300	12·83

TABLE 4. EQUILIBRIUM VALUES OF α, T, AND p FOR ARGON AS A FUNCTION OF MACH NUMBER; THE IONIZATION POTENTIAL IS A *variable*, $p_0 = 1/76$ ATM AND $T_0 = 294°K$

M_s	α	$T(°K)$	p (10^6 dyne/cm^2)
20·14	0·2997	14600	8·062
19·07	0·2557	14200	7·187
18·03	0·2153	13800	6·378
17·03	0·1788	13400	5·639
16·07	0·1462	13000	4·974
15·17	0·1178	12600	4·382
13·93	0·0824	12000	3·627
13·02	0·0591	11500	3·111
12·07	0·0378	10900	2·614
11·03	0·0189	10100	2·125

VOL.
1
1961

TABLE 5. EQUILIBRIUM VALUES OF α, T, AND p FOR ARGON AS A FUNCTION OF MACH NUMBER; THE IONIZATION POTENTIAL (15·76 eV) IS *fixed*, $p_0 = 1/76$ ATM AND $T_0 = 294°K$

M_s	α	$T(°K)$	p (10^6 dyne/cm^2)
19·72	0·2599	15000	7·688
18·79	0·2258	14600	6·940
17·88	0·1941	14200	6·243
17·00	0·1649	13800	5·600
16·15	0·1384	13400	5·012
14·96	0·1038	12800	4·233
14·22	0·0840	12400	3·780
13·95	0·0772	12250	3·623
13·11	0·0573	11750	3·153
12·02	0·0343	11000	2·582
11·11	0·0187	10250	2·134
10·60	0·01175	9750	1·934

coordinates) and the intensity then rises rapidly during the next 11 μsec to a maximum. Depending on the sensitivity of the equipment, some point of this sharp rise would be observed on drum camera pictures followed by increasing luminosity until the maximum "equilibrium luminosity" is reached. The luminosity then decreases with distance behind the shock front until the cooling of the gas by radiation losses has decreased the electron density and temperature to the point where the luminosity cannot be detected on the measuring equipment, or until the luminosity is quenched at the cold interface of the driver gas.

The time required to reach equilibrium luminosity depends strongly on the purity of the gas (see reference 5 and p. 84–85 of reference 15), and decreases rapidly with increasing strength of the shock. Moreover, the spectrophotometer oscillograms shown in Fig. 7 of reference (13) indicate that even in the case of a shock tube made of a glass (pyrex) tube of $1\frac{1}{2}$ in. interior diameter, for which one may expect the cooling due to continuum radiation to be large at the low density involved (an initial pressure of 1 cm Hg), the time interval behind the maximum is at least ten times the rise time to maximum luminosity. If the tube was much wider, or what is more important, if for the same shock strength the density of the undisturbed gas was greater, then it is expected that the greatly increased self-absorption of the continuum radiation by the gas would result in a marked decrease in the cooling rates. Measurements of the absorption of radiation in the hot gases created by strong shock waves in air indicate that there is indeed almost total absorption in a distance of 4·7 in.[58] It is the purpose of this part to show how the effect of absorption may be taken into account and how this will modify the variation of the flow variables behind the maximum luminosity front.

2. *Emission and absorption coefficients*

It was shown in Part II that for a gas with a sufficiently dense distribution of spectral lines the energy, ε_ν, emitted in 1 sec in all directions in unit frequency interval from a cubic centimeter of a partially ionized gas is

$$\varepsilon_\nu = \frac{64\pi^{3/2}e^6Z^2}{3\sqrt{6}\mu^{3/2}c^3k^{1/2}} \frac{N_e^2}{T^{1/2}} \bar{g}, \tag{1}$$

or with the constants evaluated, and Z taken equal to unity

$$\varepsilon_\nu = 6{\cdot}840 \times 10^{-38}\, \bar{g}\, N_e^2/T^{1/2} \tag{2}$$

ergs/cm^3. We note that in such a case ε_ν is independent of frequency except for the dependence of $\bar{g}$ on frequency. However over the range of frequencies corresponding to wavelengths of 2034Å to 12400Å (1 to 6·1 electron volts) at temperatures from 10,000°K to 20,000°K, $\bar{g}$ varies from 0·84 to 0·93 in a manner that it is a good approximation to use for $\bar{g}$ an average value, $\bar{g}^* \simeq 0{\cdot}9$. Similarly at other temperatures a suitable $\bar{g}^*$ may be found, and thus ε_ν becomes independent of frequency. PETSCHEK[13] implicitly took $\bar{g} = 1$.

Since ε cannot be independent of frequency for sufficiently high frequencies, a cut-off frequency must be used with equation (1). Petschek, working in a similar range of temperatures as those that are involved in this work, adopted as his upper frequency cut-off that determined by the frequency interval $\Delta\nu'$ given by

$$h\Delta\nu' = 6 \text{ eV}.$$

This number is arrived at by noting that the capture of electrons with energy greater than about $3/2kT$ to the first excited state will be fairly infrequent. The first excited state of argon is about 4·2 eV below the ionization limit and at a temperature of 14,000°K, $3/2\ kT$ corresponds roughly to 1·8 eV. The capture of electrons to the ground state can be neglected.

A simplified energy-level diagram of argon (p. 103, reference 15) indicates that for frequencies less than that corresponding to 12·8 eV above ground level, the spectral lines are sufficiently close together that one might expect equation (1) to be applicable. Thus, within good approximation, equation (1) applies, at the minimum, to a range of frequencies corresponding to 3 eV. For higher frequencies it would be necessary in a completely, rigorous treatment to employ the relatively complicated frequency (and temperature) dependent equation (69′). However, in view of the anticipated difficulties in the nature of the absorption problem to be solved, an estimate of 4·87 eV was made for the range of frequencies to be associated with equation (1) which would yield approximately the total emitted radiation.

The spontaneous emission coefficient j_s is defined as the energy emitted spontaneously per unit frequency interval by one gram of radiating matter in the directions specified by a unit solid angle. This quantity is independent of direction and here is given by

$$j_s = \frac{\varepsilon}{4\pi\rho} = \frac{6{\cdot}840 \times 10^{-38}}{4\pi\rho}\, \bar{g}^*\, \frac{N_e^2}{T^{1/2}}, \tag{3}$$

where ρ (g/cm^3) is the density of the gas. We note that j_s is frequency independent in the same manner that ε is.

Let dE_ν be the amount of radiation energy per unit frequency interval flowing per sec in the direction θ through the truncated cone defined by an element of area dA normal to the x-axis and an element of solid angle $d\tilde{\omega}$ (see Fig. 6). The specific intensity I_ν at a point 0 in the area dA in the direction θ for a unit frequency internal is defined so that

$$dE_\nu = I_\nu \cos\theta\, dA\, d\tilde{\omega}. \tag{4}$$

The change in intensity dI_ν, due to absorption alone, that is experienced by radiation of intensity I_ν in traversing normally a slab of thickness ds, is given by

$$dI_\nu = -\rho\kappa_\nu I_\nu\, ds, \tag{5}$$

VOL. 1 1961

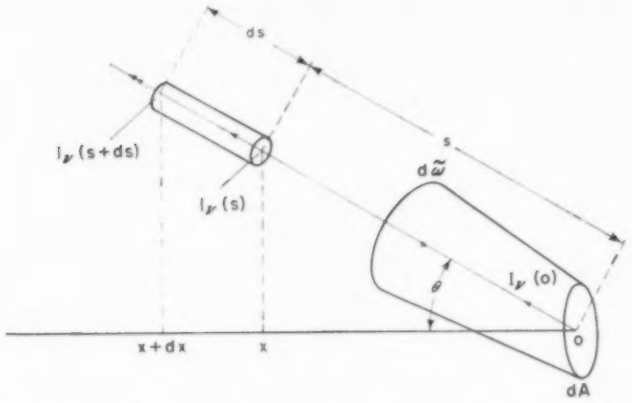

FIG. 6. Sketch illustrating specific intensity and the transfer of energy.

where the quantity $\varkappa_\nu$, assumed independent of direction, is called the mass-absorption coefficient.

To find $\varkappa_\nu$, we observe that if local occupational equilibrium is assumed to exist at every point in the gas, then the relation

$$j_s/\varkappa_\nu = 2h\nu^3/(c^2 e^{h\nu/kT}) \tag{6}$$

holds (p. 205–207, reference 59). Combining this relation with equation (3), we can write for the absorption coefficient per unit volume, $\rho\varkappa_\nu$:

$$\rho\varkappa_\nu = \frac{c^2}{8\pi h}(6{\cdot}840 \times 10^{-38})\,\bar{g}^*\,\frac{N_e^2}{T^{1/2}}\,\frac{e^{h\nu/kT}}{\nu^3} = 3{\cdot}70 \times 10^{8}\bar{g}^*\,\frac{N_e^2}{T^{1/2}}\,\frac{e^{h\nu/kT}}{\nu^3}. \tag{7}$$

It is customary to combine the absorption with the induced emission (sometimes called negative absorption), since both are determined by the intensity of the radiation. It follows from the theory of emission and absorption that the induced emission coefficient per unit mass is given by $\varkappa_\nu e^{-h\nu/kT}$. Following Chandrasekhar, we will denote the effective absorption coefficient per unit mass by the symbol $\varkappa_\nu'$. We have

$$\varkappa_\nu' = \varkappa_\nu - \varkappa_\nu e^{-h\nu/kT}. \tag{8}$$

The change in intensity dI_ν due to both absorption and induced emission that results when a pencil of intensity I_ν traverses normally a slab of thickness ds can be written analogously to equation (5) as

$$dI_\nu = -\rho\varkappa_\nu' I_\nu ds. \tag{9}$$

Integrating we obtain

$$I_\nu(s) = I_\nu(0)e^{-\int_0^s \rho(s)\varkappa_\nu'(s)ds}, \tag{10}$$

and if we define the optical depth $\tau_\nu(s)$ by

$$\tau_\nu(s) = \int_0^s \rho(s)\varkappa_\nu'(s)ds, \tag{11}$$

we can write

$$I_\nu(s) = I_\nu(0)e^{-\tau_\nu(s)}. \tag{10'}$$

If we divide both sides of equation (6) by $[1 - \exp(-h\nu/kT)]$, we obtain

$$\frac{j_\nu}{\kappa_\nu} = 2h\nu^3/c^2(e^{h\nu/kT} - 1) = B_\nu(T), \tag{12}$$

a function usually referred to as the "Planck function". The corresponding effective absorption per unit volume is

$$\rho\kappa_\nu' = 3{\cdot}70 \times 10^8\, \bar{g}^*(N_e^2/T^{1/2})([e^{h\nu/kT} - 1]/\nu^3). \tag{13}$$

The electron density N_e occurring in these equations is found from the relation

$$N_e = \alpha p/(1 + \alpha)kT. \tag{14}$$

3. *Dependence of absorption on initial, driven gas density*

In order to see whether the influence of the effective absorption of radiation behind the maximum luminosity front might be of importance, some preliminary calculations are first made for argon at the conditions that prevail behind a shock front. A uniform region is assumed to exist behind the maximum luminosity front and thus by equation (11), $\tau_\nu = \rho\kappa_\nu' s$. The quantity $I_\nu(s)/I_\nu(0) = \exp - [\tau_\nu(s)]$ for a representative frequency corresponding to $\lambda = 5000$Å is shown plotted in Fig. 7 for three different cases, curves (a), (b), and (c), corresponding to conditions behind a shock wave of about Mach number 17 advancing into argon at densities corresponding respectively to pressures of 1/76, 1/10, and 1/2 atm at a temperature of 294°K. The lowering of the ionization potential has been considered in obtaining the conditions behind the front. The quantity $I_\nu(s)$ is the value of the specific intensity which results from absorption and induced emission over the distance s. No spontaneous emission is assumed along the distance s.

In case (a) of Fig. 7 which corresponds to the conditions behind a Mach 17·03 shock wave advancing into 1/76 atm ($T_1 = 13{\cdot}400$, $\alpha_1 = 0{\cdot}1788$, $p_1 = 5{\cdot}639 \times 10^6$ dyne/cm^2 and $\rho_1 = 0{\cdot}1715 \times 10^{-3}$ g/cm^3) there is comparatively little absorption. In traversing a slab of gas 10 cm thick the emergent specific intensity is still 0·8 of the incident radiation.

In case (b), which corresponds to the conditions behind a Mach number 17·06 shock wave advancing into 1/10th atm ($T_1 = 14{,}600$, $\alpha_1 = 0{\cdot}1690$, $p_1 = 42{\cdot}42 \times 10^6$ dyne/cm^2, and $\rho_1 = 1{\cdot}1940 \times 10^{-3}$ g/cm^3) the absorption is such that the specific intensity has been reduced to 0·48 of its initial value in traversing a thickness of just one centimeter of gas. Absorption is surely important in this case.

In case (c) which corresponds to the conditions behind a Mach number 16·91 shock advancing into 1/2 atm of argon ($T_1 = 15{,}200$, $\alpha_1 = 0{\cdot}1608$, $p_1 = 203{\cdot}54 \times 10^6$ dyne/cm^2, and $\rho_1 = 5{\cdot}542 \times 10^{-3}$ g/cm^3) the absorption is very strong. The specific intensity has fallen to less than 0·08 of its initial value in 0·2 cm. The value of $\rho\kappa_\nu'$ is here 12·754 cm^{-1}, in contrast to 0·731 cm^{-1} for the case of 1/10th atm and 0·02158 cm^{-1} for the case of 1/76th atm.

We see from the above examples that for a shock wave of given strength, the initial pressure of the driven gas greatly influences the absorption of radiation. At a given radiation frequency this influence enters primarily through the N_e^2 factor in equation (13), which is the dominant factor on which the spontaneous emission coefficient j_ν depends.

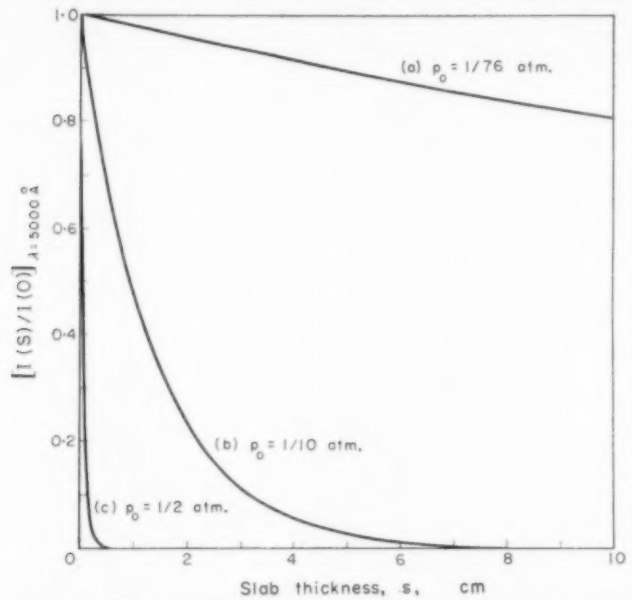

FIG. 7. Fraction of specific intensity of continuum radiation at $\lambda = 5{,}000$ Å present at distance s, calculated on basis of effective absorption behind Mach 17 shock wave advancing into 1/76, 1/10 and 1/2 atm of argon, respectively. No spontaneous emission assumed.

4. *Dependence of absorption on shock Mach number*

For a fixed initial density corresponding to a pressure of 1/10 atm for the driven gas and for a fixed wavelength of 5000Å the effective absorption coefficient per unit volume $\rho\kappa'_\nu$ was computed for various Mach numbers ranging from 11 to 20, and is shown plotted in Fig. 8. We see that $\rho\kappa'_\nu$ increases sharply with Mach number. This rise is a consequence of the increase of the electron density with Mach number.

5. *Dependence of absorption on frequency*

The variation of $\rho\kappa'_\nu$ with frequency is illustrated in Fig. 9 for the equilibrium conditions behind a Mach 17 shock wave advancing into undisturbed argon at a pressure of 1/10th atm. In the region between 2034Å and 7000Å, that is, from the near ultra-violet to the visible red, the variation with frequency is not as pronounced as it is for the longer wavelengths. This region covers a range of frequencies $\Delta\nu = 1{\cdot}0464 \times 10^{15}$ c/s. Subsequently, we shall use an average $\rho\bar{\kappa}'$ defined as

$$\rho\bar{\kappa}' = \frac{1}{\Delta\nu}\int_{\Delta\nu} \rho\kappa'_\nu d\nu, \tag{15}$$

which, of course, is a function of the state of the gas.

6. *The equation of transfer*

In the preceding section we considered the effective absorption of radiation in a medium in which there is no spontaneous emission. We will now consider a medium in which

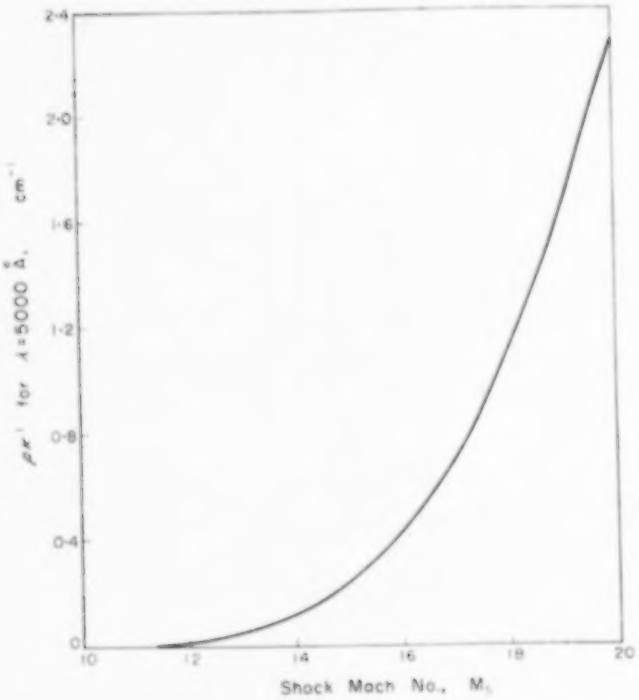

FIG. 8. The effective absorption coefficient in argon for continuum radiation at $\lambda = 5{,}000$ Å as a function of Mach number for equilibrium conditions behind shock front. Pressure in front of shock: 1/10 atm.

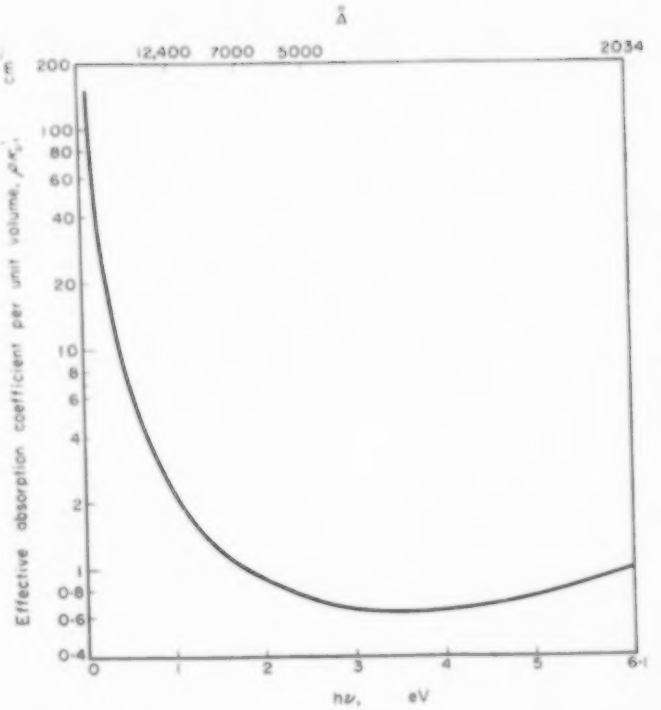

FIG. 9. The effective absorption coefficient as a function of frequency for the conditions behind a Mach number 17 shock wave advancing into 1/10 atm argon. (1 eV = 0·2148 × 10^{15} c/s)

there is present spontaneous emission as well as induced emission and absorption. Let $I_\nu(s)$ be the intensity in an arbitrary direction s at the faces of a small cylindrical element of cross section dA and height ds (see Fig. 6). The energy emerging at $s + ds$ is equal to the energy that entered at s, plus the spontaneous emission in the element in the s direction, minus the energy of the $I_\nu(s)$ pencil of rays that is absorbed, plus the energy of the induced emission caused by the pencil of rays.

$$I_\nu(s + ds)dAd\tilde{\omega} = I_\nu(s)dAd\tilde{\omega} + \\ + \rho j_s(s)dsdAd\tilde{\omega} - \rho\varkappa_\nu I_\nu(s)dsdAd\tilde{\omega} + \rho\varkappa_\nu e^{-h\nu/kT} I_\nu(s)dsdAd\tilde{\omega}. \tag{16}$$

By the use of equation (8) and dividing by $\rho\varkappa_\nu' \, ds \, dA \, d\tilde{\omega}$, we can now obtain the transfer equation

$$\frac{dI_\nu(s)}{\rho\varkappa_\nu' ds} = \frac{j_s(s)}{\varkappa_\nu'} - I_\nu(s). \tag{17}$$

In the case of the plane shock wave, the gas dynamical variables can be considered as a function of the distance behind the shock (or luminosity) front. We introduce the distance x normal to the front ($x = 0$), and the direction parameter θ which the pencil of intensity $I_\nu(x, \theta) = I_\nu(s)$ makes with the x-axis. We further assume axial symmetry, a condition which exists about the center line for a circular cylinder of finite radius, or about any line parallel to the center line for the case of a shock tube of infinite cross section. Then with the use of the relation $ds = \sec\theta \, dx$, equation (17) becomes

$$\frac{dI_\nu(x, \theta)}{\rho(x)\varkappa_\nu'(x) \sec\theta \, dx} + I_\nu(x, \theta) = \frac{j_s(x)}{\varkappa_\nu'(x)}. \tag{18}$$

Instead of $\tau_\nu(s)$ we now introduce the normal optical depth, $\tau_\nu(x)$,

$$\tau_\nu(x) = \int_0^x \rho(x')\varkappa_\nu'(x')dx' \tag{19}$$

and

$$d\tau_\nu(x) = \rho(x)\varkappa_\nu'(x)dx \tag{20}$$

for a given frequency. Equation (18) then becomes

$$\frac{dI_\nu(\tau, \theta)}{d\tau} + \sec\theta \, I_\nu(\tau, \theta) = \sec\theta \frac{j_s(\tau)}{\varkappa_\nu'(\tau)} \tag{21}$$

an equation linear in τ and of the first order, with θ as a variable parameter. With the help of the integrating factor $e^{\int \sec\theta d\tau} = e^{\tau\sec\theta}$ the solution of equation (21) is found to be

$$I_\nu(\tau, \theta) = e^{-\tau\sec\theta} \int_c^\tau \frac{j_s(\tau')}{\varkappa_\nu'(\tau')} \sec\theta \, e^{\tau'\sec\theta} \, d\tau', \tag{22}$$

where C is an arbitrary constant to be determined in terms of the boundary conditions.

At this point it is necessary to distinguish between the intensity of a pencil of rays coming from the direction of the front, and inclined at $\theta \leq \pi/2$, which we designate as $I_{\nu+}$, and the intensity of a pencil of rays from the direction of the interface or contact surface which we designate as $I_{\nu-}$. We further introduce the convention that in the latter case, too,

$\theta \leq \pi/2$. (See Fig. 10). If we assume that $I_{\nu+} = 0$ at $x = 0$, then at τ corresponding to the distance x we have

$$I_{\nu+}(\tau_\nu, \theta) = \int_0^\tau \frac{j(\tau')}{\kappa'_\nu(\tau')} \sec\theta \, e^{-(\tau-\tau')\sec\theta} d\tau'. \tag{23}$$

The subscript s denoting "spontaneous" has been dropped from j_s in the above equation and will be omitted from this point on.

7. *A stratified medium*

In astrophysics, in investigating the problem of the variation of intensity and directional distribution with depth below the surface of a star, the stellar atmosphere is idealized as a stratification of homogeneous, semi-infinite, plane-parallel layers. Similarly the region between 0 and x_c (see Fig. 10) is divided into sections in each of which the dynamic variables

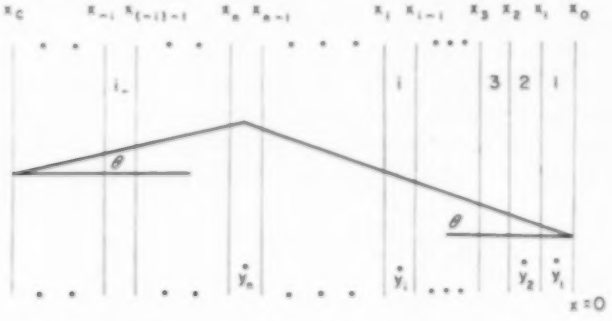

FIG. 10. Sketch illustrating notation for obtaining absorption energy.

are considered constant, and thus $j(i)$ and $\kappa'_\nu(i)$ are constant in an ith section. Let the point x lie in the nth section, and let τ be the corresponding normal optical depth. Equation (23) can then be written as

$$I_{\nu+}(\tau_\nu, \theta) = \int_0^{\tau_1} \frac{j(1)}{\kappa'_\nu(1)} \sec\theta \, e^{-(\tau-\tau')\sec\theta} \, d\tau' + \int_{\tau_1}^{\tau_2} \frac{j(2)}{\kappa'_\nu(2)} \sec\theta \, e^{-(\tau-\tau')\sec\theta} \, d\tau' + \ldots$$

$$+ \ldots + \int_{\tau_{i-1}}^{\tau_i} \frac{j(i)}{\kappa'_\nu(i)} \sec\theta \, e^{-(\tau-\tau')\sec\theta} \, d\tau' + \ldots + \int_{\tau_{n-1}}^{\tau} \frac{j(n)}{\kappa'_\nu(n)} \sec\theta \, e^{-(\tau-\tau')\sec\theta} \, d\tau'. \tag{24}$$

The τ_i refer to the optical depths at the interfaces between sections. Note that the subscript i refers to the left hand boundary of a section (i).

Similarly, for radiation from the direction of the contact surface, we have in general

$$I_{\nu-}(\tau_\nu, \theta) = \int_\tau^{\tau_c} [j(\tau')/\kappa'_\nu(\tau)] \sec\theta \, e^{-(\tau'-\tau)\sec\theta} \, d\tau', \tag{25}$$

which can be rewritten, in analogy to equation (24), as a sum.

8. *An expression for the radiation energy absorbed*

The total energy $\mathscr{E}$ absorbed at a point/sec/g over the range of frequencies $\Delta\nu$ is (including negative absorption)

$$\mathscr{E}(\tau) = \int_{\Delta\nu}\int_{\bar{\omega}} \kappa'_\nu(\tau) I_\nu(\tau, \theta) \mathrm{d}\tilde{\omega}\mathrm{d}\nu, \tag{26}$$

and if we now assume that the cross section of the shock tube is *infinite in extent* we have

$$\mathscr{E}(\tau) = \int_{\Delta\nu} \kappa'_\nu(\tau)\mathrm{d}\nu \int_0^{\pi/2} 2\pi \sin\theta [I_{\nu+}(\tau, \theta) + I_{\nu-}(\tau, \theta)]\mathrm{d}\theta. \tag{26'}$$

It was noted that j is frequency independent. If we eliminate the frequency dependence of κ'_ν for the interval $\Delta\nu$ by the use of the average absorption coefficient $\bar{\kappa}'$ defined by equation (15), considerable simplification results. With τ defined in terms of $\bar{\kappa}'$, τ is also frequency independent. In each of the n sections considered in equation (24) $j(i)/\bar{\kappa}'(i)$ is constant. We then have for the intensity at the optical depth τ due to radiation from the ith section, located to the right of τ, i.e., ($\tau' < \tau$),

$$I_{i+}(\tau, \theta) = \frac{j(i)}{\bar{\kappa}'(i)} \int_{\tau_{i-1}}^{\tau_i} \sec\theta\, \mathrm{e}^{-(\tau-\tau')\sec\theta}\mathrm{d}\tau' = \frac{j(i)}{\bar{\kappa}'(i)} [\mathrm{e}^{-(\tau-\tau_i)\sec\theta} - \mathrm{e}^{-(\tau-\tau_{i-1})\sec\theta}]. \tag{27}$$

A similar expression can be written for the intensity at τ, $I_{i-}(\tau, \theta)$, for radiation coming from some ith section to the left of τ (see Fig. 10). The specific intensities $I_+(\tau, \theta)$ and $I_-(\tau, \theta)$ obtained by summing over the sections are now independent of frequency.

The amount of energy, $\Delta\mathscr{E}_{i+}[\tau(x)]$, absorbed/sec/g at a point in the nth section, as a result of emission from an ith section located to the right of the point is by equations (26') and (27)

$$\Delta\mathscr{E}_{i+}(\tau) = 2\pi\Delta\nu\bar{\kappa}'(n)\frac{j(i)}{\bar{\kappa}(i)} \int_0^{\pi/2} \sin\theta\, [\mathrm{e}^{-(\tau-\tau_i)\sec\theta} - \mathrm{e}^{-(\tau-\tau_{i-1})\sec\theta}]\mathrm{d}\theta. \tag{28}$$

If we let $y = \sec\theta$, then $\sin\theta\,\mathrm{d}\theta = \mathrm{d}y/y^2$, and the integral becomes

$$\int_1^\infty [\mathrm{e}^{-(\tau-\tau_i)y} - \mathrm{e}^{-(\tau-\tau_{i-1})y}]y^{-2}\,\mathrm{d}y. \tag{29}$$

Now the nth exponential integral function $E_n(t)$ is defined by

$$E_n(t) = \int_1^\infty \mathrm{e}^{-ty}y^{-n}\mathrm{d}y \tag{30}$$

and has been tabulated for many values of n.[60] Equation (28) is thus given by

$$\Delta\mathscr{E}_{i+}(\tau) = 2\pi\Delta\nu\bar{\kappa}'(n)\frac{j(i)}{\bar{\kappa}'(i)}[E_2(\tau - \tau_i) - E_2(\tau - \tau_{i-1})]. \tag{31}$$

The corresponding equation for an energy absorbed as a result of emission from an ith section to the left of the absorbing element is

$$\Delta\mathscr{E}_{i-}(\tau) = 2\pi\Delta\nu\bar{\varkappa}'(n)\frac{j(i)}{\bar{\varkappa}'(i)}\left[E_2(\tau_{i-1} - \tau) - E_2(\tau_i - \tau)\right]. \tag{32}$$

The arguments of E_2 are, of course, positive in both equations (31) and (32).

The total energy $\mathscr{E}(\tau)$ absorbed at a point of optical depth τ can now be written as the sum of the contributions from all sections. We thus have

$$\mathscr{E}(\tau) = \sum\Delta\mathscr{E}_{i} + \sum\Delta\mathscr{E}_{i-}. \tag{33}$$

Having developed an expression for $\mathscr{E}(\tau)$, we can turn our attention to the variation of the gas dynamical variables due to radiation cooling.

9. *The equation of energy*

The steady-state, one dimensional equation of energy for a gas at a temperature and density high enough so that the emission and absorption of radiation have to be considered, but not sufficiently high to warrant including the radiation pressure, is

$$u\frac{\mathrm{d}}{\mathrm{d}x}(H + u^2/2) = -\frac{Q(x)}{\rho(x)} + \mathscr{E}(x), \tag{34}$$

where Q, the rate of energy loss per unit volume as a result of spontaneous emission, is here taken as

$$Q(x) = \varepsilon(x)\Delta\nu \tag{35}$$

and $\mathscr{E}$ is given by equation (33). H is the enthalpy per unit mass and u is the particle velocity behind the shock relative to the shock velocity. The enthalpy H for a partially ionized monatomic gas such as argon was written previously (equation (3), part IV) as

$$5/2(1 + \alpha_1)RT_1 + \alpha\chi/M_A,$$

but it is more convenient here to write

$$\chi/m_A = \left[\frac{(N_0k)}{(N_0m_A)}\right]\frac{\chi}{k} = RT_{\text{ion}},$$

where $T_{\text{ion}} \equiv \chi/k$ and N_0 is Avogadro's number. Thus

$$H = 5/2(1 + \alpha)RT_1 + \alpha RT_{\text{ion}}. \tag{36}$$

Equation (34) differs from Petschek's equation (10) of reference (13) in that the absorption term $\mathscr{E}$ is included here; moreover T_{ion} is a variable here, whereas Petschek took T_{ion} as a constant.

For the steady-state, one dimensional flow in a channel of constant area such as is being

VOL. 1 1961

considered, we can write the differential equations for the conservation of mass and momentum as

$$u\mathrm{d}\rho = -\rho\mathrm{d}u \tag{37}$$

$$\mathrm{d}p = -\rho_0 u_0\,\mathrm{d}u \tag{38}$$

and the equation of state and the Saha equation in differential form as

$$\frac{\mathrm{d}p}{p} = \frac{\mathrm{d}\alpha}{1+\alpha} + \frac{\mathrm{d}\rho}{\rho} + \frac{\mathrm{d}T}{T} \tag{39}$$

$$\frac{\mathrm{d}\alpha}{\alpha - \alpha^3} = -\frac{\mathrm{d}p}{2p} + \left(\frac{5}{4} + \frac{T_{\mathrm{ion}}}{2T}\right)\frac{\mathrm{d}T}{T} - \frac{\mathrm{d}T_{\mathrm{ion}}}{2T}. \tag{40}$$

(See equations (1), (2), (4) and (5) of section IV).
As previously, the values of b_0 and b_1 in equation (5) of section IV have been taken equal to unity and six, respectively, that is, independent of temperature.

On the basis of equations (37)–(39), and the differential form of the Saha equation which one obtains for constant T_{ion} (and two other approximations), Petschek found that

$$\mathrm{d}\alpha = \left[\frac{5}{4T} + \frac{T_{\mathrm{ion}}}{2T^2} + \frac{1}{2T(u_0/u - 2)}\Big/\frac{1}{\alpha} - \frac{1}{2(1+\alpha)(u_0/u - 2)}\right]\mathrm{d}T = \varphi^*\mathrm{d}T. \tag{41}$$

If equation (40) is to be used, an expression for $\mathrm{d}T_{\mathrm{ion}}$ is needed. Since

$$T_{\mathrm{ion}} = \chi/k = 11{,}605\,[\chi(\mathrm{eV})] = 11{,}605\,(\chi_0 - \Delta\chi),$$

we have

$$\mathrm{d}T_{\mathrm{ion}} = -\,11{,}605\,\mathrm{d}(\Delta\chi) \tag{42}$$

and by equations (6) and (7) of section IV

$$\Delta\chi(\mathrm{eV}) = \frac{0{\cdot}67}{10^8}\left(\frac{\alpha}{1+\alpha}\frac{p}{kT}\right)^{1/3} + \frac{0{\cdot}38}{10^7 T}\left(\frac{\alpha}{1+\alpha}\frac{p}{k}\right)^{1/2}.$$

Upon performing the indicated differentiation, one obtains after rearrangement of terms,

$$\begin{aligned}\mathrm{d}T_{\mathrm{ion}} = {} & \left[\frac{A}{3}\left(\frac{p}{kT}\right)^{1/3}\frac{1}{(1+\alpha)^{4/3}\,\alpha^{2/3}} + \frac{B}{2T}\left(\frac{p}{k}\right)^{1/2}\frac{1}{(1+\alpha)^{3/2}\,\alpha^{1/2}}\right]\mathrm{d}\alpha + \\ & + \left[\frac{A}{3}\left(\frac{\alpha}{1+\alpha}\frac{1}{kT}\right)^{1/3}\frac{1}{p^{2/3}} + \frac{B}{2T}\left(\frac{\alpha}{(1+\alpha)k}\right)^{1/2}\frac{1}{p^{1/2}}\right]\mathrm{d}p - \\ & - \left[\frac{A}{3}\left(\frac{\alpha}{1+\alpha}\frac{p}{k}\right)^{1/3}\frac{1}{T^{4/3}} + \frac{B}{T^2}\left(\frac{\alpha}{(1+\alpha)}\frac{p}{k}\right)^{1/2}\right]\mathrm{d}T,\end{aligned} \tag{43'}$$

where $A = -\,7{\cdot}77535 \times 10^{-3}$ and $B = -\,4{\cdot}4099 \times 10^{-4}$. Using symbols for the quantities in the square brackets we write, for the sake of simplicity,

$$\mathrm{d}T_{\mathrm{ion}} = C\mathrm{d}\alpha + D\mathrm{d}p + \xi\mathrm{d}T. \tag{43}$$

By combining equations (37), (38), and (39), we obtain an expression for $\mathrm{d}p$ in terms of $\mathrm{d}\alpha$ and $\mathrm{d}T$:

$$\frac{\mathrm{d}p}{p}\left[1 - \frac{p}{\rho u^2}\right] = \frac{\mathrm{d}\alpha}{1+\alpha} + \frac{\mathrm{d}T}{T}. \tag{44}$$

Substituting equations (43) and (44) into (40) we find

$$d\alpha\left[\frac{1}{\alpha-\alpha^3}-\frac{1}{2\left[\frac{p}{\rho u^2}-1\right](1+\alpha)}+\frac{C}{2T}-\frac{pD}{2T\left[\frac{p}{\rho u^2}-1\right](1+\alpha)}\right]=$$

$$=\mathrm{d}T\left[\frac{1}{2T\left[\frac{p}{\rho u^2}-1\right]}+\left(\frac{5}{4}+\frac{T_{\mathrm{ion}}}{2T}\right)\frac{1}{T}+\frac{\xi}{2T}+\frac{pD}{2T^2\left[\frac{p}{\rho u^2}-1\right]}\right].$$

Hence, we can write the derivative of α with respect to T as a function of the variables at a given point. We have

$$\mathrm{d}\alpha/\mathrm{d}T\equiv\varphi. \tag{45}$$

Combining equations (44) and (45), we obtain

$$\frac{\mathrm{d}p}{\mathrm{d}\alpha}=\frac{p}{(1-p/\rho u^2)}\left[\frac{1}{1+\alpha}+\frac{1}{T\varphi}\right]\equiv\gamma, \tag{46}$$

and, from equations (38) and (46)

$$\frac{\mathrm{d}u}{\mathrm{d}\alpha}=-\frac{\gamma}{\rho u}. \tag{47}$$

Furthermore, by the use of equations (43), (45) and (46), we obtain

$$\frac{\mathrm{d}T_{\mathrm{ion}}}{\mathrm{d}\alpha}=\left[C-\frac{\xi}{\varphi}+\gamma D\right]\equiv\psi. \tag{48}$$

With H given by equation (36) and by substituting equations (45), (47), and (48) into the energy equation (34) we obtain

$$\frac{\mathrm{d}\alpha}{\mathrm{d}x}=\frac{-Q(x)/\rho(x)+\mathscr{E}(x)}{uR\left[\left(T+\frac{1+\alpha}{\varphi}\right)\left(\frac{5}{2}+\frac{1}{[p/\rho u^2-1]}\right)+T_{\mathrm{ion}}+\alpha\psi\right.}\equiv\beta. \tag{49}$$

Equation (49) differs from an analogous equation given by Petschek in that it has the additional terms T_{ion}, $\alpha\psi$, and the absorption term $\mathscr{E}$. Petschek uses the φ^* of equation (41) instead of the more exact φ of equation (45), and furthermore he uses an approximation for the exact expression

$$\left[\frac{5}{2}+\frac{1}{(p/\rho u^2-1)}\right]$$

that occurs in the denominator of equation (49).

In terms of the preceding abbreviations the flow variables can now be expressed in terms of one independent variable x, the distance behind the plane of maximum luminosity. We have:

$$\begin{aligned}
\mathrm{d}\alpha/\mathrm{d}x&=\beta\\
\mathrm{d}T/\mathrm{d}x&=\beta/\varphi\\
\mathrm{d}T_{\mathrm{ion}}/\mathrm{d}x&=\beta\psi\\
\mathrm{d}p/\mathrm{d}x&=\beta\gamma\\
\mathrm{d}\rho/\mathrm{d}x&=\gamma\beta/u^2\\
\mathrm{d}u/\mathrm{d}x&=-\gamma\beta/\rho u.
\end{aligned} \tag{50}$$

VOL.
1
196

If the values of $\mathscr{E}(x)$ were available, then this system of equations can be solved accurately as far as third-order terms in Δx by a method for numerical integration devised by WALTON[61] for automatic digital computing machines such as the IBM calculators. A simple means of checking for the occurrence of any discrepancies in the solution is provided. An additional sensitive check for the particular system of equations (50) that was used here is the following: After α, T, and T_{ion} are found by equations (50) at a given point x, these values are substituted into the Saha equation and the pressure, $p_s(x)$, is calculated from this equation. The difference $|p_s(x) - p(x)|$ between $p_s(x)$ and the $p(x)$ found from the differential system, divided by the change in pressure, $p(x) - p(0)$, should be very small. We refer to this check as the "Saha check".

Still another check consisted of finding for each interval the quantity, $p + \rho u^2$. This quantity usually remained constant to better than a few parts in 10^8, and any departure from this was an indication that too large an interval might have been used.

10. *The development of a method for finding the absorption energy*

If the absorption term is missing, there should be little difficulty in calculating the variation of the gas dynamical variables due to simple emission, since Q is a point function. The quantity, $\mathscr{E}$, on the other hand, depends as we have seen on the complete structure of the luminous region, which we are seeking to determine.

It was found by Petschek, who did not consider the absorption, that the temperature dropped from roughly 13,750°K, 12,800°K, and 11,600°K, respectively, to 10,800°K in 10 cm and 10,000°K in 25 cm for three shocks of Mach number 17, 15, and 13 advancing into undisturbed gas at 1/76th atm (Fig. 3 of reference 11 and p. 93 of reference 13). The results of section 3 of this Part showed that the absorption of continuum radiation is small under these conditions, but that the absorption at higher densities was important. Before the detailed technique for computing the absorption was developed, equations (50) were solved with $\mathscr{E}(x)$ of equation (49) set equal to zero for a Mach 17·06 shock wave advancing into 1/10th atm of argon. This was done to gain additional information about the validity of an assumption that was under consideration and to provide a comparison with the results that would be obtained when the absorption was taken into account. Solving the system of equations (50) with $\mathscr{E} = 0$, also provides a severer test of the method of solving the equations than is provided when $\mathscr{E}(x)$ is not zero. In fact, earlier attempts at solving the system of equations for the case of $\mathscr{E} = 0$ by a method using only Δx failed to meet the "Saha check" described above, unless prohibitively small intervals of Δx were employed.

The manner in which the temperature, degree of ionization and pressure vary with distance behind the maximum luminosity front is shown in Figs. 11–13 for the case $\mathscr{E}(x) = 0$. Fig. 11 shows that the temperature diminished from 14,600°K to 10,750°K in a distance of 16 cm. Since one can anticipate much slower cooling when absorption is considered, and since the portions farther from the maximum luminosity front will influence the absorption least, it seemed reasonable to assume as a zero-order approximation that the luminous gas is all at the same equilibrium temperature. The transient region of rising ionization is very small for the higher Mach numbers and will be neglected.

Let us now take for the zero-order approximation the equilibrium conditions at the maximum luminosity front ($x = 0$) for the Mach 17·06 shock mentioned above. These are: $T_1 = 14{,}600°\text{K}$, $\alpha_1 = 0{\cdot}16900$, $T_{ion} = 165{,}259{\cdot}84°\text{K}$, $p_1 = 42{\cdot}416 \times 10^6$ dyne/cm², $\rho_1 =$

$1{\cdot}1939 \times 10^{-3}$ g/cm^3, and $u_1 = 75{\cdot}542 \times 10^2$. Except for T_{ion} the above quantities have been rounded off from the 8-place accuracy used in numerical work on the IBM machine. Let us assume that a steady state exists for a luminous region 16 cm long and of infinite cross section and that it is moving at constant speed down the "shock tube". We wish to find the absorption $\mathcal{E}$, representative of a slab 0·05 cm thick located behind $x = 0$ in the coordinate system moving with the gas. By equations (31) and (32) the absorption at any point x in this uniform region is given by

$$\mathcal{E}(\tau) = 2\pi\Delta\nu j(1)[2 - E_2(\tau) - E_2(\tau_c - \tau)], \tag{51}$$

since $\bar{\varkappa}'(n) = \bar{\varkappa}'(i) = \bar{\varkappa}'(1)$ for this case, and $E_2(0) = 1$.

For calculations with an electric computer, $E_2(\tau)$ is found from the following formula[60]:

$$E_2(\tau) = 1 + 0{\cdot}57721566\,\tau + \tau\log\tau - \tau - \frac{\tau^2}{2!1} + \frac{\tau^3}{3!2} - \frac{\tau^4}{4!3} + \frac{\tau^5}{5!4} - \cdots \tag{52}$$

From a plot of absorption versus distance one can find an average value of $\mathcal{E}$ for the 0·05 cm thick slab. However, it should be a good approximation to the average to use the absorption $\mathcal{E}[\tau(x = 0{\cdot}025)]$ at the midpoint of this slab. By inserting this value into equation (49), the system of equations (50) can be solved for the interval $\Delta x = 0{\cdot}05$ cm, and resulting values T_2, $\varkappa_2$, p_2, T_{ion2}, ρ_2 and u_2 for the point $x = 0{\cdot}05$ cm found.

As the next approximation, the 16 cm long cylinder of infinite cross section is considered as composed of two sections: one, 0·05 cm wide at conditions T_1, $\varkappa_1$, p_1, T_{ion}, ρ_1, and u_1 and the remaining section 15·95 cm long at conditions T_2, $\varkappa_2$, p_2, T_{ion_2}, ρ_2 and u_2. The width of the initial interval is multiplied by a constant factor, say 1·2, and the absorption

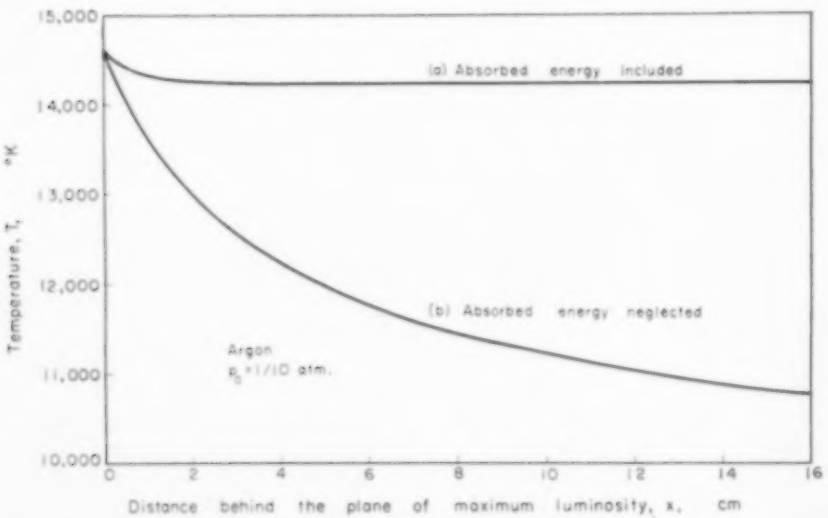

FIG. 11. Variation of temperature with the distance behind the plane of maximum luminosity when (a) the absorbed radiation energy is included in the equation of motion and (b) when it is neglected. ($M_s = 17{\cdot}06$, $p_0 = 1/10$ atm.)

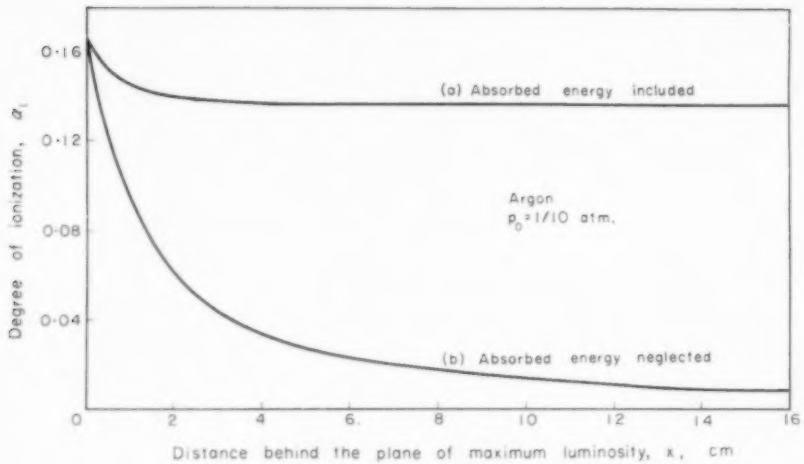

FIG. 12. Variation of degree of ionization with the distance behind the plane of maximum luminosity when (a) the absorbed radiation energy is included in the equation of motion and (b) when it is neglected. ($M_s = 17{\cdot}06$, $p_0 = 1/10$ atm.)

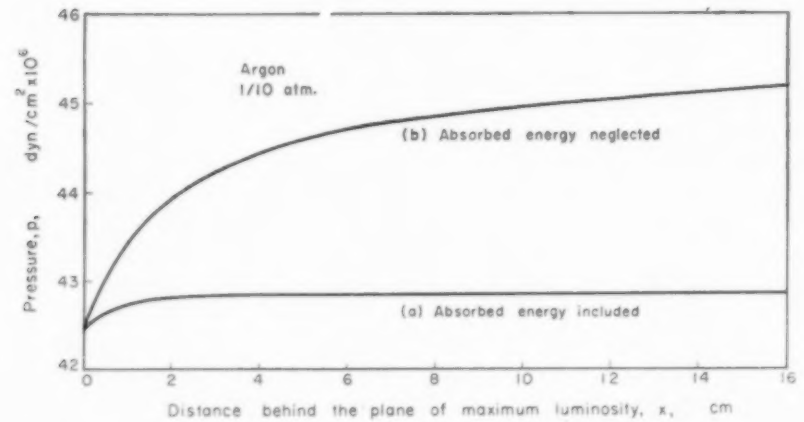

FIG. 13. Variation of pressure with the distance behind the plane of maximum luminosity when (a) the absorbed radiation energy is included in the equation of motion and (b) when it is neglected. ($M_s = 17{\cdot}06$, $p_0 = 1/10$ atm.)

found at the midpoint of a 0·06 cm wide slab adjoining the first one, namely at $x = 0{\cdot}08$ cm. If we designate the midpoint of the first interval by y_1, the midpoint of this second interval can be designated by y_2. We have (see Fig. 10) by the use of equations (31) to (33),

$$\mathscr{E}[\tau(y_2)] = 2\pi\Delta\nu\bar{\varkappa}'(2)\,\frac{j(1)}{\bar{\varkappa}'(1)}\{(E_2[\tau(y_2) - \tau(x_1)] - E_2[\tau(y_2) - \tau(0)]\} +$$

$$+ 2\pi\Delta\nu j(2)\{1 - E_2[\tau(y_2) - \tau(x_1)]\} + 2\pi\Delta\nu j(2)\{1 - E_2[\tau(x_c) - \tau(y_2)]\}. \qquad (53)$$

With this value of $\mathscr{E}(y_2)$, the conditions at x_2 ($x = 0{\cdot}11$ cm) can be found now by equations (50), and thus a third set of conditions T_3, α_3, p_3, T_{ion_3}, ρ_3 and u_3 found.

It is obvious from the above that one can continue in the same manner: the tube is divided into three sections; a new interval $(1{\cdot}2) \cdot (0{\cdot}06$ cm) is designated; the absorption at the midpoint, y_3, of this interval is found; equations (50) are integrated and a new set of values determined for the next interval (4) which begins at $x = 0{\cdot}182$ cm; and so forth, until one has divided the entire cylinder into intervals in each of which the gas dynamical variables, and $j(i)$ and $\rho(i)\overline{\alpha}'(i)$ have been found. We call a determination of the variables in all of the intervals "a completion of a cycle".

Successive intervals were increased by the factor 1·2 because the expression for $\mathscr{E}[\tau(y_n)]$ becomes lengthy as the number of intervals increase. Since the Δx's varied in size, Walton's "method of interlocked parabolas" could not be used. Instead, the sub-routine used by WALTON[61] to start his solution, a Runge-Kutta procedure was employed at each step.

After we have completed the first cycle, we can further refine the result by taking the above-found complete structure as a higher approximation. In other words, we find the energy $\mathscr{E}$ absorbed in the first interval as a result of the continuum radiation from each of the other intervals. With this value of $\mathscr{E}$ inserted in equation (49), the system of equations (50) are solved for the 0·05 cm interval, and new values T_2', α_2' . . . found for the second interval. In similar fashion, new values T_i', α_i' . . . are found for all the other intervals, and thus the second cycle is completed. In turn, the newly found complete set of values T_i', α_i', . . . may be regarded as a further, higher approximation, and taken as the basis for still another cycle or iteration.

Four complete iterations (5 cycles) were carried out for the 16 cm long, luminous region behind a shock wave of Mach number 17·06 advancing into 1/10th atm of argon, that we have been considering. Table 6 presents the values of α, T, and p, at selected distances along the cylinder for each cycle. Also given are the values of the energy absorbed/g/sec at the midpoints of the intervals which begin at the selected distances. It is seen that for all practical purposes even a first iteration is hardly necessary for this case. All subsequent calculations were iterated just once.

Comparison is made in Table 7 between the results for the 16 cm long cylinder and the results for a 40 cm long cylinder for the case of the Mach number 17·06 shock advancing into 1/10th atm of argon. The results for the second cycle were used in both cases. It is noted that up to distances of 9·33 cm, the degree of ionization, temperature, and pressure are the same for both cases when the values are rounded off to five significant figures. Very good agreement also exists at 13·55 cm.

The preceding results for the four iterations and for the cylinders of different lengths substantiate the general validity of the zero-order and subsequent approximations made in obtaining the absorbed energy.

11. *Results illustrating the influence of the absorbed radiation energy*

(a) $M_s = 17{\cdot}06$, $p_0 = 1/10$*th atm*. The values of the temperature, degree of ionization, and pressure obtained in the preceding section for the fourth iteration have been plotted (curves a) in Figs. 11, 12, and 13, respectively. The corresponding values for the case in which the absorbed energy is neglected are shown for comparison (curves b). We see that whereas the temperature diminishes from 14,600°K to 14,225°K over a distance of 16 cm

TABLE 6. THE VALUES OF α, T, p, AND $\mathscr{E}$ AT VARIOUS DISTANCES BEHIND THE PLANE OF MAXIMUM LUMINOSITY FOR SUCCESSIVE ITERATIONS. CONDITIONS CALCULATED FOR ARGON, $M_s = 17{\cdot}06$, $p_0 = 1/10$ ATM, $T_0 = 294°$K. "CYLINDER" IS 16 CM LONG AND OF INFINITE CROSS SECTION

Variable	Cycle	Distance (cm)			
		0·05	1·04	4·372	13·55
α	1	0·16648	0·14591	0·13808	0·13781
	2	0·16639	0·14506	0·13710	0·13691
	3	0·16638	0·14498	0·13685	0·13656
	4	0·16638	0·14497	0·13681	0·13645
	5	0·16638	0·14497	0·13680	0·13643
T(°K)	1	14573	14340	14246	14243
	2	14572	14330	14234	14231
	3	14572	14329	14231	14227
	4	14572	14329	14230	14226
	5	14572	14329	14230	14225
p (10^6 dyne/cm^2)	1	42·448	42·715	42·817	42·821
	2	42·449	42·726	42·830	42·833
	3	42·449	42·727	42·834	42·837
	4	42·449	42·727	42·834	42·839
	5	42·449	42·727	42·834	42·839
$\mathscr{E}$ (10^{15} erg/g sec)	1	2·4146	2·9491	2·9603	2·9615
	2	2·3499	2·9088	2·9269	2·9128
	3	2·3469	2·9031	2·9168	2·9018
	4	2·3466	2·9023	2·9147	2·8953
	5	2·3466	2·9022	2·9143	2·8944

TABLE 7. VALUES α, T, p, AND $\mathscr{E}$ AT VARIOUS DISTANCES BEHIND MAXIMUM LUMINOSITY PLANE IN "CYLINDERS" OF 16 CM AND 40 CM LENGTHS. $M_s = 17{\cdot}06$, $p_0 = 1/10$ ATM. SECOND CYCLE VALUES USED FOR BOTH

Variable	Length of cylinder (cm)	Distance (cm)			
		9·33	13·55	23·60	34·09
α	16	0·13692	0·13691	0·13697	0·13654
	40	0·13692	0·13699		
T(°K)	16	14,232	14,231	14,232	14,227
	40	14,232	14,232		
p (10^6 dyne/cm)^2	16	42·833	42·833	42·832	42·838
	40	42·833	42·832		
$\mathscr{E}$ (10^{15} erg/g sec)	16	2·9299	2·9128	2·9320	2·9164
	40	2·9307	2·9331		

when absorption is considered, it falls to 10,750°K when the absorption is not considered. Similarly, the degree of ionization diminishes in 16 cm from an initial value of 0·1690 to 0·1364 when the absorption is considered, in sharp contrast to the value of 0·00923 when the absorption is neglected. Over this same distance, the pressure rises from an initial value of $42{\cdot}416 \times 10^6$ dyne/cm^2 to $42{\cdot}840 \times 10^6$ dyne/cm^2 when the absorption is included, whereas it rises about 6·5 times as much to a value of $45{\cdot}161 \times 10^6$ dyne/cm^2 with the

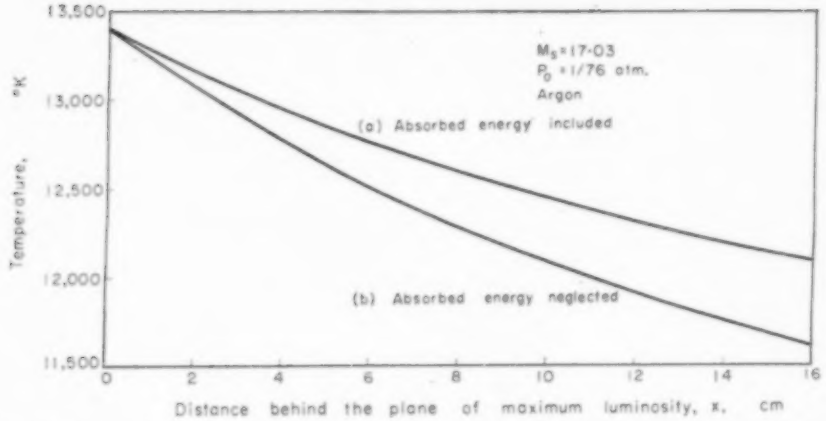

FIG. 14. The variation of temperature with distance if (a) the absorbed energy if included and (b) it is neglected.

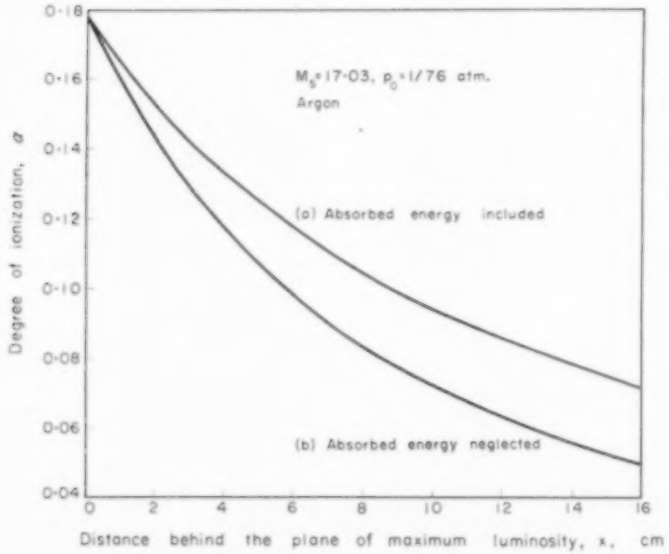

FIG. 15. The variation of the degree of ionization with distance if (a) the absorbed energy is included and (b) it is neglected.

neglect of the absorption term, $\mathscr{E}$, in the equation of energy. Moreover, Figs. 11 to 13 show that when the absorption is taken into account, the variables in this case essentially reach a constant value at a distance of about 4 cm, and change very little between 2 and 4 cm.

(b) $M_s = 17{\cdot}03$, $p_0 = 1/76$ *atm*. We noted in section 3 that the initial pressure greatly influenced the absorption coefficient, and that, in particular, the absorption coefficient for

VOL.
1
1961

a Mach number 17 shock wave advancing into 1/76 atm of argon was much smaller than that for a Mach number 17 shock wave advancing into 1/10 atm. Thus, one might anticipate that these two cases differ from one another with respect to the manner in which the absorption of radiation influences the variation of, say, temperature with distance behind the maximum luminosity plane. Figs. 14 and 15 show the manner in which temperature and degree of ionization vary with distance when the absorbed energy is taken into account (curves a) and when it is neglected (curves b) for the case of a Mach number 17·03 shock wave advancing into 1/76 atm of argon. We see that instead of an essentially constant condition being reached after several centimeters when the absorbed energy is included, as

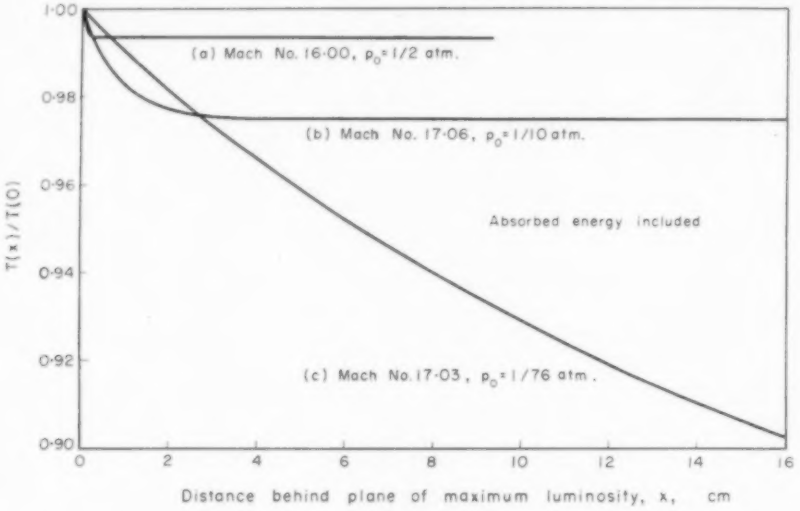

FIG. 16. The variation of normalized temperature with distance (when the absorbed energy is included) for three different initial densities.

was the case for an initial pressure of 1/10 atm, the temperature and degree of ionization continue to diminish over the 16 cm length of cylinder for which the calculation was made. We see also that there is comparatively little effect due to the absorbed energy. At 14 cm, the difference in temperature between curves (a) and (b) for the 1/76 atm results is about 430°K, in comparison with the difference of 3200°K between curves (a) and (b) for the 1/10 atm results.

(c) $M_s = 16{\cdot}00$, $p_0 = 1/2$ *atm*. It was of interest to observe the effect of an absorption greater than that present for the conditions behind a Mach number 17·06 shock wave advancing into 1/10 atm of argon. Consequently, results were obtained for a Mach number 16·00 shock wave advancing into 1/2 atm of argon. The manner in which temperature, degree of ionization, and pressure vary with distance behind the plane of maximum luminosity when the absorbed energy is considered is shown for this case as curves (a) in Figs. 16, 17, and 18, respectively. The results have been normalized with respect to the equilibrium values existing at $x = 0$, namely, $T_1 = 14{,}800°\text{K}$, $\alpha_1 = 0{\cdot}13004$, and $p_1 = 182{\cdot}53 \times 10^6$ dyne/cm². This has been done to facilitate comparison with the other two initial conditions of $p_0 = 1/10$ and 1/76 atm that we have already considered. The variables

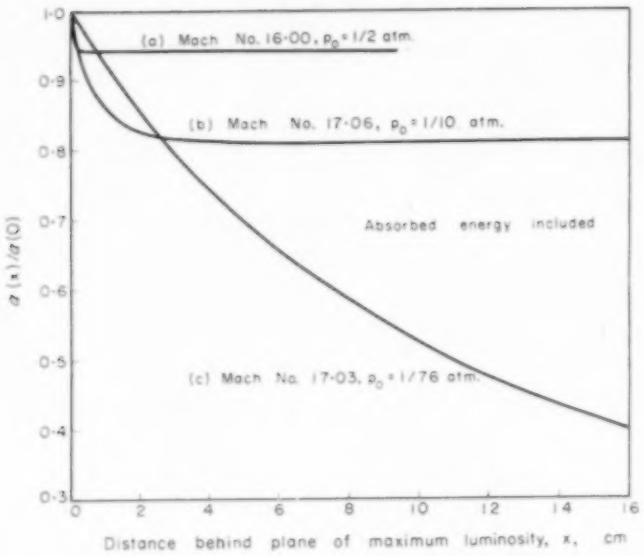
(a) Mach No. 16·00, p_0 = 1/2 atm.
(b) Mach No. 17·06, p_0 = 1/10 atm.
Absorbed energy included
(c) Mach No. 17·03, p_0 = 1/76 atm.
σ(x)/σ(0)
Distance behind plane of maximum luminosity, x, cm

FIG. 17. The variation of normalized degree of ionization with distance (when the absorbed energy is included) for three different initial densities.

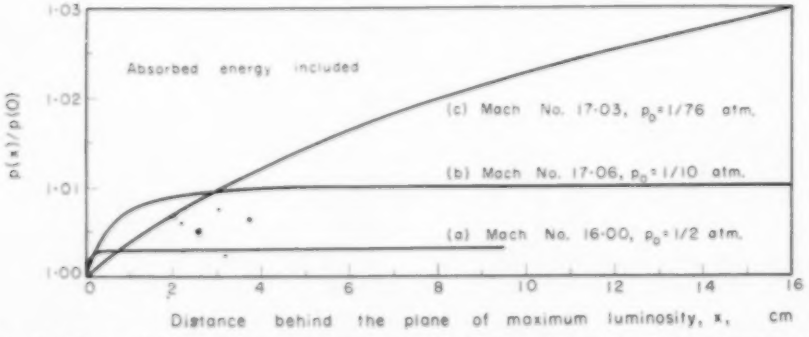
Absorbed energy included
(c) Mach No. 17·03, p_0 = 1/76 atm.
(b) Mach No. 17·06, p_0 = 1/10 atm.
(a) Mach No. 16·00, p_0 = 1/2 atm.
p(x)/p(0)
Distance behind the plane of maximum luminosity, x, cm

FIG. 18. The variation of normalized pressure with distance (when the absorbed energy is included) for three different initial densities.

T, α, and p have been normalized for the latter two cases with respect to their respective conditions at $x = 0$, and are shown plotted as curves (b) and (c), respectively. We see for the case of greatest initial density that an essentially constant condition is reached at a shorter distance, and that the magnitude of this constant value is closer to the initial value at $x = 0$, than for the other cases considered.

The values for the $M_s = 16{\cdot}00$, $p_0 = 1/2$ atm case were terminated at $x = 9{\cdot}33 \ldots$ cm, since the quantity $p + \rho u^2$ for the next point at $x = 11{\cdot}25 \ldots$ cm deviated from the initial value by 1 part in 4×10^7 (see section 9). This means, as previously indicated, that a smaller distance interval should have been used for points beyond $x = 9{\cdot}33 \ldots$ cm than

called for by the particular program used. A calculating program can be so arranged that a new set of intervals can automatically be used when certain tolerances are exceeded. However, the added complications to the program were not believed warranted in the present case.

12. *Applicability of results*

The results given in this part have been developed for conditions in a shock tube whose cross section is of infinite optical depth. In practice, this might be considered to be one of sufficient width and containing a sufficiently dense, hot plasma so that essentially no contribution of radiative energy is made to a given volume element from elements in the same cross section that are sufficiently far removed. Moreover, steady-state, one-dimensional flow has been assumed. The applicability of this assumption has to be checked for the experimental conditions in each facility.

VI. ABSORPTION AND EMISSION OF CONTINUUM RADIATION IN A SHOCK TUBE WHOSE CROSS SECTION IS OF FINITE OPTICAL DEPTH

1. *Theory*

This part will present a method for finding the effect on the gas dynamical variables of the absorption of continuum radiation at points near the center line of a shock tube of finite optical depth.

Assume that the conditions behind a plane shock wave propagating with constant speed in a shock tube of finite radius are such that the optical depth corresponding to this radius is finite for the frequency region $\Delta\nu$ defined in Part V. Assume also that the luminous region behind the plane of maximum luminosity consists of plane, parallel sections in each of which uniform conditions exist. Since axial symmetry exists in this case for points on the center line, equations (18) to (26) of Part V are applicable here. Also applicable, of course, are the equations of section 9 of Part V. Finally, we assume that the frequency dependence of $\varkappa'_\nu$ has been taken care of in the manner given in section 8 of Part V.

The differential element of intensity at the point x on the center line due to an element of volume located in the plane x' ($x > x'$) is given then by (cf. equation (23), Part V).

$$dI_+(\tau, \theta) = \Delta\nu \sec\theta \frac{j(x')}{\overline{\varkappa}'(x')} e^{-[\tau(x)-\tau'(x)]\sec\theta} d\tau \tag{1}$$

where θ is the angle between the line joining the element and x (see Fig. 19). The contribution from an elementary volume at an $x' > x$ is given, of course, by a similar expression, and has

$$-[\tau'(x) - \tau(x)] \sec\theta$$

as the exponent. The convention about θ set forth in Part V is assumed to hold here. Thus, the elementary cylinder of circular cross section which contained the elementary volume to the right of x contributes the amount

$$dI_+[\tau, \theta_{max}(x')] = \frac{j(x')}{\overline{\varkappa}'(x)'} 2\pi\Delta\nu d\tau' \int_0^{\theta_{max}(x')} e^{-[\tau(x)-\tau'(x')]\sec\theta} \sin\theta \sec\theta \, d\theta, \tag{2}$$

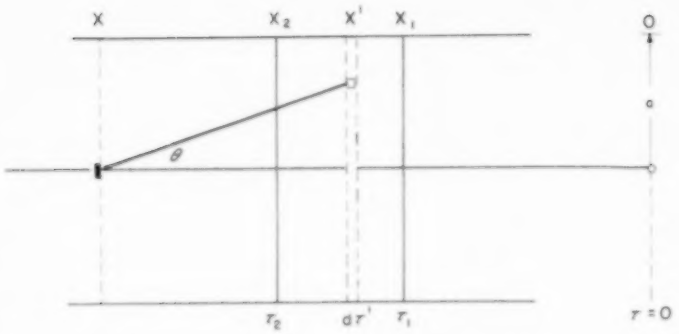

FIG. 19. Diagram showing elements of integration for cylinder of finite cross section.

where $\theta_{max} = \arctan(a/x - x')$, and a is the radius of the cylinder.

Let $y = \sec\theta$; then, as before, $\sin\theta\, d\theta = dy/y^2$, and

$$dI_+[\tau, \theta_{max}] = \frac{j(x')}{\bar{\varkappa}'(x')} 2\pi\Delta\nu d\tau' \int_1^{\sec\theta_{max}} e^{-y[\tau(x)-\tau'(x')]} \frac{dy}{y}. \tag{3}$$

Further let $z = y[\tau(x) - \tau'(x')]$,

and thus $dz = dy[\tau(x) - \tau'(x')]$.

Then, we can write for the elementary cylinder

$$dI_+ = \frac{j(x')}{\bar{\varkappa}'(x')} 2\pi\Delta\nu d\tau' \int_{[\tau(x)-\tau'(x')]}^{[\tau(x)-\tau'(x')]\sec\theta_{max}} e^{-z} \frac{dz}{z} =$$

$$= \frac{j(x)}{\bar{\varkappa}'(x)} 2\pi\Delta\nu d\tau' \left\{ E_1[\tau(x) - \tau'(x')] - E_1\left([\tau(x) - \tau'(x')] \sec \arctan \frac{a}{x - x'} \right) \right\}, \tag{4}$$

by the use of equation (30) of Part V, where $n = 1$ here.

The intensity $I(i)_+$ due to the ith uniform section between planes $x_{i-1} = x$ and $x = x_i$ is

$$I_{i+} = 2\pi\Delta\nu \frac{j(x)}{\bar{\varkappa}'(x)} \left[\int_{\tau_{i-1}}^{\tau_i} E_1[\tau(x) - \tau'(x')]\, d\tau' - \int_{\tau_{i-1}}^{\tau_i} E_1\left([\tau(x) - \tau'(x')] \sec \arctan \frac{a}{x - x'} \right) d\tau' \right]. \tag{5}$$

The first of the integrals in equation (5) can be evaluated in closed form. We obtain

$$\int_{\tau_{i-1}}^{\tau_i} E_1(\tau - \tau') d\tau' = E_2[\tau(x) - \tau(x_i)] - E_2[\tau(x) - \tau(x_{i-1})]. \tag{6}$$

The second integral however has to be evaluated numerically, and we designate it as $\mathcal{I}_{i+}$.

An equation similar to (5) can be written for the intensity from an ith uniform section to the left of x. Again it is composed of two parts, one of which can be evaluated as the

difference of two E_2 functions, as was done in equation (6), and the other integral designated $\mathscr{I}_{i-}$, has to be evaluated numerically.

The energy absorbed/sec/g at a point x on the center line in the nth section, as a result of emission from an ith section is, therefore, for $\tau > \tau'$,

$$\Delta\mathscr{E}_{i+}(\tau) = 2\pi\Delta\nu\overline{\varkappa}'(n)\,\frac{j(i)}{\overline{\varkappa}(i)}\,[E_2(\tau - \tau_i) - E_2(\tau - \tau_{i-1}) - \mathscr{I}_{i+}]\;; \tag{7}$$

and similarly, for $\tau < \tau'$,

$$\Delta\mathscr{E}_{i-}(\tau) = 2\pi\Delta\nu\overline{\varkappa}'(n)\,\frac{j(i_-)}{\overline{\varkappa}'(i_-)}\,[E_2(\tau_{(i-)-1} - \tau) - E_2(\tau_{(i-)} - \tau) - \mathscr{I}_{i-}]\;, \tag{8}$$

where we have designated the ith section to the left by the symbol $(i-)$. (The unusual subscripts in equation (8) follow from our previous convention that the section number refer to the left hand boundary.) Comparing these results with equations (31) and (32) of Part V, we see that if we sum the contribution from all sections, we obtain for the total absorption at a point on the center line of a finite shock tube:

$$\mathscr{E}(\tau) = \sum\Delta\mathscr{E}_{i+} + \sum\Delta\mathscr{E}_{i-}, \tag{9}$$

an amount which consists of the result for a shock tube of infinite cross section (equation (33) of Part V), minus the sum of the $\mathscr{I}_{i+}$ and $\mathscr{I}_{i-}$ for all the sections.

With $\mathscr{E}$ thus determined, one can proceed exactly as in Part V to find the variation of the gas dynamical variables behind the plane of maximum luminosity.

The integrals $\mathscr{I}_{i+}$ and $\mathscr{I}_{i-}$ simplify somewhat if a single, uniform condition exists throughout the whole cylinder. We have

$$\mathscr{I}_{i+} = \int_{\tau_{i-1}}^{\tau_i} E_1\,(\sqrt{a^2\rho^2\overline{\varkappa}'^2 + (\tau - \tau')^2})\,\mathrm{d}\tau'\;, \tag{10}$$

where $\rho\overline{\varkappa}'$ is the average absorption coefficient in the cylinder.

2. *Some approximations*

Conditions at points not far off the center line of a finite cylinder of large optical radius can be approximated by regarding these points as located on the center lines of circular cylinders of smaller radius. The smaller cylinder of radius r may be taken as either tangent to the larger cylinder, or an attempt can be made to compensate for the loss from farther regions by taking the radius of the cylinder a little larger than r. Similarly, points in the center of square-shaped shock tubes may under appropriate conditions be approximated by suitably chosen circular cylinders whose cross section is roughly that of the square-shaped shock tube.

VII. SUMMARY AND CONCLUSIONS

1. A semiclassical derivation of a known equation for the emission of the total continuum radiation from a partially ionized gas was presented. This equation simplified when combined with the Saha equation and remained in this form (equation (72), Part II) when the same lowering of the ionization potential was introduced in both the Saha and the continuum radiation equation.

2. A review was made of the work done by various authors on the subject of the lowering of the ionization potential. The formula given by Ecker and Weizel (equation (52), Part III) was selected as the most promising, and was used in subsequent work. It was noted that the lowering of the ionization potential was a function of the temperature and electron density of the gas.

3. The equilibrium conditions behind shocks of various strengths were found with the use of the lowered ionization potentials. (No mention is made in the literature of this having been done previously.) Results were presented for shocks varying from Mach numbers 11 to 20 for initial densities of 1/76, 1/10, and 1/2 atm. The amount by which the potential had been lowered was presented in each case.

4. Graphs were presented which illustrated the dependence of the continuum absorption on the initial driven-gas density, on the Mach number of the shock, and on the frequency of the radiation.

5. A formal expression was developed for the energy absorbed at any point in a medium, stratified into plane-parallel layers, each with known, uniform conditions.

6. To obtain an expression for the variation of the degree of ionization with distance, it was necessary to combine the energy equation with the differential forms of the following equations: the equation of state, the Saha equation, the equation for the lowering of the ionization potential, and the conservation equations for mass-flow and momentum. The resulting equation contained, of course, a term for the rate of energy loss per unit mass and a term for the rate of energy gain per unit mass by absorption. Expressions were then found for the rate of change of the other variables. The resulting system of six differential equations could be solved by numerical integrations if the absorption term were known. These equations differed from those of Petschek's in that (1) they had been developed with the ionization potential regarded as a variable, (2) they contained the absorbed radiation energy, and (3) they did not contain certain approximations made by Petschek.

7. A method was developed for finding the absorption energy term for a shock tube whose cross section was of infinite optical depth. Numerical calculations, accurate as far as third-order terms, indicated that the assumptions underlying this method were sound (see Tables 6 and 7).

8. The broad influence of the absorption of radiation in shock tube phenomena may be inferred from the comparison of the results of numerical calculations made with and without the consideration of the absorption energy term. For roughly the same Mach number, the effect of the absorption of energy was to bring the variables to an essentially constant value in a distance which depended on the density ahead of the shock. The greater the density, the shorter was this distance, and the closer was the magnitude of this constant value to the initial value at the plane of maximum luminosity.

9. A method was presented for finding the effect on the gas flow variables of the absorption of radiation at points near the center line of a shock tube of finite optical depth.

Acknowledgements—The author wishes to express his sincere appreciation to PROFESSOR J. M. BURGERS of the University of Maryland for his kind help, guidance, and inspiration.

The author is also indebted to a number of members of the staff at NOL: to DR. Z. I. SLAWSKY, DR. E. H. WINKLER and DR. A. E. SEIGEL for their interest and encouragement; and to JAMES BROWN, J. F. BUTLER, and W. J. GLOWACKI who at different times assisted in the carrying out of the calculations on the IBM Calculator.

VOL.
1
196

REFERENCES

1. J. W. Bond, Jr., *The Structure of a Shock Front in Argon*, Los Alamos Scientific Laboratory, Report LA–1693 (1954).
2. A. H. Bethe and E. Teller, *Deviations from Thermal Equilibrium in Shock Waves*, Aberdeen Proving Ground Report X–117.
3. V. H. Blackman, *J. Fluid Mech.* **1**, 61 (1956).
4. H. E. Petschek, *Ph.D. Thesis*, Cornell University (1955).
5. H. E. Petschek and S. Byron, *Ann. Phys. N.Y.* **1**, 270 (1957).
6. R. H. Christian, E. R. Duff and F. L. Yarger, *J. Chem. Phys.* **23**, 2045 (1955).
7. S. C. Lin, E. L. Resler and A. Kantrowitz, *J. Appl. Phys.* **26**, 95 (1955).
8. W. Marshall, *Proc. Roy. Soc.* A **233**, 367 (1955).
9. E. L. Resler, Jr., and W. R. Sears, *J. Aero. Sci.* **25**, 235, 258 (1958).
10. R. N. Hollyer, Jr., A. C. Hunting, O. LaPorte, E. H. Schwarcz and E. B. Turner, *Phys. Rev.* **87**, 911 (1952).
11. E. L. Resler, Shao-Chi Lin and A. Kantrowitz, *J. Appl. Phys.* **23**, 1390 (1952).
12. G. Schreffler and R. H. Christian, *J. Appl. Phys.* **25**, 324 (1954).
13. H. E. Petschek, P. H. Rose, H. S. Glick, A. Kane and A. Kantrowitz, *J. Appl. Phys.* **26**, 83 (1955).
14. L. H. Aller, *Sky & Telesc.* **14** (1954).
15. E. B. Turner, *The Production of Very High Temperatures in the Shock Tube with an Application to the Study of Spectral Line Broadening*, Univ. Mich. Rept. AFOSR TN–56–150 (May 1956).
16. W. Elenbaas, *The High Pressure Mercury Vapour Discharge*. Interscience, New York (1951).
17. Y. N. Ryabinin, N. N. Sobolev, A. M. Markevich and I. I. Tamm, *Zh. Eksp. Te. Fiz.* **23** (5), 564 (1952).
18. A. Hertzberg, H. S. Glick, W. E. Smith and W. Squire, *Modifications of the Shock Tube for the Generation of Hypersonic Flow*, Cornell Aeronautical Laboratory AEDC–TN–55–15 (March 1955).
19. J. Pomerantz, E. H. Winkler and A. E. Seigel, *Thermodynamic Properties and One-Dimensional Flow of a Partially Ionized Monatomic Gas*, Naval Ordnance Laboratory, NAVORD Report 4222 (1956).
20. L. I. Schiff, *Quantum Mechanics*, Ch. 10. McGraw-Hill, New York (1955).
21. J. Frenkel, *Wave Mechanics, Advanced General Theory*, p. 209, Oxford, New York (1934).
22. M. Stobbe, *Ann. Phys.* **7**, (5) 661 (1930).
23. W. Gordon, *Ann. Phys.* **2**, (5), 1031 (1929).
24. E. Fues, *Ann. Phys. Lpz.* **81**, (4), 281 (1926).
25. H. Bethe, *Handbuch der Physik* 24/1, Ch. 3, Berlin (1933).
26. L. McLean, *Phil. Mag.* **18**, 845 (1934).
27. D. H. Menzel and C. L. Pekeris, Absorption Coefficients and Hydrogen Line Intensities, *Mon. Not. Roy. Astr. Soc.*, **96**, 77–111 (1935).
28. L. H. Aller, *Astrophysics*, Ronald Press, New York (1953).
29. J. L. Hirschfelder, E. F. Curtiss and R. B. Bird, *Molecular Theory of Gases and Liquids*, p. 951, John Wiley, New York (1954).
30. R. V. Meghreblian, *Ph.D. Thesis*, California Institute of Technology, Pasadena, California (1953).
31. R. A. Alpher, *J. Fluid Mech.* **2**, 123 (1957).
32. J. W. Bond, Jr., *Phys. Rev.* **105**, 1683 (1957).
33. D. R. Inglis and E. Teller, *Astrophys J.* **90**, 439 (1939).
34. F. L. Mohler, *Astrophys. J.* **90**, 429 (1939).
35. David Bohm, *Quantum Theory*, p. 348, 458, 470. Prentice Hall, New York (1951).
36. J. Holtsmark, *Ann. Phys. Lpz.* **58**, 577 (1919).
37. R. G. Breene, Jr., Geophysical Research Paper No. 41, Geophysical Research Directorate, Cambridge, Mass. (1955).
38. J. Holtsmark, *Phys. Z.* **25**, 82 (1924).
39. S. Chandrasekhar, *Rev. Mod. Phys.* **15**, 1 (1943).
40. G. Ecker, *Z. Phys.* **148**, 593 (1957).
41. P. Debye and E. Hückel, *Phys. Z.* **24**, 185 (1923).
42. H. Hoffman and O. Theimer, *Astrophys. J.* **126**, 595 (1957).
43. L. Spitzer, Jr., R. S. Cohen and P. Routley, *Phys. Rev* **80**, 230 (1950).
44. B. Kivel, S. Bloom and H. Margenau, *Phys. Rev.* **98**, 495 (1955).

45. A. C. KOLB, *Theory of Hydrogen Line Broadening in High-Temperature Partially Ionized Gases*, ASTIA Doc. No. AD 115040 Univ. of Mich, Eng. Res. Inst. (1957).
46. A. UNSÖLD, *Ann. Physik.* **33**, 607 (1938).
47. A. UNSÖLD, *Z. Astrophys.* **24**, 355 (1948).
48. E. FERMI, *Z. Phys.* **26**, 54 (1924).
49. E. AMALDI and E. SEGRÉ, *Nuovo Cim.* (N.S.) **11**, 145 (1934).
50. C. FÜCHTBAUER *et al.*, *Z. Phys.* **90**, 403 (1934).
51. H. MARGENAU and D. KELLY, Abstract in *Bull. Amer. Phys. Soc.*, **2**, 67, (1957).
52. G. ECKER and W. WEIZEL, *Ann. Phys.* **17**, 126 (1956).
53. G. ECKER and W. WEIZEL, Zustandssumme und effektive Ionisierungsspannung im Inneren des Plasmas, *Z. Naturf.* **129**, 859–860 (1957).
54. CHARLES KITTEL, *Introduction to Solid State Physics*, p. 35, Wiley, New York (1953).
55. O. THEIMER, *Z. Naturf.* **129**, 518 (1957).
56. S. GASIOROWICZ, M. NEWMAN and R. J. RIDDELL, Jr., *Phys. Rev.* **101**, 922 (1956).
57. S. C. LIN, *Thesis*, Cornell University (1952).
58. I. SH. MODEL, *Soviet Phys., J. exp. theor. Phys.* **5**, 589 (1957).
59. S. CHANDRASEKHAR, *An Introduction to the Study of Stellar Structure*, The University of Chicago Press, Chicago (1939).
60. K. M. CASE, F. DE HOFFMAN and G. PLACZEK, Appendix A of *Introduction to the Theory of Neutron Diffusion*, Vol. I, Los Alamos Scientific Laboratory (1953).
61. T. S. WALTON, *Numerical Integration by a Method of Interlocked Parabolas*, NAVORD Report 3892, Naval Ordnance Laboratory (1957).

VOL.
1
1961

J. Quant. Spectrosc. Radiat. Transfer. Vol. 1, pp 249–257. Pergamon Press Ltd. Printed in Great Britain

THE COUPLING OF RADIATION AND CONVECTION IN DETACHED SHOCK LAYERS*

R. GOULARD†
Purdue University, Lafayette, Indiana

(*Received* 13 *February* 1961)

Abstract—Recent studies have shown that for sufficiently high re-entry speeds, radiation energy transfer from high temperature air becomes an appreciable part of the total energy transfer to the nose of the re-entry body. This note is concerned with the effects of this fluid energy loss on the energy distribution in the shock layer and, therefore, on the convective and radiative fluxes at the wall. A nondimensional parameter is shown to govern the resulting coupling between radiative and convective fluxes. The first approximation which consists in assuming a constant stagnation temperature layer is shown to be acceptable for most ballistic and earth satellite re-entry problems. For larger velocities or dimensions (e.g., planetary probes and heavy meteors), radiation losses become important and it is necessary to include the radiation terms into the equations which determine the flow field.

LIST OF SYMBOLS

a	radial velocity gradient in the shock layer (equation 1)
c_p	specific heat at constant pressure
E	$\rho_\infty U_\infty h_{es}$, energy flux across the shock (equation 13)
F	equation 14
h	specific enthalpy
Γ	energy ratio (equation 13)
q_c	convective heat flux to the wall
$\bar{q}_c$	dimensionless convection heat flux to the wall q_c/q_c°
q_R	radiant heat flux to the wall
$\bar{q}_R$	dimensionless radiant heat flux to the wall q_R/q_R°
r	radial coordinate (Fig. 1)
R	nose radius
$t, t_\circ$	time, initial time
T	absolute temperature
$\bar{T}$	T/T_{es}
u	radial component of the air velocity (Fig. 1)
U_∞	flight velocity

* The work described in this note was conducted by the author for the Bendix Corporation and was supported by the United States Army Rocket and Guided Missile Agency, under contracts Nos. DA-11-022-ORD-2642 and DA-11-022-ORD-3130.

† Consultant, Bendix Systems Division of Bendix Corporation.

V_E	maximum flight velocity during re-entry
w	air velocity component, normal to the wall (Fig. 1)
W/C_DA	weight–drag ratio
z	coordinate perpendicular to the wall (Fig. 1)
$\bar{z}$	z/δ
α, β	constant exponents (equation 15)
δ	shock layer thickness
θ_E	angle between the re-entry trajectory and the horizontal plane
$\varkappa$	mass absorption coefficient
ρ	density
σ	Stefan–Boltzman constant

Subscripts and superscripts

e	condition at the boundary layer edge
es	stagnation conditions
∞	upstream conditions
δ	conditions immediately behind the shock
$\circ$	stagnation approximation (constant properties across the boundary layer)

VOL.
1
1961

INTRODUCTION

THE advent of space flight has brought about the possibility of very high speed penetration of planetary atmospheres[1]. Such maneuvers communicate considerable energy to the gas particles lying in the path of the vehicle and radiative processes of appreciable intensity are likely to occur in the flow fields past the body. These radiation fluxes have been estimated for the stagnation flow of such man-made objects as ballistic missiles and planetary probes[2, 3].

In these estimates it was assumed that the radiation losses were only a small fraction of the total energy in the shock layer and that consequently, taking them into account would not appreciably affect the flow field. The properties of this flow field, notably temperature and density, were therefore determined on the basis of the familiar conservation equations, neglecting the radiation terms, and the calculation of the radiation losses was based on their value.

It is apparent, however, that for increasing velocities, the radiation losses from any group of particles streaming past the body are becoming an increasing fraction of their total energy. As a result of this cooling effect, one can expect lower flow field temperatures and consequently lower radiation fluxes than calculated for an adiabatic (loss-less) shock layer. The purpose of this note is to try to estimate this effect.

THE INCOMPRESSIBLE SHOCK LAYER MODEL

An accurate estimate of the stagnation flow field, cumbersome as it is for nonradiative media[4, 5], becomes quite intricate when radiation fluxes are included. In general, the difficulty lies in the integral character of the radiation term that must be included into the already complex set of coupled differential equations of mass, momentum and energy.

Physically, this means that the energy balance of each elementary volume of the flow field is conditioned by long range contributions from all other elementary volumes throughout the shock layer.

In this paper, radiation losses will be considered only as a perturbation to the exact

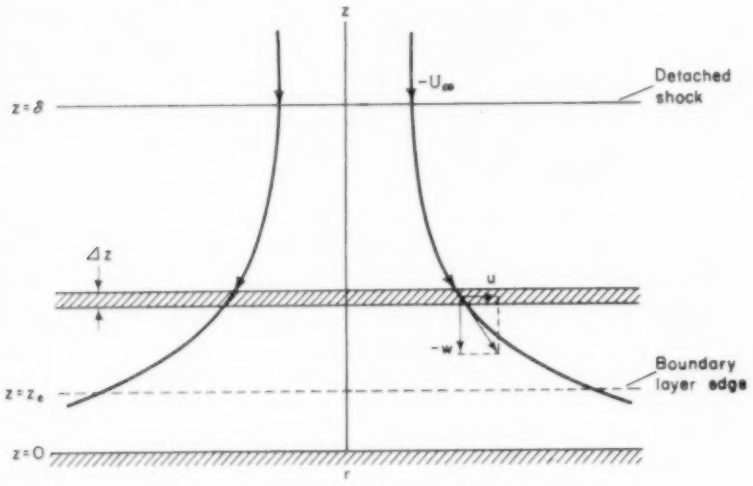

FIG. 1. Detached shock layer flow at stagnation.

nonradiant shock layer solutions[4–6]; we will make use of three important features of these solutions in the stagnation area (Fig. 1)*:

a) The shock layer thickness δ is much smaller at very high speeds than the radius R of the body $\left(\frac{\delta}{R} \simeq \frac{1}{20}\right)$.

The shock layer will therefore be considered as a plane parallel layer in the stagnation zone.

b) The shock layer is nearly incompressible in the stagnation area:

$$\rho_{es} = \text{const.}$$

c) The velocity component along the axis of the body is nearly proportional to the distance from the surface of the body[4, 6]:

$$w \equiv \frac{dz}{dt} = -2az. \tag{1}$$

The value of the parameter a will be chosen to satisfy the conservation of momentum principle in the z direction across the shock:

$$a = -\frac{w_\delta}{2\delta} = -\frac{1}{2}\frac{\rho_\infty U_\infty}{\rho_{es}\delta} \tag{2}$$

* The skillful help of T. Chen and R. Murabayashi in the calculations and the illustrations shown in this paper is gratefully acknowledged.

This value of a is in fair agreement with exact calculated values[6] and in particular with those of VAGLIO-LAURIN and FERRI[4]. We also note the close similarity between actual shock layer flow at stagnation and the classical potential flow.

THE TEMPERATURE DISTRIBUTION IN THE SHOCK LAYER

An interesting property of this incompressible stagnation flow model, from the standpoint of the mathematics of radiation (and also of those of chemical kinetics), is that for both inviscid and viscous cases[7], the time history of the particles is dependent on the coordinate z and *not* on the coordinate r (equation 1).

Therefore, all particles entering the shock layer at a time $t_\circ$ will be at z at a time t, such that:

$$t - t_\circ = -\frac{1}{2a} \ln \frac{z}{\delta} \tag{3}$$

These particles form a thin infinite layer of thickness Δz which loses its energy at the rate: $(\rho \, \Delta z) \dfrac{dh}{dt}$ per unit area. The radiative losses are made of the fluxes *towards* the wall and *away* from it. Their total value per unit area[8] is $2\,(2\,\rho\,\varkappa\,\sigma\,T^4)\Delta z$ where $\varkappa$ is the mass absorption coefficient of the gas.* No self-absorption is expected from this optically thin medium[8].

Also a look at hypersonic flow charts[9] shows that for body velocities higher than 20 kft/sec, the kinetic energy in the shock layer is always a small fraction ($< 4\%$) of the total energy, decreasing further[9] when the velocity of the body increases to values of interest in this study (35 kft/sec).

For the inviscid flow in the stagnation area (kinetic energy neglected), the principle of conservation of energy is therefore satisfied if the following two fluxes compensate† each other:

$$-\rho \frac{\mathrm{d}h}{\mathrm{d}t} = 4\,\rho\,\varkappa\,\sigma\,T^4 \tag{4}$$

Elimination of the time variable between equations (1) and (4) yields:

$$\frac{\mathrm{d}z}{z} = \frac{2\,a\,\rho\,\mathrm{d}h}{4\,\rho\,\varkappa\,\sigma\,T^4} \tag{5}$$

Since for any gas in chemical equilibrium, the enthalpy h is a known function of the temperature T, equation (5) gives implicitly a distribution $T(z)$ across the shock layer. It is also possible to bring out the shock layer thickness δ into equation (5) by using equation (2):

$$\frac{\mathrm{d}z}{z} = \frac{\rho_\infty\,U_\infty\,\mathrm{d}h}{4\,\rho_{es}\,\varkappa\,\delta\,\sigma\,T^4} \tag{6}$$

Equation (6) can be rearranged as follows:

$$\frac{\mathrm{d}z}{z} = \frac{\rho_\infty\,U_\infty\,h_{es}}{4\,\rho_{es}\,\varkappa_{es}\,\delta\,\sigma\,T^4_{es}} \frac{\varkappa_{es}}{\varkappa} \frac{T^4_{es}}{T^4} \frac{c_p \mathrm{d}T}{h_{es}} \tag{7}$$

* Note that $2\,\rho\,\varkappa = \dfrac{\varepsilon}{L}$, this latter quantity being tabulated for air in [13].

† Since, in all practical cases, the wall is assumed much cooler than the gas, its radiative emission to the gas layer will be neglected, regardless of its emissivity coefficient.

The first fraction on the right-hand side contains all the constant parameters characteristic of the problem under study. Its numerator E is the flux of total energy crossing the shock and its denominator q°_R is the flux of energy radiated by an infinite plane layer of thickness δ at uniform stagnation temperature T_{es}, across *both* its limiting planes.

This dimensionless ratio $\frac{q^{\circ}_R}{E}$ is denoted by Γ in this study; its role in radiant gas dynamics has already been recognized in their application to the problems of stellar turbulence[10] and radiant heat exchange[11]:

$$\Gamma = \frac{q^{\circ}_R}{E} = \frac{4\,\rho_{es}\,\varkappa_{es}\,\delta\,\sigma\,T^4_{es}}{\rho_{\infty}\,U_{\infty}\,h_{es}} \tag{8}$$

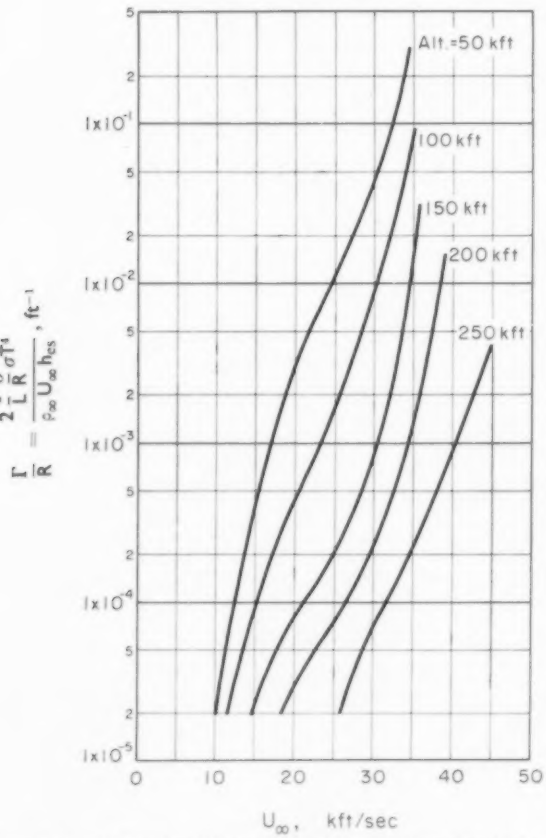

FIG. 2. Energy ratio vs. velocity for different altitudes (assuming chemical equilibrium).

The values of Γ for re-entry stagnation equilibrium conditions are shown on Figs. 2 and 3. They were calculated* using the emissivity estimates of [13].

* The value of δ used in the calculations of Γ is that derived in reference [12] for hemispherical noses: $\frac{\delta}{R} = 0{\cdot}666\left[\frac{\rho_{es}}{\rho_{\infty}} - 1\right]^{-1}$.

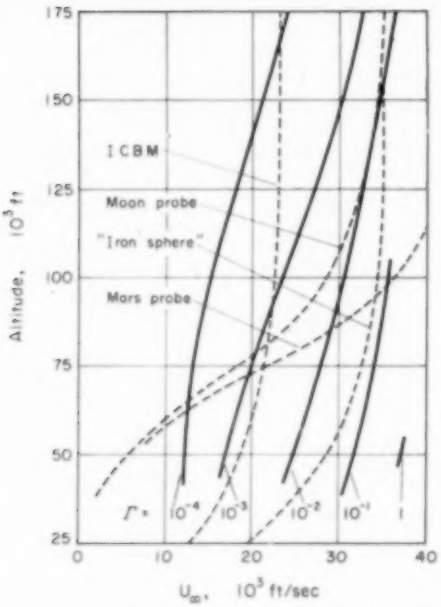

FIG. 3. Curves of constant ratio, $\Gamma = q''_R/E$ for a hemispheric nose ($R = 1$ ft) shock layer.

Coming back to equation (7), the other fractions on the right-hand side represent in dimensionless form $F(T, T_{es})$, the variation of the temperature dependent properties, when T deviates from its stagnation value T_{es}:

$$\frac{dz}{z} = \Gamma^{-1} F(T, T_{es}) \tag{9}$$

In general $F(T, T_{es})$ is not a closed function of T and equation (14) must be solved numerically. In many re-entry applications, however, a further simplification is possible:

THE CASE WHERE $\Gamma << 1$

A look at Fig. 3 shows that in many re-entry applications, Γ is small. In this case, the solution of equation (9) is not likely to yield large variations of temperature. We can then, in $F(T, T_{es})$, approximate the fluctuations of thermal properties from their stagnation value by power functions of temperature:

$$\frac{c_p}{c_{p,es}} = \left(\frac{T}{T_{es}}\right)^{\alpha}, \frac{\varkappa}{\varkappa_{es}} = \left(\frac{T}{T_{es}}\right)^{\beta}, \frac{\rho_{es}}{\rho} \simeq \frac{T}{T_{es}} \tag{10}$$

where the average specific heat $\bar{c}_p$ is defined by the identity: $h \equiv \bar{c}_p T$. Introducing also the nondimensional quantities $\overline{T} = \dfrac{T}{T_{es}}$ and $\bar{z} = \dfrac{z}{\delta}$, equation (9) becomes:

$$\frac{d\bar{z}}{\bar{z}} = \Gamma^{-1} \overline{T}^{\alpha-\beta-4} d\overline{T} \tag{11}$$

and after integration and determination of the integration constant at the shock:

$$\bar{T} = [1 + (\alpha - \beta - 3)\,\Gamma \ln \bar{z}]^{\frac{1}{\alpha-\beta-3}} \tag{12}$$

The total heat flux to the wall is the summation of the fluxes from all the elementary layers of thickness dz:

$$q_R = \int_0^{\delta} dq_R = \int_0^{\delta} 2\,\rho\,\varkappa\,\sigma\,T^4\,dz \tag{13}$$

or, in nondimensional form:

$$q_R = 2\,\rho_{es}\,\varkappa_{es}\,\delta\,\sigma\,T^4{}_{es} \int_0^1 \frac{\rho\,\varkappa}{\rho_{es}\,\varkappa_{es}} \left(\frac{T}{T_{es}}\right)^4 d\bar{z}$$

$$= q^\circ{}_R \int_0^1 \bar{T}^{\beta+3}\,d\bar{z}$$

Introducing a dimensionless flux $\bar{q}_R = q_R/q^\circ{}_R$ and replacing $\bar{T}$ by its value from equation (12):

$$\bar{q}_R = \frac{q_R}{q^\circ{}_R} = \int_0^1 [1 + (\alpha - \beta - 3)\,\Gamma \ln \bar{z}]^{\frac{\beta+3}{\alpha-\beta-3}}\,d\bar{z} \tag{14}$$

Since Γ is assumed to be small, we can expand both equation (12) and the integrand of equation (14) as Newton polynomials, and neglect the terms in powers of Γ higher than one. Equation (14) becomes:

$$\bar{q}_R = 1 + (\beta + 3)\,\Gamma \left[\lim_{\bar{z}\to 0} \int_{\bar{z}}^1 \ln \bar{z}\,d\bar{z}\right]$$

and the nondimensional radiation flux and temperature (equations 12 and 14) can finally be written:

$$\bar{q}_R = 1 - (\beta + 3)\,\Gamma \tag{15}$$

$$\bar{T} = 1 + \Gamma \ln \bar{z} \tag{16}$$

Another convenient formulation is that of the nondimensional deviations from the stagnation values:

$$\Delta\bar{q}_R = \frac{q_R - q^\circ{}_R}{q^\circ{}_R} = -(\beta + 3)\,\Gamma \tag{17}$$

$$\Delta\bar{T} = \frac{T - T_{es}}{T_{es}} = (\ln \bar{z})\,\Gamma \tag{18}$$

which are both clearly proportional to Γ.

CONVECTION AND RADIATION FLUXES

Equation (16) shows that because of the continuing radiation losses, the closer the particles get to the wall, the lower their temperature is. The temperature at the outer edge

of the viscous boundary layer must then be lower than the stagnation temperature. As a result, the convective heat transfer is expected to be reduced because of the presence of radiation.

As a first estimate, since radiation is proportional to the mass of the radiant medium, and even more dependent on temperature, the thin and cool boundary layer can be treated as if it were nonradiant.* Its calculated thickness z_e in the case of a nonradiant gas (see for instance[14], can also be used in equation (16) to determine the outer edge temperature. The convective energy transfer can then be estimated on this basis.

Both radiative fluxes q_R and boundary layer edge temperature T_e have been calculated in four typical re-entry trajectories. These trajectories are shown on Fig. 3. The values of $\bar{q}_R$ and $\bar{T}_e$ corresponding to the maximum value of Γ for each trajectory, are shown on Table 1 for a nose radius of one foot ($\beta \simeq 7$, $\bar{z}_e \simeq 0{\cdot}04$ and $\ln \bar{z}_e \simeq -3{\cdot}2$). Also shown is the dimensionless convection heat flux to the wall $\bar{q}_c = q_c/q^\circ_c$. The flux q_c is roughly proportional to the enthalpy h_e at the boundary layer edge[6] and its deviations from the stagnation value q°_c can therefore be readily calculated† from those of T_e with the help of a Mollier Chart for air[9].

TABLE 1.

Re-entry trajectory ($R = 1$ ft)	Γ_{max}	$\bar{q}_R$	$\bar{T}_e$	$\bar{q}_c$
$\theta_E = 20°$, $V_E = 23{,}000$ ft/sec, $W/C_DA = 900$ lbs ft^{-2} (ICBM)	2×10^{-3}	0·98	0·994	0·986
$\theta_E = 90°$, $V_E = 35{,}000$ ft/sec, $W/C_DA = 32$ lbs ft^{-2} (moon probe)	10^{-2}	0·90	0·97	0·93
$\theta_E = 90°$, $V_E = 35{,}000$ ft/sec, $W/C_DA = 160$ lbs ft^{-2} ("iron sphere")	5×10^{-2}	0·50	0·84	0·75
$\theta_E = 90°$, $V_E = 45{,}000$ ft/sec, $W/C_DA = 32$ lbs ft^{-2} (Mars probe)	assumption $\Gamma \ll 1$ not applicable			

CONCLUSION

Three conclusions can be drawn from Table 1 and from the form of equations (15) to (18):

1) The radiation flux in the forward direction and to the wall is, in principle, less than the quantity q°_R calculated in first approximation assuming $T = T_{es}$ throughout the layer.
2) The temperature at the edge of the boundary layer is, in principle, less than the stagnation temperature. A smaller convective flux at the wall is therefore expected. This coupling between radiation and convection is also apparent in static[8] and viscous[15] cases.
3) Calculation of radiative and convective transfer rates by assuming the temperature of the inviscid shock layer constant throughout ($\bar{q}_R = 1$, $\bar{T} = 1$), is a first order approximation to the result (equations (15) and (16)); the extent of this overestimation depends on the magnitude of Γ and on the boundary layer thickness.

* Flow contamination by the wall is not considered here.

† To help interpret the nondimensional data in Table 1, the reader is reminded that, according to estimates[2], $q^\circ_R \simeq \frac{1}{10} q^\circ_c$ for the first case in the table, $q^\circ_R \simeq q^\circ_c$ for the second case and $q^\circ_R > q^\circ_c$ for the last two cases.

In the case of air, large values of Γ correspond to high velocities, large nose radii and low altitudes. From the estimates of this paper, it appears that for ballistic and earth satellite trajectories, MEYEROTT's and KIVEL's first approximations[2, 3] are justified for nose radii of the order of one foot or less. The study of the atmospheric penetration of most planetary probes and heavy meteors present more difficulty: it will be necessary to include the radiation terms into the equations which determine the flow past the body, in order to account for radiation losses and self-absorption. For intermediate cases, such as that of a moon probe, the approximation suggested in this paper should be adequate.

REFERENCES

1. C. GAZLEY, Jr., The Penetration of Planetary Atmospheres, Transactions of the ASME, *J. Heat Transfer* **81**, Series C, No. 4, p. 315 (1959).
2. R. E. MEYEROTT, *Radiation Heat Transfer to Hypersonic Vehicles*, Third AGARD Combustion and Propulsion Panel Colloquium, Palmermo, Sicily (1958).
3. B. KIVEL, Radiation from Hot Air and Stagnation Heating, *J. Aero. Sci.* **28**, 2 (1961).
4. R. VAGLIO-LAURIN and A. FERRI, Theoretical Investigation of the Flow Field about Blunt Nosed Bodies in Supersonic Flight, *J. Aero. Sci.* **25**, 12 (1958).
5. F. G. GRAVALOS, *et al.*, *The Supersonic Flow about a Blunt Body of Revolution for Gases at Chemical Equilibrium*, Ninth International Astronautical Congress (Amsterdam 1958), Springer Verlag, Vienna (1959).
6. W. D. HAYES and R. F. PROBSTEIN, *Hypersonic Flow Theory*, p. 238–240, Academic Press, New York (1959).
7. H. SCHLICHTING, *Boundary Layer Theory*, p. 73, McGraw-Hill, New York (1955).
8. R. and M. GOULARD, One-Dimensional Energy Transfer in Radiant Media, *Int. J. Heat Mass Transfer*, **1**, 81–91 (1960).
9. S. FELDMAN, *Hypersonic Gas Dynamic Charts for Equilibrium Air*, AVCO Research Report 40 (1957).
10. A. UNSÖLD, *Physik der Sternatmosphären*, Springer Verlag, Vienna (1955).
11. V. N. ADRIANOV and S. N. SHORIN, Radiative Transfer in the Flow of a Radiating Medium, *Izv. Akad. Nauk SSSR, OTN*, 1958, **5**, 46. (Translation available from Purdue University, School of Aeronautical and Engineering Sciences, Lafayette, Indiana).
12. H. SERBIN, Supersonic Flow Around Blunt Bodies, *J. Aero. Sci.*, Readers' Forum, **25**, 58 (1958).
13. B. KIVEL and H. BAILEY, *Tables of Radiation from High Temperature Air*, AVCO Research Laboratory RR 21 (1957).
14. S. M. SCALA and C. W. BAULKNIGHT, Transport and Thermodynamic Properties in a Hypersonic Laminar Boundary Layer—Part II—Applications, *Amer. Roc. Soc. J.*, **30**, no. 4, p. 329 (1960).
15. J. P. GUIRAUD, Ecoulement plan de Couchette d'un gaz rayonnant, *C. R. Acad. Sci., Paris*, **250**, 2997 (1960).

J. Quant. Spectrosc. Radiat. Transfer, Vol. 1, pp. 258–268. Pergamon Press Ltd. Printed in Great Britain

APPROXIMATE CONTINUOUS OPACITY CALCULATIONS FOR POLYELECTRONIC ATOMS AT HIGH TEMPERATURES*

R. A. PAPPERT and S. S. PENNER†
Physics Section, Convair
A Division of General Dynamics Corporation, San Diego, California

(*Received* 5 *July* 1961)

Abstract—Approximate formulas derived by Raizer (and modifications thereof) for the Rosseland and Planck mean absorption coefficients in high-temperature gases have been compared with Armstrong's results for nitrogen at 5 and 20 eV for densities varying between $\simeq 5 \times 10^{20}$ cm^{-3} and $\simeq 5 \times 10^{15}$ cm^{-3}. Comparison has also been made with results obtained by Bernstein and Dyson for the Rosseland mean of fluorine at 10 eV in the density range $\simeq 10^{21}$ cm^{-3} to 10^{18} cm^{-3}. The modified Raizer formulas are consistently better approximations than the expressions obtained by Raizer and agree within about a factor of two with the results derived from numerical calculations.

1. INTRODUCTION

RADIATIVE transfer plays a significant, perhaps even dominant, part in the problems of energy exchange associated with high-temperature phenomena. In some cases, the calculation of Rosseland and Planck (emission) means is of importance. For heavy elements, the individual transitions which contribute to the opacity are so numerous that statistical methods must be used. Such methods have been discussed by MAYER[1] and have been extensively applied by BRODE.[2] The labor involved in carrying through these statistical methods is quite extensive and it is therefore desirable to obtain a simplified, approximate procedure for estimating the opacity under a wide variety of conditions. A useful method for calculating the continuous opacity which results from bound-free and free-free transitions has been given by RAIZER.[3] Unfortunately, Raizer made large errors in his numerical calculation of opacities. In our discussion we will stress the wide applicability of Raizer's technique and refine both his methods and numerical work.

In section II, we give a slightly modified and consistent interpretation of Raizer's model. ARMSTRONG's[4] values for the Rosseland and Planck means for nitrogen at 5 and 20 eV and for the number density range $\simeq 5 \times 10^{20}$ cm^{-3} to 5×10^{15} cm^{-3} have been compared with the values computed with Raizer's formulas (denoted by R) and the modified version of Raizer's formulas (denoted by MR) given in section II. We have also checked the (R) and (MR) formulas for the Rosseland mean against calculations by BERNSTEIN and DYSON[5] for fluorine in the number density range $\simeq 10^{21}$ cm^{-3} to $\simeq 10^{18}$ cm^{-3} at 10 eV.‡ In these

* This research was supported by the Advanced Research Projects Agency under Contract No. AF 49(638)–855, monitored by the Air Force Office of Scientific Research of the Air Research and Development Command.

† Consultant; permanent address: Division of Engineering, California Institute of Technology, Pasadena, California.

‡ We have discounted the Bernstein–Dyson data at 5 eV since omission of the weakly bound levels has presumably led to an underestimate, by about a factor of 3, of the oxygen and nitrogen opacity at this temperature (private communication from John Stewart, General Dynamics/General Atomic). However, the data at 10 eV appear to be sufficiently accurate for making comparisons.

VOL. 1 1961

cases, the (MR) formulas are the better approximations; agreement with the numerical data is good to within about a factor of two.

To illustrate that a certain measure of caution is required in applying the approximate formulas, we have made a comparison between the Bernstein–Dyson data for beryllium at 10 eV and the (R) and (MR) formulas. In this case, the (MR) formula is superior to the (R) formula but it leads nevertheless to results which differ by about a factor of 10 from the Bernstein–Dyson data. The apparent reason for this discrepancy (as discussed in section III) is the existence of a "window". Quite generally, the more proliferous the levels, the better the approximation scheme. Thus the theoretical formulas should apply reasonably well to high Z elements.

It should perhaps be emphasized that the approximation formulas allow only for the continuous opacity. At sufficiently low densities, the bound-bound contributions are expected to be negligibly small; however, at higher densities, the bound-bound contributions may become significant.* This problem deserves special attention and is beyond the scope of the present discussion.

II. APPROXIMATE CONTINUOUS OPACITY FORMULAS

The total linear absorption coefficient associated with the bound-free contribution from an m-ion (i.e., an m times ionized atom) and the free-free contribution from an $(m+1)$ ion may be written as[3, 6]

$$\varkappa_m(x) = aN_m(m+1)^2\,\Theta^{-2}\,e^{-x_{1m}}\,F_m(x) \tag{1}$$

where

$$a = \frac{16\pi^2}{3\sqrt{3}}\,\frac{e^6}{ch}\,(1{\cdot}6\times10^{-12})^{-2} \simeq 7{\cdot}3\times10^{-16}\ \text{cm}^2-(\text{eV})^2,\quad x=\frac{h\nu}{\Theta},\quad x_{1m}=\frac{I_m}{\Theta}. \tag{2}$$

I_m is the ionization potential of the m-ion, N_m is the number density (cm^{-3}) of m-ions in the ground state,† and Θ is the temperature in electron volts (in this paper, all energies are expressed in electron volts). In the following calculations, the ionization potentials have been taken from MOORE.[7] For atoms and ions more complicated than those treated here, the labor involved is increased because of the necessity of estimating the ionization potentials of the contributing ions. For the excited states, the hydrogenic approximation is made. Thus, the frequency-dependent factor is given by [3, 6]

$$F_m(x) = x^{-3}\left[2x_{1m}\sum n^{-3}\exp\left(\frac{x_{1m}}{n^2}\right)+1\right]. \tag{3}$$

The first term in the brackets represents the bound-free contribution, while the second term represents the free-free contribution to the absorption coefficient. In an ionized gas containing m-ions with $m = 0, 1, 2 \ldots$, the total continuum absorption coefficient is finally obtained by summing the contributions made by the separate m-ions. Thus,

$$\varkappa(x) = a\Theta^{-2}\sum_m N_m\,(m+1)^2\,e^{-x_{1m}}\,F_m(x)\,. \tag{4}$$

---

* John Stewart has informed us that preliminary results for oxygen at densities $\simeq 10^{20}$ cm^{-3} indicate that the bound-bound transitions contribute about two-thirds of the total opacity and that the fall off of the bound-bound contributions at lower densities is quite slow.

† For all practical purposes, N_m equals the total number of m-ions per unit volume.

For conventional calculations of radiative energy transfer, equation (4) is used to compute the Planck ($\bar{\varkappa}_{p1}$) and Rosseland ($\bar{\varkappa}_R$) mean absorption coefficients. The Rosseland mean free path is then defined by

$$\ell_R = \frac{1}{\bar{\varkappa}_R} = \int_0^\infty \frac{G(x)\mathrm{d}x}{\varkappa(x)\,(1 - \mathrm{e}^{-x})}\,,\; G(x) = \frac{15}{4\pi^4}\,\frac{x^4\mathrm{e}^{-x}}{(1 - \mathrm{e}^{-x})^2}\,, \tag{5}$$

and the reciprocal of the Planck mean free path is given by

$$\ell_{p1}^{-1} = \bar{\varkappa}_{p1} = \int_0^\infty \varkappa(x)(1 - \mathrm{e}^{-x})\, G_1(x)\mathrm{d}x,\; G_1(x) = \frac{15}{\pi^4}\,\frac{x^3}{(\mathrm{e}^x - 1)}\,. \tag{6}$$

RAIZER[3] has performed an approximate evaluation for the mean free paths ℓ_{p1} and ℓ_R by utilizing the fact that configuration splitting of the $2n^2$ degenerate hydrogenic levels makes plausible the replacement of the sum over n, which occurs in equation (3), by an integration. That is,

$$\sum \frac{2x_{1m}}{n^3} \exp\left(\frac{x_{1m}}{n^2}\right) \to \int_0^x \mathrm{e}^y\,\mathrm{d}y = \mathrm{e}^x - 1,\; x < x_{1m}\,, \tag{7}$$

whence

$$F_m(x) \simeq x^{-3}\,\mathrm{e}^x \text{ for } x < x_{1m}\,. \tag{8}$$

Thus, for the case in which the energy of the incident photon is less than the ionization potential of the m-ion, the frequency dependent factor $F_m(x)$ is a universal function of x.

For $x > x_{1m}$, Raizer assumes that the dominant role is played by the ground level $n = 1$.

Thus,

$$F_m(x) \simeq 2x_{1m}\,x^{-3} \exp(x_{1m}),\; x > x_{1m}\,. \tag{9}$$

The Planck mean absorption coefficient is now evaluated from equation (6), viz.,

$$\ell_{p1}^{-1} = \bar{\varkappa}_{p1} = \frac{45a}{\pi^4\Theta^2} \sum_m N_m(m+1)^2 x_{1m} \exp(-x_{1m})\,. \tag{10}$$

An explicit evaluation of ℓ_R is not possible without further simplification. However, it is generally a reasonable assumption that the dominant contribution to $\bar{\varkappa}_R$ comes from $x < x_{1m}$; it should be noted that this is definitely not the case for the Planck mean, which by virtue of the definition given in equation (6), is quite sensitive to the high energy photons —in fact, two-thirds of the contribution to $\bar{\varkappa}_{p1}$ in equation (10) comes from $x > x_{1m}$. Use of equation (8) for all values of x leads to the expression

$$\ell_R = \frac{0{\cdot}87\Theta^2}{a}\left[\sum_m N_m(m+1)^2 \exp(-x_{1m})\right]^{-1}. \tag{11}$$

To obtain explicit relations for ℓ_{p1} and ℓ_R, it is now necessary to evaluate the sum over the m-ions. A rigorous evaluation of the sums appearing in equations (10) and (11) requires the determination of N_m with proper allowance for each of the equilibria

$$N_m \rightleftarrows N_{m+1} + \mathrm{e}^-\,. \tag{12}$$

Instead of solving the complete set of simultaneous Saha equations, RAIZER[8] made the

observation that the mean number of electrons per atom is given, approximately, by the relationship

$$I_{\bar{m}-1/2} = \Theta \, \text{fn} \left(\frac{A \, \Theta^{3/2}}{N \bar{m}} \right) \tag{13}$$

where

$$A = 2 \left(\frac{2\pi m_e (1{\cdot}6 \times 10^{-12})}{h^2} \right)^{3/2} \simeq 6{\cdot}0 \times 10^{21} \text{ cm}^{-3} - \text{eV}^{-3/2}$$

and

N = total number density (cm^{-3}).

As before, Θ is the temperature in electron volts. The function I_m is plotted graphically by drawing a continuous curve through the discrete points I_m. In our notation, I_0 corresponds to the ionization level of the neutral atom. Representative curves showing the comparison

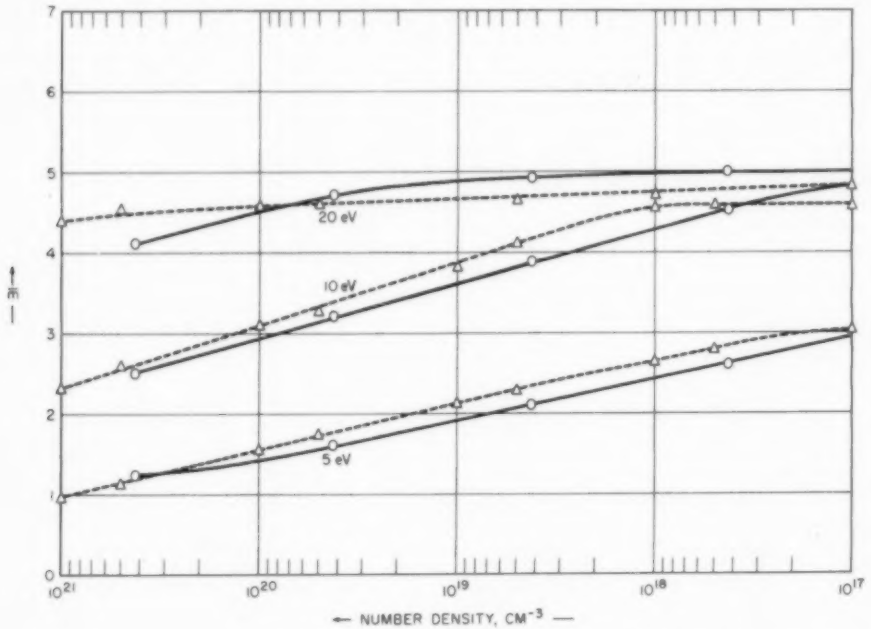

FIG. 1. Average number of electrons per atom ($\bar{m}$) for nitrogen as a function of number density N (in cm^{-3}) at various temperatures. (The dotted curve refers to results derived from Raizer's approximation (see equation 13); the solid curve is based on ARMSTRONG's data[41]).

between $\bar{m}$ as determined from equation (13) for nitrogen, and the corresponding values found by Armstrong by solving the complete set of Saha equations, are given in Fig. 1 for $\Theta = 5$, 10, and 20 eV and for number densities ranging between $\simeq 5 \times 10^{20}$ cm^{-3} and 10^{17} cm^{-3}. In view of the simplicity of the approximation, the agreement must be considered to be satisfactory.

Raizer next evaluated the sums appearing in equations (10) and (11) by replacing the

sum by an integral and N_m by $N\delta(m - \overline{m})$ where δ denotes the Dirac delta function. This scheme, along with the convention

$$x_{1\overline{m}-1/2} = I_{\overline{m}-1/2}/\Theta\,,$$

leads to the following expressions for the Rosseland and Planck means, respectively:

$$\ell_R \simeq \frac{7{\cdot}2 \times 10^{36}\,\Theta^{7/2}}{N^2\,\overline{m}\,(\overline{m}+1)^2} \tag{14}$$

and

$$\ell_{pl} \simeq \frac{1{\cdot}8 \times 10^{37}\,\Theta^{9/2}}{N^2\,\overline{m}(\overline{m}+1)^2\,I_{\overline{m}-1/2}}\,. \tag{15}$$

These are the equations derived by Raizer.

We prefer to regard the empirical relation introduced in equation (13) as being consistent with the Saha equation*

$$\frac{N_{m+1}}{N_m}\,N_e = \mathrm{A}\,\Theta^{3/2}\exp\left(-\frac{I_m}{\Theta}\right) \tag{16}$$

in the following sense: the hypothetical ion species corresponding to $m = \overline{m} + (1/2)$ and $m = \overline{m} - (1/2)$ are equal in number. This statement is clearly in accordance with equation (13) since $N_e = \overline{m}N$. Using equation (16), it is now possible† to rewrite the sums occurring in equations (10) and (11), viz.,

$$\sum_m N_m(m+1)^2\,x_{1m}\exp(-x_{1m}) = \frac{N\overline{m}}{\mathrm{A}\Theta^{3/2}}\sum_m N_{m+1}(m+1)^2\,x_{1m} \tag{17}$$

and

$$\sum_m N_m(m+1)^2\exp(-\,x_{1m}) = \frac{N\overline{m}}{A\,\Theta^{3/2}}\sum_m N_{m+1}(m+1)^2\,. \tag{18}$$

It also follows from equation (16) that

$$\frac{N_{\overline{m}+3/2}}{N_{\overline{m}+1/2}} = \exp\left(\frac{I_{\overline{m}-1/2} - I_{\overline{m}+1/2}}{\Theta}\right) = \exp(x_{1\overline{m}-1/2} - x_{1\overline{m}+1/2})\,. \tag{19}$$

and

$$\frac{N_{\overline{m}-3/2}}{N_{\overline{m}-1/2}} = \exp\left(\frac{I_{\overline{m}-3/2} - I_{\overline{m}-1/2}}{\Theta}\right) = \exp(x_{1\overline{m}-3/2} - x_{1\overline{m}-1/2})\,. \tag{20}$$

Since the exponentials appearing in equations (19) and (20) are generally much smaller than unity, we have, in good approximation,

$$N_{\overline{m}+1/2} = N_{\overline{m}-1/2} = \frac{N}{2}\,. \tag{21}$$

Thus, for all practical purposes, only two terms [$m = \overline{m} - (3/2)$ and $m = \overline{m} - (1/2)$] contribute to the sums in equations (17) and (18). We thus find the following result for the sum occurring in the expression for the Planck mean:

$$\sum_m N_m(m+1)^2\,x_{1m}\exp(-\,x_{1m}) \simeq \frac{N^2\overline{m}}{2A\Theta^{3/2}}[(\overline{m}-1/2)^2\,x_{1\overline{m}-3/2} + (\overline{m}+1/2)^2\,x_{1\overline{m}-1/2}]\,. \tag{22}$$

* In the spirit of the present approximation, the statistical weight factors are omitted.

† The authors are greatly indebted to Mr. R. Vik of the Convair Physics Section for pointing out the correct evaluation of the sums appearing in equations (17) and (18).

Similarly, the sum occurring in the expression for the Rosseland mean is

$$\sum_m N_m(m+1)^2 \exp(-x_{1m}) \approx \frac{N^2\bar{m}}{A\Theta^{3/2}}(\bar{m}^2+1/4)\,. \tag{23}$$

Insertion of these expressions into equations (10) and (11) leads to the following approximations for the Rosseland and Planck means:

$$\ell_R = \frac{7{\cdot}2\times10^{36}\,\Theta^{7/2}}{N^2\bar{m}(\bar{m}^2+1/4)}\,, \tag{24}$$

$$\ell_{p1} = \frac{3{\cdot}6\times10^{37}\,\Theta^{7/2}}{N^2\bar{m}[(\bar{m}-1/2)^2\,x_{1\bar{m}-3/2}+(\bar{m}+1/2)^2\,x_{1\bar{m}-1/2}]}\,. \tag{25}$$

Equations (24) and (25) are the modified Raizer formulas.

III. RESULTS AND CONCLUSIONS

Equations (14), (15), (24), and (25) have been compared with Armstrong's results for the Rosseland and Planck means for nitrogen at 5 and 20 eV and for the number density range $\simeq 5\times10^{20}$ cm^{-3} to 5×10^{15} cm^{-3}. The results derived from equations (14) and (24) have been checked with the Dyson–Bernstein data for fluorine at 10 eV in the density range $\simeq 10^{21}$ cm^{-3} to $\simeq 10^{18}$ cm^{-3}. The relevant plots are shown in Figs. 2 through 6. It is seen that the modified Raizer formulas are the better approximation formulas and give

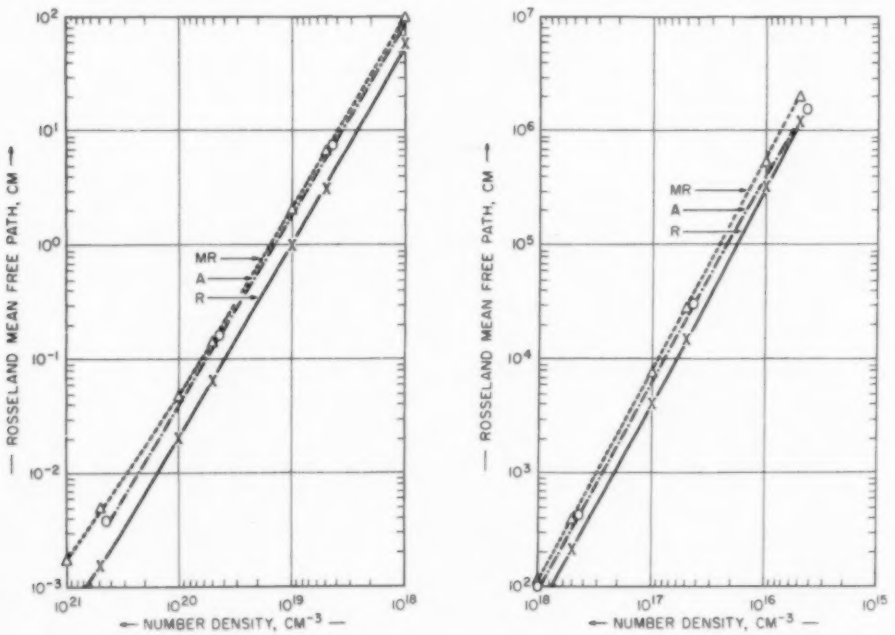

FIG. 2. The Rosseland mean free path (in cm) as a function of number density (in cm^{-3}) for nitrogen at 5 eV. (The symbols (A), (R) and (MR) identify results obtained by Armstrong (A) and derived from Raizer (R) and modified-Raizer (MR) approximations, respectively).

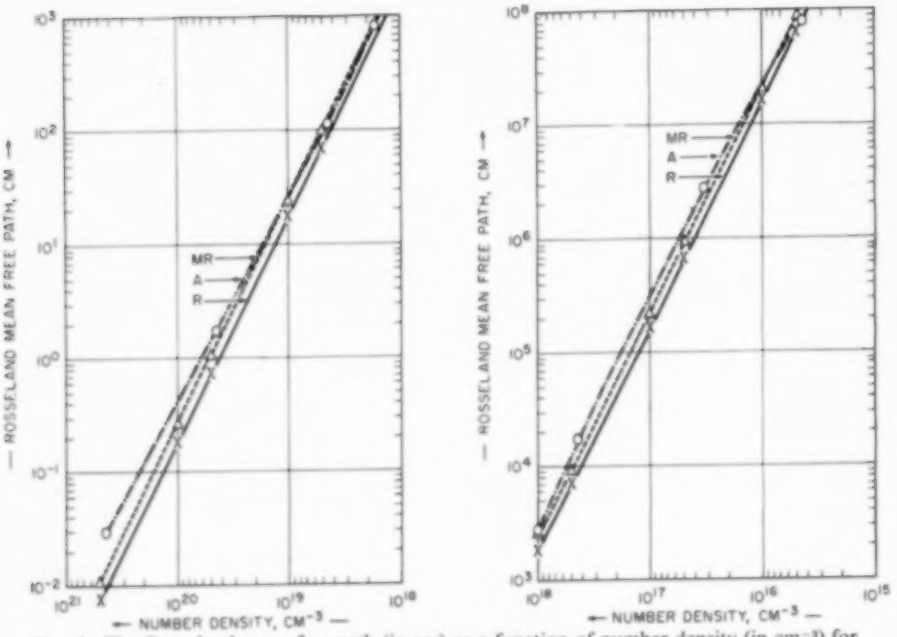

FIG. 3. The Rosseland mean free path (in cm) as a function of number density (in cm^{-3}) for nitrogen at 20 eV.

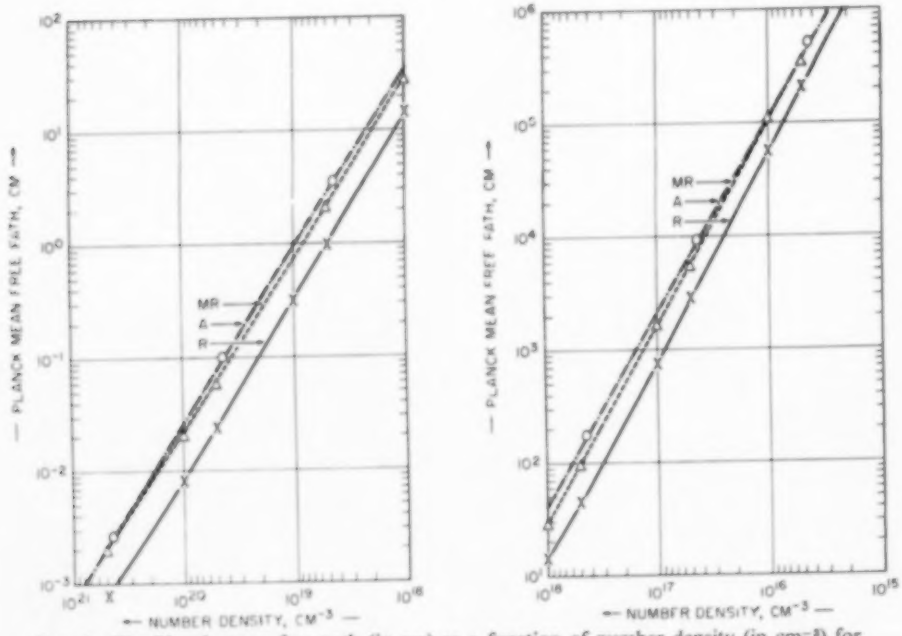

FIG. 4. The Planck mean free path (in cm) as a function of number density (in cm^{-3}) for nitrogen at 5 eV.

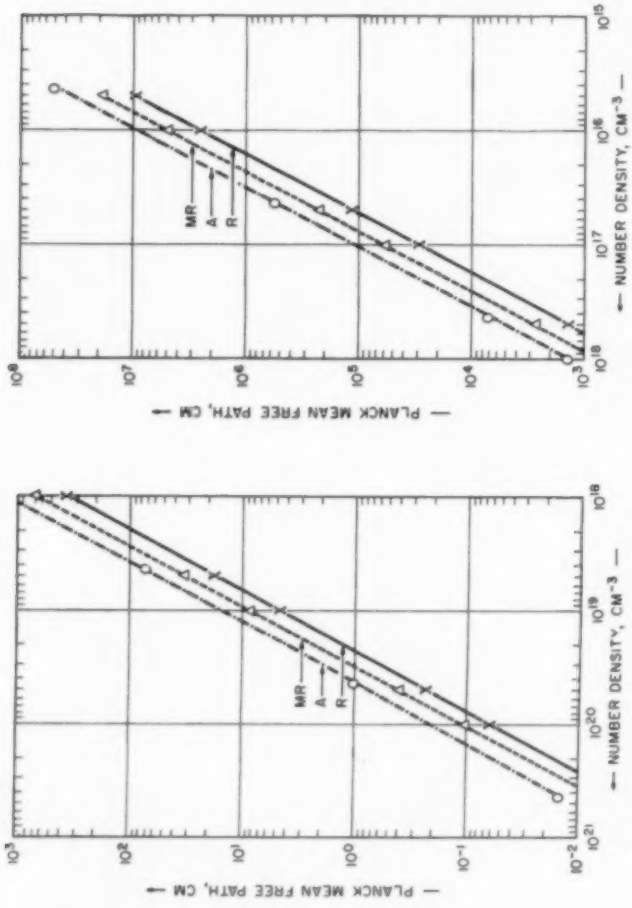

FIG. 5. The Planck mean free path (in cm) as a function of number density (in cm^{-3}) for nitrogen at 20 eV.

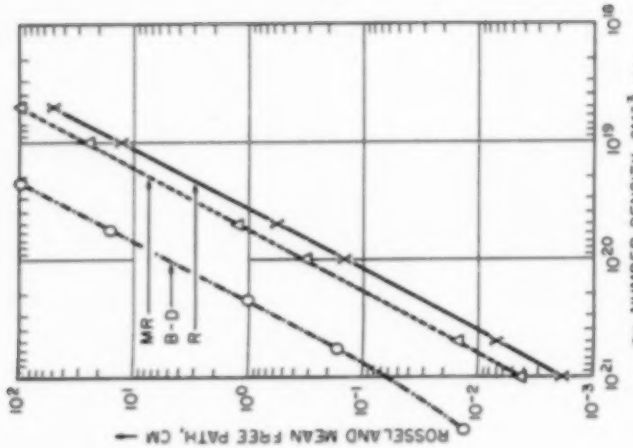

FIG. 7. The Rosseland mean free path (in cm) as a function of number density (in cm^{-3}) for beryllium at 10 eV.

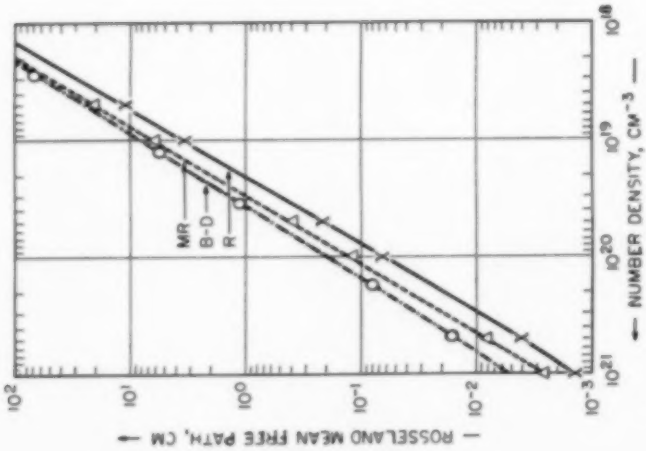

FIG. 6. The Rosseland mean free path (in cm) as a function of number density (in cm^{-3}) for fluorine at 10 eV.
(The designation B-D refers to numerical results derived by BERNSTEIN and DYSON[45]).

agreement to about a factor of two with the numerical results. However, more important than the difference between the (R) and (MR) approximations, is the fact that either set of equations provides reasonable estimates for the Rosseland and Planck means in high-temperature gases.

In conclusion, we wish to insert a word of caution. In Fig. 7 we have shown a comparison between the Bernstein–Dyson results for beryllium at 10 eV and the corresponding results

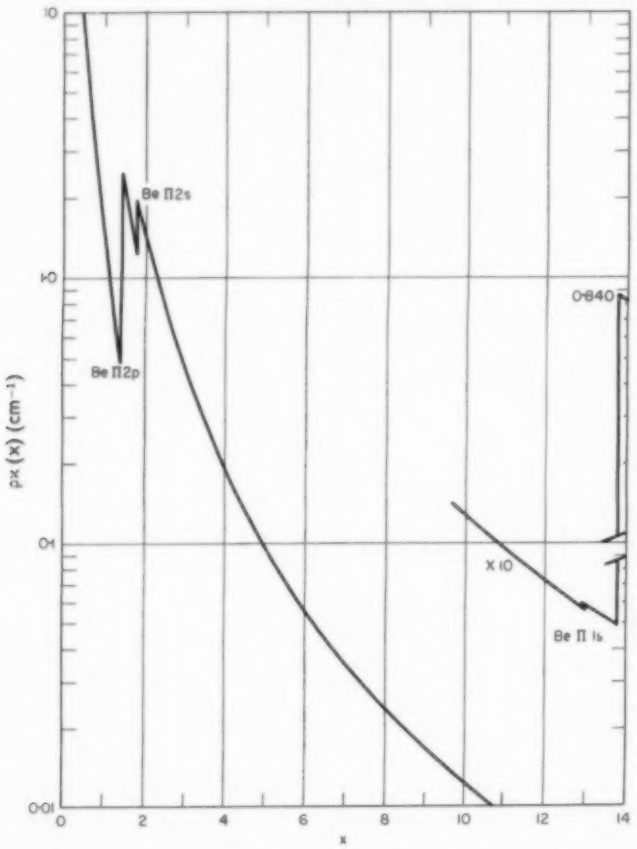

FIG. 8. The product of absorption coefficient × (x) and density (ρ) as a function of $x = h\nu/kT$ for beryllium at 10 eV for a mass density = $5{\cdot}86 \times 10^4$ g/cm³ (from BERNSTEIN and DYSON[61]).

obtained from equations (14) and (24). The reason for the large discrepancy in this case is a "window" for values of $x = h\nu/\Theta > 2$ (see Fig. 8). One of the significant approximations involved in establishing the equations for the Rosseland mean [equations (14) and (24)] is contained in equation (8). This relation should be used only if at least one of the ions which contributes significantly to the opacity has bound levels in the interval $2 \leq x \leq 8$; otherwise (compare Fig. 7) the approximation formulas will seriously underestimate the Rosseland mean.

REFERENCES

1. H. MAYER, Los Alamos Scientific Laboratory Report L-647, Los Alamos, New Mexico (1948) (unpublished).
2. H. L. BRODE (unpublished calculations), The RAND Corporation, Santa Monica, California.
3. YU. P. RAIZER, *J. exp. theor. Phys.* (U.S.S.R.) **37,** 1079 (1959).
4. B. H. ARMSTRONG, *Mean Absorption Coefficients at Air, Nitrogen, and Oxygen from* 22,000° *to* 220,000°, Lockheed Missiles and Space Division, Palo Alto, California, Report LMSD-4979, July 15 (1959).
5. J. BERNSTEIN and F. J. DYSON, *The Continuous Opacity and Equations of State of Light Elements at Low Densities*, General Atomic, A Division of General Dynamics Corporation, San Diego, California, Report GA 848, July 13 (1959).
6. A. UNSÖLD, *Physik der Sternatmosphären*, Springer, Berlin (1938).
7. C. E. MOORE, *Atomic Energy Levels*, Vol. I, National Bureau of Standards, Washington 25, D.C., Circular 467 (1949).
8. YU. P. RAIZER, *J. exp. theor. Phys.* (U.S.S.R.) **36,** 1583 (1959).

VOL.
1
1961

J. Quant. Spectrosc. Radiat. Transfer. Vol. 1, pp. 269–277. Pergamon Press Ltd. Printed in Great Britain

RADIATION FROM HOT NITROGEN*

R. A. ALLEN, J. C. CAMM, J. C. KECK
Avco–Everett Research Laboratory, Everett, Mass.

(*Received* 5 *July* 1961)

Abstract—The equilibrium radiation emitted by shock heated nitrogen has been studied in the wavelength range 3300 to 7100Å at an equilibrium temperature from 6000°–7000°K and densities 0·01 to 0·20 times atmospheric. Identification of the various radiating band systems was accomplished by spectroscopic techniques. The absolute intensity versus wave length profile at thermodynamic equilibrium was obtained using photometric methods. By comparing this profile with theoretical predictions, the electronic *f*-number for the $N_2^+(1-)$ system was found to be 0·09 ± 0·05. CN and O_2 contamination effects were also investigated. By studying the density dependence of the radiation, the collisional deactivation cross-section for this band was found to be greater than 10^{-15} cm².

I. INTRODUCTION

RECENT interest in the field of hypersonic aerodynamics and atmospheric physics has made necessary the quantitative understanding of optical radiation from air. The versatility of the shock tube for making spectroscopic study of hot gases has already been shown by many workers, and a method of obtaining electronic transition probabilities for molecules has been demonstrated by KECK *et al.*[1] in studies made of air.

This paper describes a study of the radiation from shock heated nitrogen which was undertaken as a preliminary step in an experiment to determine the dissociation rate of nitrogen. Photographic and spectroscopic methods were employed to examine the gross characteristics of the shock and to identify the various radiating species. Absolute intensity measurements were made so that theory and experiment could be compared. These intensity measurements are presented graphically along with the theoretical calculations based on the known existing electronic transition moments published by other workers. Oxygen and CN contamination effects on the equilibrium radiation were investigated quantitatively as well as qualitatively and comparison between the observations and theory was made.

II. EXPERIMENTAL EQUIPMENT

A schematic diagram of the shock tube, recording equipment and optical arrangement, is shown in Fig. 1. The shock tube has a 15 ft pyrex test section of 1·5 in. inside diameter. The high pressure driver section was separated from the low pressure test section by a steel diaphram. The driver was of stainless steel 3 ft long and 1·5 in. inside diameter. The test section was evacuated by an oil diffusion pump prior to introducing the test gas. Pressures of less than 2·0 μ of Hg and virtual leak rates of less than 1·0 μ of Hg per min were obtained.

* This work has been sponsored jointly by the Air Force Ballistic Missile Division, Air Research and Development Command, under Contract AF 04(647)–278 and by the Advanced Research Projects Agency monitored by the Army Rocket and Guided Missile Agency, Army Ordnance Missile Command, under Contract DA-19-020-ORD-4862.

A flow system was used to minimize impurities due to out gassing of the apparatus. Also used was a liquid nitrogen cold trap to remove water vapor from the N_2. Initial pressure in the test section was measured by a manometer with an estimated maximum error of 0·4 per cent.

The shock speeds were measured by observing with a single photomultiplier the radiation from the shock as it passed a series of six equally spaced slits arranged 10 in. apart along

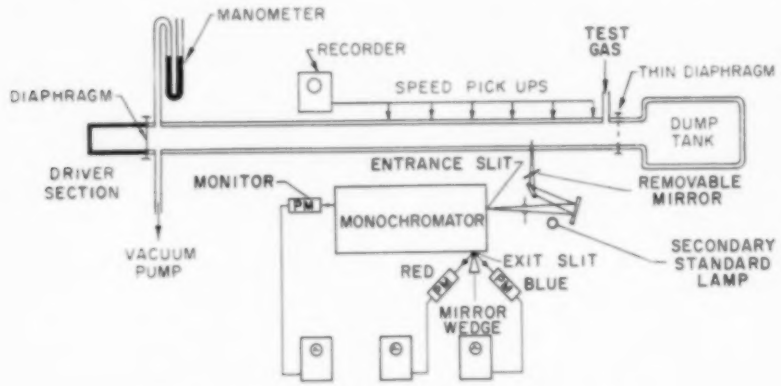

FIG. 1. Schematic diagram of experimental apparatus.

the last half of the shock tube. The output of the photomultiplier was doubly differentiated and displayed on a folded oscilloscope sweep which was normally read to the nearest 0·4 μ sec. A speed profile was constructed and the velocity at the test point was determined with a maximum error of about 1 per cent. At the position in the shock where the equilibrium measurements were made, the error in intensity measurements due to attenuation was less than 2 per cent.

III. EXPERIMENTAL RESULTS

Fig. 2a shows time resolved photograph of a typical shock wave as it passes the test point. Study of the photograph shows an abrupt onset of radiation. Also the photo shows very little change in radiation after the first 5 μ sec. This gives strong evidence that the test gas has reached thermodynamic equilibrium. Note that because of the circular cross-section of the shock tube and the thinness of the test gas, the radiation is stronger at the center then near the walls. Fig. 2c shows the radiation profile taken with a photomultiplier, the resolution of which was 0·13 μ sec, and filter, the wavelength response of which was in the 0·55–1·1 μ region. Here the radiation is observed to rise to peak value in less than a half μ sec and then decay to an equilibrium value which remains relatively constant for approximately 15 μ sec and then is terminated by the driver gas interface. Generally a slight increase in equilibrium intensity was observed as one moved back in the shock because of attenuation effects. This phenomenon would be expected since as one moved back from the shock front, one would be looking at gas which had been heated to a higher temperature than that gas which is observed nearer the shock front.

In order to be certain of the origin of the radiation being studied, spectra were taken of the shock waves using the race track techniques reported by ROSA[2]. Typical race track

VOL. 1 1961

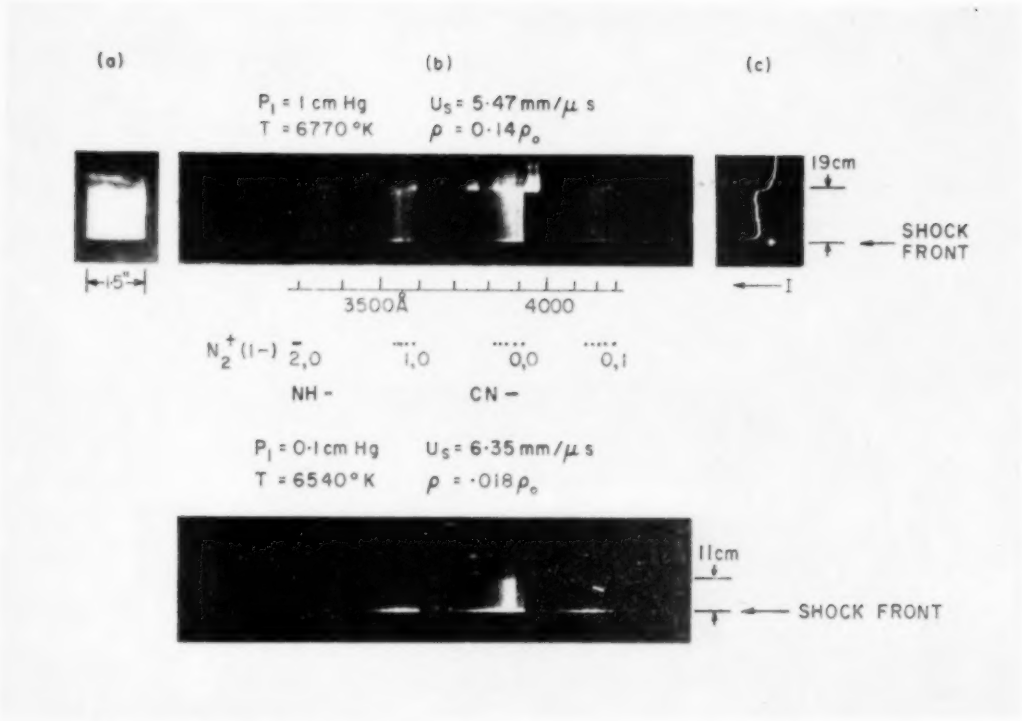

FIG. 2. (a) Time resolved photograph of normal shocks in nitrogen. (b) Race track spectrograms of shock waves in nitrogen. The overshoot and equilibrium radiation of the N_2^+(1−) radiation is clearly identified. (c) Oscillogram record of radiation observed in the 0·55–1·1 μ region showing the radiative overshoot and relatively flat equilibrium region. All pictures on the top line are scaled to the same shock thickness.

(*facing p.* 270)

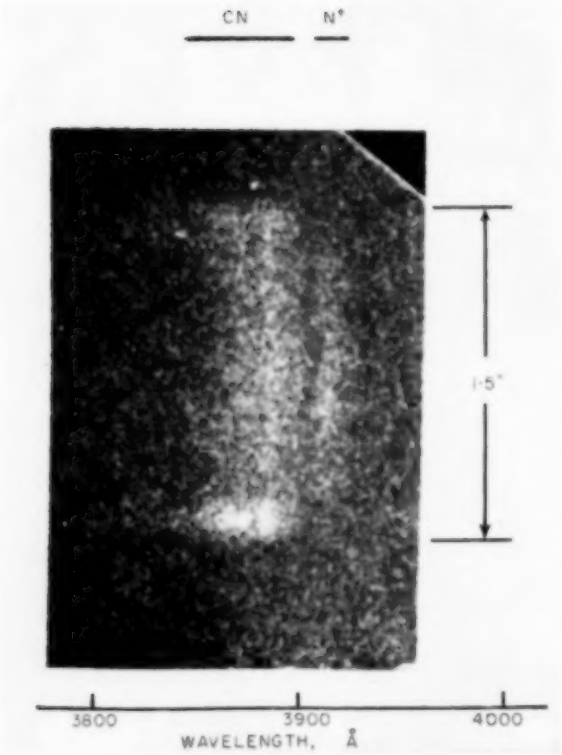

FIG. 3. Spectrogram obtained with slit of spectrograph perpendicular to axis of shock tube driver passage of a 5·1 mm/μ sec shock through nitrogen at a pressure of 1 cm Hg. The CN radiation is confined mainly to the shock tube walls.

(*facing p.* 271)

VOL
1
196

spectrograms with the radiating species identified are presented in Fig. 2b. Most of the radiation is seen to be due to N_2^+ molecules, and small amounts due to impurity CN and NH molecules. Attempts to reduce the impurity level provided evidence that most of the CN molecules were at, or near the walls of the pyrex tube. This was verified by the spectrogram shown in Fig. 3. The fact that the radiation intensity from N_2^+ appears to diminish near the edges of the tube shows that N_2^+ molecules are evenly distributed across the tube, while the fact that the radiation from CN is most intense at the edges of the tube proves that the CN molecules are more dense along the walls of the tube.

For 4–7 mm/μ sec shock waves in pure nitrogen at initial pressures from 20–1·0 mm Hg, the N_2^+ (1−) and N_2 (1+) radiation was observed to rise abruptly at the onset of the shock front to a peak value then decay in a few μ sec, corresponding to a temperature relaxation to an equilibrium level. This equilibrium level was observed to remain relatively constant for approximately 15 μ sec until the passage of the driver gas interface. Radiation from impurities was observed to be confined mainly to the shock tube walls.

IV. MEASUREMENTS

A. Apparatus and calibration

Measurements of the spectral intensity at equilibrium were made using a calibrated dual-channel grating monochromator. The experimental apparatus is shown schematically in Fig. 1. The entrance slit of the monochromator was imaged perpendicular to the shock tube at the center of the test gas by an optical train consisting of two aluminized mirrors. The monochromator was equipped with three photomultipliers; two which measured the radiation intensity in adjacent narrow wavelength bands selected by the monochromator and the third which monitored a fraction of the radiation passing through the entrance slit. Dumont 6292 and K1292 photomultipliers were used, and their outputs were fed directly to Tektronix 545 oscilloscopes equipped with 53K/54K preamplifiers.

Calibration of the complete optical train including shock tube windows and appropriate filters to prevent overlapping of orders was made using a secondary standard tungsten ribbon filament lamp which had been compared against a primary standard. The brightness temperature of the primary standard lamp was given as a function of lamp current at a wavelength of 6530Å by the National Bureau of Standards. The spectral intensity of the lamp was calculated at other wavelengths using data on the emissivity of tungsten given by DeVos[3]. The secondary standard lamp was placed permanently in position on the monochromator stand with a front surfaced aluminized mirror which could be swung into position in front of the shock tube in order to image the tungsten ribbon filament at the entrance slit of the monochromator. A section of shock tube was placed in the spectral path directly in front of the lamp to correct for transmission of light through the shock tube wall. The calibrated secondary lamp was used to calibrate from 3300Å to 7100Å and frequent checks were made on the calibration of the system. Thus, error due to voltage and photomultiplier drift was essentially eliminated.

The brightness temperature of the primary and secondary standards were checked using a Leeds and Northrup optical pyrometer. The temperatures checked to within 9° of that given by the National Bureau of Standards. The total maximum reading error of absolute intensity measurements was ±15 per cent.

The monochromator was calibrated for wavelength with a mercury lamp. The error in setting the monochromator was ±5Å.

B. Spectral distribution

Figure 4 shows absolute intensity measurements in the 3300Å–7100Å region of the equilibrium radiation from shocks in pure nitrogen at an initial pressure of 1·0 cm Hg. Since all the runs were not at exactly the same shock speed, they were extrapolated to 4·8 mm/μ sec equivalent to an equilibrium temperature of 6300°K as obtained from FELDMAN's tables.[4] The variation of intensity with shock speed given by the theory outlined in reference (1) was used as a guide in this extrapolation. For each run there were two measure-

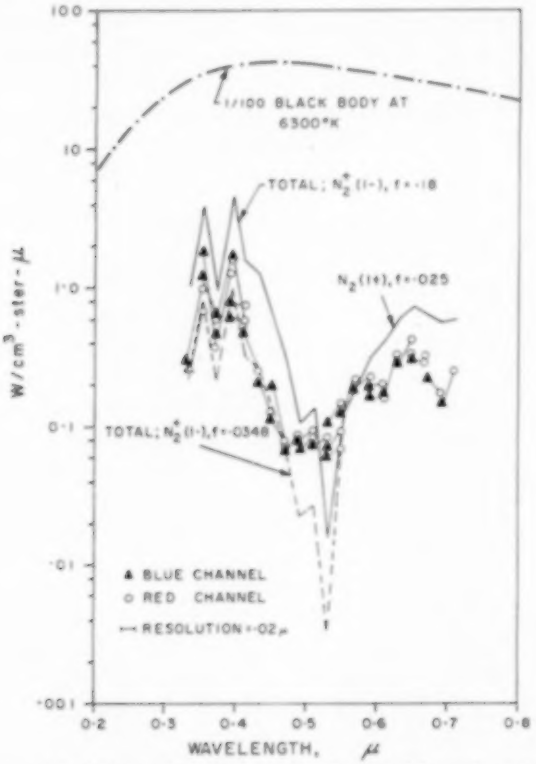

FIG. 4. Experimental and theoretical predictions of spectral intensity of nitrogen at $T = 6300°K$ and $\rho = 12\rho_0$ ($P_1 = 1$ cm Hg and $U_s = 4{\cdot}8$ mm/μ sec). The theoretical lines are based on *f*-numbers reported by the various workers mentioned in the text.

ments in adjacent monochromator channels—one represented by the solid triangle in Fig. 4 and the other by the open circles. Short lines are used to connect the two intensity measurements obtained for each run.

The theoretical lines superimposed on the experimental points are obtained using the theory outlined in reference (1), and are based upon the concentration of species in the absorbing state, the spectral distribution function averaged over the wavelength interval observed, the absolute temperature and the electronic *f*-number. The solid segmented line is the theoretical spectral distribution based on *f*-numbers reported elsewhere[1] for the N_2^+ (1−) and N_2 (1+) systems. The dashed segmented line is the theory using the *f*-number

reported by BENNET and DALBY[5] for the N_2^+ (1—) system. The discrepancy in the 0·52 μ region was attributed to a small amount of scattered radiation.

C. Shock speed dependence

The problem of extrapolating the equilibrium radiation to obtain the spectral distribution at a given temperature as well as understanding attenuation effects makes the optical

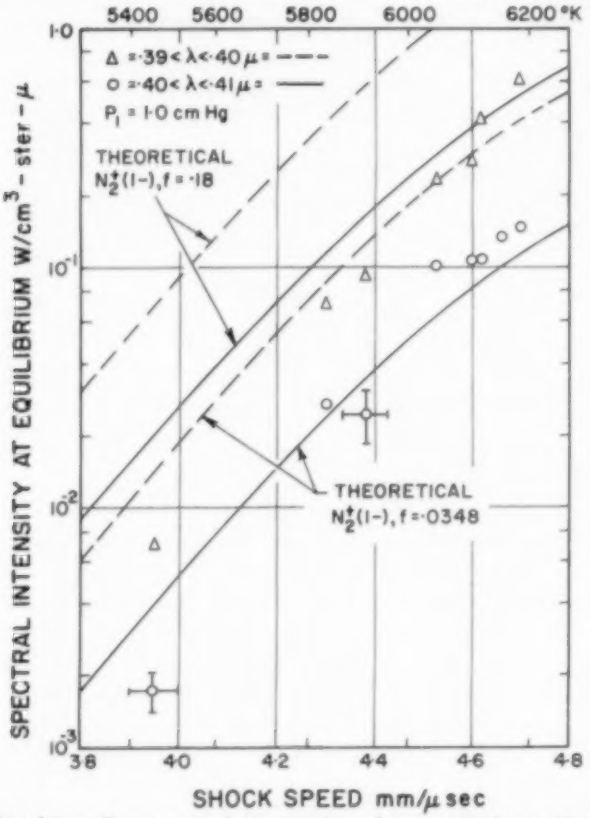

FIG. 5. Intensity of two adjacent monochromator channels versus shock speed in the N_2^+(1—) region comparing experimental observations with theoretical predictions based on the *f*-number of the N_2^+(1—) system reported by KECK *et al.*[1] (0·18) and BENNET and DALBY[5] (0·0348).

intensity dependence on shock speeds of interest. Shocks with the same monochromator setting were run at various shock speeds and are displayed in Fig. 5. Theoretical lines are constructed using the *f*-numbers for the N_2^+ (1—) system reported by both Keck *et al.* and Bennet and Dalby. It is upon these theoretical curves that the extrapolation in Fig. 4 is based. From this curve it can be seen that 1 per cent change in shock speed produces approximately 19 per cent change in radiant intensity of the N_2^+ (1—) system.

D. Effect of impurities

The presence of CN contamination has always been a problem in shock tube experiments and there has been much effort to eliminate it by such measures as using a pyrex shock tube

initially evacuating to low pressure and incorporating a flow system with a liquid N_2 trap to minimize impurities from outgassing. Under these conditions the CN radiation from shocks in pure nitrogen as observed spectroscopically (Fig. 3) is confined to the shock tube walls.

The effect of CN contamination was further investigated by introducing 2 per cent C_2H_2. One channel of the monochromator was set on the 3888 CN band head; the other on N_2^+ (1−) radiation. A Dumont K1292 photomultiplier was used as the monitor with an appropriate filter so that it monitored essentially only the N_2^+ (1+) radiation. Several runs at identical shock speeds were made with and without C_2H_2 contamination. The results for the equilibrium radiation are displayed in Table 1 and normalized to the pure N_2 run. It can

TABLE 1. SHOWING EFFECT OF 2% C_2H_2 CONTAMINATION ON EQUILIBRIUM INTENSITY MEASUREMENTS—ALL RESULTS BEING NORMALIZED TO THE RESULTS FOR THE PURE NITROGEN RUN. CN CONTAMINATION PRODUCES NO NOTICEABLE EFFECT EXCEPT IN THE CN VIOLET REGION WHERE THE RADIATION IS GREATLY ENHANCED.

Gas $P_1 = 1$ cm Hg	U_s mm/μ sec	0·38 < λ < 0·39 μ [CN band head] $I/I_{100\%N_2}$	0·39 < λ < 0·40 μ [N_2^+ (1−) band head] $I/I_{100\%N_2}$	0·55 < λ < 1·1 μ [N_2 (1+) system] $I/I_{100\%N_2}$
100% N_2	4·93	1	1	1
2% C_2H_2	4·98	8·05	1·01	1

be seen that the CN 3883 band radiation increased by a factor of 8 while there was no apparent change in the adjacent channel observing part of the N_2^+ (1−) system or in the N_2 (1+) radiation in the 0·55–1·1 μ wavelength interval. Since the CN red system radiates in the 0·55–1·1 μ region, this indicates that the red system is much less intense than the violet system and is, therefore, unlikely to effect the results of experiments carried out in the red region of the spectrum even though the CN contamination may be appreciable.

If there were NO present in the test gas excess electrons would be produced by its dissociating to NO^+ and e^- as reported by LAMB and LIN[6]. Since excess electrons would tend to suppress the N_2^+ concentration a false determination of the *f*-number for the N_2^+ (1−) system would be produced by the existence of electron contamination. To investigate this effect known amounts of oxygen up to 5 per cent were introduced into the test gas and the radiation across the 3914 N_2^+ (1−) band head was observed. The difference between the two adjacent channels versus O_2 contamination is displayed in Fig. 6. By taking the difference between the two channels, the possibility of a small contribution from impurity radiation is eliminated. The theoretical lines are based upon the chemistry of the hot gas at an equilibrium temperature of 6100°K. The results of these oxygen contamination runs show the N_2^+ (1−) radiation sensitiveness to electron concentration and also demonstrates that the nitrogen runs are reasonably pure.

E. Density dependence

"Collision limiting" of radiation occurs when the depopulation of an excited state of a molecule by radiation becomes significant compared with the depopulation of that state by collision. When this condition occurs one may have steady state radiation at a value considerably less than the equilibrium value. In this study the equilibrium radiation of the N_2 (1+) and N_2^+ (1−) systems was observed not to be "collision limited". This was deduced from the fact that there was no lowering in the apparent *f*-numbers for runs made

VOL 1 196

with initial pressures of 0·1 cm Hg as compared with runs made with initial pressures of 1·0 cm Hg. With the observation that these runs at 0.1 cm Hg were not collision limited, a minimum limiting value for the collisional deactivation cross-section can be determined based on the relations given by KECK *et al.*[1]. The results show that collisional deactivation cross-section is greater than or equal to 10^{-15} cm for the N_2^+ (1−) system and 10^{-16} cm for the N_2 (1+) system.

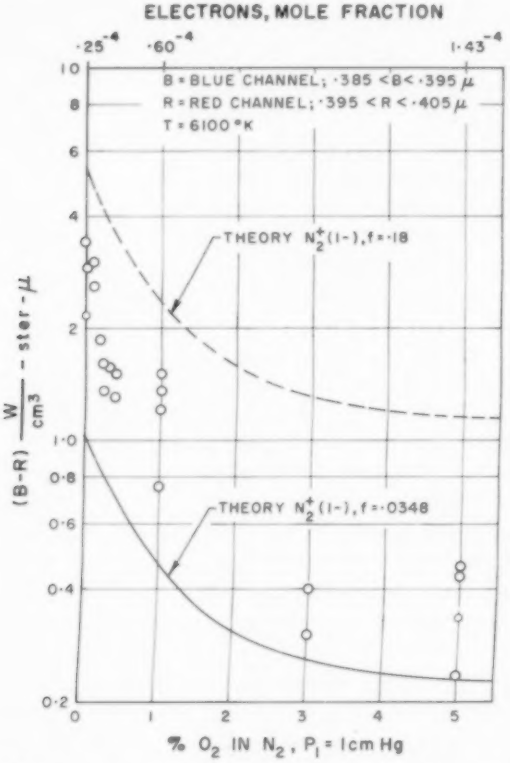

FIG. 6. Intensity difference across 3914 N^+ (1−) band head versus oxygen contamination. The two theoretical lines are based upon the *f*-number reported by KECK *et al.*[1] (0·18) and BENNET and DALBY[6] (0·0348). The depressing effect on the N_2^+ radiation by excess electrons is demonstrated here since NO readily dissociates to NO^+ and e^-.

F. Electronic f-numbers

Following the method outlined by KECK *et al.*[1], an electronic *f*-number of 0·09 ± 0·05 for the N_2^+ (1−) system was determined by fitting the data in Figs. 4, 5 and 6. Although some data were obtained in the wavelength region of the N_2 (1+) system, it was not considered sufficient to warrant a detailed analysis. As can be seen in Fig. 4, however, the data which were obtained are a little lower than expected for the *f*-number of 0·025 reported by Keck *et al.* which suggests that this value may be a little high. It was not possible to obtain any information on the N_2 (2+) radiation in these experiments due to the fact that the radiation from this band system is very small in the wavelength region covered.

The value of 0·09 ± 0·05 for the *f*-number of the N_2^+ (1−) system determined in this study lies between the values of 0·18 ± 0·09 reported by Keck *et al.* and 0·0348 ± 0·002 reported by Bennet and Dalby. It, therefore, does little to resolve the question as to which of the previous values is to be preferred. Since the method of this experiment is the same as that of Keck *et al.* the comparison of these two experiments does not give any information on the validity of the method but is primarily a check on the unfolding procedure used in the earlier experiments, and the general cleanliness of the shock tube. In this regard, it is felt that the most likely explanation of the larger *f*-number reported by Keck *et al.* is associated with the difficulty of eliminating impurity radiation from CN in the stainless steel shock tubes employed. With reference to the measurements of Bennet and Dalby we note that their method involves an observation of the decay time of the radiation from the N_2^+ (1−) system and is completely independent of the method employed here. Although it is difficult to find fault with their technique, there is the possibility that in a highly non-equilibrium situation, the population in the radiating state may be fed from higher states thus increasing the apparent lifetime and leading to a low *f*-number.

In concluding this discussion we should like to comment on a few of the problems associated with the use of the shock tube technique employed in this experiment for making *f*-number determinations.

First, there is the problem of precisely determining the gas temperature. The temperatures used in this study were obtained from Feldman's tables[4] and are based on the continuity, momentum and energy equations across the shock front and an equation of state which assumes full thermodynamic equilibrium. Parkinson and Nicholls[7], by spectroscopic methods and the use of "thermometric" molecules, obtained rotational temperatures in shock heated gases which are slightly lower (10–15 per cent) than the gas kinetic temperatures calculated from the shock velocities. Although it is our opinion that the method employed by us is the more accurate, we should like to point out that the assumption of a lower temperature would lead to higher apparent *f*-numbers further increasing the discrepancy between the shock tube measurements and those of Bennet and Dalby.

Second, there is the problem of accounting for effects of shock speed attenuation and boundary layer growth. The results of this study were relatively free of attenuation effects as indicated by the measured shock speeds and the flat region of radiation behind the shock front which rose only slightly until passage of the driver gas interface. This flat region of the equilibrium radiation and the fact that CN radiation in pure nitrogen shocks was observed to be confined along the shock tube walls also indicates that the test region was free of boundary layer effects.

Finally, there is the problem of dealing with impurities. By purposely introducing impurities, several possible sources of experimental error were found to be negligible. There was no CN red contribution to the N_2 (1+) radiation in a CN contaminated shock. Although the violet bands radiated strongly in the N_2^+ (1−) region, the N_2^+ (1−) radiation intensity could still be effectively measured in these contaminated runs by observing the radiation away from the CN violet bands. The depression of the N_2^+ (1−) radiation by excess electrons was studied by introducing small amounts of oxygen into the test gas. The observed effect was that which was predicted based on the equilibrium concentrations[8] of the various species and the gas kinetic temperature. The results indicate that the pure nitrogen runs were free of excess electrons.

VOL.
1
1961

Acknowledgements—The authors wish to acknowledge the enthusiastic support given this work by A. R. KANTROWITZ, Director of the Avco–Everett Research Laboratory. We are especially indebted to D. TEARE who carried out many of the calculations; B. KIVEL who has given many helpful suggestions; and to C. AVERITT who assisted with the experimental details.

REFERENCES

1. J. KECK, J. CAMM, B. KIVEL and T. WENTINK, Radiation from Hot Air. Part II, *Ann. Phys.* **7**, (1959).
2. R. J. ROSA, Shock Wave Spectroscopy, *Phys. Rev.* **99**, 2 (1955).
3. O. C. DEVOS, *Physica*, **20**, 690 (1954).
4. S. FELDMAN, *Hypersonic Gas Dynamic Charts for Equilibrium Air*, Avco Research Laboratory, Everett, Mass. (1957).
5. R. G. BENNET and F. W. DALBY, Experimental Determination of the Oscillator Strength of the First Negative Bands of N_2^+, *J. Chem. Phys.*, **31**, 435 (1959).
6. L. LAMB and S. C. LIN, Electrical Conductivity of Thermally Ionized Air Produced in a Shock Tube, *J. Appl. Phys.*, **28**, 754 (1957).
7. W. H. PARKINSON and R. W. NICHOLLS, Spectroscopic Measurements in a Shock Tube Using CN as a Thermometric Molecule, *Canad. J. Phys.*, **38**, 715 (1960).
8. F. R. GILMORE, Rand Corp. Research Memorandum RM–1543 (1955).

OL.
1
961